Nonlinear Hydrodynamics and Rheology of Granular and Gas-Solid Suspensions

A Thesis

Submitted for the Degree of

DOCTOR OF PHILOSOPHY

by

SAIKAT SAHA

ENGINEERING MECHANICS UNIT
JAWAHARLAL NEHRU CENTRE FOR ADVANCED SCIENTIFIC RESEARCH
(A Deemed University)
Bangalore – 560 064

December 2017

Dedicated to My Parents

DECLARATION

I hereby declare that the matter embodied in the thesis entitled "**Nonlinear Hydrodynamics and Rheology of Granular and Gas-Solid Suspensions**" is the result of investigations carried out by me at the Engineering Mechanics Unit, Jawaharlal Nehru Centre for Advanced Scientific Research, Bangalore, India under the supervision of **Prof. Meheboob Alam**, and that it has not been submitted elsewhere for the award of any degree or diploma.

In keeping with the general practice in reporting scientific observations, due acknowledgment has been made whenever the work described is based on the findings of other investigators.

Saikat Saha

CERTIFICATE

I hereby certify that the matter embodied in this thesis entitled "**Nonlinear Hydrodynamics and Rheology of Granular and Gas-Solid Suspensions**" has been carried out by **Mr. Saikat Saha** at the Engineering Mechanics Unit, Jawaharlal Nehru Centre for Advanced Scientific Research, Bangalore, India under my supervision and that it has not been submitted elsewhere for the award of any degree or diploma.

Prof. Meheboob Alam
(Research Supervisor)

Acknowledgements

I would like to thank my adviser Prof. Meheboob Alam for being an extraordinary mentor, teacher, stands as guru of my life. I express my deepest sense of gratitude for his constant encouragement and support throughout the course of the study and the thesis. Without his systematic guidance, insightful comments, vast knowledge and immense patience, this thesis would not have been possible. His dedication towards work is a quality that I hope to emulate in my academic life. Beside academics, he guided me as a mentor in other aspects of my life too, which I will try to remember and follow throughout the rest of my life.

I would also like to thank all the other faculty members of Engineering Mechanics Unit [Prof. K. R. Sreenivas, Prof. S. M. Deshpande, Prof. Ganesh Subramanian, Prof. Santosh Ansumali, Prof. Diwakar S. Venkatesan and Prof. Roddam Narasimha], Prof. Rama Govindarajan for their valuable teachings and inspiration. I gratefully thank all my professors at Calcutta University and ISI Kolkata for teaching those courses which formed the basis for my research work.

I express my gratitude to Prof. B. N. Mandal, who once taught me "hard work" is the only inevitable way to success. I would like to thank Prof. Uma Basu for her guidance and support during my M.Sc, study. I would also like to thank Prof. Nisith Das for his teaching and inspiration during my B.Sc. study, which formed as a basis of my knowledge towards mathematics. I thank Atin Kumar Das (Apu Kaku) and late Manik Bandopadhyay for teaching and guiding me during school days.

I am grateful to my friends who shared their experiences and supported me in the times of need. I would like to thank my fellow lab-mates: Dr. Nandu Gopan, Dr. Reddy, Dr. Ansari, Sunil, Ramakrishna, Deepthi, Achal, Ronak, Prateek, Prashanth, Albin and all other EMUites for their valuable advice, immeasurable help and the friendly working environment in the lab and the department. I really enjoyed my life in JNC which was particularly memorable because of playing badminton, I offer my special regards to all of those who played badminton with me and all other JNC friends. I would also like to express my sincere thanks to my senior researchers: Dr. Priyanka Shukla, Dr. Vinay Kumar Gupta, Dr. Ujjayan Paul, Dr. Ponnu Lakshmi, Dr. Dhiraj Kumar Singh, Dr. Virendra.

I would like to gratefully acknowledge my friends: Sudipto, Mayurakshi, Sourasree, Mou, Malabika, Sanjib, Haru da, Kartick Da, Sona John, Ananthu, Jyoti, Archana, Divyesh and Mahan, Rayan, Ratul. My special thanks to Dr. Shailendra Kumar Singh for his valuable suggestions as a senior cum friend from last eight years. I would like to thank all Bharat Soka Gakkai members; specially to Abhiroop, Aishwariya, Nikita, Papri, Srimayee, Sutanuka, Vijay, Uttam and Suman.

I am thankful to CSIR for my Ph.D scholarship. I thank DST, JNCASR, CSIR for providing me financial assistance to attend conferences. I thank our A.O sir A N Jayachandra, admin staffs and academic staffs for their invaluable support from time to time. I thank all other members (especially the Dhanvantari staffs, Security staffs, Cleaning staffs, Chandraiya staffs and the Mess staffs) of JNC community who made my life possible at JNC.

Finally, I take this opportunity to express my deeply profound gratitude to my beloved parents, my sisters (Bardi, Mejdi, Sejdi and Chordi), my brother-in-laws (Baro Jamaibabu, Sona Da, Sejo Jamaibabu and Tapas Da) and my grandparents for their love and continuous support. My love to all my nieces (sonu, mom) and nephews (papan, montu), for giving me all that lovely moments during my visits to home.

Synopsis

A brief introduction about dry granular materials and gas-solid suspensions and their importance, along with the objective and motivation of the present research work, are given in **Chapter 1**. The remaining chapters of this thesis are sub-divided into two parts: (i) Part-A and (ii) Part-B. In Part-A, an extended hydrodynamic theory for dry granular materials and its rheological behaviour under plane shearing conditions are analysed in Chapter-2 and Chapter-3, respectively. In Part-B, the related analyses for gas-solid suspensions are described in Chapters 4 and 5.

The major focus of the present work has been to develop a complete theory for "rapid" granular and gas-solid suspensions that includes normal-stress differences and shear-thinning and shear-thickening behaviour, and the theory must be valid for the whole range of density spanning from the dilute limit to the (close to) freezing density. The theoretical approach adopted in this thesis is based on (i) the Enskog-Boltzmann equation of dense-gas kinetic theory and (ii) the moment-method of Harold Grad. The present theory has been validated via comparisons of transport coefficients with (i) the previous theories and (ii) the existing particle-level simulations.

In **Chapter 2**, a 14/10-moment theory for a dense granular gas using Grad's moment method is developed. An effort has been made to develop a complete theory that can be applicable to granular flows for any choice of inelasticity and particle volume fraction. An expansion around the Maxwellian is performed to obtain the non-equilibrium distribution function. A Grad-like moment theory has been developed in terms of fourteen field variables: (i) the mass density (ρ), (ii) the macroscopic flow velocity ($\boldsymbol{u} = \langle \boldsymbol{c} \rangle$), (iii) the kinetic stress ($\boldsymbol{P}^k = \rho \langle \boldsymbol{CC} \rangle \equiv \rho \boldsymbol{M}$), (iv) the kinetic heat-flux ($\boldsymbol{q}^k = \rho \langle \boldsymbol{C} C^2 \rangle$) and (v) the contracted fourth-moment P_{iijj}. The collisional source and flux terms at different orders are calculated by including all nonlinear terms arising from these hydrodynamic fields and their gradients. The collisional dissipation or the cooling rate is derived for the whole range of volume fraction that includes second-order derivatives of the hydrodynamic variables as well. A generalized Fourier law for granular heat flux is established using Maxwell-iteration technique, leading to a 10-moment theory in terms of (i) the mass density (ρ), (ii) the macroscopic velocity ($\boldsymbol{u}$)

and (iii) the kinetic stress ($\boldsymbol{P}^k$). It is shown that the thermal conductivity is described by an anisotropic-asymmetric tensor and the anisotropy follows from the presence of higher-order nonlinear terms in the respective collisional source/production term $\aleph_{\alpha\beta\beta}$; the gradients of density and kinetic stress also drive a heat current; the above features of heat-flux vector are distinct signatures of the non-Fourier rheology of the medium. Finally, the 14-moment theory is applied to analyse the uniform shear flow of a dense granular fluid; the analytical expressions of transport coefficients are determined as functions of the coefficient of restitution (e) and the solid volume fraction (ν). The theoretical results on pressure, shear viscosity and two normal-stress differences are compared with data from previous molecular dynamics (MD) simulations of granular shear flow. It is found that while the pressure and viscosity are well-predicted by the present theory for a wide range of density, there are large quantitative differences between theory and simulation for the prediction of two normal-stress differences. The resolution of the latter discrepancy is attempted in Chapter-3 that follows a different ansatz on the distribution function.

In **Chapter 3**, the rheology of the steady uniform shear flow of smooth inelastic hard-spheres is analysed using an anisotropic Maxwellian distribution function; the latter ansatz follows from the maximum entropy principle (E. T. Jaynes, 1957, Phys. Rev.) and seems to be appropriate for a granular gas for which an equilibrium-state does not exist. For the simple shear flow, the second-moment tensor $\boldsymbol{M}$ is assumed to be anisotropic, characterized by three parameters: (i) the non-coaxiality angle (ϕ, the angle between the principal eigen-directions of $\boldsymbol{M}$ and the shear tensor $\boldsymbol{D}$), (ii) the shear-plane temperature-anisotropy (η, the difference between the principal eigenvalues of $\boldsymbol{M}$ on the shear plane, $\propto T_x - T_y$) and (iii) the excess temperature ($\lambda^2 \propto T - T_z$) along the vorticity direction. The balance equations governing the kinetic stress tensor (or, the balance of second moment) has been solved using anisotropic Maxwellian as the single particle distribution function. An exact analytical solution at the Burnett order (second order in the shear rate) and a perturbative solution at the super-super-Burnett order (fourth order in shear rate) have been derived leading to analytical determination of the first ($\mathscr{N}_1$) and second ($\mathscr{N}_2$) normal-stress differences and other transport coefficients. The theoretical expressions for the two normal-stress differences, along with those of pressure (p) and shear viscosity (μ), are compared with (i) the full numerical solution of the second-moment equation and (ii) the previous MD simulation data. An excellent agreement with the simulation data is found when the solutions are considered at the super^2-Burnett order, valid for the whole range of volume fraction spanning from the dilute limit ($\nu \to 0$) to the freezing point density ($\nu \to 0.5$). The origins of two normal-stress differences are discussed in terms of the non-coaxiality of the eigen-directions of the stress and strain tensors and the excess

temperature in the vorticity direction. This chapter is based on two recently published papers in J. Fluid Mech. [(i) vol. 757 (2014), pp. 251-296 and (ii) vol. 795 (2016), pp. 549-580].

In **Chapter 4**, the normal stress differences and other transport coefficients are analysed for the simple shear flow of a dense gas-solid suspension of inelastic hard spheres suspended in a Newtonian gas of viscosity μ_g and experiencing a Stokesian drag force; this work is a direct extension of chapter-3 ($St \to \infty$), including the effects of interstitial gas ($St =$ finite). The viscous heating from the boundaries is compensated by dissipation via two mechanisms (i) the inelastic collisions between particles characterized by a coefficient of normal restitution e $(0 < e < 1)$ and (ii) the drag force which the surrounding fluid exerts on the particles. Rheology of the particle phase is analysed with anisotropic-Maxwelliian as the single-particle distribution function as in Chapter-3. The pressure, shear viscosity and the first and second normal-stress differences are computed for the whole range of density (ν) and inelasticity (e), with the scaled Stokes number ($St_d = St/R_{diss}$) varying from a small value (~ 10) to the dry granular limit of $St \to \infty$. An exact solution of the second-moment balance of velocity fluctuations at the Burnett order (i.e. second order in the shear rate) has been derived, leading to analytical expressions for the first ($\mathscr{N}_1$) and the second ($\mathscr{N}_2$) normal stress differences. Expanding around the Burnett order solution, a perturbative solution at the super-super-Burnett order (i.e. fourth order in the shear rate) is also derived which is found to improve the second-order solution. It is found that the first normal-stress difference is maximum in the dilute regime and tends to zero in the dense limit and remains positive throughout; on the other hand, the second normal-stress difference is negative in the dilute limit, undergoes a sign change at some finite density and becomes positive in the dense limit. The effect of the gas-phase is found to (i) decrease the values of both pressure and shear viscosity, and (ii) increase the magnitude of both normal-stress differences. The location of the critical density, where the second normal-stress difference changes its sign, is determined and plotted as a critical surface in the (ν, e, St_d)-plane. Finally, as the limit of $St \to \infty$ ($\mu_g \to 0$) is approached, the results for the dry granular flows of chapter 3 are recovered.

In **Chapter 5**, the dilute limit of a sheared gas-solid suspension is reanalysed, with a focus to understand the hysteresis behaviour in the particle phase rheology (H.-K. Tsao & D. L. Koch, J. Fluid Mech, 1995, vol. 296). Another focus of this chapter is to analyse and quantify the anisotropy of the second-moment tensor, $\boldsymbol{M} = \langle \boldsymbol{CC} \rangle$, of fluctuation velocity, and subsequently tie and explain the rheological/transport coefficients of a sheared gas-solid suspension in terms of the anisotropies of $\boldsymbol{M}$. In analysing this problem three qualitatively different states of solutions are found. Firstly, the "quenched" state, in which the individual particles follow the local fluid motion, corresponds to a very low value of particle agitation and appears below a critical value of Stokes number $St_{c_2}(\nu, e)$; this state is followed by an unstable state

of solution that exists over a range of intermediate Stokes numbers $St_{c_1} < St < St_{c_2}$. Finally, the agitated state corresponds to a very high value of temperature which is termed as the "ignited" state and exists beyond a critical value of Stokes number $St_{c_1}(e)$. The phase diagram is constructed in the three-dimensional (ν, St, e)-space that delineates the regions of ignited and quenched states and their coexistence. Analytical expressions for the particle-phase shear viscosity and the normal stress differences are obtained, along with related scaling relations on the quenched and ignited states. At any e, the shear-viscosity undergoes a discontinuous jump with increasing shear rate (i.e. discontinuous shear-thickening, DST) at the "quenched-ignited" transition. The first ($\mathscr{N}_1$) and second ($\mathscr{N}_2$) normal-stress differences also undergo similar first-order transitions: (i) $\mathscr{N}_1$ jumps from large to small positive values and (ii) $\mathscr{N}_2$ from positive to negative values with increasing St, with the sign-change of $\mathscr{N}_2$ identified with the system making a transition from the quenched to ignited states. It is shown that for both granular and gas-solid suspensions, the excess temperature ($T^{ex} = T = T_z \propto \lambda^2$) along the vorticity direction is responsible for $\mathscr{N}_2 \neq 0$, while the shear-plane anisotropies (ϕ and η) are responsible for $\mathscr{N}_1 \neq 0$.

Finally, the conclusions are drawn in **Chapter 6** with an overall summary of the thesis.

Table of contents

List of figures

List of tables

Chapter 1

Introduction

Granular matter is a collection of large number of solid particles where the particle size ranges from 1mm to meters (Saturn's ring) and it is found everywhere in nature (avalanche, debris flows, Planetary rings, etc.) as well as in industry (Jackson 2000; Rao & Nott 2008).

At rest the 'dry' granular materials (for which the effect of interstitial fluid can be neglected) behave like a solid, having a compressive strength but no tensile strength, and hence dubbed a 'peculiar' solid. On the other hand, a collection of particles can flow like a liquid as in an hour-glass or behave like a gas under strong shaking (Forterre & Pouliquen 2008; Rao & Nott 2008). In the case of a granular gas (Campbell 1990; Goldhirsch 2003; Brilliantov & Pöschel 2004), the particle collisions are inelastic, leading to the dissipation of the kinetic energy of colliding particles. The inelastic dissipation is known to be the progenitors of many interesting properties of a granular fluid, and is also responsible for the loss of 'microscopic' reversibility at the level of Liouville and Boltzmann equations that calls for non-standard statistical mechanics (Jenkins & Richman 1985*a*; Sela & Goldhirsch 1998; Garzó & Dufty 1999; Lutsko 2005; Rongali & Alam 2014) to develop coarse-grained theories for flowing granular matter. Because of its rich properties it is still an interesting and unexplored topic of research.

Granular matter is found in all three forms of matter viz. solid, liquid and gas. It can behave like a solid when undisturbed and can support large load or can form a pile. The frictional bond among the particles support that large load (Campbell 1990). Once this bond is overcome because of an external shear or some other form of disturbance, the system will start to flow. The initial stage of the flow will be movement of the particle-blocks relative to one another and this stage is the quasi static state. When the external disturbance is increased beyond a certain limit, the system reaches to the rapid-flow regime. Where the system is under a very strong external force, each particle moves randomly and independent of each other, as it happens in a gas flow. Therefore granular matter can work as a solid when undisturbed and can flow in response to an external influence. For example the sands in an hour glass flows

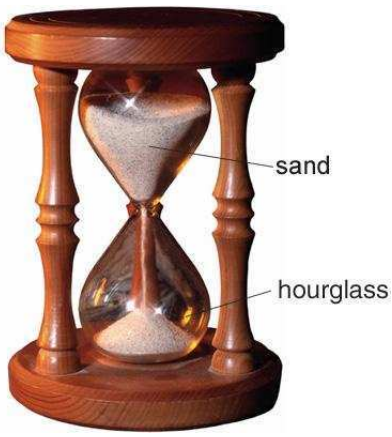

Fig. 1.1 Granular matter appears as solid and fluid phases simultaneously.

under gravity. Hourglass is an example where quasi-static, fluid and solid, all three phases of granular matter, can be seen. The flow through the orifice is the signature of a fluid, the sand-slides above the orifice shows the quasi-static behaviour whereas the stored sands at the bottom is the form of a solid (see figure 1.1).

Interestingly the flow rate through the orifice of an hour glass is independent of the height (Jaeger *et al.* 1996) of the substance above. This is unconventional and the behaviour is exactly opposing the characteristic of an usual fluid. This property of granular fluid being flowing at an almost constant speed is used in hour glasses. It is the contact forces between the grains and the static friction with the glass of the container enables the wall to support the extra load of the sand above (Janssen 1895). Because of it's stature and exhibition of properties of all three forms of matter, granular matter can be thought of as a different state of matter in it's own right.

Once the external influence is increased by means of increasing the shear rate, granular matter comes out of the quasi-static regime and flows like a fluid. At this stage an individual particle flows independent of others and it is called a rapid granular flow. This thesis addresses the behaviours of rapid granular flow in particular, when the substance is uniformly sheared.

Therefore, a driven system of macroscopic/non-Brownian particles (e.g. driven by external vibration or shearing) resemble a molecular gas in which the particles move around randomly but they loose energy upon collisions, with the latter being a major difference of the granular gas from its molecular counterpart. Such a non-equilibrium state of agitated particles is actually known as rapid granular fluid (Goldhirsch 2003) for which the dense gas kinetic theory (Chapman & Cowling 1970) has been appropriately modified and successfully used for a variety of flow configurations over the last three decades (Savage & Jeffrey 1981; Jenkins &

Richman 1985*b*,*a*; Sela & Goldhirsch 1998; Brey *et al.* 1998; Garzó & Dufty 1999; Brilliantov & Pöschel 2004; Rao & Nott 2008).

When a granular matter is rapidly sheared, each individual particle moves randomly independent of the presence of the neighbouring particles, it collides with other particles and the collisions are instantaneous, therefore the motion of these grains in a granular system can be thought of analogous to the thermal motion of the molecules in a molecular gas. The analogy between the random motion of the granules and the thermal motion of the molecular gas is so onto mapped that, all the definitions used in statistical mechanics of molecular gases have been employed to analyse the properties of a flowing granular media. Following the definition of temperature in molecular gases, the granular temperature is also defined as the mean of the square of particle's fluctuation velocity (Ogawa 1978; Campbell 1990). One point we must emphasize here that this granular temperature is not a thermodynamic temperature, it is not possible to maintain a constant granular temperature just by keeping it in contact with an isothermal heat hub albeit both the thermodynamic and granular temperatures have the act similar in their respective systems.

Despite the similarities between the molecular and granular gases there are certain differences also. The first one is the difference in size. The diameter of the particles in a granular system varies from 1 μm to some meters (for example, in Saturn's ring), much much larger than the diameter of an atom or molecule. The second and most important difference is that the collisions in a granular system are inherently "inelastic" leading to a continuous energy dissipation (Kadanoff 1999; Brilliantov & Pöschel 2004; Goldhirsch 2003). Because of this continuous energy dissipation, granular system needs a constant supply of energy in order to keep itself alive. If the energy source is stopped the system becomes dead. It can be experienced in our daily life examples. The grains kept in a container shows random temperature like motions when it is shaken but immediately becomes inert if the shaking is stopped. Therefore we have to constantly shake it in order to maintain the motions of these grains. The inelastic nature of the particles leads to so many interesting implications regarding the behaviours of a granular gas which will be discussed in the main chapters of the present thesis.

1.1 Coefficient of Restitution

The inelastic collisions between the grains are characterized by a coefficient of normal restitution e. It relates the post $(\boldsymbol{c}_1', \boldsymbol{c}_2')$ and pre-collisional $(\boldsymbol{c}_1, \boldsymbol{c}_2)$ velocities of disks/spheres labelled by 1 and 2 as (Brilliantov & Pöschel 2004; Rao & Nott 2008)

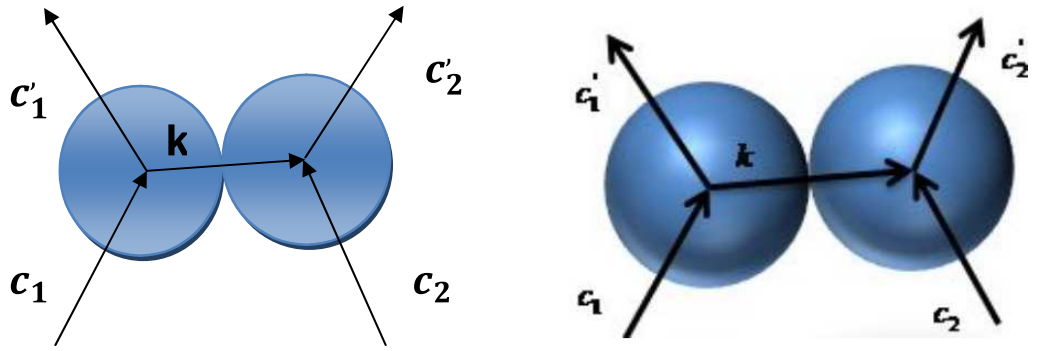

Fig. 1.2 Collision sketch of pairs of inelastic disks and spheres.

$$\left.\begin{aligned} \boldsymbol{c}_1' &= \boldsymbol{c}_1 - \frac{(1+e)}{2}(\boldsymbol{g}\cdot\boldsymbol{k})\boldsymbol{k} \\ \boldsymbol{c}_2' &= \boldsymbol{c}_2 + \frac{(1+e)}{2}(\boldsymbol{g}\cdot\boldsymbol{k})\boldsymbol{k} \end{aligned}\right\}, \tag{1.1}$$

where $\boldsymbol{g} = \boldsymbol{c}_1 - \boldsymbol{c}_2$ denotes the relative velocity of the colliding pair before the collision and $\boldsymbol{k}$ is the unit contact vector along the line joining the centres of the particles (figure 1.2). This coefficient of restitution mainly separates a granular gas from the molecular gas and is responsible for some rich features that granular matter possesses.

In general, for a granular gas of realistic particles, the coefficient of restitution is a function of the relative velocity $e \equiv e(\boldsymbol{g})$ and the explicit functional dependence on g must be worked out. Many attempts have been made (Schwager & Pöschel 1998; Ramírez *et al.* 1999) to derive a general closed form expression for $e(\boldsymbol{g})$. The most compact expression can be found in Brilliantov & Pöschel (2004), which is an infinite series representation of the form:

$$e = 1 - Ag^{1/5} + Bg^{2/5} \mp \cdots, \tag{1.2}$$

where $A, B, \cdots$ are functions of the Young modulus Y, Poisson ratio, mass density ρ, etc. But in this present thesis, for simplicity, we have assumed e to be a constant that belongs to the closed interval $[0,1]$. The supremum of the set $(e = 1)$ corresponds to a conserved system, where collision occurs elastically and the infimum $(e = 0)$ corresponds to a perfectly sticky collision, where complete energy of the relative motion is lost and the particles are bound together after a collision. Therefore the open interval $(0,1)$ corresponds to a dissipative system and causes energy loss.

We have also assumed that the particles are smooth in nature, which means that there is no change in the tangential direction of the relative velocity during a collision and the only

change along the normal direction is governed by

$$\left.\begin{aligned}(\boldsymbol{g}'\cdot\boldsymbol{k}) &= -e(\boldsymbol{g}\cdot\boldsymbol{k})\\ (\boldsymbol{g}'\times\boldsymbol{k}) &= \ \ (\boldsymbol{g}\times\boldsymbol{k})\end{aligned}\right\}, \tag{1.3}$$

where $\boldsymbol{g}' = \boldsymbol{c}_1' - \boldsymbol{c}_2'$ is the relative velocity after the collision. There are some studies that deal with the rough particles (Lun 1991; Abu-Zaid & Ahmadi 1993; Luding *et al.* 1998; Cafiero & Luding 2000; Gayen & Alam 2006, 2008, 2011; Rongali & Alam 2014) including the spin degrees of freedom. The particles that actually appear in real world are rough and frictional, therefore system composed of particles like these must deserves an attention. Several scientists have studied granular system of rough particles via theory (Alam & Nott 1997; Brilliantov *et al.* 2007; Goldhirsch *et al.* 2005; Huthmann & Zippelius 1997; Jenkins & Zhang 2002; Gayen & Alam 2006; Santos *et al.* 2011) and simulation (Cafiero *et al.* 2002; Gayen & Alam 2008, 2011). In their studies of rough particles the collision model includes energy loss due to changes in the normal as well as tangential components of momentum of the colliding particles, and relative velocity changes according to the rule (Pidduck 1922; Maw *et al.* 1976):

$$\left.\begin{aligned}(\boldsymbol{g}'\cdot\boldsymbol{k}) &= -e_n(\boldsymbol{g}\cdot\boldsymbol{k})\\ (\boldsymbol{g}'\times\boldsymbol{k}) &= -e_t(\boldsymbol{g}\times\boldsymbol{k})\end{aligned}\right\}, \tag{1.4}$$

where

$$\boldsymbol{g} = \boldsymbol{c}_1 - \boldsymbol{c}_2 + \left(\frac{\sigma}{2}\right)\boldsymbol{k}\times(\omega_1+\omega_2), \tag{1.5}$$

is the relative velocity before the collision. In equations (1.4-1.5) ω_1, ω_2 are the angular velocities of particles levelled with 1, 2 respectively and e_n, e_t stand for the coefficients of normal, tangential restitution respectively. The parameter e_t measures the particle's surface roughness and belongs to the interval $[-1,1]$, it accounts for the amount of change in the tangential direction during a collision. The boundary points $e_t = -1$ and $e_t = 1$ correspond to perfectly smooth and perfectly rough collisions respectively. As in the present thesis we are interested in granular flows for smooth particles we must take $e_t = -1$ and replace $e_n = e$, for which the collision dynamics given in (1.4) simplifies to the equation (1.3). Polydispersity is not a concern of the present thesis although it has great practical importance (Ottino & Khakhar 2000) and some scientists have studied them (Garzó & Dufty 2002; Montanero & Garzó 2003; Alam & Luding 2002, 2003*b*; Trujillo *et al.* 2003; Serero *et al.* 2006) in recent days. Some people have worked with non-spherical grains as well (Buchholtz *et al.* 1995; Pöschel & Buchholtz 1995). But for the present thesis we focus on the simplest model that consists of identical smooth spherical particles following hard sphere binary collisions.

In general the interstices between the solid particles are filled with air or with some other fluid and therefore, technically, the granular matter is a multiphase system. However when the density ratio between the fluid phase and the solid phase becomes very low, the presence of the interstitial fluid can be neglected and it is called the "dry" granular system. On the other hand, when the presence of the ambient fluid becomes important, the particle fluid interaction plays a significant role in momentum transport. The latter class of system is considered to be a suspension and the presence of an interstitial fluid leads to interesting physical phenomena. This thesis deals with both of these classes of systems, the dry granular flows and gas-solid suspensions. In the fast two chapters of this thesis, we have concentrated in analysing the dry granular system, while the last two chapters are devoted to analyse flows of gas-solid suspensions.

1.2 Non-Newtonian Rheology: Normal Stress Differences and Rate Dependent Viscosity in Granular Fluids

In a Newtonian fluid the shear stress varies linearly with the shear rate, passing thorough the origin in a response to an external disturbance. The proportionality constant, called the coefficient of shear viscosity or simply the viscosity, is the measure of fluidity or the measure of fluid's ability to resist deformation in response to shear stresses. In general for a Newtonian fluid the total stress tensor can be expressed as

$$P_{\alpha\beta} = p\delta_{\alpha\beta} + \widehat{P}_{\alpha\beta}. \tag{1.6}$$

The deviatoric part $\widehat{P}_{\alpha\beta}$ of the stress tensor for a Newtonian fluid takes the form

$$\widehat{P}_{\alpha\beta} = \begin{bmatrix} 0 & P_{xy} & P_{xz} \\ P_{yx} & 0 & P_{yz} \\ P_{zx} & P_{zy} & 0 \end{bmatrix}, \tag{1.7}$$

where P_{xy} is the shear stress, connects the strain rate $\frac{\partial u_x}{\partial r_y}$ via the constant shear viscosity (μ) as

$$P_{xy} = -\mu \frac{\partial u_x}{\partial r_y}, \tag{1.8}$$

and called the Newton's law of viscosity.

When a fluid disobeys any one of these (1.7- 1.8) laws, in terms of showing non-zero normal components in the deviatoric stress or/and non-constant μ, it is categorized as a non-Newtonian fluid. The occurrence of finite normal stress differences and the dependence of shear viscosity on shear rate in non-Newtonian fluids are briefly discussed in following sub-sections.

1.2.1 Normal Stress Differences and their consequences

The studies on normal stresses has a long and rich history in the area of particulate suspensions (Bagnold 1954; Brady & Morris 1997; Sierou & Brady 2002; Singh & Nott 2003; Guazzelli & Morris 2011), with the early works being carried out in the dense regime of such systems. More recent experimental work (Boyer *et al.* 2011; Couturier *et al.* 2011) on the behaviour of normal stresses in non-Brownian suspensions has generated renewed interest to understand the non-Newtonian rheology of suspensions and dense granular media via simulation and experiment (Lerner *et al.* 2012; Trulsson *et al.* 2012; Dbouk *et al.* 2013; Denn & Morris 2014). Even after 60 years' of research starting from (Bagnold 1954), there remain debates about the sign of two normal stresses in the dense regime of a suspension. In any case, studying the non-Newtonian behaviour is also important since the normal stresses themselves are responsible for many interesting flow-features (e.g. rod-climbing or Weissenberg-effect, see figure 1.3, die-swelling, secondary flows, etc.) in non-Newtonian fluids. Moreover, it is also known from the literature on in polymeric fluids and suspensions that the non-Newtonian fluids can support additional instability modes whose origin can solely be tied to normal stresses. From the modelling viewpoint, the presence of large normal-stress differences readily calls for higher-order constitutive models even at the minimal level. Of course, to make meaningful progress in developing such constitutive models, a prior knowledge of rheology is also needed.

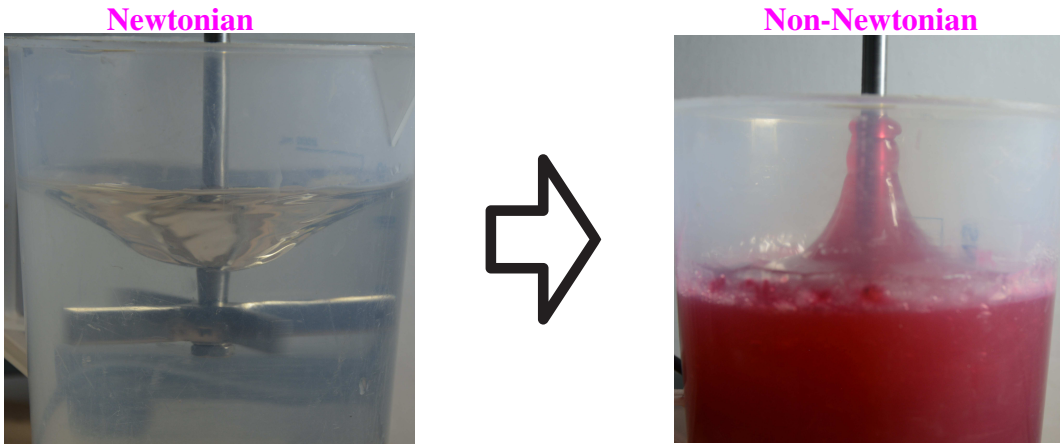

Fig. 1.3 Manifestation of normal-stress differences as observed in an experiment. In the left figure for a Newtonian fluid (water), the free surface is a parabola whereas the right figure shows prominent non-Newtonian rheology as the fluid (water+polymer solution) is climbing up along the rod.

In this thesis we investigate the non-Newtonian rheology of a sheared (i) granular and (ii) gas-solid systems via kinetic theory. For an N-particle system, the stress tensor has contributions from both kinetic and collisional mechanisms of transport:

$$\boldsymbol{P} = \boldsymbol{P}_{kin} + \boldsymbol{P}_{coll}, \tag{1.9}$$

the first term is dominant in the dilute regime, whereas the second-one dominates in the dense regime. This can be further decomposed as

$$\boldsymbol{P} = p\boldsymbol{I} + \widehat{\boldsymbol{P}}, \tag{1.10}$$

where $p \equiv P_{ii}/\text{dim}$ is the isotropic pressure (dim is the dimension), $\boldsymbol{I}$ is the identity tensor and the deviatoric stress is $\widehat{\boldsymbol{P}}$. The off-diagonal components of $\widehat{\boldsymbol{P}}$ are related to shear viscosity which, in general, depends on the deformation rate.

At the Navier-Stokes (NS) order, the stress tensor (1.10) is Newtonian (i.e. linear in the shear rate, with the proportionality constant being the shear viscosity) and its diagonal components are equal. The latter implies that the first and second normal stress differences, $\mathscr{N}_1 \sim (P_{xx} - P_{yy})$ and $\mathscr{N}_2 \sim (P_{yy} - P_{zz})$, respectively, are identically zero. The non-zero normal stresses and/or the shear-rate dependence of viscosity are signatures of the non-Newtonian rheology of the medium. In kinetic theory, the normal stresses appear at the Burnett-order

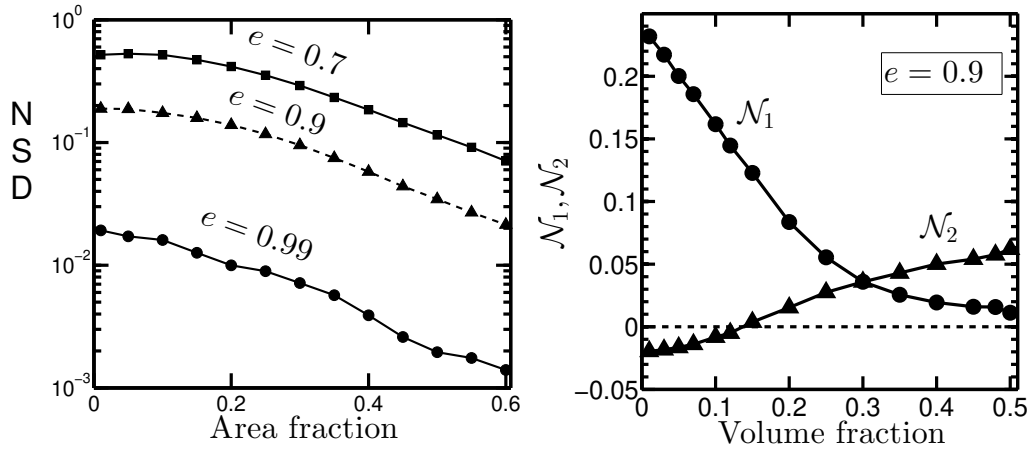

Fig. 1.4 Variations of the (a) first normal stress difference with area fraction of disks for different values of the restitution coefficient e and (b) first and second normal stress differences with volume fraction of particles for restitution coefficient $e = 0.9$. Data (symbols) correspond to event-driven simulations (Alam & Luding 2003*b*, 2005*b*) for a sheared system of smooth inelastic hard-disks (panel a) and hard-spheres (panel b) with Lees-Edward boundary condition; lines are drawn to guide the eye. These two figures constitute the primary motivation of the theoretical work embodied in the present thesis.

(Burnett 1935; Grad 1949; Chapman & Cowling 1970) and hence cannot be taken into account in the standard NS-order hydrodynamic equations. The higher-order theories like the Burnett equations (Burnett 1935; Sela & Goldhirsch 1998), or, Grad's 13-moment equations (Grad 1949; Jenkins & Richman 1985*b*,*a*; Torrilhon & Struchtrup 2004) should therefore be used to correctly model the nonlinear rheology of granular fluids. Although the rest state of Burnett equations is known to be unstable for molecular gases, there are ways to regularize these equations (Rosenau 1989); moreover, it has been established recently (Santos 2008) that the partial sum of the shear stress converges in the uniform shear of a granular fluid, with its radius of convergence increasing with increasing dissipation/inelasticity. On the other hand, in Grad's method the distribution function is expanded in a Hermite series around the local Maxwellian of thermal equilibrium, and the moment equations for an extended set of hydrodynamic fields are given in the main chapters.

The sheared granular fluid is known to possess finite normal stress differences for the whole range of densities (Walton & Braun 1986; Campbell 1990; Sela & Goldhirsch 1998; Alam & Luding 2003*a*,*b*, 2005*a*,*b*; Montanero *et al.* 2006; Reyes *et al.* 2013; Saha & Alam 2014, 2016) and the rate-dependence of viscosity seems to be an inherent feature of the uniform shear state of a granular fluid (Santos *et al.* 2004). Figure 1.4 indicates that the first normal stress difference is finite in a sheared granular fluid for a range of density and its

magnitude increases with increasing dissipation. Detailed simulations in two-dimensions (2D, i.e. for disks, (Alam & Luding 2003*b*)) and three-dimensions (3D, i.e. for spheres, (Alam & Luding 2005*b*)) have uncovered the following distinguishing features of normal stresses in a sheared granular fluid: (i) the first normal stress difference is positive in the dilute limit and undergo a sign-reversal at a finite density near the freezing point (depending on dissipation) in the dense limit; (ii) the second normal stress difference is negative in the dilute limit and becomes positive beyond a moderate density. Both theory and simulation suggest that the magnitude of both first and second normal stress differences increases with increasing dissipation.

Variations of the two normal stress differences ($\mathscr{N}_1$ and $\mathscr{N}_2$) for uniform shear flow of smooth inelastic spheres, at a restitution coefficient $e = 0.9$ are displayed in figure 1.4(b). It is observed that the scaled first normal stress difference ($\mathscr{N}_1 = (P_{xx} - P_{yy})/p$, where $P_{\alpha\alpha}$ is the diagonal component of the stress tensor along the α-direction, and $p = (P_{xx} + P_{yy} + P_{zz})/3$ is the mean pressure) is positive and maximal in the dilute limit ($\nu \to 0$) and decreases in magnitude with increasing density. On the other hand, the second normal stress difference ($\mathscr{N}_2 = (P_{yy} - P_{zz})/p$) is negative in the dilute limit, increases with increasing density, becomes *positive* at a critical density $\nu_{cr} \approx 0.13$, and increases monotonically thereafter. Alam & Luding (2005*b*) also postulated a frame-indifferent phenomenological constitutive model for granular fluids to predict the sign-reversals of both first and second normal stress differences.

Large normal stresses, such as those in figure 1.4, must be taken into account to correctly model a dissipative granular fluid in the rapid shear regime. Jenkins & Richman (1988) have incorporated normal stresses in their study of steady uniform shear flow (USF) of inelastic disks, following earlier kinetic theory works of (Goldreich & Tremaine 1978) and (Araki & Tremaine 1986) that used the anisotropic Gaussian as a reference state. They solved the second moment balance equation in the two extreme limits of density, and derived analytical results for the stress tensor in dilute and dense flows, but the solutions for the full range of density remain unexplored for the shear flow of inelastic disks. Chou & Richman (1998) analysed the USF of inelastic spheres and provided numerical solutions for the stress tensor for the full range of density. More recently, Lutsko (2004) used an arbitrary Gaussian as a reference to solve the Enskog equation for a polydisperse mixture of inelastic hard-spheres via the Hermite expansion (Grad 1949) around the anisotropic reference state, and the related kinetic integrals were simplified using a generating function technique. Focussing attention to the uniform shear state, he evaluated the stress tensor numerically and confirmed the previous numerical results of (Chou & Richman 1998). It was further shown (Lutsko 2004) that the moment-theory predictions for normal stress differences agree well with those obtained from the direct simulation Monte Carlo (DSMC) solution of the Enskog equation for a range of densities but can differ considerably from molecular dynamic simulations of the same system

for moderately dense binary mixtures. The reason for the latter disagreement remains unclear. It would greatly help our understanding of nonlinear/non-Newtonian rheology of particulate media if such higher-order theories can be tackled analytically or semi-analytically to obtain closed-form constitutive relations– this forms the primary motivation of the present thesis.

Therefore the primary objective of the present thesis is to develop a unified theory and the related non-Newtonian and non-Fourier constitutive relations of a granular fluid for a large range of density encompassing the dilute and dense regimes that incorporates the normal stress differences and the heat flux. Explaining figure1.4 theoretically is the major motivation of this thesis as explained in Chapters 2 and 3.

1.2.2 Shear rate dependent viscosity: shear thinning and shear thickening

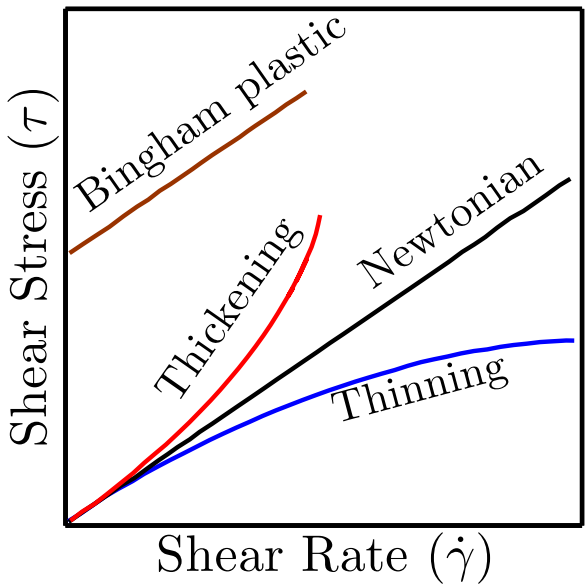

Fig. 1.5 Schematic classifying different categories of fluid in terms of showing variations of shear stress with shear rate. The raw data of the figure have been extracted from the wikipedia article on "Non-Newtonian fluid".

The decrease and increase of shear viscosity with increasing shear rate are, respectively, defined as the shear thinning and shear thickening behaviours. In general viscosity (μ) of a system as a function of the shear rate $\dot{\gamma}$ is connected via the power law

$$\mu = K\dot{\gamma}^{n-1}, \tag{1.11}$$

where K is a constant based on the material itself. The shear thinning and thickening behaviours correspond to $n < 1$ and $n > 1$ respectively. Finally the intermediate value $n = 1$ corresponds to the Newtonian fluid, where viscosity is independent of the shear rate and remains constant throughout.

- Newtonian fluid

In this case the apparent viscosity of the fluid remains constant during flow (black solid line in figure 1.5) and Navier-Stokes level hydrodynamics remain the valid theory to analyse the flow behaviour. Blood plasma, water are very commonly seen examples of Newtonian fluid.

Fig. 1.6 Paint: a shear thinning fluid. Cornstarch in water solution : a shear thickening fluid. The first figure has been taken from an internet resource, the second figure is taken from Brown & Jaeger (2014).

- Shear thinning fluid

It is also known as pseudoplastic. In this case unlike Newtonian fluid the viscosity of the substance decreases with increasing shear rate (blue solid line in figure 1.5). This fluid is very common in our daily life and some examples of shear thinning fluids are nail polish, ketchup, syrups, latex paint, ice, blood and etc. Paint is a very well cited example of a shear thinning fluid, it flows continuously when applied a shear with a brush without much drip (left panel in figure 1.6). Similar technique is used in nail polish and spreading of butter over a bread. Blood, a suspension of red blood cells in Newtonian plasma, is also an example of a shear thinning fluid.

- Shear thickening fluid

Fluids that behave exactly opposite to the case discussed above are called as shear thickening fluids. The apparent viscosity in a shear thickening fluid increases with increasing shear rate (red solid line in figure 1.5). Highly concentrated suspensions like cornstarch dissolved in water is an example of shear thickening fluid. Figure 1.6 (right panel), taken from Brown & Jaeger (2014), is a snapshot of an experiment showing a person running on the cornstarch solution of water, a highly dense suspension. The suspension works like a normal fluid when undisturbed but can support the weight of a person running over it. While running over it, the man actually applies a shear stress onto the fluid that leads to an increase of viscosity. Therefore the fluid behaves like a solid and supports the person's weight. But if the person tries to remain static over the fluid without running, he would sink into the fluid as it would happen in a normal Newtonian fluid.

Discontinuous shear thickening is the phenomena, where this increment of shear viscosity shows a sudden jump in the shear stress versus shear rate plot [figure 1.5]. This corresponds to a very high value of shear viscosity and appears when index n becomes larger than 2 in the power law (1.11).

Therefore, from equation (1.11), we can classify fluids according to different values of n:

- $n < 1$ Shear thinning.
- $n = 1$ Newtonian.
- $1 < n < 2$ Continuous shear thickening.
- $n \geqslant 2$ Discontinuous shear thickening.

Beside this there is another class of fluid, in which the viscosity changes with time as the fluid is continuously sheared. Fluids that show time dependent viscosity are called the memory materials. Like shear thinning/thickening the time dependent feature can also be categorized into two types, viz. thixotropic and rheopectic. When the viscosity of a fluid decreases with time, it is called thixotropic and if it increases with time, it is called rheopectic. Examples of thixotropic fluids are gelatine, cream, paints, yogurt, whereas the rheopectic behaviour is less common in nature and can be observed in highly concentrated starch solutions.

As far as the present thesis is concerned, we are mostly interested in the shear rate dependence of viscosity. The shear rate history (time) dependence is left for future.

Recently in a review article by Brown & Jaeger (2014), three different mechanisms for discontinuous shear thickening in a densely packed suspension are proposed: (i) hydroclustering, (ii) order-disorder transition and (iii) the dialatancy. In hydroclustering there is an increase of lubrication drag force between particles and particles form larger clusters (Brady & Bossis 1985). Flow structure changes from ordered layers to disordered in order-disorder transition. Finally in dialatancy the volume of the particulate packing increases, leading to a total increase of stresses. However neither of these conditions are necessary or sufficient for a DST to happen. For example, these mechanisms are not able to explain the DST observed in dry jammed frictional grains without presence of any interstitial fluid (Otsuki & Hayakawa 2011), nor it can explain why there has not been any DST for frictionless particles. Also in the review article by Barnes (1989) it is said that all suspensions can exhibit shear thickening provided a proper condition is being imposed. Depending upon the types of particles being suspended and the suspended fluid, a complex fluid can exhibit all three natures viz. the (i) Newtonian regime, (ii) shear thinning and finally the (iii) shear thickening with a change in the shear rate. On the other hand, not all suspensions show all these behaviours. Therefore, clarifying the conditions and identifying the proper mechanism behind DST still remains a fundamental problem of research.

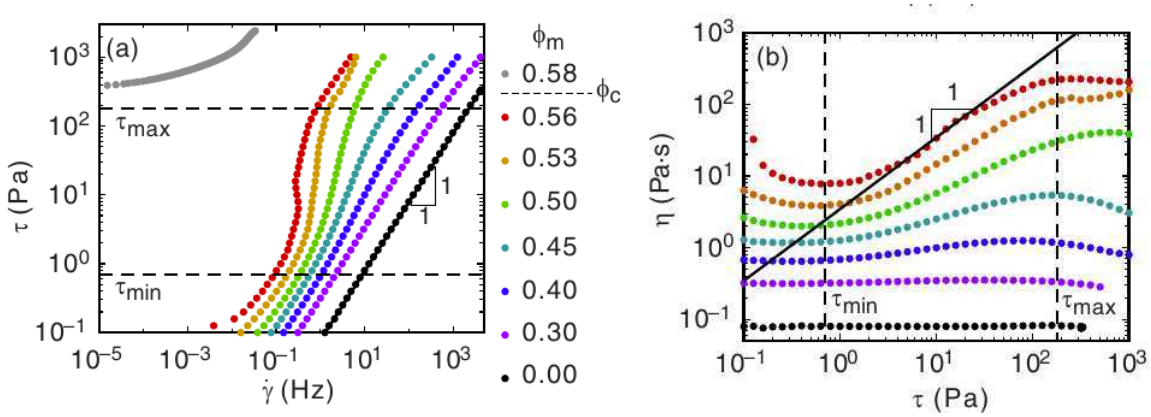

Fig. 1.7 Evolution diagram showing (a) shear stress against shear rate, (b) shear viscosity versus against stress; for a concentrated suspension of cornstarch suspended in water at different mass fractions ϕ_m. The figure has been adopted from the works of Brown & Jaeger (2012, 2014).

Figure 1.7 has been taken from Brown & Jaeger (2012, 2014), it tells (a) the dependence of shear stress (τ) versus shear rate $(\dot{\gamma})$ and (b) the shear viscosity (η) versus shear stress (τ) for a suspension; cornstarch suspended in a solution of 85% glycerol and 15% water, with different mass fraction ϕ_m. The mass fraction is proportional to the volume fraction ν. Here

the shear viscosity and shear stress in a steady flow are related via

$$\tau = \eta(\dot{\gamma})\dot{\gamma}. \tag{1.12}$$

The portion of the plot (b), where the slope is greater than 0, is the region of continuous shear thickening. It is observed that there is a threshold value $\tau_{\min}$ beyond which shear thickening starts. This value of minimum critical shear stress $\tau_{\min}$ (marked by left dashed vertical line in fig. 1.7) is almost independent of volume fraction (Maranzano & Wagner 2001; Wagner & Brady 2009) and below $\tau_{\min}$ a shear thinning or Newtonian behaviour may be observed. The continuous shear thickening does not generally appear in dilute suspensions, it is observed in the range $0.3 \leqslant \nu \leqslant 0.4$. On the other hand the portion of the plot (b), where the slope becomes 1 corresponds to point of discontinuous jump in viscosity. Therefore beyond the point $\tau_{\min}$ viscosity gradually increases with increasing shear rate but as it can be seen in fig. 1.7, this increase of viscosity is not indefinite, in fact there exists a critical value of shear stress $\tau_{\max}$, where this increasing phenomenon stops. This critical value of maximum shear stress $\tau_{\max}$ (marked by right dashed vertical line in fig. 1.7) is also independent of volume fraction (Brown & Jaeger 2009; Maranzano & Wagner 2001) and beyond this value cracking, breakup can be seen (Laun 1994). Therefore determining these critical values of shear stresses ($\tau_{\min}$ and $\tau_{\max}$) and their explicit functional dependence with volume fraction remain an interesting problem of research.

Extensive research on the appearance of discontinuous shear thickening in a densely packed suspension has been done in the last few decades [Hoffman (1972, 1974); Barnes (1989); Brown & Jaeger (2012); Fernandez *et al.* (2013); Seto *et al.* (2013); Brown & Jaeger (2014); Wyart & Cates (2014); Xu *et al.* (2014); Clavaud *et al.* (2017)]. On the other hand there are a few articles focusing on the dilute suspension. Tsao & Koch (1995) have identified DST for a dilute suspension of elastic particles. Sangani *et al.* (1996) have extended their work for a non-dilute suspension and it is shown that the DST disappears beyond a finite density. The appearance of discontinuous shear thickening in simple shear flow of a "dilute" suspension of elastic/inelastic particles along-with their conditions of existence are discussed thoroughly in Chapter-5 of the present thesis. However uncovering the same conditions for a non-dilute inelastic suspension remains an unsolved problem and must be worked out in future.

Figure 1.8 displays the variations of the effective viscosity μ_s/μ versus Pećlet number for a colloidal Brownian suspension at different values of volume fraction $\nu = 0.49$ (solid line on the top), $\nu = 0.47$ (dashed line) and $\nu = 0.419$ (dot-dashed line). This is a schematic of the results obtained from Stokesian simulation data adapted from Foss & Brady (2000) and Guazzelli & Morris (2011). Here μ_s is the effective viscosity of the suspension and μ is the viscosity of the suspending fluid. The suspended particles are small enough that than

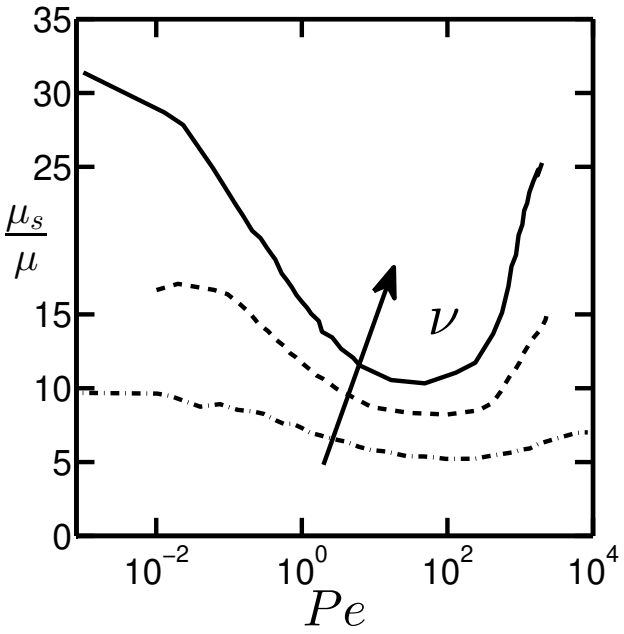

Fig. 1.8 Variation of the effective viscosity versus Pećlet number for different values of volume fraction. The raw data for this figure have been taken from Foss & Brady (2000); Guazzelli & Morris (2011).

can respond to thermal fluctuations in the suspending fluid. Therefore unlike non-Brownian suspensions, the effective viscosity is a function of volume fraction ν, shear rate $\dot{\gamma}$, the thermal energy and viscosity of the suspending fluid and also of suspended particle's diameter σ. The combined effect is captured via defining the Pećlet number

$$Pe \sim \mu \dot{\gamma} \sigma^3 / T_f, \tag{1.13}$$

is a dimensionless measure of the shear rate, T_f is the temperature of the fluid. It is clear from the above figure that at any value of volume fraction ν, as the shear rate is increased the effective viscosity shows a shear thinning behaviour reaches a minimum and then eventually shows a shear thickening behaviour at large shear rate. The increase of effective viscosity with increasing volume fraction is also shown with an arrow. Figure 1.8 works as a secondary motivation of the present thesis and our interest is to find the rheological properties of the particle phase in suspensions composed of non-Brownian hard spheres (elastic or inelastic) dense (Chapter 4) and dilute (Chapter 5) gas-solid suspensions.

1.3 Organization of the Present Thesis

Chapters 2 to 5 are fairly independent and can be read as follows.

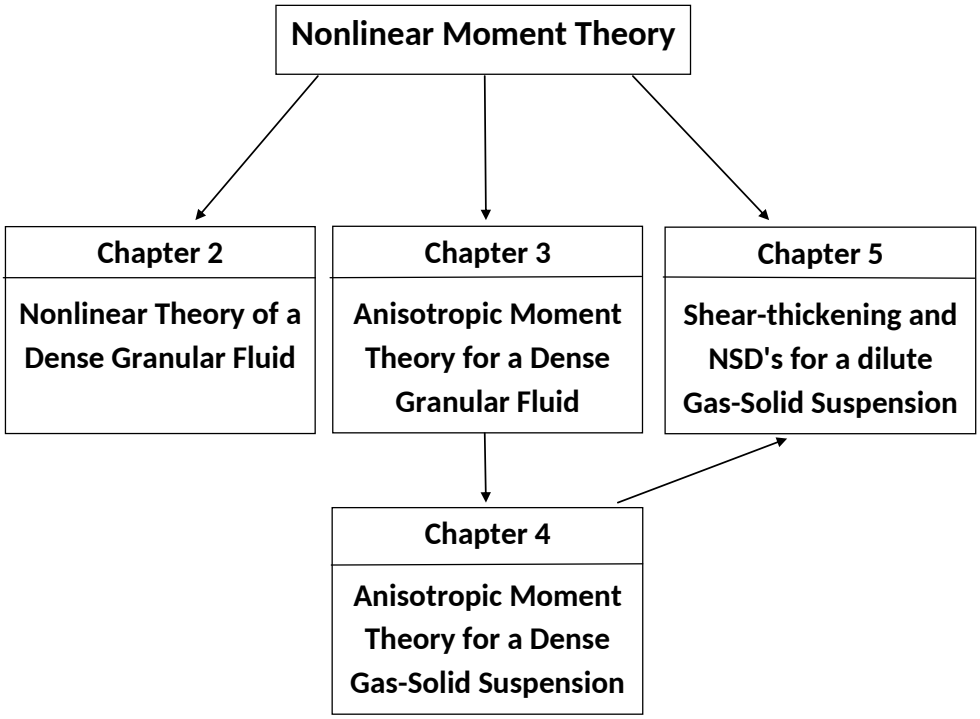

Chapter 2

Nonlinear Theory for a Granular Gas at Finite Density : Fourteen and Ten Moment Theories[1]

2.1 Introduction

In this chapter, we are interested in a dense-granular system of N randomly moving *identical smooth* particles of mass m and diameter σ. By using the word "dense" we mean granular systems of finite density, spanning from the extreme dilute limit to close to the freezing point density. Particles are colliding with each other randomly and unlike in a molecular gas these collisions are inelastic in a granular gas and the system dissipates energy upon collisions. It is assumed that the granules are solid balls/disks and collide according to the hard-sphere potential for which the potential function works like a delta function: it becomes infinity when two particles come into contact and remain zero otherwise. All these collisions are instantaneous in the sense that particle-particle collision time is much much lesser than the particle's mean free time and we have accounted for binary collisions only. Cases like multi-particle collisions, clustering, finite collision time, polydispersity are not considered in this thesis.

[1]By the word "dense" I tried to refer flows of granular matter at any "finite" density (non-dilute). In granular research community scientists have used the term "dense" to mean granular flows having volume fractions > 0.01; mathematically any value of volume fraction slightly greater than zero. In the works of Garzó *et al.* (2012); Garzó (2013), they have mentioned volume fraction of 0.1 as "dense" granular fluid. Also in the works of Herdegen & Hess (1982) and Ugawa & Cordero (2007), these authors have considered a volume fraction of $\nu = 0.015$ as dense. On the other hand, in soil mechanics and geophysical context a volume fraction of $\nu > 0.5$ is considered as dense where frictional contacts are important.

We have assumed the non-equilibrium distribution function is an expansion around the isotropic Gaussian state. This isotropic Gaussian works as the equilibrium distribution function (Chapman & Cowling 1970; Huang 1987) in a dilute molecular gas at rest and is termed as the Maxwell-Boltzmann distribution:

$$f^M = \frac{n}{2\pi\left(\frac{k_B T}{m}\right)^{\frac{3}{2}}} e^{-mC^2/2k_B T}, \tag{2.1}$$

where n is the number density, m denotes the mass of a molecule, k_B is the Boltzmann constant, T is the energy of the system and $\boldsymbol{C}$ is the peculiar velocity. Unlike in molecular gases the particles in a granular gas are inherently inelastic, and therefore the system constantly dissipates energy upon collisions. Because of the continuous energy loss, it is not possible to keep a granular system alive without proper inclusion of an external energy resource. Therefore we do not have any concept of a granular fluid at equilibrium and hence f^M is not exactly the same as the Maxwell-Boltzmann distribution for molecular gases at equilibrium/rest. Although their functional forms look same, there exits certain difference as well. The base state isotropic distribution function for flows of granular medium contains field variables n and T, which are not constants as they are in a molecular gas but are functions of space and time [Jenkins & Richman (1985*a*); Lun *et al.* (1984); Campbell (1990); Goldhirsch (2003)].

The macroscopic state of the granular system is assumed to be characterized by the fourteen field variables: the mass density (ρ), macroscopic flow velocity $(\boldsymbol{u})$, full stress tensor $(\boldsymbol{P})$, heat flux $(\boldsymbol{q})$ and the contracted fourth moment P_{iijj}, for which the evolution equations are given. The nonlinear production terms at different orders are calculated by including all the second order nonlinearities which regularize this moment description. The collisional dissipation is derived for the whole range of volume fraction that includes double derivatives of the hydrodynamic field variables as well. In the dilute limit the balance of contracted third order balance is solved to obtain a relation for granular heat flux. It is observed that, gradient of kinetic stress also drives a heat current and thermal conductivity is characterized by an asymmetric anisotropic tensor. Therefore a generalized Fourier law for granular heat flux in the dilute limit is established. Lastly, uniform shear flow of spherical granular particles is analysed using the theory and all the transport coefficients are computed for the whole range of density. The non-Newtonian rheology appears in the uniform shear flow in terms of the normal stress differences is also appreciated. Although discrepancy is observed in normal stress differences but for pressure and shear viscosity an excellent agreement with the particle simulation data (Alam & Luding 2005*b*) is found. The theory we propose gives better predictions over all other existing Grad-level theories (Jenkins & Richman 1985*a*; Kremer & Marques Jr 2011; Garzó 2012, 2013) in terms of predicting the non-Newtonian transport coefficients. Overall,

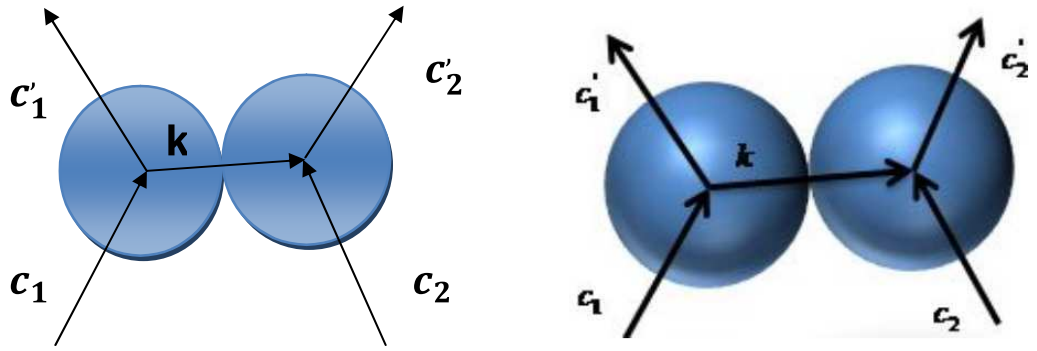

Fig. 2.1 Collision sketch of pairs of inelastic disks and spheres.

we have tried to establish a complete Grad-level theory for a dense granular system which can be applied to flows of finite density and inelasticity.

This work is a direct extension of the work by (Kremer & Marques Jr 2011; Jenkins & Richman 1985*a*), in the sense that we have a "nonlinear" 14-moment theory for the whole range of volume fraction including all nonlinear terms. It may be noted that Jenkins & Richman (1985*a*) developed a 13-moment theory of a dense granular gas, but the source and flux terms of each balance equation were not calculated. On the other hand, the 14-moment theory of Kremer & Marques Jr (2011) holds only for a "dilute" granular gas; they calculated only the "linear" part of source terms in each balance equation. Deficiencies of all previous moment models will become clearer as we move through this chapter.

This chapter is organized as follows. A brief overview of kinetic theory is provided in §2.2. The fourteen field variables and their corresponding balance equations are given in §2.3 and §2.4. The non-equilibrium distribution function is proposed in §2.5. Mathematical formulation of the nonlinear production terms at different orders are given in §2.6. The balance of granular energy and the complete expression for the collisional dissipation for the whole range of density that includes all the second order nonlinear terms are given in §2.7. Balance of second and contracted third moment of velocity fluctuations along-with their closures are discussed in §2.8 and §2.9. In §2.10 we outline a generalized Fourier law for granular heat flux. In §2.11 the simple shear flow is analysed using this 14 moment nonlinear theory to determine the non-Newtonian transport coefficients. Finally the summary is provided in §2.12.

2.2 Brief Overview of Kinetic Theory

We consider flows of a dry granular material consisting of identical, smooth, inelastic spheres of mass m and diameter σ. Particles are in random motion colliding in an inelastic manner and share information among themselves. Let $\boldsymbol{c}_1$ and $\boldsymbol{c}_2$ denote the pre-collisional velocities

of a colliding pair of particles, with $\boldsymbol{c}_1'$ and $\boldsymbol{c}_2'$ denoting the post-collisional one, respectively. Then the collision dynamics is governed by (Brilliantov & Pöschel 2004; Rao & Nott 2008)

$$\left.\begin{aligned}\boldsymbol{c}_1' &= \boldsymbol{c}_1 - \frac{(1+e)}{2}(\boldsymbol{g}\cdot\boldsymbol{k})\boldsymbol{k}\\ \boldsymbol{c}_2' &= \boldsymbol{c}_2 + \frac{(1+e)}{2}(\boldsymbol{g}\cdot\boldsymbol{k})\boldsymbol{k}\end{aligned}\right\}, \tag{2.2}$$

where $\boldsymbol{g} = \boldsymbol{c}_1 - \boldsymbol{c}_2$ denotes the relative velocity of the colliding pair before the collision and $\boldsymbol{k}$ is the unit contact vector along the line joining the centres of the particles (figure 2.1).

The particles are considered to be smooth and therefore the tangential component of the relative velocity $\boldsymbol{g}$ remains unaltered during any collision. On the other hand as the collisions are inelastic, there is a change in the relative velocity $\boldsymbol{g}$ along the normal direction after a collision. This change of $\boldsymbol{g}$ along the normal direction is measured using the inelasticity parameter e, as introduced in eq.(2.2), which is called the coefficient of normal restitution, or simply the restitution coefficient. In general the coefficient of restitution e is a function of the relative velocity $\boldsymbol{g}$ [see Goldsmith (1960); Bizon *et al.* (1999); Brilliantov & Pöschel (2004)] but for simplicity, we have assumed it to be a constant with its range being $[0,1]$, where $e = 0$ and $e = 1$ correspond to perfectly sticky and elastic collisions, respectively.

Now, the post-collisional relative velocity, denoted by $\boldsymbol{g}' = \boldsymbol{c}_1' - \boldsymbol{c}_2'$, changes according to

$$\left.\begin{aligned}(\boldsymbol{g}'\cdot\boldsymbol{k}) &= -e(\boldsymbol{g}\cdot\boldsymbol{k})\\ (\boldsymbol{g}'\times\boldsymbol{k}) &= (\boldsymbol{g}\times\boldsymbol{k})\end{aligned}\right\}. \tag{2.3}$$

Therefore the total change in the kinetic energy $(E = mc^2/2)$ during a collision can be easily obtained from eqs.(2.2-2.3) as

$$\Delta E = \frac{1}{2}m\boldsymbol{c}_1'^2 + \frac{1}{2}m\boldsymbol{c}_2'^2 - \frac{1}{2}m\boldsymbol{c}_1^2 - \frac{1}{2}m\boldsymbol{c}_2^2 = -\frac{m}{4}(1-e^2)(\boldsymbol{g}\cdot\boldsymbol{k})^2. \tag{2.4}$$

It is clear from equation (2.4) that in the elastic limit $e = 1$, $\Delta E = 0$. Therefore when the collisions are elastic the total energy of the system remains conserved. On the other hand, for the case of granular matter, the collisions are inelastic and the system continuously dissipates energy upon collisions. Hence we must supply energy from some external source in order to maintain a steady state.

In kinetic theory of granular/molecular gases at the mesoscopic level, this system is described by the Liouville equation for an N-particle distribution function which can be reduced to an infinite hierarchy of evolution equations of distribution functions (one-body, two-body, three-body, ...), known as the BBGKY-hierarchy (Chapman & Cowling 1970). The first

member of this hierarchy deals with the evolution of the single-particle distribution function $f^{(1)}(\boldsymbol{c},\boldsymbol{r},t)$ reads as:

$$\left(\frac{\partial}{\partial t}+\boldsymbol{c}\cdot\boldsymbol{\nabla}_{\boldsymbol{r}}+\boldsymbol{F}\cdot\boldsymbol{\nabla}_{\boldsymbol{p}}\right)f^{(1)}=J(f^{(2)}), \tag{2.5}$$

where $\boldsymbol{\nabla}_{\boldsymbol{r}}$ is the gradient operator in the configuration space, $\boldsymbol{\nabla}_{\boldsymbol{p}}$ is the gradient operator in the momentum space and $\boldsymbol{F}(\boldsymbol{r},t)$ is the velocity-independent external force field (such as gravity) acting on particles. On the right hand side of equation (2.5), $J(f^{(2)})$ is the collision integral that depends on two-particle distribution function $f^{(2)}(\boldsymbol{c}_1,\boldsymbol{r}_1,\boldsymbol{c}_2,\boldsymbol{r}_2,t)$.

The single particle distribution function $f^{(1)}(\boldsymbol{c},\boldsymbol{r},t)$ is defined such that $f^{(1)}(\boldsymbol{c},\boldsymbol{r},t)d\boldsymbol{r}d\boldsymbol{c}$ denotes the probable number of particles in an elementary volume $d\boldsymbol{r}$ about the point $\boldsymbol{r}$ with the velocities in the range $d\boldsymbol{c}$ around $\boldsymbol{c}$ at time t. Therefore, from the above information about $f^{(1)}$, the total number (N) of particles in the system is

$$N=\int f^{(1)}(\boldsymbol{c},\boldsymbol{r},t)d\boldsymbol{r}d\boldsymbol{c}, \tag{2.6}$$

and the local number density n at a point $\boldsymbol{r}$ at time t is defined as

$$n(\boldsymbol{r},t)=\int f^{(1)}(\boldsymbol{c},\boldsymbol{r},t)d\boldsymbol{c}. \tag{2.7}$$

The mean value of a physical property $\psi(\boldsymbol{c})$ is calculated using the single particle distribution function $f^{(1)}$ as

$$\langle\psi(\boldsymbol{c})\rangle=\int\psi(\boldsymbol{c})f^{(1)}(\boldsymbol{c},\boldsymbol{r},t)d\boldsymbol{c}. \tag{2.8}$$

$\langle\psi\rangle$ describes the macroscopic analog of a microscopic property ψ at the particle level. Therefore equation (2.8) establishes a connection between the microscopic and macroscopic fields.

The evolution equations for the hydrodynamic fields are obtained from the kinetic equation (2.5) by multiplying it with $\psi(\boldsymbol{c})$ and integrating over the velocity space, resulting in the following master balance (Chapman & Cowling 1970; Trulsen 1971; Reif 2009) equation :

$$\frac{\partial}{\partial t}\langle n\psi\rangle=\left\langle n\frac{\boldsymbol{F}}{m}\cdot\frac{\partial\psi}{\partial\boldsymbol{c}}\right\rangle-\boldsymbol{\nabla}\cdot\langle n\boldsymbol{c}\psi\rangle+\mathfrak{C}[\psi], \tag{2.9}$$

where

$$\left.\begin{aligned}\mathfrak{C}[\psi] &= \textstyle\int_{\boldsymbol{g}\cdot\boldsymbol{k}>0}(\psi_2'-\psi_2)f^{(2)}(\boldsymbol{c}_1,\boldsymbol{x}-\sigma\boldsymbol{k},\boldsymbol{c}_2,\boldsymbol{x},t)\sigma(\boldsymbol{k}\cdot\boldsymbol{g})d\boldsymbol{k}d\boldsymbol{c}_1d\boldsymbol{c}_2\\ &= \textstyle\int_{\boldsymbol{g}\cdot\boldsymbol{k}>0}(\psi_1'-\psi_1)f^{(2)}(\boldsymbol{c}_1,\boldsymbol{x},\boldsymbol{c}_2,\boldsymbol{x}+\sigma\boldsymbol{k},t)\sigma(\boldsymbol{k}\cdot\boldsymbol{g})d\boldsymbol{k}d\boldsymbol{c}_1d\boldsymbol{c}_2\end{aligned}\right\}, \tag{2.10}$$

is the collisional rate of production of ψ per unit volume, with $\boldsymbol{g}\cdot\boldsymbol{k}>0$ referring to the constraint of impending collisions. It is straightforward to decompose (2.10) into the following form (Jenkins & Richman 1985*b*,*a*; Rao & Nott 2008):

$$\mathfrak{C}[\psi]=\aleph[\psi]-\boldsymbol{\nabla}\cdot\boldsymbol{\Theta}[\psi]-\boldsymbol{\nabla u}:\boldsymbol{\Theta}\left[\frac{\partial\psi}{\partial\boldsymbol{C}}\right], \tag{2.11}$$

where $\boldsymbol{\Theta}[\psi]$ and $\aleph[\psi]$ are the collisional flux and production/source terms, respectively, whose integral expressions are given by

$$\aleph[\psi]=\frac{1}{2}\iiint\limits_{\boldsymbol{g}\cdot\boldsymbol{k}>0}(\psi_1'+\psi_2'-\psi_1-\psi_2)f^{(2)}(\boldsymbol{c}_1,\boldsymbol{r}-\sigma\boldsymbol{k},\boldsymbol{c}_2,\boldsymbol{r})\sigma^2(\boldsymbol{g}\cdot\boldsymbol{k})d\boldsymbol{k}d\boldsymbol{c}_1d\boldsymbol{c}_2, \tag{2.12}$$

$$=\frac{1}{2}\iiint\limits_{\boldsymbol{g}\cdot\boldsymbol{k}>0}(\psi_1'+\psi_2'-\psi_1-\psi_2)f^{(2)}(\boldsymbol{c}_1,\boldsymbol{r},\boldsymbol{c}_2,\boldsymbol{r}+\sigma\boldsymbol{k})\sigma^2(\boldsymbol{g}\cdot\boldsymbol{k})d\boldsymbol{k}d\boldsymbol{c}_1d\boldsymbol{c}_2, \tag{2.13}$$

and

$$\boldsymbol{\Theta}[\psi]=-\frac{1}{2}\iiint\limits_{\boldsymbol{g}\cdot\boldsymbol{k}>0}(\psi_1'-\psi_1)\boldsymbol{k}\Sigma_{m=0}^{\infty}\frac{(-\sigma\boldsymbol{k}\cdot\boldsymbol{\nabla})^m}{(m+1)!}f^{(2)}(\boldsymbol{c}_1,\boldsymbol{r},\boldsymbol{c}_2,\boldsymbol{r}+\sigma\boldsymbol{k})\sigma^2(\boldsymbol{g}\cdot\boldsymbol{k})d\boldsymbol{k}d\boldsymbol{c}_1d\boldsymbol{c}_2. \tag{2.14}$$

Note that the origin of the collisional flux $\boldsymbol{\Theta}[\psi]$ is tied to the excluded volume of the "macroscopic" particles and hence this term vanishes for a "dilute" system of point particles. Combining (2.11) and (2.9), the master balance equation simplifies to (Jenkins & Richman 1985*b*,*a*, 1988)

$$\frac{\partial}{\partial t}\langle n\psi\rangle=\left\langle n\left(\frac{\boldsymbol{F}}{m}-\left(\frac{\partial}{\partial t}+\boldsymbol{c}\cdot\boldsymbol{\nabla}\right)u\right)\cdot\frac{\partial\psi}{\partial\boldsymbol{C}}\right\rangle-\boldsymbol{\nabla}\cdot(\langle n\boldsymbol{c}\psi\rangle+\boldsymbol{\Theta}[\psi])-\boldsymbol{\nabla u}:\boldsymbol{\Theta}\left[\frac{\partial\psi}{\partial\boldsymbol{C}}\right]+\aleph[\psi], \tag{2.15}$$

where $\boldsymbol{C}$ is the peculiar velocity.

2.3 Fourteen Field Variables

The macroscopic state of a flowing granular media is characterized here by 14 hydrodynamic variables as defined below. The connection from the microscopic level to the mesoscopic/macroscopic level is set by the single particle distribution function $f^{(1)}(\boldsymbol{c},\boldsymbol{r},t)$ in (2.8). From lower to higher order, the filed variables are defined as:

(i) the mass density

$$\rho \equiv mn(\boldsymbol{r},t) \equiv \langle m \rangle = m \int f^{(1)}(\boldsymbol{c},\boldsymbol{r},t) d\boldsymbol{c}, \tag{2.16}$$

(ii) the macroscopic flow velocity

$$\boldsymbol{u} \equiv \langle \boldsymbol{c} \rangle = \int \boldsymbol{c} f^{(1)}(\boldsymbol{c},\boldsymbol{r},t) d\boldsymbol{c}. \tag{2.17}$$

(iii) the full second moment tensor

$$\boldsymbol{M}(\boldsymbol{r},t) \equiv \langle \boldsymbol{CC} \rangle = \frac{1}{n(\boldsymbol{r},t)} \int \boldsymbol{CC} f(\boldsymbol{c},\boldsymbol{r},t) d\boldsymbol{c}, \tag{2.18}$$

where $\boldsymbol{C} \equiv \boldsymbol{c} - \boldsymbol{u}$ is the peculiar/fluctuation velocity of particles. The granular temperature is defined as the trace of the second moment tensor $\boldsymbol{M}$ (2.18) (Savage & Jeffrey 1981; Lun *et al.* 1984; Jenkins & Richman 1985*b*,*a*; Goldhirsch 2003)

$$T(\boldsymbol{r},t) \equiv \frac{1}{3} \langle \boldsymbol{C} \cdot \boldsymbol{C} \rangle = \frac{1}{3n(\boldsymbol{r},t)} \int \boldsymbol{C}^2 f(\boldsymbol{c},\boldsymbol{r},t) \mathrm{d}\boldsymbol{c}. \tag{2.19}$$

In some articles the definition (Chapman & Cowling 1970) of temperature incorporating the mass (m) and the Boltzmann constant (k_B) has also been adopted (Garzó & Dufty 1999; Santos *et al.* 2004; Lutsko 2005; Brilliantov & Pöschel 2004). In either case, it must be noted that the granular temperature is not a thermodynamic temperature (Goldhirsch 2003).

Finally, (iv) the kinetic part of the heat flux vector is defined as

$$\boldsymbol{q}^k(\boldsymbol{r},t) \equiv \frac{1}{2} \rho \langle \boldsymbol{C}^2 \boldsymbol{C} \rangle = \frac{m}{2} \int \boldsymbol{C}^2 \boldsymbol{C} f(\boldsymbol{c},\boldsymbol{r},t) d\boldsymbol{c}, \tag{2.20}$$

and the (v) contracted fourth moment is

$$P_{\alpha\alpha\beta\beta} \equiv \rho \langle \boldsymbol{C}^4 \rangle = m \int \boldsymbol{C}^4 f(\boldsymbol{c},\boldsymbol{r},t) d\boldsymbol{c}. \tag{2.21}$$

Equations (2.16,2.17,2.18,2.20,2.21) represent 14 hydrodynamic fields for which a macroscopic theory will be developed as detailed in the remaining part of this chapter.

This last quantity (2.21) is added to highlight some crucial features of granular flows, like the anomalous heat current from lower to higher density regime (Brey *et al.* 2001; Candela & Walsworth 2007; Ansari & Alam 2016) is due to the dependence of the heat flux vector on spatial gradient of density, etc. The last quantity (Dufour current) vanishes in the elastic limit ($e = 1$) but becomes finite for granular flows ($e \neq 1$) (Van Noije & Ernst 1998; Sela &

Goldhirsch 1998; Garzó & Dufty 1999; Brilliantov & Pöschel 2003; Kremer & Marques Jr 2011; Garzó 2013).

2.4 Balance Equations for Fourteen Field Variables

The balance equations for the fourteen field variables are obtained by substituting $\psi = 1$, c_α, $C_\alpha C_\beta$, $\boldsymbol{C}^2 C_\alpha$ and C^4 into the master balance equation (2.15), yielding

$$\frac{\mathrm{D}\rho}{\mathrm{D}t} = -\rho u_{\alpha,\alpha}, \tag{2.22}$$

$$\rho\frac{\mathrm{D}u_\alpha}{\mathrm{D}t} = -P_{\alpha\beta,\beta}, \tag{2.23}$$

$$\rho\frac{\mathrm{D}M_{\alpha\beta}}{\mathrm{D}t} = -Q_{\gamma\alpha\beta,\gamma} - P_{\delta\beta}u_{\alpha,\delta} - P_{\delta\alpha}u_{\beta,\delta} + \aleph_{\alpha\beta}, \tag{2.24}$$

$$\begin{aligned}\frac{\mathrm{D}q^k_\alpha}{\mathrm{D}t} = &-\frac{1}{2}Q_{\gamma\alpha\beta\beta,\gamma} - q^k_\alpha u_{\delta,\delta} - q^k_\beta u_{\alpha,\beta} - Q_{\gamma\alpha\beta}u_{\beta,\gamma} + \left(M_{\alpha\beta} + \frac{1}{2}M_{\gamma\gamma}\delta_{\alpha\beta}\right)P_{\beta n,n} \\ &- \frac{1}{2}\Theta_{\gamma\beta\beta}u_{\alpha,\gamma} + \frac{1}{2}\aleph_{\alpha\beta\beta},\end{aligned} \tag{2.25}$$

$$\frac{\mathrm{D}P_{\alpha\alpha\beta\beta}}{\mathrm{D}t} = -Q_{\gamma\alpha\alpha\beta\beta,\gamma} - P_{\alpha\alpha\beta\beta}u_{\delta,\delta} - 4Q_{\gamma\beta\alpha\alpha}u_{\beta,\gamma} + \frac{8}{\rho}q^k_\alpha P_{\alpha\gamma,\gamma} + \aleph_{\alpha\alpha\beta\beta}, \tag{2.26}$$

the balance of mass, momentum, second moment, heat flux and contracted fourth moment, respectively.

In the above, $\mathrm{D}/\mathrm{D}t = \partial/\partial t + u_\alpha(\partial/\partial x_\alpha)$ is the convective derivative, the subscript following a comma denotes a partial derivative (i.e. $u_{\alpha,\alpha} \equiv \partial u_\alpha/\partial x_\alpha$) with Einstein's summation convention over repeated indices, and

$$P_{\alpha\beta} = \rho\langle \boldsymbol{C}_\alpha \boldsymbol{C}_\beta\rangle + \Theta_\alpha\left[mC_\beta\right] \equiv \rho M_{\alpha\beta} + \Theta_{\alpha\beta}, \tag{2.27}$$

$$Q_{\gamma\alpha\beta} = \rho\langle C_\gamma C_\alpha C_\beta\rangle + \Theta_\gamma\left[mC_\alpha C_\beta\right] \equiv \rho M_{\gamma\alpha\beta} + \Theta_{\gamma\alpha\beta}, \tag{2.28}$$

$$\aleph_{\alpha\beta} = \aleph\left[mC_\alpha C_\beta\right], \tag{2.29}$$

are the total stress tensor (momentum flux), the flux of the third moment, and the collisional source of the second moment (dissipation), respectively. In (2.27) and (2.28), the first term represents the kinetic contribution and the second term is its collisional contribution. Similarly the flux and production terms can be written as :

$$q_\alpha = \frac{1}{2}\rho\langle \boldsymbol{C}^2 C_\alpha\rangle + \frac{1}{2}\Theta_\alpha\left[m\boldsymbol{C}^2\right] \equiv \frac{1}{2}\rho M_{\alpha\beta\beta} + \frac{1}{2}\Theta_{\gamma\alpha\alpha} = q^k_\alpha + q^c_\alpha, \tag{2.30}$$

$$Q_{\gamma\alpha\beta\beta} = \rho\langle \boldsymbol{C}^2 C_\gamma C_\alpha\rangle + \Theta_\gamma\left[m\boldsymbol{C}^2 C_\alpha\right] \equiv \rho M_{\gamma\alpha\beta\beta} + \Theta_{\gamma\alpha\beta\beta}, \tag{2.31}$$

$$\aleph_{\alpha\beta\beta} = \aleph\left[m\boldsymbol{C}^2 C_\alpha\right], \tag{2.32}$$

$$Q_{\gamma\alpha\alpha\beta\beta} = \rho\langle \boldsymbol{C}^4 C_\gamma\rangle + \Theta_\gamma\left[m\boldsymbol{C}^4\right] \equiv \rho M_{\gamma\alpha\alpha\beta\beta} + \Theta_{\gamma\alpha\alpha\beta\beta}, \tag{2.33}$$

$$\aleph_{\alpha\alpha\beta\beta} = \aleph\left[m\boldsymbol{C}^4\right]. \tag{2.34}$$

For a complete 14-moment theory of a "dense" gas, all the above terms (2.27-2.34) must be calculated by an appropriate choice of the single-particle distribution function.

2.5 Non-equilibrium Distribution Function

Let f^M denotes the isotropic/base state Maxwellian distribution defined via

$$f^M = \frac{n(\boldsymbol{r},t)}{(2\pi T(\boldsymbol{r},t))^{\frac{3}{2}}} e^{-C^2/2T(\boldsymbol{r},t)}. \tag{2.35}$$

Equation (2.35) corresponds to distribution function of a five field theory at Eulerian level hydrodynamics [Chapman & Cowling (1970)]. As we are interested in the theory beyond Eulerian and Navier-Stokes order, we must include higher order moments in the distribution function.

2.5.1 Expansion around Maxwellian

The full non-equilibrium distribution function in terms of all fourteen field variables is assumed to be of the form (Grad 1949; Jenkins & Richman 1985*a*; Kremer & Marques Jr 2011)

$$f = f^M\left(a + a_i C_i + a_{ij} C_i C_j + b_i C^2 C_i + bC^4\right). \tag{2.36}$$

The solution for the fourteen unknown coefficients a, a_i, a_{ij}, b_i, b follows from the compatibility conditions (2.16-2.21), and are found to be

$$\left.\begin{aligned} a &= 1+\frac{15\mathfrak{a}_2}{8},\\ a_i &= -\frac{1}{\rho T^2}q_i^k,\\ a_{ij} &= -\frac{5\mathfrak{a}_2}{4T}\delta_{ij}+\frac{1}{2\rho T^2}P^k_{\langle ij\rangle},\\ b_i &= \frac{1}{5\rho T^3}q_i^k,\\ b &= \frac{\mathfrak{a}_2}{8T^2}, \end{aligned}\right\} \tag{2.37}$$

where $\mathfrak{a}_2$ is defined as the deviation of the contracted fourth moment P_{iijj} from it's isotropic measure

$$\mathfrak{a}_2 = \frac{P_{\alpha\alpha\beta\beta}-P^M_{\alpha\alpha\beta\beta}}{P^M_{\alpha\alpha\beta\beta}}. \tag{2.38}$$

Note that $\mathfrak{a}_2$ is a measure of "excess" Kurtosis of the distribution function. Therefore the full from of the distribution function corresponding to this 14-moment theory for a general non-equilibrium system is (Kremer & Marques Jr 2011; Garzó 2012, 2013) given by

$$f^{(1)} = f^{(0)}\left\{1+\frac{1}{2\rho T^2}P^k_{\langle ij\rangle}C_iC_j+\frac{q_i^k}{5\rho T^3}\left(C^2C_i-5TC_i\right)+\underline{\left(\frac{15}{8}-\frac{5}{4T}C^2+\frac{C^4}{8T^2}\right)\mathfrak{a}_2}\right\}. \tag{2.39}$$

The underlined term in equation (2.39) is an addition over the distribution function proposed by Jenkins & Richman (1985*a*) who developed a 13-moment theory. Therefore at the level of distribution function, the present work differs from that of Jenkins & Richman (1985*a*) by including the "excess" Kurtosis of the distribution function.

2.5.2 Assumption of Molecular Chaos

To evaluate the collisional source and flux terms and in order to close the system we must relate the two particle distribution function $f^{(2)}$ with the single particle distribution function $f^{(1)}$. This has been done by adopting the molecular chaos assumption (Chapman & Cowling 1970) for which

$$f^{(2)}(\boldsymbol{c}_1,\boldsymbol{r}-\sigma\boldsymbol{k},\boldsymbol{c}_2,\boldsymbol{r},t) = g_0(\boldsymbol{r}-\frac{1}{2}\sigma\boldsymbol{k})f(\boldsymbol{c}_1,\boldsymbol{r}-\sigma\boldsymbol{k},t)f(\boldsymbol{c}_2,\boldsymbol{r},t), \tag{2.40}$$

where g_0 is the contact value of the pair distribution function. The functional forms of the radial distribution functions for flows of uniform disks (2-dimension) and spheres (3-dimension) are as follows (Verlet & Levesque 1982; Carnahan & Starling 1969)

$$g_0(\nu) = \frac{(1-7\nu/16)}{(1-\nu)^2}, \qquad \nu = n\pi\sigma^2/4; \tag{2.41}$$

$$g_0(\nu) = \frac{(1-\nu/2)}{(1-\nu)^3}, \qquad \nu = n\pi\sigma^3/6; \tag{2.42}$$

with ν being the area/volume fractions (density) of particles.

2.6 Nonlinear Production and Flux Terms at Different Orders

We re-write the expressions for the collisional source ($\aleph[\psi]$) and flux ($\boldsymbol{\Theta}[\psi]$) terms as obtained on decomposing the collisional production term $\mathfrak{C}[\psi]$, appeared in the right hand side of the Enskog-Boltzmann equation (2.9):

$$\mathfrak{C}[\psi] = \aleph[\psi] - \boldsymbol{\nabla}\cdot\boldsymbol{\Theta}[\psi] - \boldsymbol{\nabla}\boldsymbol{u} : \boldsymbol{\Theta}[\boldsymbol{\nabla}_C\psi], \tag{2.43}$$

where

$$\aleph[\psi] = \frac{1}{2}\iiint_{\boldsymbol{g}\cdot\boldsymbol{k}>0} (\psi_1' + \psi_2' - \psi_1 - \psi_2) f^{(2)}(\boldsymbol{c}_1, \boldsymbol{r} - \sigma\boldsymbol{k}, \boldsymbol{c}_2, \boldsymbol{r})\sigma^2(\boldsymbol{g}\cdot\boldsymbol{k}) d\boldsymbol{k} d\boldsymbol{c}_1 d\boldsymbol{c}_2 \tag{2.44}$$

$$= \frac{1}{2}\iiint_{\boldsymbol{g}\cdot\boldsymbol{k}>0} (\psi_1' + \psi_2' - \psi_1 - \psi_2) f^{(2)}(\boldsymbol{c}_1, \boldsymbol{r}, \boldsymbol{c}_2, \boldsymbol{r} + \sigma\boldsymbol{k})\sigma^2(\boldsymbol{g}\cdot\boldsymbol{k}) d\boldsymbol{k} d\boldsymbol{c}_1 d\boldsymbol{c}_2, \tag{2.45}$$

is the collisional source term.

On expanding the two particle distribution function $f^{(2)}$ in Taylor series yields the following expression for collisional flux of ψ :

$$\boldsymbol{\Theta}[\psi] = -\frac{1}{2}\iiint_{\boldsymbol{g}\cdot\boldsymbol{k}>0} (\psi_1' - \psi_1)\boldsymbol{k}\Sigma_{m=0}^{\infty}\frac{(-\sigma\boldsymbol{k}\cdot\boldsymbol{\nabla})^m}{(m+1)!} f^{(2)}(\boldsymbol{c}_1, \boldsymbol{r}, \boldsymbol{c}_2, \boldsymbol{r} + \sigma\boldsymbol{k})\sigma^2(\boldsymbol{g}\cdot\boldsymbol{k}) d\boldsymbol{k} d\boldsymbol{c}_1 d\boldsymbol{c}_2$$

$$\Rightarrow \Theta_i[\psi] \approx -\frac{1}{2}\iiint_{\boldsymbol{g}\cdot\boldsymbol{k}>0} (\psi_1' - \psi_1)k_i\left(1 - \frac{\sigma}{2!}k_j\frac{\partial}{\partial r_j}\right) f^{(2)}(\boldsymbol{c}_1, \boldsymbol{r}, \boldsymbol{c}_2, \boldsymbol{r} + \sigma\boldsymbol{k})\sigma^2(\boldsymbol{g}\cdot\boldsymbol{k}) d\boldsymbol{k} d\boldsymbol{c}_1 d\boldsymbol{c}_2, \tag{2.46}$$

is the collisional flux of ψ. Note that the derivatives of second and higher orders are neglected on deriving the collisional flux (2.46).

Combining (2.44) and (2.45), we can re-write the collisional source term as

$$\aleph[\psi] = \frac{1}{2}\iiint\limits_{\boldsymbol{g}\cdot\boldsymbol{k}>0} \Delta\psi \frac{\Big(f^{(2)}(\boldsymbol{c}_1,\boldsymbol{r}-\sigma\boldsymbol{k},\boldsymbol{c}_2,\boldsymbol{r}) + f^{(2)}(\boldsymbol{c}_1,\boldsymbol{r},\boldsymbol{c}_2,\boldsymbol{r}+\sigma\boldsymbol{k})\Big)}{2}\sigma^2(\boldsymbol{g}\cdot\boldsymbol{k})d\boldsymbol{k}d\boldsymbol{c}_1d\boldsymbol{c}_2, \tag{2.47}$$

where

$$\Delta\psi = \psi_1' + \psi_2' - \psi_1 - \psi_2. \tag{2.48}$$

Applying the molecular chaos assumption (2.40) on $f^{(2)}$, we have

$$\begin{aligned} f^{(2)}(\boldsymbol{c}_1,\boldsymbol{r}-\sigma\boldsymbol{k},\boldsymbol{c}_2,\boldsymbol{r}) &= g_0\Big(\boldsymbol{r}-\frac{1}{2}\sigma\boldsymbol{k}\Big)f^{(1)}(\boldsymbol{c}_1,\boldsymbol{r}-\sigma\boldsymbol{k})f^{(1)}(\boldsymbol{c}_2,\boldsymbol{r}) \\ &\approx \Big\{g_0(\boldsymbol{r}) \underbrace{-\frac{1}{2}\sigma\boldsymbol{k}\cdot\boldsymbol{\nabla}g_0(\boldsymbol{r}) + \frac{1}{8}(\sigma\boldsymbol{k}\cdot\boldsymbol{\nabla})^2 g_0(\boldsymbol{r})}\Big\} \\ &\times \Big\{f^{(1)}(\boldsymbol{c}_1,\boldsymbol{r}) \underbrace{-\sigma\boldsymbol{k}\cdot\boldsymbol{\nabla}f^{(1)}(\boldsymbol{c}_1,\boldsymbol{r}) + \frac{1}{2}(\sigma\boldsymbol{k}\cdot\boldsymbol{\nabla})^2 f^{(1)}(\boldsymbol{c}_1,\boldsymbol{r})}\Big\}f^{(1)}(\boldsymbol{c}_2,\boldsymbol{r}), \end{aligned} \tag{2.49}$$

where the under-braced terms represent spatial-gradients upto second order.

Similarly we can write,

$$\begin{aligned} f^{(2)}(\boldsymbol{c}_1,\boldsymbol{r},\boldsymbol{c}_2,\boldsymbol{r}+\sigma\boldsymbol{k}) &= g_0\Big(\boldsymbol{r}+\frac{1}{2}\sigma\boldsymbol{k}\Big)f^{(1)}(\boldsymbol{c}_1,\boldsymbol{r})f^{(1)}(\boldsymbol{c}_2,\boldsymbol{r}+\sigma\boldsymbol{k}) \\ &\approx \Big\{g_0(\boldsymbol{r}) + \underbrace{\frac{1}{2}\sigma\boldsymbol{k}\cdot\boldsymbol{\nabla}g_0(\boldsymbol{r}) + \frac{1}{8}(\sigma\boldsymbol{k}\cdot\boldsymbol{\nabla})^2 g_0(\boldsymbol{r})}\Big\}f^{(1)}(\boldsymbol{c}_1,\boldsymbol{r})\Big\} \\ &\times \Big\{f^{(1)}(\boldsymbol{c}_2,\boldsymbol{r}) + \underbrace{\sigma\boldsymbol{k}\cdot\boldsymbol{\nabla}f^{(1)}(\boldsymbol{c}_2,\boldsymbol{r}) + \frac{1}{2}(\sigma\boldsymbol{k}\cdot\boldsymbol{\nabla})^2 f^{(1)}(\boldsymbol{c}_2,\boldsymbol{r})}\Big\}. \end{aligned} \tag{2.50}$$

Using eqs.(2.49)-(2.50) on (2.47), we have the final expression for the collisional source/production term as

$$\begin{aligned}\aleph[\psi] = &\frac{g_0}{2}\iiint\limits_{\boldsymbol{g}\cdot\boldsymbol{k}>0}\Delta\psi f_1 f_2\left\{1+\frac{1}{2}\sigma k_i\frac{\partial}{\partial r_i}\log\frac{f_2}{f_1}\right\}\sigma^2(\boldsymbol{g}\cdot\boldsymbol{k})d\boldsymbol{k}d\boldsymbol{c}_1d\boldsymbol{c}_2\\ &+\frac{g_0}{8}\iiint\limits_{\boldsymbol{g}\cdot\boldsymbol{k}>0}\Delta\psi k_ik_j\left(f_2\frac{\partial^2 f_1}{\partial r_i\partial r_j}+f_1\frac{\partial^2 f_2}{\partial r_i\partial r_j}\right)\sigma^4(\boldsymbol{g}\cdot\boldsymbol{k})d\boldsymbol{k}d\boldsymbol{c}_1d\boldsymbol{c}_2\\ &+\frac{1}{8}\iiint\limits_{\boldsymbol{g}\cdot\boldsymbol{k}>0}\Delta\psi k_ik_j\frac{\partial g_0}{\partial r_i}\left(f_2\frac{\partial f_1}{\partial r_j}+f_1\frac{\partial f_2}{\partial r_j}\right)\sigma^4(\boldsymbol{g}\cdot\boldsymbol{k})d\boldsymbol{k}d\boldsymbol{c}_1d\boldsymbol{c}_2\\ &+\frac{1}{16}\iiint\limits_{\boldsymbol{g}\cdot\boldsymbol{k}>0}\Delta\psi k_ik_j\frac{\partial^2 g_0}{\partial r_i\partial r_j}f_1f_2\sigma^4(\boldsymbol{g}\cdot\boldsymbol{k})d\boldsymbol{k}d\boldsymbol{c}_1d\boldsymbol{c}_2,\end{aligned}\tag{2.51}$$

and the collisional flux as

$$\begin{aligned}\Theta_i[\psi] = &-\frac{g_0}{2}\iiint\limits_{\boldsymbol{g}\cdot\boldsymbol{k}>0}(\psi_1'-\psi_1)k_if_1f_2\left\{1+\frac{1}{2}\sigma k_l\frac{\partial}{\partial r_l}\log\frac{f_2}{f_1}\right\}\sigma^3(\boldsymbol{g}\cdot\boldsymbol{k})d\boldsymbol{k}d\boldsymbol{c}_1d\boldsymbol{c}_2\\ &+\frac{g_0}{4}\iiint\limits_{\boldsymbol{g}\cdot\boldsymbol{k}>0}(\psi_1'-\psi_1)k_ik_mk_n\frac{\partial f_1}{\partial r_m}\frac{\partial f_2}{\partial r_n}\sigma^5(\boldsymbol{g}\cdot\boldsymbol{k})d\boldsymbol{k}d\boldsymbol{c}_1d\boldsymbol{c}_2\\ &+\frac{1}{8}\iiint\limits_{\boldsymbol{g}\cdot\boldsymbol{k}>0}(\psi_1'-\psi_1)k_ik_mk_n\frac{\partial g_0}{\partial r_m}\left(f_2\frac{\partial f_1}{\partial r_n}+f_1\frac{\partial f_2}{\partial r_n}\right)\sigma^5(\boldsymbol{g}\cdot\boldsymbol{k})d\boldsymbol{k}d\boldsymbol{c}_1d\boldsymbol{c}_2,\end{aligned}\tag{2.52}$$

where the following abbreviations have been used

$$\Delta\psi=\psi_1'+\psi_2'-\psi_1-\psi_2,\qquad f_1=f^{(1)}(\boldsymbol{c}_1,\boldsymbol{r},t),\qquad f_2=f^{(1)}(\boldsymbol{c}_2,\boldsymbol{r},t).\tag{2.53}$$

To evaluate the integrals (2.51-2.52) we will make use of the following change of co-ordinate system

$$\left.\begin{aligned}&(\boldsymbol{c}_1,\boldsymbol{c}_2)\Rightarrow(\boldsymbol{C}_1,\boldsymbol{C}_2)\Rightarrow(\boldsymbol{G},\boldsymbol{g}),\\ &\boldsymbol{G}=\frac{\boldsymbol{C}_1+\boldsymbol{C}_2}{2};\ \boldsymbol{g}=\boldsymbol{C}_1-\boldsymbol{C}_2\text{ and }d\boldsymbol{c}_1d\boldsymbol{c}_2=d\boldsymbol{G}d\boldsymbol{g},\end{aligned}\right\}\tag{2.54}$$

and compute all the integrals in the $(\boldsymbol{G},\boldsymbol{g})$ co-ordinate space.

Equations (2.51-2.52) remain the backbone of the present analysis and will be used subsequently to determine the collisional sources $(\aleph_{\alpha\beta},\aleph_{\alpha\beta\beta},\aleph_{\alpha\alpha\beta\beta})$ and the collisional fluxes $(\Theta_{\alpha\beta},\Theta_{\gamma\alpha\beta},\Theta_{\gamma\alpha\beta\beta})$. These production terms will then be substituted into the balance equations (2.24-2.26) and hence will yield a "nonlinear" theory for a "dense" granular system

which is valid upto "second-order" in gradients. The evaluation of these quantities at different orders and their physical interpretations will be discussed in following sections.

It may be noted that Ugawa & Cordero (2007) have considered extended hydrodynamic equations for a moderately dense flow of an "elastic" hard disks system using Grad's moment expansion method. In their work, although all the integrals appearing in (2.51) have been taken care of in calculating $\aleph$, but while calculating the collisional flux terms Θ only the first integral of (2.52) has been considered. Contributions from the gradients of hydrodynamic fields in the collisional flux terms Θ have been neglected in the work of Ugawa & Cordero (2007). Therefore there is a lack of consistency in their work. Unlike all previous works (Ugawa & Cordero 2007; Jenkins & Richman 1985*a*; Garzó 2013), we have calculated all the source $\aleph$ and flux Θ terms by retaining terms of second order in spatial gradients as well as products of first-order gradients.

2.6.1 Dealing with Integrands

In this section we will give explicit expressions of different integrands that appear in the integral expressions of the collisional source and flux terms (2.51-2.52).

For the first integrand in (2.51-2.52), we use the following relation

$$\log(x/y) = \log x - \log y;\ \log(1+x) = x - \frac{1}{2}x^2 + \frac{1}{3}x^3 - ...;\ |x| \ll 1, \tag{2.55}$$

and hence we can write

$$\begin{aligned}
\log\frac{f_2}{f_1} = \log\frac{f_{02}}{f_{01}} &+ \frac{P^k_{\langle ab\rangle}}{2\rho T^2}(\boldsymbol{C}_2\boldsymbol{C}_2 - \boldsymbol{C}_1\boldsymbol{C}_1)_{ab} + \frac{q^k_a}{5\rho T^3}\Big\{(C^2\boldsymbol{C}|_2 - C^2\boldsymbol{C}|_1) - 5T(\boldsymbol{C}_2 - \boldsymbol{C}_1)\Big\}_a \\
&- \frac{5\mathfrak{a}_2}{4T}\Big(C^2|_2 - C^2|_1\Big) + \frac{\mathfrak{a}_2}{8T^2}\Big(C^4|_2 - C^4|_1\Big) \\
&- \frac{1}{2}\Big[\frac{1}{4\rho^2T^4}P^k_{\langle ab\rangle}P^k_{\langle lm\rangle}(\boldsymbol{C}_2\boldsymbol{C}_2\boldsymbol{C}_2\boldsymbol{C}_2 - \boldsymbol{C}_1\boldsymbol{C}_1\boldsymbol{C}_1\boldsymbol{C}_1)_{ablm} \\
&+ \frac{1}{25\rho^2T^6}q^k_a q^k_b\Big\{(C^2C_a - 5TC_a)(C^2C_b - 5TC_b)|_2 - (C^2C_a - 5TC_a)(C^2C_b - 5TC_b)|_1\Big\} \\
&+ \mathfrak{a}_2^2\Big\{\Big(\frac{15}{8} - \frac{5}{4T}C^2 + \frac{C^4}{8T^2}\Big)^2\Big|_2 - \Big(\frac{15}{8} - \frac{5}{4T}C^2 + \frac{C^4}{8T^2}\Big)^2\Big|_1\Big\}\Big],
\end{aligned} \tag{2.56}$$

which implies that

$$
\begin{aligned}
&f^{(1)}(\boldsymbol{C}_1,\boldsymbol{r})f^{(1)}(\boldsymbol{C}_2,\boldsymbol{r})\left\{1+\frac{1}{2}\sigma k_i\frac{\partial}{\partial r_i}\log\frac{f^{(1)}(\boldsymbol{C}_2,\boldsymbol{r})}{f^{(1)}(\boldsymbol{C}_1,\boldsymbol{r})}\right\}\\
&\quad\approx\frac{n^2}{(8\pi^3T^3)}\exp\left(-\frac{4G^2+g^2}{4T}\right)\\
&\quad\times\left\{1+\frac{P^k_{\langle ij\rangle}}{2\rho T^2}C_iC_j+\frac{q^k_i}{5\rho T^3}\left(C^2C_i-5TC_i\right)+\left(\frac{15}{8}-\frac{5}{4T}C^2+\frac{C^4}{8T^2}\right)\mathfrak{a}_2\right\}_1\\
&\quad\times\left\{1+\frac{P^k_{\langle lm\rangle}}{2\rho T^2}C_lC_m+\frac{q^k_l}{5\rho T^3}\left(C^2C_l-5TC_l\right)+\left(\frac{15}{8}-\frac{5}{4T}C^2+\frac{C^4}{8T^2}\right)\mathfrak{a}_2\right\}_2\\
&\quad\times\Bigg[1-\frac{\sigma k_i}{2T}g_a\frac{\partial u_a}{\partial r_i}-\frac{\sigma k_i}{2T^2}\frac{\partial T}{\partial r_i}G_ag_a+\frac{\sigma k_i}{4\rho T^2}P^k_{\langle ab\rangle}\left(\frac{\partial u_a}{\partial r_i}g_b+\frac{\partial u_b}{\partial r_i}g_a\right)\\
&\qquad+\frac{\sigma k_i}{20\rho^2T^3}\frac{\partial\rho}{\partial r_i}\left\{5TP^k_{\langle ab\rangle}(G_ag_b+G_bg_a)+2q^k_a(G^2g_a+\frac{1}{4}g^2g_a+2G_aG_bg_b-5Tg_a)\right\}\\
&\qquad+\frac{\sigma k_i}{5\rho T^3}q^k_a\left\{\frac{\partial u_b}{\partial r_i}(G_ag_b+G_bg_a)+\frac{\partial u_a}{\partial r_i}G_bg_b\right\}+\frac{\sigma k_i}{16T^2}\mathfrak{a}_2\frac{\partial u_a}{\partial r_i}(4G^2g_a+g^2g_a+8G_aG_bg_b-20Tg_a)\\
&\qquad+\frac{\sigma k_i}{40\rho T^4}\frac{\partial T}{\partial r_i}\Big\{20TP^k_{\langle ab\rangle}(G_ag_b+G_bg_a)+q^k_a(12G^2g_a+3g^2g_a+24G_aG_bg_b-40Tg_a)\\
&\qquad\qquad+5\rho T\mathfrak{a}_2G_ag_a(4G^2+g^2-10T)\Big\}\\
&\qquad-\frac{\sigma k_i}{4\rho T^2}\frac{\partial P^k_{\langle ab\rangle}}{\partial r_i}(G_ag_b+G_bg_a)-\frac{\sigma k_i}{10\rho T^3}\frac{\partial q^k_a}{\partial r_i}(G^2g_a+\frac{1}{4}g^2g_a+2G_aG_bg_b-5Tg_a)\\
&\qquad-\frac{\sigma k_i}{16T^2}\frac{\partial\mathfrak{a}_2}{\partial r_i}G_ag_a(4G^2+g^2-20T)\\
&\qquad-\frac{\sigma k_i}{4}\left\{\frac{1}{4\rho^2T^4}\frac{\partial}{\partial r_i}(P^k_{\langle ab\rangle}P^k_{\langle lm\rangle})(\boldsymbol{C}_2\boldsymbol{C}_2\boldsymbol{C}_2\boldsymbol{C}_2-\boldsymbol{C}_1\boldsymbol{C}_1\boldsymbol{C}_1\boldsymbol{C}_1)_{ablm}\right.\\
&\qquad+\frac{1}{25\rho^2T^6}\frac{\partial}{\partial r_i}(q^k_aq^k_b)\left\{(C^2C_a-5TC_a)(C^2C_b-5TC_b)|_2-(C^2C_a-5TC_a)(C^2C_b-5TC_b)|_1\right\}\\
&\qquad\left.+\frac{\partial}{\partial r_i}(\mathfrak{a}_2^2)\left\{\left(\frac{15}{8}-\frac{5}{4T}C^2+\frac{C^4}{8T^2}\right)^2\Big|_2-\left(\frac{15}{8}-\frac{5}{4T}C^2+\frac{C^4}{8T^2}\right)^2\Big|_1\right\}\right\}\Bigg].
\end{aligned}
\tag{2.57}
$$

2.6.2 Ordering Approximation : Second-order Gradients

In evaluating the collision integrals, we will consider terms that satisfy the following constraint

$$\left(P^k_{\langle ab\rangle}\right)^A \left(q^k_c\right)^B \left(\mathfrak{a}_2\right)^C \left(\frac{\partial n}{\partial r_i}\right)^D \left(\frac{\partial u_p}{\partial r_j}\right)^E \left(\frac{\partial T}{\partial r_k}\right)^F \left(\frac{\partial P^k_{\langle lm\rangle}}{\partial r_s}\right)^G \left(\frac{\partial q^k_t}{\partial r_d}\right)^H \left(\frac{\partial \mathfrak{a}_2}{\partial r_n}\right)^I ;$$

$$A+B+C+D+E+F+G+H+I \leq 2. \qquad (2.58)$$

Assumption (2.58) implies that all the terms involving second-order nonlinearities are taken into account.

With (2.58), equation (2.57) simplifies to:

$$
\begin{aligned}
&f^{(1)}(\boldsymbol{C}_1,\boldsymbol{r})f^{(1)}(\boldsymbol{C}_2,\boldsymbol{r})\left\{1+\frac{1}{2}\sigma k_i\frac{\partial}{\partial r_i}\log\frac{f^{(1)}(\boldsymbol{C}_2,\boldsymbol{r})}{f^{(1)}(\boldsymbol{C}_1,\boldsymbol{r})}\right\}\\
&\quad=\frac{n^2}{(8\pi^3T^3)}\exp\left(-\frac{4G^2+g^2}{4T}\right)\\
&\quad\times\Bigg[1_{(i)}+\frac{P^k_{\langle ab\rangle}}{2\rho T^2}(\boldsymbol{C}_1\boldsymbol{C}_1+\boldsymbol{C}_2\boldsymbol{C}_2)_{ab|(ii)}+\underline{\frac{q^k_a}{5\rho T^3}\left\{(C^2C_a-5TC_a)|_1+(C^2C_a-5TC_a)|_2\right\}_{(i)}}\\
&\qquad+\mathfrak{a}_2\left(\frac{15}{4}-\frac{5}{4T}(C^2|_1+C^2|_2)+\frac{1}{8T^2}(C^4|_1+C^4|_2)\right)_{(iii)}\\
&\qquad+\frac{1}{4\rho^2T^4}P^k_{\langle ab\rangle}P^k_{\langle lm\rangle}(\boldsymbol{C}_1\boldsymbol{C}_1\boldsymbol{C}_2\boldsymbol{C}_2)_{ablm|(iv)}\\
&\qquad\underline{+\frac{1}{10\rho^2T^5}P^k_{\langle ab\rangle}q^k_l\left\{C_aC_b|_1(C^2C_l-5TC_l)|_2+C_aC_b|_2(C^2C_l-5TC_l)|_1\right\}_{(ii)}}\\
&\qquad+\frac{1}{2\rho T^2}P^k_{\langle ab\rangle}\mathfrak{a}_2\left\{C_aC_b|_1\left(\frac{15}{8}-\frac{5}{4T}C^2+\frac{C^4}{8T^2}\right)_2+C_aC_b|_2\left(\frac{15}{8}-\frac{5}{4T}C^2+\frac{C^4}{8T^2}\right)_1\right\}_{(v)}\\
&\qquad+\frac{1}{25\rho^2T^6}q^k_aq^k_b\left\{(C^2C_a-5TC_a)_1(C^2C_b-5TC_b)_2\right\}_{(vi)}\\
&\qquad+\frac{1}{5\rho T^3}q^k_a\mathfrak{a}_2\Bigg\{(C^2C_a-5TC_a)_1\left(\frac{15}{8}-\frac{5}{4T}C^2+\frac{C^4}{8T^2}\right)_2\\
&\qquad\qquad\underline{+(C^2C_a-5TC_a)_2\left(\frac{15}{8}-\frac{5}{4T}C^2+\frac{C^4}{8T^2}\right)_1\Bigg\}_{(iii)}}\\
&\qquad+\mathfrak{a}_2^2\left\{\left(\frac{15}{8}-\frac{5}{4T}C^2+\frac{C^4}{8T^2}\right)_1\left(\frac{15}{8}-\frac{5}{4T}C^2+\frac{C^4}{8T^2}\right)_2\right\}_{(vii)}\\
&\qquad-\frac{\sigma k_i}{2T}\frac{\partial u_l}{\partial r_i}g_l|_{(viii)}-\frac{\sigma k_i}{2\rho T^3}\frac{\partial u_l}{\partial r_i}P^k_{\langle ab\rangle}g_l(G_aG_b+\frac{1}{4}g_ag_b)|_{(ix)}\\
&\qquad\underline{-\frac{\sigma k_i}{10\rho T^4}\frac{\partial u_l}{\partial r_i}q^k_ag_l(2G^2G_a+\frac{1}{2}g^2G_a+G_bg_bg_a-10TG_a)_{(iv)}}\\
&\qquad-\frac{\sigma k_i}{2T}\frac{\partial u_l}{\partial r_i}\mathfrak{a}_2g_l\left(\frac{15}{4}-\frac{5}{2T}(G^2+\frac{1}{4}g^2)+\frac{1}{64T^2}(g^4+8g^2G^2+16G^4+16g_ag_bG_aG_b)\right)|_{(x)}\\
&\qquad\underline{-\frac{\sigma k_i}{2T^2}\frac{\partial T}{\partial r_i}G_lg_{l(v)}}-\underline{\frac{\sigma k_i}{2\rho T^4}\frac{\partial T}{\partial r_i}P^k_{\langle ab\rangle}G_lg_l(G_aG_b+\frac{1}{4}g_ag_b)_{(vi)}}\\
&\qquad-\frac{\sigma k_i}{10\rho T^5}\frac{\partial T}{\partial r_i}q^k_aG_lg_l(2G^2G_a+\frac{1}{2}g^2G_a+G_bg_bg_a-10TG_a)|_{(xi)}\\
&\qquad\underline{-\frac{\sigma k_i}{2T^2}\frac{\partial T}{\partial r_i}\mathfrak{a}_2G_lg_l\left(\frac{15}{4}-\frac{5}{2T}(G^2+\frac{1}{4}g^2)+\frac{1}{64T^2}(g^4+8g^2G^2+16G^4+16g_ag_bG_aG_b)\right)_{(vii)}}\\
&\qquad+\frac{\sigma k_i}{4\rho T^2}P^k_{\langle ab\rangle}\left(\frac{\partial u_a}{\partial r_i}g_b+\frac{\partial u_b}{\partial r_i}g_a\right)|_{(xii)}
\end{aligned}
$$

$$
\begin{aligned}
&+\frac{\sigma k_i}{20\rho^2T^3}\frac{\partial\rho}{\partial r_i}\Big\{\underline{5TP^k_{\langle ab\rangle}(G_ag_b+G_bg_a)_{(viii)}}+2q^k_a(G^2g_a+\frac{1}{4}g^2g_a+2G_aG_bg_b-5Tg_a)|_{(xiii)}\Big\}\\
&\underline{+\frac{\sigma k_i}{5\rho T^3}q^k_a\Big\{\frac{\partial u_b}{\partial r_i}(G_ag_b+G_bg_a)+\frac{\partial u_a}{\partial r_i}G_bg_b\Big\}_{(ix)}}\\
&+\frac{\sigma k_i}{16T^2}\mathfrak{a}_2\frac{\partial u_a}{\partial r_i}(4G^2g_a+g^2g_a+8G_aG_bg_b-20Tg_a)|_{(xiv)}\\
&+\frac{\sigma k_i}{40\rho T^4}\frac{\partial T}{\partial r_i}\Big\{\underline{20TP^k_{\langle ab\rangle}(G_ag_b+G_bg_a)_{(x)}}+q^k_a(12G^2g_a+3g^2g_a+24G_aG_bg_b-40Tg_a)|_{(xv)}\\
&\qquad\qquad\underline{+5\rho T\mathfrak{a}_2G_ag_a(4G^2+g^2-10T)_{(xi)}}\Big\}\\
&-\frac{\sigma k_i}{4\rho T^2}\frac{\partial P^k_{\langle ab\rangle}}{\partial r_i}(G_ag_b+G_bg_a)\\
&\times\Big\{\underline{1_{(xii)}+\frac{P^k_{\langle lm\rangle}}{\rho T^2}(G_lG_m+\frac{1}{4}g_lg_m)_{(xiii)}}+\frac{q^k_l}{5\rho T^3}(2G^2G_l+\frac{1}{2}g^2G_l+G_mg_mg_l-10TG_l)|_{(xvi)}\\
&\qquad\underline{+\mathfrak{a}_2\Big(\frac{15}{4}-\frac{5}{2T}(G^2+\frac{1}{4}g^2)+\frac{1}{64T^2}(g^4+8g^2G^2+16G^4+16g_ag_bG_aG_b)\Big)_{(xiv)}}\Big\}\\
&-\frac{\sigma k_i}{10\rho T^3}\frac{\partial q^k_a}{\partial r_i}(G^2g_a+\frac{1}{4}g^2g_a+2G_aG_bg_b-5Tg_a)\\
&\times\Big\{1|_{(xvii)}+\frac{P^k_{\langle lm\rangle}}{\rho T^2}(G_lG_m+\frac{1}{4}g_lg_m)|_{(xviii)}+\underline{\frac{q^k_l}{5\rho T^3}(2G^2G_l+\frac{1}{2}g^2G_l+G_mg_mg_l-10TG_l)_{(xv)}}\\
&\qquad+\mathfrak{a}_2\Big(\frac{15}{4}-\frac{5}{2T}(G^2+\frac{1}{4}g^2)+\frac{1}{64T^2}(g^4+8g^2G^2+16G^4+16g_ag_bG_aG_b)\Big)|_{(xix)}\Big\}\\
&-\frac{\sigma k_i}{16T^2}\frac{\partial\mathfrak{a}_2}{\partial r_i}G_ag_a(4G^2+g^2-20T)\\
&\times\Big\{\underline{1_{(xvi)}+\frac{P^k_{\langle lm\rangle}}{\rho T^2}(G_lG_m+\frac{1}{4}g_lg_m)_{(xvii)}}+\frac{q^k_l}{5\rho T^3}(2G^2G_l+\frac{1}{2}g^2G_l+G_mg_mg_l-10TG_l)|_{(xx)}\\
&\qquad\underline{+\mathfrak{a}_2\Big(\frac{15}{4}-\frac{5}{2T}(G^2+\frac{1}{4}g^2)+\frac{1}{64T^2}(g^4+8g^2G^2+16G^4+16g_ag_bG_aG_b)\Big)_{(xviii)}}\Big\}\\
&\underline{-\frac{\sigma k_i}{4}\Big\{\frac{1}{4\rho^2T^4}\frac{\partial}{\partial r_i}(P^k_{\langle ab\rangle}P^k_{\langle lm\rangle})(\boldsymbol{C}_2\boldsymbol{C}_2\boldsymbol{C}_2\boldsymbol{C}_2-\boldsymbol{C}_1\boldsymbol{C}_1\boldsymbol{C}_1\boldsymbol{C}_1)_{ablm(xix)}}\\
&\underline{+\frac{1}{25\rho^2T^6}\frac{\partial}{\partial r_i}(q^k_aq^k_b)\Big\{(C^2C_a-5TC_a)(C^2C_b-5TC_b)|_2-(C^2C_a-5TC_a)(C^2C_b-5TC_b)|_1\Big\}_{(xx)}}\\
&\underline{+\frac{\partial}{\partial r_i}(\mathfrak{a}_2^2)\Big\{\Big(\frac{15}{8}-\frac{5}{4T}C^2+\frac{C^4}{8T^2}\Big)^2\Big|_2-\Big(\frac{15}{8}-\frac{5}{4T}C^2+\frac{C^4}{8T^2}\Big)^2\Big|_1\Big\}_{(xxi)}}\Big\}\Big]. \qquad (2.59)
\end{aligned}
$$

Table 2.1 Truncation of equation (2.59)

Herdegen & Hess (1982)	$(i)+(ii)+(iv)$
Kremer & Marques Jr (2011)	$(i)+(ii)+(iii)+(v)$ $(i)+(iii)$
Jenkins & Richman (1985*a*)	$(i)+(ii)+(viii)$ $(i)+(v)$
Garzó (2013)	$(i)+(ii)+(iii)+(v)+(viii)+(x)+(xiv)$ $(i)+(iii)+(v)+(vii)$
Present 14-moment theory	$(i)+(ii)+....+(xx)$ $(i)+(ii)+....+(xxi)$

Different truncated versions of (2.59) have been used by several authors, as shown the Table 2.1

Similarly, for the third-term in (2.51-2.52) we have

$$
\begin{aligned}
&f_2\frac{\partial f_1}{\partial r_j}+f_1\frac{\partial f_2}{\partial r_j}= \\
&\frac{n^2}{(8\pi^3T^3)}\exp\left(-\frac{4G^2+g^2}{4T}\right)\left[\left(\frac{2}{n}\frac{\partial n}{\partial x_j}-\frac{3}{T}\frac{\partial T}{\partial r_j}+\frac{15}{4}\frac{\partial \mathfrak{a}_2}{\partial r_j}\right)+\underline{\frac{2}{T}\frac{\partial u_a}{\partial r_j}G_a}\right. \\
&\quad+\left(\frac{1}{T^2}\frac{\partial T}{\partial r_j}-\frac{5}{2T}\frac{\partial \mathfrak{a}_2}{\partial r_j}\right)(G^2+\frac{1}{4}g^2)+\frac{1}{\rho T^2}\frac{\partial P^k_{\langle ab\rangle}}{\partial r_i}(G_aG_b+\frac{1}{4}g_ag_b) \\
&\quad+\underline{\frac{1}{5\rho T^3}\frac{\partial q^k_a}{\partial r_j}(2G^2G_a+\frac{1}{2}g^2G_a+G_bg_bg_a-10TG_a)} \\
&\quad\left.+\frac{1}{64T^2}\frac{\partial \mathfrak{a}_2}{\partial r_i}(g^4+8g^2G^2+16G^4+16g_ag_bG_aG_b)\right].
\end{aligned}
\tag{2.60}
$$

For the second-term in eqn. (2.52), we can write :

$$
\begin{aligned}
&\frac{\partial f_2}{\partial r_a}\frac{\partial f_1}{\partial r_b} = \\
&\frac{n^2}{(8\pi^3T^3)}\exp\left(-\frac{4G^2+g^2}{4T}\right)\left[\frac{1}{n^2}\frac{\partial n}{\partial r_a}\frac{\partial n}{\partial r_b}-\frac{3}{2nT}\left(\frac{\partial n}{\partial r_a}\frac{\partial T}{\partial r_b}+\frac{\partial n}{\partial r_b}\frac{\partial T}{\partial r_a}\right)+\frac{9}{4T^2}\frac{\partial T}{\partial r_b}\frac{\partial T}{\partial r_a}\right.\\
&+\underline{\frac{1}{nT}\left(\frac{\partial n}{\partial r_a}\frac{\partial u_m}{\partial r_b}C_m|_1+\frac{\partial n}{\partial r_b}\frac{\partial u_m}{\partial r_a}C_m|_2\right)-\frac{3}{2T^2}\left(\frac{\partial T}{\partial r_a}\frac{\partial u_m}{\partial r_b}C_m|_1+\frac{\partial T}{\partial r_b}\frac{\partial u_m}{\partial r_a}C_m|_2\right)}\\
&+\frac{1}{T^2}\left(\frac{\partial u_l}{\partial r_a}\frac{\partial u_m}{\partial r_b}\right)C_m|_1C_l|_2+\frac{1}{2nT^2}\left(\frac{\partial n}{\partial r_a}\frac{\partial T}{\partial r_b}C^2|_1+\frac{\partial n}{\partial r_b}\frac{\partial T}{\partial r_a}C^2|_2\right)\\
&-\frac{3}{4T^3}\frac{\partial T}{\partial r_a}\frac{\partial T}{\partial r_b}(C^2|_1+C^2|_2)+\underline{\frac{1}{2T^3}\left(\frac{\partial T}{\partial r_a}\frac{\partial u_m}{\partial r_b}C^2|_2C_m|_1+\frac{\partial T}{\partial r_b}\frac{\partial u_m}{\partial r_a}C^2|_1C_m|_2\right)}\\
&+\frac{1}{4T^4}\frac{\partial T}{\partial r_a}\frac{\partial T}{\partial r_b}C^2|_1C^2|_2+\frac{1}{4\rho^2T^4}\frac{\partial P^k_{\langle ij\rangle}}{\partial r_a}\frac{\partial P^k_{\langle rs\rangle}}{\partial r_b}C_rC_s|_1C_iC_j|_2\\
&+\underline{\frac{1}{10\rho^2T^5}\left(\frac{\partial P^k_{\langle ij\rangle}}{\partial r_a}\frac{\partial q^k_m}{\partial r_b}C_iC_j|_2\left(C^2C_m-5TC_m\right)|_1+\frac{\partial P^k_{\langle ij\rangle}}{\partial r_b}\frac{\partial q^k_m}{\partial r_a}C_iC_j|_1\left(C^2C_m-5TC_m\right)|_2\right)}\\
&+\frac{1}{25\rho^2T^6}\frac{\partial q^k_l}{\partial r_a}\frac{\partial q^k_m}{\partial r_b}\left(C^2C_l-5TC_l\right)|_1\left(C^2C_m-5TC_m\right)|_2\\
&+\frac{1}{2\rho T^2}\left(\frac{\partial P^k_{\langle ij\rangle}}{\partial r_a}\frac{\partial \mathfrak{a}_2}{\partial r_b}C_iC_j|_2\left(\frac{15}{8}-\frac{5}{4T}C^2+\frac{C^4}{8T^2}\right)\Big|_1\right.\\
&\qquad\left.+\frac{\partial P^k_{\langle ij\rangle}}{\partial r_b}\frac{\partial \mathfrak{a}_2}{\partial r_a}C_iC_j|_1\left(\frac{15}{8}-\frac{5}{4T}C^2+\frac{C^4}{8T^2}\right)\Big|_2\right)\\
&+\underline{\frac{1}{5\rho T^3}\left(\frac{\partial q^k_m}{\partial r_a}\frac{\partial \mathfrak{a}_2}{\partial r_b}\left(C^2C_m-5TC_m\right)|_2\left(\frac{15}{8}-\frac{5}{4T}C^2+\frac{C^4}{8T^2}\right)\Big|_1\right.}\\
&\qquad\underline{\left.+\frac{\partial q^k_m}{\partial r_b}\frac{\partial \mathfrak{a}_2}{\partial r_a}\left(C^2C_m-5TC_m\right)|_1\left(\frac{15}{8}-\frac{5}{4T}C^2+\frac{C^4}{8T^2}\right)\Big|_2\right)}\\
&\left.+\frac{\partial \mathfrak{a}_2}{\partial r_a}\frac{\partial \mathfrak{a}_2}{\partial r_b}\left(\frac{15}{8}-\frac{5}{4T}C^2+\frac{C^4}{8T^2}\right)\Big|_1\left(\frac{15}{8}-\frac{5}{4T}C^2+\frac{C^4}{8T^2}\right)\Big|_2.\right. \qquad (2.61)
\end{aligned}
$$

The underlined terms of (2.59-2.61) do not contribute to any of the "even order" production terms $\aleph_{\alpha\beta}$, $\aleph_{\alpha\alpha\beta\beta}$, $\Theta_{\alpha\beta}$ and $\Theta_{\gamma\alpha\beta\beta}$ since they are odd functions of the centre of mass-velocity (G) and therefore cancel out and become identically zero.

On the other hand while calculating the "odd-order" moments like $\aleph_{\alpha\beta\beta}$ and $\Theta_{\gamma\alpha\beta}$, the underlined terms in (2.59-2.61) only contribute and will produce non-zero values. We have marked the terms with different colours. Note in (2.59-2.61) that the terms marked with red

contribute to the "even-order" production terms whereas the terms marked with blue contribute to the "odd-order" production terms.

2.7 Balance of Granular Energy and Collisional Dissipation

The granular temperature T, (2.19), is defined as the trace of the second moment tensor $\boldsymbol{M}$ and the balance of granular energy directly follows from the trace of the second moment balance (2.24), yielding

$$\frac{3}{2}\rho\frac{\mathrm{D}T}{\mathrm{D}t} = -q_{\alpha,\alpha} - P_{\alpha\beta}\, u_{\beta,\alpha} - \mathscr{D}, \tag{2.62}$$

where

$$\mathscr{D} \equiv -\frac{1}{2}\aleph_{\beta\beta} = -\frac{1}{2}\aleph[mC^2] \tag{2.63}$$

is the rate of dissipation of fluctuation kinetic energy per unit volume and

$$q_\alpha \equiv \frac{1}{2}Q_{\alpha\beta\beta} = \frac{1}{2}\rho M_{\alpha\beta\beta} + \frac{1}{2}\Theta_{\alpha\beta\beta} = q^k_\alpha + q^c_\alpha \tag{2.64}$$

is the total (kinetic and collisional) heat-flux. In equation (2.64), $\frac{1}{2}\rho M_{\alpha\beta\beta}$ is the transport/kinetic part and $\frac{1}{2}\Theta_{\alpha\beta\beta}$ is the collisional part of the energy flux vector, denoted by q^k and q^c, respectively. The kinetic components of the energy flux vector and other constitutive variables are dominant in the dilute limit whereas the collisional components become significant in the dense limit. Therefore, in dilute granular flows of point particles, the collisional component vanishes and the kinetic component serves as the only contributor to any transport coefficient.

The collisional dissipation rate $\mathscr{D}$ appearing in the right hand side of the energy balance equation (2.62) is the source of energy dissipation due to inelastic collisions and termed as the *cooling rate* in granular literature (with some multiplicative constant). The most general form of $\mathscr{D}$ including second order gradients can be written as :

$$
\begin{aligned}
\mathscr{D} = {} & \mathscr{D}_0 + \mathscr{D}_u(\boldsymbol{\nabla}\cdot\boldsymbol{u}) + \mathscr{D}_q\boldsymbol{\nabla}\cdot\boldsymbol{q}^k + \mathscr{D}_{u\Pi}(\boldsymbol{\nabla}\boldsymbol{u}\colon\boldsymbol{\Pi}) + \mathscr{D}_{q\Pi}\Big((\boldsymbol{q}^k\boldsymbol{\nabla}\colon\boldsymbol{\Pi}) + (\boldsymbol{\nabla}\boldsymbol{q}^k\colon\boldsymbol{\Pi})\Big) \\
& + \mathscr{D}_{q\rho}(\boldsymbol{q}^k\cdot\boldsymbol{\nabla}\rho) + \mathscr{D}_{q\mathfrak{a}_2}(\boldsymbol{q}^k\cdot\boldsymbol{\nabla}\mathfrak{a}_2) \\
& + \mathscr{D}_\rho\boldsymbol{\nabla}^2\rho + \mathscr{D}_T\boldsymbol{\nabla}^2T + \mathscr{D}_\Pi\Big(\boldsymbol{\nabla}\cdot(\boldsymbol{\nabla}\cdot\boldsymbol{\Pi})\Big) + \mathscr{D}_{\mathfrak{a}_2}\boldsymbol{\nabla}^2\mathfrak{a}_2 \\
& + \mathscr{D}_{\rho T}\boldsymbol{\nabla}\rho\cdot\boldsymbol{\nabla}T + \mathscr{D}_{\rho\Pi}\boldsymbol{\nabla}\rho\cdot(\boldsymbol{\nabla}\cdot\boldsymbol{\Pi}) + \mathscr{D}_{\rho\mathfrak{a}_2}\boldsymbol{\nabla}\rho\cdot\boldsymbol{\nabla}\mathfrak{a}_2 \\
& + \mathscr{D}_{TT}(\boldsymbol{\nabla}T)^2 + \mathscr{D}_{T\Pi}\boldsymbol{\nabla}T\cdot(\boldsymbol{\nabla}\cdot\boldsymbol{\Pi}) + \mathscr{D}_{T\mathfrak{a}_2}\boldsymbol{\nabla}T\cdot\boldsymbol{\nabla}\mathfrak{a}_2 \\
& + \mathscr{D}_{uu}\Big(\boldsymbol{\nabla}\boldsymbol{u}\colon\boldsymbol{\nabla}\boldsymbol{u} + \boldsymbol{\nabla}\boldsymbol{u}\colon\boldsymbol{\nabla}\boldsymbol{u}' + (\boldsymbol{\nabla}\cdot\boldsymbol{u})^2\Big) \\
& + \mathscr{D}_{uq}\Big(\boldsymbol{\nabla}\boldsymbol{u}\colon\boldsymbol{\nabla}\boldsymbol{q}^k + \boldsymbol{\nabla}\boldsymbol{u}\colon\boldsymbol{\nabla}\boldsymbol{q}^{k'} + (\boldsymbol{\nabla}\cdot\boldsymbol{q}^k)^2\Big). \qquad (2.65)
\end{aligned}
$$

The coefficients $\mathscr{D}_\rho$, $\mathscr{D}_T$ corresponding to the terms $\boldsymbol{\nabla}^2\rho$ and $\boldsymbol{\nabla}^2T$ have been calculated by Brey *et al.* (1998) for a "dilute" granular gas whereas the coefficients $\mathscr{D}_\rho$, $\mathscr{D}_T$, $\mathscr{D}_{TT}$, $\mathscr{D}_{\rho T}$, $\mathscr{D}_{uu}$ have been determined by Brilliantov & Pöschel (2003) for a dilute granular system of "viscoelastic" particles. As a reference supporting the above statement we quote the text from the work by (Garzó 2013) and put it below as an paragraph in italic font.

It must be noted that Navier-Stokes hydrodynamics retains terms up through second order in the spatial gradients. Since the cooling rate ζ is a scalar, its most general form at this order is

$$
\begin{aligned}
\zeta \;=\; & \zeta_0 + \zeta_U\boldsymbol{\nabla}\cdot\mathbf{U} + \zeta_n\boldsymbol{\nabla}^2n + \zeta_T\boldsymbol{\nabla}^2T + \zeta_{nn}(\boldsymbol{\nabla}n)^2 + \zeta_{TT}(\boldsymbol{\nabla}T)^2 \\
& + \zeta_{nT}\boldsymbol{\nabla}n\cdot\boldsymbol{\nabla}T + \zeta_{1,uu}\partial_iU_j\partial_iU_j + \zeta_{2,uu}\partial_jU_i\partial_iU_j.
\end{aligned}
$$

The first two second-order terms ζ_n and ζ_T have been determined for dilute granular gases by Brey et al., while all the set of coefficients $\{\zeta_n, \zeta_T, \zeta_{nn}, \zeta_{nT}, \zeta_{1,uu}, \zeta_{2,uu}\}$ have been computed for granular gases of viscoelastic particles by Brilliantov and Pöschel. The evaluation of the above set of coefficients for dense gases is a quite intricate problem. In fact, to the best of my knowledge, no explicit results for these coefficients have been reported for granular dense gases.

2.7.1 Collisional Dissipation Rate for Whole Range of Density

The determination of the collisional dissipation $\mathscr{D}$ (2.65) for the whole range of density including all the terms (which also includes double derivatives of all the transport coefficients) is a quite intricate problem and has not been worked out till date. The complete expression for

collisional dissipation for the whole range of density including the terms involving derivatives of second order in hydrodynamic variables has been computed in this thesis work. In order to determine it, we have to take care of all the integrals appearing in eq.(2.51).

The total change of mC^2 in a collision is

$$\Delta mC^2 = -\frac{m}{2}(1-e^2)\,(\boldsymbol{g}\cdot\boldsymbol{k})^2\,. \tag{2.66}$$

Substituting this into the expression for collisional source [(2.51) and 2.63] and after performing the integrals term by term we have the final expression for collisional dissipation as

$$
\begin{aligned}
\mathcal{D} &= -\frac{1}{2}\aleph_{\alpha\alpha} \\
&= \underbrace{\frac{12\rho\nu g_0(1-e^2)T^{\frac{3}{2}}}{\pi^{\frac{1}{2}}\sigma}\left(1+\frac{3}{16}\mathfrak{a}_2+\frac{9}{1024}\mathfrak{a}_2^2\right)}\ \underbrace{-3\rho\nu g_0(1-e^2)T(\boldsymbol{\nabla}\cdot\boldsymbol{u})} \\
&-\frac{3}{10}(1-e^2)\nu g_0(2+21\mathfrak{a}_2)\boldsymbol{\nabla}\cdot\boldsymbol{q}^k+\frac{3\nu g_0(1-e^2)}{5\pi^{\frac{1}{2}}\sigma\rho T^{\frac{1}{2}}}\boldsymbol{\Pi}\colon\boldsymbol{\Pi}+\frac{3\nu g_0(1-e^2)}{50\pi^{\frac{1}{2}}\rho\sigma T^{\frac{3}{2}}}(\boldsymbol{q}^k\cdot\boldsymbol{q}^k) \\
&-\frac{6}{5}\nu g_0(1-e^2)(\boldsymbol{\nabla}\boldsymbol{u}\colon\boldsymbol{\Pi})-\frac{399}{175\rho T}\nu g_0(1-e^2)\Big((\boldsymbol{q}^k\boldsymbol{\nabla}\colon\boldsymbol{\Pi})+(\boldsymbol{\nabla}\boldsymbol{q}^k\colon\boldsymbol{\Pi})\Big) \\
&+\frac{3}{5\rho}\nu g_0(1-e^2)(\boldsymbol{q}^k\cdot\boldsymbol{\nabla}\rho)-\frac{63}{10}\nu g_0(1-e^2)(\boldsymbol{q}^k\cdot\boldsymbol{\nabla}\mathfrak{a}_2) \\
&+\frac{\rho\nu(1-e^2)\sigma}{16\sqrt{\pi}T^{\frac{3}{2}}} \\
&\quad\times\Bigg[g_0(\boldsymbol{r})\Bigg\{32\left(\frac{T^3}{\rho}\right)\boldsymbol{\nabla}^2\rho+24T^2\boldsymbol{\nabla}^2T+\frac{48}{5}\left(\frac{T^2}{\rho}\right)\Big(\boldsymbol{\nabla}\cdot(\boldsymbol{\nabla}\cdot\boldsymbol{\Pi})\Big)+3T^3\boldsymbol{\nabla}^2\mathfrak{a}_2 \\
&\qquad+48\left(\frac{T^2}{\rho}\right)\boldsymbol{\nabla}\rho\cdot\boldsymbol{\nabla}T+6T(\boldsymbol{\nabla}T)^2+\frac{24}{5}\left(\frac{T}{\rho}\right)\boldsymbol{\nabla}T\cdot(\boldsymbol{\nabla}\cdot\boldsymbol{\Pi}) \\
&\qquad+6\left(\frac{T^3}{\rho}\right)\boldsymbol{\nabla}\rho\cdot\boldsymbol{\nabla}\mathfrak{a}_2-237T^2\boldsymbol{\nabla}T\cdot\boldsymbol{\nabla}\mathfrak{a}_2 \\
&\qquad+\frac{48}{5}T^2\Big(\boldsymbol{\nabla}\boldsymbol{u}\colon\boldsymbol{\nabla}\boldsymbol{u}+\boldsymbol{\nabla}\boldsymbol{u}\colon\boldsymbol{\nabla}\boldsymbol{u}'+(\boldsymbol{\nabla}\cdot\boldsymbol{u})^2\Big) \\
&\qquad+\frac{48}{25}\left(\frac{T}{\rho}\right)\Big(\boldsymbol{\nabla}\boldsymbol{u}\colon\boldsymbol{\nabla}\boldsymbol{q}^k+\boldsymbol{\nabla}\boldsymbol{u}\colon\boldsymbol{\nabla}\boldsymbol{q}^{k'}+(\boldsymbol{\nabla}\cdot\boldsymbol{q}^k)^2\Big)\Bigg\} \\
&\qquad+16T^3\left\{\boldsymbol{\nabla}\cdot\left(\frac{\partial g_0}{\partial\rho}\boldsymbol{\nabla}\rho\right)\right\} \\
&\qquad+\frac{\partial g_0}{\partial\rho}\boldsymbol{\nabla}\rho\cdot\left\{32\left(\frac{T^3}{\rho}\right)\boldsymbol{\nabla}\rho+24T^2\boldsymbol{\nabla}T+3T^3\boldsymbol{\nabla}\mathfrak{a}_2+\frac{48}{5}\left(\frac{T^2}{\rho}\right)(\boldsymbol{\nabla}\cdot\boldsymbol{\Pi})\right\}\Bigg],
\end{aligned}
\tag{2.67}
$$

where a $(')$ over a quantity means its transpose and the following notation is used for the deviatoric part of the kinetic pressure tensor :

$$
\Pi_{\alpha\beta}=P^k_{\langle\alpha\beta\rangle}. \tag{2.68}
$$

The under-bracket terms in (2.67) are the contributions from the recent work by Garzó (2013)

$$\mathcal{D}_{\text{Garzo}} = \frac{12\rho\nu g_0(1-e^2)T^{\frac{3}{2}}}{\pi^{\frac{1}{2}}\sigma}\left(1+\frac{3}{16}\mathfrak{a}_2\right) - 3\rho\nu g_0(1-e^2)T(\boldsymbol{\nabla}\cdot\boldsymbol{u}), \tag{2.69}$$

where a 14-moment theory for a granular gas at a moderate density has been proposed. It is clear that the 14-moment theory of Garzó (2013) is incomplete since he has not calculated all source and flux terms consistently upto the second-order.

The 13-moment theory of Jenkins & Richman (1985*a*) is also incomplete for similar reasons and their expression for collisional dissipation $\mathcal{D}$ is

$$\mathcal{D}_{\text{Jenkins}} = \frac{12\rho\nu g_0(1-e^2)T^{\frac{3}{2}}}{\pi^{\frac{1}{2}}\sigma} - 3\rho\nu g_0(1-e^2)T(\boldsymbol{\nabla}\cdot\boldsymbol{u}). \tag{2.70}$$

2.7.2 Collisional Dissipation in the Dilute limit

In the dilute limit of a granular gas ($\nu\to 0; g_0\to 1$), eq. (2.67) reduces into

$$\begin{aligned}
\mathcal{D} = {} & \frac{12\rho\nu(1-e^2)T^{\frac{3}{2}}}{\pi^{\frac{1}{2}}\sigma}\left(1+\frac{3}{16}\mathfrak{a}_2+\frac{9}{1024}\mathfrak{a}_2^2\right) + \frac{3\nu(1-e^2)}{5\pi^{\frac{1}{2}}\sigma\rho T^{\frac{1}{2}}}\boldsymbol{\Pi}\colon\boldsymbol{\Pi} + \frac{3\nu(1-e^2)}{50\pi^{\frac{1}{2}}\rho\sigma T^{\frac{3}{2}}}(\boldsymbol{q}^k\cdot\boldsymbol{q}^k) \\
& + \frac{\rho\nu(1-e^2)\sigma}{16\sqrt{\pi}T^{\frac{3}{2}}}\Bigg\{32\left(\frac{T^3}{\rho}\right)\boldsymbol{\nabla}^2\rho + 24T^2\boldsymbol{\nabla}^2T + \frac{48}{5}\left(\frac{T^2}{\rho}\right)\Big(\boldsymbol{\nabla}\cdot(\boldsymbol{\nabla}\cdot\boldsymbol{\Pi})\Big) + 3T^3\boldsymbol{\nabla}^2\mathfrak{a}_2 \\
& \qquad + 48\left(\frac{T^2}{\rho}\right)\boldsymbol{\nabla}\rho\cdot\boldsymbol{\nabla}T + 6T(\boldsymbol{\nabla}T)^2 + \frac{24}{5}\left(\frac{T}{\rho}\right)\boldsymbol{\nabla}T\cdot(\boldsymbol{\nabla}\cdot\boldsymbol{\Pi}) \\
& \qquad + 6\left(\frac{T^3}{\rho}\right)\boldsymbol{\nabla}\rho\cdot\boldsymbol{\nabla}\mathfrak{a}_2 - 237T^2\boldsymbol{\nabla}T\cdot\boldsymbol{\nabla}\mathfrak{a}_2 \\
& \qquad + \frac{48}{5}T^2\Big(\boldsymbol{\nabla}\boldsymbol{u}\colon\boldsymbol{\nabla}\boldsymbol{u} + \boldsymbol{\nabla}\boldsymbol{u}\colon\boldsymbol{\nabla}\boldsymbol{u}' + (\boldsymbol{\nabla}\cdot\boldsymbol{u})^2\Big) \\
& \qquad + \frac{48}{25}\left(\frac{T}{\rho}\right)\Big(\boldsymbol{\nabla}\boldsymbol{u}\colon\boldsymbol{\nabla}\boldsymbol{q}^k + \boldsymbol{\nabla}\boldsymbol{u}\colon\boldsymbol{\nabla}\boldsymbol{q}^{k'} + (\boldsymbol{\nabla}\cdot\boldsymbol{q}^k)^2\Big)\Bigg\}.
\end{aligned} \tag{2.71}$$

Our expression of collisional dissipation (2.71) in the dilute limit contains all the terms obtained by Kremer & Marques Jr (2011) and Garzó (2012); moreover, the terms proportional to the nonlinear transport coefficients ($\sim \mathfrak{a}_2^2, P^k_{\langle kl\rangle}P^k_{\langle kl\rangle}, q^{k^2}$) match exactly with the expressions of the cooling rate as computed in a recent article by Gupta *et al.* (2017).

It should be noted here that the cooling rate obtained in this present theory is proportional to $(1-e^2)$, like it is found in the previous literature (Jenkins & Richman 1985*b*; Sela & Goldhirsch 1998; Garzó & Dufty 1999; Van Noije & Ernst 1998; Kremer & Marques Jr 2011). The cooling rate computed via the present nonlinear theory also contains terms proportional to the

double derivatives of number density ($\sim \boldsymbol{\nabla}^2 n$), granular temperature ($\sim \boldsymbol{\nabla}^2 T$), kinetic stress ($\sim \boldsymbol{\nabla}^2 \widehat{\boldsymbol{P}}^k$) and cumulant ($\sim \boldsymbol{\nabla}^2 \mathfrak{a}_2$). Establishing the dependence of collisional dissipation on these higher-order terms is a new finding of our work.

2.7.3 Remaining Higher-order Terms and the Nonlinear 5-Field Theory

The expression for $\Theta_{\alpha\beta\beta}$ is calculated and given in (2.95) and serves as the collisional contribution to the heat flux vector (2.64). It is noteworthy that with the information given for $\Theta_{\alpha\beta\beta}$, along with the dissipation rate (2.67), gives a "nonlinear" 5-moment theory for a granular gas at finite density that includes (i) the mass density (ρ), (ii) the macroscopic velocity $(\boldsymbol{u})$ and (iii) the granular temperature (T) as field variables; the corresponding balance equations are as follows:

$$\frac{\mathrm{D}\rho}{\mathrm{D}t} + \rho u_{\alpha,\alpha} = 0, \tag{2.72}$$

$$\rho \frac{\mathrm{D}u_\alpha}{\mathrm{D}t} + P_{\alpha\beta,\beta} = 0, \tag{2.73}$$

$$\frac{3}{2}\rho \frac{\mathrm{D}T}{\mathrm{D}t} + q_{\alpha,\alpha} + P_{\alpha\beta}\, u_{\beta,\alpha} + \mathscr{D} = 0. \tag{2.74}$$

Using Maxwell-iteration technique [Truesdell & Muncaster (1980)] the laws of Navier-Stokes and Fourier can be recovered as we shall demonstrate in §2.10.

This nonlinear 5-field theory can be applied to analyse molecular/granular flow phenomena that have negligible normal stress differences and replicates the Navier-Stokes level hydrodynamics (Garzó & Dufty 1999; Lutsko 2005) with second-order nonlinearities.

The hydrodynamics beyond Navier-Stokes that incorporates the normal stress differences and generalized Fourier's law are the main focus of the present work and will be considered in the following sections. We will discuss about the higher-order moment equations where the stress tensor $\boldsymbol{P}$ and heat flux vector $\boldsymbol{q}$ do not remain constitutive quantities but are considered as independent hydrodynamic variables.

2.8 Balance of Second Moment and the 10-moment System

We re-write the balance of second moment

$$\rho \frac{\mathrm{D}M_{\alpha\beta}}{\mathrm{D}t} + Q_{\gamma\alpha\beta,\gamma} + P_{\delta\beta} u_{\alpha,\delta} + P_{\delta\alpha} u_{\beta,\delta} = \aleph_{\alpha\beta}, \tag{2.75}$$

where the definitions of various production terms are as

$$\aleph_{\alpha\beta} = \aleph[mC_\alpha C_\beta],\ \Theta_{\alpha\beta} = \Theta_\alpha[mC_\beta] \text{ and } \Theta_{\gamma\alpha\beta} = \Theta_\alpha[mC_\alpha C_\beta], \tag{2.76}$$

and

$$P_{\alpha\beta} = \rho\langle \boldsymbol{C}_\alpha \boldsymbol{C}_\beta\rangle + \Theta_\alpha\left[mC_\beta\right] \equiv \rho M_{\alpha\beta} + \Theta_{\alpha\beta} = P^k_{\alpha\beta} + P^c_{\alpha\beta}, \tag{2.77}$$

$$Q_{\gamma\alpha\beta} = \rho\langle C_\gamma C_\alpha C_\beta\rangle + \Theta_\gamma\left[mC_\alpha C_\beta\right] \equiv \rho M_{\gamma\alpha\beta} + \Theta_{\gamma\alpha\beta}. \tag{2.78}$$

In this section we focus on the evolution equation for the second moment of velocity fluctuations $M_{\alpha\beta}(=\langle C_\alpha C_\beta\rangle)$, or, the balance of second moment as given in (2.75) and discuss about its closure. We evaluate the collisional source of second moment ($\aleph_{\alpha\beta}$) as appeared in the right hand side of (2.75) along with the collisional flux at second ($\Theta_{\alpha\beta}$) and third ($\Theta_{\gamma\alpha\beta}$) orders, respectively. The calculations involve terms correct up-to linear order in spatial gradients and the terms containing derivatives of second and higher order are neglected. The collisional flux of momentum ($\Theta_{\alpha\beta}$) is also termed as the collisional contribution to the stress tensor (2.77), $\boldsymbol{P}^c$, whereas the second moment of velocity fluctuations $\rho\langle C_\alpha C_\beta\rangle$ contributes the kinetic counterpart, $\boldsymbol{P}^k$, of the stress tensor.

2.8.1 Collisional Source and Flux at Second Order: Whole Range of Density

The total change of the dyadic product $\boldsymbol{C}C$ and the particle momentum $m\boldsymbol{C}$ in a collision is given by the formulae

$$\Delta(mC_\alpha C_\beta) = \frac{m}{2}(1+e)(\boldsymbol{g}\cdot\boldsymbol{k})\Big\{(1+e)(\boldsymbol{g}\cdot\boldsymbol{k})k_\alpha k_\beta - (k_\alpha g_\beta + g_\alpha k_\beta)\Big\}, \tag{2.79}$$

$$m(C'_\beta - C_\beta)|_1 = -\frac{m}{2}(1+e)(\boldsymbol{g}\cdot\boldsymbol{k})k_\beta, \tag{2.80}$$

where the subscript 1 in 2.80 corresponds to granule levelled with 1. Plugging the above set of information into the integral expressions of collisional source (2.51) and flux (2.52), we obtain

$$\begin{aligned}
\aleph_{\alpha\beta} = \frac{m(1+e)\sigma^2 g_0}{4} \iiint\limits_{\boldsymbol{g}\cdot\boldsymbol{k}>0} \Big\{(1+e)(\boldsymbol{g}\cdot\boldsymbol{k})^3 k_\alpha k_\beta - (\boldsymbol{g}\cdot\boldsymbol{k})^2(k_\alpha g_\beta + g_\alpha k_\beta)\Big\} \\
\times f_1 f_2 \Big\{1 + \frac{1}{2}\sigma k_i \frac{\partial}{\partial r_i}\log\frac{f_2}{f_1}\Big\} d\boldsymbol{k}d\boldsymbol{G}d\boldsymbol{g} \\
+ \frac{m(1+e)\sigma^4}{16} \iiint\limits_{\boldsymbol{g}\cdot\boldsymbol{k}>0} \Big\{(1+e)(\boldsymbol{g}\cdot\boldsymbol{k})^3 k_\alpha k_\beta - (\boldsymbol{g}\cdot\boldsymbol{k})^2(k_\alpha g_\beta + g_\alpha k_\beta)\Big\} \\
\times k_i k_j \frac{\partial g_0}{\partial r_i}\left(f_2\frac{\partial f_1}{\partial r_j} + f_1\frac{\partial f_2}{\partial r_j}\right) d\boldsymbol{k}d\boldsymbol{G}d\boldsymbol{g},
\end{aligned} \tag{2.81}$$

$$\begin{aligned}
\Theta_{\alpha\beta} = \frac{m(1+e)\sigma^3 g_0}{4} \iiint\limits_{\boldsymbol{g}\cdot\boldsymbol{k}>0} (\boldsymbol{g}\cdot\boldsymbol{k})^2 k_\alpha k_\beta f_1 f_2 \Big\{1 + \frac{1}{2}\sigma k_i \frac{\partial}{\partial r_i}\log\frac{f_2}{f_1}\Big\} d\boldsymbol{k}d\boldsymbol{G}d\boldsymbol{g} \\
- \frac{m(1+e)\sigma^5 g_0}{8} \iiint\limits_{\boldsymbol{g}\cdot\boldsymbol{k}>0} (\boldsymbol{g}\cdot\boldsymbol{k})^2 k_\alpha k_\beta k_m k_n \frac{\partial f_1}{\partial r_m}\frac{\partial f_2}{\partial r_n} d\boldsymbol{k}d\boldsymbol{G}d\boldsymbol{g} \\
- \frac{m(1+e)\sigma^5}{16} \iiint\limits_{\boldsymbol{g}\cdot\boldsymbol{k}>0} (\boldsymbol{g}\cdot\boldsymbol{k})^2 k_\alpha k_\beta k_m k_n \frac{\partial g_0}{\partial r_m}\left(f_2\frac{\partial f_1}{\partial r_n} + f_1\frac{\partial f_2}{\partial r_n}\right) d\boldsymbol{k}d\boldsymbol{G}d\boldsymbol{g}.
\end{aligned} \tag{2.82}$$

Evaluating above integrals, the expressions for collisional source of second moment is found as

$$
\begin{aligned}
&\aleph \equiv [\aleph_{\alpha\beta}] = \\
&\underbrace{-\frac{8\rho\nu g_0(1-e^2)T^{\frac{3}{2}}}{\pi^{\frac{1}{2}}\sigma}\Big(1+\frac{3\mathfrak{a}_2}{16}+\frac{9}{1024}\mathfrak{a}_2^2\Big)\mathbf{I}}\underbrace{-\frac{24\nu g_0(1+e)(3-e)T^{\frac{1}{2}}}{5\pi^{\frac{1}{2}}\sigma}\Big(1-\frac{\mathfrak{a}_2}{32}\Big)\mathbf{\Pi}} \\
&\underbrace{-\frac{6\rho\nu g_0(1+e)T}{5}\Big\{2(e-2)\mathbf{D}+\Big(e-\frac{1}{3}\Big)(\boldsymbol{\nabla}\cdot\boldsymbol{u})\mathbf{I}\Big\}} \\
&+\frac{(1+e)\nu g_0}{25}(2+21\mathfrak{a}_2)\Big[(1-3e)(\boldsymbol{\nabla}\cdot\boldsymbol{q})\mathbf{I}+3(2-e)\Big\{\boldsymbol{\nabla}\boldsymbol{q}^k+(\boldsymbol{\nabla}\boldsymbol{q}^k)'\Big\}\Big] \\
&+\frac{(1+e)\nu g_0}{35\pi^{\frac{1}{2}}\rho\sigma T^{\frac{1}{2}}}\Big\{(3e+5)(\mathbf{\Pi}\colon\mathbf{\Pi})\mathbf{I}+12(e-3)(\mathbf{\Pi}\cdot\mathbf{\Pi})\Big\} \\
&+\frac{(1+e)\nu g_0}{125\pi^{\frac{1}{2}}\rho\sigma T^{\frac{3}{2}}}\Big\{(1+3e)(\mathbf{q}^\mathbf{k}\cdot\mathbf{q}^\mathbf{k})\mathbf{I}-6(3-e)(\mathbf{q}^\mathbf{k}\mathbf{q}^\mathbf{k})\Big\} \\
&+\frac{2(1+e)\nu g_0}{35}\Big[(1-27e)(\boldsymbol{\nabla}\boldsymbol{u}\colon\mathbf{\Pi})\mathbf{I}+(50-27e)\Big\{(\boldsymbol{\nabla}\boldsymbol{u}\cdot\mathbf{\Pi})+(\boldsymbol{\nabla}\boldsymbol{u}\cdot\mathbf{\Pi})'\Big\} \\
&\qquad\qquad+2(11-3e)\Big\{(\mathbf{\Pi}\cdot\boldsymbol{\nabla}\boldsymbol{u})+(\mathbf{\Pi}\cdot\boldsymbol{\nabla}\boldsymbol{u})'+(\boldsymbol{\nabla}\cdot\boldsymbol{u})\mathbf{\Pi}\Big\}\Big] \\
&-\frac{2(1+e)\nu g_0}{5}\Big\{(1-3e)(\boldsymbol{\nabla}\boldsymbol{u}\colon\mathbf{\Pi})\mathbf{I}+3(2-e)\Big((\boldsymbol{\nabla}\boldsymbol{u}\cdot\mathbf{\Pi})+(\boldsymbol{\nabla}\boldsymbol{u}\cdot\mathbf{\Pi})'\Big)\Big\} \\
&+\frac{2(1+e)\nu g_0}{175\rho T}\Big[4(11-3e)\Big\{\Big((\boldsymbol{q}^k\cdot\boldsymbol{\nabla})\mathbf{\Pi}+\boldsymbol{q}^k(\boldsymbol{\nabla}\cdot\mathbf{\Pi})+\{\boldsymbol{q}^k(\boldsymbol{\nabla}\cdot\mathbf{\Pi})\}'\Big) \\
&\qquad\qquad+\Big((\boldsymbol{\nabla}\cdot\boldsymbol{q}^k)\mathbf{\Pi}+(\mathbf{\Pi}\cdot\boldsymbol{\nabla})\boldsymbol{q}^k+\{(\mathbf{\Pi}\cdot\boldsymbol{\nabla})\boldsymbol{q}^k\}'\Big)\Big\} \\
&\qquad\qquad+(9-75e)\Big\{(\boldsymbol{q}^k\boldsymbol{\nabla}\colon\mathbf{\Pi})+(\boldsymbol{\nabla}\boldsymbol{q}^k\colon\mathbf{\Pi})\Big\}\mathbf{I} \\
&\qquad\qquad+(142-75e)\Big\{(\boldsymbol{\nabla}\mathbf{\Pi})\cdot\boldsymbol{q}^k+\{(\boldsymbol{\nabla}\mathbf{\Pi})\cdot\boldsymbol{q}^k\}'+(\boldsymbol{\nabla}\boldsymbol{q}^k)\cdot\mathbf{\Pi}+\{(\boldsymbol{\nabla}\boldsymbol{q}^k)\cdot\mathbf{\Pi}\}'\Big\}\Big] \\
&-\frac{2(1+e)\nu g_0}{25\rho}\Big\{(1-3e)(\boldsymbol{q}^k\cdot\boldsymbol{\nabla}\rho)\mathbf{I}+3(2-e)\Big(\boldsymbol{q}^k\boldsymbol{\nabla}\rho+(\boldsymbol{q}^k\boldsymbol{\nabla}\rho)'\Big)\Big\} \\
&+\frac{21(1+e)\nu g_0}{25}\Big\{(1-3e)(\boldsymbol{q}^k\cdot\boldsymbol{\nabla}\mathfrak{a}_2)\mathbf{I}+3(2-e)\Big(\boldsymbol{q}^k\boldsymbol{\nabla}\mathfrak{a}_2+(\boldsymbol{q}^k\boldsymbol{\nabla}\mathfrak{a}_2)'\Big)\Big\} \\
&-\frac{\rho\nu\sigma(1+e)T^{\frac{1}{2}}}{40\pi^{\frac{1}{2}}}\Big[\Big\{\boldsymbol{\nabla}g_0\Big(32(1-e)\frac{T}{n}\boldsymbol{\nabla}n+24(1-e)\boldsymbol{\nabla}T+3(1-e)T\boldsymbol{\nabla}\mathfrak{a}_2+\frac{48(2-e)}{7}\frac{1}{\rho}\boldsymbol{\nabla}\cdot\mathbf{\Pi}\Big)\Big\} \\
&\qquad+\Big\{\boldsymbol{\nabla}g_0\Big(32(1-e)\frac{T}{n}\boldsymbol{\nabla}n+24(1-e)\boldsymbol{\nabla}T+3(1-e)T\boldsymbol{\nabla}\mathfrak{a}_2+\frac{48(2-e)}{7}\frac{1}{\rho}\boldsymbol{\nabla}\cdot\mathbf{\Pi}\Big)\Big\}' \\
&\qquad+\Big\{\boldsymbol{\nabla}g_0\cdot\Big(32(1-e)\frac{T}{n}\boldsymbol{\nabla}n+24(1-e)\boldsymbol{\nabla}T+3(1-e)T\boldsymbol{\nabla}\mathfrak{a}_2-\frac{16(1+3e)}{7}\frac{1}{\rho}\boldsymbol{\nabla}\cdot\mathbf{\Pi}\Big)\Big\}\mathbf{I} \\
&\qquad+\frac{48(2-e)}{7}\frac{1}{\rho}\Big\{(\boldsymbol{\nabla}\mathbf{\Pi}\cdot\boldsymbol{\nabla}g)+(\boldsymbol{\nabla}\mathbf{\Pi}\cdot\boldsymbol{\nabla}g)'\Big\}+\frac{16(13-3e)}{7}\frac{1}{\rho}(\boldsymbol{\nabla}g\cdot\boldsymbol{\nabla}\mathbf{\Pi})\Big],
\end{aligned}
\tag{2.83}
$$

and the expression for the collisional flux of momentum is

$$
\begin{aligned}
&\boldsymbol{\Theta} \equiv [\Theta_{\alpha\beta}] = \\
&\underbrace{\Big(2(1+e)\rho\nu g_0 T\Big)\mathbf{I} + \frac{4}{5}\nu g_0(1+e)\boldsymbol{\Pi} - \frac{4\rho\nu g_0(1+e)\sigma T^{\frac{1}{2}}}{5\pi^{\frac{1}{2}}}\Big(1-\frac{\mathfrak{a}_2}{16}\Big)\Big(\boldsymbol{\nabla u}+\boldsymbol{\nabla u}'+(\boldsymbol{\nabla}\cdot\boldsymbol{u})\mathbf{I}\Big)}\\
&-\frac{(1+e)\nu g_0\sigma}{200\pi^{\frac{1}{2}}T^{\frac{1}{2}}}(16+239\mathfrak{a}_2)\Big(\boldsymbol{\nabla q}^k+(\boldsymbol{\nabla q}^k)'+(\boldsymbol{\nabla}\cdot\boldsymbol{q})\mathbf{I}\Big)\\
&-\frac{4(1+e)\nu g_0\sigma}{35\pi^{\frac{1}{2}}T^{\frac{1}{2}}}\Big[8\Big\{(\boldsymbol{\nabla u}\colon\boldsymbol{\Pi})\mathbf{I}+(\boldsymbol{\nabla u}\cdot\boldsymbol{\Pi})+(\boldsymbol{\nabla u}\cdot\boldsymbol{\Pi})'\Big\}\\
&\qquad\qquad+\Big\{(\boldsymbol{\Pi}\cdot\boldsymbol{\nabla u})+(\boldsymbol{\Pi}\cdot\boldsymbol{\nabla u})'+(\boldsymbol{\nabla}\cdot\boldsymbol{u})\boldsymbol{\Pi}\Big\}\Big]\\
&+\frac{4(1+e)\nu g_0\sigma}{5\pi^{\frac{1}{2}}T^{\frac{1}{2}}}\Big\{(\boldsymbol{\nabla u}\colon\boldsymbol{\Pi})\mathbf{I}+(\boldsymbol{\nabla u}\cdot\boldsymbol{\Pi})+(\boldsymbol{\nabla u}\cdot\boldsymbol{\Pi})'\Big\}\\
&-\frac{2(1+e)\nu g_0\sigma}{175\pi^{\frac{1}{2}}\rho T^{\frac{3}{2}}}\\
&\quad\times\Big[4\Big\{(\boldsymbol{q}^k\cdot\boldsymbol{\nabla})\boldsymbol{\Pi}+\boldsymbol{q}^k(\boldsymbol{\nabla}\cdot\boldsymbol{\Pi})+\{\boldsymbol{q}^k(\boldsymbol{\nabla}\cdot\boldsymbol{\Pi})\}'\Big\}\\
&\qquad+3\Big\{(\boldsymbol{\nabla}\cdot\boldsymbol{q}^k)\boldsymbol{\Pi}+(\boldsymbol{\Pi}\cdot\boldsymbol{\nabla})\boldsymbol{q}^k+\{(\boldsymbol{\Pi}\cdot\boldsymbol{\nabla})\boldsymbol{q}^k\}'\Big\}\\
&\qquad+39\Big\{(\boldsymbol{\nabla\Pi})\cdot\boldsymbol{q}^k+\{(\boldsymbol{\nabla\Pi})\cdot\boldsymbol{q}^k\}'+(\boldsymbol{q}^k\boldsymbol{\nabla}\colon\boldsymbol{\Pi})\mathbf{I}\Big\}\\
&\qquad+38\Big\{(\boldsymbol{\nabla q}^k)\cdot\boldsymbol{\Pi}+\{(\boldsymbol{\nabla q}^k)\cdot\boldsymbol{\Pi}\}'+(\boldsymbol{\nabla q}^k\colon\boldsymbol{\Pi})\mathbf{I}\Big\}\Big]\\
&+\frac{2(1+e)\nu g_0\sigma}{25\pi^{\frac{1}{2}}\rho T^{\frac{1}{2}}}\Big(\boldsymbol{q}^k\boldsymbol{\nabla}\rho+(\boldsymbol{q}^k\boldsymbol{\nabla}\rho)'+(\boldsymbol{q}^k\cdot\boldsymbol{\nabla}\rho)\mathbf{I}\Big)\\
&-\frac{59(1+e)\nu g_0\sigma}{50\pi^{\frac{1}{2}}T^{\frac{1}{2}}}\Big(\boldsymbol{q}^k\boldsymbol{\nabla}\mathfrak{a}_2+(\boldsymbol{q}^k\boldsymbol{\nabla}\mathfrak{a}_2)'+(\boldsymbol{q}^k\cdot\boldsymbol{\nabla}\mathfrak{a}_2)\mathbf{I}\Big)\\
&-\frac{\rho(1+e)\nu g_0\sigma^2}{5n}\Big[\frac{T}{n}\Big\{(\boldsymbol{\nabla}n\cdot\boldsymbol{\nabla}n)\mathbf{I}+2(\boldsymbol{\nabla}n\boldsymbol{\nabla}n)\Big\}+\Big\{(\boldsymbol{\nabla}n\cdot\boldsymbol{\nabla}T)\mathbf{I}+(\boldsymbol{\nabla}n\boldsymbol{\nabla}T)+(\boldsymbol{\nabla}n\boldsymbol{\nabla}T)'\Big\}\Big]\\
&+\frac{\rho(1+e)\nu g_0\sigma^2}{35}\Big[\Big\{\boldsymbol{\nabla u}\colon\boldsymbol{\nabla u}+\boldsymbol{\nabla u}\colon(\boldsymbol{\nabla u})'+(\boldsymbol{\nabla}\cdot\boldsymbol{u})^2\Big\}\mathbf{I}\\
&\quad+2\Big\{\boldsymbol{\nabla u}\cdot\boldsymbol{\nabla u}+(\boldsymbol{\nabla u}\cdot\boldsymbol{\nabla u})'+\boldsymbol{\nabla u}\cdot(\boldsymbol{\nabla u})'+(\boldsymbol{\nabla u})'\cdot\boldsymbol{\nabla u}+\Big(\boldsymbol{\nabla u}+(\boldsymbol{\nabla u})'\Big)(\boldsymbol{\nabla}\cdot\boldsymbol{u})\Big\}\Big]\\
&-\frac{\rho(1+e)\nu\sigma^2}{10}\Big[\frac{2T}{n}\Big\{(\boldsymbol{\nabla}g_0\cdot\boldsymbol{\nabla}n)\mathbf{I}+(\boldsymbol{\nabla}g_0\boldsymbol{\nabla}n)+(\boldsymbol{\nabla}g_0\boldsymbol{\nabla}n)'\Big\}\\
&\qquad\qquad+\Big\{(\boldsymbol{\nabla}g_0\cdot\boldsymbol{\nabla}T)\mathbf{I}+(\boldsymbol{\nabla}g_0\boldsymbol{\nabla}T)+(\boldsymbol{\nabla}g_0\boldsymbol{\nabla}T)'\Big\}\Big]\\
&-\frac{(1+e)\nu\sigma^2}{35\rho}\Big[(\boldsymbol{\nabla}g_0\cdot\boldsymbol{\nabla})\boldsymbol{\Pi}+\Big\{(\boldsymbol{\nabla}g_0)\cdot(\boldsymbol{\nabla}\cdot\boldsymbol{\Pi})\Big\}\mathbf{I}+(\boldsymbol{\nabla\Pi})\cdot\boldsymbol{\nabla}g_0+\Big\{(\boldsymbol{\nabla\Pi})\cdot\boldsymbol{\nabla}g_0\Big\}'\\
&\qquad\qquad+(\boldsymbol{\nabla}g_0)(\boldsymbol{\nabla}\cdot\boldsymbol{\Pi})+\Big\{(\boldsymbol{\nabla}g_0)(\boldsymbol{\nabla}\cdot\boldsymbol{\Pi})\Big\}'\Big],
\end{aligned}
\tag{2.84}
$$

The under-braced terms in (2.83) and (2.84) are contributions from work by Garzó (2013); the remaining terms are new contributions of the present work.

2.8.2 Collisional Flux at Third Order: Whole Range of Density

The second moment of velocity fluctuations (2.75) contains the third order flux $\Theta_{\gamma\alpha\beta}$, see eq.(2.78). In order to close the system of equations (2.75), we need to calculate this higher order term. The detailed calculation is beyond the scope of the thesis and we give the final expression as follows:

$$
\begin{aligned}
\Theta_{\gamma\alpha\beta} &= \frac{2}{25}\nu g_0(1+e)\Big(4q_\gamma\delta_{\alpha\beta}+9q_\alpha\delta_{\beta\gamma}+9q_\beta\delta_{\alpha\gamma}\Big)\\
&-\frac{2\nu g_0\sigma(1+e)}{175\sqrt{\pi}\sqrt{T}}\left[4\left\{\frac{\partial u_\alpha}{\partial r_\beta}+\frac{\partial u_\beta}{\partial r_\alpha}+(\boldsymbol{\nabla}\cdot u)\,\delta_{\alpha\beta}\right\}q^k_\gamma\right.\\
&+4\left\{\frac{\partial u_\alpha}{\partial r_l}\delta_{\beta\gamma}+\frac{\partial u_\beta}{\partial r_l}\delta_{\alpha\gamma}+\frac{\partial u_\gamma}{\partial r_l}\delta_{\alpha\beta}\right\}q^k_l+4\left\{\frac{\partial u_l}{\partial r_\alpha}\delta_{\beta\gamma}+\frac{\partial u_l}{\partial r_\beta}\delta_{\alpha\gamma}+\frac{\partial u_l}{\partial r_\gamma}\delta_{\alpha\beta}\right\}q^k_l\\
&\left.+11\left\{\frac{\partial u_\alpha}{\partial r_\gamma}+\frac{\partial u_\gamma}{\partial r_\alpha}+(\boldsymbol{\nabla}\cdot u)\,\delta_{\alpha\gamma}\right\}q^k_\beta+11\left\{\frac{\partial u_\beta}{\partial r_\gamma}+\frac{\partial u_\gamma}{\partial r_\beta}+(\boldsymbol{\nabla}\cdot u)\,\delta_{\beta\gamma}\right\}q^k_\alpha\right]\\
&-\frac{\rho\nu g_0\sigma(1+e)}{20\sqrt{\pi}}(16+7\mathfrak{a}_2)\sqrt{T}\left(\frac{\partial T}{\partial r_\gamma}\delta_{\alpha\beta}+\frac{\partial T}{\partial r_\alpha}\delta_{\beta\gamma}+\frac{\partial T}{\partial r_\beta}\delta_{\alpha\gamma}\right)\\
&-\frac{4\nu g_0\sigma(1+e)}{35\sqrt{\pi}\sqrt{T}}\left\{\left(P^k_{\langle\alpha l\rangle}\delta_{\beta\gamma}+P^k_{\langle\beta l\rangle}\delta_{\alpha\gamma}+P^k_{\langle\gamma l\rangle}\delta_{\alpha\beta}\right)\frac{\partial T}{\partial r_l}\right.\\
&\qquad\left.+P^k_{\langle\alpha\beta\rangle}\frac{\partial T}{\partial r_\gamma}+P^k_{\langle\beta\gamma\rangle}\frac{\partial T}{\partial r_\alpha}+P^k_{\langle\alpha\gamma\rangle}\frac{\partial T}{\partial r_\beta}\right\}\\
&+\frac{2\nu g_0\sigma(1+e)\sqrt{T}}{5\sqrt{\pi}\rho}\left\{\left(P^k_{\langle\alpha\beta\rangle}\delta_{\gamma l}+P^k_{\langle\alpha l\rangle}\delta_{\beta\gamma}+P^k_{\langle\beta l\rangle}\delta_{\alpha\gamma}\right)\frac{\partial\rho}{\partial r_l}\right.\\
&\qquad\left.+P^k_{\langle\alpha\beta\rangle}\frac{\partial\rho}{\partial r_\gamma}+P^k_{\langle\beta\gamma\rangle}\frac{\partial\rho}{\partial r_\alpha}+P^k_{\langle\alpha\gamma\rangle}\frac{\partial\rho}{\partial r_\beta}\right\}\\
&-\frac{2\nu g_0\sigma(1+e)\sqrt{T}}{5\sqrt{\pi}}\left(\frac{\partial P^k_{\langle\alpha\beta\rangle}}{\partial r_\gamma}+\frac{\partial P^k_{\langle\beta\gamma\rangle}}{\partial r_\alpha}+\frac{\partial P^k_{\langle\alpha\gamma\rangle}}{\partial r_\beta}+\frac{\partial P^k_{\langle\alpha\beta\rangle}}{\partial r_l}\delta_{\gamma l}+\frac{\partial P^k_{\langle\alpha l\rangle}}{\partial r_l}\delta_{\beta\gamma}+\frac{\partial P^k_{\langle\beta l\rangle}}{\partial r_l}\delta_{\alpha\gamma}\right)\\
&-\frac{\nu g_0\sigma(1+e)\sqrt{T}\mathfrak{a}_2}{280\sqrt{\pi}}\left(354\frac{\partial P^k_{\langle\alpha\beta\rangle}}{\partial r_\gamma}+193\frac{\partial P^k_{\langle\beta\gamma\rangle}}{\partial r_\alpha}+193\frac{\partial P^k_{\langle\alpha\gamma\rangle}}{\partial r_\beta}\right.\\
&\qquad\left.+32\frac{\partial P^k_{\langle\gamma l\rangle}}{\partial r_l}\delta_{\alpha\beta}+193\frac{\partial P^k_{\langle\alpha l\rangle}}{\partial r_l}\delta_{\beta\gamma}+193\frac{\partial P^k_{\langle\beta l\rangle}}{\partial r_l}\delta_{\alpha\gamma}\right)\\
&-\frac{\nu g_0\sigma(1+e)}{35\sqrt{\pi}\rho\sqrt{T}}\left\{2\left(\frac{\partial P^k_{\langle\alpha\beta\rangle}}{\partial r_l}P^k_{\langle\gamma l\rangle}-\frac{\partial P^k_{\langle\gamma l\rangle}}{\partial r_l}P^k_{\langle\alpha\beta\rangle}\right)\right.\\
&\quad+\frac{\partial P^k_{\langle\alpha l\rangle}}{\partial r_\beta}P^k_{\langle\gamma l\rangle}-\frac{\partial P^k_{\langle\gamma l\rangle}}{\partial r_\beta}P^k_{\langle\alpha l\rangle}+\left(\frac{\partial P^k_{\langle\beta m\rangle}}{\partial r_l}P^k_{\langle ml\rangle}-\frac{\partial P^k_{\langle ml\rangle}}{\partial r_l}P^k_{\langle\beta m\rangle}\right)\delta_{\alpha\gamma}\\
&\quad\left.+\frac{\partial P^k_{\langle\beta l\rangle}}{\partial r_\alpha}P^k_{\langle\gamma l\rangle}-\frac{\partial P^k_{\langle\gamma l\rangle}}{\partial r_\alpha}P^k_{\langle\beta l\rangle}+\left(\frac{\partial P^k_{\langle\alpha m\rangle}}{\partial r_l}P^k_{\langle ml\rangle}-\frac{\partial P^k_{\langle ml\rangle}}{\partial r_l}P^k_{\langle\alpha m\rangle}\right)\delta_{\beta\gamma}\right\}\\
&-\frac{\nu g_0\sigma(1+e)}{250\sqrt{\pi}\rho T^{\frac{3}{2}}}\left\{\frac{\partial q^k_\alpha}{\partial r_\beta}q^k_\gamma-\frac{\partial q^k_\gamma}{\partial r_\beta}q^k_\alpha+\frac{\partial q^k_\beta}{\partial r_\alpha}q^k_\gamma-\frac{\partial q^k_\gamma}{\partial r_\alpha}q^k_\beta\right.\\
&\qquad\left.+\left(\frac{\partial q^k_\beta}{\partial r_l}q^k_l-\frac{\partial q^k_l}{\partial r_l}q^k_\beta\right)\delta_{\alpha\gamma}+\left(\frac{\partial q^k_\alpha}{\partial r_l}q^k_l-\frac{\partial q^k_l}{\partial r_l}q^k_\alpha\right)\delta_{\beta\gamma}\right\}. \qquad (2.85)
\end{aligned}
$$

It may be noted that third-order flux (2.85) has not been calculated in previous works [Jenkins & Richman (1985*a*); Garzó (2013)].

2.8.3 Nonlinear 10-moment System

The following set of 10-equations

$$\frac{\mathrm{D}\rho}{\mathrm{D}t} = -\rho u_{\alpha,\alpha}, \tag{2.86}$$

$$\rho\frac{\mathrm{D}u_\alpha}{\mathrm{D}t} = -P_{\alpha\beta,\beta}, \tag{2.87}$$

$$\rho\frac{\mathrm{D}M_{\alpha\beta}}{\mathrm{D}t} = -Q_{\gamma\alpha\beta,\gamma} - P_{\delta\beta}u_{\alpha,\delta} - P_{\delta\alpha}u_{\beta,\delta} + \aleph_{\alpha\beta}, \tag{2.88}$$

along with the constitutive expressions (2.83), (2.84) and (2.85) serve as the nonlinear 10-moment theory of $\{\rho,\, \boldsymbol{u},\, \boldsymbol{P}\}$ for a dense granular gas at finite densities. It may be noted that the third-order flux (2.85) has not been calculated before.

For a closure of second moment balance (2.88), we need a constitutive expression for the kinetic part of the third moment tensor $Q_{\gamma\alpha\beta}$. This can be accomplished via Maxwell-iteration technique as discussed in §2.10.

2.9 Collisional Source and Flux at Third Order : Whole Range of Density

In this section we determine the collisional source of contracted third moment $\aleph_{\alpha\beta\beta}$ and the collisional flux of third moment $\Theta_{\gamma\alpha\beta}$ for the whole range of density. The contracted third-order production term $\aleph_{\alpha\beta\beta}$ appears on the right hand side of the balance equation for kinetic heat-flux (2.25), which after re-writing reads as

$$\frac{\mathrm{D}q^k_\alpha}{\mathrm{D}t} + \frac{1}{2}Q_{\gamma\alpha\beta\beta,\gamma} + q^k_\alpha u_{\delta,\delta} + q^k_\beta u_{\alpha,\beta} + Q_{\gamma\alpha\beta}u_{\beta,\gamma} - \left(M_{\alpha\beta} + \frac{1}{2}M_{\gamma\gamma}\delta_{\alpha\beta}\right)P_{\beta n,n} + \frac{1}{2}\Theta_{\gamma\beta\beta}u_{\alpha,\gamma} = \frac{1}{2}\aleph_{\alpha\beta\beta}, \tag{2.89}$$

which determines the evolution of the kinetic contribution $\boldsymbol{q}^k$ to granular heat flux. On the other hand, the third order flux term $\Theta_{\gamma\alpha\beta}$ on the left hand side of (2.89) also appears on the left hand side of the balance of second moment (2.24) which is required to close the 10-moment theory. Furthermore, the contraction over the last two indices of $\Theta_{\gamma\alpha\beta}$ produces the

collisional component of the heat flux vector $q^c_\gamma(=\frac{1}{2}\Theta_{\gamma\alpha\alpha})$ and therefore the total heat flux vector can be obtained using

$$q_\alpha = q^k_\alpha + q^c_\alpha = \frac{1}{2}M_{\alpha\beta\beta} + \frac{1}{2}\Theta_{\alpha\beta\beta}. \tag{2.90}$$

Now

$$\aleph_{\alpha\beta\beta} = \aleph[mC^2C_\alpha], \qquad \Theta_{\gamma\alpha\beta} = \Theta_\gamma[mC_\alpha C_\beta], \tag{2.91}$$

$$\Delta(mC^2C_\alpha) = \frac{m}{2}(1+e)(\boldsymbol{g}\cdot\boldsymbol{k})\Big\{2(1+e)(\boldsymbol{g}\cdot\boldsymbol{k})k_\alpha k_\beta G_\beta - (1-e)(\boldsymbol{g}\cdot\boldsymbol{k})G_\alpha - 2G_\beta(g_\alpha k_\beta + k_\alpha g_\beta)\Big\}, \tag{2.92}$$

$$m\left(C'_\alpha C'_\beta - C_\alpha C_\beta\right) = \frac{m}{2}(1+e)(\boldsymbol{g}\cdot\boldsymbol{k})\Big\{\frac{1}{2}(1+e)(\boldsymbol{g}\cdot\boldsymbol{k})k_\alpha k_\beta - (G_\alpha k_\beta + k_\alpha G_\beta) - \frac{1}{2}(g_\alpha k_\beta + k_\alpha g_\beta)\Big\}. \tag{2.93}$$

Plugging the above set of information into (2.51-2.52) and performing some tedious steps, we obtain the expressions for the contracted third order source and flux:

$$\begin{aligned}
\aleph_{\alpha\beta\beta} = &-\frac{4(1+e)\nu g_0\sqrt{T}}{5\sqrt{\pi}\sigma}\Big[\Big\{(49-33e)+\frac{\mathfrak{a}_2}{32}(19-3e)\Big\}q^k_\alpha + \frac{3(7+e)}{10\rho T}P^k_{\langle\alpha l\rangle}q^k_l\Big] \\
&-\frac{1}{5\rho}\nu g_0(1+e)(29-27e)TP^k_{\langle\alpha l\rangle}\frac{\partial\rho}{\partial r_l} \\
&+\frac{2(1+e)\nu g_0}{25}\Big[(55-39e)\frac{\partial u_l}{\partial r_l}q^k_\alpha + 2(25-12e)\frac{\partial u_\alpha}{\partial r_l}q^k_l + 6(5-4e)\frac{\partial u_l}{\partial r_\alpha}q^k_l\Big] \\
&+\frac{1}{5}\rho\nu g_0(1+e)\Big\{5(13-9e)(1+\mathfrak{a}_2)T\delta_{\alpha l} + 2(19-9e)\frac{P^k_{\langle\alpha l\rangle}}{\rho}\Big\}\frac{\partial T}{\partial r_l} \\
&+\frac{1}{5}\nu g_0(1+e)\Big\{(29-27e)+24(4-3e)\mathfrak{a}_2\Big\}T\frac{P^k_{\langle\alpha l\rangle}}{\partial r_l} \\
&+\frac{1}{10}\rho\nu g_0(1+e)\Big\{5(13-9e)\delta_{l\alpha} + 48(4-3e)\frac{P^k_{\langle\alpha l\rangle}}{\rho T}\Big\}T^2\frac{\partial\mathfrak{a}_2}{\partial r_l},
\end{aligned} \tag{2.94}$$

and

$$\Theta_{\alpha\beta\beta} = \frac{12(1+e)\nu g_0}{5} q_\alpha - \frac{12(1+e)\nu g_0\sigma}{25\sqrt{\pi}\sqrt{T}}\left(\frac{\partial u_l}{\partial r_l} q^k_\alpha + \frac{\partial u_\alpha}{\partial r_l} q^k_l + \frac{\partial u_l}{\partial r_\alpha} q^k_l\right)$$
$$+ \frac{8\nu g_0\sigma(1+e)\sqrt{T}}{5\sqrt{\pi}\rho} P^k_{\langle\alpha l\rangle}\frac{\partial \rho}{\partial r_l} - \frac{\rho\nu g_0\sigma(1+e)\sqrt{T}}{20\sqrt{\pi}}\left\{5(16+7\mathfrak{a}_2)\delta_{\alpha l} + 16\frac{P^k_{\langle\alpha l\rangle}}{\rho T}\right\}\frac{\partial T}{\partial r_l}$$
$$- \frac{\nu g_0(1+e)\sigma\sqrt{T}}{10\sqrt{\pi}}(16+31\mathfrak{a}_2)\frac{P^k_{\langle\alpha l\rangle}}{\partial r_l} - \frac{\rho\nu g_0(1+e)\sigma T^{\frac{3}{2}}}{\sqrt{\pi}}\left(\delta_{\alpha l} + 3\frac{P^k_{\langle\alpha l\rangle}}{\rho T}\right)\frac{\partial \mathfrak{a}_2}{\partial r_l}, \quad (2.95)$$

respectively.

The expression for $\Theta_{\alpha\beta\beta}$ given in (2.95) is twice the collisional contribution to the heat flux vector (2.64) and gives a closure for the "nonlinear" 5-moment theory of (i) the mass density (ρ), (ii) the macroscopic flow velocity $(\boldsymbol{u})$ and (iii) the granular temperature (T) as discussed in §2.7.3:

$$\frac{\mathrm{D}\rho}{\mathrm{D}t} + \rho u_{\alpha,\alpha} = 0, \quad (2.96)$$
$$\rho\frac{\mathrm{D}u_\alpha}{\mathrm{D}t} + P_{\alpha\beta,\beta} = 0, \quad (2.97)$$
$$\frac{3}{2}\rho\frac{\mathrm{D}T}{\mathrm{D}t} + q_{\alpha,\alpha} + P_{\alpha\beta}\, u_{\beta,\alpha} + \mathscr{D} = 0. \quad (2.98)$$

The constitutive relation for the heat-flux must be determined at finite densities which is left for a future work. In the following, we outline a procedure on how to determine "nonlinear" constitutive relation for heat flux of a "dilute" granular gas.

2.10 Granular Heat Flux and Thermal Conductivity in the Dilute Limit

In this section we focus on the dilute limit of of a granular gas and determine the granular heat heat flux along with the corresponding thermal conductivity tensor in a non-uniform shear flow. In dilute limit, the collisional component of any quantity becomes negligible and the kinetic component is the only relevant parameter. Therefore in this limit ($\nu \to 0$) the governing equation (2.89) for heat flux reduces to

$$\frac{\mathrm{D}q_\alpha}{\mathrm{D}t} + q_\alpha u_{\delta,\delta} + \frac{1}{2}Q_{\gamma\alpha\beta\beta,\gamma} + \underbrace{Q_{\gamma\alpha\beta}u_{\beta,\gamma} + q_\beta u_{\alpha,\beta}} - \left(M_{\alpha\beta} + \frac{1}{2}M_{\gamma\gamma}\delta_{\alpha\beta}\right)P_{\beta n,n} = \frac{1}{2}\aleph_{\alpha\beta\beta}, \quad (2.99)$$

where the heat flux vector is defined via

$$q_\alpha = q^k_\alpha = \frac{m}{2}\int C^2 C_\alpha f d\boldsymbol{C} = \frac{1}{2}\rho M_{\alpha\beta\beta}. \tag{2.100}$$

The other related quantities appearing in (2.99) take the form

$$\left.\begin{aligned} Q_{\gamma\alpha\beta\beta} = \rho M_{\gamma\alpha\beta\beta} = \rho\langle C^2 C_\alpha C_\gamma\rangle = 5\rho T^2(1+\mathfrak{a}_2)\delta_{\gamma\alpha} + 7TP^k_{\langle\gamma\alpha\rangle},\\ Q_{\gamma\alpha\beta} = \rho M_{\gamma\alpha\beta} = \rho\langle C_\gamma C_\alpha C_\beta\rangle,\\ P_{\alpha\beta} = P^k_{\alpha\beta} = \rho M_{\alpha\beta} = \rho T + P^k_{\langle\alpha\beta\rangle},\\ \aleph_{\alpha\beta\beta} = -\frac{4(1+e)\nu g_0\sqrt{T}}{5\sqrt{\pi}\sigma}\left[\left\{(49-33e)+\frac{\mathfrak{a}_2}{32}(19-3e)\right\}q^k_\alpha + \frac{3(7+e)}{10\rho T}P^k_{\langle\alpha l\rangle}q^k_l\right]. \end{aligned}\right\} \tag{2.101}$$

Now we assume the third-order tensor $Q_{\gamma\alpha\beta}$ is trace-free, therefore, using (2.100), we can write

$$Q_{\gamma\alpha\beta} = \frac{1}{5}\left(Q_\gamma\delta_{\alpha\beta} + Q_\alpha\delta_{\beta\gamma} + Q_\beta\delta_{\alpha\gamma}\right) \equiv \frac{2}{5}\left(q_\gamma\delta_{\alpha\beta} + q_\alpha\delta_{\beta\gamma} + q_\beta\delta_{\alpha\gamma}\right). \tag{2.102}$$

Therefore the under-braced term in (2.99) simplifies to

$$Q_{\gamma\alpha\beta}u_{\beta,\gamma} + q_\beta u_{\alpha,\beta} = \frac{9}{5}D_{\alpha\gamma}q_\gamma + W_{\alpha n}q_\gamma + \frac{2}{5}q_\alpha\frac{\partial u_\beta}{\partial x_\beta}, \tag{2.103}$$

where the following definitions of

$$D_{\alpha\gamma} = \frac{1}{2}\left(\frac{\partial u_\alpha}{\partial x_\gamma} + \frac{\partial u_\gamma}{\partial x_\alpha}\right) \tag{2.104}$$

$$W_{\alpha\gamma} = \frac{1}{2}\left(\frac{\partial u_\alpha}{\partial x_\gamma} - \frac{\partial u_\gamma}{\partial x_\alpha}\right), \tag{2.105}$$

strain and vorticity tensors, respectively, have been used. Inserting (2.101) and (2.103) into the balance equation for heat flux (2.100), we get

$$2\frac{Dq_\alpha}{Dt} + \frac{14}{5}q_\alpha\frac{\partial u_\gamma}{\partial r_\gamma} + \frac{\partial(\rho M_{\gamma\alpha\beta\beta})}{\partial r_\gamma} - (2M_{\alpha\beta} + 3T\delta_{\alpha\beta})\frac{\partial P_{\beta\gamma}}{\partial r_\gamma} = \aleph_{\alpha\gamma\gamma} - \frac{18}{5}q^k_\gamma D_{\alpha\gamma} - 2q^k_\gamma W_{\alpha\gamma}$$

$$\begin{aligned} 2\frac{Dq_\alpha}{Dt} + \frac{14}{5}q_\alpha\frac{\partial u_n}{\partial x_n} + 5\left\{\rho T(1+2\mathfrak{a}_2)\delta_{\alpha\beta} + P^k_{\langle\alpha\beta\rangle}\right\}\frac{\partial T}{\partial r_\beta} + \left(5\mathfrak{a}_2T^2\delta_{\alpha\beta} - \frac{2T}{\rho}P^k_{\langle\alpha\beta\rangle}\right)\frac{\partial\rho}{\partial r_\beta}\\ + 5\rho T^2\frac{\partial\mathfrak{a}_2}{\partial r_\alpha} + 2\left(T\delta_{\alpha\beta} - \frac{P^k_{\langle\alpha\beta\rangle}}{\rho}\right)\frac{\partial P^k_{\langle\beta\gamma\rangle}}{\partial r_\gamma} = -\frac{4\nu(1+e)\sqrt{T}}{5\sigma\sqrt{\pi}}\mathscr{Q}_{\alpha\gamma}q_\gamma, \end{aligned} \tag{2.106}$$

where

$$\mathscr{Q}_{\alpha\gamma} = \left\{(49-33e)+\frac{\mathfrak{a}_2}{32}(19-3e)\right\}\delta_{\alpha\gamma} + \underbrace{\frac{3(7+e)}{10\rho T}P^k_{\langle\alpha\gamma\rangle} + \frac{9\sigma\sqrt{\pi}}{2\nu(1+e)\sqrt{T}}D_{\alpha\gamma} + \frac{5\sigma\sqrt{\pi}}{2\nu(1+e)\sqrt{T}}W_{\alpha\gamma}}, \tag{2.107}$$

is a second rank tensor.

Equation (2.106) remains the central equation to determine the heat flux vector ($\boldsymbol{q}$) for a dilute non-uniform granular shear flow. We will apply Maxwell iteration technique [Truesdell & Muncaster (1980)] on (2.106) to obtain $\boldsymbol{q}$.

2.10.1 Maxwell Iteration : Heat-flux for 5-Moment Theory of a Dilute Granular Gas

In Maxwell iteration scheme [Maxwell (1867, 1879); Truesdell & Muncaster (1980)] the heat-flux vector $\boldsymbol{q}$ and pressure deviator no longer remain field variables but they are constitutive quantities. This method is based on the five-field theory of density, macroscopic velocity and granular temperature and any other quantity other than these appearing on the left hand side of (2.106) must be set to be zero. Therefore following the procedure as described in Ikenberry & Truesdell (1956) and Kremer & Marques Jr (2011), and substituting $P^k_{\langle\alpha\beta\rangle} = q^k = 0$ on the left hand side of (2.106), we obtain

$$q_\gamma = -\frac{25\sqrt{\pi}\rho_p\sigma\sqrt{T}}{4(1+e)}(1+2\mathfrak{a}_2)[\mathscr{Q}^{-1}_{\gamma\alpha}]\frac{\partial T}{\partial x_\alpha} - \frac{25\sqrt{\pi}\rho_p\sigma T^{\frac{3}{2}}}{4(1+e)\rho}\mathfrak{a}_2[\mathscr{Q}^{-1}_{\gamma\alpha}]\frac{\partial \rho}{\partial x_\alpha} \tag{2.108}$$

$$= -\mathscr{K}^T_{\gamma\alpha}\frac{\partial T}{\partial x_\alpha} - \mathscr{K}^\rho_{\gamma\alpha}\frac{\partial \rho}{\partial x_\alpha}, \tag{2.109}$$

where the thermal conductivity and Dufour tensors are given by

$$\mathscr{K}^T_{\gamma\alpha} = \frac{25\sqrt{\pi}\rho_p\sigma\sqrt{T}}{4(1+e)}(1+2\mathfrak{a}_2)[\mathscr{Q}^{-1}_{\gamma\alpha}], \tag{2.110}$$

$$\mathscr{K}^\rho_{\gamma\alpha} = \frac{25\sqrt{\pi}\rho_p\sigma T^{\frac{3}{2}}}{4(1+e)\rho}\mathfrak{a}_2[\mathscr{Q}^{-1}_{\gamma\alpha}], \tag{2.111}$$

and the expression for $\mathscr{Q}$ is given by (2.107).

The Fourier's law for heat flux obtained in (2.108) is a modification over the conventional Fourier's law [as obtained in the articles of Kremer & Marques Jr (2011) and Garzó (2012)] in the sense that thermal conductivity (also Dufour tensor) is not just a scalar but an asymmetric

anisotropic second-rank tensor. The asymmetry is due to the under-braced term in the governing equation for heat flux (2.99) manifested as the shear rate dependence in $\mathscr{Q}_{\alpha\gamma}$ and hence in the thermal conductivity tensor $\mathscr{K}^T$. The anisotropy of conductivity tensors [2.110 and 2.111] follows from the inclusion of the higher order term in calculating $\aleph_{\alpha\beta\beta}$, the term underlined in the expression for $\mathscr{Q}_{\alpha\gamma}$ in (2.107). The law established in (2.108) must be treated as generalized Fourier law for granular heat flux.

2.10.2 Linear 5-Moment Theory : The Navier-Stokes Limit

The Navier-Stokes limit corresponds to a theory that is linear order in shear rate ($\sim \dot{\gamma}$) and is a special case of the proposition proposed in §2.10.1. This also gives a complete 5-field theory of (i) the mass density (ρ), (ii) the macroscopic velocity $(\boldsymbol{u})$ and (iii) the granular temperature (T); but unlike previous section, only linear order terms must be retained and nonlinear terms like $P^k_{\langle\alpha l\rangle}q^k_l$ should be ignored. . Therefore at linear order, (2.107) reduces to

$$\mathscr{Q}_{\gamma\alpha} = \Big\{(49-33e)+\frac{a_2}{32}(19-3e)\Big\}\delta_{\alpha\gamma}. \tag{2.112}$$

Substituting (2.112) into (2.108), we obtain the conventional Fourier's law for heat flux

$$q_\gamma = -\mathscr{K}^T_{\gamma\alpha}\frac{\partial T}{\partial x_\alpha} - \mathscr{K}^\rho_{\gamma\alpha}\frac{\partial \rho}{\partial x_\alpha}, \tag{2.113}$$

with

$$\mathscr{K}^T_{\gamma\alpha} = \frac{25\sqrt{\pi}\rho_p\sigma\sqrt{T}}{4(1+e)\Big\{(49-33e)+\frac{a_2}{32}(19-3e)\Big\}}(1+2\mathfrak{a}_2), \tag{2.114}$$

$$\mathscr{K}^\rho_{\gamma\alpha} = \frac{25\sqrt{\pi}\rho_p\sigma T^{\frac{3}{2}}}{4(1+e)\rho\Big\{(49-33e)+\frac{a_2}{32}(19-3e)\Big\}}\mathfrak{a}_2, \tag{2.115}$$

are the expressions for "scalar" thermal conductivity and Dufour tensors at Navier-Stokes order (Jenkins & Richman 1985*a*; Garzó 2012).

2.10.3 Nonlinear 10-Moment Theory for a Granular Gas

In the 10-moment theory the hydrodynamic field variables are the the mass density (ρ), macroscopic flow velocity $(\boldsymbol{u})$, granular temperature (T) and the kinetic stress deviator $(P^k_{\langle\alpha\beta\rangle})$. Therefore, in addition to the 5-field theory, $P^k_{\langle\alpha\beta\rangle}$ is treated as a separate hydrodynamic field and will remain non-zero in the iteration scheme for obtaining heat flux. The only constitutive

quantity is the heat-flux vector and upon substituting $q^k = 0$ on the left hand side of (2.106) we obtain

$$\begin{aligned} q_\gamma = &-\frac{25\sqrt{\pi}\rho_p\sigma}{4(1+e)\rho\sqrt{T}}[\mathscr{Q}^{-1}_{\gamma\alpha}]\Big\{(1+2\mathfrak{a}_2)\rho T\delta_{\alpha\beta}+P^k_{\langle\alpha\beta\rangle}\Big\}\frac{\partial T}{\partial x_\beta} \\ &-\frac{5\sqrt{\pi}\rho_p\sigma}{4(1+e)\rho\sqrt{T}}[\mathscr{Q}^{-1}_{\gamma\alpha}]\Big\{5\mathfrak{a}_2T^2\delta_{\alpha\beta}-\frac{2T}{\rho}P^k_{\langle\alpha\beta\rangle}\Big\}\frac{\partial \rho}{\partial x_\beta} \\ &-\frac{5\sqrt{\pi}\rho_p\sigma}{2(1+e)\rho\sqrt{T}}[\mathscr{Q}^{-1}_{\gamma\alpha}]\Big\{T\delta_{\alpha\beta}-\frac{P^k_{\langle\alpha\beta\rangle}}{\rho}\Big\}\frac{\partial P^k_{\langle\beta n\rangle}}{\partial x_n} \qquad (2.116) \\ \equiv &-\mathscr{K}^T_{\gamma\alpha}\frac{\partial T}{\partial x_\alpha}-\mathscr{K}^\rho_{\gamma\alpha}\frac{\partial \rho}{\partial x_\alpha}-\mathscr{K}^\Pi_{\gamma\beta}\frac{\partial P^k_{\langle\beta n\rangle}}{\partial x_n} \qquad (2.117) \end{aligned}$$

where the thermal conductivity, Dufour and stress conductivity tensors are given by

$$\mathscr{K}^T_{\gamma\alpha} = \frac{25\sqrt{\pi}\rho_p\sigma}{4(1+e)\rho\sqrt{T}}[\mathscr{Q}^{-1}_{\gamma\alpha}]\Big\{(1+2\mathfrak{a}_2)\rho T\delta_{\alpha\beta}+P^k_{\langle\alpha\beta\rangle}\Big\}, \qquad (2.118)$$

$$\mathscr{K}^\rho_{\gamma\alpha} = \frac{5\sqrt{\pi}\rho_p\sigma}{4(1+e)\rho\sqrt{T}}[\mathscr{Q}^{-1}_{\gamma\alpha}]\Big\{5\mathfrak{a}_2T^2\delta_{\alpha\beta}-\frac{2T}{\rho}P^k_{\langle\alpha\beta\rangle}\Big\}, \qquad (2.119)$$

$$\mathscr{K}^\Pi_{\gamma\beta} = \frac{5\sqrt{\pi}\rho_p\sigma}{2(1+e)\rho\sqrt{T}}[\mathscr{Q}^{-1}_{\gamma\alpha}]\Big\{T\delta_{\alpha\beta}-\frac{P^k_{\langle\alpha\beta\rangle}}{\rho}\Big\}, \qquad (2.120)$$

and the expression for $\mathscr{Q}$ is given by (2.107).

The generalized Fourier's law obtained in (2.117) using the 10-moment theory is also different from the conventional law for heat flux. Because of the presence of non-zero off-diagonal terms in the conductivity tensor, there exists heat flow in the direction perpendicular to the temperature gradient. The gradient of kinetic stress also drives a heat current governed by the stress conductivity tensor $\mathscr{K}^\Pi_{\gamma\beta}$ (2.120). These are signatures of the non-Fourier rheology. The occurrence of the heat current parallel to the flow and the stress-gradient-driven heat flux is a well known phenomena in rarefied gas study (Grad 1949; Kogan 1969; Chapman & Cowling 1970). The establishment of a generalized Fourier law (2.117) for a non-uniform dilute granular shear flow is a new finding of our work.

In order to obtain a complete information about the total heat flux vector ($\boldsymbol{q} = \boldsymbol{q}^k + \boldsymbol{q}^c$), the kinetic component $\boldsymbol{q}^k$ must be calculated from the general contracted third order balance (2.64), valid for the whole range of density but not from the dilute version (2.99). The original equation (2.25) governing the kinetic part of the granular heat flux contains the fourth-order collisional flux term $\Theta_{\gamma\alpha\beta\beta}$ that must be calculated to complete this equation. The total heat

flux vector $\boldsymbol{q}$ can then be determined upon summing the kinetic $\boldsymbol{q}^k$ and collisional components $\boldsymbol{q}^c$ (2.95) of the heat flux vector (2.64).

The determination of the fourth order flux $\Theta_{\gamma\alpha\beta\beta}$ and consequently the generalized Fourier's law for a "dense" granular gas using full 14 moments and the issues related to the closure of this 14 moment DG14 theory are left for a future work.

2.11 Application of Nonlinear DG14 Moment Theory to Uniform Shear Flow

We apply the above developed theory to analyse the uniform shear flow (USF) problem of a dense granular gas. In USF, the number density $n(=\rho/m)$, the velocity gradient $\boldsymbol{\nabla} u$, the granular temperature T remain constant and heat flux along with the third-order moment vanish. The velocity profile in simple shear flow is given by

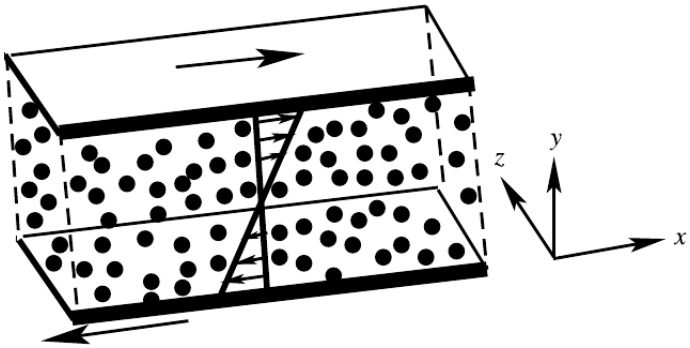

Fig. 2.2 Schematic of the uniform shear flow, with x denoting the flow direction. The y axis is along the gradient and z axis is along the vorticity direction.

$$\boxed{u = 2\dot{\gamma} y, \qquad v = 0, \qquad w = 0}, \tag{2.121}$$

where $2\dot{\gamma} y$ is the constant/uniform shear rate. In this case the mass and momentum balance equations are identically satisfied and the balance of second moment (2.75) reduces into

$$P_{\delta\beta} u_{\alpha,\delta} + P_{\delta\alpha} u_{\beta,\delta} = \aleph_{\alpha\beta}, \tag{2.122}$$

with

$$[\boldsymbol{P}]_{\alpha\beta} = P^k_{\alpha\beta} + P^c_{\alpha\beta} = \rho T + P^k_{\langle\alpha\beta\rangle} + \Theta_{\alpha\beta}, \tag{2.123}$$

is total stress tensor and the expressions for the collisional source and flux at second order are to be calculated from (2.83) and (2.84) respectively. Note that, for the present case of uniform shear flow $[\nabla(n,\dot{\gamma},T)=0]$, the balance of contracted third moment (2.99) also satisfies trivially and we are remaining with

$$4Q_{\gamma\beta\alpha\alpha}u_{\beta,\gamma}=\aleph_{\alpha\alpha\beta\beta}, \tag{2.124}$$

to determine the excess Kurtosis $\mathfrak{a}_2$ in the present context. The contribution of $\mathfrak{a}_2$ in determining the non-Newtonian transport coefficients for USF is assumed to be negligible and therefore for the present circumstance we neglect (2.124) leading to eq.(2.122) as the central equation to solve for.

The system of equations given in (2.122) is solved in the context of the velocity profile given in (2.121). It represents a system of equations with the set of unknowns being $\left\{T,P^k_{\langle xx\rangle},P^k_{\langle yy\rangle},P^k_{\langle zz\rangle},P^k_{\langle xy\rangle};\boxed{P^k_{\langle xx\rangle}+P^k_{\langle yy\rangle}+P^k_{\langle zz\rangle}=0}\right\}$ when the volume fraction ν, the radial distribution function g_0 and the coefficient of restitution e are specified. The radial distribution function g_0 is a function of the volume fraction ν and the exact functional dependence follows from (Carnahan & Starling 1969):

$$g_0=\frac{(2-\nu)}{2(1-\nu)^3};\qquad \nu=\frac{1}{6}n\pi\sigma^3. \tag{2.125}$$

All the transport coefficients viz. the total pressure $(p=P_{\alpha\alpha}/3)$, shear viscosity $(\mu\simeq -P_{xy}/\frac{du}{dy})$, granular temperature and normal stress differences are computed and compared with the molecular dynamics simulation results (Alam & Luding 2003*b*, 2005*b*). The most important result is the finding of the nonzero normal stress differences which are signatures of the non-Newtonian rheology.

The total pressure, shear viscosity, granular temperature and the scaled first and second normal stress differences are defined in the following way

$$p=\frac{\nu}{\rho(2\dot{\gamma}\sigma^2)}\left(\frac{P_{xx}+P_{yy}+P_{zz}}{3}\right), \tag{2.126}$$

$$\mu=-\frac{\nu}{\rho(2\dot{\gamma}\sigma^2)}P_{xy}, \tag{2.127}$$

$$\mathscr{N}_1=\frac{3(P_{xx}-P_{yy})}{(P_{xx}+P_{yy}+P_{zz})}, \tag{2.128}$$

and

$$\mathscr{N}_2=\frac{3(P_{yy}-P_{zz})}{(P_{xx}+P_{yy}+P_{zz})}, \tag{2.129}$$

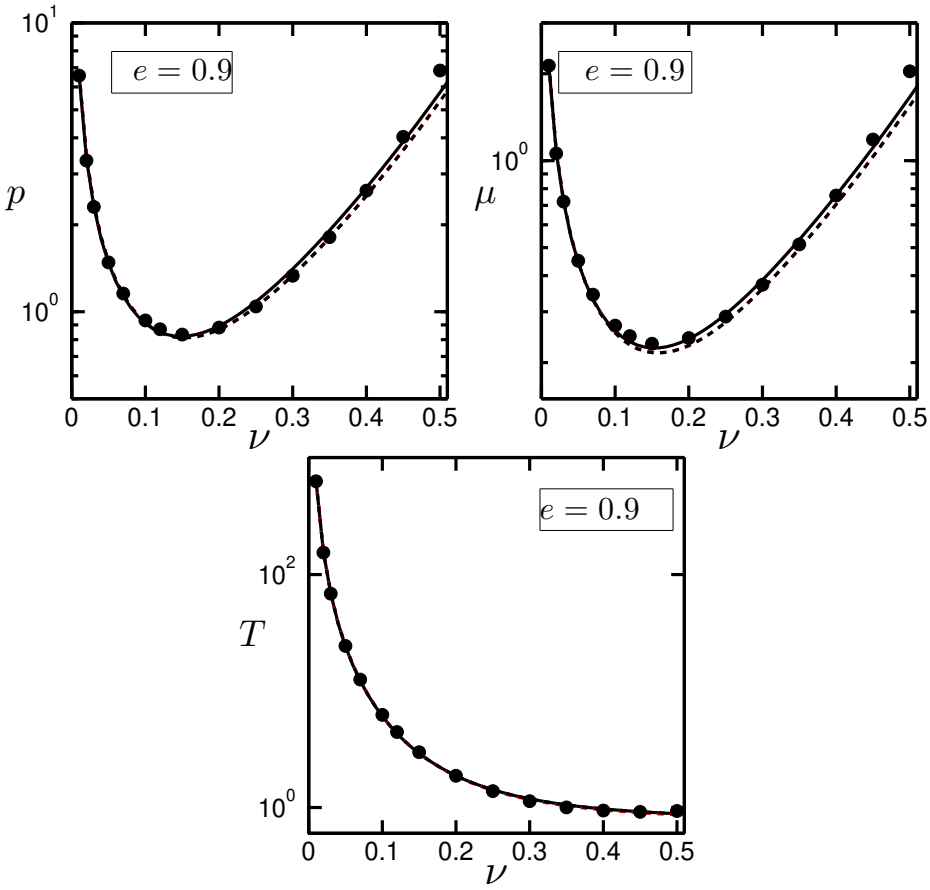

Fig. 2.3 Variations of the (a) total pressure (p), (b) shear viscosity (μ) and (c) granular temperature (T) against volume fraction (ν) for coefficient of restitution $e = 0.9$. The black solid lines, black and red dashed lines present the current DG14 moment theory, the dense gas theories by Jenkins & Richman (1985*a*) and Garzó (2013) respectively. The symbols are molecular dynamics simulation results (Alam & Luding 2005*b*).

respectively, are calculated for the whole range of density (ν) for some specific choices of restitution coefficients (e).

The density variations of (a) pressure (p), (b) shear viscosity (μ) and (c) granular temperature (T) at a restitution coefficient $e = 0.9$ are shown in figure 2.3(a)-(c). It is seen that the DG14 moment theory (continuous black lines) predictions for p and μ agrees well with the simulations as compared to the theory by (Garzó 2013) (red dashed lines) and this agreement holds uniformly for the whole range of density. In panel (b) the density variations of the viscosity is displayed and it is observed that although both of these theories are almost indistinguishable up-to volume fraction $\nu = 0.1$ but beyond this point the theory of Garzó (2013) starts deviating from simulation data and the deviation continues thereafter. Both theories are

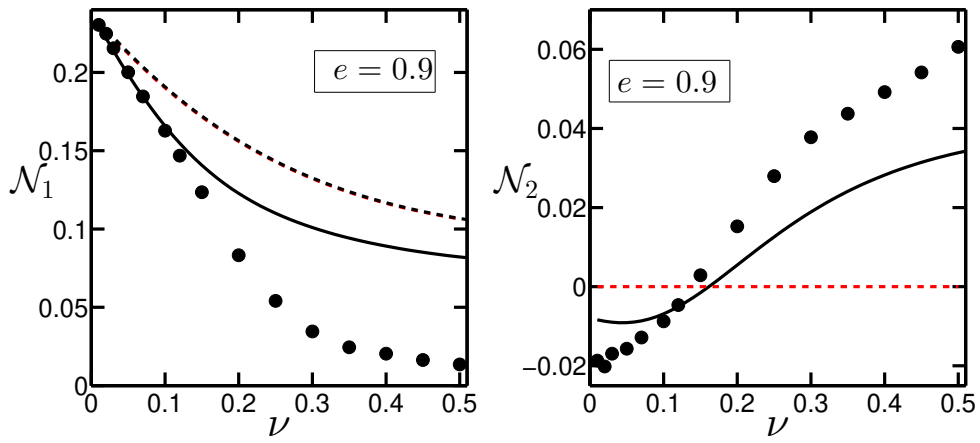

Fig. 2.4 Variations of the (a) first ($\mathcal{N}_1$) and (b) second ($\mathcal{N}_2$) normal stress differences (2.128-2.129) against volume fraction (ν) for restitution coefficient $e = 0.9$. The black solid lines are the results from the current DG14 moment theory whereas the black dashed and red dashed lines represent the work of Jenkins & Richman (1985*a*) and Garzó (2013) respectively. The symbols are simulation results.

able to well predict the behaviour of granular temperature and they agree with the simulation data [see figure 2.3.*c*]. Overall, the present 14-moment nonlinear theory well predicts p and μ over the other Grad-level theories (Jenkins & Richman 1985*a*; Garzó 2013) for the whole range of density.

The normal stress differences and other transport coefficients obtained in this way are compared with another Grad-level theory of (Garzó 2013) for a restitution coefficient $e = 0.9$ and are depicted in figure 2.4. In each panel the results from the molecular dynamics simulation (Alam & Luding 2003*b*, 2005*b*) are also superimposed for a relative qualitative study between these two Grad-level theories.

Figure 2.4 displays the variations of the two normal stress differences against density at $e = 0.9$ and it shows that the theory presented here is unable to predict the correct qualitative behaviours of the normal stress differences. It is observed that, for the first normal stress difference ($\mathcal{N}_1$), the DG14 moment theory (black solid line) shows an excellent agreement with the simulation up-to $\nu = 0.1$ but then starts deviating and the deviation continues with increasing density. For the second normal stress difference ($\mathcal{N}_2$), although our theory is able to capture the sign change of $\mathcal{N}_2$ at some finite density but underestimates its magnitude throughout the span the volume fraction. Nevertheless, our theory is superior as compared to other Grad level theories (Garzó 2013) in the sense that it is successful in capturing the qualitative behaviour of the second normal stress difference ($\mathcal{N}_2$) along with its correct signs

in the two extreme limits of the volume fraction ($\nu \to 0$ and $\nu \to \nu_{\max}$), which the standard Grad-level theories cannot predict.

The works of Jenkins & Richman (1985*a*) (black dashed line in figure 2.4) and Garzó (2013) (red dashed line in figure 2.4), which also are based on an expansion around the Maxwellian state, when applied to the USF, the second normal stress difference is found to be identically zero $\mathscr{N}_2 \equiv 0$. On the other hand, the kinetic theory work (based on a BGK-type model) by Montanero *et al.* (1999) predicts $\mathscr{N}_2$ to be positive for all ν. Therefore, the present DG14 moment theory is preferable over the other Grad-like theories because of its qualitative match with the simulation-data for normal stress differences over all densities.

2.12 Summary

On using the present nonlinear DG14-moment (Dense Grad 14-moment) theory, we have established a generalized Fourier's law for the granular heat flux in a dilute non-uniform shear flow. It is observed that the gradient of kinetic stress also drives a heat current parallel to the flow which clearly shows the non-Fourier phenomena. The anisotropy in the thermal conductivity and Dufour tensors along with its asymmetry are also discussed briefly. A thorough analysis regarding the asymmetry and anisotropy of these thermal, Dufour and stress conductivity tensors and the establishment of a generalized Fourier's law for a dense granular flow will be considered in a future work. To complete the present DG14-moment theory, three additional terms need to be determined as noted in Table 2.2. The DG14 theory discussed above

Collisional Source and Flux Terms	
Calculated	Yet to determine
$\aleph_{\alpha\beta}$	
$\Theta_{\alpha\beta}$	$\aleph_{\alpha\alpha\beta\beta}$
$\Theta_{\gamma\alpha\beta}$	$\Theta_{\gamma\alpha\beta\beta}$
$\Theta_{\gamma\alpha\alpha}$	$\Theta_{\gamma\alpha\alpha\beta\beta}$
$\aleph_{\alpha\beta\beta}$	

Table 2.2 Production terms worksheet

has been tested in the context of an uniform shear flow at any arbitrary density. It is clear from the discussions in §2.11 and from figures 2.3-2.4 that the DG14-moment theory gives excellent predictions for pressure (p), viscosity (μ), granular temperature (T) and a qualitatively correct prediction for two normal-stress differences over the whole range of density. It is successful in predicting the qualitative variation of the second normal stress difference, the

correct signs in the dilute and dense limits and its sign reversal at some finite density. The success of our theory originates from the inclusion of the higher order nonlinear terms ($\sim P^2_{\langle ij\rangle}, q_i^2$ etc.) in calculating the collision integrals.

Finally, it remains to find a theory that can improve the present analysis and match with the simulation data for normal stress differences throughout the whole range of volume fraction $\nu\varepsilon(0, 0.5)$. An effort to predict the correct behaviours of the normal stress differences and other transport coefficients in uniform shear flow of a dense granular fluid will be discussed in the next chapter.

Chapter 3

Non-Newtonian and Non-Fourier Rheology of Sheared Granular Fluid: Expansion around Anisotropic Maxwellian[2]

3.1 Introduction

In chapter 2 it was found that the nonlinear DG14 (Dense Grad 14 moment theory) moment theory has a drawback in the sense that it is not possible to predict the "quantitative" behaviours of two normal-stress differences (black solid lines) for the whole range of density, see figure 3.1. In this chapter we have followed a complementary approach to sort out the issues raised in Chapter 2.

Here we assume that the single particle distribution function is an anisotropic Maxwellian, which also gives a complete 10-moment system for the uniform shear flow. An exact solution of the second-moment of velocity fluctuations at Burnett order (i.e second order in shear rate) is derived which determines all the transport coefficients as functions of the coefficient of restitution e and the volume fraction ν. A perturbative solution at the fourth order (super-super-Burnett) is also determined which improves the second order analytical solution. Particle simulation data (Alam & Luding 2005*b*) for the uniform shear flow of inelastic hard-spheres

[2]This chapter is an extended version of the work published in Journal of Fluid Mechanics [Saha & Alam (2016), J. Fluid Mech. 795, 549-580]. Additionally, a Burnett order analytical solution for the related 2-dimensional problem is described in Appendix M of this chapter. The complete 2-dimensional analogue has been published in the same journal [Saha & Alam (2014), J. Fluid Mech. 757, 251-296], which is attached as a supplementary material at the end of this thesis.

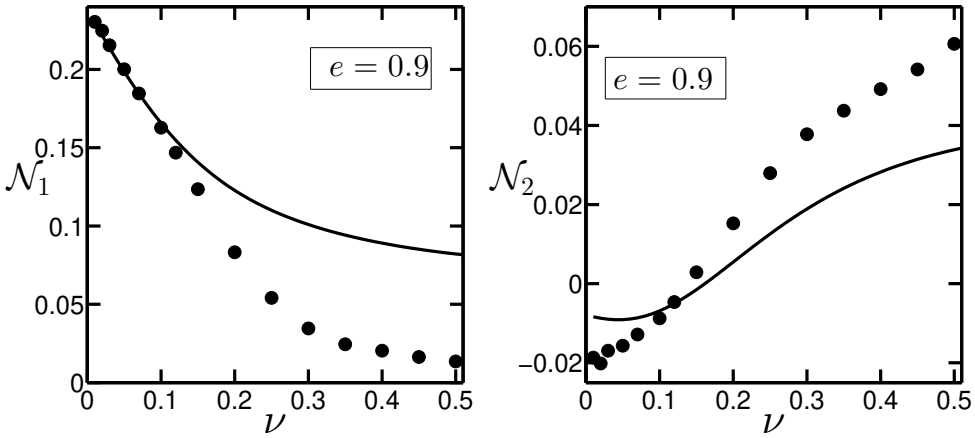

Fig. 3.1 Variations of the first ($\mathcal{N}_1$) and second ($\mathcal{N}_2$) normal stress differences with particle volume-fraction (ν) in the uniform shear flow of smooth inelastic spheres; the symbols represent the particle-dynamics simulation data of (Alam & Luding 2005*b*) for a restitution coefficient of $e = 0.9$. The solid lines denote the "Dense Grad 14" (DG14) moment theory as discussed in Chapter 2.

is compared with the theoretical model, with excellent agreement for pressure, shear viscosity and two normal stress differences over a range of densities spanning from the dilute to close to the freezing point. The origins of two normal stress differences in both dilute and dense limits are discussed. Lastly, a generalized Fourier law for the granular heat flux is derived for a dilute granular gas by analysing the non-uniform shear flow via an expansion around the anisotropic Maxwellian state; this determination of granular heat flux makes the theory closed at least in the dilute limit. It is observed that the gradient of kinetic stress drives a heat current in addition to parallel heat flow, which certainly is a signature of non-Fourier rheology. The thermal conductivity is characterized by an asymmetric anisotropic second-rank tensor, for which explicit analytical expressions are given. It is observed that the asymmetry or/and anisotropy appears at Burnett order and beyond, and therefore we can say that the non-Fourier rheology is a Burnett order effect.

This chapter is organized as follows. The extended-hydrodynamic theory is outlined in §3.2. The second moment tensor of velocity fluctuations is constructed and analysed for the uniform shear flow in §3.4.1 and the origin of stress anisotropy is discussed in §3.4.2. Working in a rotated coordinate frame and using a series expansion for certain integrals, the balance equation for the second moment is reduced to a set of algebraic equations as described in §3.5. Two sets of analytical solutions of these algebraic equations at different orders in the perturbation parameter are derived in §3.6. The closed-form expressions for (i) all components of the stress tensor, (ii) the shear viscosity, (iii) the pressure, (iv) two normal stress differences,

and (v) the source of the second-moment tensor as well as the collisional dissipation rate are provided in §3.7 for the whole range of density. The analytical forms of the above transport coefficients are validated in §3.10.1; an analytical solution of the second-moment equation valid near the dense-limit is derived and validated in §3.11. In §3.12 we consider the non-uniform shear state and outline a procedure to derive the constitutive relation for the 'non-Fourier' heat flux. The summary and conclusion are given in §3.13.

3.2 Extended Hydrodynamic Equations: the 10-Moment System with Heat Flux

We consider a dense granular gas consisting of N randomly moving smooth inelastic hard-spheres of diameter σ and mass m. The particles loose energy upon collisions which is characterized by a single parameter e, called the coefficient of normal restitution, with $e=1$ and 0 referring to perfectly elastic and sticking collisions, respectively. The first member of BBGKY (Bogoliubov-Born-Green-Kirkwood-Yvon, Chapman & Cowling (1970)) hierarchy, that deals with the evolution of the single-particle distribution function $f(\boldsymbol{c},\boldsymbol{x},t)$ for a dense granular gas, reads as (Chapman & Cowling 1970; Jenkins & Richman 1985*a*)

$$\left(\frac{\partial}{\partial t}+\boldsymbol{c}\cdot\boldsymbol{\nabla}\right)f=\sigma^2\int \mathrm{d}\boldsymbol{c}_2\int_{\boldsymbol{g}\cdot\boldsymbol{k}>0}\mathrm{d}\boldsymbol{k}(\boldsymbol{g}\cdot\boldsymbol{k})\left[e^{-2}f^{(2)}(\boldsymbol{c}_1,\boldsymbol{x},\boldsymbol{c}_2,\boldsymbol{x}-\sigma\boldsymbol{k};t)\right.$$
$$\left.-f^{(2)}(\boldsymbol{c}_1',\boldsymbol{x},\boldsymbol{c}_2',\boldsymbol{x}+\sigma\boldsymbol{k};t)\right], \tag{3.1}$$

where $\boldsymbol{g}=\boldsymbol{c}_1-\boldsymbol{c}_2$ is the pre-collisional relative velocity between two colliding spheres, with $\boldsymbol{c}_1$ and $\boldsymbol{c}_2$ denoting their pre-collisional instantaneous velocities and their post-collisional velocities being denoted by primes, and $\boldsymbol{g}\cdot\boldsymbol{k}>0$ accounts for the constraint of impending collisions; $\boldsymbol{k}\equiv\boldsymbol{k}_{12}=(\boldsymbol{x}_2-\boldsymbol{x}_1)/|\boldsymbol{x}_2-\boldsymbol{x}_1|$ is the unit contact vector joining the center of sphere-1 to that of sphere-2 at collision. In (5.4), $f^{(2)}$ is the two-body distribution function such that

$$f^{(2)}(\boldsymbol{c}_1,\boldsymbol{x}_1,\boldsymbol{c}_2,\boldsymbol{x}_2)d\boldsymbol{c}_1d\boldsymbol{x}_1d\boldsymbol{c}_2d\boldsymbol{x}_2$$

is the probability of finding a pair of spheres with the first sphere being centered within $d\boldsymbol{x}_1$ about $\boldsymbol{x}_1$, with its velocity in $d\boldsymbol{c}_1$ about $\boldsymbol{c}_1$ and the second one being centered within $d\boldsymbol{x}_2$ about $\boldsymbol{x}_2$, with its velocity in $d\boldsymbol{c}_2$ about $\boldsymbol{c}_2$. For a pair of colliding *smooth* spheres, the tangential component of their relative velocity remains invariant but the normal component changes ac-

cording to the following the collision rule:

$$(\boldsymbol{g}' \cdot \boldsymbol{k}) = -e(\boldsymbol{g} \cdot \boldsymbol{k}), \tag{3.2}$$

where $\boldsymbol{g} \equiv \boldsymbol{g}_{12} = \boldsymbol{c}_1 - \boldsymbol{c}_2$ and $\boldsymbol{g}' = \boldsymbol{c}_1' - \boldsymbol{c}_2'$ are the pre- and post-collisional relative velocities, respectively.

To derive hydrodynamic balance equations, let us consider any particle property $\psi(\boldsymbol{C})$ which is a function of the peculiar/fluctuation velocity $\boldsymbol{C} = (\boldsymbol{c} - \langle \boldsymbol{c} \rangle)$, with the angular bracket, $\langle \cdot \rangle$, denoting an average over the velocity space. Multiplying (5.4) by $\psi(\boldsymbol{C})$ and integrating over the velocity space and after tedious algebra, the master balance equation is obtained (Jenkins & Richman 1985*a*; Saha & Alam 2014)

$$\frac{\partial}{\partial t}\langle n\psi \rangle = -\left\langle n\left(\frac{\partial}{\partial t} + \boldsymbol{c}\cdot\boldsymbol{\nabla}\right) u_\alpha \frac{\partial \psi}{\partial C_\alpha}\right\rangle - \boldsymbol{\nabla}\cdot(\langle n\boldsymbol{c}\psi\rangle + \boldsymbol{\Theta}[\psi]) - \boldsymbol{\Theta}\left[\frac{\partial \psi}{\partial \boldsymbol{C}}\right] : \boldsymbol{\nabla}\boldsymbol{u} + \aleph[\psi], \tag{3.3}$$

where

$$n(\boldsymbol{r},t) \equiv \frac{N}{V} = \int f(\boldsymbol{c},\boldsymbol{r},t)\mathrm{d}\boldsymbol{c}, \tag{3.4}$$

is the number density of particles, $\boldsymbol{\Theta}(\psi)$ is the collisional flux of ψ,

$$\boldsymbol{\Theta}(\psi) = -\frac{\sigma^3}{2}\int\int\int_{\boldsymbol{g}\cdot\boldsymbol{k}>0} (\psi_1' - \psi_1)\boldsymbol{k}\int_0^1 f^{(2)}(\boldsymbol{c}_1, \boldsymbol{x} - \omega\sigma\boldsymbol{k}, \boldsymbol{c}_2, \boldsymbol{x} + \sigma\boldsymbol{k} - \omega\sigma\boldsymbol{k}) \\ (\boldsymbol{k}\cdot\boldsymbol{g})\mathrm{d}\omega\mathrm{d}\boldsymbol{k}\mathrm{d}\boldsymbol{c}_1\mathrm{d}\boldsymbol{c}_2, \tag{3.5}$$

and $\aleph(\psi)$ is the collisional source of ψ,

$$\aleph(\psi) = \frac{\sigma^2}{2}\int\int\int_{\boldsymbol{g}\cdot\boldsymbol{k}>0} \left(\psi_1' + \psi_2' - \psi_1 - \psi_2\right) f^{(2)}(\boldsymbol{c}_1, \boldsymbol{x} - \sigma\boldsymbol{k}, \boldsymbol{c}_2, \boldsymbol{x})(\boldsymbol{k}\cdot\boldsymbol{g})\mathrm{d}\boldsymbol{k}\mathrm{d}\boldsymbol{c}_1\mathrm{d}\boldsymbol{c}_2. \tag{3.6}$$

Note that the origin of the collisional flux term (3.5) is tied to the 'macroscopic' natures of particles (and hence to the "denseness" of the matter) and this term is zero in a dilute gas of point particles.

3.2.1 The 10-Moment System

As in our previous works [Saha & Alam (2014) and Chapter 2], we will work with an extended set of 10 hydrodynamic fields: (i) the mass density

$$\rho(\boldsymbol{r},t) \equiv mn(\boldsymbol{r},t) = m\int f(\boldsymbol{c},\boldsymbol{r},t)\mathrm{d}\boldsymbol{c}, \tag{3.7}$$

(ii) the coarse-grained velocity

$$\boldsymbol{u}(\boldsymbol{r},t) \equiv \langle \boldsymbol{c} \rangle = \frac{1}{n(\boldsymbol{r},t)} \int \boldsymbol{c} f(\boldsymbol{c},\boldsymbol{r},t) \mathrm{d}\boldsymbol{c}, \tag{3.8}$$

and (iii) the second moment tensor

$$\boldsymbol{M}(\boldsymbol{r},t) \equiv \langle \boldsymbol{CC} \rangle = \frac{1}{n(\boldsymbol{r},t)} \int \boldsymbol{CC} f(\boldsymbol{c},\boldsymbol{r},t) d\boldsymbol{c}, \tag{3.9}$$

where $\boldsymbol{C} \equiv \boldsymbol{c} - \boldsymbol{u}$ is the peculiar/fluctuation velocity of particles. The last hydrodynamic field (3.9) is required to account for normal stress differences which is the major focus of the present work.

Putting $\psi = 1$, $\boldsymbol{c}$ and $\boldsymbol{CC}$ into (3.3), the mass, momentum and second-moment balance equations, respectively, are obtained as

$$\left(\frac{\partial}{\partial t} + \boldsymbol{u} \cdot \boldsymbol{\nabla} \right) \rho = -\rho \boldsymbol{\nabla} \cdot \boldsymbol{u}, \tag{3.10}$$

$$\rho \left(\frac{\partial}{\partial t} + \boldsymbol{u} \cdot \boldsymbol{\nabla} \right) \boldsymbol{u} = -\boldsymbol{\nabla} \cdot \boldsymbol{P}, \tag{3.11}$$

$$\rho \left(\frac{\partial}{\partial t} + \boldsymbol{u} \cdot \boldsymbol{\nabla} \right) \boldsymbol{M} = -\boldsymbol{\nabla} \cdot \boldsymbol{Q} - \boldsymbol{P} \cdot \boldsymbol{\nabla} \boldsymbol{u} - (\boldsymbol{P} \cdot \boldsymbol{\nabla} \boldsymbol{u})^T + \boldsymbol{\aleph} \tag{3.12}$$

where $\boldsymbol{P}$ is the total stress, a second-rank tensor, given by

$$\boldsymbol{P} \equiv \rho \langle \boldsymbol{CC} \rangle + \boldsymbol{\Theta}(m\boldsymbol{C}), \tag{3.13}$$

$\boldsymbol{Q}$ is the flux of the second moment, a third-rank tensor, given by

$$\boldsymbol{Q} \equiv \rho \langle \boldsymbol{CCC} \rangle + \boldsymbol{\Theta}(m\boldsymbol{CC}), \tag{3.14}$$

and $\boldsymbol{\aleph}$ is the collisional source of second moment, a second-rank tensor, given by

$$\boldsymbol{\aleph} \equiv \boldsymbol{\aleph}(m\boldsymbol{CC}). \tag{3.15}$$

In (3.13-3.14), the first and second terms refer to the corresponding kinetic and collisional contributions, respectively.

Defining the granular temperature as

$$T \equiv \frac{1}{3} M_{\alpha\alpha} \tag{3.16}$$

and taking the trace of (3.12), we obtain the balance equation for the granular energy

$$\frac{3}{2}\rho\left(\frac{\partial}{\partial t}+\boldsymbol{u}\cdot\boldsymbol{\nabla}\right)T=-\frac{\partial q_\alpha}{\partial x_\alpha}-P_{\alpha\beta}\frac{\partial u_\beta}{\partial x_\alpha}-\mathscr{D}, \tag{3.17}$$

and that of the deviator of the second-moment

$$\left.\begin{aligned}\tfrac{1}{2}\rho\left(\tfrac{\partial}{\partial t}+\boldsymbol{u}\cdot\boldsymbol{\nabla}\right)\widehat{M}_{\alpha\beta}=&-\tfrac{1}{2}\tfrac{\partial}{\partial x_\gamma}\left(Q_{\gamma\alpha\beta}-\tfrac{2}{3}q_\gamma\delta_{\alpha\beta}\right)\\&-\left\{\tfrac{1}{2}\left(P_{\gamma\alpha}\tfrac{\partial u_\beta}{\partial x_\gamma}+P_{\gamma\beta}\tfrac{\partial u_\alpha}{\partial x_\gamma}\right)-\tfrac{1}{3}P_{\gamma\xi}\tfrac{\partial u_\xi}{\partial x_\gamma}\delta_{\alpha\beta}\right\}+\tfrac{1}{2}\widehat{\aleph}_{\alpha\beta}\end{aligned}\right\}. \tag{3.18}$$

In above equations,

$$q_\alpha\equiv\frac{1}{2}Q_{\alpha\beta\beta}=\frac{1}{2}\rho M_{\alpha\beta\beta}+\frac{1}{2}\Theta_{\alpha\beta\beta} \tag{3.19}$$

is the total energy flux vector (i.e. the heat flux vector), whose first term is the kinetic contribution and the second term is the collisional contribution, and

$$\mathscr{D}\equiv-\frac{1}{2}\aleph_{\beta\beta}=-\frac{1}{2}\aleph\left(mC^2\right) \tag{3.20}$$

is the rate of dissipation of kinetic energy per unit volume.

The balance equations (3.10-3.11) and (3.17), along with constitutive relations for (3.13), (3.19) and (3.20), constitute the Navier-Stokes-order hydrodynamics for a fluidized granular matter; clearly, the equation for the deviatoric part of the second moment tensor (3.18) satisfies identically at NS-order.

For an extended hydrodynamic description of granular matter, incorporating normal stress differences, we need the balance equation (3.12) for full second moment tensor, along with mass and momentum balances (3.10-3.11). For a closure of (3.12), the deviatoric part of the third-order $Q_{\gamma\alpha\beta}$,

$$\widehat{Q}_{\gamma\alpha\beta}=Q_{\gamma\alpha\beta}-\frac{1}{5}\left(Q_{\gamma\xi\xi}\delta_{\alpha\beta}+Q_{\alpha\xi\xi}\delta_{\gamma\beta}+Q_{\beta\xi\xi}\delta_{\alpha\gamma}\right), \tag{3.21}$$

is assumed to be zero, leaving only its isotropic part, the heat flux vector (3.19), to be evaluated as a constitutive relation. In addition to (3.19), we need to determine constitutive relations for the stress tensor (3.13) and the source of second-moment (3.15) in terms of the gradients of the hydrodynamic fields (ρ, $\boldsymbol{u}$, $\boldsymbol{M}$). While the expressions for the latter two constitutive quantities are derived for the uniform shear state as discussed in §3.7.1, §3.7.2 and §3.9, the heat flux (3.19) requires a consideration of the *non-uniform* shear flow since the temperature gradient vanishes in the uniform shear flow (USF) which is dealt in §3.12.

3.2.2 Why 10-moment System?

In Chapter 2, we dealt with a 14-moment system and showed how a 10-moment system with heat-flux can be obtained via Maxwell-iteration technique. For the sake of simplicity, we will restrict to the 10-moment theory of a dense granular fluid in the present and subsequent chapters. The 10-moment theory is sufficient to analyse normal stress differences [Saha & Alam (2014, 2016)] which constitute the major goal of this thesis.

3.3 Single-Particle Velocity Distribution Function

3.3.1 Maximum Entropy Principle and the Anisotropic Maxwellian Distribution

In order to obtain the explicit expressions of the single-particle distribution function using the maximum entropy principle [Jaynes (1957); Holway Jr (1966)], we write down the definitions of the 10 hydrodynamic fields that form the set $\{\rho, \boldsymbol{u}, \boldsymbol{M}\}$

$$\left.\begin{aligned} \rho(\boldsymbol{r},t) &\equiv mn(\boldsymbol{r},t) = m\int f(\boldsymbol{c},\boldsymbol{r},t)\mathrm{d}\boldsymbol{c}, \\ \boldsymbol{u}(\boldsymbol{r},t) &\equiv \langle \boldsymbol{c}\rangle = \frac{1}{n(\boldsymbol{r},t)}\int \boldsymbol{c} f(\boldsymbol{c},\boldsymbol{r},t)\mathrm{d}\boldsymbol{c}, \\ \boldsymbol{M}(\boldsymbol{r},t) &\equiv \langle \boldsymbol{CC}\rangle = \frac{1}{n(\boldsymbol{r},t)}\int \boldsymbol{CC} f(\boldsymbol{c},\boldsymbol{r},t)d\boldsymbol{c} \end{aligned}\right\}. \tag{3.22}$$

The optimum distribution function f is such that it maximizes the uncertainty about the velocity, subject to a set of compatibility conditions given in (3.22). In information theory, the entropy is defined following Shannon (1948)

$$S = -\int f(\boldsymbol{c},\boldsymbol{r},t)\ln f(\boldsymbol{c},\boldsymbol{r},t)\mathrm{d}\boldsymbol{c}, \tag{3.23}$$

which is the same as the Boltzmann's entropy (negative of H-function) without the multiplicative factor of $k_B T$ (Chapman & Cowling 1970).

The final probability distribution function is the one which maximizes the Shanon entropy (3.23) subject to the constraints (3.22). The variation of S can be written as

$$\delta S = -\int \delta f \underbrace{\left(\ln f + 1 - \alpha - \alpha_i c_i - \alpha_{ij} C_i C_j\right)}\mathrm{d}\boldsymbol{c}, \tag{3.24}$$

where α, α_i, and α_{ij} are Lagrange multipliers. For a maximum value of S, the variation δS must be equal to zero. Using the basic principle of integral calculus we can say that vanishing of δS for an arbitrary choice of δf imposes vanishing of the under-braced term in (3.24) as well which yields

$$f = \exp(\alpha - 1 + \alpha_i c_i + \alpha_{ij} C_i C_j). \tag{3.25}$$

The solution set for 10 Lagrange multipliers $\{\alpha, \alpha_i, \alpha_{ij}\}$ appeared in eq.(3.25) follows from (3.22):

$$\alpha = 1 - \frac{1}{2}\ln\left(8\pi^3|\boldsymbol{M}|\right), \tag{3.26}$$

$$\alpha_i = 0, \tag{3.27}$$

$$\alpha_{ij} = -\frac{1}{2}\boldsymbol{M}^{-1}. \tag{3.28}$$

Using this, we obtain the final form of the distribution function as (Holway Jr 1966)

$$f^{(1)}(\boldsymbol{c},\boldsymbol{x},t) = \frac{n}{(8\pi^3|\boldsymbol{M}|)^{\frac{1}{2}}}\exp\left(-\frac{1}{2}\boldsymbol{C}\cdot\boldsymbol{M}^{-1}\cdot\boldsymbol{C}\right), \tag{3.29}$$

which is called the anisotropic Maxwell distribution (AMD) function.

3.3.2 Molecular Chaos Ansatz

To relate the two-particle distribution function with the single-particle velocity distribution function, we adopt the molecular chaos assumption for which

$$f^{(2)}(\boldsymbol{c}_1,\boldsymbol{x}-\sigma\boldsymbol{k},\boldsymbol{c}_2,\boldsymbol{x}) = g_0(\nu)f^{(1)}(\boldsymbol{c}_1,\boldsymbol{x}-\sigma\boldsymbol{k})f^{(1)}(\boldsymbol{c}_2,\boldsymbol{x}), \tag{3.30}$$

where $g_0(\nu)$ is the well-known contact radial distribution function (Carnahan & Starling 1969),

$$g_0(\nu) = \frac{(2-\nu)}{2(1-\nu)^3}, \tag{3.31}$$

with

$$\nu = n\pi\sigma^3/6 \tag{3.32}$$

being the local volume fraction of particles.

Following the principle of maximum entropy we assume that the single particle velocity distribution is an anisotropic Maxwellian/Gaussian

$$f^{(1)}(\boldsymbol{c},\boldsymbol{x},t) = \frac{n}{(8\pi^3|\boldsymbol{M}|)^{\frac{1}{2}}} \exp\left(-\frac{1}{2}\boldsymbol{C}\cdot\boldsymbol{M}^{-1}\cdot\boldsymbol{C}\right), \tag{3.33}$$

with $|\boldsymbol{M}| = \det(\boldsymbol{M})$, which contains complete information about the second moment tensor $\boldsymbol{M}$. This form (3.33) was originally used by Holway Jr (1966) to improve certain problems in the BGK (Bhatnagar-Gross-Krook) model of gas dynamics, resulting in what is popularly known as the 'Ellipsoidal' BGK-model.

While (3.33) is an appropriate leading-order distribution function for a non-equilibrium steady state, such as the steady uniform shear flow (Goldreich & Tremaine 1978; Shukhman 1984; Araki & Tremaine 1986; Araki 1988; Jenkins & Richman 1988; Richman 1989; Chou & Richman 1998; Lutsko 2004; Saha & Alam 2014), the isotropic Maxwellian/Gaussian

$$f^{(1)}(\boldsymbol{c},\boldsymbol{x},t) = \frac{n}{(2\pi T)^{\frac{3}{2}}} \exp\left(-\frac{C^2}{2T}\right), \tag{3.34}$$

(i.e. eq.(3.33) with $M_{\alpha\beta} = T\delta_{\alpha\beta}$) holds for the rest state of a gas at equilibrium.

3.4 Second Moment Tensor and Its Anisotropies

We consider a collection of smooth inelastic spheres of mass m and diameter σ, subjected to uniform shear flow in the (x,y)-plane:

$$u = 2\dot{\gamma}y, \qquad v = 0 \qquad \text{and} \qquad w = 0, \tag{3.35}$$

where $2\dot{\gamma}$ is the uniform/constant shear rate. Note that x and y denote flow and gradient directions, respectively, and the z direction is perpendicular to x-y plane, see figure 3.2; in the following, the (x,y)-plane is referred to as the *shear plane*, with the z-direction being the *vorticity direction*. The velocity gradient tensor completely characterizes the uniform shear flow:

$$\boldsymbol{\nabla u} = \begin{bmatrix} 0 & 2\dot{\gamma} & 0 \\ 0 & 0 & 0 \\ 0 & 0 & 0 \end{bmatrix} \equiv \boldsymbol{D} + \boldsymbol{W}, \tag{3.36}$$

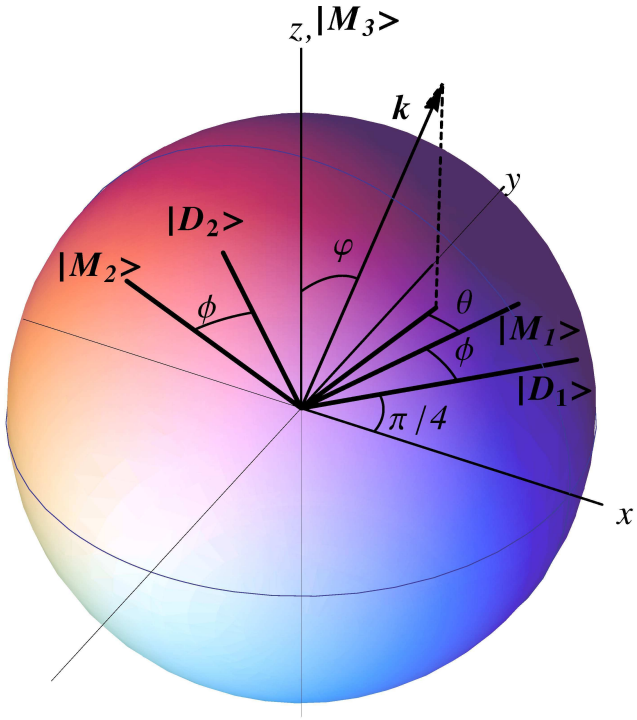

Fig. 3.2 (Colour online) Sketch of the spherical coordinate system showing the eigendirections of the shear tensor $\boldsymbol{D}$ and the second moment tensor $\boldsymbol{M}$.

with the shear ($\boldsymbol{D}$) and spin ($\boldsymbol{W}$) tensors, respectively, are given by

$$\boldsymbol{D} = \begin{bmatrix} 0 & \dot{\gamma} & 0 \\ \dot{\gamma} & 0 & 0 \\ 0 & 0 & 0 \end{bmatrix} \quad \text{and} \quad \boldsymbol{W} = \begin{bmatrix} 0 & \dot{\gamma} & 0 \\ -\dot{\gamma} & 0 & 0 \\ 0 & 0 & 0 \end{bmatrix}. \tag{3.37}$$

It is straightforward to verify that $\dot{\gamma}$, $-\dot{\gamma}$ and 0 are the eigenvalues of $\boldsymbol{D}$ and the corresponding orthonormal eigenvectors are, respectively,

$$|D_1\rangle = \begin{bmatrix} \cos\frac{\pi}{4} \\ \sin\frac{\pi}{4} \\ 0 \end{bmatrix}, \quad |D_2\rangle = \begin{bmatrix} -\sin\frac{\pi}{4} \\ \cos\frac{\pi}{4} \\ 0 \end{bmatrix} \quad \text{and} \quad |D_3\rangle = \begin{bmatrix} 0 \\ 0 \\ 1 \end{bmatrix}, \tag{3.38}$$

that are sketched in figure 3.2. While $|D_3\rangle$ is directed along the z-axis, the shear-plane eigenvectors $|D_1\rangle$ and $|D_2\rangle$ are rotated by 45° anticlockwise from the xy-axes.

3.4.1 Construction of Second Moment Tensor from its Eigen Vectors

In this section we follow the seminal works of Goldreich & Tremaine (1978), Shukhman (1984), Araki & Tremaine (1986), Araki (1988), Jenkins & Richman (1988), Richman (1989) and Chou & Richman (1998) to construct the second moment tensor in terms of its eigen-basis.

Recalling that the granular temperature $T = M_{\alpha\alpha}/3$ is the isotropic measure of the second moment tensor $\boldsymbol{M}$, we can decompose $\boldsymbol{M}$ into an isotropic tensor and a traceless deviatoric tensor:

$$\frac{\boldsymbol{M}}{T} = \boldsymbol{I} + \frac{\widehat{\boldsymbol{M}}}{T} \tag{3.39}$$

where $\widehat{\boldsymbol{M}}/T$ is the dimensionless counterpart of its deviatoric/traceless tensor whose eigenvalues ξ, ς and ζ satisfy

$$\xi + \varsigma + \zeta = 0. \tag{3.40}$$

From (3.39) it follows that the eigenvalues of $\boldsymbol{M}$ are $T(1+\xi)$, $T(1+\varsigma)$ and $T(1+\zeta)$, and let us assume that the corresponding orthonormal set of eigen-directions are $|M_1\rangle$, $|M_2\rangle$ and $|M_3\rangle$, respectively. Since $|M_1\rangle$, $|M_2\rangle$ and $|M_3\rangle$ constitute an orthonormal triad of eigenvectors in the three-dimensional Euclidean space (see figure 3.2), we can express the second-moment tensor $\boldsymbol{M}$ as

$$\boldsymbol{M} = T(1+\xi)|M_1\rangle\langle M_1| + T(1+\varsigma)|M_2\rangle\langle M_2| + T(1+\zeta)|M_3\rangle\langle M_3|, \tag{3.41}$$

The expression for $\widehat{\boldsymbol{M}}$ follows from (3.39) and (5.20). The determinant of $\boldsymbol{M}$ is given by

$$|\boldsymbol{M}| = T^3(1+\xi)(1+\varsigma)(1+\zeta). \tag{3.42}$$

Referring to figure 3.2, we assume that the shear-plane eigenvectors $|M_1\rangle$ and $|M_2\rangle$ can be obtained by rotating the system of axes at an angle $(\pi/4+\phi)$, with ϕ being unknown, in the anti-clockwise sense about the z-axis which coincides with $|M_3\rangle$:

$$|M_1\rangle = \begin{bmatrix} \cos\left(\phi+\frac{\pi}{4}\right) \\ \sin\left(\phi+\frac{\pi}{4}\right) \\ 0 \end{bmatrix}, \quad |M_2\rangle = \begin{bmatrix} -\sin\left(\phi+\frac{\pi}{4}\right) \\ \cos\left(\phi+\frac{\pi}{4}\right) \\ 0 \end{bmatrix} \quad \text{and} \quad |M_3\rangle = \begin{bmatrix} 0 \\ 0 \\ 1 \end{bmatrix}. \tag{3.43}$$

We further assume that the contact vector $\boldsymbol{k}$ makes an angle φ with $|M_3\rangle$, and θ is the angle between $|M_1\rangle$ and $\boldsymbol{k} - (\boldsymbol{k}\cdot\boldsymbol{z})\boldsymbol{z}$, the projection of $\boldsymbol{k}$ on the shear plane, as shown in figure 3.2.

Inserting (5.21) into (5.20), we obtain the following expression for the second moment tensor,

$$\boldsymbol{M} = T\begin{bmatrix} 1+\lambda^2+\eta\sin 2\phi & -\eta\cos 2\phi & 0 \\ -\eta\cos 2\phi & 1+\lambda^2-\eta\sin 2\phi & 0 \\ 0 & 0 & 1-2\lambda^2 \end{bmatrix} \equiv T[\delta_{\alpha\beta}] + \widehat{\boldsymbol{M}}, \tag{3.44}$$

and its deviatoric part is

$$\widehat{\boldsymbol{M}} = T\begin{bmatrix} \lambda^2+\eta\sin 2\phi & -\eta\cos 2\phi & 0 \\ -\eta\cos 2\phi & \lambda^2-\eta\sin 2\phi & 0 \\ 0 & 0 & -2\lambda^2 \end{bmatrix}, \tag{3.45}$$

where we have introduced the following notations

$$\eta \equiv \frac{1}{2}(\varsigma - \xi) \geq 0, \tag{3.46}$$

$$\lambda^2 \equiv \frac{1}{2}(\varsigma + \xi) = -\frac{\zeta}{2} \geq 0, \tag{3.47}$$

and $T = M_{\alpha\alpha}/3$ is the granular temperature. It is straightforward to verify that the eigenvalues in the shear-plane can be expressed in terms of η and λ via

$$\xi = \lambda^2 - \eta \quad \text{and} \quad \varsigma = \lambda^2 + \eta > \xi, \tag{3.48}$$

with the eigenvalue, ζ, along the vorticity direction (z), being given by (5.44).

Let us define the dimensionless shear rate (Savage & Jeffrey 1981)

$$R \equiv \frac{\dot{\gamma}}{4\sqrt{T/\sigma^2}} = \left(\frac{\sqrt{T}}{\sigma\dot{\gamma}/4}\right)^{-1} \equiv \frac{v_{sh}}{v_{th}}, \tag{3.49}$$

which can be interpreted as the inverse of the square root of dimensionless temperature. Equation (3.49) is called the Savage-Jeffrey parameter (Savage & Jeffrey 1981) which is a measure of the mean shear velocity ($v_{sh} = \sigma\dot{\gamma}/2$ over a particle diameter) relative to the thermal velocity ($v_{th} \propto \sqrt{T}$) associated with the random motion of particles. The second-moment tensor (5.22) in USF, constructed from its eigen-basis, is, therefore, completely determined when R, η, ϕ and λ^2 are specified.

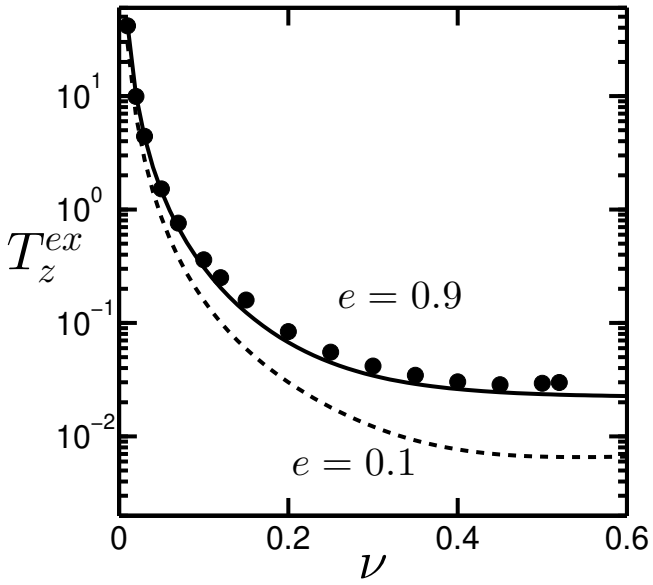

Fig. 3.3 Variation of *excess* temperature (3.50) with density for different restitution coefficients: $e = 0.9$ (solid line) and $e = 0.1$ (dashed line). While the lines denote the present theory, the circles denote the simulation data of Alam (2005) for $e = 0.9$.

3.4.2 Anisotropy of Second Moment and Excess Temperature

It is clear from (5.23) that the second moment tensor $\boldsymbol{M}$ is anisotropic, and the measure of its anisotropy is given by η, ϕ and λ^2. Note that η [(5.43)] is the difference between the two shear-plane eigenvalues of $\boldsymbol{M}$ which, in physical terms, is a measure of the anisotropy of the second-moment tensor $\boldsymbol{M}$ on the shear plane. On the other hand, λ^2 [(5.44)] is a measure of the *excess* temperature,

$$T_z^{ex} \equiv (T - T_z) = -\zeta T \equiv 2\lambda^2 T > 0, \tag{3.50}$$

along the vorticity direction (which is proportional to the out-of-plane eigenvalue ζ of $\boldsymbol{M}$).

Equation (3.50) implies that, when a granular material is sheared, the kinetic temperature along the vorticity direction is always smaller than the mean temperature [$T = (T_x + T_y + T_z)/3$]. This theoretical result has been verified via a comparison of molecular dynamic event-driven simulations for a sheared granular fluid, see figure 3.3. It is seen that the excess temperature T_z^{ex} decreases with increasing density but remains positive for all ν and e. Due to the linear relationship (3.50) between λ^2 and T_z^{ex}, λ^2 will henceforth be termed as excess temperature too.

3.5 Balance Equations for Uniform Shear Flow and Their Algebraic Form

In the steady uniform shear flow, the number density n, the velocity gradient $\boldsymbol{\nabla u}$ and the components of the second moment tensor $\boldsymbol{M}$ are constants and the contracted third moment vanishes. The mass and momentum balance equations, (3.10) and (3.11), are identically satisfied; the remaining balance equation (3.12) for the second moment tensor needs to be solved.

3.5.1 The Balance of Second Moment

The balance equation (3.12) for $\boldsymbol{M}$ in USF simplifies to

$$P_{\delta\beta}u_{\alpha,\delta}+P_{\delta\alpha}u_{\beta,\delta}=\aleph_{\alpha\beta}, \tag{3.51}$$

where

$$P_{\alpha\beta}=\rho M_{\alpha\beta}+\Theta_{\alpha\beta}, \tag{3.52}$$

is the total stress tensor, with $\rho M_{\alpha\beta}\equiv\rho\langle C_\alpha C_\beta\rangle$ being its kinetic contribution and $\Theta_{\alpha\beta}\equiv m\Theta_\alpha[C_\beta]$ is its collisional contribution, given by [explicit derivation is given in Appendix K]

$$\Theta_{\alpha\beta}=\frac{3(1+e)\rho\nu g_0(\nu)}{\pi^{3/2}}\int k_\alpha k_\beta(\boldsymbol{k}\cdot\boldsymbol{M}\cdot\boldsymbol{k})\mathfrak{G}(\chi)\,d\boldsymbol{k}. \tag{3.53}$$

In (3.51), $\aleph_{\alpha\beta}$ represents the collisional source of second moment whose integral expression [see Appendix L] can be written as (Chou & Richman 1998):

$$\aleph_{\alpha\beta}=A_{\alpha\beta}+\widehat{E}_{\alpha\beta}+\widehat{G}_{\alpha\beta}+\Theta_{\alpha\delta}W_{\beta\delta}+\Theta_{\beta\delta}W_{\alpha\delta}, \tag{3.54}$$

with

$$A_{\alpha\beta}=-\frac{6(1-e^2)\rho\nu g_0(\nu)}{\sigma\pi^{3/2}}\int k_\alpha k_\beta(\boldsymbol{k}\cdot\boldsymbol{M}\cdot\boldsymbol{k})^{3/2}\mathfrak{F}(\chi)\,d\boldsymbol{k}, \tag{3.55}$$

and the traceless tensors, $\widehat{E}_{\alpha\beta}$ and $\widehat{G}_{\alpha\beta}$, are

$$\widehat{E}_{\alpha\beta}=-\frac{12(1+e)\rho\nu g_0}{\sigma\pi^{\frac{3}{2}}}\int(k_\alpha j_\beta+j_\alpha k_\beta)(\boldsymbol{k}\cdot\boldsymbol{M}\cdot\boldsymbol{j})(\boldsymbol{k}\cdot\boldsymbol{M}\cdot\boldsymbol{k})^{\frac{1}{2}}\mathfrak{F}(\chi)d\boldsymbol{k}, \tag{3.56}$$

$$\widehat{G}_{\alpha\beta}=\frac{6(1+e)\rho\nu g_0}{\pi^{\frac{3}{2}}}\int(k_\alpha j_\beta+j_\alpha k_\beta)[(\boldsymbol{k}\cdot\boldsymbol{M}\cdot\boldsymbol{k})(\boldsymbol{k}\cdot\boldsymbol{D}\cdot\boldsymbol{j})-(\boldsymbol{k}\cdot\widehat{\boldsymbol{M}}\cdot\boldsymbol{j})(\boldsymbol{k}\cdot\boldsymbol{D}\cdot\boldsymbol{k})]\mathfrak{G}(\chi)d\boldsymbol{k}. \tag{3.57}$$

The above integrals are to be evaluated over $d\boldsymbol{k}$ such that $d\boldsymbol{k} = \sin\varphi d\varphi d\theta$, with the limits of the integrations being $\theta \in (0, 2\pi)$ and $\varphi \in (0, \pi)$. Note that $\boldsymbol{j}$ is an unit vector perpendicular to the contact vector $\boldsymbol{k}$ that lies in the plane formed by $\boldsymbol{g}$ and $\boldsymbol{k}$ such that

$$\boldsymbol{k} = \begin{bmatrix} \cos(\theta+\phi+\frac{\pi}{4})\sin\varphi \\ \sin(\theta+\phi+\frac{\pi}{4})\sin\varphi \\ \cos\varphi \end{bmatrix} \quad \text{and} \quad \boldsymbol{j} = \frac{1}{\sqrt{2}} \begin{bmatrix} \cos\varphi\cos(\theta+\phi+\frac{\pi}{4}) - \sin(\theta+\phi+\frac{\pi}{4}) \\ \cos\varphi\sin(\theta+\phi+\frac{\pi}{4}) + \cos(\theta+\phi+\frac{\pi}{4}) \\ -\sin\varphi \end{bmatrix} \tag{3.58}$$

It is straightforward to verify the following relations:

$$\left.\begin{aligned} \boldsymbol{k}\cdot\boldsymbol{M}\cdot\boldsymbol{k} &= T\left(1-\eta\sin^2\varphi\cos 2\theta + \lambda^2(3\sin^2\varphi - 2)\right) \\ \boldsymbol{k}\cdot\boldsymbol{M}\cdot\boldsymbol{j} &= \tfrac{1}{\sqrt{2}}T\sin\varphi[\eta(\sin 2\theta - \cos\varphi\cos 2\theta) + 3\lambda^2\cos\varphi] \equiv \boldsymbol{k}\cdot\widehat{\boldsymbol{M}}\cdot\boldsymbol{j} \\ \boldsymbol{k}\cdot\boldsymbol{D}\cdot\boldsymbol{j} &= \tfrac{1}{\sqrt{2}}\dot{\gamma}\sin\varphi[\cos\varphi\cos(2\phi+2\theta) - \sin(2\phi+2\theta)] \\ \boldsymbol{k}\cdot\boldsymbol{D}\cdot\boldsymbol{k} &= \dot{\gamma}\sin^2\varphi\cos(2\phi+2\theta) \end{aligned}\right\}. \tag{3.59}$$

In the integrand of (3.53-3.57), the following two analytic functions appear (Araki & Tremaine 1986):

$$\mathfrak{F}(\chi) \equiv -\sqrt{\pi}\left(\frac{3}{2}\chi + \chi^3\right)\operatorname{erfc}(\chi) + (1+\chi^2)\exp(-\chi^2), \tag{3.60}$$

$$\mathfrak{G}(\chi) \equiv \sqrt{\pi}\left(\frac{1}{2} + \chi^2\right)\operatorname{erfc}(\chi) - \chi\exp(-\chi^2), \tag{3.61}$$

where

$$\chi(R,\eta,\phi,\lambda;\theta,\varphi) \equiv \frac{\sigma(\boldsymbol{k}\cdot\boldsymbol{\nabla u}\cdot\boldsymbol{k})}{2\sqrt{(\boldsymbol{k}\cdot\boldsymbol{M}\cdot\boldsymbol{k})}} = \frac{2R\sin^2\varphi\cos(2\phi+2\theta)}{\sqrt{(1-\eta\sin^2\varphi\cos 2\theta + \lambda^2(3\sin^2\varphi - 2))}}. \tag{3.62}$$

The origin of χ can be traced to the excluded volume effects of macroscopic particles (Jenkins & Richman 1988; Saha & Alam 2014), and hence $\chi = 0$ in the dilute limit and, consequently,

$$\mathfrak{F}(\chi) = 1 \quad \text{and} \quad \mathfrak{G}(\chi) = \frac{\sqrt{\pi}}{2}, \quad \text{as} \quad \nu \to 0. \tag{3.63}$$

With (3.63), the integrals $\Theta_{\alpha\beta}$, $A_{\alpha\beta}$, $\widehat{E}_{\alpha\beta}$ and $\widehat{G}_{\alpha\beta}$ can be expressed in terms of elliptic integrals (Goldreich & Tremaine 1978) and further approximations are needed to evaluate them explicitly. On the other hand, it has not been possible to evaluate the above integrals analytically when the dense-gas corrections are incorporated due to the dependence of (3.60-3.61) on

the integration variable θ and φ. We shall outline an approximate method in §3.5.3 to evaluate these integrals analytically for the whole range of density.

Substituting (5.17), (3.52) and (3.54) into (3.51), the balance equation for the second moment tensor reduces to

$$\rho M_{\delta\beta}(D_{\alpha\delta}+W_{\alpha\delta})+\rho M_{\delta\alpha}(D_{\beta\delta}+W_{\beta\delta})+\Theta_{\delta\beta}D_{\alpha\delta}+\Theta_{\delta\alpha}D_{\beta\delta}=A_{\alpha\beta}+\widehat{E}_{\alpha\beta}+\widehat{G}_{\alpha\beta}. \quad (3.64)$$

With the integrals for $\Theta_{\alpha\beta}$, $A_{\alpha\beta}$, $\widehat{E}_{\alpha\beta}$ and $\widehat{G}_{\alpha\beta}$ being evaluated in terms of R, η, ϕ and λ as discussed above, the equation (3.64) yields four independent algebraic equations that needs to be solved to obtain the rheological properties of USF for the whole range of volume fraction ν. The collisional dissipation rate (3.54) can also be evaluated simultaneously.

3.5.2 Second Moment Balance in Rotated Co-ordinate Frame

Let us now rewrite (3.64) in a new co-ordinate system $x'y'z'$, formed by the orthonormal triad of eigenvectors of $\boldsymbol{M}$, i.e., with respect to the co-ordinate system whose axes coincide with $|M_1\rangle$, $|M_2\rangle$ and $|M_3\rangle$, respectively. This amounts to a transformation, see figure 3.2, via the following rotation matrix,

$$\mathscr{R}=\begin{bmatrix}\cos(\phi+\frac{\pi}{4}) & -\sin(\phi+\frac{\pi}{4}) & 0\\ \sin(\phi+\frac{\pi}{4}) & \cos(\phi+\frac{\pi}{4}) & 0\\ 0 & 0 & 1\end{bmatrix}, \quad (3.65)$$

that transforms the second moment tensor,

$$\boldsymbol{M}'=T\begin{bmatrix}1+\lambda^2-\eta & 0 & 0\\ 0 & 1+\lambda^2+\eta & 0\\ 0 & 0 & 1-2\lambda^2\end{bmatrix}, \quad (3.66)$$

into a diagonal matrix. It is evident from (3.66) that the anisotropy of the second moment in the rotated co-ordinate frame is quantified in terms of (i) the temperature difference η [eqn. (5.43)] in the shear-plane and (ii) the "excess" temperature T_z^{ex} ($\propto \lambda^2$ eqn. (3.50)) along the vorticity direction. With a prime over a quantity denoting its value in the new co-ordinate

frame, the following relations hold:

$$\boldsymbol{k}' = \cos\theta\sin\varphi|M_1\rangle + \sin\theta\sin\varphi|M_2\rangle + \cos\varphi|M_3\rangle, \tag{3.67}$$

$$\boldsymbol{j}' = \frac{1}{\sqrt{2}}\left[(\cos\varphi\cos\theta - \sin\theta)|M_1\rangle + (\cos\varphi\sin\theta + \cos\theta)|M_2\rangle - \sin\varphi|M_3\rangle\right], \tag{3.68}$$

$$\boldsymbol{u}' = 2\dot{\gamma}\left[x'\sin\left(\phi+\frac{\pi}{4}\right) + y'\cos\left(\phi+\frac{\pi}{4}\right)\right]\left[\cos\left(\phi+\frac{\pi}{4}\right)|M_1\rangle - \sin\left(\phi+\frac{\pi}{4}\right)|M_2\rangle\right], \tag{3.69}$$

$$\boldsymbol{D}' = \dot{\gamma}\begin{bmatrix} \cos 2\phi & -\sin 2\phi & 0 \\ -\sin 2\phi & -\cos 2\phi & 0 \\ 0 & 0 & 0 \end{bmatrix} \qquad \text{and} \qquad \boldsymbol{W}' = \boldsymbol{W}. \tag{3.70}$$

The last equation confirms that the spin tensor $\boldsymbol{W}$ is invariant under the planar rotation (3.65).

With the aid of (3.66-3.70), the second moment balance equation (3.64) transforms into four independent equations in the rotated co-ordinate frame:

(i) the trace of (3.64),

$$-4\eta\rho T\dot{\gamma}\cos 2\phi + 2\dot{\gamma}\left[\left(\Theta_{x'x'} - \Theta_{y'y'}\right)\cos 2\phi - 2\Theta_{x'y'}\sin 2\phi\right] = A_{x'x'} + A_{y'y'} + A_{z'z'}, \tag{3.71}$$

(ii) the z'-z' component of its deviatoric part

$$-4\eta\rho T\dot{\gamma}\cos 2\phi + 2\dot{\gamma}[(\Theta_{x'x'} - \Theta_{y'y'})\cos 2\phi - 2\Theta_{x'y'}\sin 2\phi] = -3\widehat{\Gamma}_{z'z'}, \tag{3.72}$$

(iii) the difference between the x'-x' and y'-y' components

$$4\left(1+\lambda^2\right)\rho T\dot{\gamma}\cos 2\phi + 2\dot{\gamma}\left(\Theta_{x'x'} + \Theta_{y'y'}\right)\cos 2\phi = \Gamma_{x'x'} - \Gamma_{y'y'}, \tag{3.73}$$

and, finally, (iv) the off-diagonal x'-y' component

$$2\rho T\dot{\gamma}\left[\eta - \left(1+\lambda^2\right)\sin 2\phi\right] - \left(\Theta_{x'x'} + \Theta_{y'y'}\right)\dot{\gamma}\sin 2\phi = \Gamma_{x'y'}, \tag{3.74}$$

where

$$\Gamma_{\alpha\beta} = A_{\alpha\beta} + \widehat{E}_{\alpha\beta} + \widehat{G}_{\alpha\beta}, \tag{3.75}$$

see (3.54-3.57). The various collision integrals (viz. §3.5.1) appearing in (3.71-3.74) can be compactly written as

$$\left.\begin{aligned}
\Theta_{x'x'}-\Theta_{y'y'} &= \tfrac{3(1+e)\rho\nu g_0 T}{\pi^{\frac{3}{2}}}\mathscr{J}^{30}_{012}(\eta,\lambda^2,R,\phi),\\
2\Theta_{x'y'} &= \tfrac{3(1+e)\rho\nu g_0 T}{\pi^{\frac{3}{2}}}\mathscr{J}^{30}_{102}(\eta,\lambda^2,R,\phi),\\
\Theta_{x'x'}+\Theta_{y'y'} &= \tfrac{3(1+e)\rho\nu g_0 T}{\pi^{\frac{3}{2}}}\mathscr{J}^{30}_{002}(\eta,\lambda^2,R,\phi),\\
A_{x'x'}+A_{y'y'}+A_{z'z'} &= -\tfrac{6(1-e^2)\rho\nu g_0 T^{\frac{3}{2}}}{\sigma\pi^{\frac{3}{2}}}\mathscr{H}^{10}_{003}(\eta,\lambda^2,R,\phi),
\end{aligned}\right\}, \tag{3.76}$$

$$\left.\begin{aligned}
\widehat{\Gamma}_{z'z'} &= -\tfrac{6(1+e)\rho\nu g_0 T^{\frac{3}{2}}}{\sigma\pi^{\frac{3}{2}}}\Big[\tfrac{1}{3}(1-e)\left(2\mathscr{H}^{12}_{003}-\mathscr{H}^{30}_{003}\right)-2\eta\left(\mathscr{H}^{31}_{101}-\mathscr{H}^{32}_{011}\right)\\
&\qquad -6\lambda^2\mathscr{H}^{32}_{001}-4R\mathscr{K}^{31}_{00}\Big],\\
\Gamma_{x'x'}-\Gamma_{y'y'} &= -\tfrac{6(1+e)\rho\nu g_0 T^{\frac{3}{2}}}{\sigma\pi^{\frac{3}{2}}}\Big[(1-e)\mathscr{H}^{30}_{013}+2\eta\left(2\mathscr{H}^{31}_{111}-\mathscr{H}^{30}_{201}-\mathscr{H}^{32}_{021}\right)\\
&\qquad +6\lambda^2\left(\mathscr{H}^{32}_{011}-\mathscr{H}^{31}_{101}\right)-4R\left(\mathscr{K}^{30}_{10}-\mathscr{K}^{31}_{01}\right)\Big],\\
\Gamma_{x'y'} &= -\tfrac{6(1+e)\rho\nu g_0 T^{\frac{3}{2}}}{\sigma\pi^{\frac{3}{2}}}\Big[\tfrac{1}{2}(1-e)\mathscr{H}^{30}_{103}+\eta\left(\mathscr{H}^{31}_{201}+\mathscr{H}^{30}_{111}-\mathscr{H}^{32}_{111}-\mathscr{H}^{31}_{021}\right)\\
&\qquad +3\lambda^2\left(\mathscr{H}^{32}_{101}+\mathscr{H}^{31}_{011}\right)+2R\left(\mathscr{K}^{31}_{10}+\mathscr{K}^{30}_{01}\right)\Big].
\end{aligned}\right\}. \tag{3.77}$$

In (3.76-3.77), $\mathscr{H}^{\delta p}_{\alpha\beta\gamma}$, $\mathscr{J}^{\delta p}_{\alpha\beta\gamma}$ and $\mathscr{K}^{\delta p}_{\alpha\beta\gamma}$ have integral expressions over θ and φ:

$$\begin{aligned}
\mathscr{H}^{\delta p}_{\alpha\beta\gamma}(\eta,R,\phi,\lambda) &\equiv \int_{\theta=0}^{2\pi}\int_{\varphi=0}^{\pi}\sin^{\alpha}2\theta\cos^{\beta}2\theta\sin^{\delta}\varphi\cos^{p}\varphi\\
&\quad\times\left(1-\eta\sin^2\varphi\cos 2\theta+\lambda^2(3\sin^2\varphi-2)\right)^{\frac{\gamma}{2}}\mathfrak{F}\left(\chi\left[\eta,R,\phi,\lambda;\theta,\varphi\right]\right)d\varphi d\theta, \qquad (3.78)\\
\mathscr{J}^{\delta p}_{\alpha\beta\gamma}(\eta,R,\phi,\lambda) &\equiv \int_{\theta=0}^{2\pi}\int_{\varphi=0}^{\pi}\sin^{\alpha}2\theta\cos^{\beta}2\theta\sin^{\delta}\varphi\cos^{p}\varphi\\
&\quad\times\left\{1-\eta\sin^2\varphi\cos 2\theta+\lambda^2(3\sin^2\varphi-2)\right\}^{\frac{\gamma}{2}}\mathfrak{G}\left(\chi\left[\eta,R,\phi,\lambda;\theta,\varphi\right]\right)d\varphi d\theta, \qquad (3.79)\\
\mathscr{K}^{\delta p}_{\alpha\beta}(\eta,R,\phi,\lambda) &\equiv \int_{\theta=0}^{2\pi}\int_{\varphi=0}^{\pi}\sin^{\alpha}2\theta\cos^{\beta}2\theta\sin^{\delta}\varphi\cos^{p}\varphi\left[(1-2\lambda^2)\{\sin(2\phi+2\theta)-\cos\varphi\right.\\
&\quad\left.\times\cos(2\phi+2\theta)\}+\sin^2\varphi\{3\lambda^2\sin(2\phi+2\theta)-\eta\sin 2\phi\}\right]\mathfrak{G}\left(\chi\left[\eta,R,\phi,\lambda;\theta,\varphi\right]\right)d\varphi d\theta, \qquad (3.80)
\end{aligned}$$

where $\mathfrak{F}(\chi)$ and $\mathfrak{G}(\chi)$ are given by (3.60) and (3.61), respectively. The integrals (3.78-3.80) can be evaluated *numerically* via any quadrature method.

In the following section, we outline an approximate method to evaluate the integrals (3.78-3.80) analytically via a power-series expansion. As illustrated in §3.5.3 below, the series expansion would help (i) to reduce the integro-algebraic equations (3.71-3.74) into a set of algebraic equations for four unknowns η, R, ϕ and λ as well as (ii) to obtain closed-from analytical expressions for nonlinear transport coefficients and collisional dissipation (see §3.7). More importantly, we shall derive 'closed-form' analytical solutions of the second moment balance at the Burnett order and beyond.

3.5.3 Series Expansion and the Algebraic form of Second-moment Balance

Recall that the integrand in (3.78-3.80) depend on two analytic functions $\mathfrak{F}(\chi)$ and $\mathfrak{G}(\chi)$ as defined in (3.60) and (3.61), respectively, with χ being given by (3.62). Substituting the power-series representation for the complementary error function and the exponential and after some straightforward algebra, the expressions for $\mathfrak{F}(\chi)$ and $\mathfrak{G}(\chi)$ can be written as (Saha & Alam 2014)

$$\begin{aligned}\mathfrak{F}(\eta,R,\phi,\lambda;\theta,\varphi) = -\sqrt{\pi}\Bigg[&\frac{3R\sin^2\varphi\cos(2\phi+2\theta)}{\{1-\eta\sin^2\varphi\cos 2\theta+\lambda^2(3\sin^2\varphi-2)\}^{\frac{1}{2}}}\\ &+\left\{\frac{2R\sin^2\varphi\cos(2\phi+2\theta)}{\{1-\eta\sin^2\varphi\cos 2\theta+\lambda^2(3\sin^2\varphi-2)\}^{\frac{1}{2}}}\right\}^3\Bigg]\\ +\sum_{n=0}^{\infty}\frac{(-1)^n}{n!}&\frac{3}{(2n-1)(2n-3)}\left[\frac{2R\sin^2\varphi\cos(2\phi+2\theta)}{\{1-\eta\sin^2\varphi\cos 2\theta+\lambda^2(3\sin^2\varphi-2)\}^{\frac{1}{2}}}\right]^{2n},\end{aligned} \tag{3.81}$$

$$\begin{aligned}\mathfrak{G}(\eta,R,\phi,\lambda;\theta,\varphi) = \sqrt{\pi}\Bigg[&\frac{1}{2}+\frac{4R^2\sin^4\varphi\cos^2(2\phi+2\theta)}{1-\eta\sin^2\varphi\cos 2\theta+\lambda^2(3\sin^2\varphi-2)}\Bigg]\\ +\sum_{n=0}^{\infty}\frac{(-1)^n}{n!}&\frac{2}{(2n-1)(2n+1)}\left[\frac{2R\sin^2\varphi\cos(2\phi+2\theta)}{\{1-\eta\sin^2\varphi\cos 2\theta+\lambda^2(3\sin^2\varphi-2)\}^{\frac{1}{2}}}\right]^{2n+1}.\end{aligned} \tag{3.82}$$

Substituting (3.81-3.82) into (3.78-3.80) and carrying out term-by-term integrations over $\theta\in(0,2\pi)$ and $\varphi\in(0,\pi)$ results in an infinite series in η, R and λ for each integral in (3.78-3.80), see Appendix F. To progress further, we need to truncate each series after a finite number of terms.

Retaining terms up-to third order $O(\eta^m\lambda^n R^p\sin^q(2\phi))$, $m+n+p+q\leq 3$ in the resulting infinite series for each integral (3.78-3.80) and substituting them into (3.71-3.74), we obtain

the following set of coupled nonlinear algebraic equations

$$\left.\begin{aligned}
&20\sqrt{\pi}\Big\{1+\tfrac{4}{5}(1+e)\nu g_0\Big\}\eta R\cos 2\phi+128(1+e)\nu g_0R^2\\
&\qquad -3(1-e^2)\nu g_0(10+\eta^2+32R^2+8\sqrt{\pi}R\eta\cos 2\phi)=0\\
&35\sqrt{\pi}\eta R\cos 2\phi+(1+e)\nu g_0\Big\{32(1+3e)R^2-3(3-e)(\eta^2+21\lambda^2)\\
&\qquad -8\sqrt{\pi}(4-3e)\eta R\cos 2\phi\Big\}=0\\
&210\sqrt{\pi}(1+\lambda^2)R\cos 2\phi-(1+e)\nu g_0\big[12\sqrt{\pi}\big\{7(1-3e)+4(4-3e)\lambda^2\\
&-32(1+e)R^2\big\}R\cos 2\phi+\eta\big\{126(3-e)-3(3-e)\eta^2+36(3-e)\lambda^2\\
&+64(4-3e)R^2-32(5+3e)R^2\cos 4\phi\big\}\big]=0\\
&105\sqrt{\pi}\big\{\eta-(1+\lambda^2)\sin 2\phi\big\}-2(1+e)\nu g_0\sin 2\phi\big[16(5+3e)\eta R\cos 2\phi\\
&-3\sqrt{\pi}\big\{7(1-3e)+4(4-3e)\lambda^2-32(1+e)R^2\big\}\big]=0
\end{aligned}\right\}. \tag{3.83}$$

for four unknowns η, λ, R and ϕ, given that the restitution coefficient (e) and the volume fraction (ν) are known.

Similarly, retaining terms up-to fourth order $O(\eta^m\lambda^nR^p\sin^q(2\phi))$, $m+n+p+q\leq 4$, the equations (3.71-3.74) simplify to

$$\left.\begin{aligned}
&1680\sqrt{\pi}\eta R\cos 2\phi-3(1-e^2)\nu g_0\big(840+84\eta^2+3\eta^4+2688R^2+1024R^4\\
&-128R^2\eta^2+768R^2\lambda^2-24\eta^2\lambda^2+252\lambda^4+672\sqrt{\pi}\eta R\cos 2\phi-64\eta^2R^2\cos 4\phi\big)\\
&+64(1+e)\nu g_0R\big\{21\sqrt{\pi}\eta\cos 2\phi+4R(42-2\eta^2+12\lambda^2+32R^2-\eta^2\cos 4\phi)\big\}=0\\
&2310\sqrt{\pi}\eta R\cos 2\phi+(1+e)\nu g_0\big[32R^2\big\{66+8\eta^2-165\lambda^2+3e(66-4\eta^2+33\lambda^2)\big\}\\
&-9(3-e)\big\{\eta^4+11\eta^2(2-\lambda^2)+66\lambda^2(7-\lambda^2)\big\}+1024(5+3e)R^4\\
&-16R\eta\big\{33\sqrt{\pi}(4-3e)\cos 2\phi-4R\eta(2-3e)\cos 4\phi\big\}\big]=0\\
&210\sqrt{\pi}(1+\lambda^2)R\cos 2\phi-(1+e)\nu g_0\big[12\sqrt{\pi}\big\{7(1-3e)+4(4-3e)\lambda^2\\
&-32(1+e)R^2\big\}R\cos 2\phi+\eta\big\{126(3-e)-3(3-e)\eta^2+36(3-e)\lambda^2\\
&+64(4-3e)R^2-32(5+3e)R^2\cos 4\phi\big\}\big]=0\\
&105\sqrt{\pi}\big\{\eta-(1+\lambda^2)\sin 2\phi\big\}-2(1+e)\nu g_0\sin 2\phi\big[16(5+3e)\eta R\cos 2\phi\\
&-3\sqrt{\pi}\big\{7(1-3e)+4(4-3e)\lambda^2-32(1+e)R^2\big\}\big]=0
\end{aligned}\right\}. \tag{3.84}$$

For specified values of the restitution coefficient (e) and the density (ν), we can use the standard Newton-Raphson's method to solve both (3.83) and (3.84), yielding solutions for η, λ^2, R and ϕ that are correct up-to orders $O(\eta^m\lambda^nR^p\sin^q(2\phi))$, $m+n+p+q\leq 3$ and $O(\eta^m\lambda^nR^p\sin^q(2\phi))$, $m+n+p+q\leq 4$, respectively. However we have solved (3.83) and (3.84) analytically using regular perturbation theory with the exact Burnett order solution as the solution at leading order. We shall show in §3.10.1 that the terms up-to the fourth-order must be retained in the above series expansion to recover the exact numerical solution of (3.71-3.74).

It must be noted that equations (3.83) and (3.84) belong to the 'super-Burnett' and 'super-super-Burnett' orders since they incorporate terms that are at most 'cubic' and 'quartic' in the shear-rate (R) respectively. Therefore, the resulting solutions of (3.83) and (3.84) for η, λ, R and ϕ and the transport coefficients will be dubbed 'super-Burnett' and 'super^2-Burnett' solutions (see §3.10) respectively.

3.6 Closed-form Solution of "Truncated" Second Moment Equations

3.6.1 Approximate Solution in the Dilute Limit and its Comparison

Let us consider the dilute limit ($\nu \to 0$) of the second-moment balance (3.71-3.74) which was analysed previously by Richman (1989). In this limit, the collisional contribution to flux terms vanishes (e.g. $\Theta_{\alpha\beta} = 0$) and consequently the stress tensor is given by its kinetic contribution:

$$P_{\alpha\beta} = \rho M_{\alpha\beta}. \tag{3.85}$$

Moreover, $\chi = 0$ as $\nu \to 0$ and hence $\mathfrak{F}(\chi \to 0) = 1$, $\mathfrak{G}(\chi \to 0) = \sqrt{\pi}/2$, see (3.63); it can be verified that the integrals $\widehat{G}_{\alpha\beta}(\nu \to 0) = 0$ and $\Gamma_{x'y'}(\chi \to 0) = 0$ vanish too. Therefore, the balance equations (3.71-3.74) for the second moment simplify to

$$\left.\begin{aligned} -4\eta\rho T\dot{\gamma}\cos 2\phi &= A_{x'x'} + A_{y'y'} + A_{z'z'}, \\ -4\eta\rho T\dot{\gamma}\cos 2\phi &= -3\widehat{\Gamma}_{z'z'}, \\ 4(1+\lambda^2)\rho T\dot{\gamma}\cos 2\phi &= (\Gamma_{x'x'} - \Gamma_{y'y'}), \\ 2\rho T\dot{\gamma}[\eta - (1+\lambda^2)\sin 2\phi] &= \Gamma_{x'y'} = 0. \end{aligned}\right\} \tag{3.86}$$

The last equation of (3.86) yields an expression for the non-coaxiality angle ϕ in terms of η and λ:

$$\frac{\eta}{1+\lambda^2} = \sin 2\phi \quad \Rightarrow \quad \phi = \frac{1}{2}\sin^{-1}\left(\frac{\eta}{1+\lambda^2}\right). \tag{3.87}$$

By evaluating the integrals on the right-hand side of (3.86) and retaining terms up-to super-super-Burnett order $O(\eta^m\lambda^n R^p \sin^q(2\phi)\ m+n+p+q \le 4)$, the remaining three equations simplify to

$$\left.\begin{aligned} 8\pi^{\frac{3}{2}}R\eta\cos 2\phi - \tfrac{3}{70}(1-e^2)\pi\nu(280+28\eta^2+\eta^4-8\eta^2\lambda^2+84\lambda^4) &= 0, \\ 8\pi^{\frac{3}{2}}R\eta\cos 2\phi - \tfrac{24}{35}(3-e)(1+e)\pi\nu\{\eta^2+3\lambda^2(7-\lambda^2)\} &= 0, \\ 35\sqrt{\pi}R(1+\lambda^2)\cos 2\phi - 3(3+2e-e^2)\nu\eta(7+2\lambda^2) &= 0. \end{aligned}\right\} \tag{3.88}$$

The solutions for R is given by

$$R = \frac{3(1-e^2)\nu}{560\sqrt{\pi}\eta\cos 2\phi}\left(280+28\eta^2+\eta^4-8\eta^2\lambda^2+84\lambda^4\right), \tag{3.89}$$

where λ^2 satisfies a cubic equation, which after truncating at the second-order, takes the form

$$\lambda^4+\left(\frac{7}{e}+\frac{53}{24}\left(e^{-1}-1\right)\right)\lambda^2-\frac{5}{2}\left(e^{-1}-1\right)=0. \tag{3.90}$$

yielding an approximate solution for λ^2. And finally, the solution for η^2 follows form

$$(14+3\lambda^2)\eta^4-33(12+3\lambda^2+\lambda^4)\eta^2+198\lambda^2(7+6\lambda^2-\lambda^4)=0. \tag{3.91}$$

A comparison of the present analytical solutions (3.87, 3.89, 3.90, 3.91) for η, ϕ, R and λ^2 with those of Richman (1989) is made in figure 3.4(*a-d*) respectively: the dashed and dot-dashed lines denote the present 4th-order solution and that of Richman respectively. To understand the quality of our solution (the red dot-dashed line), the exact variations of η, ϕ, R and λ^2 with e, obtained by solving (3.86) numerically, are superimposed in each panel as denoted by the solid lines. It is clear that the present solutions are better than those of Richman (1989) at lower values of the restitution coefficient ($e<0.5$), but are almost indistinguishable for $e>0.5$.

3.6.2 Exact Solution at Leading Order for Whole Range of Density

Here we discuss an exact solution of the 'leading-order' second-moment equations that helps to understand the scaling relations of η, R, λ^2 and ϕ in terms of the restitution coefficient (e).

Exact solution at Burnett order

Retaining terms up to second order $O(\eta^m\lambda^n R^n\sin^q(2\phi),\ m+n+p+q\leq 2)$ in the resulting infinite series for $\mathscr{H}^{\delta p}_{\alpha\beta\gamma}$, $\mathscr{J}^{\delta p}_{\alpha\beta\gamma}$ and $\mathscr{K}^{\delta p}_{\alpha\beta}$ [see (F.4-F.18) in Appendix F], the following set of

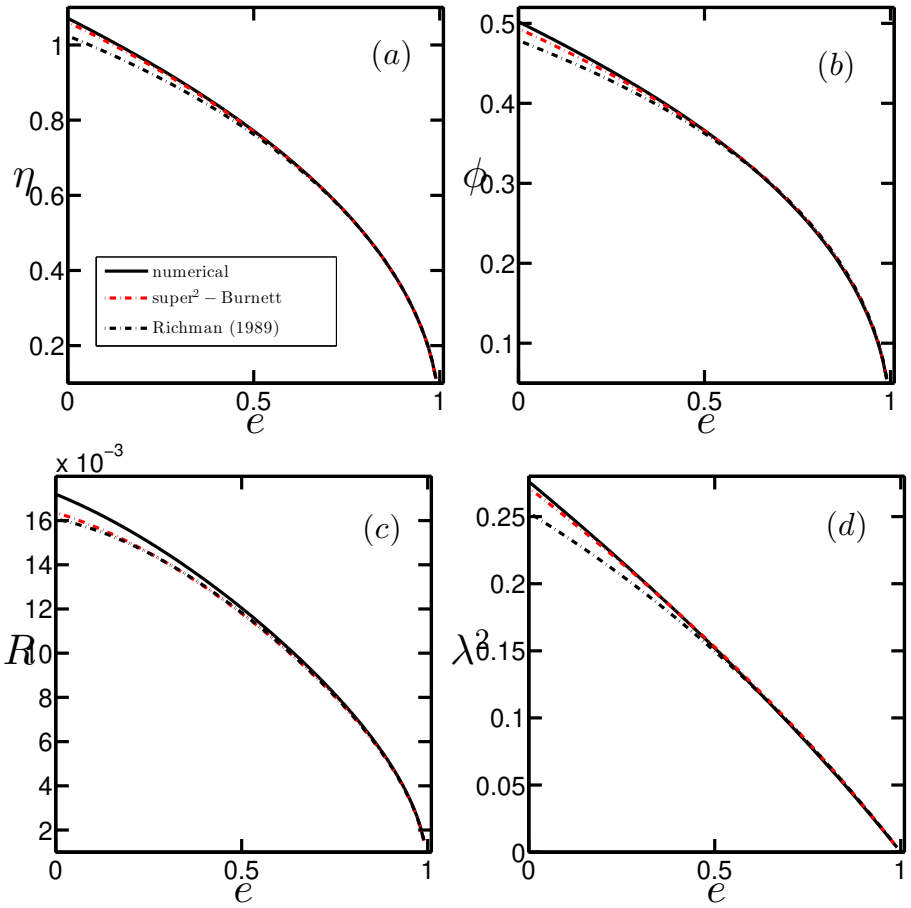

Fig. 3.4 Comparison of the "dilute-limit" analytical solution (red dot-dashed line) with that of Richman (1989) (black dot-dashed line) and the full numerical solution (black solid line): Variations of (*a*) η, (*b*) ϕ, (*c*) R and (*d*) λ^2 with the restitution coefficient e.

equations for the second moment balance (3.71-3.74) is obtained:

$$\left.\begin{aligned} 20\sqrt{\pi}\left\{1+\tfrac{4}{5}(1+e)\nu g_0\right\}\eta R\cos 2\phi + 128(1+e)\nu g_0 R^2 \\ -3(1-e^2)\nu g_0(10+\eta^2+32R^2+8\sqrt{\pi}\eta R\cos 2\phi)=0 \\ 35\sqrt{\pi}\eta R\cos 2\phi + (1+e)\nu g_0\{32(1+3e)R^2-3(3-e)(\eta^2+21\lambda^2) \\ -8\sqrt{\pi}(4-3e)\eta R\cos 2\phi\}=0 \\ 5\sqrt{\pi}R\cos 2\phi-(1+e)\nu g_0\{3(3-e)\eta+2(1-3e)\sqrt{\pi}R\cos 2\phi\}=0 \\ 5(\eta-\sin 2\phi)+2(1+e)(1-3e)\nu g_0\sin(2\phi)=0. \end{aligned}\right\} \tag{3.92}$$

These equations represent the second-moment balance equations at "Burnett order" (Burnett 1935) since all terms up to the second order in the shear rate have been retained.

These equations admit an exact solution

$$\left.\begin{aligned} \eta &= \tfrac{\{5-2(1+e)(1-3e)\nu g_0\}}{5}\sin 2\phi \\ \lambda^2 &= \tfrac{10(1-e)}{21(3-e)} + \tfrac{\left[(7-3e)\{5-2(1+e)(1-3e)\nu g_0\}-18(1+e)^2(3-e)\nu g_0\right]}{525(3-e)} \\ &\quad\times\{5-2(1+e)(1-3e)\nu g_0\}\sin^2 2\phi \\ R &= \tfrac{3(1+e)(3-e)}{5\sqrt{\pi}}\nu g_0\tan 2\phi \\ \tfrac{\eta}{R}\cos(2\phi) &= \tfrac{\sqrt{\pi}}{3(1+e)(3-e)}\cos^2(2\phi)\left(\tfrac{5}{\nu g_0}+2(1+e)(3e-1)\right), \end{aligned}\right\} \tag{3.93}$$

where $\sin^2(2\phi)=\mathscr{Y}$ is the real positive root of the quadratic equation

$$\begin{aligned} &(11-3e)\{5-2(1+e)(1-3e)\nu g_0\}^2\pi\mathscr{Y}^2- \\ &\left[(11-3e)\{5-2(1+e)(1-3e)\nu g_0\}^2\pi+96(1+3e)(1+e)^2(3-e)^2\nu^2 g_0^2+250\pi(1-e)\right]\mathscr{Y} \\ &+250\pi(1-e)=0. \end{aligned} \tag{3.94}$$

For specified values of ν and e, the non-coaxiality angle ϕ is determined from (3.94) and the remaining quantities are from (3.93). This provides the 'Burnett-order' solution for ϕ, η, λ^2 and R as functions of ν and e.

From (3.93-3.94), it is straightforward to verify the following scaling relations as $\nu\to 0$:

$$\eta\sim\sin 2\phi\sim R\sim\lambda\sim(1-e)^{1/2}. \tag{3.95}$$

Equation (3.95) holds strictly in the dilute limit ($\nu\to 0$), and therefore η, $\sin 2\phi$, R and λ are of the same order and scale with inelasticity as $\sqrt{(1-e)}$. The above scaling also holds in the dense limit as we shall verify in §3.11. The validity of the leading-order solution (3.93) to

accurately predict the transport coefficients (pressure, viscosity and normal stress differences, see §3.7) for the whole range of density will be checked in §3.10.1.

Beyond Burnett Order: Perturbation Solution

To obtain solutions beyond the Burnett order, i.e. at $O(\eta^m \lambda^n R^n \sin^q(2\phi),\ m+n+p+q>2)$, we must solve the related nonlinear algebraic equations as given by (3.83-3.84) valid at third and fourth orders in shear rate respectively. We could not find an 'exact' solution of (3.83-3.84) either at super-Burnett or super-super-Burnett order. Therefore we look for perturbation solution of (3.83-3.84) be taking Burnett-order solution (3.93-3.94) as the leading solution:

$$\left.\begin{aligned} \eta &= \eta^{(2)} + \varepsilon\eta^{(3)} + \varepsilon^2\eta^{(4)} + \cdots \\ \lambda^2 &= \lambda^{(2)} + \varepsilon\lambda^{(3)} + \varepsilon^2\lambda^{(4)} + \cdots \\ R &= R^{(2)} + \varepsilon R^{(3)} + \varepsilon^2 R^{(4)} + \cdots \\ \sin 2\phi &= \sin 2\phi^{(2)} + \varepsilon \sin 2\phi^{(3)} + \varepsilon^2 \sin 2\phi^{(4)} + \cdots \end{aligned}\right\}. \tag{3.96}$$

In the above expressions $\varepsilon \sim \dot{\gamma}$ and the superscript "2" corresponds to the "Burnett-order" solution and the superscripts "3" and "4" correspond to the corrections at the third and fourth order, respectively, in the shear rate. Plugging (3.96) into the corresponding third- and fourth-order equations and after performing some cumbersome algebra, we obtain the following solution for the correction terms at third order:

$$\eta^{(3)} = \lambda^{(3)} = R^{(3)} = \sin 2\phi^{(3)} = 0. \tag{3.97}$$

The fourth order correction terms are found to be non-zero and are given in Appendix H.

3.7 Constitutive Relations for Non-Newtonian Stress and Collisional Dissipation

The dimensionless stress tensor in USF can be written as

$$\begin{aligned}\boldsymbol{P}^* = \frac{\boldsymbol{P}}{\rho_p U_R^2} &= \begin{pmatrix} P_{xx}^* & P_{xy}^* & 0 \\ P_{yx}^* & P_{yy}^* & 0 \\ 0 & 0 & P_{zz}^* \end{pmatrix} \\ &\equiv \begin{pmatrix} p^* & 0 & 0 \\ 0 & p^* & 0 \\ 0 & 0 & p^* \end{pmatrix} + \begin{pmatrix} \frac{2}{3}\mathscr{N}_1^* + \frac{1}{3}\mathscr{N}_2^* & -\mu^* & 0 \\ -\mu^* & -\frac{1}{3}\mathscr{N}_1^* + \frac{1}{3}\mathscr{N}_2^* & 0 \\ 0 & 0 & -\frac{1}{3}\mathscr{N}_1^* - \frac{2}{3}\mathscr{N}_2^* \end{pmatrix}, \end{aligned} \tag{3.98}$$

where

$$p^* = \frac{1}{3}\left(P_{xx}^* + P_{yy}^* + P_{zz}^*\right), \tag{3.99}$$

$$\mu^* = -P_{xy}^*, \tag{3.100}$$

$$\mathscr{N}_1^* = \left(P_{xx}^* - P_{yy}^*\right), \tag{3.101}$$

$$\mathscr{N}_2^* = \left(P_{yy}^* - P_{zz}^*\right) \tag{3.102}$$

is the pressure, the shear viscosity, the first and second normal stress differences respectively; here ρ_p is material/intrinsic density of particles and $U_R = 2\dot{\gamma}\sigma$ is the reference velocity scale.

The power-series (3.82) for $\mathfrak{G}(\eta, R, \phi, \lambda)$ is inserted into (3.53) to evaluate the collisional stress, and the total stress tensor is subsequently obtained from (3.52) by summing the kinetic stress and the collisional stress. We will express constitutive relations in terms of the dimensionless temperature, which is defined as

$$T^* = \frac{T}{U_R^2} \equiv \frac{1}{64R^2}. \tag{3.103}$$

The final analytical expressions for the components of the stress tensor are presented in the following subsections, and the related algebraic details can be found in Appendix G.

3.7.1 Shear Stress and Viscosity

Retaining terms up-to the fourth-order in temperature anisotropy (η), shear rate (R), excess temperature along the vorticity direction ($\propto \lambda$) and $\sin(2\phi)$ $O(\eta^m \lambda^n R^n \sin^q(2\phi)$, $m+n+p+$

$q \leq 4$), the dimensionless shear stress can be written as (see Appendix G):

$$\frac{P_{xy}^*}{\nu T^*} = -\eta\cos 2\phi - \frac{4(1+e)\nu g_0}{105\sqrt{\pi}}\Big[21R\Big\{8+\sqrt{\pi}\frac{\eta\cos 2\phi}{R}\Big\}+48\lambda^2 R \\ +4R^3\Big\{32-\frac{\eta^2}{R^2}\Big(2+(1+2\cos^2 2\phi)\Big)\Big\}\Big], \tag{3.104}$$

with the dimensionless temperature T^* being given by (3.103). The expression for the dimensionless shear viscosity, $\mu^*{=}{-}P_{xy}/\rho_p U_R^2{=}{-}P_{xy}^*$, follows from (3.104):

$$\mu^* = \frac{\nu\sqrt{T^*}}{8}\Bigg[\frac{\eta\cos 2\phi}{R}+\frac{4(1+e)\nu g_0}{105\sqrt{\pi}}\Big(21\Big\{8+\sqrt{\pi}\frac{\eta\cos 2\phi}{R}\Big\} \\ \underbrace{+48\lambda^2+128R^2-4\eta^2\Big\{2+(1+2\cos^2 2\phi)\Big\}}\Big)\Bigg], \tag{3.105}$$

where the under-braced terms represent nonlinear contributions beyond the Navier-Stokes (NS) order.

Neglecting quadratic- and higher-order terms in (5.50), we obtain the NS-order expression for the shear viscosity:

$$\mu_{NS}^* = \frac{\nu\sqrt{T^*}}{8}\Bigg[\frac{\eta\cos 2\phi}{R}+\frac{4(1+e)\nu g_0}{5}\Big(\frac{8}{\sqrt{\pi}}+\frac{\eta\cos 2\phi}{R}\Big)\Bigg]+O(R^2). \tag{3.106}$$

The elastic limit of the Burnett-order solution (3.93) for $\eta\cos 2\phi/R$, with $\phi\to 0$ (which holds at NS order),

$$\frac{\eta\cos 2\phi}{R}\xrightarrow[\phi=0]{e=1}\frac{5\sqrt{\pi}}{12}\left(\frac{1}{\nu g_0}+\frac{8}{5}\right), \tag{3.107}$$

can be substituted into (3.106) to arrive at

$$\mu_{NS}^{elastic} = \sqrt{T^*}\left[\frac{5\sqrt{\pi}}{96 g_0}\left(1+\frac{8}{5}\nu g_0\right)^2+\frac{8}{5\sqrt{\pi}}\nu^2 g_0\right]. \tag{3.108}$$

This expression (3.108) matches exactly with the shear viscosity for an elastic hard-sphere system (Chapman & Cowling 1970).

3.7.2 Normal Stress Components and the Pressure

The diagonal components of the stress tensor, correct up-to $O(\eta^m\lambda^n R^n \sin^q(2\phi),\ m+n+p+q\leq 4)$, have following expressions:

$$\frac{P^*_{xx}}{\nu T^*} = (1+\lambda^2+\eta\sin 2\phi)+\frac{2(1+e)\nu g_0}{1155}\Big[33(35+96R^2+14\eta\sin 2\phi+14\lambda^2) + \frac{8}{\sqrt{\pi}}\eta R\cos 2\phi\Big\{3(66+5\eta^2-22\lambda^2)-160R^2-22\eta\sin 2\phi\Big\}\Big], \tag{3.109}$$

$$\frac{P^*_{yy}}{\nu T^*} = (1+\lambda^2-\eta\sin 2\phi)+\frac{2(1+e)\nu g_0}{1155}\Big[33(35+96R^2-14\eta\sin 2\phi+14\lambda^2) + \frac{8}{\sqrt{\pi}}\eta R\cos 2\phi\Big\{3(66+5\eta^2-22\lambda^2)-160R^2+22\eta\sin 2\phi\Big\}\Big], \tag{3.110}$$

$$\frac{P^*_{zz}}{\nu T^*} = (1-2\lambda^2)+\frac{2(1+e)\nu g_0}{1155}\Big[33(35+32R^2-28\lambda^2) + \frac{8}{\sqrt{\pi}}\eta R\cos 2\phi\Big\{(66+3\eta^2-32R^2)\Big\}\Big]. \tag{3.111}$$

The dimensionless mean pressure, correct up-to $O(\eta^m\lambda^n R^n \sin^q(2\phi),\ m+n+p+q\leq 4)$, is given by

$$p^* = \nu T^*\Big[1+\frac{2(1+e)\nu g_0}{315}\Big\{315+\underbrace{672R^2+\frac{8}{\sqrt{\pi}}\eta R\cos 2\phi(42+3\eta^2-32R^2-12\lambda^2)}\Big\}\Big]. \tag{3.112}$$

Neglecting the 'under-braced' non-linear terms in (3.112), we obtain the well-known expression for pressure,

$$p^*_{NS} = \nu T^*(1+2(1+e)\nu g_0), \tag{3.113}$$

at the NS-order.

3.8 Normal Stress Differences and Their Origin

3.8.1 First Normal Stress Difference and Its Origin

Subtracting (3.110) from (3.109) the expression for the first normal stress difference (3.101) is found to be

$$\mathscr{N}_1^* = 2\eta\sin(2\phi)\left(1+\frac{4(1+e)\nu g_0}{105}\left[21-\frac{8}{\sqrt{\pi}}\eta R\cos(2\phi)\right]\right)\nu T^* + O(\eta^m\lambda^n R^n\sin^q(2\phi),\ m+n+p+q\geq 5), \tag{3.114}$$

with its kinetic and collisional contributions ($\mathscr{N}_1^* = \mathscr{N}_1^{k*} + \mathscr{N}_1^{c*}$), respectively, being given by

$$\mathscr{N}_1^{k*} = 2\eta\sin(2\phi)\nu T^* \tag{3.115}$$

$$\mathscr{N}_1^{c*} = \frac{8(1+e)\nu g_0}{1155}\left[231-\frac{8}{\sqrt{\pi}}\eta R\cos(2\phi)\right]\eta\sin(2\phi)\nu T^*. \tag{3.116}$$

Note that both (3.115) and (3.116) vanish in the limits of $\eta\to 0$ and/or $\phi\to 0$: while the former represents the limit of vanishing temperature anisotropy in the shear-plane (5.43), the latter correspond to the eigendirections of the second moment tensor $\boldsymbol{M}$ and the shear tensor $\boldsymbol{D}$ being *coaxial* (viz. figure 3.2). Therefore we conclude that the origin of first normal stress difference is tied to (i) the 'finite' temperature anisotropy and/or (ii) the 'non-coaxiality' between the eigendirections of $\boldsymbol{M}$ and $\boldsymbol{D}$ at any density.

The leading terms in both (3.115) and (3.116) are,

$$\eta\sin 2\phi = O\left(\dot{\gamma}^2\right), \tag{3.117}$$

of Burnett-order in the shear rate. The leading-order corrections in (3.116) are

$$R^2\eta\sin(2\phi)\left(\frac{\eta}{R}\cos(2\phi)\right) = O\left(\dot{\gamma}^4\right). \tag{3.118}$$

It is noteworthy that the excess temperature along the mean-vorticity direction (3.50), $T_z^{ex}\propto\lambda^2$, does not affect the kinetic part of first NSD, but it affects the collisional part of the first NSD at sixth-order and beyond in the shear rate.

3.8.2 Second Normal Stress Difference, Sign-reversal and Origin

Similarly, the expression for the second normal stress difference (3.102) is obtained from (3.110) and from (3.111):

$$\begin{aligned}\mathscr{N}_2^* &= \mathscr{N}_2^{k*} + \mathscr{N}_2^{c*} \\ &= \left[3\lambda^2 - \eta\sin(2\phi)\right]\nu T^* + \frac{32(1+e)\nu^2 T^* g_0}{1155}\left[264\left(\frac{1}{2}+\frac{7}{\nu}\mathscr{N}_2^{k*}\right)R^2\right. \\ &\left. + \frac{1}{\sqrt{\pi}}\eta R\cos 2\phi\left\{(66+6\eta^2-64R^2-33\lambda^2)+11\eta\sin 2\phi\right\}\right] \\ &\qquad + O(\eta^m\lambda^n R^n \sin^q(2\phi),\ m+n+p+q\geq 5), \end{aligned} \tag{3.119}$$

with its kinetic and collisional components at $O(\eta^m\lambda^{2n}R^p,\ m+n+p\leq 4)$ being given by

$$\mathscr{N}_2^{k*} = \left[3\lambda^2 - \eta\sin(2\phi)\right]\nu T^* \tag{3.120}$$

$$\begin{aligned}\mathscr{N}_2^{c*} = \frac{32(1+e)\nu^2 T^* g_0}{1155}&\left[264\left(\frac{1}{2}+\frac{7}{\nu}\mathscr{N}_2^{k*}\right)R^2 + \frac{1}{\sqrt{\pi}}\eta R\cos 2\phi\right. \\ &\left.\times\left\{(66+6\eta^2-64R^2-33\lambda^2)+11\eta\sin 2\phi\right\}\right].\end{aligned} \tag{3.121}$$

where T^* is the dimensionless temperature (3.103). In the limit of vanishing of the 'shear-plane' temperature-anisotropy ($\eta\to 0$) and/or the coaxiality ($\phi\to 0$) between the eigendirections of $\boldsymbol{M}$ and $\boldsymbol{D}$, we have

$$\mathscr{N}_2^{k*} = 3\lambda^2\nu T^* \propto T_z^{ex} \geq 0, \tag{3.122}$$

$$\mathscr{N}_2^{c*} = \frac{4(1+e)\nu^2 T^* g_0}{35}\left[32R^2+21\lambda^2\right] \geq 0, \tag{3.123}$$

where T_z^{ex} is the excess temperature (3.50). Both (3.122) and (3.123) hold strictly in the dense limit since η and ϕ approach zero as $\nu\to\nu_{\max}$. Equation (3.122) suggests that even the kinetic part of the second normal stress difference remains positive in the dense limit since $\lambda^2\propto T_z^{ex}>0$ in the dense limit (see figure 3.3).

It is evident from (3.122) and (3.123) that the second normal-stress difference in the dense limit (3.123) remains finite and positive which is in contrast to zero first normal stress difference in the same limit. Moreover, even if $\lambda^2=0$ and $\eta=0$, $\mathscr{N}_2$ remains finite as $\nu\to\nu_{\max}$ as long as the shear-rate is finite ($R^2>0$) and hence this is 'shear-induced'. Therefore, *the origin of non-zero second normal-stress difference in the dense limit is tied to the imposed shear field*.

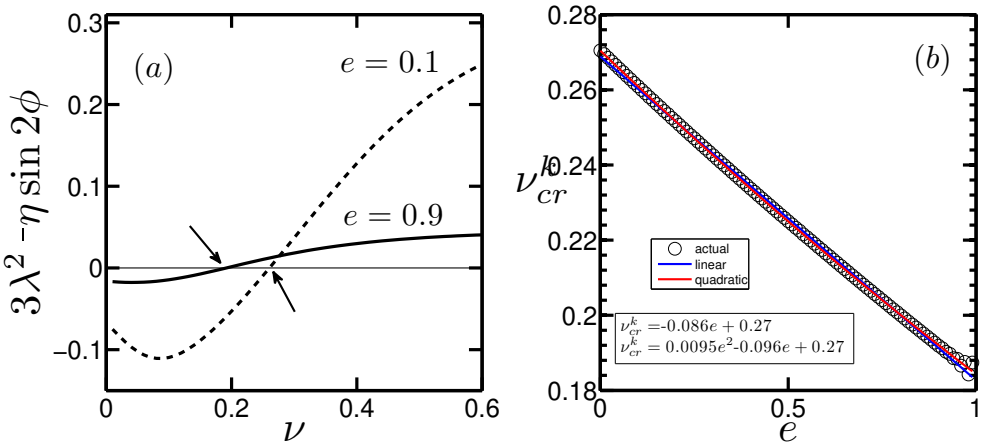

Fig. 3.5 (*a*) Variation of $(3\lambda^2 - \eta \sin 2\phi)$ with density ν for two values of restitution coefficient $e = 0.9$ (solid line) and $e = 0.1$ (dashed line). (*b*) Variation of the critical density ν^k_{cr}, at which $\eta \sin 2\phi = 3\lambda^2$, with e.

Equation (3.120) indicates that the $\mathscr{N}_2^{k*}$ can be positive or negative depending on the relative magnitudes of $3\lambda^2$ and $\eta \sin(2\phi)$ and can undergo a *sign-change* at a finite density if

$$3\lambda^2 - \eta \sin(2\phi) = 0. \tag{3.124}$$

The density-variation of (3.124), obtained by solving (3.71-3.74) numerically, as depicted in figure 3.5(a) clarifies the above point: $3\lambda^2 < \eta \sin(2\phi)$ in the dilute limit and $3\lambda^2 > \eta \sin(2\phi)$ in the dense limit for any value of the restitution coefficient. The variation of the critical density ν^k_{cr}, at which (3.124) holds, with the restitution coefficient is shown in figure 3.5(b) – clearly, $\nu^k_{cr}(e)$ is a decreasing function of e and can be fitted via the following linear function:

$$\nu^k_{cr}(e) = 0.27 - 0.086e. \tag{3.125}$$

Since $\mathscr{N}_2^c = 0$ at $\nu = 0$ and is a monotonically increasing function of ν, the critical density, ν_{cr}, at which total second normal stress difference ($\mathscr{N}_2 = \mathscr{N}_2^k + \mathscr{N}_2^c = 0$) changes sign from negative to positive would be slightly lower than (3.125).

In summary the second normal stress difference is negative and positive in the dilute and dense limits, respectively, and the 'sign-reversal' of $\mathscr{N}_2$ at some finite density is directly tied to the sign-reversal of its kinetic component $\mathscr{N}_2^k$. The above analysis further confirms that the origin of $\mathscr{N}_2$ is tied to the 'excess' temperature ($T_z^{ex} \propto \lambda^2$, viz. (3.50)) along the mean vorticity direction in the dilute limit, but its origin in the dense limit is tied to the imposed shear field.

3.9 Source of Second Moment and the Collisional Dissipation

In USF the collisional source of second moment (3.54) takes the following form:

$$\aleph = \begin{pmatrix} \aleph_{xx} & \aleph_{xy} & 0 \\ \aleph_{yx} & \aleph_{yy} & 0 \\ 0 & 0 & \aleph_{zz} \end{pmatrix}, \tag{3.126}$$

with its non-zero components being given by

$$\left.\begin{aligned} \aleph_{xx} &= A_{xx} + \widehat{E}_{xx} + \widehat{G}_{xx} + 2\dot{\gamma}\Theta_{xy} \\ \aleph_{yy} &= A_{yy} + \widehat{E}_{yy} + \widehat{G}_{yy} - 2\dot{\gamma}\Theta_{xy} \\ \aleph_{zz} &= A_{zz} + \widehat{E}_{zz} + \widehat{G}_{zz} \\ \aleph_{xy} &= A_{xy} + \widehat{E}_{xy} + \widehat{G}_{xy} + \dot{\gamma}(\Theta_{yy} - \Theta_{xx}) \end{aligned}\right\}. \tag{3.127}$$

The integral expressions for $\Theta_{\alpha\beta}$ (3.53), $A_{\alpha\beta}$ (3.55), $E_{\alpha\beta}$ (3.56) and $G_{\alpha\beta}$ (3.57) have been evaluated in terms of η, λ and R, correct up-to $O(\eta^m\lambda^n R^p \sin^q(2\phi), m+n+p+q \leq 4)$, and the resulting truncated series for (3.127) are written down in Appendix I.

3.9.1 Collisional Dissipation

The constitutive expression for the collisional dissipation rate (3.20) follows directly from the trace of (3.126):

$$\begin{aligned} \mathscr{D} &= -\frac{1}{2}\aleph_{\beta\beta} = -\frac{1}{2}(A_{xx} + A_{yy} + A_{zz}) = \frac{3(1-e^2)\rho\nu g_0 T^{\frac{3}{2}}}{\sigma\pi^{\frac{3}{2}}}\mathscr{H}^{10}_{003}(\eta, \lambda^2, R, \phi) \\ &= \frac{\rho\nu g_0(1-e^2)T^{\frac{3}{2}}}{70\sigma\sqrt{\pi}}\Big[840 + 32\Big\{\Big(84 + 21\sqrt{\pi}\frac{\eta}{R}\cos 2\phi\Big) + 32R^2 - 2\eta^2(2+\cos 4\phi) + 24\lambda^2\Big\}R^2 \\ &\qquad + 3(28\eta^2 + \eta^4 - 8\eta^2\lambda^2 + 84\lambda^4)\Big], \end{aligned} \tag{3.128}$$

where we have made use of the last equation in (3.76) and the related series expansion for $\mathscr{H}^{10}_{003}$ by retaining terms up-to $O(\eta^m\lambda^n R^n \sin^q(2\phi),\ m+n+p+q \leq 4)$. In the isotropic limit ($\eta \to 0$ and $\lambda^2 \to 0$), we obtain

$$\mathscr{D} = \mathscr{D}^0\left(1 + \frac{16}{5}R^2 + \frac{128}{105}R^4\right), \tag{3.129}$$

where

$$\mathscr{D}^0 = \frac{12\rho_p \nu^2 g_0 (1-e^2) T^{\frac{3}{2}}}{\sigma\sqrt{\pi}} \tag{3.130}$$

is the corresponding bare part valid at NS-order (Jenkins & Richman 1985*a*). Returning to (3.128), we note that the correction terms beyond the NS-order depend quadratically on (i) the shear rate ($\dot{\gamma} \sim R$), (ii) the temperature anisotropy η, and (iii) the excess temperature, $\lambda^2 \propto T_z^{ex}$, along the vorticity direction. The quadratic-order shear rate dependence in (3.129) agrees qualitatively with that calculated by Sela & Goldhirsch (1998) via a Burnett-order Chapman-Enskog expansion of inelastic Boltzmann equation. The latter two findings (ii-iii) indicate that the collisional dissipation depends on both normal stress differences,

$$\mathscr{D} \equiv \mathscr{D}(\cdots; \mathscr{N}_1, \mathscr{N}_2), \tag{3.131}$$

since $(\eta, \lambda) \sim (\mathscr{N}_1, \mathscr{N}_2)$ as we demonstrate below.

3.9.2 Dilute Limit: Dependence on NSDs

To clarify the dependence of collisional dissipation (3.131) on normal stress differences, here we consider the dilute limit of (3.128). Recall that the leading-order moment equations admit an exact solution in the dilute limit ($\nu \to 0$):

$$\left.\begin{array}{rl} \eta^2 & = \frac{1}{12}\left(6 + \mathscr{N}_1^k + 2\mathscr{N}_2^k\right)\mathscr{N}_1^k \\ \lambda^2 & = \frac{1}{6}\left(\mathscr{N}_1^k + 2\mathscr{N}_2^k\right) \end{array}\right\}, \tag{3.132}$$

where $\mathscr{N}_1^k = (P_{xx}^k - P_{yy}^k)/p$ and $\mathscr{N}_2^k = (P_{yy}^k - P_{zz}^k)/p$ are the kinetic parts of the 'scaled' first and second normal stress differences, respectively. Substituting (3.132) into (3.128) and retaining terms up-to quadratic-order in $\mathscr{N}_1^k$ and $\mathscr{N}_2^k$, we obtain the following expression for the collisional dissipation rate,

$$\begin{aligned} \mathscr{D} &= \frac{3\rho_p \nu^2 (1-e^2) T^{\frac{3}{2}}}{70\sigma\sqrt{\pi}} \left[280 + \eta^2(28 + \eta^2 - 8\lambda^2) + 84\lambda^4\right] + h.o.t., \\ &= \frac{3\rho_p \nu^2 (1-e^2) T^{\frac{3}{2}}}{70\sigma\sqrt{\pi}} \left[280 + \frac{\mathscr{N}_1^k}{2}\left(28 + \frac{1}{2}\mathscr{N}_1^k + \frac{10}{3}\left(\mathscr{N}_1^k + 2\mathscr{N}_2^k\right)\right)\right. \\ &\qquad \left. + \frac{7}{3}\left(\mathscr{N}_1^k + 2\mathscr{N}_2^k\right)^2\right] + O\left((N_i^k)^3\right), \end{aligned} \tag{3.133}$$

which holds in the dilute limit. That the Grad-level dissipation rate depends on the normal stress difference was pointed out previously (Saha & Alam 2014) for the case of granular shear flow in two-dimensions.

3.10 Validation of Constitutive Relations

In this section we probe the range of validity of the analytical constitutive relations for the shear viscosity (§3.7.1), the pressure (§3.7.2), and the two normal stress differences (§3.8) that are obtained by solving the 'truncated' second-moment equations (3.92), (3.83) and (3.84) at second- third- and fourth-order, respectively. These approximate solutions are then compared with the numerical solution of the full second moment equation (3.71-3.74) as functions of the density (ν) and the restitution coefficient (e). It may be recalled from the analysis in §3.5.3 that the transport coefficients obtained using the solutions of (3.92), (3.83) and (3.84) for η, λ, R and ϕ are referred as the 'Burnett' 'super-Burnett' and 'super^2-Burnett' solutions, respectively.

For the 'exact' numerical solution of (3.71-3.74), first we evaluate the integrals $\mathscr{H}^{\delta p}_{\alpha\beta\gamma}$ (3.78), $\mathscr{J}^{\delta p}_{\alpha\beta\gamma}$ (3.79), and $\mathscr{K}^{\delta p}_{\alpha\beta}$ (3.80), that appear in (3.76-3.77), numerically using the standard quadrature rule. Substituting the numerically evaluated integrals into (3.71-3.74) results in a system of nonlinear algebraic equations which again is solved by the same Newton's method. The values of η,λ, R and ϕ thus obtained are inserted into the expressions for pressure (p, G.6), viscosity (μ, G.8) and the normal stress differences ($\mathscr{N}_1$ and $\mathscr{N}_2$, G.9) as given in Appendix G. Such numerically obtained transport coefficients are dubbed 'exact' numerical solution since a very high accurate solution can be obtained, limited only by (i) the truncation error of the quadrature rule and (ii) the machine precision.

In the following, such exact numerical solutions for p, μ, T, $\mathscr{N}_1$ and $\mathscr{N}_2$ are compared with those obtained from (i) the (exact) Burnett-order solution and (ii) the perturbation solution at fourth order for η, λ, R and ϕ.

3.10.1 Comparison Between Analytical and Exact Numerical Solutions

Figure 3.6(a-d) shows a comparison within the 'exact' numerical solution of second-moment equations, the exact Burnett order solutions and the perturbative fourth order solutions for the variations of the shear-plane anisotropy η, the excess temperature λ^2, the dimensionless shear rate R, and the non-coaxiality angle ϕ (degrees) with density (ν) for three values of the restitution coefficient $e = 0.9,\ 0.7,\ 0.5$. In each panel, while the solid black lines denote the exact solution, the blue dashed lines and red dot-dashed lines denote the series solutions at second-order and fourth-order, respectively. It is seen that while the second-order solution provides a good agreement for η, λ^2, ϕ and R up-to a restitution coefficient of $e \geq 0.9$, the fourth-order solution is required for more dissipative particles ($e = 0.7$) for a reasonable agreement over the whole range of density (for λ^2 and R, see panels b and c respectively). On the other hand, panels a and d indicate that even the 4th-order solution for the shear-plane anisotropy η and

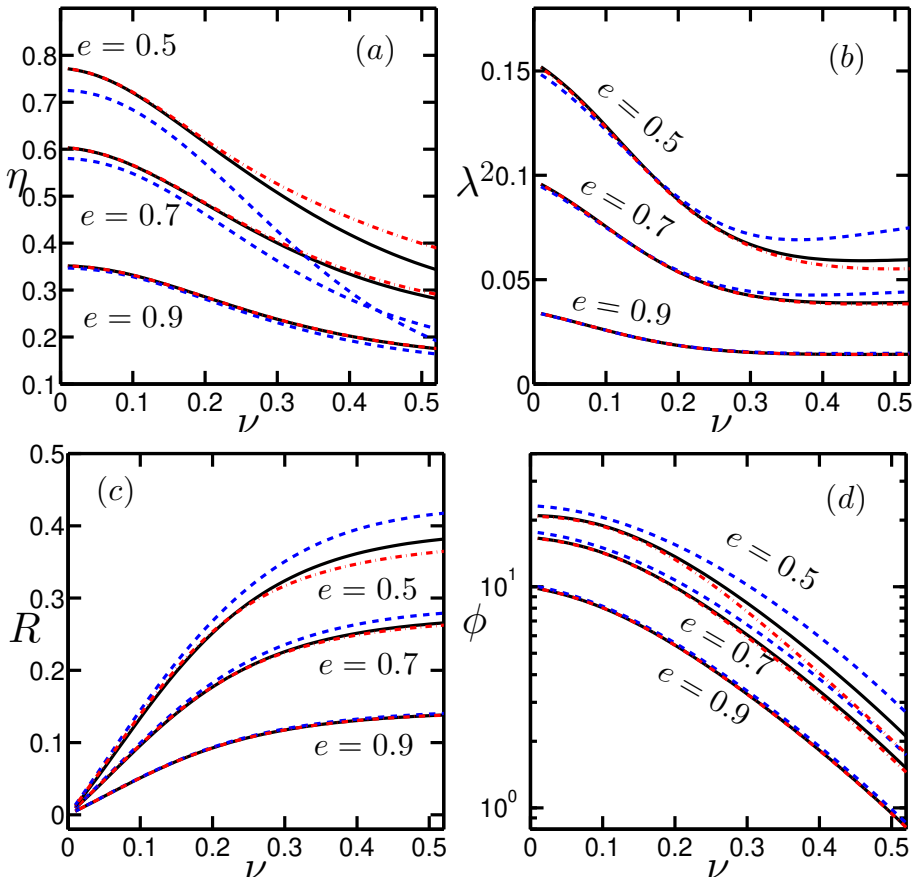

Fig. 3.6 Variations of (a) η, (b) λ^2, (c) R, and (d) ϕ (degrees) with density (ν). While the solid black lines denote the exact numerical solution of second moment equations, the blue dashed and red dot-dashed lines denote the exact Burnett-order solution and the perturbation solution at fourth-order, respectively.

the non-coaxiality angle ϕ is not adequate at $e = 0.5$ in the dense limit (for $\nu > 0.3$). Since all transport coefficients in USF are functions of η, λ^2, ϕ and R, next we will check the ability of the exact second- (Burnett) and fourth-order approximations (super-super-Burnett) of the second-moment equation to predict p, μ, T, $\mathscr{N}_1$ and $\mathscr{N}_2$.

Figure 3.7(*a-c*) displays the density variations of (*a*) the pressure p, (*b*) the shear viscosity μ and (*c*) granular temperature T for three different values of the restitution coefficient $e = 0.9$, 0.7 and 0.5. In each panel, the 'exact' numerical solution (denoted by the black solid line) is compared with (i) Burnett order (blue dashed line) and (ii) the perturbation solution at fourth-order (red dot-dash line) It is seen that the Burnett-order solutions for p, μ and T are almost indistinguishable from their exact numerical value for small dissipation ($e = 0.9$); moreover, this agreement seems to hold uniformly for the whole range of density. On the other hand, retaining the fourth order terms yields a better agreement for p, μ and T at large dissipation ($e = 0.5$).

The ability of the fourth-order series solution to quantitatively predict p and μ at any density also holds for both the first and second normal stress differences, see figures 3.8(*a*,*b*). Note that the plotted quantities in figure 3.8 are the 'scaled' first and second normal stress differences defined via

$$\mathscr{N}_1 = \frac{P_{xx} - P_{yy}}{p} \tag{3.134}$$

$$\mathscr{N}_2 = \frac{P_{yy} - P_{zz}}{p} \tag{3.135}$$

respectively, with the expressions for P_{xx}, P_{yy}, P_{zz} and p given in (3.109-3.112); equations (3.134) and (3.135) are measures of two normal stress differences with respect to the mean pressure. In figure 3.8(*b*) we find that $\mathscr{N}_2$ undergoes a sign reversal at some finite density. The location ($\nu = \nu_{cr}$) of the sign-reversal of $\mathscr{N}_2$ appears to be independent of the restitution coefficient as it is evident from figure 3.8(*b*). This finding should be contrasted with the sign-reversal of the kinetic component ($\mathscr{N}_2^k$) of the second normal stress difference in figure 3.5 which indicates that ν_{cr}^k (at which $\mathscr{N}_2^k = 0$, figure 3.5*b*) is a decreasing function of e. The dependence of the collisional component of the stress on e is likely to be responsible for the independence of this critical density (ν_{cr} at which $\mathscr{N}_2 = \mathscr{N}_2^k + \mathscr{N}_2^c = 0$) on the restitution coefficient.

3.10.2 Comparison with Simulation

The molecular dynamic event-driven simulations data for the uniform shear flow of inelastic hard-spheres, previously carried out by Alam & Luding (2005*b*) for a restitution coefficient

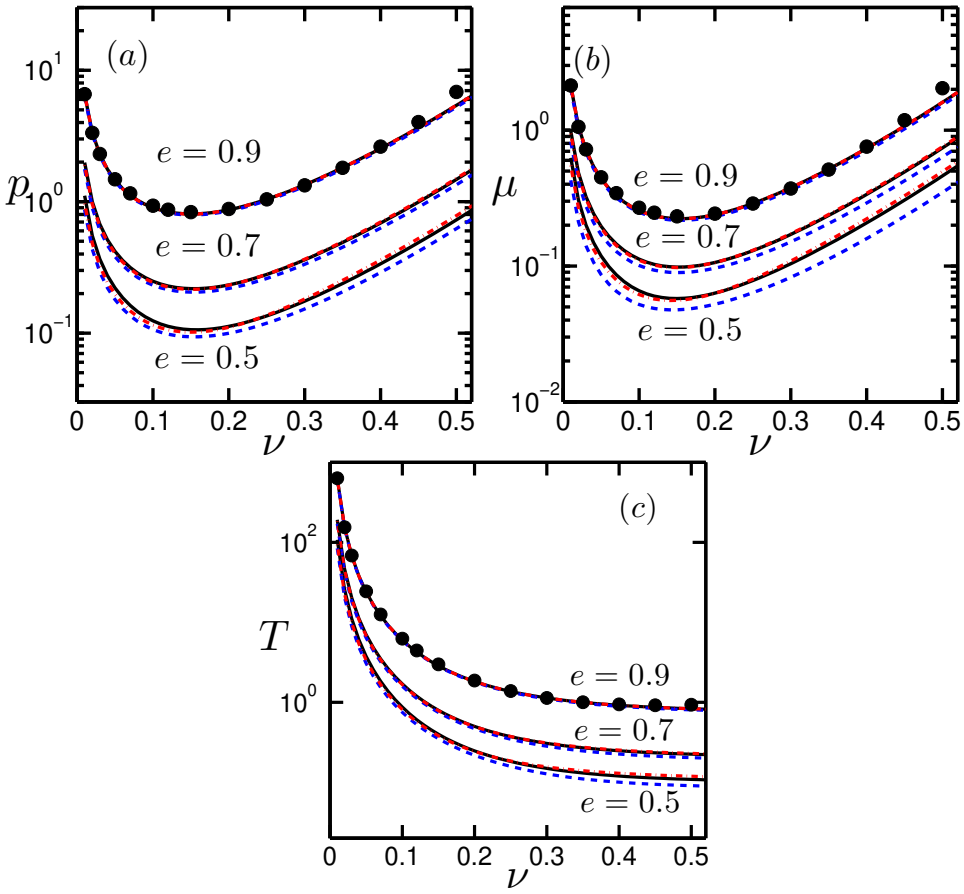

Fig. 3.7 Comparison between the 'Burnett-order' analytical solution (blue dashed lines), fourth order perturbation solution (red dot-dashed lines) and the 'exact' numerical solution (solid black lines) for (*a*) pressure, (*b*) shear viscosity and (*c*) granular temperature with volume fraction (ν) for different values of e. The filled circles represent the molecular dynamic event-driven simulations data of (Alam & Luding 2005*b*) for $e = 0.9$.

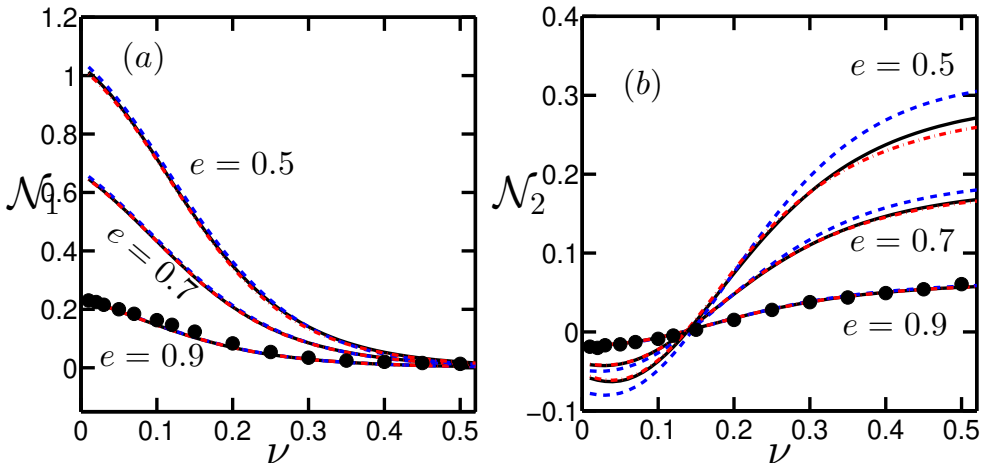

Fig. 3.8 Same as figure 3.7 but for the variations of (a) the first ($\mathscr{N}_1$,) and (b) the second ($\mathscr{N}_2$) normal stress differences with density (ν).

of $e = 0.9$, are superimposed in figures 3.7 and 3.8. Note that Alam & Luding (2005*b*) used event-driven techniques to conduct these simulations of smooth inelastic hard-spheres in a cubic box by implementing the Lees-Edwards boundary condition (Lees & Edwards 1972) along the gradient (y) direction with periodic boundary conditions along the stream-wise (x) and span-wise (z) directions – the other details of simulation can be obtained from the original paper. Figure 3.7(*a-c*) indicates that our theoretical predictions are in good agreement with the simulation data for p, μ and T as well as for two normal stress differences $\mathscr{N}_1$ and $\mathscr{N}_2$ (figure 3.8).

The above comparative study in figures 3.6, 3.7, 3.8 and 3.9 suggests that the terms retained up-to the fourth-order (super^2-Burnett solutions) in the series expansion (3.81–3.82) of the second-moment equation provide an adequate accuracy to predict all transport coefficients (p, μ, $\mathscr{N}_1$ and $\mathscr{N}_2$) in the uniform shear flow. This in turn implies that the super-super-Burnett terms (i.e. fourth-order in the shear rate) must be retained to predict the correct behaviour of p, μ, $\mathscr{N}_1$ and $\mathscr{N}_2$ for all values of ν and e.

3.11 Dense limit: Approximate Solution and Its Validation

Here we determine an approximate solution of the second-moment balance equations (3.71-3.74) which is likely to hold in the dense limit ($\nu \to \nu_{\max}$). Since the collisional mechanism of momentum transfer dominates over its kinetic contribution as $\nu \to \nu_{\max}$, the stress tensor can be approximated by

$$P_{\alpha\beta} = \Theta_{\alpha\beta}. \tag{3.136}$$

Therefore the balance equations (3.71-3.74) simplify to

$$\left.\begin{aligned} 2\dot{\gamma}[(\Theta_{x'x'}-\Theta_{y'y'})\cos 2\phi - 2\Theta_{x'y'}\sin 2\phi] &= (A_{x'x'}+A_{y'y'}+A_{z'z'}),\\ 2\dot{\gamma}[(\Theta_{x'x'}-\Theta_{y'y'})\cos 2\phi - 2\Theta_{x'y'}\sin 2\phi] &= -3\widehat{\Gamma}_{z'z'},\\ 2\dot{\gamma}(\Theta_{x'x'}+\Theta_{y'y'})\cos 2\phi &= (\Gamma_{x'x'}-\Gamma_{y'y'}),\\ -(\Theta_{x'x'}+\Theta_{y'y'})\dot{\gamma}\sin 2\phi &= \Gamma_{x'y'}, \end{aligned}\right\} \tag{3.137}$$

Substituting the expressions of the integrals $(\Theta_{x'x'}+\Theta_{y'y'})$ and $\Gamma_{x'y'}$ into the last equation yields $\phi = 0$, which implies that the eigenvectors of the shear tensor $\boldsymbol{D}$ and the second-moment tensor $\boldsymbol{M}$ becomes *co-axial* at $\nu \to \nu_{\max}$. We are now left with η, λ^2 and R to solve for.

3.11.1 Approximate Solutions in the Dense Limit

Let us simplify (3.137) by retaining terms up-to $O(\eta\lambda^2 R)^2$:

$$\left.\begin{aligned} &32(1+3e)R^2 - 8(1-3e)\sqrt{\pi}R\eta - 3(1-e)\eta^2 - 9(1-e)\lambda^4 - 30(1-e) = 0,\\ &32(1+3e)R^2 - 8(4-3e)\sqrt{\pi}R\eta - 3(3-e)\eta^2 - 63(3-e)\lambda^2 + 9(3-e)\lambda^4 = 0,\\ &8(4-3e)\sqrt{\pi}R\lambda^2 + 6(3-e)\eta\lambda^2 + 14(1-3e)\sqrt{\pi}R + 21(3-e)\eta = 0. \end{aligned}\right\} \tag{3.138}$$

The solutions of these equations are given by

$$\left.\begin{aligned} \eta^2 &= \tfrac{1}{(-238+42e-40\mathscr{X})}\Big\{70 - 281\mathscr{X} - 924\mathscr{X}^2 + 192\mathscr{X}^3\\ &-e(280 - 1190\mathscr{X} - 798\mathscr{X}^2 + 240\mathscr{X}^3) + 3e^2(70 - 107\mathscr{X} - 42\mathscr{X}^2 + 24\mathscr{X}^3)\Big\},\\ R^2 &= \tfrac{1}{64(1+3e)(-119+21e-20\mathscr{X})}\Big[3\Big\{3e^3(210 - 401\mathscr{X} + 42\mathscr{X}^2 + 24\mathscr{X}^3)\\ &-3(1050 - 1457\mathscr{X} + 378\mathscr{X}^2 + 72\mathscr{X}^3) - e^2(3570 - 8621\mathscr{X} + 546\mathscr{X}^2 + 456\mathscr{X}^3)\\ &+e(6090 - 16493\mathscr{X} + 882\mathscr{X}^2 + 792\mathscr{X}^3)\Big\}\Big], \end{aligned}\right\} \tag{3.139}$$

where $\lambda^2 = \mathscr{X}$. Inserting (3.139) into (3.138) yields a fourth-order equation in $\mathscr{X}$, which after retaining terms only up-to quadratic-order in $\lambda^2 = \mathscr{X}$ yields

$$\begin{aligned} &(81792 + 199824e - 130560e^2 + 18288e^3 + 20666\pi - 88562e\pi + 74982e^2\pi - 11790e^3\pi)\mathscr{X}^2\\ &+(202104 + 485016e - 345912e^2 + 53928e^3 - 6601\pi - 26201e\pi + 83433e^2\pi - 17703e^3\pi)\mathscr{X}\\ &-35280 - 58800e + 129360e^2 - 35280e^3 - 7350\pi + 33810e\pi - 39690e^2\pi + 13230e^3\pi = 0. \end{aligned} \tag{3.140}$$

The above solution (3.139) and (3.140) can be further simplified if we remove λ^4-terms from (3.138). The resulting equations admit an explicit solution (Alam & Saha 2017):

$$\left.\begin{aligned} \eta &= 0, \\ \lambda^2 &= \tfrac{10(1-e)}{21(3-e)}, \\ R^2 &= \tfrac{15(1-e)}{16(1+3e)}, \\ \phi &= 0. \end{aligned}\right\} \tag{3.141}$$

Since $\eta, \phi \to 0$, the first normal stress difference ($\mathscr{N}_1 \propto \eta \sin 2\phi$) vanishes as $\nu \to \nu_{\max}$, but the second normal stress difference remains finite ($\mathscr{N}_2 \propto \lambda^2 \neq 0$) in the dense limit. The solution (3.141) indicates that $R, \lambda \sim \sqrt{(1-e)}$ and therefore both the shear-rate and the excess temperature scale with inelasticity as $\sqrt{(1-e)}$ in the dense limit.

Employing (3.141), all transport coefficients (p, μ, $\mathscr{N}_1$ and $\mathscr{N}_2$) can now be calculated as functions of ν and e as follows:

$$\begin{aligned}
p^* \approx p^{c*} &\equiv \frac{(1+e)\nu^2 g_0}{110880R^2}\Big\{3465+7392R^2 \\
&+\frac{8}{\sqrt{\pi}}\eta R\cos 2\phi(462+33\eta^2-352R^2-132\lambda^2+99\lambda^4)\Big\}, \\
&= \frac{(1+e)\nu^2 g_0}{32R^2}\left(1+\frac{32}{15}R^2\right) \qquad (3.142)\\
\mu^* \approx \mu^{c*} &\equiv \frac{(1+e)\nu^2 g_0}{18480\sqrt{\pi}R}\Big[3\Big\{616+77\sqrt{\pi}\frac{\eta\cos 2\phi}{R}+4\lambda^2(44+8\eta^2-11\lambda^2+4\lambda^4\Big\} \\
&+128(11-4\lambda^2)R^2-4\eta^2\Big\{22+(11-12\lambda^2)(1+2\cos^2 2\phi)\Big\}\Big], \\
&= \frac{(1+e)\nu^2 g_0}{4620\sqrt{\pi}R}\Big[3\Big\{154+\lambda^2(44-11\lambda^2+4\lambda^4\Big\}+32(11-4\lambda^2)R^2\Big], \qquad (3.143)\\
\mathscr{N}_1 \approx &\frac{P^c_{xx}-P^c_{yy}}{p^c} \\
&= \frac{12\Big\{231-\frac{8}{\sqrt{\pi}}\eta R(11-12\lambda^2)\cos 2\phi\Big\}\eta\sin 2\phi}{\Big\{231(15+32R^2)+\frac{8}{\sqrt{\pi}}\eta R\cos 2\phi(462+33\eta^2-352R^2-132\lambda^2+99\lambda^4)\Big\}}, \\
&= 0 \qquad (3.144)\\
\mathscr{N}_2 \approx &\frac{P^c_{yy}-P^c_{zz}}{p^c} = \\
&6\Big[33(32R^2-7\eta\sin 2\phi+21\lambda^2)+ \\
&\frac{\frac{8}{\sqrt{\pi}}\eta R\cos 2\phi\Big\{66+6\eta^2-64R^2-33\lambda^2+18\lambda^4+\eta(11-12\lambda^2)\sin 2\phi\Big\}\Big]}{\Big\{231(15+32R^2)+\frac{8}{\sqrt{\pi}}\eta R\cos 2\phi(462+33\eta^2-352R^2-132\lambda^2+99\lambda^4)\Big\}}, \\
&= \frac{6(32R^2+21\lambda^2)}{7(15+32R^2)}, \qquad (3.145)
\end{aligned}$$

where we have retained only the collisional contributions to the stress tensor.

3.11.2 Validation of the Dense Limit Solution

The density-variations of the pressure, shear viscosity and granular temperature for $\nu=(0.5,0.64)$ are displayed in figures 3.9(a), 3.9(b) and 3.9(c), respectively. In each panel, while the blue solid line denotes the 'exact' numerical solution of the second-moment equation with the radial distribution function being given by (3.31) of Carnahan & Starling (1969), the black solid

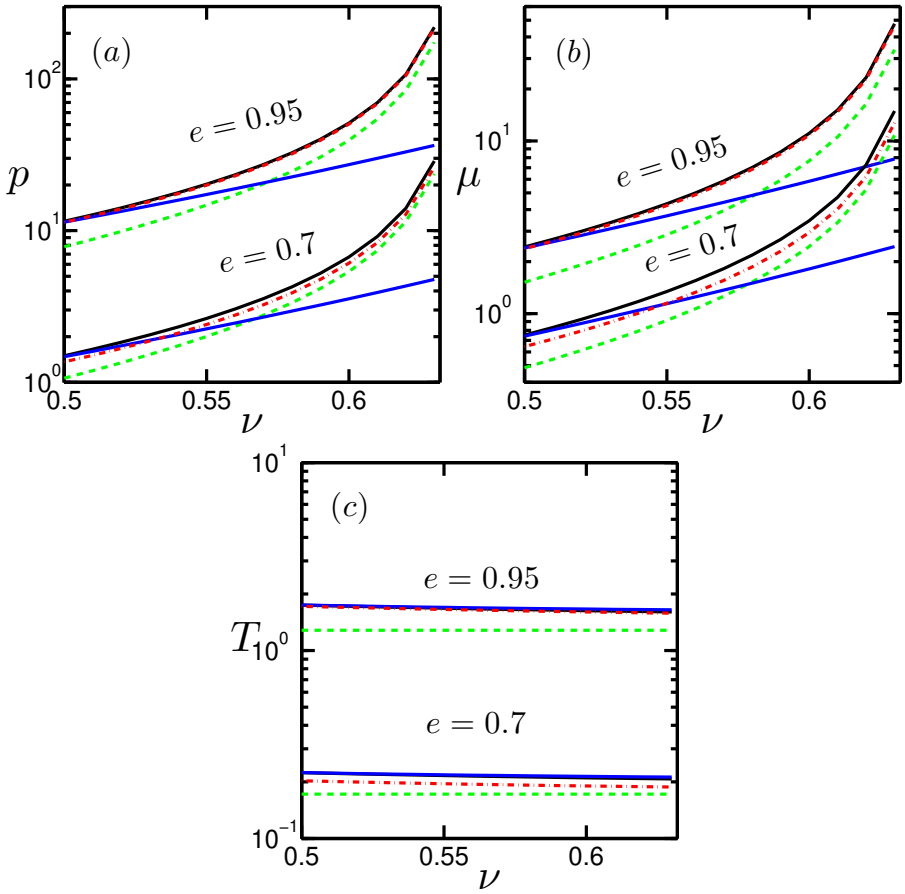

Fig. 3.9 Comparison of 'dense-limit' analytical solution (green dashed lines) for (a) pressure (3.142), (b) shear viscosity (3.143) and (c) granular temperature with their 'exact' numerical solution for (i) Carnahan-Starling (3.31, blue solid line) and (ii) Torquato's (3.146, black solid line) radial distribution function. The red dot-dash line in each panel represents the 'leading-order' closed-form solution (3.93-3.94).

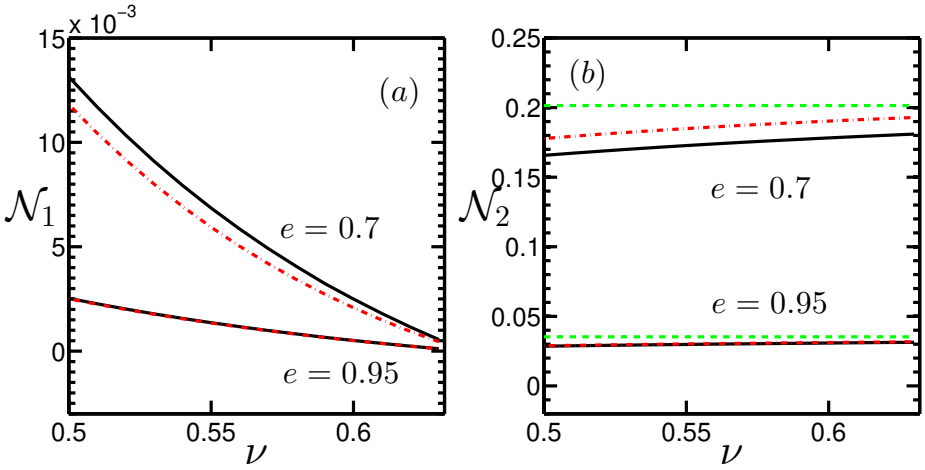

Fig. 3.10 Same as figure 3.9 but for (*a*) the first ($\mathcal{N}_1$) and (*b*) the second ($\mathcal{N}_2$) normal stress differences. The black solid line, the green dashed line and the red dot-dash line represent the exact numerical solution, approximate dense-limit solution (3.144-3.145) and the leading-order solution (3.93-3.94), respectively.

line represents the same with the following radial distribution function (Torquato 1995)

$$g_0(\nu) = \begin{cases} \frac{2-\nu}{2(1-\nu)^3}, & \text{if} \quad \nu \leq 0.49 \\ \frac{2-0.49}{2(1-0.49)^3}\frac{(\nu_{\max}-0.49)}{(\nu_{\max}-\nu)}, & 0.49 < \nu < 0.64, \end{cases} \tag{3.146}$$

where $\nu_{\max} = 0.64$ is taken as the random packing limit (or, the jamming density) and $\nu = 0.49 \approx \nu_f$ represents the freezing-density of a hard-sphere system. Our approximate dense-limit solution (3.142-3.143) is marked by the green dash-line in each panel of figure 3.9; we have also superimposed the leading-order solution (3.93-3.94) denoted by the red dot-dash line. It is seen that while the dense-limit solution (3.142-3.143) agrees qualitatively with with the respective exact (black solid line) numerical solution, the leading-order solution (3.93-3.94) agree quantitatively (for $e = 0.95$) with the exact (black solid line) numerical solution. Expectedly, the pressure (figure 3.9*a*) and shear viscosity (figure 3.9*b*) calculated using the Carnahan-Starling radial distribution function (3.31) deviates from those calculated using (3.146) since the former has a singularity at $\nu = 1$. In fact, Torquato's expression (3.146) is valid for the whole range of density (for an 'equilibrium' hard-sphere system) up-to the maximum packing limit ($\nu_{\max} \sim 0.64$), while the Carnahan-Starling form (3.31) may be used up-to the freezing density ($\nu_f \sim 0.49$).

Figures 3.10(*a*) and 3.10(*b*) compare the above two dense-limit solutions for the first and second normal stress differences, respectively, with the respective exact numerical-solution

(the black solid line, with (3.146)). It may be noted that $\mathscr{N}_1 = 0$ for our approximate dense-limit solution (3.144) since the non-coaxiality angle (ϕ) is zero, but $\mathscr{N}_2 \neq 0$ as in (3.145). On the other hand, our leading-order solution (3.93-3.94) for the whole range of density predicts a non-zero $\mathscr{N}_1$ for $\nu < \nu_{\max}$ (denoted by the red dot-dash line in figure 3.10*a*) which closely follows the exact numerical solution for $\mathscr{N}_1$. In particular, the agreement between the leading-order (red dot-dash line) and exact (black line) solutions for both $\mathscr{N}_1$ and $\mathscr{N}_2$ is very good at $e = 0.95$, but the deviation increases with decreasing restitution coefficient.

Collectively, the comparative analysis in figures 3.9 and 3.10 suggests that our leading-order solution (3.93-3.94) can be used as a first approximation to predict all transport coefficients (p, μ, $\mathscr{N}_1$ and $\mathscr{N}_2$) in the dense limit. On the other hand, the present dense-limit solution (3.141) can also be improved by incorporating next higher-order terms in future.

3.12 Granular Heat Flux and Thermal Conductivity

For the uniform shear flow, the granular heat flux vanishes identically since the gradients of hydrodynamic fields (the number density, the shear rate and the second moment) are zero for which the anisotropic Maxwellian (3.33) was chosen as the single-particle distribution function. Therefore we need to determine the distribution function for the 'non-USF' having finite gradients of hydrodynamic fields. To do this, we carry out a perturbation expansion around the USF with the anisotropic Maxwellian being zeroth-order distribution function. The resultant analysis is similar to our previous work (Saha & Alam 2014) on inelastic hard-disks, and the related details for the present case of hard-spheres are discussed below.

With respect to the anisotropic Maxwellian as the weight function and applying Gram-Schmidt orthogonalization procedure along with the following definition of the inner product

$$\langle \phi, \psi \rangle = \frac{1}{2\pi |\boldsymbol{M}|^{\frac{1}{2}}} \int \phi \psi \exp\Big(-\frac{1}{2} \boldsymbol{C} \cdot \boldsymbol{M}^{-1} \cdot \boldsymbol{C} \Big) d\mathbf{C}, \tag{3.147}$$

we obtain a set of orthonormal polynomials $\Big\{ \mathscr{P}^{(0)}, \mathscr{P}^{(1)}_1, \mathscr{P}^{(1)}_2, \mathscr{P}^{(1)}_3, \mathscr{P}^{(2)}_{11}, \mathscr{P}^{(2)}_{12}, \mathscr{P}^{(2)}_{22}, \mathscr{P}^{(2)}_{33}, \mathscr{P}^{(3)}_{ii1}, \mathscr{P}^{(3)}_{ii2}, \mathscr{P}^{(3)}_{ii3} \Big\}$. The explicit expressions of $\mathscr{P}^{(k)}_i$ and $\mathscr{P}^{(k)}_{ij}$ are omitted for the sake of brevity. In an analogous approach, the distribution function for the non-USF can be written as

$$f^{(1)} = f^{(0)} \Big(a + a_i C_i + a_{xx} C_x^2 + 2 a_{xy} C_x C_y + a_{yy} C_y^2 + a_{zz} C_z^2 + b_i C^2 C_i \Big). \tag{3.148}$$

where $f^{(0)}$ represents the anisotropic-Maxwellian state (3.33). To determine a, a_i, a_{xx}, a_{xy}, a_{yy}, a_{zz} and b_i, the following compatibility conditions must be satisfied

$$\int f^{(1)}(\boldsymbol{c},\boldsymbol{x},t)d\boldsymbol{c} = n(\boldsymbol{x},t) = \int f^{(0)}(\boldsymbol{c},\boldsymbol{x},t)d\boldsymbol{c}, \tag{3.149}$$

$$\int \boldsymbol{C} f^{(1)}(\mathbf{c},\boldsymbol{x},t)d\mathbf{c} = 0 = \int \boldsymbol{C} f^{(0)}(\mathbf{c},\boldsymbol{x},t)d\mathbf{c}, \tag{3.150}$$

$$m\int C_\alpha C_\beta f^{(1)}(\mathbf{c},\boldsymbol{x},t)d\mathbf{c} = P_{\alpha\beta} = m\int C_\alpha C_\beta f^{(0)}(\mathbf{c},\boldsymbol{x},t)d\mathbf{c}, \tag{3.151}$$

along with the definition of the heat-flux vector

$$q_\alpha = \frac{m}{2}\int C^2 C_\alpha f^{(1)}(\mathbf{c},\boldsymbol{x},t)d\mathbf{c}. \tag{3.152}$$

The solutions for the constants are

$$\left.\begin{aligned}
&a = 1, \qquad a_{xx} = a_{xy} = a_{yy} = a_{zz} = 0,\\
&a_x = \tfrac{1}{\rho\mathfrak{d}}\Big[\Big\{8M_{xy}^4 - 2\Big[(3M_{yy}-M_{zz})M_{zz} + M_{xx}(8M_{yy}+M_{zz})\Big]M_{xy}^2\\
&\quad -M_{yy}(3M_{xx}+M_{yy}+M_{zz})(M_{xx}^2+3M_{yy}^2+M_{zz}^2)\Big\}q_x\\
&\quad +M_{xy}\Big\{3(M_{xx}+M_{yy})^3 + (3M_{xx}^2+2M_{xx}M_{yy}+3M_{yy}^2+4M_{xy}^2)M_{zz}\\
&\quad +(M_{xx}+M_{yy}+M_{zz})M_{zz}^2\Big\}q_y\Big],\\
&a_y = \tfrac{1}{\rho\mathfrak{d}}\Big[M_{xy}\Big\{3(M_{xx}+M_{yy})^3 + (3M_{xx}^2+2M_{xx}M_{yy}+3M_{yy}^2+4M_{xy}^2)M_{zz}\\
&\quad +(M_{xx}+M_{yy}+M_{zz})M_{zz}^2\Big\}q_x\\
&\quad +\Big\{8M_{xy}^4 - 2\Big[(3M_{xx}-M_{zz})M_{zz} + M_{yy}(8M_{xx}+M_{zz})\Big]M_{xy}^2\\
&\quad -M_{xx}(M_{xx}+3M_{yy}+M_{zz})(3M_{xx}^2+M_{yy}^2+M_{zz}^2)\Big\}q_y\Big],\\
&a_z = -\tfrac{(M_{xx}+M_{yy}+3M_{zz})q_z}{\rho M_{zz}(M_{xx}^2+M_{yy}^2+3M_{zz}^2+2M_{xy}^2)},\\
&b_x = \tfrac{1}{\rho\mathfrak{d}}\Big[\Big\{M_{xx}^2M_{yy} + M_{yy}M_{zz}^2 + 3M_{yy}^3 + 2(M_{xx}+3M_{yy})M_{xy}^2\Big\}q_x\\
&\quad -M_{xy}\Big\{3M_{xx}^2+2M_{xx}M_{yy}+3M_{yy}^2+M_{zz}^2+4M_{xy}^2\Big\}q_y\Big],\\
&b_y = \tfrac{1}{\rho\mathfrak{d}}\Big[-M_{xy}\Big\{3M_{xx}^2+2M_{xx}M_{yy}+3M_{yy}^2+M_{zz}^2+4M_{xy}^2\Big\}q_x\\
&\quad +\Big\{3M_{xx}^3 + M_{xx}M_{yy}^2 + M_{xx}M_{zz}^2 + 2(3M_{xx}+M_{yy})M_{xy}^2\Big\}q_y\Big],\\
&b_z = \tfrac{q_z}{\rho M_{zz}(M_{xx}^2+M_{yy}^2+3M_{zz}^2+2M_{xy}^2)}.
\end{aligned}\right\}$$

where

$$\mathfrak{d} = \left(M_{xx}M_{yy} - M_{xy}^2\right)\Big\{3M_{xx}^4 + 10M_{xx}^2M_{yy}^2 + 4M_{xx}^2M_{zz}^2 + 3M_{yy}^4 + 4M_{yy}^2M_{zz}^2 \tag{3.153}$$

$$+ M_{zz}^4 + M_{xy}^2\left(12M_{xx}^2 + 16M_{xy}^2 - 8M_{xx}M_{yy} + 12M_{yy}^2 + 8M_{zz}^2\right)\Big\}. \tag{3.154}$$

Equation (3.148) along with (3.153) and (3.154) constitute the single particle distribution function for the non-uniform shear flow.

This completes the determination of the distribution function (3.148) for the non-USF which we shall use in the next section to calculate the source term in the balance equation for the third-order moment.

3.12.1 The Third Order Balance

The balance equation for the contracted third-order moment is

$$\rho\frac{\mathrm{D}M_{\alpha\beta\beta}}{\mathrm{D}t} + Q_{n\alpha\beta\beta,n} - 3M_{(\alpha\beta}P_{\beta)n,n} + 3Q_{n(\alpha\beta}u_{\beta),n} = \aleph_{\alpha\beta\beta}, \tag{3.155}$$

where

$$Q_{n\alpha\beta} = \rho M_{n\alpha\beta} = \int C_nC_\alpha C_\beta f^{(1)}(\mathbf{c},\boldsymbol{x},t)d\mathbf{c} \tag{3.156}$$

$$Q_{n\alpha\beta\beta} = \rho M_{n\alpha\beta\beta} = \int C^2C_nC_\alpha f^{(1)}(\mathbf{c},\boldsymbol{x},t)d\mathbf{c}, \tag{3.157}$$

and

$$M_{(\alpha\beta}P_{\beta)n,n} = \frac{1}{3}(2M_{\alpha\beta}P_{\beta n,n} + M_{\beta\beta}P_{\alpha n,n}) = \frac{1}{3}(2M_{\alpha\beta}P_{\beta n,n} + 3TP_{\alpha n,n}), \tag{3.158}$$

$$Q_{n(\alpha\beta}u_{\beta),n} = \frac{1}{3}(2Q_{n\alpha\beta}u_{\beta,n} + Q_{n\beta\beta}u_{\alpha,n}) = \frac{1}{3}(2Q_{n\alpha\beta}u_{\beta,n} + 2q_nu_{\alpha,n}). \tag{3.159}$$

The source term in (3.155), $\aleph_{\alpha\beta\beta}$, is defined as

$$\aleph_{\alpha\beta\beta} = \aleph[mC^2C_\alpha]$$

$$= \frac{m\sigma^2}{2}\int\int\int_{\boldsymbol{g}\cdot\boldsymbol{k}>0}\Delta(C^2C_\alpha)f^{(1)}(\boldsymbol{c}_1,\boldsymbol{x})f^{(1)}(\boldsymbol{c}_2,\boldsymbol{x})(\boldsymbol{g}\cdot\boldsymbol{k})d\boldsymbol{k}d\boldsymbol{c}_1d\boldsymbol{c}_2. \tag{3.160}$$

By using the distribution function (3.148) we can carry out the integration in (3.160) as detailed in Appendix J. The final expression for the third-order source term (see Appendix J)

is

$$\aleph_{\alpha\beta\beta} = -\frac{2\rho(1+e)\sqrt{T}}{385\rho_p\sigma\sqrt{\pi}}\mathfrak{Q}_{\alpha\gamma}q_\gamma. \tag{3.161}$$

The expressions for different elements of $\mathfrak{Q}$ are given below.

3.12.2 Elements of $\mathfrak{Q}$

The expressions for the non-zero elements of $\mathfrak{Q}$ in (J.38) are given by

$$\begin{aligned}\mathfrak{Q}_{11} = \frac{1}{25+24\eta^2+40\lambda^2+16\alpha^4+96\lambda^4}\Big[&(188650+341880\lambda^2+849783\lambda^4+639606\lambda^6\\&+586074\lambda^8)-e\{(127050+221760\lambda^2+569151\lambda^4+403722\lambda^6+427258\lambda^8)\\&+\eta^2(144309+45606\lambda^2+331524\lambda^4+71192\lambda^6)+2\eta^4(50529+20800\lambda^2-2968\lambda^4)\\&-8\eta^6(210-739\lambda^2)\}+\eta^2(205997+68618\lambda^2+354132\lambda^4-161304\lambda^6)\\&+2\eta^4(63017-7780\lambda^2-94424\lambda^4)-8\eta^6(1751+3309\lambda^2)-10400\eta^8\\&+2\eta[4(5005+9680\lambda^2+12067\lambda^4+4856\lambda^6)-e\{9240-2\eta^2(759+6740\lambda^2+5367\lambda^4)\\&+\eta^4(5756-3264\lambda^2)+660\eta^6+22440\lambda^2+16566\lambda^4+24008\lambda^8\}\\&+\eta^2(6116-44640\lambda^2-43578\lambda^4)+\eta^4(8961-12948\lambda^2)-2156\eta^6]\sin 2\phi\Big],\end{aligned} \tag{3.162}$$

$$\begin{aligned}\mathfrak{Q}_{12} = -\frac{2\eta\cos 2\phi}{25+24\eta^2+40\lambda^2+16\alpha^4+96\lambda^4}\Big[&4(5005+9680\lambda^2+12067\lambda^4+4856\lambda^6)-e\{9240\\&-2\eta^2(759+6740\lambda^2+5367\lambda^4)+\eta^4(5756-3264\lambda^2)+660\eta^6+22440\lambda^2+16566\lambda^4\\&+24008\lambda^8\}+\eta^2(6116-44640\lambda^2-43578\lambda^4)+\eta^4(8961-12948\lambda^2)-2156\eta^6\Big],\end{aligned} \tag{3.163}$$

$$\mathfrak{Q}_{22}=\frac{1}{25+24\eta^2+40\lambda^2+16\alpha^4+96\lambda^4}\Big[(188650+341880\lambda^2+849783\lambda^4+639606\lambda^6 +586074\lambda^8)-e\{(127050+221760\lambda^2+569151\lambda^4+403722\lambda^6+427258\lambda^8) +\eta^2(144309+45606\lambda^2+331524\lambda^4+71192\lambda^6)+2\eta^4(50529+20800\lambda^2-2968\lambda^4) -8\eta^6(210-739\lambda^2)\}+\eta^2(205997+68618\lambda^2+354132\lambda^4-161304\lambda^6) +2\eta^4(63017-7780\lambda^2-94424\lambda^4)-8\eta^6(1751+3309\lambda^2)-10400\eta^8 -2\eta[4(5005+9680\lambda^2+12067\lambda^4+4856\lambda^6)-e\{9240-2\eta^2(759+6740\lambda^2+5367\lambda^4) +\eta^4(5756-3264\lambda^2)+660\eta^6+22440\lambda^2+16566\lambda^4+24008\lambda^8\} +\eta^2(6116-44640\lambda^2-43578\lambda^4)+\eta^4(8961-12948\lambda^2)-2156\eta^6]\sin 2\phi\Big], \quad (3.164)$$

$$\mathfrak{Q}_{33}=\frac{1}{(5+2\eta^2-8\lambda^2)}\Big[37730-25410e+18733\eta^2-13101e\eta^2-1028\eta^4-4e\eta^4 -520\eta^6-2\{616(62-39e)-11(71-147e)\eta^2+(889+167e)\eta^4\}\lambda^2 +\{33(4471-2967e)-80(76-3e)\eta^2\}\lambda^4-2(21373-11121e)\lambda^6\Big]. \quad (3.165)$$

3.12.3 Heat Flux and Thermal Conductivity: Maxwell Iteration

Inserting (3.158-3.159) in (3.155), the equation for the heat-flux vector $\boldsymbol{q}$ can be written as:

$$\aleph_{\alpha\beta\beta}=2\frac{Dq_\alpha}{Dt}+2q_\alpha\frac{\partial u_\beta}{\partial x_\beta}+\frac{\partial Q_{n\alpha\beta\beta}}{\partial x_n}-(2M_{\alpha\beta}+3T\delta_{\alpha\beta})\frac{\partial P_{\beta n}}{\partial x_n} \underbrace{+2(Q_{n\alpha\beta}+q_n\delta_{\alpha\beta})\frac{\partial u_\beta}{\partial x_n}}. \quad (3.166)$$

Following the same closure assumption of vanishing $\widehat{Q}_{n\alpha\beta}$ as in (3.21), we can write

$$Q_{n\alpha\beta}=\frac{1}{5}\left(Q_n\delta_{\alpha\beta}+Q_\alpha\delta_{n\beta}+Q_\beta\delta_{n\alpha}\right)\equiv\frac{2}{5}\left(q_n\delta_{\alpha\beta}+q_\alpha\delta_{n\beta}+q_\beta\delta_{n\alpha}\right). \quad (3.167)$$

Therefore, the under-braced term in (3.166) can be simplified as

$$2(Q_{n\alpha\beta}+q_n\delta_{\alpha\beta})\frac{\partial u_\beta}{\partial x_n}=\frac{18}{5}D_{\alpha n}q_n+2W_{\alpha n}q_n+\frac{4}{5}q_\alpha\frac{\partial u_\beta}{\partial x_\beta}, \quad (3.168)$$

where we have used the following definitions

$$\frac{\partial u_\alpha}{\partial x_n} = \frac{1}{2}\left(\frac{\partial u_\alpha}{\partial x_n} + \frac{\partial u_n}{\partial x_\alpha}\right) + \frac{1}{2}\left(\frac{\partial u_\alpha}{\partial x_n} - \frac{\partial u_n}{\partial x_\alpha}\right) = D_{\alpha n} + W_{\alpha n} \tag{3.169}$$

$$\frac{\partial u_n}{\partial x_\alpha} = D_{\alpha n} - W_{\alpha n}. \tag{3.170}$$

Inserting (3.168) into (3.166), the governing equation for the heat flux reduces to

$$2\frac{Dq_\alpha}{Dt} + \frac{14}{5}q_\alpha\frac{\partial u_n}{\partial x_n} + \frac{\partial Q_{n\alpha\beta\beta}}{\partial x_n} - (2M_{\alpha\beta} + 3T\delta_{\alpha\beta})\frac{\partial P_{\beta n}}{\partial x_n} = -\frac{4\nu(1+e)\sqrt{T}}{5\sigma\sqrt{\pi}}\mathscr{Q}_{\alpha\gamma}q_\gamma, \tag{3.171}$$

where

$$\mathscr{Q}_{\alpha\gamma} = \frac{1}{154}\mathfrak{Q}_{\alpha\gamma} + \frac{9\sigma\sqrt{\pi}}{2\nu(1+e)\sqrt{T}}D_{\alpha\gamma} + \frac{5\sigma\sqrt{\pi}}{2\nu(1+e)\sqrt{T}}W_{\alpha\gamma} \tag{3.172}$$

is a rank-two tensor field.

Now to determine the constitutive relation for the heat flux, we apply the anisotropic Maxwell-iteration scheme (Truesdell & Muncaster 1980; Saha & Alam 2014) for which the following relations hold at the zeroth-order:

$$\left.\begin{aligned} P^{(0)}_{\alpha\beta} &= \rho M^{(0)}_{\alpha\beta} = \rho M_{\alpha\beta}, \\ Q^{(0)}_{n\alpha\beta\beta} &= \rho(3T\delta_{\alpha\beta} + 2M_{\alpha\beta})M_{n\beta}, \end{aligned}\right\} \tag{3.173}$$

and hence

$$\left.\begin{aligned} M^{(0)}_{\alpha\beta}\frac{\partial P^{(0)}_{\beta n}}{\partial x_n} &= \rho M_{\alpha\beta}\frac{\partial M_{\beta n}}{\partial n} + \frac{\partial \rho}{\partial x_n}M_{\alpha\beta}M_{\beta n}, \\ \frac{\partial Q^{(0)}_{n\alpha\beta\beta}}{\partial x_n} &= 3\frac{\partial \rho}{\partial x_n}TM_{\alpha n} + 3\rho\frac{\partial T}{\partial x_n}M_{\alpha n} + 3\rho T\frac{\partial M_{\alpha n}}{\partial x_n} \\ &\quad + 2\frac{\partial \rho}{\partial x_n}M_{n\beta}M_{\alpha\beta} + 2\rho\frac{\partial M_{n\beta}}{\partial x_n}M_{\alpha\beta} + 2\rho M_{n\beta}\frac{\partial M_{\alpha\beta}}{\partial x_n}. \end{aligned}\right\} \tag{3.174}$$

Inserting (3.173-3.174) into (3.171) we obtain the expression for the heat-flux vector

$$q_\gamma = -\frac{5\rho_p\sigma\sqrt{\pi}}{4(1+e)\sqrt{T}}\mathscr{Q}^{-1}_{\gamma\alpha}\left(5M_{\alpha n}\frac{\partial T}{\partial x_n} + 2M_{\beta n}\frac{\partial \widehat{M}_{\alpha\beta}}{\partial x_n}\right), \tag{3.175}$$

with $\mathscr{Q}_{\gamma\alpha}$ being given by (3.172). Equation (3.175) is dubbed the 'generalized' Fourier law since the gradient of the kinetic stress drives a heat-current in addition to the standard Fourier heat-current driven by the gradient of the temperature. The coefficient of the temperature gradient term in (3.175)

$$\kappa_{\gamma n} = \frac{25\rho_p\sigma\sqrt{\pi}}{4(1+e)\sqrt{T}}\mathscr{Q}^{-1}_{\gamma\alpha}M_{\alpha n}, \tag{3.176}$$

is identified as the thermal conductivity which is a rank-two tensor field.

3.12.4 Navier-Stokes's Limit

When the shear-plane temperature anisotropy ($\eta \to 0$) and the excess temperature along the vorticity direction ($\lambda^2 \to 0$) approach zero, we have $\widehat{M}_{\alpha\beta} = 0$ and $M_{\alpha\beta} = T\delta_{\alpha\beta}$, along with

$$\mathscr{Q}^{-1}_{\gamma\alpha} M_{\alpha n} = \frac{T}{(49-33e)} \begin{bmatrix} \left(1 - \frac{224\pi R^2}{(1+e)^2(49-33e)^2\nu^2}\right)^{-1} & 0 & 0 \\ 0 & \left(1 - \frac{224\pi R^2}{(1+e)^2(49-33e)^2\nu^2}\right)^{-1} & 0 \\ 0 & 0 & 1 \end{bmatrix}. \tag{3.177}$$

At linear order in the shear rate ($\sim R$), (3.177) reduces to

$$\mathscr{Q}^{-1}_{\gamma\alpha} M_{\alpha n} = \frac{T\delta_{\gamma n}}{(49-33e)}. \tag{3.178}$$

Substituting (3.178) into (3.175), we obtain an expression for the heat-flux

$$q_\gamma = -\frac{75m\sqrt{T}}{2\sqrt{\pi}\sigma^2(1+e)(49-33e)}\frac{\partial T}{\partial x_\gamma} = -\kappa\frac{\partial T}{\partial x_\gamma}, \tag{3.179}$$

with

$$\kappa = \frac{25\sqrt{\pi}\rho_p\sigma\sqrt{T}}{4(1+e)(49-33e)} \tag{3.180}$$

being the expression for the 'scalar' thermal conductivity at NS-order (Jenkins & Richman 1985*a*). Therefore, at linear-order in the shear rate (the NS-order), the heat flux follows the standard Fourier law (3.179) and the thermal conductivity, $\kappa_{\gamma n} = \kappa\delta_{\gamma n}$, is an isotropic tensor.

3.12.5 Comparison with Previous Work

As cited in the work of (Simon & Jenkins 1994), similar expressions for the heat flux (3.175) and thermal conductivity (3.176) were derived by Zhang (1993). Here we make a comparison between our work and the constitutive expression derived by Zhang (1993) by analysing the different components of the tensor $\mathscr{Q}$ as given in (3.172).

For the uniform shear flow and after truncating the terms beyond $O(\eta\lambda^2)^2$, we can explicitly evaluate different components of $\mathscr{Q}$: the diagonal elements of $\mathscr{Q}$ are given by

$$\left.\begin{aligned}
\mathscr{Q}_{xx} &= \tfrac{1}{14(25+24\eta^2+40\lambda^2+96\beta^4)}\Big[17150+18727\eta^2+31080\lambda^2+77253\lambda^4 \\
&-3e(3850+4373\eta^2+6720\lambda^2+17247\lambda^4)+40\eta\Big\{91+176\lambda^2-6e(7+17\lambda^2)\Big\}\sin 2\phi\Big], \\
\mathscr{Q}_{yy} &= \tfrac{1}{14(25+24\eta^2+40\lambda^2+96\beta^4)}\Big[17150+18727\eta^2+31080\lambda^2+77253\lambda^4 \\
&-3e(3850+4373\eta^2+6720\lambda^2+17247\lambda^4)-40\eta\Big\{91+176\lambda^2-6e(7+17\lambda^2)\Big\}\sin 2\phi\Big], \\
\mathscr{Q}_{zz} &= \tfrac{1}{154(5+2\eta^2-8\lambda^2+14\lambda^4)}\Big[37730-25410e+18733\eta^2-13101e\eta^2 \\
&\qquad -1232(62-39e)\lambda^2+33(4471-2967e)\lambda^4\Big],
\end{aligned}\right\} \tag{3.181}$$

and the non-zero off-diagonal elements are

$$\left.\begin{aligned}
\mathscr{Q}_{xy} &= -\tfrac{20\eta\cos 2\phi}{7(25+24\eta^2+40\lambda^2+96\beta^4)}\Big[91+176\lambda^2-6e(7+17\lambda^2)\Big]+\tfrac{28\sqrt{\pi}}{\nu(1+e)}R \\
\mathscr{Q}_{yx} &= -\tfrac{20\eta\cos 2\phi}{7(25+24\eta^2+40\lambda^2+96\beta^4)}\Big[91+176\lambda^2-6e(7+17\lambda^2)\Big]+\tfrac{8\sqrt{\pi}}{\nu(1+e)}R,
\end{aligned}\right\} \tag{3.182}$$

with $R=\dot{\gamma}\sigma/4\sqrt{T}$ being the Savage-Jeffrey parameter (3.49). Clearly, $\mathscr{Q}_{\alpha\beta}\neq\mathscr{Q}_{\beta\alpha}$ for any $R\neq 0$, and hence $\mathscr{Q}_{\alpha\beta}$ is asymmetric. We conclude that the thermal conductivity tensor $\kappa_{\alpha\beta}$ is anisotropic in the uniform shear flow having dependence on the shear rate and, moreover, the off-diagonal anisotropy of $\kappa_{\alpha\beta}$ (i.e. $\kappa_{\alpha\beta}\neq\kappa_{\beta\alpha}$) results from the imposed shear-field in USF.

Before closing this section, we make a comparison of the different elements of $\mathscr{Q}$ as given by our expressions in (3.181-3.182) with the approximate solutions derived by Zhang (1993); the related expression of $\mathscr{Q}$ is given in Simon & Jenkins (1994). To evaluate each element $\mathscr{Q}_{\alpha\beta}$, we used the reference state of USF for which η, λ^2, R and ϕ are calculated as before and they are subsequently substituted into (3.181-3.182). Figure 3.11(a) displays the diagonal elements of $\mathscr{Q}$, while figure 3.11(b) displays the non-zero off-diagonal elements $\mathscr{Q}_{xy}$ and $\mathscr{Q}_{yx}$. It is seen in figure 3.11(b) that our second-order solution (3.182) for $\mathscr{Q}_{xy}$ and $\mathscr{Q}_{yx}$ agree well with those of Zhang (1993) for the whole range of restitution coefficient. On the other hand, while the agreement for the longitudinal component $\mathscr{Q}_{xx}$ is excellent between two theories, there are significant differences for $\mathscr{Q}_{yy}$ and $\mathscr{Q}_{zz}$ for $e<0.9$. It may be noted the analysis of Zhang (1993) considers only leading-order terms, while our analysis is based on second-order corrections. In any case, the particle simulation data are required to verify the constitutive expressions for the heat flux.

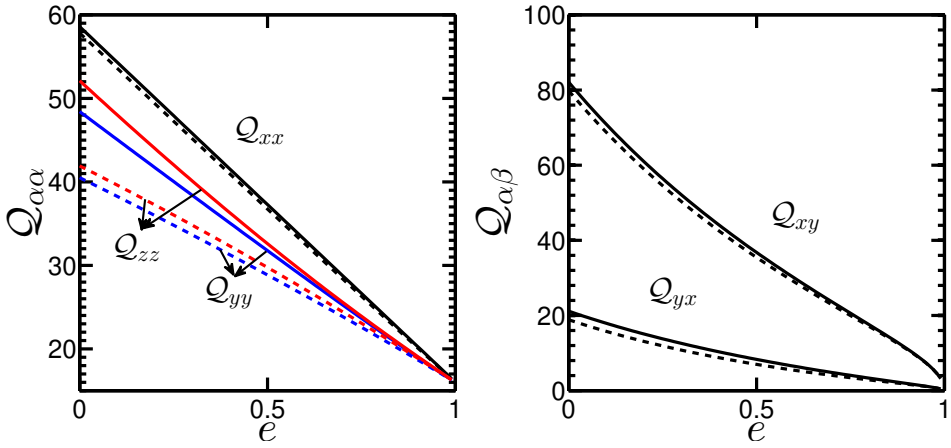

Fig. 3.11 Variations of the different components of $\mathscr{Q}_{\alpha\beta}$ with e in the dilute limit ($\nu = 0.01$): the values of η, λ^2, R and ϕ correspond to the solution of the USF problem. The solid lines represent the present solution as given in (3.181-3.182) and the dashed lines represent the work of Zhang (1993) as cited in (Simon & Jenkins 1994).

3.13 Summary and Comparison with Standard Moment Theory

3.13.1 Summary of Theory and Its Predictions

The motivation to develop a higher-order hydrodynamic-like theory for a flowing granular matter came from the fact that the normal stress differences remain order-one quantities (see figures 3.1 and 3.8) in a granular fluid and hence cannot be neglected. This ruled out Navier-Stokes-order models (for which $\mathscr{N}_1 = 0 = \mathscr{N}_2$) and the 'minimal' model that incorporates normal stress differences is the well-known "10-moment" model of (Grad 1949) in terms of an extended set of 10 hydrodynamic fields (density, velocity vector and the second moment tensor) as detailed in §3.2. The constitutive relations were then derived by choosing the anisotropic Maxwellian as the single-particle distribution function which is the zeroth-order distribution function (Goldreich & Tremaine 1978; Araki & Tremaine 1986; Jenkins & Richman 1988; Richman 1989; Lutsko 2004; Saha & Alam 2014) for a non-equilibrium system like the steady uniform shear flow of smooth inelastic spheres. The equation for the second moment tensor has been solved semi-analytically, and the closed-form expressions for the "non-Newtonian" stress tensor, the shear viscosity and the collisional dissipation rate are provided for the whole range of density as detailed in §3.7.1, §3.7.2 and §3.9. In addition, the origin of two normal stress differences has been identified in §3.8.

We found that the normal stress differences and the anisotropy of the second-moment tensor $\boldsymbol{M} = \langle \boldsymbol{CC} \rangle$ (where $\boldsymbol{C} = (\boldsymbol{c} - \boldsymbol{u})$ is the peculiar velocity of a particle, $\boldsymbol{c}$ is its instantaneous velocity and $\boldsymbol{u}$ is the coarse-grained/hydrodynamic velocity) are intertwined with each other in uniform shear flow. This can be easily appreciated by focussing on the dilute limit of shear flow for which the following relations hold:

$$\eta^2 = \frac{1}{12}\left(6 + \mathscr{N}_1 + 2\mathscr{N}_2\right)\mathscr{N}_1 \tag{3.183}$$

$$\lambda^2 = \frac{1}{6}\left(\mathscr{N}_1 + 2\mathscr{N}_2\right) \tag{3.184}$$

$$\sin 2\phi = \sqrt{\frac{3\mathscr{N}_1}{\left(6 + \mathscr{N}_1 + 2\mathscr{N}_2\right)}} \tag{3.185}$$

Therefore, the temperature anisotropy in the shear-plane (η), the non-coaxiality angle (ϕ) and the excess temperature ($T_z^{ex} = (T - T_z) \propto \lambda^2$, where T_z and T are the z-component and the average of the granular temperature respectively) along the mean-vorticity (z) direction vanish if the two normal stress differences are zero. This results in an 'isotropic' second-moment tensor for which only the granular temperature is a field variable, in addition to density and velocity, leading to the standard NS-order hydrodynamic model.

The 'scaled' first normal stress difference ($\mathscr{N}_1 = (P_{xx} - P_{yy})/p$, scaled with respect to the mean pressure) is positive in the dilute limit and decreases monotonically to zero in the dense limit. In contrast, the scaled second normal stress difference ($\mathscr{N}_2 = (P_{yy} - P_{zz})/p$) is negative and positive in the dilute and dense limits, respectively, and the sign-change of $\mathscr{N}_2$ at some finite density is directly tied to the sign-change of its kinetic component $\mathscr{N}_2^k$. In physical terms, the vanishing of the first normal stress difference is tied to the 'coaxiality' (i.e. the non-coaxiality angle is $\phi = 0$) of the eigendirections of the shear tensor $\boldsymbol{D} = (\boldsymbol{\nabla u} + (\boldsymbol{\nabla u})^T)/2$ and the second-moment tensor $\boldsymbol{M}$. On the other hand, the second normal stress difference can be non-zero even if the above coaxiality condition ($\phi = 0$) is satisfied since the 'excess' temperature ($T_z^{ex} = (T - T_z) \propto \lambda^2$, where T and T_z are the average and z-component of the granular temperature) along the mean vorticity (z) direction could differ from zero in uniform shear flow.

A detailed comparison between the 'exact' numerical solution of the second-moment equation and two different (approximate) semi-analytical solutions has been made (see figures 3.6, 3.7 and 3.8). We found that the super-super-Burnett terms (i.e. fourth-order in the shear rate) must be retained in the series expansion (3.81–3.82) of the second-moment equation to quantitatively predict the behaviour of the pressure (p), the shear viscosity (μ) and two normal stress differences ($\mathscr{N}_1$ and $\mathscr{N}_2$) for all values of density (ν) and restitution coefficient (e).

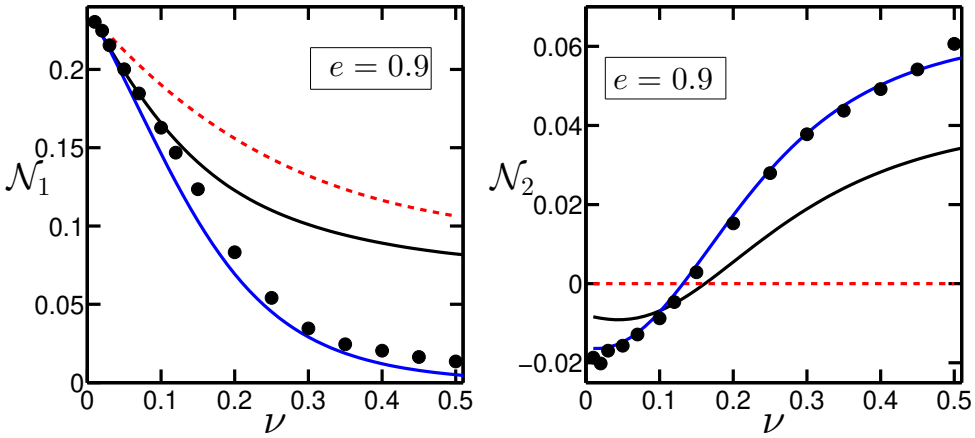

Fig. 3.12 Variations of the (a) first $\mathscr{N}_1$ and (b) second $\mathscr{N}_2$ normal stress differences against volume fraction ν for coefficient of restitution $e = 0.9$. The blue solid lines, black solid lines and red dashed lines represent the Burnett order analytical solution of current anisotropic Gaussian theory, DG14 theory (chapter 2) and 14 moment theory of Garzó (2013) respectively. The symbols are simulation results from Alam & Luding (2005*b*).

Furthermore, a similar comparison with the molecular dynamic event-driven simulations data of Alam & Luding (2005*b*) for the uniform shear flow of inelastic hard-spheres confirmed the reliability of our theoretical expressions for transport coefficients over a large range of density (see figures 3.7 and 3.9). Therefore we conclude that the beyond-Navier-Stokes contributions up-to the super-super-Burnett order must be retained in all transport coefficients.

Lastly, we derived a constitutive relation for the granular heat-flux in the dilute limit by utilizing an expansion around the anisotropic Maxwellian state. The resulting generalized heat flux (3.175) depends on the gradients of (i) the granular temperature and (ii) the kinetic stress. We found that the thermal conductivity tensor $\kappa_{\alpha\beta}$ (3.176) is anisotropic in the uniform shear flow having dependence on the shear rate and, moreover, the off-diagonal anisotropy of $\kappa_{\alpha\beta}$ (i.e. $\kappa_{\alpha\beta} \neq \kappa_{\beta\alpha}$) results from the imposed shear-field in USF.

To complete the present 10-moment theory, the collisional contribution to the heat flux needs to be calculated in future. This is required for the applicability of the present theory over the whole range of density.

3.13.2 Comparison with GME (Grad's Moment Expansion) Theory

Figure 3.12 shows a comparison of first ($\mathscr{N}_1$) and second ($\mathscr{N}_2$) normal stress differences within (i) Burnett order analytical solution of present anisotropic Gaussian theory, (ii) Dense Grad 14 moment (DG14) theory established in Chapter 2, (iii) Grad's 14 moment theory by Garzó (2013) and (iv) molecular dynamics solution by Alam & Luding (2005*b*), against volume

fraction ν for $e = 0.9$. It is seen that the theory based on standard Grad's moment expansion (GME) (Jenkins & Richman 1985*a*; Garzó 2013) grossly over-predicts $\mathscr{N}_1$ and predicts $\mathscr{N}_2$ to be identically zero. Therefore questions the applicability of GME at a finite density as far as normal stress differences are concerned. The DG14 moment theory predicts $\mathscr{N}_1$ up-to a volume fraction of 0.1 and then over-predicts it. The $\mathscr{N}_2$ predictions of DG14 is better compared to the GME in a sense that DG14 theory predicts the corrects signs of $\mathscr{N}_2$ at the dilute and dense limits, and also predicts the sign reversal of it at some finite density. Overall, the DG14 moment theory gives a qualitatively correct predictions for $\mathscr{N}_1$ and $\mathscr{N}_2$ both but there is quantitative disagreement with the simulation. However the anisotropic Maxwellian expansion (AME) discussed in this chapter predicts the correct behaviours of both the normal stress differences and an excellent quantitative agreement with the simulation is observed throughout the span of density. Here lies the success of AME theory.

The quantitative predictions of the AME theory for two normal stress differences and other transport coefficients motivate us to apply this anisotropic theory to analyse the simple shear flows of gas-solid suspensions. The particle phase rheology of a uniformly sheared gas-solid suspension using anisotropic Maxwellian as the single particle distribution function will be discussed in the remaining two chapters.

Chapter 4

Dense Gas-Solid Suspension: Stress Tensor and Normal Stress Differences

4.1 Introduction

This chapter is devoted to analyse the non-Newtonian stress tensor in a sheared gas-solid suspension, and is a direct extension of the anisotropic Maxwellian theory described in Chapter 3. A detailed review of pertinent works on gas-solid suspensions is deferred to Chapter-5; in the following we discuss a few papers from which the present work is motivated. The simple shear flow of a gas-solid suspension has been analysed by Tsao & Koch (1995) and Sangani *et al.* (1996) for the cases of (i) the elastic particles in dense suspension and for (ii) the inelastic particles in very dilute suspension. Their theory is based on the standard Grad's moment-expansion (GME) around a Maxwellian using Hermite polynomials yielding (i) finite first normal stress difference ($\mathscr{N}_1$) in the dense limit ($\nu \to \nu_{\max}$) and (ii) vanishing second normal stress difference ($\mathscr{N}_2 \equiv 0$) at any density. But the particle simulation data (Alam & Luding 2005*b*,*a*) and related theory works (Jenkins & Richman 1988; Saha & Alam 2014, 2016) clearly suggest non-vanishing $\mathscr{N}_2 \neq 0$ at any density and vanishing $\mathscr{N}_1 \to 0$ in the dense regime. Finding the correct behaviour of two normal stress differences ($\mathscr{N}_1$, $\mathscr{N}_2$) and other transport coefficients for a "non-dilute" suspension of dissipative particles is the main objective of the present chapter.

In figure 4.1 we have shown the density variations of the two normal stress differences [$\mathscr{N}_1$ and $\mathscr{N}_2$] for $e = 0.5$ (upper panel) and $e = 0.9$ (lower panel) respectively.[3] The continuous lines are the results that correspond to a Stokes number (St_d) of 10, whereas the dashed lines correspond to its dry granular analogue ($St_d \to \infty$). This analysis is based on an adjusted

[3]The mathematical definitions of all the transport coefficients remain same as they are defined in previous chapters.

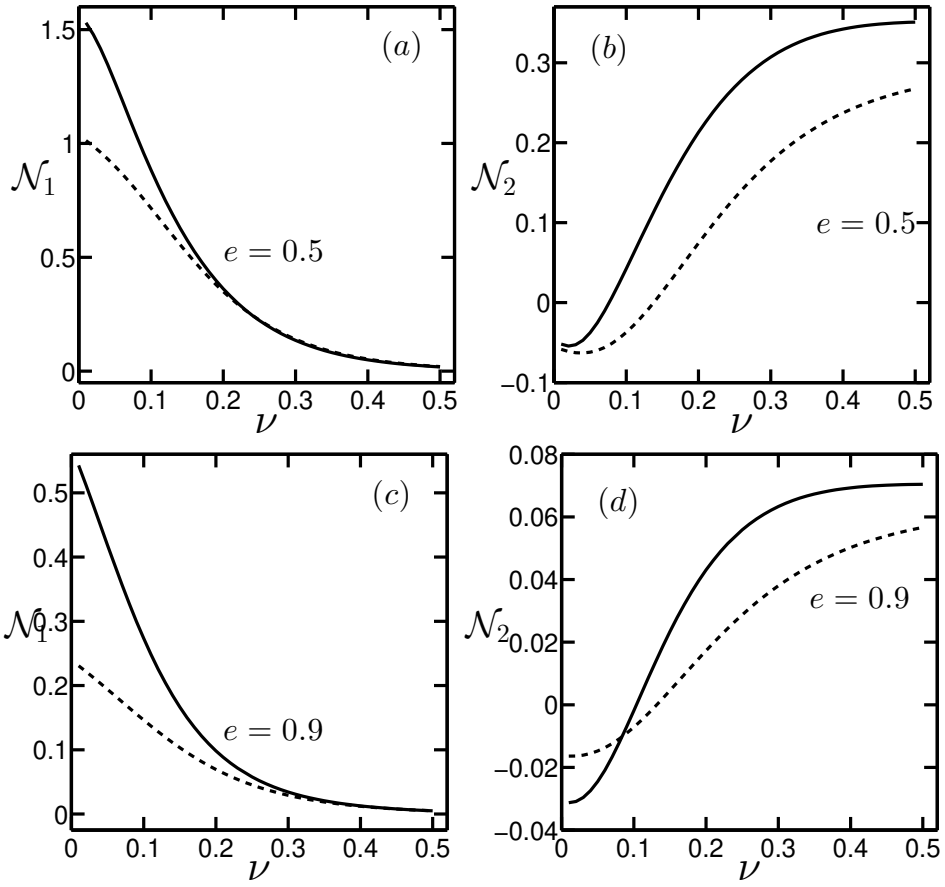

Fig. 4.1 Variations of the first ($\mathscr{N}_1$) and second ($\mathscr{N}_2$) normal stress differences with particle volume fraction (ν) in a uniformly sheared gas solid suspension of smooth inelastic spheres. The dashed lines represent the theory of Saha & Alam (2016), in the limit of infinite Stokes number ($St_d \to \infty$) and the solid lines denote the present anisotropic moment theory at a finite Stokes number of $St_d = 10$. The results depicted above are at restitution coefficients of $e = 0.5$ and $e = 0.9$ respectively.

Stokes number (Sangani *et al.* 1996)

$$St_d = St/R_{diss}, \tag{4.1}$$

defined via a correction factor R_{diss}, for which the clarification will be given in the main text.

Figure 4.1 works as a motivation for our present work. It shows that the normal stress differences are $\mathscr{O}(1)$ quantities in dry granular flows and as well in gas-solid suspensions. The presence of an interstitial fluid increases the first ($\mathscr{N}_1$) normal stress difference [panel (a) and (c)] significantly in the dilute limit but its effect remains small near the dense regime. On the other hand, for the case of second ($\mathscr{N}_2$) normal stress difference [panel (b) and (d)], the interstitial fluid shows its effect throughout the span of volume fraction. Such large normal stress differences must be taken into account to study the flow of a driven system of dissipative particles. It is also important to understand the effects of the interstitial fluid on the particle phase normal-stress differences and other transport coefficients in a dissipative gas-solid suspension relative to its dry granular counterpart.

Sangani *et al.* (1996) has proposed a linear theory for a gas-solid suspension of elastic and inelastic particles based on an expansion around the Maxwellian. Their work is an application of the theory described in Jenkins & Richman (1985*a*) for a suspension problem and an extension of the work by Tsao & Koch (1995) for a dense suspension. They have included finite-density effects for elastic particles but the second normal stress difference was found to be identically zero. This is due to the removal of certain nonlinear terms while calculating the production terms. A small portion of their work has been devoted towards the dissipative particles but focusing only in the dilute limit and $\mathscr{N}_2$ was again found to be zero. The extension of their proposed model for the whole range density with inelastically colliding particles gives rise to a finite first normal stress difference ($\mathscr{N}_1$) in the dense limit with second normal stress difference ($\mathscr{N}_2$) being zero throughout. The behaviours of the two normal stress differences as obtained from their theory are represented by brown dash-dotted lines in figure 4.1.

Recently, Parmentier & Simonin (2012) prescribed a theory for elastic and inelastic particles valid for arbitrary Stokes numbers. A comparison with the simulation (Abbas *et al.* 2009) has been made and a qualitatively good agreement is observed. But they have only considered the kinetic contribution to the stress tensor ($P^k_{ij} = \rho\langle C_i C_j\rangle$) but nothing regarding the collisional stress ($P^c_{ij} = \Theta_{ij}$) has been mentioned. We know from the kinetic theory of molecular and granular gases that collisional stresses are very important in determining the correct transport properties at finite densities. All transport coefficients like the pressure (p), viscosity (μ), normal-stress differences ($\mathscr{N}_1, \mathscr{N}_2$) have contributions from kinetic as well as collisional transport of momentum; the collisional contribution to each transport coefficient becomes significant as we consider flows of a "non-dilute" system.

In this chapter our focus is in the evaluation of the complete stress tensor P_{ij} $(= P^k_{ij} + P^c_{ij})$ for a non-dilute suspension of dissipative particles, which can be valid for arbitrary values of Stokes number and inelasticity, and this has not been worked out till date. The present work fills this gap by determining the non-Newtonian stress tensor and related transport coefficients for a "non-dilute" gas-solid suspension of inelastic particles. The resulting theory is nonlinear since super-super-Burnett order terms are retained to evaluate the transport coefficients.

4.2 Governing Equations for Gas and Particles

Here we follow the work of Sangani *et al.* (1996) to formulate the problem and the analysis/solution of this problem follows methodologies and tools developed in Chapter 3.

4.2.1 Equations for the Fluid Phase: Stokes Equations

The gas phase is assumed to be a Newtonian fluid of constant viscosity μ_g and obeys the Navier-Stokes equations of motion

$$\rho_g \frac{Dv_i}{Dt} = -\nabla_i p_g + \mu_g \nabla^2 v_i. \tag{4.2}$$

Under the assumption of small particle Reynolds number

$$Re \sim \rho_g \dot{\gamma} \sigma^2 / \mu_g \ll 1, \tag{4.3}$$

where ρ_g stands for density of the fluid, σ is the particle diameter and $\dot{\gamma}$ is the shear rate of the flow, the inertial terms on the left hand side of (4.2) can be left out and we have the equations for the fluid phase as the well known Stokes equations of motion :

$$\mu_g \nabla^2 v_i = \nabla_i p_g, \qquad \nabla_i v_i = 0. \tag{4.4}$$

For a homogeneous sheared suspension at steady state, $\dot{\gamma}$ is a constant and the ensemble averaged velocity of the particles (the macroscopic velocity of the particle phase) is related to the shear rate via

$$\langle \boldsymbol{c} \rangle = \boldsymbol{u} = \gamma_{ij} x_j = \dot{\gamma} y \boldsymbol{e}_x + 0\boldsymbol{e}_y + 0\boldsymbol{e}_z, \tag{4.5}$$

where $\boldsymbol{c}$ is the instantaneous velocity of a particle at time t and $\boldsymbol{e}_i$ corresponds to the unit vector in i-th direction. The velocity profile (4.5) satisfies (4.4) for a sheared suspension.

4.2.2 Equations for the Particle Motion: Stokes Number

The motion of an individual "smooth" particle follows

$$m\frac{d\boldsymbol{c}}{dt} = \mathscr{F}, \tag{4.6}$$

where $\mathbf{c}$ is the translational velocity of the particle at time t, and $\mathscr{F}$ is the force acting on it, exerted by the surrounding fluid. With $\mathscr{F}$ to be the Stokes drag, we can have the definition of Stokes number

$$St = \frac{m\dot{\gamma}}{3\pi\mu_g\sigma} = \left(\frac{m}{3\pi\mu_g\sigma}\right)\left(\frac{1}{\dot{\gamma}^{-1}}\right) = \frac{\tau_v}{\dot{\gamma}^{-1}}, \tag{4.7}$$

the non-dimensional measure of the particle inertia.

It can be interpreted as the ratio between the viscous relaxation time scale, $\tau_v = \frac{m}{3\pi\mu_g\sigma}$ to an imposed time scale $(\dot{\gamma}^{-1})$ by shear. With $m = \rho_p\pi\sigma^3/6$, where ρ_p is the material density, we have

$$St = \frac{2}{9}(\rho_p/\rho_g)Re. \tag{4.8}$$

On omitting the numerical pre-factor, the Stokes number is (ρ_p/ρ_g) times the Reynolds number based on particle diameter. The interstitial fluid here is a gas and that leads to a very high value of the density ratio

$$\rho_p/\rho_g \gg 1. \tag{4.9}$$

Hence, we can still have a very large value of the Stokes number even if the particle Reynolds number (4.3) remains very small. In addition to that, the viscous forces of the fluid are large enough as compared to the fluid inertial forces ($Re \ll 1$) but small enough in compare to the inertia of the particles ($St \gg 1$). In that case the inelastic collisions between the particles are mainly responsible for changes in particle velocities and the viscous drag exerted by the gas plays a less significant role. Nevertheless when the Stokes number becomes very small for a dilute suspension the viscous effects must be given equal importance and the detailed analysis will be given in chapter 5. Finally, in the limit of $St \to \infty$ the particles will not feel the presence of any interstitial fluid and the dry granular theory (Chapter 2 and 3) remains relevant. The inelastic inter-particle collisions between particles demands a statistical approach to elucidate the collective behaviour of these granules. We will use the methods from kinetic theory to determine the balance laws that govern the dynamics of the particle phase.

In the following we will analyse the particle phase rheology of a sheared gas-solid non-dilute suspension in the case of vanishingly small Reynolds number and moderate Stokes number in absence of gravity.

4.3 Extended Hydrodynamic Equations for a Gas-Solid Suspension

As it is mentioned in Chapters 2 and 3, the dynamics governing the particle/granular phase will be followed from the non-equilibrium statistical mechanics (Zwanzig 2001; De Groot & Mazur 2013). We adopt the kinetic theory of granular gases (Chapman & Cowling 1970; Jenkins & Richman 1985*a*; Sela & Goldhirsch 1998; Brey *et al.* 1998; Brilliantov & Pöschel 2003) in determining this. At the particle phase, the probabilistic/statistical approach is governed by the single particle distribution function $f^{(1)}$, where $f^{(1)}(\boldsymbol{c},\boldsymbol{r},t)d\boldsymbol{c}d\boldsymbol{r}$ is the probable number of particles in $B_{d\boldsymbol{r}}(\boldsymbol{r})$[3] having velocities within $B_{d\boldsymbol{c}}(\boldsymbol{c})$ at time t. Then the evolution equation for the single particle distribution function $[f^{(1)}(\boldsymbol{c},\boldsymbol{r},t)d\boldsymbol{c}d\boldsymbol{r}]$ follows from the Enskog-Boltzmann equation (Chapman & Cowling 1970)

$$\left(\frac{\partial}{\partial t}+\boldsymbol{c}\cdot\nabla\right)f+\nabla_{\boldsymbol{c}}\cdot\left(\frac{d\boldsymbol{c}}{dt}f\right)=\sigma^2\int \mathrm{d}\boldsymbol{c}_2\int_{\boldsymbol{g}\cdot\boldsymbol{k}>0}\mathrm{d}\boldsymbol{k}(\boldsymbol{g}\cdot\boldsymbol{k})\left[e^{-2}f^{(2)}(\boldsymbol{c}_1,\boldsymbol{r},\boldsymbol{c}_2,\boldsymbol{r}-\sigma\boldsymbol{k};t)\right.$$
$$\left.-f^{(2)}(\boldsymbol{c}_1',\boldsymbol{r},\boldsymbol{c}_2',\boldsymbol{r}+\sigma\boldsymbol{k};t)\right], \quad (4.10)$$

where $\nabla_{\boldsymbol{c}}$ is the divergence operator in the velocity space and $\frac{d\boldsymbol{c}}{dt}$ is the acceleration of the particle due to the external forces acting on it (viscous drag etc.). For the present problem, it is assumed that the dynamics of individual particle follows the linear Stokes's drag

$$\frac{d\boldsymbol{c}}{dt}=-\frac{\boldsymbol{c}-\boldsymbol{v}}{\tau_v}, \quad (4.11)$$

where

$$\tau_v=m/(3\pi\mu_g\sigma), \quad (4.12)$$

is the viscous relaxation time of the particles.

The pre-collisional relative velocity between two colliding spheres is given by $\boldsymbol{g}=\boldsymbol{c}_1-\boldsymbol{c}_2$, with $\boldsymbol{c}_1$ and $\boldsymbol{c}_2$ denoting their pre-collisional instantaneous velocities and their post-collisional velocities being denoted by primes, and $\boldsymbol{g}\cdot\boldsymbol{k}>0$ accounts for the constraint of impending

[3] $B_a(\boldsymbol{r})$: Volume of the sphere having radius a with centre at $\boldsymbol{r}$.

collisions; $\boldsymbol{k} \equiv \boldsymbol{k}_{12} = (\boldsymbol{r}_2 - \boldsymbol{r}_1)/|\boldsymbol{r}_2 - \boldsymbol{r}_1|$ is the unit contact vector joining the centre of sphere-1 to that of sphere-2 at collision. In (4.10), $f^{(2)}$ is the two-body distribution function such that

$$f^{(2)}(\boldsymbol{c}_1, \boldsymbol{r}_1, \boldsymbol{c}_2, \boldsymbol{r}_2) d\boldsymbol{c}_1 d\boldsymbol{r}_1 d\boldsymbol{c}_2 d\boldsymbol{r}_2$$

is the probability of finding a pair of spheres with the first sphere being centred within $d\boldsymbol{r}_1$ about $\boldsymbol{r}_1$, with its velocity in $d\boldsymbol{c}_1$ about $\boldsymbol{c}_1$ and the second one being centred within $d\boldsymbol{r}_2$ about $\boldsymbol{r}_2$, with its velocity in $d\boldsymbol{c}_2$ about $\boldsymbol{c}_2$. For a pair of colliding *smooth* spheres, the tangential component of their relative velocity remains invariant but the normal component changes according to the following collision rule:

$$(\boldsymbol{g}' \cdot \boldsymbol{k}) = -e(\boldsymbol{g} \cdot \boldsymbol{k}), \tag{4.13}$$

where $\boldsymbol{g}' = \boldsymbol{c}_1' - \boldsymbol{c}_2'$ is the post-collisional relative velocity.

4.3.1 The 10-Moment System for Particle Phase

Any physical quantity at the macroscopic level is defined as the ensemble averaged value of the same at the particle level, using the single particle distribution $f(\boldsymbol{c}, \boldsymbol{r}, t)$ function as

$$\langle \psi \rangle \equiv \frac{1}{n} \int \psi f(\boldsymbol{c}, \boldsymbol{r}, t) d\boldsymbol{c}. \tag{4.14}$$

Here $n \equiv n(\boldsymbol{r}, t)$ denotes the number density which represents the number of particles in an unit volume around the point $\boldsymbol{r}$ at time t. The macroscopic velocity $\boldsymbol{u} = \langle \boldsymbol{c} \rangle$, granular temperature $T = \langle C^2/3 \rangle$ and the second moment of fluctuation velocity $\boldsymbol{M} = \langle \boldsymbol{CC} \rangle$ are obtained by substituting $\psi = \boldsymbol{c}$, $\frac{1}{3}\boldsymbol{C}^2$ and $\boldsymbol{CC}$ respectively in equation(4.14) (Jenkins & Richman 1985*a*; Saha & Alam 2014, 2016), where $\boldsymbol{C} = \boldsymbol{c} - \boldsymbol{u}$, is the peculiar velocity.

The master balance equation governing the evolution equations for all the hydrodynamic field variables are obtained by multiplying the Enskog-Boltzmann equation (4.10) (Jenkins & Richman 1985*a*; Sangani *et al.* 1996; Saha & Alam 2016) with particle property ψ and integrating over the velocity space, yields:

$$\frac{D\langle \rho \psi \rangle}{Dt} + \langle \rho \psi \rangle \frac{\partial u_i}{\partial r_i} + \frac{\partial}{\partial r_i}\Big(\langle \rho C_i \psi \rangle + \Theta_i[m\psi] \Big) + \rho \frac{Du_i}{Dt} \Big\langle \frac{\partial \psi}{\partial C_i} \Big\rangle - \rho \Big\langle \frac{dc_i}{dt} \frac{\partial \psi}{\partial C_i} \Big\rangle + \Big(\Big\langle \rho C_i \frac{\partial \psi}{\partial C_j} \Big\rangle + \Theta_i \Big[m \frac{\partial \psi}{\partial C_j} \Big] \Big) \frac{\partial u_j}{\partial r_i} = \aleph[m\psi]. \tag{4.15}$$

Equation (4.15) holds as the key equation to obtain the individual moment equation at any order. The balance equations for the set of 10 variables $\left\{n, \boldsymbol{u}, \boldsymbol{M}\right\}$ follow from the master balance equation (4.15) upon successive substitution of $\psi = 1$, $\boldsymbol{C}$ and $\boldsymbol{CC}$, respectively:

$$\left(\frac{\partial}{\partial t} + \boldsymbol{u}\cdot\nabla\right)\rho = -\rho\nabla\cdot\boldsymbol{u}, \tag{4.16}$$

$$\rho\left(\frac{\partial}{\partial t} + \boldsymbol{u}\cdot\nabla\right)\boldsymbol{u} = -\nabla\cdot\boldsymbol{P} + \frac{\dot{\gamma}}{St_d}\rho\left\langle\frac{d\boldsymbol{c}}{dt}\right\rangle, \tag{4.17}$$

$$\begin{aligned}\rho\left(\frac{\partial}{\partial t} + \boldsymbol{u}\cdot\nabla\right)\boldsymbol{M} = &-\nabla\cdot\boldsymbol{Q} - \boldsymbol{P}\cdot\nabla\boldsymbol{u} - (\boldsymbol{P}\cdot\nabla\boldsymbol{u})^T \\ &- \frac{2\dot{\gamma}}{St_d}\rho\langle\boldsymbol{CC}\rangle \underbrace{- \frac{\dot{\gamma}}{St_d}\rho\langle(\boldsymbol{u}-\boldsymbol{v})\boldsymbol{C}\rangle - \frac{\dot{\gamma}}{St_d}\rho\langle\boldsymbol{C}(\boldsymbol{u}-\boldsymbol{v})\rangle}_{} + \aleph,\end{aligned} \tag{4.18}$$

where $\boldsymbol{P}$ is the total stress, a second-rank tensor, given by

$$\boldsymbol{P} \equiv \rho\langle\boldsymbol{CC}\rangle + \Theta(m\boldsymbol{C}) = \boldsymbol{P}^k + \boldsymbol{P}^c, \tag{4.19}$$

$\boldsymbol{Q}$ is the flux of the second moment, a third-rank tensor, given by

$$\boldsymbol{Q} \equiv \rho\langle\boldsymbol{CCC}\rangle + \Theta(m\boldsymbol{CC}) = \boldsymbol{Q}^k + \boldsymbol{Q}^c, \tag{4.20}$$

and $\aleph$ is the collisional source of second moment, a second-rank tensor, given by

$$\aleph \equiv \aleph(m\boldsymbol{CC}). \tag{4.21}$$

In (4.19-4.20), the first and second terms refer to the corresponding kinetic and collisional contributions, respectively. The balance equations (4.16-4.18) constitute the 10-moment system for the particle-phase of a gas-solid suspension. These equations are supplemented by the conservation equation (4.4) for the gas phase.

On deriving (4.18), we have used the following relation (Sangani *et al.* 1996)

$$\left\langle\left(\delta_{ik}C_j + \delta_{jk}C_i\right)\frac{d\boldsymbol{c}}{dt}\right\rangle = -\left(\frac{2}{\tau_v}\right)R_{diss}\langle C_iC_j\rangle, \tag{4.22}$$

where $R_{diss}(\nu)$ is an effective drag coefficient. The functional dependence of R_{diss} on ν has been explicitly determined by Sangani *et al.* (1996)

$$R_{diss} = k_1(\nu) - k_1(\nu) - k_2(\nu)\ln\varepsilon_m, \tag{4.23}$$

where

$$k_1(\nu) = 1 + 3\sqrt{\frac{\nu}{2}} + \frac{135}{64}\nu \ln \nu + 11.26\nu(1 - 5.1\nu + 16.57\nu^2 - 21.77\nu^3), \tag{4.24}$$

$$k_2(\nu) = \nu g_0, \tag{4.25}$$

$$\varepsilon_m = 9.76\lambda_{MFP}/\sigma, \tag{4.26}$$

g_0 and λ_{MFP} are the radial distribution function and mean free path respectively.

One point we should emphasize here that the hydrodynamic interactions between particles are not considered explicitly in this study. This may appear as a very serious issue at initial instant, but the hydrodynamic interaction is incorporated implicitly in the correction function R_{diss} as shown in Sangani *et al.* (1996). The whole analysis is based on an adjusted Stokes number defined via :

$$St_d = \frac{St}{R_{diss}}. \tag{4.27}$$

In the dilute limit of volume fraction $(\nu \to 0)$ $R_{diss} \to 1$ and consequently we have $St_d = St$.

The integral expressions for the collisional source and flux of ψ are given by (Jenkins & Richman 1985*a*, 1988; Chou & Richman 1998; Saha & Alam 2016),

$$\aleph(\psi) = \frac{\sigma^2}{2}\int\int\int_{\boldsymbol{g}\cdot\boldsymbol{k}>0} \left(\psi_1' + \psi_2' - \psi_1 - \psi_2\right) f^{(2)}(\boldsymbol{c}_1, \boldsymbol{r} - \sigma\boldsymbol{k}, \boldsymbol{c}_2, \boldsymbol{r})(\boldsymbol{k}\cdot\boldsymbol{g})\mathrm{d}\boldsymbol{k}\mathrm{d}\boldsymbol{c}_1\mathrm{d}\boldsymbol{c}_2, \tag{4.28}$$

and

$$\boldsymbol{\Theta}(\psi) = -\frac{\sigma^3}{2}\int\int\int_{\boldsymbol{g}\cdot\boldsymbol{k}>0} (\psi_1' - \psi_1)\boldsymbol{k}\int_0^1 f^{(2)}(\boldsymbol{c}_1, \boldsymbol{r} - \omega\sigma\boldsymbol{k}, \boldsymbol{c}_2, \boldsymbol{r} + \sigma\boldsymbol{k} - \omega\sigma\boldsymbol{k})$$
$$(\boldsymbol{k}\cdot\boldsymbol{g})\mathrm{d}\omega\mathrm{d}\boldsymbol{k}\mathrm{d}\boldsymbol{c}_1\mathrm{d}\boldsymbol{c}_2, \tag{4.29}$$

respectively. The collisional flux term (4.29) takes care of the finite volume effect of the particles and the magnitude of this term decreases with decreasing volume fraction and becomes zero for a dilute gas of point particles.

The integral expressions for the collisional source and flux terms given above are identical with the ones derived in Chapter 3, in analysing the shear flow of a dry granular medium. This point is clear from the fact that the presence of an interstitial fluid is assumed not to affect (no St number dependence on $\aleph$ and $\boldsymbol{\Theta}$) the collision integrals.

4.3.2 Granular Energy : Inelastic and Viscous Dissipations

The balance of granular temperature can be obtained by taking trace of (4.18):

$$\frac{3}{2}\rho\left(\frac{\partial}{\partial t}+\boldsymbol{u}\cdot\nabla\right)T=-\frac{\partial q_\alpha}{\partial x_\alpha}-P_{\alpha\beta}\frac{\partial u_\beta}{\partial x_\alpha}-\mathscr{D}, \tag{4.30}$$

and that of the deviator of the second-moment

$$\left.\begin{aligned}\tfrac{1}{2}\rho\left(\tfrac{\partial}{\partial t}+\boldsymbol{u}\cdot\nabla\right)\widehat{M}_{\alpha\beta}=&-\tfrac{1}{2}\tfrac{\partial}{\partial x_\gamma}\left(Q_{\gamma\alpha\beta}-\tfrac{2}{3}q_\gamma\delta_{\alpha\beta}\right)\\&-\left\{\tfrac{1}{2}\left(P_{\gamma\alpha}\tfrac{\partial u_\beta}{\partial x_\gamma}+P_{\gamma\beta}\tfrac{\partial u_\alpha}{\partial x_\gamma}\right)-\tfrac{1}{3}P_{\gamma\xi}\tfrac{\partial u_\xi}{\partial x_\gamma}\delta_{\alpha\beta}\right\}-\tfrac{R_{diss}}{\tau_v}\rho\widehat{M}_{\alpha\beta}+\tfrac{1}{2}\widehat{\aleph}_{\alpha\beta}\end{aligned}\right\}. \tag{4.31}$$

In above equations,

$$q_\alpha\equiv\frac{1}{2}Q_{\alpha\beta\beta}=\frac{1}{2}\rho M_{\alpha\beta\beta}+\frac{1}{2}\Theta_{\alpha\beta\beta} \tag{4.32}$$

is the total energy flux vector (i.e. the heat flux vector), and

$$\mathscr{D}=\mathscr{D}_{viscous}+\mathscr{D}_{inelastic} \tag{4.33}$$

is the rate of dissipation of kinetic energy per unit volume.

The total energy dissipation rate $\mathscr{D}$ is a sum of energy sink via two mechanisms viz. energy dissipation due to viscous drag and energy dissipation due to inelastic collisions within the particles. For a suspension of zero mean velocity between the particles and the fluid, the rate of viscous energy dissipation $\mathscr{D}_{viscous}$ is (Sangani *et al.* 1996)

$$\mathscr{D}_{viscous}=9\pi\mu_g n\sigma T R_{diss}. \tag{4.34}$$

And the rate of energy dissipation due to inelastic collisions within the particles is given by

$$\mathscr{D}_{inelastic}=-\frac{1}{2}\aleph\left(mC^2\right), \tag{4.35}$$

which must have to be calculated using a proper choice of the single-particle distribution function. Therefore from eqns.(4.30) and (4.33), we can say that for a suspension of inelastic particles, energy input into the system is compensated by two mechanisms viz. (i) the viscous drag and (ii) the dissipative collisions. In absence of any interstitial fluid $\mathscr{D}_{viscous}$ becomes zero and $\mathscr{D}_{inelastic}$ balances the energy input analogous to the dry granular flow as discussed in Chapters (2-3). On the other hand, for suspension of elastic particles $(e\equiv 1)$ the energy input is solely compensated by $\mathscr{D}_{viscous}$ and $\mathscr{D}_{inelastic}$ vanishes identically. Finally, for a suspension

composed of elastic particles, both these terms $\mathscr{D}_{viscous}$, $\mathscr{D}_{inelastic}$ become zero which leads to a continuous increase of energy and we need a thermostat to balance the system.

The moment equations (4.16-4.17) and (4.30), along with constitutive relations for (4.19), (4.32) and (4.33), constitute the Navier-Stokes-order hydrodynamics for a fluidized granular matter; the equation for the deviatoric part of the second moment tensor (4.31) satisfies identically at NS-order.

As clarified in Chapter 3, for an extended hydrodynamic description of granular matter, incorporating normal stress differences, we need the balance equation (4.18) for full second moment tensor, along with mass and momentum balances (4.16-4.17). For a closure of (4.18), the deviatoric part of the third-order $Q_{\gamma\alpha\beta}$,

$$\widehat{Q}_{\gamma\alpha\beta} = Q_{\gamma\alpha\beta} - \frac{1}{5}\left(Q_{\gamma\xi\xi}\delta_{\alpha\beta} + Q_{\alpha\xi\xi}\delta_{\gamma\beta} + Q_{\beta\xi\xi}\delta_{\alpha\gamma}\right), \tag{4.36}$$

is assumed to be zero, and its isotropic part, the heat flux vector (4.32), remain to be evaluated as a constitutive relation. In addition to (4.32), we need to determine constitutive relations for the stress tensor (4.19) and the source of second-moment (4.21) in terms of the gradients of the hydrodynamic fields (ρ, $\boldsymbol{u}$, $\boldsymbol{M}$).

In this present work, as we are focusing on the uniform shear flow problem, the heat flux vector defined in (4.32) is identically zero and we are left to determine constitutive relations for the full stress tensor $\boldsymbol{P}$ (4.19) and the collisional source of second moment $\mathfrak{K}$(4.21).

4.3.3 Molecular Chaos assumption and the Anisotropic Maxwellian Distribution Function

In order to evaluate the collision integrals (4.28) and (4.29), we make the following two assumptions as in Chapter 3.

(i) Assumption of molecular chaos (Chapman & Cowling 1970):

$$f^{(2)}(\boldsymbol{c}_1,\boldsymbol{x}-\boldsymbol{\sigma k},\boldsymbol{c}_2,\boldsymbol{x}) = g_0(\nu) f^{(1)}(\boldsymbol{c}_1,\boldsymbol{x}-\boldsymbol{\sigma k}) f^{(1)}(\boldsymbol{c}_2,\boldsymbol{x}), \tag{4.37}$$

where $g_0(\nu)$ contact radial distribution function of Carnahan & Starling (1969),

$$g_0(\nu) = \frac{(2-\nu)}{2(1-\nu)^3}, \tag{4.38}$$

where

$$\nu = n\pi\sigma^3/6 \tag{4.39}$$

is the local volume fraction of particles.

(ii) The single particle velocity distribution is an anisotropic Maxwellian

$$f^{(1)}(\boldsymbol{c},\boldsymbol{r},t)=\frac{n}{(8\pi^3|\boldsymbol{M}|)^{\frac{1}{2}}}\exp\left(-\frac{1}{2}\boldsymbol{C}\cdot\boldsymbol{M}^{-1}\cdot\boldsymbol{C}\right), \tag{4.40}$$

with $|\boldsymbol{M}|=\det(\boldsymbol{M})$, which contains complete information about the second moment tensor $\boldsymbol{M}$. The choice of (4.40) follows from the maximum entropy principle which has been discussed in Chapter 3.

4.4 Balance of Second Moment in Uniform Shear Flow

For the present problem of steady uniform shear flow ($u_x=\dot{\gamma}y$, $u_y=u_z=0$) of a gas-solid suspension, the number density n, the velocity gradient $\nabla\boldsymbol{u}$ and the components of the second moment tensor $\boldsymbol{M}$ are constants, and the heat flux vector q_α vanishes. As a consequence of this, the ensemble averaged velocity of the particles equals with the local fluid velocity:

$$\boldsymbol{u}=\langle\boldsymbol{c}\rangle=\boldsymbol{v}. \tag{4.41}$$

Therefore the motion between the particles and the suspension has a zero mean relative velocity, yields

$$\boldsymbol{u}-\boldsymbol{v}=0, \tag{4.42}$$

and the under-braced term in eqn.(4.18) vanishes.

Therefore in that case, the mass and momentum balance equations, (4.16) and (4.17), are trivially satisfied and the remaining balance equation (4.18) for the second moment of velocity fluctuations $\boldsymbol{M}=\langle\boldsymbol{CC}\rangle$ simplifies to

$$P_{\delta\beta}u_{\alpha,\delta}+P_{\delta\alpha}u_{\beta,\delta}+2P^k_{\alpha\beta}\frac{\dot{\gamma}}{St_d}=\aleph_{\alpha\beta}, \tag{4.43}$$

where

$$P_{\alpha\beta}=\rho M_{\alpha\beta}+\Theta_{\alpha\beta}=P^k_{\alpha\beta}+P^c_{\alpha\beta}, \tag{4.44}$$

is the total stress tensor. The integral expressions for the collisional stress/collisional flux of second moment $\Theta_{\alpha\beta}\equiv m\Theta_\alpha[C_\beta]$ and the collisional source of second moment $\aleph_{\alpha\beta}=$

$\aleph[mC_\alpha C_\beta]$:

$$\aleph_{\alpha\beta} = A_{\alpha\beta} + \widehat{E}_{\alpha\beta} + \widehat{G}_{\alpha\beta} + \Theta_{\alpha\delta}W_{\beta\delta} + \Theta_{\beta\delta}W_{\alpha\delta}, \tag{4.45}$$

remain same as for dry granular flow and are explicitly given in Chapter-3. Substituting (4.44) and (4.45) into (4.43), the balance equation for the second moment tensor reduces to

$$\rho M_{\delta\beta}(D_{\alpha\delta} + W_{\alpha\delta}) + \rho M_{\delta\alpha}(D_{\beta\delta} + W_{\beta\delta}) + \Theta_{\delta\beta}D_{\alpha\delta} + \Theta_{\delta\alpha}D_{\beta\delta} + 2\rho M_{\alpha\beta}\frac{\dot{\gamma}}{St_d} = A_{\alpha\beta} + \widehat{E}_{\alpha\beta} + \widehat{G}_{\alpha\beta}. \tag{4.46}$$

In the limit of $St_d \to \infty$, eqn. (4.46) reduces to that for dry granular flow as discussed in Chapter- *chapter* : 3.

4.4.1 Second Moment Balance in Rotated Co-ordinate Frame

We can decompose the velocity gradient tensor as

$$\boldsymbol{\nabla} u = \boldsymbol{D} + \boldsymbol{W} = \begin{bmatrix} 0 & \dot{\gamma}/2 & 0 \\ \dot{\gamma}/2 & 0 & 0 \\ 0 & 0 & 0 \end{bmatrix} + \begin{bmatrix} 0 & \dot{\gamma}/2 & 0 \\ -\dot{\gamma}/2 & 0 & 0 \\ 0 & 0 & 0 \end{bmatrix}, \tag{4.47}$$

where $\boldsymbol{D}$ and $\boldsymbol{W}$ are the strain and vorticity tensors, respectively and $\dot{\gamma}$ is the constant shear rate of the flow. Now with the help of figure 4.2 and in terms of following parameters (i) the temperature anisotropy $\eta \propto (T_x - T_y)$, (ii) the non-coaxiality angle $\phi \propto |D_1\rangle \measuredangle |M_1\rangle$ and (iii) the excess temperature along the vorticity direction $\lambda^2 \propto (T - T_z)$, the expressions for the second moment tensor of velocity fluctuations can be written as

$$\boldsymbol{M} = T\begin{bmatrix} 1+\lambda^2+\eta\sin 2\phi & -\eta\cos 2\phi & 0 \\ -\eta\cos 2\phi & 1+\lambda^2-\eta\sin 2\phi & 0 \\ 0 & 0 & 1-2\lambda^2 \end{bmatrix} \equiv T[\delta_{\alpha\beta}] + \widehat{\boldsymbol{M}}. \tag{4.48}$$

The detailed derivation of the second moment tensor (4.48) and the definitions of η, ϕ, λ^2 are given in Chapter-3.

Let us now rewrite (4.46) in a new co-ordinate system $x'y'z'$, formed by the orthonormal triad of eigen-vectors of $\boldsymbol{M}$, i.e., with respect to the co-ordinate system whose axes coincide with the eigen-directions $|M_1\rangle$, $|M_2\rangle$ and $|M_3\rangle$ of the second moment tensor $\boldsymbol{M}$, respectively.

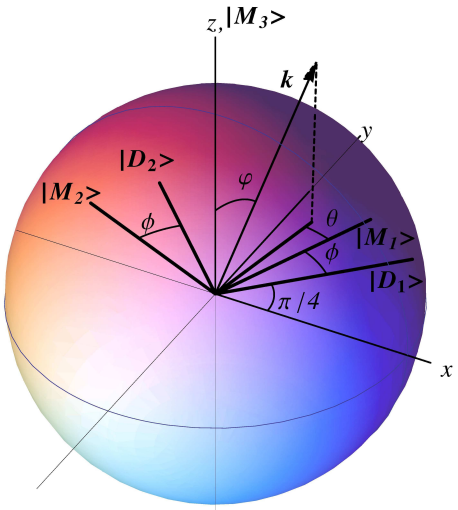

Fig. 4.2 Sketch of the spherical coordinate system showing the eigendirections of the shear tensor $\boldsymbol{D}$ and the second moment tensor $\boldsymbol{M}$.

This amounts to a transformation, see figure 4.2, via the following rotation matrix,

$$\mathscr{R} = \begin{bmatrix} \cos(\phi+\frac{\pi}{4}) & -\sin(\phi+\frac{\pi}{4}) & 0 \\ \sin(\phi+\frac{\pi}{4}) & \cos(\phi+\frac{\pi}{4}) & 0 \\ 0 & 0 & 1 \end{bmatrix}, \tag{4.49}$$

that transforms the second moment tensor,

$$\boldsymbol{M}' = T \begin{bmatrix} 1+\lambda^2-\eta & 0 & 0 \\ 0 & 1+\lambda^2+\eta & 0 \\ 0 & 0 & 1-2\lambda^2 \end{bmatrix}, \tag{4.50}$$

into a diagonal matrix. It is evident from (4.50) that for the present suspension problem also the anisotropy of the second moment in the rotated co-ordinate frame is quantified in terms of (i) the temperature difference η in the shear-plane and (ii) the "excess" temperature T_z^{ex} ($\propto \lambda^2$) along the vorticity direction. With a prime over a quantity denoting its value in the new co-ordinate frame, the second moment balance equation (4.46) transforms into four independent equations in the rotated co-ordinate frame:

(i) the trace of (4.46),

$$-4\eta\rho T\dot{\gamma}\cos 2\phi + 2\dot{\gamma}\left[\left(\Theta_{x'x'}-\Theta_{y'y'}\right)\cos 2\phi - 2\Theta_{x'y'}\sin 2\phi\right] + \underline{\frac{6\rho T\dot{\gamma}}{St_d}} = A_{x'x'}+A_{y'y'}+A_{z'z'}, \tag{4.51}$$

(ii) the z'-z' component of its deviatoric part

$$-4\eta\rho T\dot{\gamma}\cos 2\phi + 2\dot{\gamma}[(\Theta_{x'x'}-\Theta_{y'y'})\cos 2\phi - 2\Theta_{x'y'}\sin 2\phi] + \underline{\frac{12\rho T\dot{\gamma}\lambda^2}{St_d}} = -3\widehat{\Gamma}_{z'z'}, \tag{4.52}$$

(iii) the difference between the x'-x' and y'-y' components

$$4\left(1+\lambda^2\right)\rho T\dot{\gamma}\cos 2\phi + 2\dot{\gamma}\left(\Theta_{x'x'}+\Theta_{y'y'}\right)\cos 2\phi - \underline{\frac{4\rho T\dot{\gamma}\eta}{St_d}} = \Gamma_{x'x'}-\Gamma_{y'y'}, \tag{4.53}$$

and, finally, (iv) the off-diagonal x'-y' component

$$2\rho T\dot{\gamma}\left[\eta - \left(1+\lambda^2\right)\sin 2\phi\right] - \left(\Theta_{x'x'}+\Theta_{y'y'}\right)\dot{\gamma}\sin 2\phi = \Gamma_{x'y'}, \tag{4.54}$$

where

$$\Gamma_{\alpha\beta} = A_{\alpha\beta} + \widehat{E}_{\alpha\beta} + \widehat{G}_{\alpha\beta}. \tag{4.55}$$

The explicit expressions for the various integrals $A_{\alpha\beta}$, $\widehat{E}_{\alpha\beta}$, $\widehat{G}_{\alpha\beta}$ and $\Theta_{\alpha\beta}$ appearing in (4.51-4.54) remain the same as for the dry granular flow and we refer to Chapter-3 for details. The underlined terms in (4.51)-(4.54) are the contributions from the fluid phase.

Equations (4.51-4.54) represent a system of four nonlinear algebraic equations with four unknowns viz. (i) the temperature anisotropy $\eta \propto (T_x - T_y)$, (ii) the non-coaxiality angle $\phi \propto |D_1\rangle \measuredangle |M_1\rangle$, (iii) the excess temperature along the vorticity direction $\lambda^2 \propto (T - T_z)$ and (iv) the Savage-Jeffrey parameter (Savage & Jeffrey 1981) $R = \dot{\gamma}\sigma/8\sqrt{T}$ when the volume fraction ν, dissipation coefficient e and Stokes number St_d are specified. We must solve this system of equations at different orders in shear rate to obtain the rheological properties of the particle phase for the whole range of volume fraction, restitution coefficient and Stokes number.

4.5 Exact Solution at Burnett Order for the Whole Range of Density

Retaining terms up to second order $O(\eta^m \lambda^n R^p \sin^q(2\phi),\ m+n+p+q \leq 2)$ in the corresponding equations for the second moment balance 4.51-4.54, we obtain the following set of coupled nonlinear algebraic equations

$$\left.\begin{aligned}
20\sqrt{\pi}\left\{1+\tfrac{4}{5}(1+e)\nu g_0\right\}\eta R\cos 2\phi + 128(1+e)\nu g_0 R^2 \\
-3(1-e^2)\nu g_0(10+\eta^2+32R^2+8\sqrt{\pi}\eta R\cos 2\phi) - \frac{60\sqrt{\pi}R}{St_d} = 0 \\
35\sqrt{\pi}\eta R\cos 2\phi + (1+e)\nu g_0\{32(1+3e)R^2 - 3(3-e)(\eta^2+21\lambda^2) \\
-8\sqrt{\pi}(4-3e)\eta R\cos 2\phi\} - \frac{210\sqrt{\pi}\lambda^2 R}{St_d} = 0 \\
5\sqrt{\pi}R\cos 2\phi - (1+e)\nu g_0\{3(3-e)\eta + 2(1-3e)\sqrt{\pi}R\cos 2\phi\} - \frac{10\sqrt{\pi}\eta R}{St_d} = 0 \\
5(\eta - \sin 2\phi) + 2(1+e)(1-3e)\nu g_0 \sin(2\phi) = 0
\end{aligned}\right\} \quad (4.56)$$

These equations represent the second-moment balance equations at "Burnett order" (Burnett 1935) since all terms up to the second order in the shear rate have been retained.

Equations (4.56) admit an exact solution

$$\left.\begin{aligned}
\eta^2 &= \frac{30(1-e^2)St_d\nu g_0 + 60\sqrt{\pi}R - 32(1+e)(1+3e)St_d\nu g_0 R^2}{40\sqrt{\pi}R + 3(1+e)(11-3e)St_d\nu g_0} \\
\phi &= \tfrac{1}{2}\sin^{-1}\left[\frac{5}{\{5-2(1+e)(1-3e)\nu g_0\}}\eta\right] \\
\lambda^2 &= \frac{140\sqrt{\pi}R + (1+e)\nu g_0 St_d\{70(1-e) - 32(1+3e)R^2 - (5+3e)\eta^2\} - 24\sqrt{\pi}(1+e)^2\nu g_0\eta R\cos(2\phi)}{28\{3(1+e)(3-e)\nu g_0 St_d + 10\sqrt{\pi}R\}} \\
\frac{\eta}{R}\cos(2\phi) &= \frac{\sqrt{\pi}}{\left\{3(1+e)(3-e)\nu g_0 + 10\sqrt{\pi}\left(\frac{R}{St_d}\right)\right\}}\cos^2(2\phi)\{5+2(1+e)(3e-1)\nu g_0\}
\end{aligned}\right\} \quad (4.57)$$

where R is the real positive root of the quadratic equation

$$\begin{aligned}
&\Big[200(23-11e)\pi + 250(1-e)\pi St_d^2 - 96(3-e)^2(1+e)^2(1+3e)St_d^2\nu^2 g_0^2 \\
&\qquad -(11-3e)\pi St_d^2\{5-2(1+e)(1-3e)\nu g_0\}^2\Big]R^2 \\
&+60(1+e)(3-e)(19-13e)\sqrt{\pi}(St_d)\nu g_o R + 90(1+e)(1-e^2)(3-e)^2 St_d^2\nu^2 g_0^2 = 0.
\end{aligned} \quad (4.58)$$

For specified values of ν, e and St_d, the Savage-Jeffrey parameter R is determined from (4.58) and the remaining quantities are from (4.57). This provides the "exact" solution for R, η, λ and ϕ as functions of ν, e and St_d. The super-Burnett [(4.65)] and super-super-Burnett [(4.66)] equations are solved via regular perturbation expansion around the exact Burnett-order solution (4.57-4.58), see §4.5.2.

4.5.1 Dry Granular Limit ($St \to \infty$): Recovering Results of Chapter 3

In this section we take the limit $St \to \infty$ of the Burnett order solution described above in §4.5 and recover the related results of Chapter 3 (Saha & Alam 2016) fro dry granular flow.

The second equation of (4.57) gives

$$\sin 2\phi = \frac{5}{\{5-2(1+e)(1-3e)\nu g_0\}}\eta, \tag{4.59}$$

and the third equation of (4.56) in the limit of $St \to \infty$ simplifies to

$$\cos(2\phi) = \frac{3(1+e)(3-e)\nu g_0}{\sqrt{\pi}\{5-2(1+e)(1-3e)\nu g_0\}R}\eta. \tag{4.60}$$

Upon division (4.59) by (4.60) we get

$$R = \frac{3(1+e)(3-e)}{\sqrt{\pi}}\nu g_0 \tan 2\phi, \tag{4.61}$$

also from (4.59)

$$\eta = \frac{\{5-2(1+e)(1-3e)\nu g_0\}}{5}\sin 2\phi, \tag{4.62}$$

are respectively equations 3.93-(c) and 3.93-(a) of of Chapter 3.

Now from (4.57) $(St \to \infty)$

$$-32(1+e)(1+3e)\nu g_0 R^2 = -30(1-e^2)\nu g_0 + 3(1+e)(11-3e)\nu g_0 \eta^2. \tag{4.63}$$

Substituting eqns. (4.60) and (4.63) into (4.57) and dropping the terms containing effects from the gas phase, we get,

$$\begin{aligned}\lambda^2 \;=\; & \frac{10(1-e)}{21(3-e)} + \frac{[(7-3e)\{5-2(1+e)(1-3e)\nu g_0\} - 18(1+e)^2(3-e)\nu g_0]}{525(3-e)} \\ & \times\{5-2(1+e)(1-3e)\nu g_0\}\sin^2 2\phi,\end{aligned} \tag{4.64}$$

equation 3.93-(b) of Chapter 3.

Two points we would like to mention here

(i) The Burnett order solution for the present suspension problem [§4.5] eventually boils down to an equation (4.58) for determining R. On the other hand the corresponding Burnett order solution for the dry counterpart reduces to an equation determining the non-coaxial angle ϕ, nevertheless both of these two approaches give rise to identical results for $St \to \infty$.

(ii) Secondly, the off-diagonal x-y component (4.54) of the second moment balance (4.46) remains same for the dry granular flows and gas-solid suspensions. This is because of the fact that the term containing the effect of interstitial fluid becomes a diagonal matrix in the rotated co-ordinate frame of axes; consequently, the off-diagonal component vanishes, leads to identical x-y components of equations for both of these (dry and wet) cases.

4.5.2 Beyond Burnett Order: Perturbation Solutions at Super and Super-Super Burnett Orders

Retaining terms up-to third order $O(\eta^m\lambda^n R^p \sin^q(2\phi))$, $m+n+p+q \leq 3$ in the related integrals appearing in (4.51-4.54), we obtain the following set of coupled nonlinear algebraic equations

$$\left.\begin{array}{c} 20\sqrt{\pi}\Big\{1+\frac{4}{5}(1+e)\nu g_0\Big\}\eta R\cos 2\phi + 128(1+e)\nu g_0 R^2 \\ -3(1-e^2)\nu g_0(10+\eta^2+32R^2+8\sqrt{\pi}R\eta\cos 2\phi) - \underline{\frac{60\sqrt{\pi}R}{St_d}} = 0 \\ 35\sqrt{\pi}\eta R\cos 2\phi + (1+e)\nu g_0\Big\{32(1+3e)R^2 - 3(3-e)(\eta^2+21\lambda^2) \\ -8\sqrt{\pi}(4-3e)\eta R\cos 2\phi\Big\} - \underline{\frac{210\sqrt{\pi}\lambda^2 R}{St_d}} = 0 \\ 210\sqrt{\pi}(1+\lambda^2)R\cos 2\phi - (1+e)\nu g_0\big[12\sqrt{\pi}\big\{7(1-3e)+4(4-3e)\lambda^2 \\ -32(1+e)R^2\big\}R\cos 2\phi + \eta\big\{126(3-e) - 3(3-e)\eta^2 + 36(3-e)\lambda^2 \\ +64(4-3e)R^2 - 32(5+3e)R^2\cos 4\phi\big\}\big] - \underline{\frac{420\sqrt{\pi}\eta R}{St_d}} = 0 \\ 105\sqrt{\pi}\big\{\eta - (1+\lambda^2)\sin 2\phi\big\} - 2(1+e)\nu g_0 \sin 2\phi\big[16(5+3e)\eta R\cos 2\phi \\ -3\sqrt{\pi}\big\{7(1-3e)+4(4-3e)\lambda^2 - 32(1+e)R^2\big\}\big] = 0 \end{array}\right\}. \quad (4.65)$$

for four unknowns η, λ, R and ϕ, given that the restitution coefficient (e), Stokes number (St_d) and the volume fraction (ν) are known. Similarly, retaining terms up-to fourth order $O(\eta^m\lambda^n R^p \sin^q(2\phi))$, $m+n+p+q \leq 4$, the equations (4.51-4.54) simplify to

$$\left.\begin{aligned}
&1680\sqrt{\pi}\eta R\cos 2\phi - 3(1-e^2)\nu g_0\big(840+84\eta^2+3\eta^4+2688R^2+1024R^4\\
&-128R^2\eta^2+768R^2\lambda^2-24\eta^2\lambda^2+252\lambda^4+672\sqrt{\pi}\eta R\cos 2\phi-64\eta^2R^2\cos 4\phi\big)\\
&+64(1+e)\nu g_0 R\big\{21\sqrt{\pi}\eta\cos 2\phi+4R(42-2\eta^2+12\lambda^2+32R^2-\eta^2\cos 4\phi)\big\}\\
&-\frac{5040\sqrt{\pi}R}{St_d}=0\\
&2310\sqrt{\pi}\eta R\cos 2\phi+(1+e)\nu g_0\big[32R^2\big\{66+8\eta^2-165\lambda^2+3e(66-4\eta^2+33\lambda^2)\big\}\\
&-9(3-e)\big\{\eta^4+11\eta^2(2-\lambda^2)+66\lambda^2(7-\lambda^2)\big\}+1024(5+3e)R^4\\
&-16R\eta\big\{33\sqrt{\pi}(4-3e)\cos 2\phi-4(2-3e)\eta R\cos 4\phi\big\}\big]-\frac{13860\sqrt{\pi}\lambda^2R}{St_d}=0\\
&210\sqrt{\pi}(1+\lambda^2)R\cos 2\phi-(1+e)\nu g_0\big[12\sqrt{\pi}\big\{7(1-3e)+4(4-3e)\lambda^2\\
&-32(1+e)R^2\big\}R\cos 2\phi+\eta\big\{126(3-e)-3(3-e)\eta^2+36(3-e)\lambda^2\\
&+64(4-3e)R^2-32(5+3e)R^2\cos 4\phi\big\}\big]-\frac{420\sqrt{\pi}\eta R}{St_d}=0\\
&105\sqrt{\pi}\big\{\eta-(1+\lambda^2)\sin 2\phi\big\}-2(1+e)\nu g_0\sin 2\phi\big[16(5+3e)\eta R\cos 2\phi\\
&-3\sqrt{\pi}\big\{7(1-3e)+4(4-3e)\lambda^2-32(1+e)R^2\big\}\big]=0
\end{aligned}\right\}\tag{4.66}$$

For specified values of the restitution coefficient (e) and the density (ν), we can use the standard Newton-Raphson's method to solve both (4.65) and (4.66), yielding solutions for η, λ^2, R and ϕ that are correct up-to orders $O(\eta^m\lambda^nR^p\sin^q(2\phi))$, $m+n+p+q\leq 3$ and $O(\eta^m\lambda^nR^p\sin^q(2\phi))$, $m+n+p+q\leq 4$, respectively.

It must be noted that equations (4.65) and (4.66) belong to the 'super-Burnett' and 'super-super-Burnett' orders since they incorporate terms that are at most 'cubic' and 'quartic' in the shear-rate ($R\sim\dot{\gamma}$) respectively. Therefore, the resulting solutions of (4.65) and (4.66) for η, λ, R and ϕ and the transport coefficients will be dubbed 'super-Burnett' and 'super^2-Burnett' solutions, respectively.

But below we present a methodology to solve these higher order system analytically, by opting for a regular perturbation technique. We assume the solution of the form

$$\left.\begin{aligned}
\eta &= \eta^{(2)}+\varepsilon\eta^{(3)}+\varepsilon^2\eta^{(4)}+\cdots\\
\lambda^2 &= \lambda^{(2)}+\varepsilon\lambda^{(3)}+\varepsilon^2\lambda^{(4)}+\cdots\\
R &= R^{(2)}+\varepsilon R^{(3)}+\varepsilon^2R^{(4)}+\cdots\\
\sin 2\phi &= \sin 2\phi^{(2)}+\varepsilon\sin 2\phi^{(3)}+\varepsilon^2\sin 2\phi^{(4)}+\cdots
\end{aligned}\right\}.\tag{4.67}$$

In the above expressions $\varepsilon\sim\dot{\gamma}$ and the superscript "2" corresponds to the "Burnett-order" solution (closed form expressions (4.57-4.58) are given in the previous section which is valid

for the whole range of density) and the superscripts “3” and “4" correspond to the corrections beyond second order.

Plugging (4.67) into corresponding third (super-Burnett, 4.65) and fourth (super-super-Burnett, 4.66) order equations and after performing some cumbersome algebra we obtain the solutions at third-order as

$$\left.\begin{aligned}\eta^{(3)} &= 0\\ \lambda^{(3)} &= 0\\ R^{(3)} &= 0\\ \sin 2\phi^{(3)} &= 0\end{aligned}\right\}. \tag{4.68}$$

The solutions at fourth-order are given by :

$$\begin{aligned}
\varepsilon^2\eta^{(4)} = &-\Bigg[\Big[\sqrt{\pi}(1+e)\nu g_0\cos 2\phi^{(2)}\{5-2(1+e)(1-3e)\nu g_0\}\Big\{1024(5+3e){R^{(2)}}^4\\
&-192(1+3e){R^{(2)}}^2\Big({\eta^{(2)}}^2-4{\lambda^{(2)}}^2\Big)-9(1-e)\Big({\eta^{(2)}}^4-8{\eta^{(2)}}^2{\lambda^{(2)}}^2+84{\lambda^{(2)}}^4\Big)\Big\}\Big]\\
&-\Big[8\Big\{5\sqrt{\pi}\eta^{(2)}\cos 2\phi^{(2)}+2(1+e)\nu g_0\Big(8(1+3e)R^{(2)}-(1-3e)\sqrt{\pi}\eta^{(2)}\cos 2\phi^{(2)}\Big)\Big\}\\
&\times\Big\{210\sqrt{\pi}{\lambda^{(2)}}^2R^{(2)}\cos 2\phi^{(2)}-48(1+e)\sqrt{\pi}\nu g_0R^{(2)}\cos 2\phi^{(2)}\Big((4-3e){\lambda^{(2)}}^2-8(1+e){R^{(2)}}^2\Big)\\
&\qquad -3(1+e)\nu g_0\eta^{(2)}\Big(32(1-3e){R^{(2)}}^2-(3-e)({\eta^{(2)}}^2-{\lambda^{(2)}}^2)\Big)\Big\}\Big]\Bigg]\\
&\overline{168\Big[\sqrt{\pi}\cos 2\phi^{(2)}\Big\{2\sqrt{\pi}\cos 2\phi^{(2)}\{5-2(1+e)(1-3e)\nu g_0\}R^{(2)}-3(1-e^2)\nu g_0\eta^{(2)}\Big\}}\\
&\times\{5-2(1+e)(1-3e)\nu g_0\}+2\Big\{3(1+e)(3-e)\nu g_0+10\sqrt{\pi}\underline{\Big(\frac{R}{St}\Big)}\Big\}\Big\{5\sqrt{\pi}\eta^{(2)}\cos 2\phi^{(2)}\\
&+2(1+e)\nu g_0\Big(8(1+3e)R^{(2)}-(1-3e)\sqrt{\pi}\eta^{(2)}\cos 2\phi^{(2)}\Big)\Big\}\Big]
\end{aligned} \tag{4.69}$$

$$
\begin{aligned}
&\varepsilon^2\lambda^{(4)} = \\
&\frac{1}{77616\lambda^{(2)}}\Bigg(\Bigg[_a \frac{28(1+e)\nu g_0}{\left\{3(1+e)(3-e)\nu g_0+10\sqrt{\pi}\underline{\left(\frac{R}{St}\right)}\right\}}\Big\{1024(5+3e)R^{(2)^4} \\
&+96R^{(2)^2}\left(2(2-3e)\eta^{(2)^2}-11(5-3e)\lambda^{(2)^2}\right)-9(3-e)\left(\eta^{(2)^4}-11\eta^{(2)^2}\lambda^{(2)^2}-66\lambda^{(2)^4}\right)\Big\}\Bigg]_a \\
&-\Bigg[_b \frac{132}{\left\{3(1+e)(3-e)\nu g_0+10\sqrt{\pi}\underline{\left(\frac{R}{St}\right)}\right\}\sqrt{\pi}\{5-2(1+e)(1-3e)\nu g_0\}\nu g_0\cos 2\phi^{(2)}} \\
&\times\left[35\sqrt{\pi}\eta^{(2)}\cos 2\phi^{(2)}+8(1+e)\nu g_0\left\{8(1+3e)R^{(2)}-(4-3e)\sqrt{\pi}\eta^{(2)}\cos 2\phi^{(2)}\right\}\right] \\
&\times\Big[70\sqrt{\pi}\lambda^{(2)^2}R^{(2)}\cos 2\phi^{(2)}+(1+e)\nu g_0\Big\{16\sqrt{\pi}R^{(2)}\cos 2\phi^{(2)}\left(8(1+e)R^{(2)^2}-(4-3e)\lambda^{(2)^2}\right) \\
&-32(1-3e)\eta^{(2)^2}R^{(2)}+(3-e)\eta^{(2)}\left(\eta^{(2)^2}-12\lambda^{(2)^2}\right)\Big\}\Big]\Bigg]_b \\
&+\Bigg[_c 1848\varepsilon^2\eta^{(4)}\Big[\frac{\sqrt{\pi}\{35-8(1+e)(4-3e)\nu g_0\}R^{(2)}\cos 2\phi^{(2)}-6(3-e)(1+e)\nu g_0\eta^{(2)}}{\left\{3(1+e)(3-e)\nu g_0+10\sqrt{\pi}\underline{\left(\frac{R}{St}\right)}\right\}} \\
&+\frac{\left\{35\sqrt{\pi}\eta^{(2)}\cos 2\phi^{(2)}+8(1+e)\nu g_0\left(8(1+3e)R^{(2)}-(4-3e)\sqrt{\pi}\eta^{(2)}\cos 2\phi^{(2)}\right)\right\}}{\sqrt{\pi}\{5-2(1+e)(1-3e)\nu g_0\}\cos 2\phi^{(2)}}\Big]\Bigg]_c\Bigg)
\end{aligned}
\tag{4.70}
$$

$$
\begin{aligned}
\varepsilon^2 R^{(4)} = \frac{1}{42\sqrt{\pi}\{5-2(1+e)(1-3e)\nu g_0\}\cos 2\phi^{(2)}}\Big[&-210\sqrt{\pi}\lambda^{(2)^2}R^{(2)}\cos^{(2)}2\phi \\
&+48(1+e)\sqrt{\pi}\nu g_0 R^{(2)}\cos^{(2)}2\phi\left\{(4-3e)\lambda^{(2)^2}-8(1+e)R^{(2)^2}\right\} \\
&+3(1+e)\nu g_0\eta\left\{32(1-3e)R^{(2)^2}-(3-e)\left(\eta^{(2)^2}-12\lambda^{(2)^2}\right)\right\} \\
&+42\varepsilon^2\eta^{(4)}\left\{3(3-e)(1+e)\nu g_0+10\sqrt{\pi}\underline{\left(\frac{R}{St}\right)}\right\}\Big]
\end{aligned}
\tag{4.71}
$$

$$
\begin{aligned}
&\varepsilon^2\sin 2\phi^{(4)} = \Big[105\sqrt{\pi}\left(\varepsilon^2\eta^{(4)}-\lambda^{(2)^2}\sin^{(2)}2\phi\right) \\
&-\frac{2(1+e)\nu g_0\sin^{(2)}2\phi\left\{16(5+3e)\eta^{(2)}R^{(2)}\cos^{(2)}2\phi-3\sqrt{\pi}\left(4(4-3e)\lambda^{(2)^2}-32(1+e)R^{(2)^2}\right)\right\}\Big]}{21\sqrt{\pi}\{5-2(1+e)(1-3e)\nu g_0\}}
\end{aligned}
\tag{4.72}
$$

In absence of any interstitial fluid i.e in the limit of $St \to \infty$, the underlying terms in (4.69-4.72) disappear and we obtain the corresponding super-super-Burnett order solutions for the dry-granular flow. On removing the terms containing St number dependence from (4.69-4.72), the resulted expressions match exactly with the solution provided in Chapter 3 (Saha & Alam 2016) for uniform shear flow of dry granular matter.

4.6 Stress Tensor and Transport Coefficients

The dimensionless stress tensor in this uniformly sheared gas-solid suspension problem, takes the form

$$\begin{aligned} \boldsymbol{P}^* &= \frac{\boldsymbol{P}}{\rho_p U_R^2} = \begin{pmatrix} P_{xx}^* & P_{xy}^* & 0 \\ P_{yx}^* & P_{yy}^* & 0 \\ 0 & 0 & P_{zz}^* \end{pmatrix} \\ &\equiv \begin{pmatrix} p^* & 0 & 0 \\ 0 & p^* & 0 \\ 0 & 0 & p^* \end{pmatrix} + \begin{pmatrix} \frac{2}{3}\mathscr{N}_1^* + \frac{1}{3}\mathscr{N}_2^* & -\mu^* & 0 \\ -\mu^* & -\frac{1}{3}\mathscr{N}_1^* + \frac{1}{3}\mathscr{N}_2^* & 0 \\ 0 & 0 & -\frac{1}{3}\mathscr{N}_1^* - \frac{2}{3}\mathscr{N}_2^* \end{pmatrix} \end{aligned} \tag{4.73}$$

where

$$p^* = \frac{1}{3}\left(P_{xx}^* + P_{yy}^* + P_{zz}^*\right), \tag{4.74}$$

$$\mu^* = -P_{xy}^*, \tag{4.75}$$

$$\mathscr{N}_1^* = \left(P_{xx}^* - P_{yy}^*\right), \tag{4.76}$$

$$\mathscr{N}_2^* = \left(P_{yy}^* - P_{zz}^*\right) \tag{4.77}$$

is the pressure, the shear viscosity, the first and second normal stress differences respectively; here ρ_p is material/intrinsic density of particles and $U_R = \dot{\gamma}\sigma$ is the reference velocity scale.

The dimensionless temperature, scaled first and second normal stress differences are defined in the following way

$$T^* = \frac{T}{U_R^2}, \tag{4.78}$$

$$\mathscr{N}_1 = \frac{3(P_{xx} - P_{yy})}{(P_{xx} + P_{yy} + P_{zz})}, \tag{4.79}$$

and

$$\mathscr{N}_2 = \frac{3(P_{yy} - P_{zz})}{(P_{xx} + P_{yy} + P_{zz})}, \tag{4.80}$$

where the explicit expressions of all these above transport coefficients are given below.

4.6.1 Shear Stress and Viscosity

Retaining terms up-to the fourth-order $O(\eta^m \lambda^n R^n \sin^q(2\phi),\ m+n+p+q \leq 4)$, the dimensionless shear stress can be written as :

$$\begin{aligned}\frac{P^*_{xy}}{\nu T^*} &= -\eta\cos 2\phi - \frac{4(1+e)\nu g_0}{105\sqrt{\pi}}\Big[21R\Big\{8+\sqrt{\pi}\frac{\eta\cos 2\phi}{R}\Big\} \\ &\quad +48\lambda^2 R + 4R^3\Big\{32-\frac{\eta^2}{R^2}\Big(2+(1+2\cos^2 2\phi)\Big)\Big\}\Big], \end{aligned} \tag{4.81}$$

with the dimensionless temperature T^* being given by (4.78). The expression for the dimensionless shear viscosity, $\mu^*{=}{-}P_{xy}/\rho_p U_R^2{=}{-}P^*_{xy}$, follows from (4.81):

$$\begin{aligned}\mu^* &= \frac{\nu\sqrt{T^*}}{8}\Big[\frac{\eta\cos 2\phi}{R}+\frac{4(1+e)\nu g_0}{105\sqrt{\pi}}\Big(21\Big\{8+\sqrt{\pi}\frac{\eta\cos 2\phi}{R}\Big\} \\ &\quad \underbrace{+48\lambda^2+128R^2-4\eta^2\Big\{2+(1+2\cos^2 2\phi)\Big\}}\Big)\Big], \end{aligned} \tag{4.82}$$

where the under-braced terms represent nonlinear contributions beyond the Navier-Stokes (NS) order.

Neglecting quadratic- and higher-order terms in (4.82), we obtain the NS-order expression for the shear viscosity:

$$\mu^*_{NS} = \frac{\nu\sqrt{T^*}}{8}\Big[\frac{\eta\cos 2\phi}{R}+\frac{4(1+e)\nu g_0}{5}\Big(\frac{8}{\sqrt{\pi}}+\frac{\eta\cos 2\phi}{R}\Big)\Big]. \tag{4.83}$$

4.6.2 Expression for Shear Viscosity in Dry Granular Limit

For the case of dry granular flow ($St_d \to \infty$), we have from (4.57)

$$\frac{\eta}{R}\cos(2\phi) = \frac{\sqrt{\pi}}{3(1+e)(3-e)}\cos^2(2\phi)\Big(\frac{5}{\nu g_0}+2(1+e)(3e-1)\Big) \tag{4.84}$$

$$\xrightarrow{\phi=0} \frac{\sqrt{\pi}}{3(1+e)(3-e)}\Big(\frac{5}{\nu g_0}+2(1+e)(3e-1)\Big), \tag{4.85}$$

with last expression holds at Navier-Stokes ($\phi \to 0$) order. Substituting (4.85) into (4.83), we obtain the expression for shear viscosity at Navier-Stokes order

$$\begin{aligned}\mu_{NS}^{inelastic} &= \sqrt{T^*}\Bigg[\frac{5\sqrt{\pi}}{24(1+e)(3-e)g_0}\left(1+\frac{2(1+e)(3e-1)}{5}\nu g_0\right)\left(1+\frac{4(1+e)}{5}\nu g_0\right) \\ &\qquad +\frac{4(1+e)}{5\sqrt{\pi}}\nu^2 g_0\Bigg] \\ &= \mu_k^* + \mu_c^*, \end{aligned} \tag{4.86}$$

where

$$\mu_k^* = \frac{5\sqrt{\pi}\sqrt{T^*}}{24(1+e)(3-e)g_0}\left(1+\frac{2(1+e)(3e-1)}{5}\nu g_0\right), \tag{4.87}$$

$$\mu_c^* = \frac{(1+e)\nu^2 g_0\sqrt{T^*}}{10\sqrt{\pi}}\left\{8+\frac{5\pi}{3(1+e)(3-e)\nu g_0}\left(1+\frac{2(1+e)(3e-1)}{5}\nu g_0\right)\right\} \tag{4.88}$$

are respectively the kinetic and collisional components of viscosity.

Equation (4.86) matches exactly with the expression for the shear viscosity (with a factor $\rho_p\dot{\gamma}\sigma^2$) of a dense granular gas given as equation (69) in Jenkins & Richman (1985*a*).

4.6.3 Normal Stress Components and the Pressure

The diagonal components of the stress tensor, correct up-to $O(\eta^m\lambda^n R^n \sin^q(2\phi),\ m+n+p+q\leq 4)$, have following expressions:

$$\begin{aligned}\frac{P_{xx}^*}{\nu T^*} &= (1+\lambda^2+\eta\sin 2\phi)+\frac{2(1+e)\nu g_0}{1155}\Big[33(35+96R^2+14\eta\sin 2\phi+14\lambda^2) \\ &\quad +\frac{8}{\sqrt{\pi}}\eta R\cos 2\phi\left\{3(66+5\eta^2-22\lambda^2)-160R^2-22\eta\sin 2\phi\right\}\Big], \end{aligned} \tag{4.89}$$

$$\begin{aligned}\frac{P_{yy}^*}{\nu T^*} &= (1+\lambda^2-\eta\sin 2\phi)+\frac{2(1+e)\nu g_0}{1155}\Big[33(35+96R^2-14\eta\sin 2\phi+14\lambda^2) \\ &\quad +\frac{8}{\sqrt{\pi}}\eta R\cos 2\phi\left\{3(66+5\eta^2-22\lambda^2)-160R^2+22\eta\sin 2\phi\right\}\Big], \end{aligned} \tag{4.90}$$

$$\begin{aligned}\frac{P_{zz}^*}{\nu T^*} &= (1-2\lambda^2)+\frac{2(1+e)\nu g_0}{1155}\Big[33(35+32R^2-28\lambda^2) \\ &\quad +\frac{8}{\sqrt{\pi}}\eta R\cos 2\phi\left\{(66+3\eta^2-32R^2)\right\}\Big]. \end{aligned} \tag{4.91}$$

The dimensionless mean pressure, correct up-to $O(\eta^m\lambda^n R^n \sin^q(2\phi),\ m+n+p+q\leq 4)$, is given by

$$p^* = \nu T^*\Big[1+\frac{2(1+e)\nu g_0}{315}\Big\{315+\underbrace{672R^2+\frac{8}{\sqrt{\pi}}\eta R\cos 2\phi(42+3\eta^2-32R^2-12\lambda^2)}\Big\}\Big]. \tag{4.92}$$

Neglecting the 'under-braced' non-linear terms in (4.92), we obtain the well-known expression for pressure,

$$p^*_{NS} = \nu T^*(1+2(1+e)\nu g_0), \tag{4.93}$$

at the NS-order.

4.6.4 First and Second Normal Stress Differences

Subtracting (4.90) from (4.89) the expression for the first normal stress difference (4.76) is found to be

$$\begin{aligned}\mathscr{N}_1^* &= 2\eta\sin(2\phi)\left(1+\frac{4(1+e)\nu g_0}{105}\Big[21-\frac{8}{\sqrt{\pi}}\eta R\cos(2\phi)\Big]\right)\nu T^* \\ &\quad +O(\eta^m\lambda^n R^n\sin^q(2\phi),\ m+n+p+q\geq 5),\end{aligned} \tag{4.94}$$

with its kinetic and collisional contributions ($\mathscr{N}_1^* = \mathscr{N}_1^{k*}+\mathscr{N}_1^{c*}$), respectively, being given by

$$\mathscr{N}_1^{k*} = 2\eta\sin(2\phi)\nu T^* \tag{4.95}$$

$$\mathscr{N}_1^{c*} = \frac{8(1+e)\nu g_0}{1155}\Big[231-\frac{8}{\sqrt{\pi}}\eta R\cos(2\phi)\Big]\eta\sin(2\phi)\nu T^*. \tag{4.96}$$

Similarly, the expression for the second normal stress difference (4.77) is obtained from (4.90) and from (4.91):

$$\begin{aligned}\mathscr{N}_2^* &= \mathscr{N}_2^{k*}+\mathscr{N}_2^{c*} \\ &= \big[3\lambda^2-\eta\sin(2\phi)\big]\nu T^*+\frac{32(1+e)\nu^2T^*g_0}{1155}\Big[264\left(\frac{1}{2}+\frac{7}{\nu}\mathscr{N}_2^{k*}\right)R^2 \\ &\quad +\frac{1}{\sqrt{\pi}}\eta R\cos 2\phi\Big\{(66+6\eta^2-64R^2-33\lambda^2)+11\eta\sin 2\phi\Big\}\Big] \\ &\quad +O(\eta^m\lambda^n R^n\sin^q(2\phi),\ m+n+p+q\geq 5)\end{aligned} \tag{4.97}$$

with its kinetic and collisional components at $O(\eta^m \lambda^{2n} R^p,\ m+n+p \leq 4)$ being given by

$$\mathscr{N}_2^{k*} = \left[3\lambda^2 - \eta \sin(2\phi)\right] \nu T^* \tag{4.98}$$

$$\mathscr{N}_2^{c*} = \frac{32(1+e)\nu^2 T^* g_0}{1155}\left[264\left(\frac{1}{2}+\frac{7}{\nu}\mathscr{N}_2^{k*}\right)R^2 + \frac{1}{\sqrt{\pi}}\eta R\cos 2\phi \times\left\{(66+6\eta^2-64R^2-33\lambda^2)+11\eta\sin 2\phi\right\}\right]. \tag{4.99}$$

where T^* is the dimensionless temperature (4.78).

4.6.5 Universal Expressions for Transport Coefficients

One point should be noted here that all the expressions for transport coefficients obtained above are exactly the same as those obtained for the dry-granular shear flow (**Chapter** refer). But a careful look at these expressions reveals that the difference follows via the individual expressions of η, λ, R and ϕ. These parameters obtained for the dry granular flows and gas-solid suspensions are different in the sense that the latter contains an explicit Stokes number (St_d) dependence, clearly shown in §4.5 and §4.5.2.

$$\left.\begin{aligned}\eta &\equiv \eta(\nu, e, St_d)\\ \phi &\equiv \phi(\nu, e, St_d)\\ \lambda &\equiv \lambda(\nu, e, St_d)\\ R &\equiv R(\nu, e, St_d).\end{aligned}\right\}. \tag{4.100}$$

In the limit of $St_d \to \infty$ the interstitial fluid effect vanishes and both the theories yield identical results.

4.7 Anisotropy of Second-moment Tensor

As discussed in §4.4.1, the anisotropy of the second-moment tensor is characterized by three parameters: η, ϕ and λ^2,

$$\left.\begin{aligned}\eta &\equiv \eta(\nu, e, St_d)\\ \phi &\equiv \phi(\nu, e, St_d)\\ \lambda &\equiv \lambda(\nu, e, St_d)\end{aligned}\right\}. \tag{4.101}$$

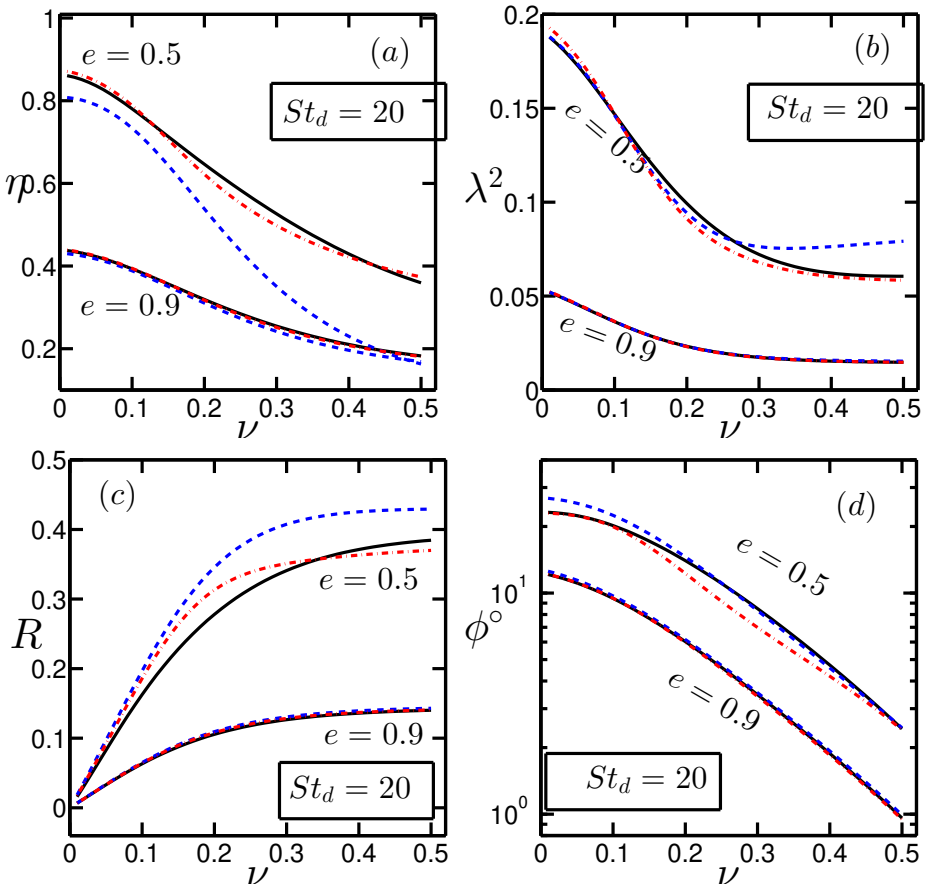

Fig. 4.3 Variations of (a) η, (b) λ^2, (c) R and (d) ϕ (degrees) with density (ν) at $St_d = 20$. While the solid black lines denote the exact numerical solution, the blue dashed and the red dot-dashed lines denote the Burnett-order solution and the perturbation solution at fourth order, respectively.

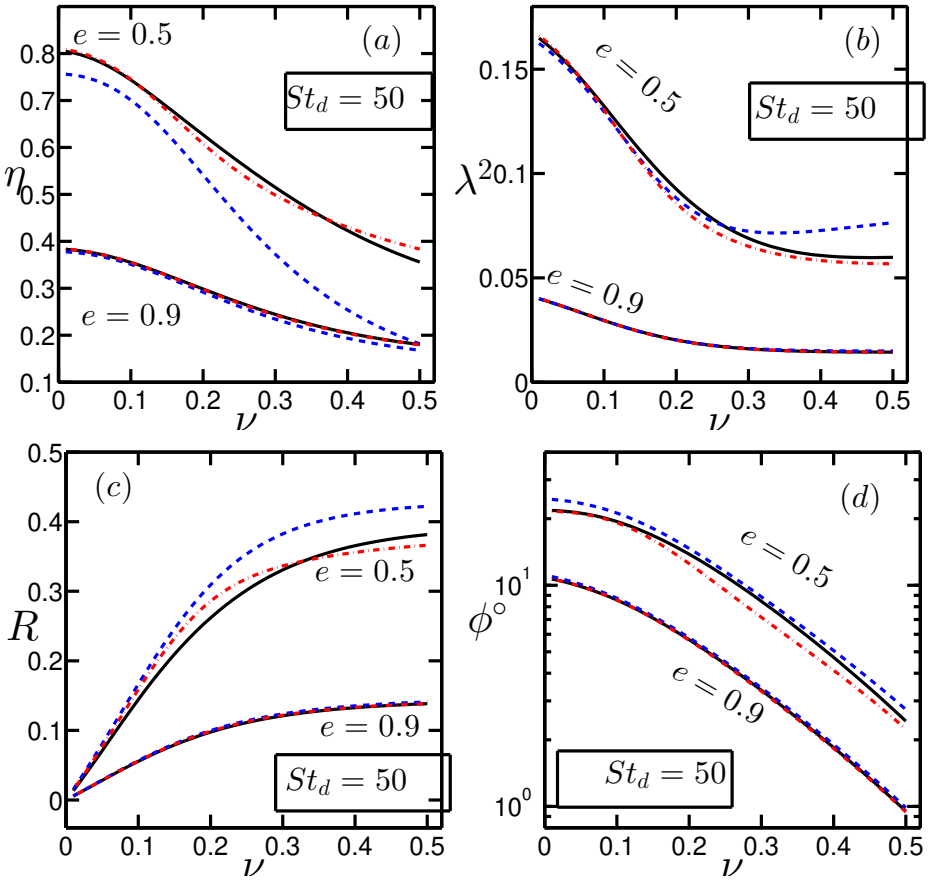

Fig. 4.4 Same as FIG. 4.3 but for modified Stokes number equals to $St_d = 50$.

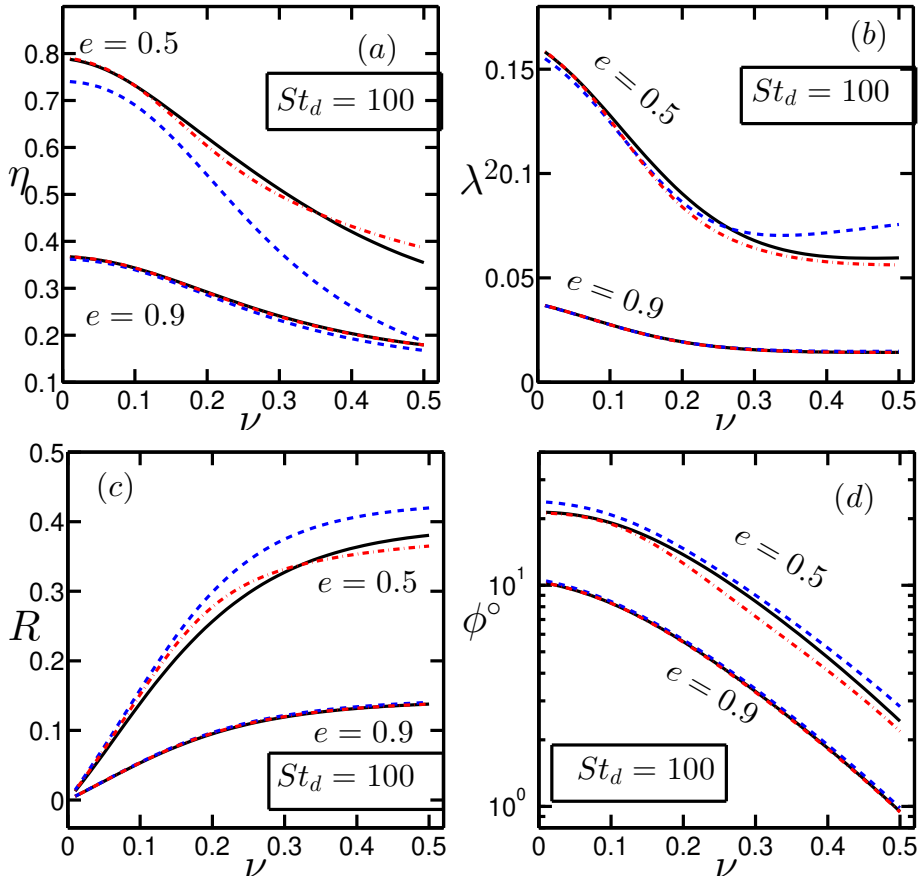

Fig. 4.5 Same as FIG. 4.3 but for modified Stokes number equals to $St_d = 100$.

whereas the parameter "R" is measure of the isotropic part of $\boldsymbol{M}$ (i.e. inverse of granular temperature)

$$R \equiv R(\nu, e, St_d). \tag{4.102}$$

The nonzero values of (η,ϕ,λ^2) are a measure of the non-Newtonian character of rheology.

Figures 4.3-4.5 present a comparison within the second-order analytical solution §4.5 (blue dashed lines), the fourth order perturbative solution §4.5.2 (red dot-dashed lines) and the full numerical solution (black solid lines) of (4.51-4.54) for four unknowns η, λ^2, R and ϕ (in degrees) against a range of density at specified values of Stokes number (St_d) and coefficient of restitution (e). In each of theses figures 4.3-4.5, the variations are shown for two different values of restitution coefficients: $e = 0.5$ corresponds to a highly dissipative and $e = 0.9$ corresponds to a relatively less dissipative system, respectively. It is observed that at $St_d = 20$ and for $e = 0.9$ three solutions for each of four parameters η, λ^2, R and ϕ almost fall on top of each other (however the temperature anisotropy η slightly differs above $\nu \sim 0.25$) and remain indistinguishable. Therefore at $e = 0.9$ the Burnett order solution is good enough for successful determination of $(\eta, \lambda^2, R, \phi)$ even at a low value of Stokes number $St_d = 20$.

On the other hand at $e = 0.5$ the Burnett order solution grossly underestimates η throughout the span of density and the deviation is more in the dense limit, whereas the fourth-order perturbative solution is closer to the full numerical solution except a slight deviation near $\nu \sim 0.25$. For λ^2, although the Burnett order analytical solution gives a relatively better approximation near the dilute limit, the fourth-order solution is better when the density is increased. However, none of these analytical solutions are able to give a quantitative good agreement for λ^2 for the whole range of density, which clearly will be manifested in the second normal difference, therefore demands a numerical study when Stokes number becomes very low $St_d \sim 20$. For Savage-Jeffrey parameter R and non-coaxiality angle ϕ, the fourth-order solution gives a fairly good prediction for the whole range of density with a slight disagreement near $\nu = 0.2$.

In figure 4.4, we have shown the variations of the parameters at $St_d = 50$. It is seen that the differences within the analytical and numerical solutions decrease when the Stokes number is increased and eventually at a very high value of Stokes number $St_d = 100$ the super-super-Burnett order solution almost agree with the full numerical solution of (4.51-4.54) for the whole range of density. One interesting point to note here that although increasing the number of terms in the related algebraic equations (4.51-4.54) gives a relatively better agreement with the full numerical solution, a closer look at these plots tells us that this series solution is in fact oscillatory. Therefore one cannot have a better agreement just by increasing the number of terms indefinitely. It may also appear that adding a certain number of terms in the series expansion can make the solution worsen. One reason behind this behaviour could be due to

the fact that the Chapman-Enskog expansion is actually a non-convergent series (McLennan 1965; Santos *et al.* 1986; Santos 2008). The related issues are not addressed in this thesis.

4.8 Validation of the Theoretical Model

4.8.1 Pressure, Shear Viscosity and Normal-Stress Differences

Here we focus on the behaviours of transport coefficients with varying Stokes number. Figure 4.6 display the density variations of (a) the pressure, (b) the shear viscosity and (c) the granular temperature at $e = 0.5, e = 0.9$ for three different values of Stokes number $St_d = 20$, 50 and 100. It is seen that the Burnett-order solutions for p, μ and T are almost indistinguishable from their exact numerical value at small dissipation $(e = 0.9)$; moreover, this agreement seems to hold uniformly for the whole range of density even for a very low value of Stokes number $St_d = 20$. On the other hand, retaining the fourth-order terms yields a better agreement for p, μ and T at large dissipation $(e = 0.5)$ and the agreement becomes better when we increase the Stokes number.

The ability of the fourth-order series solution to quantitatively predict p and μ at any density and Stokes number also holds reasonably well for both first and second normal-stress differences (4.79-4.80) which are displayed in figure 4.7. For nearly elastic particles $(e = 0.9)$ our Burnett order analytical solution is able to qualitatively predict both $\mathscr{N}_1$ and $\mathscr{N}_2$ in the uniform shear flow of a gas-solid suspension for the whole range of density (ν) and at any value of Stokes number (St_d). However, there are quantitative differences between numerical and analytical solutions in the prediction of $\mathscr{N}_2$ for highly dissipative particles $(e = 0.5)$ as it is evident from the right panel of figure 4.7 (denoted by dashed and dash-dot lines).

4.8.2 Three-dimensional Representation : Comparison Between Numerical and 4-th-order Perturbation Solution

The variations of all transport coefficients against inverse of Stokes number St_d^{-1} and density ν are shown in the three dimensional figures 4.8-4.12. In each of these plots the first row shows the variations of the transport coefficient obtained by solving the system (4.51-4.54) numerically for two values values of $e = 0.5$ and 0.9 respectively. In the second rows we have shown the respective variations at (c) $\nu = 0.01$ and (d) $\nu = 0.5$. Therefore the second row tells us about the inverse Stokes (St_d^{-1}) variations of these transport coefficients at two extreme (dilute and dense) limits of volume fractions. The results from the fourth-order perturbative

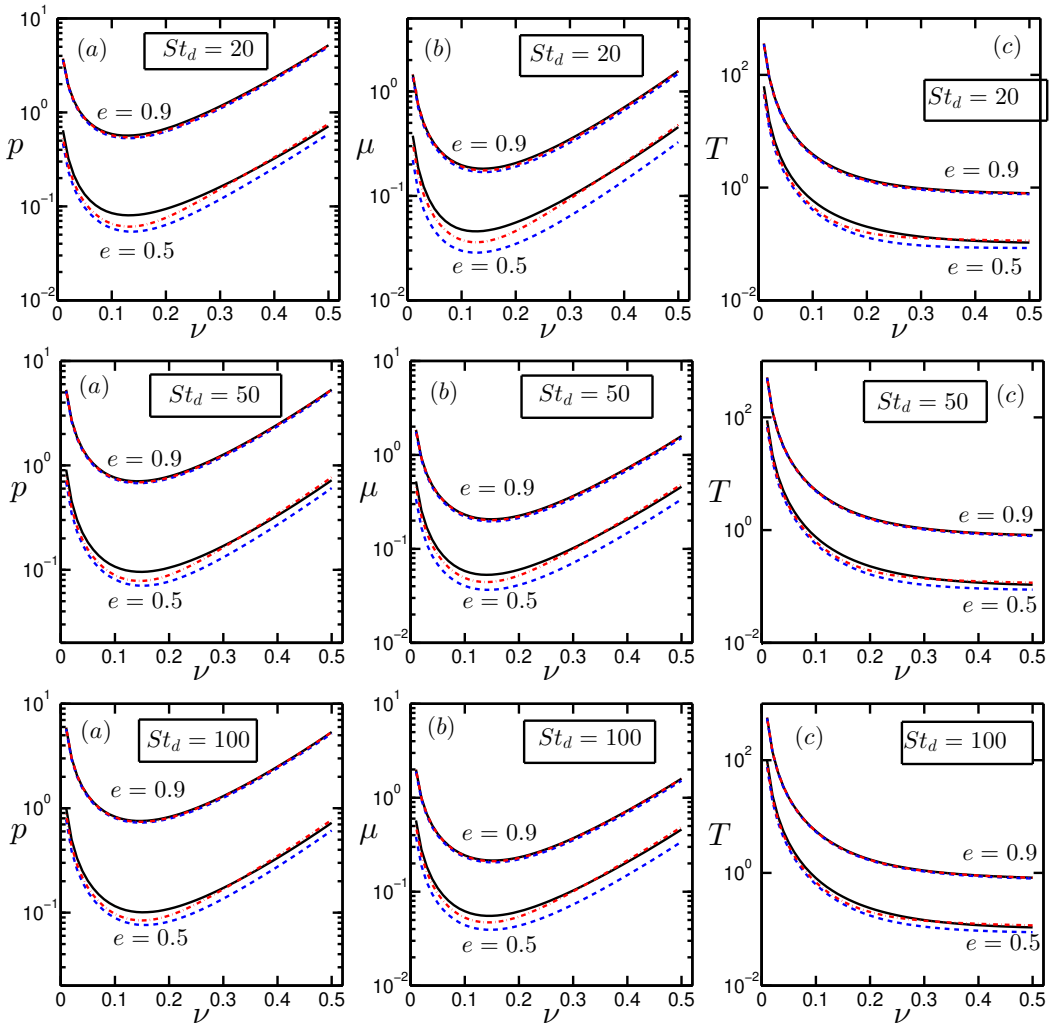

Fig. 4.6 Comparison between the "Burnett-order" analytical solution (blue dashed lines), fourth-order perturbation solution (red dot-dashed lines) and the "exact" numerical solution (black solid lines) for the variations of the (a) pressure, (b) shear viscosity and (c) granular temperature with volume fraction (ν) at coefficient of restitution $e = 0.5$ and $e = 0.9$ for $St_d = 20$ (top row), 50 (middle row) and 100 (bottom row) respectively.

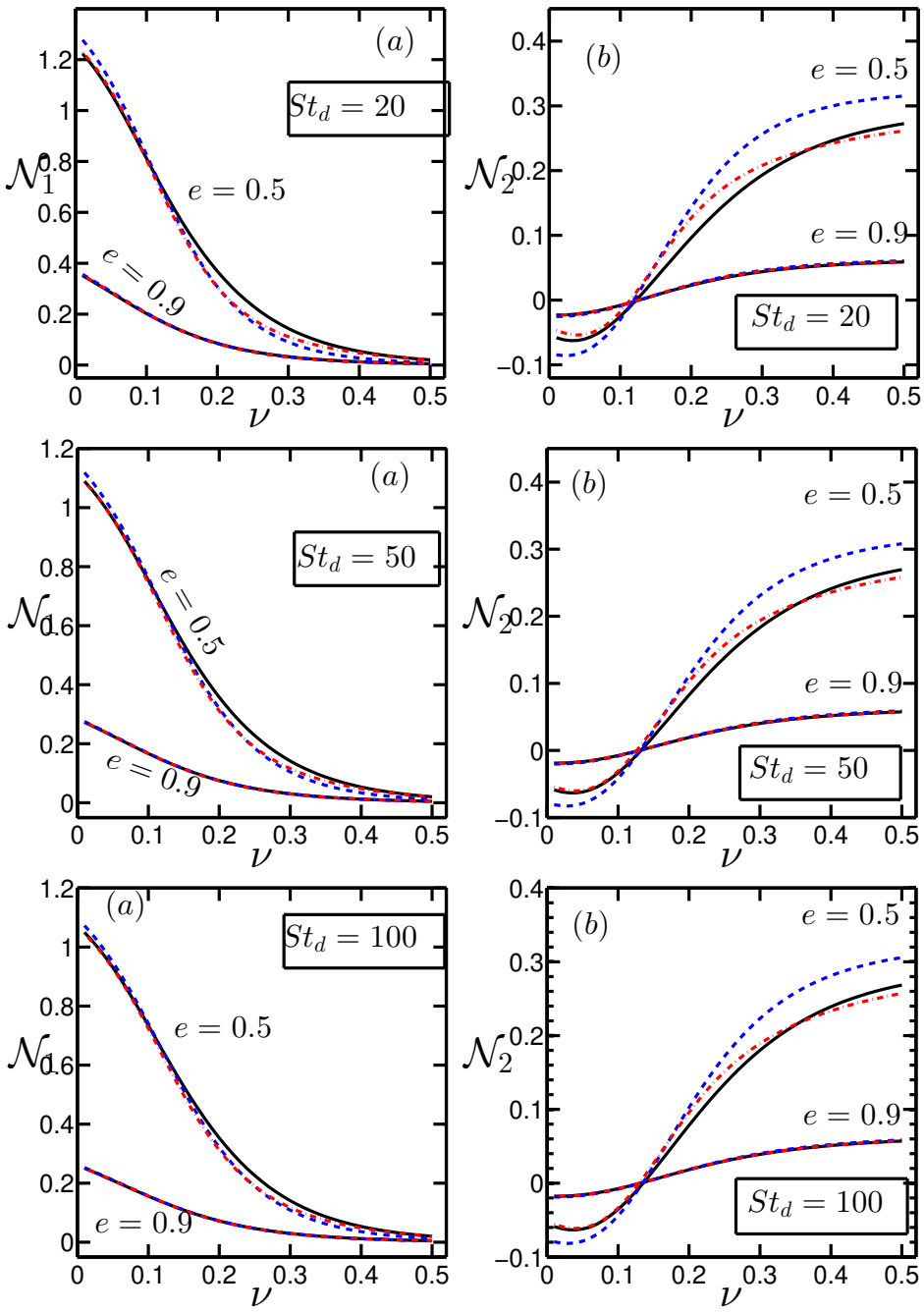

Fig. 4.7 Same as 4.6 but for the variations of the two normal stress differences (a) $\mathcal{N}_1$ and (b) $\mathcal{N}_2$ with volume fraction (ν).

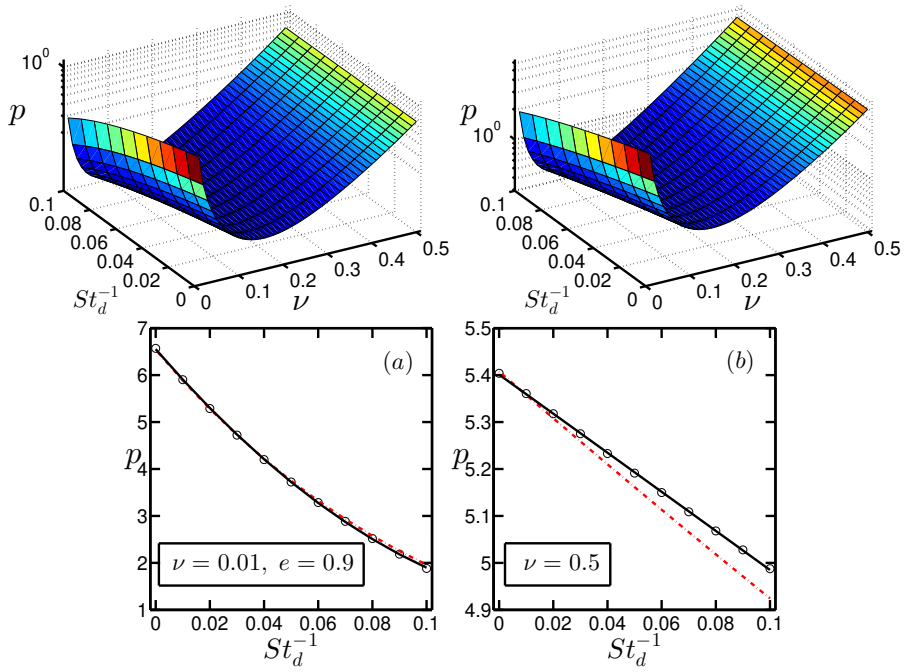

Fig. 4.8 Variations of the total pressure ($p = \frac{1}{3}P_{\alpha\alpha}$) against volume fraction (ν) and full range of $(St_d)^{-1}$ at $e = 0.5$ and $e = 0.9$ respectively. Panel (a) and (b) describe the variations of this transport coefficient (circles) when projected into the planes $\nu = 0.01$ (dilute limit) and $\nu = 0.5$ (dense limit) at $e = 0.9$. The red dot-dashed lines represent the fourth order analytical solutions (4.69)-(4.72) and the black solid lines are the quadratic (a) $y = 9x^2 - 66.63x + 6.552$ and linear fits (b) $y = -4.16x + 5.401$ respectively.

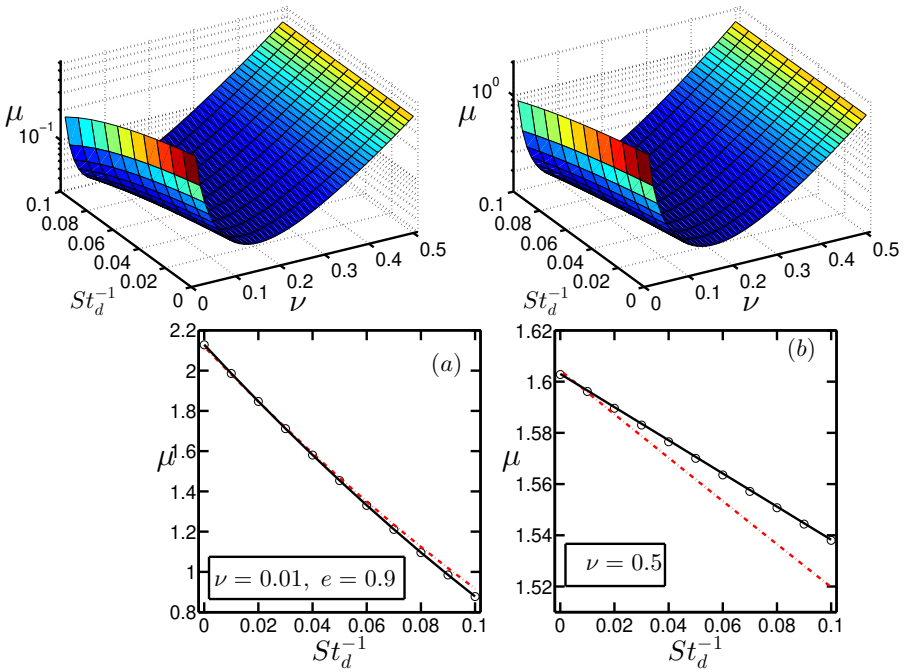

Fig. 4.9 Same as figure 4.8 but for the variations of shear viscosity (μ). The equations behind the quadratic and linear fits are $(a)\ y = 19.8x^2 - 14.49x + 2.129$ and $(b)\ y = -0.6475x + 1.603$ respectively.

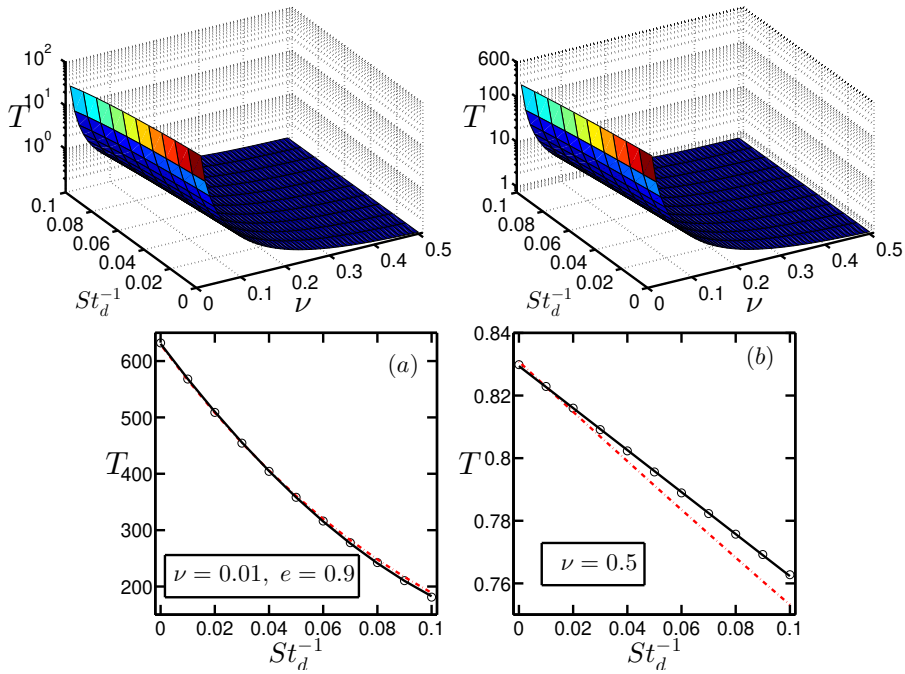

Fig. 4.10 Same as figure 4.8 but for the variations of granular temperature (T). The equations are $(a)\ y = 1.934 + e04x^2 - 6413x + 630.6$ and $(b)\ y = -0.6708x + 0.8294$ respectively.

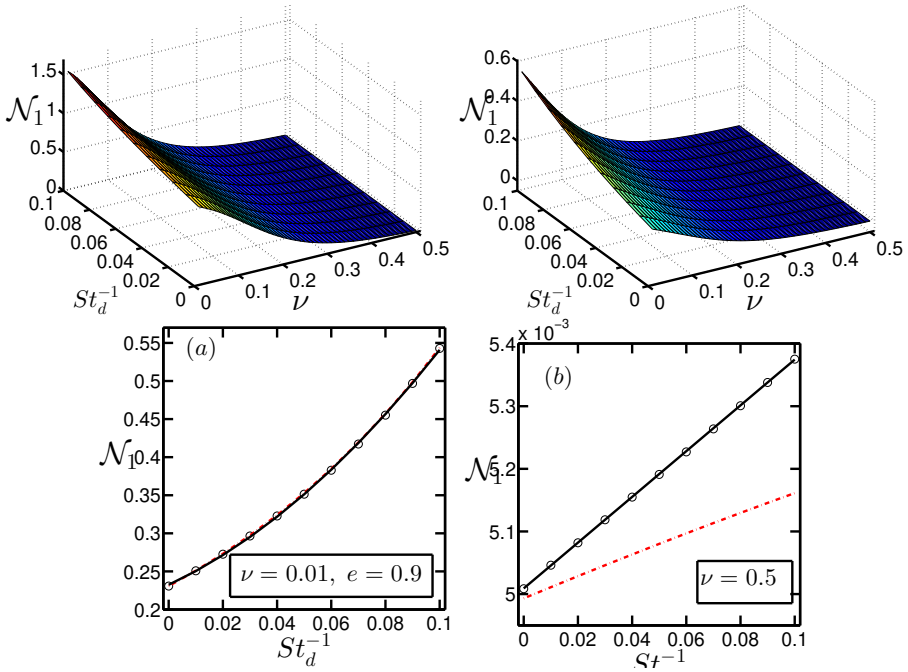

Fig. 4.11 Variations of the first normal stress difference ($\mathscr{N}_1 = \frac{P_{xx}-P_{yy}}{p}$) with density (ν) and inverse of (St_d) at coefficients of restitution $e = 0.5,\ 0.7$ and 0.9 respectively. In panel (a) and (b) we have shown the behaviours of $\mathscr{N}_1$ (circles) at $e = 0.9$ in the dilute and dense limits upon projecting the cartoon into the respective planes of $\nu = 0.01$ and $\nu = 0.5$ respectively. It is observed that $\mathscr{N}_1$ varies in a quadratic manner (a) $y = 14.15x^2 + 1.67x + 0.2324$ in the dilute limit whereas the variation is observed to be linear (b) $y = 0.003654x + 0.005009$ in the dense limit. The red dot-dashed lines are the fourth order perturbation solution (4.69)-(4.72).

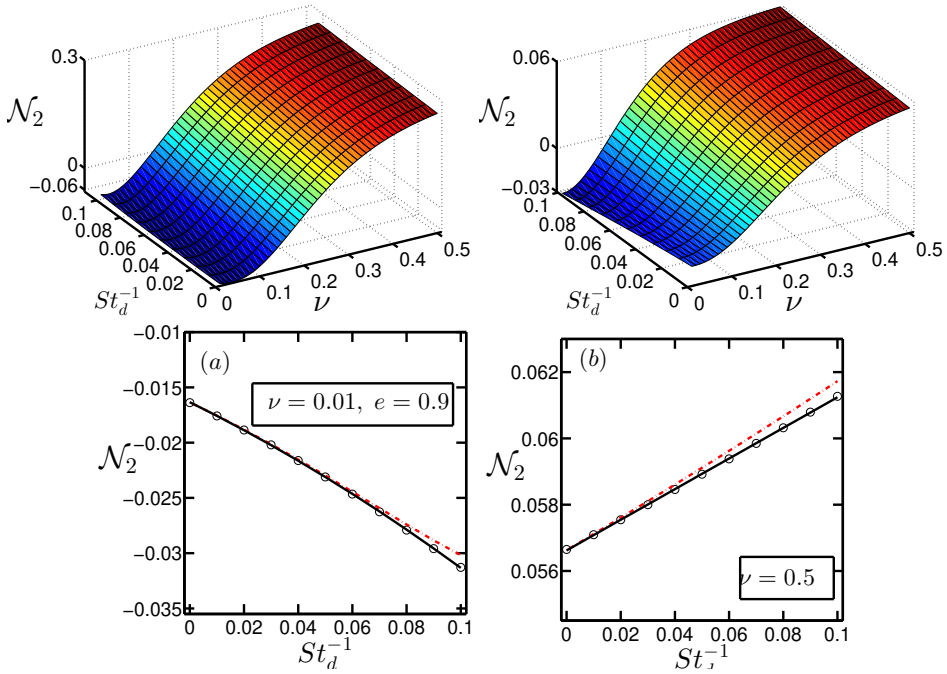

Fig. 4.12 Same as figure 4.11 but for the variations of the second normal stress difference ($\mathcal{N}_2 = \frac{P_{yy}-P_{zz}}{p}$). The governing equations for the parabola and straight line in the dilute and dense limit are $(a)\ y = -0.2914x^2 - 0.1208x - 0.01634$, $(b)\ y = 0.04621x + 0.05662$ respectively.

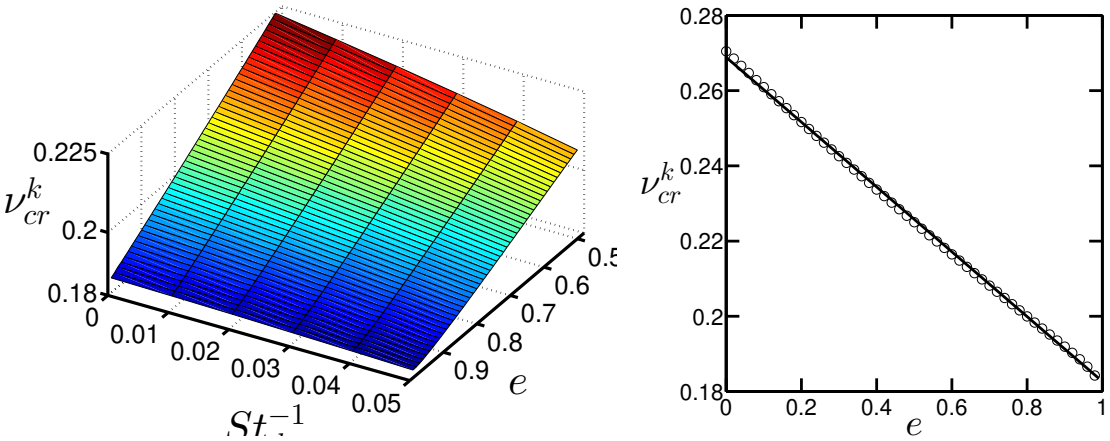

Fig. 4.13 Variation of the critical density ν_{cr}^k, at which $\eta \sin 2\phi = 3\lambda^2$ against $(St_d)^{-1}$ and e. The figure in the right is the corresponding dry granular analogue where $(St_d)^{-1} = 0 (St \to \infty)$.

solutions are superimposed in latter plots for a comparison between analytical (dot-dashed line) and numerical schemes ("circles").

It is observed that the dilute limit variations (left panels of second rows in figures) of p, μ, T and $\mathcal{N}_1$ are well predicted by the perturbative fourth order solution even at a very low value of Stokes number $(St_d = 10; St_d^{-1} = 0.1)$. The prediction for $\mathcal{N}_2$ is good up-to $St_d = 50$ but for Stokes number less than 50 the fourth-order solution underestimates $\mathcal{N}_2$ and the deviation increases with decreasing St_d.

The dense limit variations are shown in the right panels of second rows of figures (4.8-4.12), corresponding to a volume fraction $\nu = 0.5$. It is seen that the fourth order analytical solutions agree with the full numerical solution up-to $St_d^{-1} = 0.05$ ($\sim St_d = 20$) and beyond this value we need an improvement over our analytical approach. Also the variations of all transport coefficients at these extreme limits of volume fractions are checked by fitting them with proper choices of polynomials. In the dilute limit all the quantities vary quadratically with St_d^{-1} whereas in the dense limit the variations are linear and the equations of each of these parabolas and straight lines are given explicitly in the captions.

4.8.3 Sign-change of $\mathcal{N}_2$: Surface of Critical Density ν_{cr}^k

In the plots for the second normal stress difference (figure 4.12), we find that $\mathcal{N}_2$ changes its sign at some finite density similar to the case of dry granular flow, for any choice of Stokes number and coefficient of restitution. The location $(\nu = \nu_{cr}^k)$ of the point at which $\mathcal{N}_2$ changes its sign appears to be a slowly varying function of the restitution coefficient and Stokes number. The variations of the critical density as a function of the Stokes number St_d and and coefficient of restitution e are shown in figures 4.13-4.15.

$$\nu_{cr}^k = 0.2598 - 0.07683e, \qquad \nu_{cr}^k = 0.2541 - 0.0717e, \qquad \nu_{cr}^k = 0.2353 - 0.05476e \tag{4.103}$$

$$\nu_{cr}^k = 0.2245 - 0.2594(St_d)^{-1} - 1.289(St_d)^{-2}, \tag{4.104}$$

$$\nu_{cr}^k = 0.2077 - 0.1816(St_d)^{-1} - 0.7398(St_d)^{-2}, \tag{4.105}$$

$$\nu_{cr}^k = 0.1916 - 0.09537(St_d)^{-1} - 0.4298(St_d)^{-2}. \tag{4.106}$$

Combining the planar equations (4.103)-(4.106), the best fit for ν_{cr}^k is the surface

$$\boxed{\nu_{cr}^k = 0.2668 - 0.08424e - (0.4964 - 0.4360e)\alpha - (2.048 - 2.092e)\alpha^2}, \tag{4.107}$$

where

$$\alpha = (St_d)^{-1}. \tag{4.108}$$

Equation (4.107) represents the critical surface in ν-e-ST_d space. The significance of this surface is as follows: corresponding to any point (St_d, e) in the ST_d-e plane, there exists a unique point ν_{cr}^k which satisfies equation (4.107) and above this value $\mathcal{N}_2$ is positive, whereas $\mathcal{N}_2$ remains negative below this point. Therefore the surface (4.107) acts as the surface of degeneracy for $\mathcal{N}_2$. Finally, when this surfaces is projected onto the plane St_d^{-1} (i.e $St \to \infty$) the critical density curve for dry granular flow Saha & Alam (2016)

$$\nu_{cr}^k(St_d \to \infty) \equiv 0.27 - 0.084e \tag{4.109}$$

is recovered.

4.9 Summary and Outlook

4.9.1 Summary

We have studied the uniform shear flow of a gas solid suspension where inertial inelastic particles are suspended in a Newtonian gas and experiencing a Stokes drag force. Viscous heating from the boundaries is compensated by dissipation via two mechanisms (i) the inelastic collisions between particles characterized by a coefficient of normal restitution e $(0 < e < 1)$ and (ii) the Stokes drag force which the surround fluid exerts on the particles. The hydrodynamic interactions has been not taken into account but as shown in Sangani *et al.* (1996), the hydro-

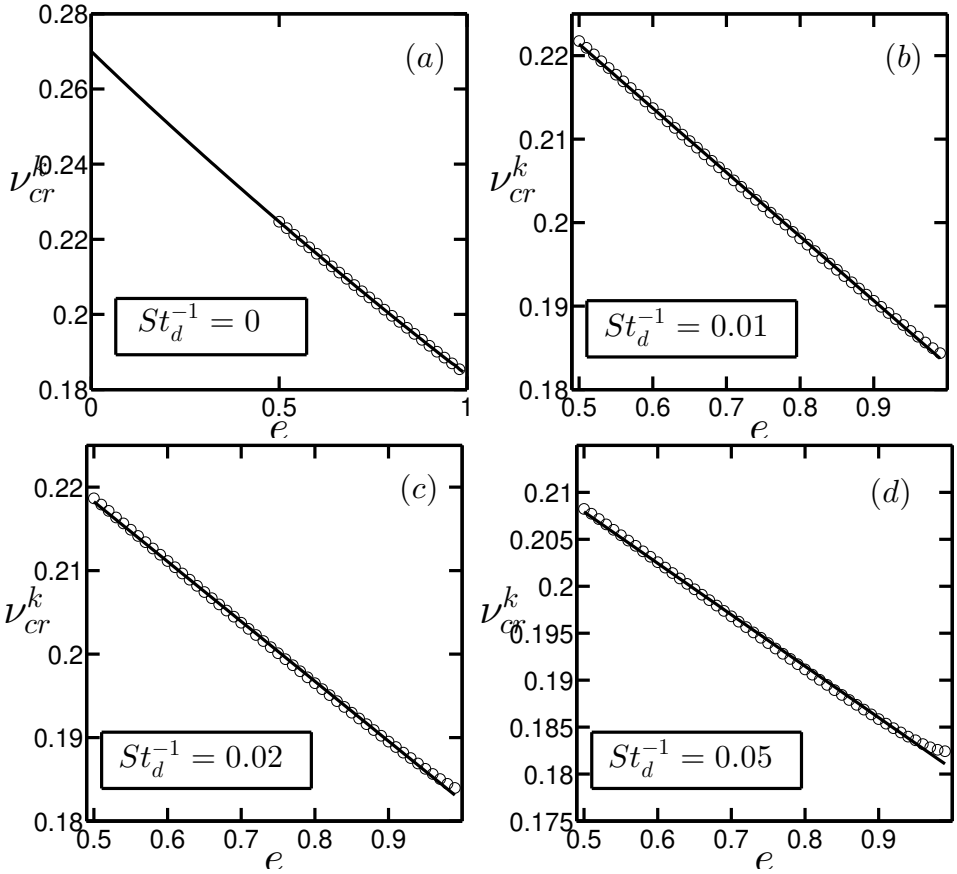

Fig. 4.14 Variations of the critical density ν_{cr}^k, at which $\eta \sin 2\phi = 3\lambda^2$ against e. Panel (a) is a comparison between our present theory (circles) at $(St_d)^{-1} = 0$ and the theory of (Saha & Alam 2016) (solid line) for dry granular flow. Panel (b), (c) and (d) are variations of the critical density at non zero values of $(St_d)^{-1} = 0.01$, 0.02 and 0.05 (presence of an interstitial fluid is considered). The solid lines depicted in the last three figures are linear fittings (4.103).

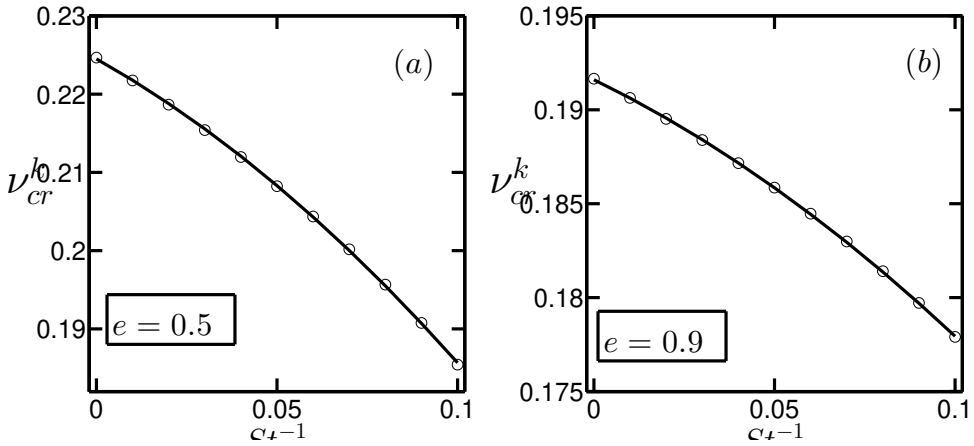

Fig. 4.15 Same as 4.14 but for variations of the critical density ν_{cr}^k against $(St_d)^{-1}$ for $e = 0.5$ and $e = 0.9$ respectively. The solid lines are quadratic fittings as given in (4.104)–(4.106).

dynamic interaction is incorporated within a corrected factor $R_{\text{diss}}(\nu)$, where ν is the particle volume fraction and the analysis is based on an adjusted Stokes number $St_d = St/R_{\text{diss}}$.

The particle-phase rheology is analysed using the anisotropic Maxwellian as the single particle distribution function. The balance equation for the second-moment of velocity fluctuations is solved analytically and perturbatively to obtain the transport coefficients viz. pressure, viscosity, normal stress differences etc.. The Burnett order analytical solution and perturbative solution at super-super-Burnett order are compared with the full numerical solutions in terms of the particle phase transport coefficients and a good agreement within these approaches has been found for the whole range of density. Although a slight disagreement between the analytical and numerical solutions is observed when the Stokes number becomes very low $St \sim 20$ and the dissipation becomes very large $e \sim 0.5$ but for a nearly-elastic system $e \sim 0.9$ these two solutions become almost identical.

In a recent work, Parmentier & Simonin (2012) have prescribed a theory for simple sheared homogeneous suspension of elastic and inelastic particles, valid for the whole range of density and Stokes number. But in their work, the collisional component of the stress tensor has not been calculated. Their main focus was to predict the behaviours of the collisional source terms with varying Stokes number and density, and a comparison of these quantities with simulations were given. In our anisotropic Maxwellian theory, we have taken care of the kinetic $(P^k_{\alpha\beta})$ as well as the collisional components of the stress tensor $(\Theta_{\alpha\beta})$ that yield correct behaviours of the transport coefficients for the whole range of density. It also improves the results presented in Parmentier & Simonin (2012) in the sense that results obtained using anisotropic Gaussian theory agrees well with the simulation data which can be seen from the figure 4.16

Figure 4.16 shows the density variation of the off-diagonal anisotropy of the second moment tensor for $St_d = 3.5$ and $e = 1$ and the improvement over the work by Parmentier & Simonin (2012) is clearly seen at lower volume fraction. Finally, when $St_d \to \infty$ the conventional results for the dry granular flows are recovered.

The simulation data on transport coefficients of gas-solid suspensions at finite densities are scarce, and future work should focus on molecular dynamics simulation of gas-solid suspension of inelastic particles. In the next chapter, we will make a detailed comparison of present theory with available simulation data in the dilute limit of a gas-solid suspension.

4.9.2 Next Chapter

When the particle volume fraction becomes very low, two distinct states can be expected (Tsao & Koch 1995): the "quenched" state, in which particle inertia is less and the "ignited" state, where particles are mostly agitated. A transition between these two states depending upon the Stokes number and volume fraction has been analysed by Tsao & Koch (1995) in simple shear

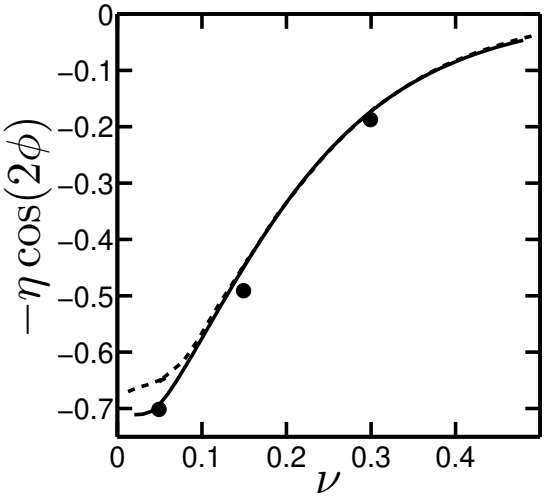

Fig. 4.16 Variation of the anisotropy coefficient against volume fraction for $St = 3.5$ and $e = 1$. The solid line corresponds to the current anisotropic Gaussian theory whereas the dashed line and symbols correspond to the theory and simulation work of Parmentier & Simonin (2012) and Abbas *et al.* (2009) respectively.

flows of dilute gas-solid suspensions of elastic particles. In the next chapter we will extend their work for inelastic particles, where the effects of inelasticity on the transport coefficients in these two states will be discussed. The hysteresis in the particle-phase rheology along with behavioural dependency of the transit points on inelasticity will also be addressed.

Chapter 5

Dilute Gas-Solid Suspension : Shear-thickening Behaviour and Normal Stress Differences[4]

5.1 Introduction

During the last few decades, a lot of research has been done to understand the behaviours of rapid granular flows (Savage & Jeffrey 1981; Lun *et al.* 1984; Jenkins & Richman 1985*a*; Campbell 1990; Sela & Goldhirsch 1998; Brey *et al.* 1998; Goldhirsch 2003; Rao & Nott 2008; Forterre & Pouliquen 2008), a collection macroscopic inelastic (the restitution coefficient $e < 1$) hard-particles for which the effect of the interstitial fluid is neglected, and the tools from dense-gas kinetic theory have been successfully employed to understand its hydrodynamics and rheology. The closely related research-area of gas-solid suspensions (Davidson & Harrison 1963; Anderson & Jackson 1967; Buyevich 1971; Gidaspow 1994; Jackson 2000; Guazzelli & Morris 2011), in which the viscous drag due to interstitial fluid and other related hydrodynamic effects must be incorporated, has also been extensively studied over the last century due to its importance in fluidized-bed and FCC reactors (Davidson & Harrison 1963; Gidaspow 1994) encountered in chemical and process industries. For continuum models of gas-solid suspensions, the kinetic-theory-based rheological models have been suggested by considering elastically colliding particles (Koch 1990; Tsao & Koch 1995) as well as for in-

[4]This chapter is a slightly edited version of a paper submitted to J. Fluid Mech. (May 2017): "Revisiting ignited-quench transition and the non-Newtonian rheology of a sheared dilute gas-solid suspension" by S. Saha and M. Alam (Saha & Alam 2017*a*). The revised version has been published in the Journal of Fluid Mechanics [Saha & Alam (2017*b*), J. Fluid Mech. 833, 240-246].

elastic particles (Louge *et al.* 1991; Sangani *et al.* 1996; Lun & Savage 2003) interacting in a bath of a Newtonian gas.

For the present problem of a sheared gas-solid suspension of inelastic particles, the energy input due to shear is compensated by two mechanisms, (i) inelastic inter-particle collisions, characterized by a coefficient of normal restitution (e) and (ii) the drag force which the surrounding fluid exerts on the particles. The volume fraction of the suspended particles (of diameter σ and mass m) is assumed to be small, i.e. $\nu = \pi\sigma^3 n/6 \ll 1$, representing a 'dilute' suspension, along with the conditions of (ii) small Reynolds number $Re = \rho_g \dot{\gamma}\sigma^2/\mu_g \ll 1$ (where ρ_g and μ_g are the gas density and its viscosity, respectively, and $\dot{\gamma}$ is the imposed shear rate on the suspension) and (iii) finite Stokes number

$$St = \dot{\gamma}\tau_v, \quad \text{with} \quad \tau_v = m/(3\pi\mu_g\sigma) \tag{5.1}$$

being the viscous relaxation time which is a measure of the time a typical particle takes to relax back to the local fluid velocity. The limit of $St \to \infty$ represents the 'dry' granular gas (Campbell 1990; Goldhirsch 2003). Under the above assumptions, Tsao & Koch (1995) analysed the hydrodynamics and the non-Newtonian rheology of a dilute suspension of elastic ($e = 1$) hard-particles employing the Grad's moment-expansion method (i.e. an expansion in terms of Hermite polynomials around a Maxwellian, Grad (1949)). They discovered two qualitatively different states, dubbed (i) "quenched" (low temperature) and (ii) "ignited" (high temperature) states, corresponding to the time intervals (i) $\tau_c \gg \tau_v \gg \dot{\gamma}^{-1}$ and (ii) $\tau_c \ll \dot{\gamma}^{-1} \ll \tau_v$, respectively, where τ_c is the collision time (i.e, the average time between two successive collisions). They analytically determined two critical Stokes numbers St_{c_1} and St_{c_2} (with $St_{c_2} > St_{c_1}$), below and above which the flow remains in the quenched and ignited states, respectively. They also determined the shear viscosity and the first and second normal-stress differences, and compared their theory with DSMC (direct simulation Monte Carlo) data.

Sangani *et al.* (1996) extended the work of Tsao & Koch (1995) to (i) a 'dense' gas-solid suspension of elastic ($e = 1$) particles as well as to (ii) a 'dilute' suspension of inelastic ($e < 1$) particles. The same Grad moment-expansion was used to derive constitutive relations from the underlying Enskog-Boltzmann equation; but their analysis is deficient in the sense that they found zero value for the second normal stress difference as they did not incorporate certain non-linear terms (see §5.5 in this work). They briefly discussed about the lower limit of Stokes number St_{c_1}, but a thorough analysis of the "ignited-quenched" transitions, identifying the regions for the existence of different states, in terms of Stokes number (St), particle volume fraction (ν) and the coefficient of restitution (e) has not been worked out till date. The latter effect of the restitution coefficient is important for dissipative particles which forms one motivation of the present work.

In the current decade, Parmentier & Simonin (2012) analysed a sheared gas-solid suspension by considering a distribution function that sandwiches both the ignited and quenched states – the resulting rheological fields are reasonably well-predicted over a range of density and Stokes number, although quantitative mis-match with simulation data exists that increase with increasing dissipation (i.e. at smaller e). A Navier-Stokes-order continuum model has been developed by Garzó *et al.* (2012) for a moderately-dense gas-solid suspension following dense-gas kinetic theory. They solved the underlying Enskog-Boltzmann equation using a Chapman-Enskog-like expansion around a time-dependent homogeneous cooling state for a gas-solid suspension, and the particle motion has been modelled via a Langevin-type stochastic model with Stokesian drag. The resulting transport coefficients for the particle-phase are found to have explicit dependence on the gas-phase parameters. However, the prediction of the latter model for the shear viscosity of a suspension indicates large discrepancies with simulation data in the dilute limit of low-St suspension, presumably due to the presence of order-one values of normal stress differences and other non-Newtonian effects. A related work to uncover the non-Newtonian rheology of a 'dilute' gas-solid suspension has been done recently by Chamorro *et al.* (2015). They followed the standard Grad's method to analyse the ignited state of a gas-solid suspension, and the related predictions on the granular temperature and the non-Newtonian stress tensor are found to be quantitatively similar to the earlier work of Tsao & Koch (1995); for example, the suspension viscosity is over-predicted by the Grad's moment-theory at smaller values of e, although the discrepancy decreases with increasing Stokes number. Collectively, the above literature review points toward the need to go beyond the well-studied Newtonian rheology (of Navier-Stokes-order) for both dry granular and gas-solid suspensions.

In this chapter, we revisit and extend the work of Tsao & Koch (1995) by considering a dilute system of inelastic ($e \leq 1$) particles suspended in a bath of a Newtonian gas, and interacting via (i) a Stokeian drag force and (ii) hard-core inelastic collisions. Our work differs from all previous works on gas-solid suspensions as we adopt the anisotropic Maxwellian distribution function (Goldreich & Tremaine 1978; Jenkins & Richman 1988; Richman 1989) to analyse the underlying Boltzmann equation under homogeneous shearing conditions. The latter assumption is motivated from our recent work (Saha & Alam 2014, 2016; Alam & Saha 2017) on 'dry' ($St \to \infty$) sheared granular fluid which established that the transport coefficients for highly inelastic system ($e \ll 1$) of a sheared granular fluid (both dilute and dense) can be accurately predicted by the anisotropic Maxwellian [in comparison to (i) the standard Grad's moment expansion (in terms of a truncated Hermite series around a Maxwellian) as well as (ii) the Burnett-order solutions obtained from Chapman-Enskog expansion]. Here we demonstrate the superiority of the former for the case of a sheared gas-solid suspension via a one-to-one

comparison of two theories with simulation data. Another focus of the present work is to analyse and quantify the anisotropy of the second-moment, $\boldsymbol{M} = \langle \boldsymbol{CC} \rangle$, of fluctuation/peculiar velocity, and subsequently tie and explain the rheological/transport coefficients of a sheared gas-solid suspension in terms of the anisotropies of $\boldsymbol{M}$. The underlying analysis utilizes the geometric structure of the eigen-basis of both the shear tensor and the second-moment tensor; this provides geometric insight into the origin of normal stress differences as found for the case of a sheared granular fluid (Saha & Alam 2016). It must be noted that the analysis of stress anisotropy in this form was initiated in a seminal work by Goldreich & Tremaine (1978) and subsequently by others (Araki & Tremaine 1986; Araki 1988; Shukhman 1984; Jenkins & Richman 1988; Richman 1989) and the present effort is a continuation of the same legacy to the case of a sheared gas-solid suspension.

This chapter is organized as follows. A brief account of the problem and the governing equations for the gas and particle phases are given in §5.2. The anisotropic-Maxwellian distribution function is introduced in §5.2.1 which is employed to analyse the "ignited" state of sheared gas-solid suspension; the second moment tensor for the uniform shear flow is constructed in §5.2.1 in terms of its eigen-basis. The source term of the second moment balance equation is calculated in §5.2.1 and §5.2.2 for the ignited and quenched states, respectively. The second-moment balance combining both ignited (I) and quenched (Q) states is analysed in §5.2.3. The multi-stability and hysteresis transitions in granular temperature are analysed in detail in §5.3, along with (i) the validation and superiority of the present analysis in §5.3.1, (ii) analytical solutions for temperatures in three states in §5.3.2 and (iii) the critical Stokes numbers for "$I \leftrightarrow Q$" transitions in §5.3.3. The non-Newtonian rheology (shear-thickening, normal stress differences) is analysed in §5.4.2 and §5.4.3, in terms of the anisotropies of the second-moment tensor (§5.4.1). The relative merits of the present theory over the standard Grad's moment-expansion and Chapman-Enskog expansion are analysed in §5.5 via comparisons with available simulation data. The conclusions are given in §5.6. The mathematical details of various analyses are relegated to Appendices A to E.

5.2 Problem description and the kinetic-theory analysis

We examine the uniform shear flow of a "dilute" gas-solid suspension in the absence of gravity, with a collection of smooth inelastic spheres of mass m and diameter σ being suspended in a gas; with x, y and z pointing the velocity, gradient and vorticity directions (see figure 5.1), respectively, the velocity field for the suspension is given by

$$\boldsymbol{u} \equiv (u_x, u_y, u_z) = (\dot{\gamma} y, 0, 0), \tag{5.2}$$

where $\dot{\gamma}$ is the overall shear rate. We are interested in a steady state suspension where the fluid inertia is very small but the particle inertia remains finite. Under the assumptions of the smallness of particle Reynolds number, the gas-phase obeys the Stokes equations of motion

$$\mu_g \nabla^2 v_i = \nabla_i p_g, \qquad \nabla_i v_i = 0, \tag{5.3}$$

where μ_g is the shear viscosity of the gas.

For the particle-phase, we adopt the kinetic theory of gases as pursued in granular gases (Chapman & Cowling 1970; Savage & Jeffrey 1981; Lun *et al.* 1984; Jenkins & Richman 1985*a*; Brey *et al.* 1998; Sela & Goldhirsch 1998; Brilliantov & Pöschel 2004; Rongali & Alam 2014)as well as in gas-solid suspensions (koch1990kinetic,louge1991role,tsao1995simple,sangani1996s The evolution of the single particle distribution function $(f(\boldsymbol{c},\boldsymbol{x},t))$ follows the celebrated Boltzmann equation (Chapman & Cowling 1970)

$$\left(\frac{\partial}{\partial t} + \boldsymbol{c}\cdot\nabla\right) f + \nabla_{\boldsymbol{c}} \cdot \left(f\frac{\mathrm{d}\boldsymbol{c}}{\mathrm{d}t}\right) = \left(\frac{\partial f}{\partial t}\right)_{coll}, \tag{5.4}$$

where $\nabla_{\boldsymbol{c}}$ is divergence operator in the velocity space and $(\partial f/\partial t)_{coll}$ is the well-known collision operator (chapman1970mathematical). The acceleration of the particles is assumed to follow the Stokes's linear drag law:

$$\frac{\mathrm{d}\boldsymbol{c}}{\mathrm{d}t} = -\frac{\boldsymbol{c}-\boldsymbol{v}}{\tau_v}, \tag{5.5}$$

with $\tau_v = m/(3\pi\mu_g\sigma)$ being the viscous relaxation time of the particles. Equation (5.5) holds if the particle Reynolds number and the density-ratio (ρ_f/ρ_p) are very small; for large Reynolds numbers, a nonlinear form of the drag-law would be necessary (Jackson 2000). Any physical quantity at the macroscopic level is defined as the ensemble averaged value of the same at the particle level, using the single particle distribution $f(\boldsymbol{c},\boldsymbol{x},t)$ function

$$\langle\psi\rangle = \frac{1}{n(\boldsymbol{x},t)}\int \psi\boldsymbol{c} f(\boldsymbol{c},\boldsymbol{x},t)d\boldsymbol{c} \equiv \frac{1}{n(\boldsymbol{x},t)}\int \psi\boldsymbol{C} f\boldsymbol{C}d\boldsymbol{C}, \tag{5.6}$$

with $\psi(\boldsymbol{c})$ being any particle-level quantity. Here $n \equiv n(\boldsymbol{x},t)$ denotes the number density and $\rho(\boldsymbol{x},t) = mn \equiv \rho_p\nu$ is the mass-density of the particle-phase, with $\nu = \pi\sigma^3 n/6$ being the volume fraction of particles and $\rho_p = m/(\pi\sigma^3/6)$ is its intrinsic/material density. The macroscopic/hydrodynamic velocity $\boldsymbol{u} = \langle\boldsymbol{c}\rangle$, the granular temperature $T = \langle\boldsymbol{C}^2/3\rangle$ and the particle-phase stress tensor $\boldsymbol{P} = \langle m\boldsymbol{C}\boldsymbol{C}\rangle$ are obtained by substituting $\psi = \boldsymbol{c}$, $\frac{1}{3}\boldsymbol{C}^2$ and $m\boldsymbol{C}C$, respectively, in (5.6), where $\boldsymbol{C} = \boldsymbol{c} - \boldsymbol{u}$, is the peculiar velocity.

Focussing on a steady homogeneous sheared suspension, the Boltzmann equation (5.4) for the distribution function $f(\boldsymbol{C};\boldsymbol{x},t)$ reads (Chapman & Cowling 1970)

$$-C_m\dot{\gamma}_{km}\frac{\partial f}{\partial C_k}+\frac{\partial}{\partial C_k}\left(\frac{dc_k}{dt}f\right)=\left(\frac{\partial f}{\partial t}\right)_{coll}, \tag{5.7}$$

where $\dot{\gamma}_{\alpha\beta}=\dot{\gamma}\delta_{\alpha x}\delta_{\beta y}$ is the velocity gradient tensor of the uniform shear flow. On multiplying (5.7) by $m\psi(\boldsymbol{C})$ and integrating over the velocity space, the master balance equation is obtained (Jenkins & Richman 1985*a*; Sangani *et al.* 1996) as

$$\rho_f\left(\dot{\gamma}_{km}\left\langle C_m\frac{\partial\psi}{\partial C_k}\right\rangle-\left\langle\frac{dc_k}{dt}\frac{\partial\psi}{\partial C_k}\right\rangle\right)=\aleph(m\psi) \tag{5.8}$$

where

$$\aleph(m\psi)=\int m\psi\left(\frac{\partial f}{\partial t}\right)d\boldsymbol{C} \tag{5.9}$$

represents the collisional source of $m\psi$.

Putting $\psi=1$ and $\boldsymbol{c}$ into (5.8), the mass and momentum balance equations for the particle phase, respectively are obtained. For the steady uniform shear flow $(u=(\dot{\gamma}y,0,0))$ the mass balance $(\cdot u=0)$ is identically satisfied since (i) the stress tensor is constant and the 'mean' drag on the particle phase (due to the gas phase) is zero. The latter follows from the assumption that there is no 'slip' between the coarse-grained velocity of the particle phase $(\boldsymbol{u})$ and the 'local' gas velocity $(\boldsymbol{v})$, i.e $\boldsymbol{u}_s=\boldsymbol{u}-\boldsymbol{v}=0$. The hydrodynamic interactions among the particles are neglected in the present analysis which can be justified for a dilute suspension (Koch 1990; Tsao & Koch 1995) at moderate to high values of Stokes number. For moderately dense gas-solid suspensions, Sangani *et al.* (1996) developed a Grad-type moment theory by incorporating hydrodynamic interactions in an *ad hoc* manner (via a corrective function $R_{diss}(\nu)$ to the Stokes drag, with its dilute limit being $R_{diss}(\nu\to 0)\to 1$. This theory was found to be in good agreement with full dynamic simulations of gas-solid suspensions even at a small Stokes number of $St\gg 5$. The mean-field arguments of Sangani *et al.* (1996) were also used in a more recent work (Parmentier & Simonin 2012) on dense suspensions. The reader is referred to a review article (Koch & Hill 2001) for further details on hydrodynamic interactions.

Inserting $\psi=\boldsymbol{CC}$ into (5.8), we obtain the balance equation for the second moment:

$$\boldsymbol{P}\cdot\nabla\boldsymbol{u}+(\boldsymbol{P}\cdot\nabla\boldsymbol{u})^T+\frac{2}{\tau_v}\rho\langle\boldsymbol{CC}\rangle+\frac{1}{\tau_v}\rho\langle(\boldsymbol{u}-\boldsymbol{v})\boldsymbol{C}\rangle+\frac{1}{\tau_v}\rho\langle((\boldsymbol{u}-\boldsymbol{v})\boldsymbol{C})^T\rangle=\aleph(m\boldsymbol{CC}), \tag{5.10}$$

where $\boldsymbol{P} = \rho \boldsymbol{CC}$ is the particle-phase stress tensor and $\aleph(m\boldsymbol{CC})$ is the collisional source of the second moment as defined in (5.9). The third term on the left hand side of (5.10) embodies the Stokes drag law (5.5), along with the following assumption

$$\left\langle (\delta_{ik}C_j + \delta_{jk}C_i)\frac{dc_k}{dt} \right\rangle = -\frac{2}{\tau_v}\langle C_i C_j \rangle, \tag{5.11}$$

which holds if the microstructure of the suspension is nearly isotropic (Sangani *et al.* 1996). The fourth and fifth terms in (5.10) vanish due to the zero-slip ($\boldsymbol{u}_s = \boldsymbol{u} - \boldsymbol{v} = 0$) assumption, leading to the final form of the second moment balance equation

$$\boldsymbol{P}\cdot\nabla\boldsymbol{u} + (\boldsymbol{P}\cdot\nabla\boldsymbol{u})^T + \frac{2}{\tau_v}\boldsymbol{P} = \aleph(m\boldsymbol{CC}), \tag{5.12}$$

which must be solved for the homogeneously sheared gas-solid suspension. The integral expression for the source term in (5.12) is given by Jenkins & Richman (1985*a*); Saha & Alam (2014)

$$\aleph = \int m\boldsymbol{CC}\left(\frac{\partial f}{\partial t}\right)_{coll} d\boldsymbol{C} = \frac{\sigma^2}{2}\int \Delta\Big(m\boldsymbol{CC}\Big) f(\boldsymbol{C}_1) f(\boldsymbol{C}_2) d\boldsymbol{C}_1 d\boldsymbol{C}_2, \tag{5.13}$$

with

$$\Delta\Big(m\boldsymbol{CC}\Big) = \frac{m}{2}(1+e)(\boldsymbol{g}\cdot\boldsymbol{k})\left[(1+e)(\boldsymbol{g}\cdot\boldsymbol{k})\boldsymbol{kk} - \boldsymbol{kw} - \boldsymbol{wk}\right], \tag{5.14}$$

where $\boldsymbol{g} = \boldsymbol{c}_1 - \boldsymbol{c}_2$ and $\boldsymbol{w} = \boldsymbol{C}_1 - \boldsymbol{C}_2 \equiv \boldsymbol{g} - (\boldsymbol{u}_1 - \boldsymbol{u}_2)$ are the relative velocity and the relative fluctuation velocity respectively, between two colliding particles 1 and 2; $\boldsymbol{k} \equiv \boldsymbol{k}_{12} = (\boldsymbol{x}_1 - \boldsymbol{x}_2)/|\boldsymbol{x}_1 - \boldsymbol{x}_2|$ is the unit contact vector joining the center of particle-1 to that particle-2. The molecular chaos ansatz, $f(\boldsymbol{C}_1, \boldsymbol{C}_2) = f(\boldsymbol{C}_1) f(\boldsymbol{C}_2)$ (i.e. the two-particle distribution function can be written as the product of two single-particle distribution functions), has been adopted in 5.13.

With an appropriate choice of the distribution function $f(\boldsymbol{c}, \boldsymbol{x}, t)$, the collision integral (5.13) can be evaluated, which will be plugged into (5.12) to carry out the analysis for the particle-phase rheology and hydrodynamics of a sheared gas-solid suspension.

5.2.1 Analysis in the ignited sate

The "*ignited*" state (Tsao & Koch 1995) represents the hydrodynamic state of fluidized-particles in rapid granular flow (Goldhirsch 2003), where the particles fly around randomly in between two collisions without getting much affected by the viscous drag of the interstitial fluid. A

typical particle encounters successive collisions with other particles again and again before it can relax back to the local fluid velocity and hence the collision time is much smaller than the viscous relaxation time ($\tau_c \ll \tau_v$). In this state, the particles have strong velocity fluctuations, resulting in $T/\dot{\gamma}\sigma \gg 1$.

As in our recent work (Saha & Alam 2014, 2016), the distribution function in the ignited state of a sheared suspension is assumed to be an anisotropic Maxwellian,

$$f(\boldsymbol{c},\boldsymbol{x},t) = \frac{n}{(8\pi^3|\boldsymbol{M}|)^{1/2}}\exp\Big(-\frac{1}{2}\boldsymbol{C}\cdot\boldsymbol{M}\cdot\boldsymbol{C}\Big), \tag{5.15}$$

where $|\boldsymbol{M}| = det(\boldsymbol{M})$. This form of the distribution function has been used previously in studying the velocity dispersions in Saturn's rings (Goldreich & Tremaine 1978; Shukhman 1984; Araki & Tremaine 1986; Araki 1988) as well as to analyse the shear flow of dry rapid granular flows (Jenkins & Richman 1988; Richman 1989; Lutsko 2004).

In the isotropic limit, (5.15) reduces to the Maxwellian distribution function, and an Hermite expansion of the form

$$\begin{aligned} f(\boldsymbol{c},\boldsymbol{x},t) &= \frac{n}{(2\pi T)^{3/2}}\exp\Big(-C^2/2T\Big)\sum_i a^{(i)}\mathscr{H}^{(i)} \\ &= \frac{n}{(2\pi T)^{3/2}}\exp\Big(-C^2/2T\Big)\Big\{1+\frac{1}{2\rho T^2}P_{\langle\alpha\beta\rangle}C_\alpha C_\beta\Big\}+HOT, \end{aligned} \tag{5.16}$$

represents the well-known Grad's moment expansion (GME) (Grad 1949) – such moment expansion has subsequently been employed to solve the Boltzmann equation for molecular gases (Herdegen & Hess 1982; Kremer 2010), granular gases (Jenkins & Richman 1985*a*; Kremer & Marques Jr 2011) and gas-solid suspensions (Tsao & Koch 1995; Sangani *et al.* 1996; Chamorro *et al.* 2015). Equation (5.16) with leading-order term ($P_{\langle\alpha\beta\rangle} = \rho M_{\alpha\beta} - T\delta_{\alpha\beta}$ is the stress deviator) yields the 10-moment system of Grad (1949), with density, velocity, temperature and stress-deviator constituting the extended set of ten hydrodynamic fields (Saha & Alam 2016).

Uniform shear flow (USF) and the second moment tensor

The analysis in this section closely follows the theoretical framework introduced by (Goldreich & Tremaine 1978; Shukhman 1984; Araki & Tremaine 1986; Jenkins & Richman 1988; Richman 1989). For the uniform shear flow, the velocity gradient tensor can be decomposed

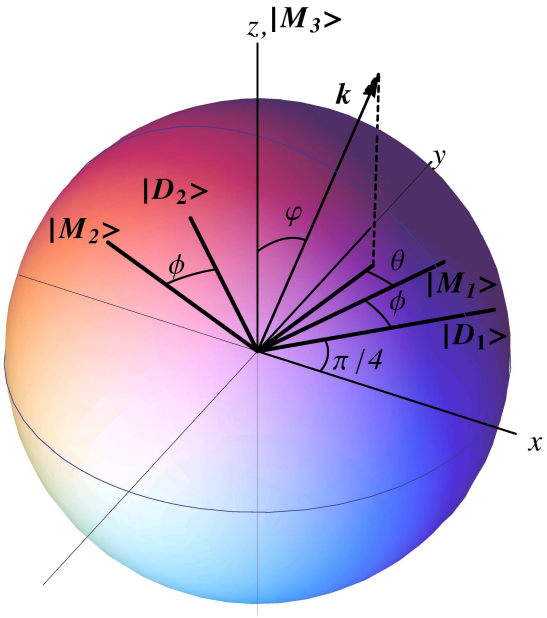

Fig. 5.1 Schematic of the co-ordinate system and the eigen-basis for analysis; the eigen-directions of the shear tensor $\boldsymbol{D}$ and the second moment tensor $\boldsymbol{M}$ are decpicted. The uniform shear flow, $\boldsymbol{u} = (\dot{\gamma}y, 0, 0)$, is directed along the x-direction, with the velocity gradient along the y-direction and the mean-vorticity along the z-direction.

as

$$\boldsymbol{\nabla u} = \boldsymbol{D} + \boldsymbol{W} \equiv \begin{bmatrix} 0 & \dot{\gamma}/2 & 0 \\ \dot{\gamma}/2 & 0 & 0 \\ 0 & 0 & 0 \end{bmatrix} + \begin{bmatrix} 0 & \dot{\gamma}/2 & 0 \\ -\dot{\gamma}/2 & 0 & 0 \\ 0 & 0 & 0 \end{bmatrix}, \tag{5.17}$$

where $\boldsymbol{D}$ and $\boldsymbol{W}$ are the shear and spin tensors, respectively. Referring to figure 5.1, the (x,y)-plane is dubbed the *shear plane* and the z-direction is the *vorticity direction*. The eigenvalues of $\boldsymbol{D}$ are $\dot{\gamma}/2$, $-\dot{\gamma}/2$ and 0, with the corresponding orthonormal eigenvectors, respectively,

$$|D_1\rangle = \begin{bmatrix} \cos\frac{\pi}{4} \\ \sin\frac{\pi}{4} \\ 0 \end{bmatrix}, \quad |D_2\rangle = \begin{bmatrix} -\sin\frac{\pi}{4} \\ \cos\frac{\pi}{4} \\ 0 \end{bmatrix} \quad \text{and} \quad |D_3\rangle = \begin{bmatrix} 0 \\ 0 \\ 1 \end{bmatrix}, \tag{5.18}$$

that are sketched in figure 5.1. While $|D_3\rangle$ is directed along the z-axis, the shear-plane eigenvectors $|D_1\rangle$ and $|D_2\rangle$ are rotated by 45° anticlockwise from the xy-axes.

Since the granular temperature $T = M_{\alpha\alpha}/3$ is the isotropic measure of the second moment tensor $\boldsymbol{M} = \langle \boldsymbol{CC} \rangle$, we can decompose it as $\boldsymbol{M}/T = \boldsymbol{I} + \widehat{\boldsymbol{M}}/T$, where $\widehat{\boldsymbol{M}}/T$ is the dimensionless counterpart of its deviatoric/traceless tensor. The eigenvalues of $\boldsymbol{M}$ are denoted by $T(1+\xi)$, $T(1+\varsigma)$ and $T(1+\zeta)$, with ξ, ς and ζ being the eigenvalues of $\widehat{\boldsymbol{M}}/T$ such that

$$\xi + \varsigma + \zeta = 0. \tag{5.19}$$

The corresponding orthonormal set of eigen-directions are assumed to be $|M_1\rangle$, $|M_2\rangle$ and $|M_3\rangle$, respectively, as depicted in figure 5.1. Therefore, the second-moment tensor $\boldsymbol{M}$ can be written in terms of its eigen-basis:

$$\boldsymbol{M} = T(1+\xi)|M_1\rangle\langle M_1| + T(1+\varsigma)|M_2\rangle\langle M_2| + T(1+\zeta)|M_3\rangle\langle M_3|. \tag{5.20}$$

Referring to figure 5.1, we assume that the shear-plane eigenvectors $|M_1\rangle$ and $|M_2\rangle$ can be obtained by rotating the system of axes at an angle $(\pi/4+\phi)$, with ϕ being unknown, in the anti-clockwise sense about the z-axis which coincides with $|M_3\rangle$:

$$|M_1\rangle = \begin{bmatrix} \cos\left(\phi+\frac{\pi}{4}\right) \\ \sin\left(\phi+\frac{\pi}{4}\right) \\ 0 \end{bmatrix}, \quad |M_2\rangle = \begin{bmatrix} -\sin\left(\phi+\frac{\pi}{4}\right) \\ \cos\left(\phi+\frac{\pi}{4}\right) \\ 0 \end{bmatrix} \quad \text{and} \quad |M_3\rangle = \begin{bmatrix} 0 \\ 0 \\ 1 \end{bmatrix}. \tag{5.21}$$

We further assume that the contact vector $\boldsymbol{k}$ makes an angle φ with $|M_3\rangle$, and θ is the angle between $|M_1\rangle$ and $\boldsymbol{k} - (\boldsymbol{k}\cdot\boldsymbol{z})\boldsymbol{z}$, the projection of $\boldsymbol{k}$ on the shear plane, as shown in figure 5.1.

Inserting (5.21) into (5.20), we obtain the following expression for the second moment tensor

$$\boldsymbol{M} = T[\delta_{\alpha\beta}] + \widehat{\boldsymbol{M}}, \tag{5.22}$$

with its deviatoric part being given by

$$\widehat{\boldsymbol{M}} = T \begin{bmatrix} \lambda^2 + \eta \sin 2\phi & -\eta \cos 2\phi & 0 \\ -\eta \cos 2\phi & \lambda^2 - \eta \sin 2\phi & 0 \\ 0 & 0 & -2\lambda^2 \end{bmatrix}. \tag{5.23}$$

Here we have introduced the following notations

$$\eta \equiv \frac{1}{2}(\varsigma - \xi) \geq 0 \quad \text{and} \quad \lambda^2 \equiv \frac{1}{2}(\varsigma + \xi) = -\frac{\zeta}{2} \geq 0, \tag{5.24}$$

such that the eigenvalues in the shear-plane can be expressed in terms of η and λ via

$$\xi = \lambda^2 - \eta \quad \text{and} \quad \varsigma = \lambda^2 + \eta > \xi, \tag{5.25}$$

with the eigenvalue, ζ, along the vorticity direction (z), being given by (5.24).

Since $\phi = 0$ implies that the shear tensor ($\boldsymbol{D}$) and the second-moment tensor ($\boldsymbol{M}$) have same principal directions, a non-zero value of ϕ is a measure of the *non-coaxiality* angle between the principal directions of $\boldsymbol{D}$ and $\boldsymbol{M}$. It is straightforward to show that $\eta \sim (T_x - T_y)$ is proportional to the difference between two temperatures T_x and T_y on the shear-plane (x, y), and hence $\eta \neq 0$ is indicative of the degree of *temperature-anisotropy* on the shear plane. On the other hand, a non-zero value of λ^2 is a measure of the *excess temperature* (Saha & Alam 2016),

$$T_z^{ex} = (T - T_z) = 2\lambda^2 T \quad \Rightarrow \quad \lambda^2 = \frac{T_z^{ex}}{2T}, \tag{5.26}$$

along the mean vorticity direction. In summary, the anisotropy of $\boldsymbol{M}$ is quantified in terms of three dimensionless quantities: (i) $\eta \propto (T_x - T_y) \neq 0$, or, $\phi \neq 0$ and (ii) $\lambda^2 \propto T_z^{ex} \neq 0$.

The second-moment tensor (5.22-5.23) in the USF of suspension, constructed from its eigen-basis, is therefore completely determined when T, η, ϕ and λ^2 are specified; the dependence on the Stokes number St and the particle volume fraction (ν) is implicit as will be made clear below.

Source term in the ignited state

Employing (5.15), the collisional production term (5.13) for the ignited state has been evaluated

$$\aleph_{\alpha\beta}^{is} = -\frac{6(1+e)\rho_p \nu^2}{\pi^{\frac{3}{2}}\sigma}\Big\{(1-e)\int k_\alpha k_\beta (\boldsymbol{k}\cdot\boldsymbol{M}\cdot\boldsymbol{k})^{\frac{3}{2}} d\boldsymbol{k} + 2\int (k_\alpha j_\beta + j_\alpha k_\beta)(\boldsymbol{k}\cdot\boldsymbol{M}\cdot\boldsymbol{k})^{\frac{1}{2}}(\boldsymbol{k}\cdot\boldsymbol{M}\cdot\boldsymbol{j}) d\boldsymbol{k}\Big\}. \tag{5.27}$$

$$= -\frac{4(1+e)\rho_p \nu^2 T^{3/2}}{35\sigma\sqrt{\pi}}\Big\{(1-e)\times \begin{bmatrix} 70+9\eta^2+42\lambda^2+42\eta\sin 2\phi & -42\eta\cos 2\phi & 0 \\ -42\eta\cos 2\phi & 70+9\eta^2+42\lambda^2-42\eta\sin 2\phi & 0 \\ 0 & 0 & 70+3\eta^2-84\lambda^2 \end{bmatrix} + 4\begin{bmatrix} \eta^2+21\lambda^2+21\eta\sin 2\phi & -21\eta\cos 2\phi & 0 \\ -21\eta\cos 2\phi & \eta^2+21\lambda^2-21\eta\sin 2\phi & 0 \\ 0 & 0 & -2(\eta^2+21\lambda^2) \end{bmatrix}\Big\}, \tag{5.28}$$

which is a function of ν, e, T, η, ϕ and λ^2. In the final expression (5.28), we have retained terms that are up-to second-order in η, $\sin\phi$ and λ – we shall show in the end that this is sufficient to yield accurate predictions of transport coefficients of a sheared dilute suspension for a wide range of (i) restitution coefficient e and (ii) Stokes number St.

5.2.2 Analysis in the quenched sate

Tsao & Koch (1995) envisaged a scenario of a dilute gas-solid suspension in which the particle inertia is very low such that the particles tend to align with fluid streamlines after a collision. Most of the particles will be having their individual velocity equal to the fluid velocity ($\boldsymbol{c} \approx \boldsymbol{u}$) which implies that the peculiar velocity $\boldsymbol{C} \approx 0$ and therefore the particle agitation is very small ($T/\dot{\gamma}\sigma \ll 1$) – this is dubbed the *quenched* state. The collisions in this state are mainly shear-induced with some occasional variance-driven collisions and the particles relax back to the local fluid velocity after such a collision before they encounter a second collision and therefore the viscous relaxation time is much smaller than the collision time $\tau_v \ll \tau_c$. The velocity distribution function of the quenched state is taken to be a delta function

$$f = n\delta(\boldsymbol{C}), \tag{5.29}$$

which is a solution of the Boltzmann equation. Using (5.29), the collisional production term at second-order can be evaluated as

$$\aleph^{qs}_{\alpha\beta} = -\rho\dot{\gamma}^3\sigma^2\frac{3(1+e)^2\nu}{2\pi}\int_{k_xk_y>0}(k_xk_y)^3k_\alpha k_\beta d\boldsymbol{k},$$
$$= \rho_p\dot{\gamma}^3\sigma^2\frac{(1+e)^2\nu^2}{16}\begin{bmatrix}\frac{512}{315\pi} & -\frac{16}{35} & 0\\ -\frac{16}{35} & \frac{512}{315\pi} & 0\\ 0 & 0 & \frac{128}{315\pi}\end{bmatrix}. \tag{5.30}$$

Note that this expression differs from that of Tsao & Koch (1995) by a numerical-factor 2 which was also noted previously (Parmentier & Simonin 2012).

5.2.3 Second moment balance combining quenched and ignited states

Combining the ignited and quenched states, the second-order moment balance equation (5.12) for a 'dilute' gas-solid suspension undergoing uniform shear flow is

$$P_{\delta\beta}u_{\alpha,\delta} + P_{\delta\alpha}u_{\beta,\delta} + \frac{2\dot{\gamma}}{St}P_{\alpha\beta} = \aleph_{\alpha\beta} \equiv \aleph^{qs}_{\alpha\beta} + \aleph^{is}_{\alpha\beta}, \tag{5.31}$$

where the superscripts *qs* and *is* stand for the source of second moment in quenched and ignited states, respectively. Following (5.22-5.23), the expression for the stress tensor can be written as

$$\boldsymbol{P} = \rho\boldsymbol{M} = \rho_p\nu T\begin{bmatrix}1+\lambda^2+\eta\sin 2\phi & -\eta\cos 2\phi & 0\\ -\eta\cos 2\phi & 1+\lambda^2-\eta\sin 2\phi & 0\\ 0 & 0 & 1-2\lambda^2\end{bmatrix}. \tag{5.32}$$

Substituting (5.27), (5.30) and (5.32) into (5.31), we obtain the following four independent equations:

$$\left.\begin{aligned}
-2T\eta\cos 2\phi+\tfrac{2}{St}T(1+\lambda^2+\eta\sin 2\phi) &= \Big[-\tfrac{2(1-e^2)\nu T^{\frac{3}{2}}}{35\sqrt{\pi}}(70+9\eta^2+42\lambda^2+42\eta\sin 2\phi)\\
&\quad -\tfrac{8(1+e)\nu T^{\frac{3}{2}}}{35\sqrt{\pi}}(\eta^2+21\lambda^2+21\eta\sin 2\phi)\Big]\\
&\quad +\Big[\tfrac{128(1+e)^2\nu}{315\pi}\Big],\\
\tfrac{2}{St}T(1+\lambda^2-\eta\sin 2\phi) &= \Big[-\tfrac{2(1-e^2)\nu T^{\frac{3}{2}}}{35\sqrt{\pi}}(70+9\eta^2+42\lambda^2-42\eta\sin 2\phi)\\
&\quad -\tfrac{8(1+e)\nu T^{\frac{3}{2}}}{35\sqrt{\pi}}(\eta^2+21\lambda^2-21\eta\sin 2\phi)\Big]\\
&\quad +\Big[\tfrac{128(1+e)^2\nu}{315\pi}\Big],\\
\tfrac{2}{St}T(1-2\lambda^2) &= \Big[-\tfrac{2(1-e^2)\nu T^{\frac{3}{2}}}{35\sqrt{\pi}}(70+3\eta^2-84\lambda^2)\\
&\quad +\tfrac{16(1+e)\nu T^{\frac{3}{2}}}{35\sqrt{\pi}}(\eta^2+21\lambda^2)\Big]+\Big[\tfrac{32(1+e)^2\nu}{315\pi}\Big],\\
T(1+\lambda^2-\eta\sin 2\phi)-\tfrac{2}{St}T\eta\cos 2\phi &= \Big[\tfrac{12(1-e)(3-e)\nu T^{\frac{3}{2}}}{5\sqrt{\pi}}\eta\cos 2\phi-\tfrac{4(1+e)^2\nu}{35\pi}\Big].
\end{aligned}\right\}, \tag{5.33}$$

Note that the terms involving the Stokes number (St) on the left-hand sides of (5.33) vanish in the limit of $St\to\infty$, thereby recovering the second-moment balance for the shear flow of a 'dry' granular gas (Saha & Alam 2016).

In (5.33), we have made temperature dimensionless via $T=T/(\dot\gamma\sigma/2)^2$. The coupled system of equations (5.33) must be solved to determine η, λ, ϕ and T for specified values of (i) particle volume fraction (ν), (ii) Stokes number (St) and (iii) restitution coefficient (e). Analytical progress can be made to solve (5.33) as discussed in §5.3 and §5.4.

Before proceeding further, it may be noted that the analysis of the second moment balance (5.31) or (5.33) in the ignited state (i.e. with $\aleph^{qs}_{\alpha\beta}=0$) is considerably simplified for elastically-colliding ($e=1$) particles, see Appendix A. The related analytical results on the temperature field provide a lower-bound on the Stokes number for the existence of the ignited state (and consequently on the multiple states and hysteresis, §5.3.2) in a dilute gas-solid suspension.

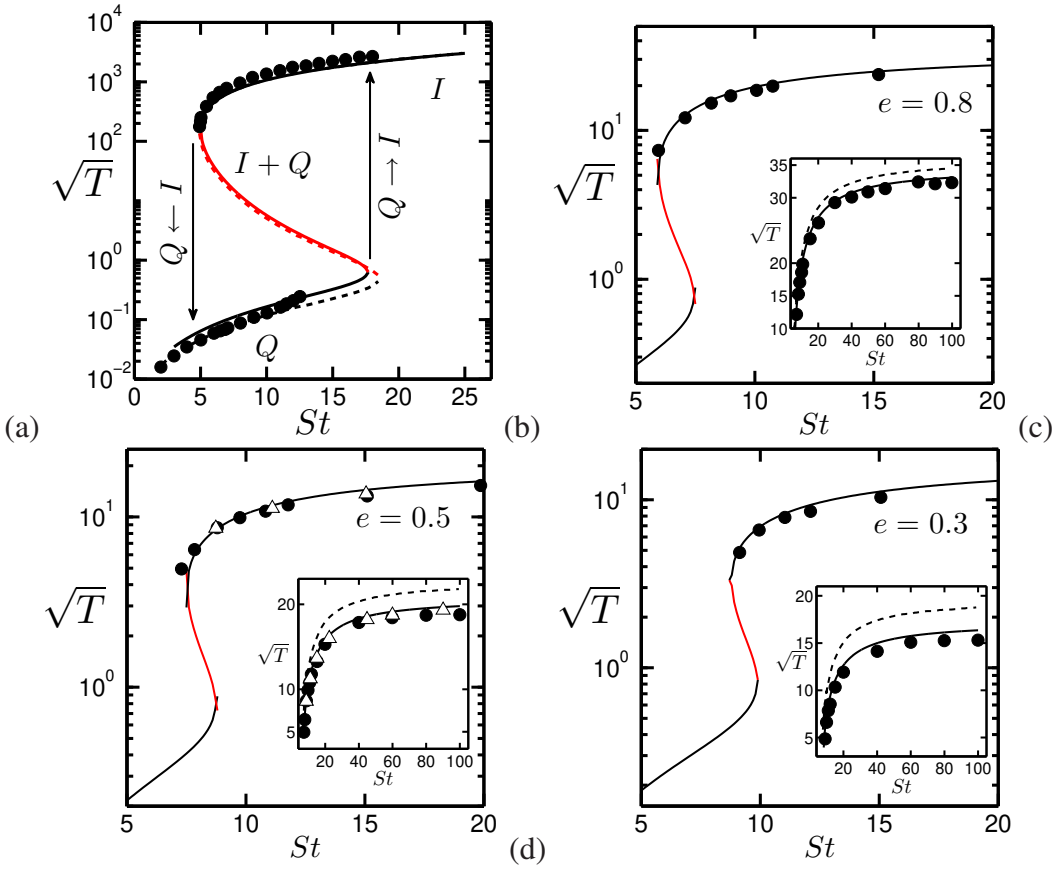

Fig. 5.2 Hysteretic/first-order transitions of granular temperature for (a) $e = 1$ and $\nu = 5 \times 10^{-4}$; (b) $e = 0.8$, (c) $e = 0.5$ and (d) $e = 0.3$ with $\nu = 0.01$. The solid and dashed (inset) lines denote the present anisotropic-Maxwellian theory and the Maxwellian theory (Tsao & Koch 1995; Sangani *et al.* 1996), respectively. The filled-circles represent the DSMC data of Sangani *et al.* (1996); the open-triangles in panel *c* denote the DSMC data of Chamorro *et al.* (2015). In each panel, the black and red lines represent stable and unstable solutions, respectively, of Eq. (3.1).

5.3 Granular temperature: Multi-stability and ignited-to-quenched state transitions

After some tedious algebra, we found that (5.33) can be decoupled to yield a 10-th degree polynomial for granular temperature $\xi = \sqrt{T}$:

$$\mathscr{G}(\xi) \equiv a_{10}\xi^{10} + a_9\xi^9 + a_8\xi^8 + a_7\xi^7 + a_6\xi^6 + a_5\xi^5 + a_4\xi^4 + a_3\xi^3 + a_2\xi^2 + a_1\xi + a_0 = 0, \tag{5.34}$$

the explicit expressions of the coefficients a_i are given in Appendix B. It is straightforward to verify that for the case of elastically colliding particles ($e = 1$), $a_{10} = 0 = a_9 = a_8$ and hence (5.34) reduces to a polynomial of 7th-degree; in fact these three roots vapourize to $-\infty$ at $e = 1$ and remain negative for $e < 1$ and hence unphysical. It has been verified numerically (as well as via an ordering analysis, see Appendix C) that at most three roots of (5.34) are real positive, depending on the values of ν, St and e, and the remaining roots are negative and/or complex.

5.3.1 Validation of present anisotropic-Maxwellian theory

First, we solve the temperature equation (5.34) numerically and compare it with simulation data in order to validate the present theory.

Figure 5.2(a,b,c,d) shows the variations of the granular temperature with Stokes number (St) at particle volume fractions of (a) $\nu = 5 \times 10^{-4}$ and (b,c,d) $\nu = 0.01$, with different values of the restitution coefficient (a) $e = 1$, (b) $e = 0.8$, (c) $e = 0.5$ and $e = 0.3$. In each panel and inset, the symbols represent the DSMC (direct simulation Monte Carlo) data of Sangani *et al.* (1996) which are compared with the (i) present anisotrpic-Maxwellian theory (solid line) and (ii) the standard moment expansion (dashed line) of Tsao & Koch (1995, for $e = 1$) and Sangani et al. (1996, for $e \neq 1$), Figure 5.2(a) indicates that for the case of elastically colliding particles, the present theory is on par with Tsao-Koch theory. On the other hand, for inelastic particles ($e < 1$), the insets of figure 5.2(b,c,d) confirm that the present theory is able to better predict the temperature-variation with St; however, the agreement with Tsao-Koch theory worsens with increasing dissipation. In panel c, the recent DSMC data (open triangles) of Chamorro *et al.* (2015) for $e = 0.5$ also agree quantitatively with the present theory.

Overall, the moment theory with anisotropic-Maxwellian as the leading term seems better suited for a dilute gas-solid suspension of inelastic particles undergoing shear flow for a large range of $e < 1$ at small and moderate values of Stokes number. It may be noted that a similar analysis (Saha & Alam 2014, 2016) for a sheared granular gas ($St = \infty$) provides excellent predictions for temperature and rheological quantities for highly dissipative particles. The

same conclusions seem to carry over to the limit of small Stokes numbers of a sheared gas-solid suspension too – this issue is further discussed in §5.5 (with respect to predictions for viscosity and normal stress differences).

5.3.2 Analytical solution for three temperatures: hysteresis and multi-stability

Returning to figure 5.2, we note that the temperature is a multi-valued function of Stokes number for a range of St over which there are three possible solutions; there are hysteretic/discontinuous jumps in temperature from the low/high temperature branches with increasing/decreasing St. For a better understanding of this hysteresis phenomenon, equation (5.34) has been solved in the asymptotic limit $\nu \ll 1$, $St \gg 1$, and $St^3\nu \ll 1$ via an ordering analysis, the details of which are given in Appendix C. Three real solutions have been found,

$$\sqrt{T_{is}} = \frac{5(1+e)^{-1}(1691+539e-1223e^2+337e^3)\sqrt{\pi}}{48(3-e)(12607-19952e+10099e^2-1746e^3)}\left(\frac{St}{\nu}\right) \overset{e=1}{\equiv} \frac{5\sqrt{\pi}}{144}\frac{St}{\nu}, \tag{5.35}$$

$$\sqrt{T_{qs}} = \sqrt{\frac{32(1+e)^2}{945\pi}}St^{3/2}\nu^{1/2} \overset{e=1}{\equiv} \frac{8\sqrt{2}}{3\sqrt{105\pi}}St^{3/2}\nu^{1/2}, \tag{5.36}$$

$$\sqrt{T_{us}} = \frac{840\sqrt{\pi}}{(1+e)(107+193e)}\left(\frac{1}{St^3\nu}\right) \overset{e=1}{\equiv} \frac{7\sqrt{\pi}}{5}\left(\frac{1}{St^3\nu}\right), \tag{5.37}$$

which correspond to the temperatures in the ignited (T_{is}), quenched (T_{qs}) and unstable (T_{us}) states, respectively. These three solutions (5.35-5.37) can be identified in figure 5.2 as the high-, low-, and intermediate-temperature branches, respectively; the red-colored solution branch in each panel of figure 5.2 represent T_{us} which is of course *unstable* from stability viewpoint (see §5.4.2 for related discussions).

It is clear from (5.35) that T_{is} increases with increasing Stokes number St, but decreases with increasing particle volume fraction ν. On the other hand, the quenched-state temperature (5.36) increases with increasing St and ν, whereas the unstable temperature (5.37) decreases with increasing St and ν. These overall predictions are verified in figure 5.3 which display the variations of granular temperature as functions of (ν, e) for two values of Stokes number (a) $St = 10$ and (b) $St = 20$. In each panel, the upper-most branch corresponds to the ignited-state of high temperature T_{is}; the middle and the lower-most planes represent the unstable and quenched states, respectively. The latter two states are connected via a line of turning-points, resulting in saddle-node bifurcations (jump-transitions) from "$Q \to I$" with increasing ν, above which the ignited state is the only solution. The critical density $\nu = \nu_c(St, e)$ for this transition increases with increasing inelasticity but decreases with increasing St (see panel b).

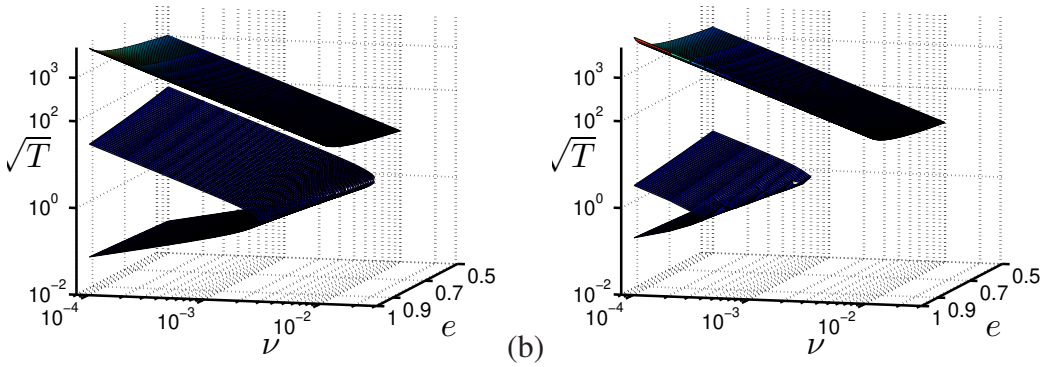

Fig. 5.3 Multiple states of granular temperature as functions of the mean volume fraction ν and restitution coefficient e for (a) $St = 10$ and (b) $St = 20$.

The corresponding Stokes number for "$Q \to I$"-transition is denoted by $St_{c_2}(\nu, e)$ which can also be identified with the right limit-point in figure 5.2.

A noteworthy feature of figure 5.3 is that the ignited branch [$T \propto \nu^{-2}$, see (5.35)] is disconnected from the quenched and unstable branches, and therefore there is no jump-transitions (on decreasing ν) from $I \to Q$ at $St = 10$ (panel a) and 20 (panel b). However, on further decreasing the Stokes number (below $St = 10$), the ignited state solution disappears below a minimum St – how this process occurs is explained in figures 5.4(a,b,c) for $e = 1$, 0.8 and 0.5, respectively. In particular, at any e, the unstable branch (red line) and the ignited-branch come closer with decreasing St and merge with each other at some minimum St below which only the quenched-state solution [$T \propto \nu$, see (5.36)] survives. Similarly, by fixing the Stokes number at $St = 6$ but increasing the inelasticity (decreasing e) also results in the disappearance of the ignited state solution, see figure 5.4(d). Therefore, the quenched state is the only possible solution below a minimum Stokes number $St = St_{c_1}(e, \nu)$ – this can be identified with the left limit-point in figure 5.2 for "$I \to Q$" transition.

5.3.3 Critical Stokes numbers (St_{c_1}, St_{c_2}) and the master phase-diagram

Referring to figure 5.2, two critical/limit points (at $St = St_{c_1}$ and St_{c_2}, with $St_{c_2} > St_{c_1}$) correspond to the double roots of (5.34) at which the following conditions must be satisfied:

$$\mathscr{G}(\xi_c) = 0 \quad \text{and} \quad \mathscr{G}'(\xi_c) = 0. \tag{5.38}$$

This implies that two solution branches, corresponding to two different states [(i) ignited (T_{is}), (ii) quenched (T_{qs}) and (iii) unstable (T_{us})] meet at $\xi = \xi_c$, leading to saddle-node bifurcations from one stable state to another stable state.

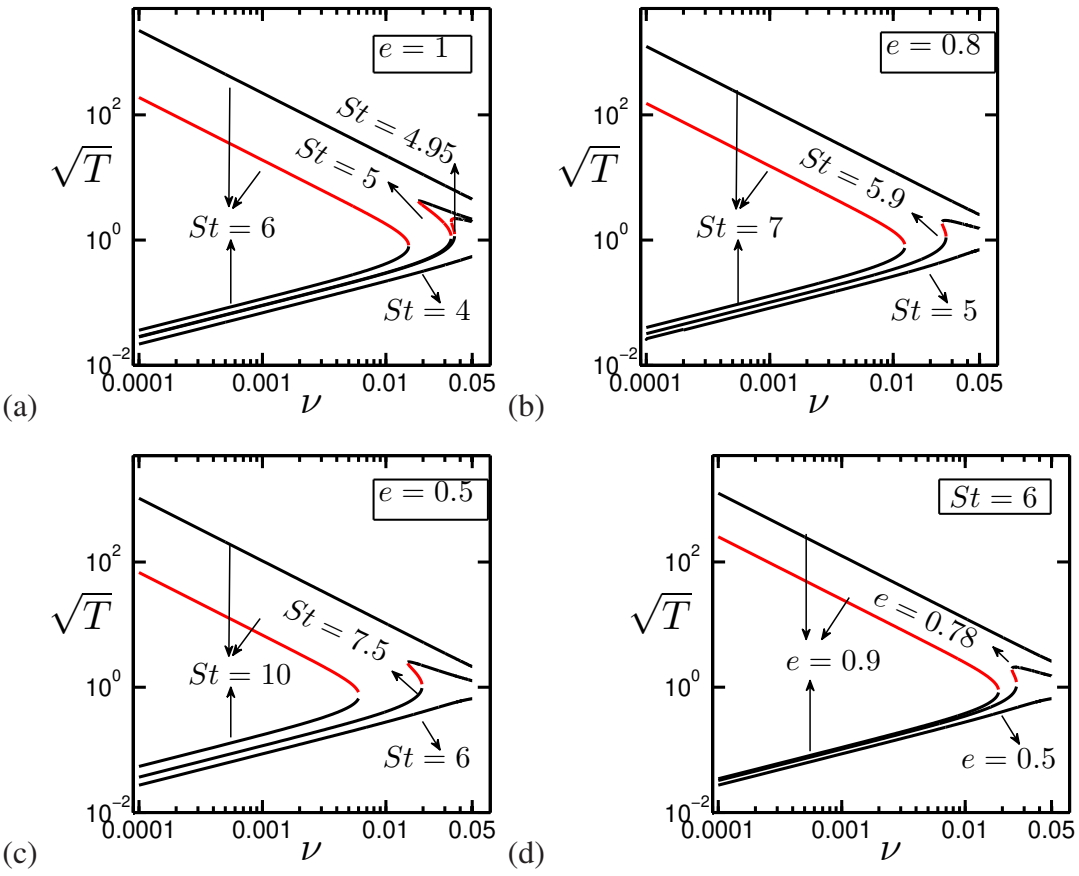

Fig. 5.4 Disappearance of the ignited-state branch with (a,b,c) decreasing Stokes number at (a) $e = 1$, (b) $e = 0.8$ and (c) $e = 0.5$, and (d) the same with decreasing restitution coefficient at $St = 6$.

The discontinuous "$Q \rightarrow I$" transition corresponds to a limit point ($St = St_{c_2}$, viz. figure 5.2*a*) at which the quenched and unstable solution branches meet. Carrying out the asymptotic analysis of (5.34) with $T_{qs} = T_{us}$ and satisfying (5.38) (see Appendix D for details), we obtain the following relation

$$St_{c_2}^3 \nu_c = \left(\frac{3087000\pi^2}{(1+e)^4(107+193e)^2} \right)^{\frac{1}{3}}, \tag{5.39}$$

that represents a *critical-surface* in the (ν, St, e)-plane, above which only the ignited state exists. Equation (5.39) is depicted in figure 5.5 as a blue-surface. In the elastic limit of $e = 1$, (5.39) reduces to $St_{c_2}^3 \nu_c = 2.7685$ which differs from the prediction (≈ 3.23) of Tsao & Koch (1995).

The critical Stokes number, St_{c_1}, for the "$I \rightarrow Q$" transition (on decreasing St) corresponds to the limit point at which $T_{is} = T_{us}$. The asymptotic analysis of (5.34) yields the following expression for St_{c_1} (see Appendix D for details):

$$St_{c_1} \approx 9.9 - 4.91e, \tag{5.40}$$

which is marked as a brown-shaded plane in figure 5.5, to the left of which only the quenched state exists. For elastically colliding particles ($e = 1$), we have $St_{c_1} \approx 4.99$ which is close to our numerical solution of 4.94...; both are close to the result of $\sqrt{169.5/7} \approx 4.92$ obtained by Tsao & Koch (1995). Note that (5.40) depends only on the restitution coefficient, and therefore the minimum value of Stokes number (St_{c_1}), below which only the quenched-state exists, is independent of the volume fraction for a dilute gas-solid suspension.

The master phase-diagram in figure 5.5 summarizes all possible states in the (ν, St, e)-plane: (i) the ignited state (I) exists above the blue-surface, (ii) the quenched state (Q) is the only solution to the left of the brown surface and (iii) the coexistence of ignited and quenched ($I + Q$) states occurs for parameter values lying between the blue and brown surfaces. Two critical surfaces in figure 5.5 would meet along a curve, thus acting as an upper bound for the existence of the unstable state (T_{us}) solution (and hence the existence of the mixed state $I + Q$). By equating $St_{c_1} = St_{c_2}$, the equation of this curve is obtained as

$$\nu_{us}^{l}(e) = \left(\frac{3087000\pi^2}{(1+e)^4(107+193e)^2} \right)^{\frac{1}{3}} / (9.9 - 4.91e)^3, \tag{5.41}$$

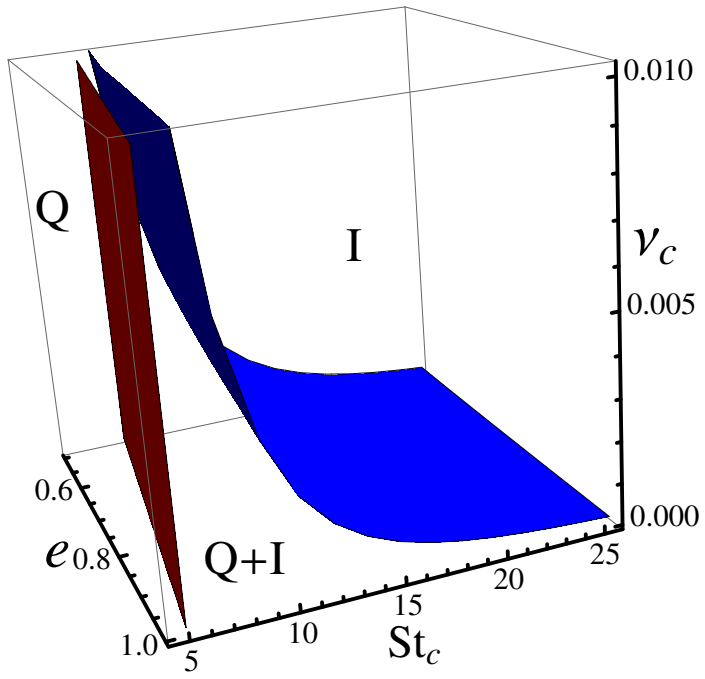

Fig. 5.5 Complete phase diagram of different states ["ignited" (I), "quenched" (Q) and their co-existence (Q+I)] in the (ν, St, e)-plane. The blue- and brown-colored planes, above and below which, respectively, the ignited and quenched states exist, have been determined analytically from an ordering analysis of (5.34) in the dilute limit; for details, see the text in §5.3.3 and Appendix D.

which is a decreasing function of the restitution coefficient. Note that (5.41) is not a critical point, rather it represents an upper-bound on density below which the phase-coexistence [$I+Q$] occurs in the small-St regime of a sheared gas-solid suspension.

It is clear from from (5.40) and (5.39) that the critical Stokes numbers St_{c_1} and St_{c_2} increase with decreasing e (i.e. increasing inelasticity) at a fixed volume fraction $\nu < \nu_{us}^{l}$, When dissipative particles ($e \ll 1$) collide with each other they loose more energy and hence loose more of their inertia; in that case the recovery time (τ_v) reduces and the adjustment with the local fluid velocity becomes faster, leading to the quenched state. On the other hand, for nearly elastic ($e \sim 1$) collisions, the particles lose very little kinetic energy during collisions and take much more time to come back to the bulk flow and hence the recovery process becomes slow. Therefore, at higher values of e, both ignited and quenched states exist but only the quenched state is possible if we increase inelasticity of the system, leading to the behaviour of St_{c_1} as in (5.40). Similar argument holds for the variation of St_{c_2} with inelasticity as well.

5.4 Non-Newtonian rheology: second-moment anisotropy, discontinuous shear-thickening and normal stress differences

Once the temperature field is solved from (5.34) for specified values of ν, St and e, the non-coaxiality angle ϕ, the temperature-anisotropy η and the excess temperature λ^2 can be calculated from the remaining equations of (5.33) – these are amenable to analytical solutions as described in §5.4.1. The behaviour of shear viscosity and normal stress differences are analysed in §5.4.2 and §5.4.3, respectively.

5.4.1 Anisotropies of second-moment tensor: analytical solution for ϕ, η and λ^2

After some algebra and rearrangement of terms in (5.33), the closed-form solutions for ϕ, η^2 and λ^2 have been found:

$$\phi = \frac{1}{2}\tan^{-1}\left(\frac{2}{St} + \frac{12(1+e)(3-e)\nu\sqrt{T}}{5\sqrt{\pi}}\right)^{-1}, \tag{5.42}$$

$$\eta^2 = -\frac{\mathfrak{b}}{2\mathfrak{a}} - \frac{1}{2\mathfrak{a}}\sqrt{\mathfrak{b}^2 - 4\mathfrak{a}\mathfrak{c}}, \tag{5.43}$$

$$\lambda^2 = \frac{\frac{5\sqrt{\pi}}{2St}T + (1+e)\nu T^{3/2}[5(1-e) - (5+3e)\frac{\eta^2}{14}] - \frac{8(1+e)^2\nu}{63\sqrt{\pi}}}{\left(\frac{5\sqrt{\pi}}{St}T + 6(1+e)(3-e)\nu T^{3/2}\right)}, \tag{5.44}$$

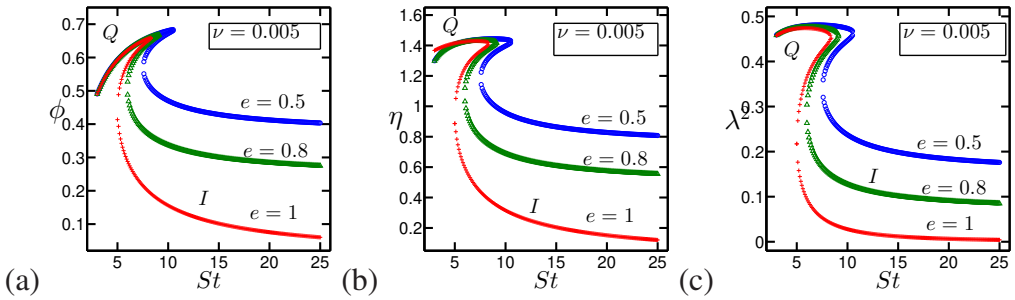

Fig. 5.6 Variations of (a) the non-coaxiality angle ϕ, (b) the shear-plane anisotropy η and (c) the excess temperature λ^2 with Stokes number for different e. The mean volume fraction is set to $\nu = 0.005$.

with T being calculated from (5.34) for specified values of St, ν and e. The solution for the temperature-anisotropy η follows from the quadratic equation $\mathfrak{a}\eta^4 + \mathfrak{b}\eta^2 + \mathfrak{c} = 0$, where

$$\left.\begin{aligned} \mathfrak{a} &= \frac{9(1-e^2)^2\nu^2T^3}{25\pi} > 0 \\ \mathfrak{b} &= \frac{6(1-e^2)\nu T^{3/2}}{5\sqrt{\pi}}\left(\frac{3}{St}T - \frac{16\nu(1+e)^2}{35\pi} + \frac{6(1-e^2)\nu T^{3/2}}{\sqrt{\pi}}\right) - T^2\cos^2 2\phi \\ \mathfrak{c} &= \left(\frac{3}{St}T - \frac{16\nu(1+e)^2}{35\pi} + \frac{6(1-e^2)\nu T^{3/2}}{\sqrt{\pi}}\right)^2 > 0 \end{aligned}\right\}. \tag{5.45}$$

For a suspension of elastically colliding particles ($e = 1$, with finite St), we have $\mathfrak{a} = 0$ and $\mathfrak{b} = -T^2\cos^2 2\phi$, and hence the above solutions (5.42-5.44) simplify to

$$\left.\begin{aligned} \phi(e=1) &= \tfrac{1}{2}\tan^{-1}\left(\frac{2}{St} + \frac{48\nu\sqrt{T}}{5\sqrt{\pi}}\right)^{-1} > 0, \\ \eta^2(e=1) &= -\frac{\mathfrak{c}}{\mathfrak{b}} \equiv \left(\frac{3}{St}T - \frac{64\nu}{35\pi}\right)^2 T^{-2}\sec^2 2\phi > 0, \\ \lambda^2(e=1) &= \frac{\frac{5\sqrt{\pi}}{2St}T - \frac{8}{7}\nu T^{3/2}\eta^2 - \frac{32\nu}{63\sqrt{\pi}}}{\left(\frac{5\sqrt{\pi}}{St}T + 24\nu T^{3/2}\right)} > 0. \end{aligned}\right\} \tag{5.46}$$

Recall from (2.17) that the non-zero values of (ϕ, η, λ^2) quantify the degree of anisotropy of the second-moment tensor $\boldsymbol{M}$ (and hence is a measure of the anisotropy of the kinetic stress tensor, $\boldsymbol{P} = \langle\rho\boldsymbol{CC}\rangle = \rho\boldsymbol{M}$, too).

The positivity of (5.42-5.44) is verified in figures 5.6(a), 5.6(b) and 5.6(c), respectively, which display the variations of ϕ, η and λ^2 with Stokes number for different values of the restitution coefficient $e \leq 1$, at a mean volume fraction of $\nu = 0.005$ – the results look qualitatively similar at other values of $\nu < \nu_{us}^{l}$ (5.41). It is seen from figure 5.6 that the increasing inelasticity markedly increases the values of (ϕ, η, λ^2) on the ignited state, thereby enhancing the anisotropy of the second-moment tensor. In contrast, the inelasticity does not noticeably affect (ϕ, η, λ^2) on the quenched state in which the particle collisions are rare and the dynamics

is primarily dictated by fluid inertia. Interestingly, increasing shear makes the second-moment tensor more anisotropic on the quenched branch – this can be understood by considering the scaling relations of (ϕ, η, λ^2) at $St \sim 0$ as follows. Using the closed-form solutions for three temperatures (3.2-3.4), the non-coaxiality angle for $e = 1$ can be rewritten as

$$\tan 2\phi_{qs} = \frac{St}{2 + \frac{128\sqrt{2}}{5\sqrt{105}\pi} \nu^{3/2} St^{5/2}} \sim St/2 \quad \text{at} \quad St \sim 0. \tag{5.47}$$

Therefore, in the limit of small St, the inertia enhances the non-coaxiality angle in the quenched state. On the other hand, increasing St decreases ϕ in the ignited state, reaching some asymptotic value (depending on e) at large enough St as seen in figure 5.6(a). This can be explained from an analysis of the ignited branch solution, leading to:

$$\tan 2\phi_{is} = \frac{3St}{6 + St^2} \sim \frac{3}{St}, \quad \text{for} \quad St \gg 1. \tag{5.48}$$

Similar scalings (5.47-5.48) hold for the temperature anisotropy η and the excess temperature λ^2 too, that explain the observed behaviour in figures 5.6(b) and 5.6(c), respectively. In summary, the degree of anisotropy of the second-moment tensor in the quenched and ignited states is primarily dictated by the background shear and inelasticity, respectively. The latter effect of inelasticty can be understood from following scaling arguments.

It may be noted that the scaling relation (5.48) is not strictly valid at $St \to \infty$ since the double-limit of $e \to 1$ and $St \to \infty$ leads to a singular behaviour of temperature $T \to \infty$ (and hence a thermostat is necessary to achieve a steady shearing state of elastically colliding particles in the absence of fluid drag). The case of a sheared granular gas ($St = \infty$ at $e \neq 1$) has been analysed previously (Jenkins & Richman 1988; Richman 1989; Saha & Alam 2014, 2016); it can be verified that the above solutions (5.42-5.44) for the ignited-branch reduce to the low-density solution of Saha & Alam (2016):

$$\left.\begin{aligned}
\lambda^2 &\approx \tfrac{1}{48e}\left(168 + 53(1-e)\right)\left[\sqrt{1 + 5760e(1-e)(168+53(1-e))^{-2}} - 1\right] \\
&\approx \tfrac{5}{14}(1-e)\left(1 + \tfrac{53}{168}(1-e)\right)\left(1 - \tfrac{53}{84}(1-e)\right) \\
\eta^2 &= \tfrac{3\lambda^2(7+6\lambda^2)}{6+\lambda^2} \approx \tfrac{7}{2}\lambda^2 = \tfrac{5}{4}(1-e)\left(1 + \tfrac{53}{168}(1-e)\right)\left(1 - \tfrac{53}{84}(1-e)\right) \\
\sin 2\phi &= \tfrac{\eta}{1+\lambda^2} \approx \eta \sim \sqrt{1-e} \\
\sqrt{T} &= \tfrac{5\sqrt{\pi}\eta\cos\phi}{3(1-e^2)\nu(10+\eta^2)} \approx \tfrac{\sqrt{\pi}}{6(1-e^2)\nu}\eta(1-\eta^2/10)(1-\eta^2/2) \\
&\approx \tfrac{\sqrt{\pi}}{6(1-e^2)\nu}\eta(1-\tfrac{3}{5}\eta^2) \sim (1-e)^{-1/2}
\end{aligned}\right\} \tag{5.49}$$

Therefore, in the limit ($St \to \infty$) of a granular gas, $\eta \sim \lambda \sim \sin 2\phi \sim \sqrt{(}1-e)$, with the granular temperature diverging like $T \sim (1-e)^{-1}$ – the latter finding rules out the possibility

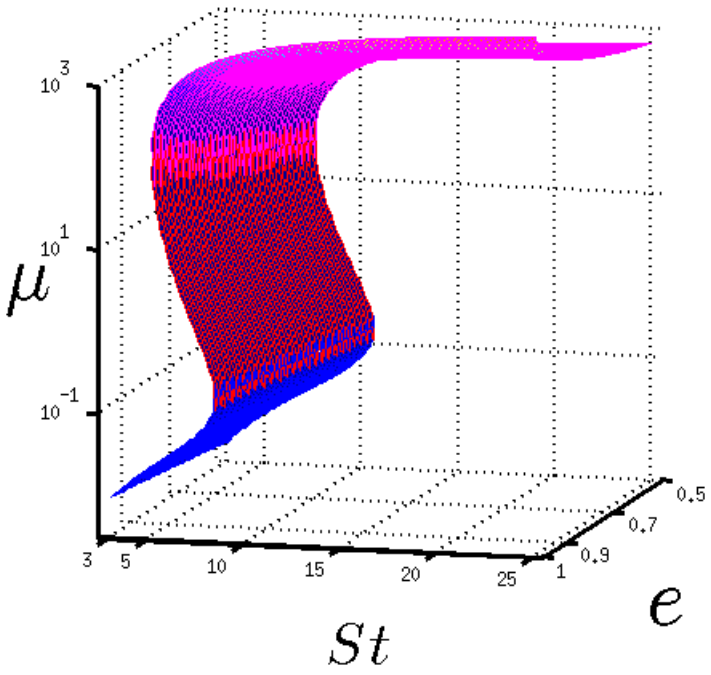

(a)

Fig. 5.7 (a) Hysteretic behaviour of particle-phase viscosity (μ) as functions of (St, e) for a volume fraction of $\nu = 0.005$; this represents DST (discontinuous shear-thickening) behaviour for any e at $\nu < \nu_{us}^{l}$ [(5.41)].

of the quenched-state solution in a sheared granular gas. The scaling relations (5.49) hold at leading-order in $\sqrt{1-e}$ for $St \gg 1$, and therefore we conclude that the inelasticty enhances the degree of anisotropy of $\boldsymbol{M}$ on the ignited branch, see figure 5.6.

5.4.2 Shear viscosity: continuous and discontinuous shear-thickening (DST)

The dimensionless shear viscosity for the particle phase is given by

$$\begin{aligned}
\mu &= -\frac{P_{xy}}{\rho_p \nu (\dot{\gamma}\sigma/2)^2} = \eta \cos(2\phi) T \\
&\equiv \frac{3}{St} T - \frac{16\nu(1+e)^2}{35\pi} + \frac{3(1-e^2)\nu T^{3/2}}{5\sqrt{\pi}}(10+\eta^2), \qquad (5.50) \\
&\overset{St\to\infty}{\equiv} -\frac{16\nu(1+e)^2}{35\pi} + \frac{3(1-e^2)\nu T^{3/2}}{5\sqrt{\pi}}(10+\eta^2) > 0, \qquad \forall \quad e < 1. \qquad (5.51)
\end{aligned}$$

For the ignited-state solution only (i.e. $\aleph \equiv \aleph^{is}$), it can be verified that the shear viscosity for elastically colliding particles ($e = 1$) is $\mu = 3T/St$ which represents the first term in (5.50).

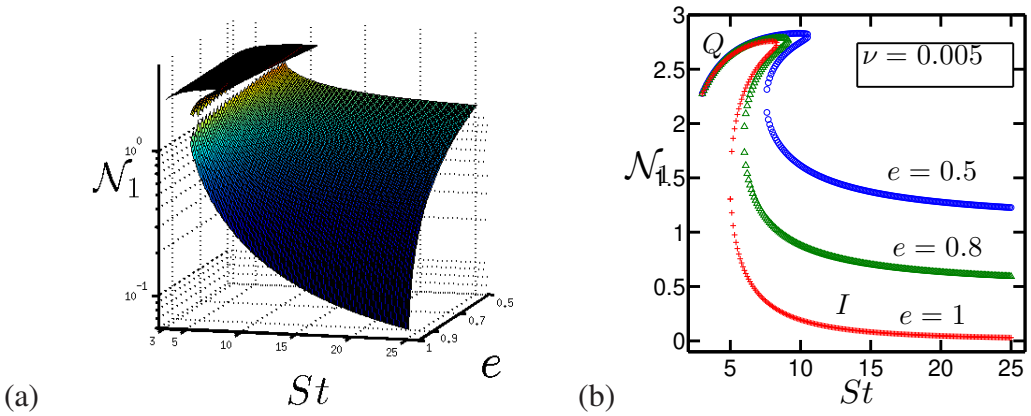

Fig. 5.8 Variations of the first $(\mathcal{N}_1)$ normal stress differences against Stokes number (St) and restitution coefficient (e) at $\nu = 0.005$. In panel b the projection of panel a is displayed for different e.

The variation of (5.50) as functions of (St, e) is depicted in figure 5.7(a) for particle volume fraction of $\nu = 0.005$. Similar to granular temperature, the shear viscosity undergoes hysteretic jumps at $St = St_{c_2}$ ("$Q \to I$") and St_{c_1} ("$I \to Q$") on increasing and decreasing St, respectively. The effect of dissipation ($e < 1$) is to reduce the viscosity of the particle-phase in each state, see figure 5.7(b). On the other hand, the effect of Stokes number can be understood by considering the viscosity of elastically colliding ($e = 1$) particles as given by

$$\mu_{is} \approx \frac{75\pi}{20736}\frac{St}{\nu^2}, \quad \mu_{qs} \approx \frac{384}{945\pi}\nu St^2, \quad \text{and} \quad \mu_{us} \approx \frac{147\pi}{25}\nu^{-2}St^{-7}, \tag{5.52}$$

in the ignited, quenched and unstable states, respectively. Clearly, two shear-thickening branches (Q and I) are connected via a shear-thinning branch.

The 'discontinuous shear thickening' (DST) behaviour, such as in figure 5.7(a,b), occurs only in the small Stokes-number limit of a dilute gas-solid suspension at $\nu < \nu^l_{us}$, (5.41), for any restitution coefficient. The middle-branch in figure 5.7(a,b), over which μ decreases with increasing St (i.e. the shear-thinning branch), is unstable. This is a thermodynamic/constitutive instability which can be understood from a phenomenological viewpoint (Saha & Alam 2017*a*).

In the area of liquid-solid suspensions, the shear-thickening and its discontinuous analog are well-known since the original work of Hoffman (1972). There have been a renewed research activity to understand the origin of DST in the "dense" regime of colloidal and non-colloidal suspensions as well as in dense granular media (Brown & Jaeger 2014; Denn & Morris 2014). Extending the present theoretical formalism to the dense regime of suspensions, by incorporating frictional interactions and related physics (Seto *et al.* 2013; Fernandez *et al.* 2013; Wyart & Cates 2014; Clavaud *et al.* 2017), would be an interesting future work.

5.4.3 First and second normal stress differences

The expression for the first normal stress difference is

$$\mathscr{N}_1 = \frac{P_{xx} - P_{yy}}{p} = 2\eta \sin 2\phi, \tag{5.53}$$

which has been 'scaled' by the mean pressure $p = (P_{xx} + P_{yy} + P_{zz})/3$; in (5.53), ϕ and η are calculated from (5.42) and (5.43), respectively. The variation of (5.53) as functions of (St, e) is displayed in figure 5.8(a,b). The quenched-branch $\mathscr{N}_1$ remains unaffected by inelasticity (see panel b), however, on the ignited branch, increasing inelasticity increases $\mathscr{N}_1$; the effect of the gas-phase (i.e. decreasing St) also increases the ignited branch $\mathscr{N}_1$. On the whole, the dependence of $\mathscr{N}_1$ on both St and e mirrors that of the non-coaxiality angle (ϕ) and the shear-plane temperature-anisotropy (η), compare figure 5.8(b) with figure 5.6(a,b). It is clear from (5.53) that the origin of the first normal stress difference is tied to the shear-plane anisotropies (η and ϕ) of the second-moment tensor as in the case of a sheared granular gas (Jenkins & Richman 1988; Saha & Alam 2016) – the dependence of St on its origin remains implicit via two anisotropy parameters (ϕ, η).

The scaled second normal stress difference is given by

$$\mathscr{N}_2 = \frac{P_{yy} - P_{zz}}{p} = 3\lambda^2 - \eta \sin 2\phi = 3\lambda^2 - \frac{1}{2}\mathscr{N}_1. \tag{5.54}$$

The variation of (5.54) with St is shown in figure 5.9(a) for different values of the restitution coefficient e. Similar to $\mathscr{N}_1$, the effect of inelasticity is to increase the magnitude of the second normal stress difference on the ignited branch, but the quenched-branch $\mathscr{N}_2$ remains unaffected (expectedly) by changing e. It is noteworthy in figure 5.9(a) that $\mathscr{N}_2$ is positive and negative in the quenched and ignited states, respectively. This sign-change can be understood from figure 5.9(b) which display the variations of two terms in (5.54) with St. In the quenched state the excess temperature ($3\lambda^2 \propto T_z^{ex}$) dominates over the shear-plane anisotropies ($\eta \sin 2\phi \equiv \mathscr{N}_1/2$), whereas the latter dominates over the former in the ignited state, resulting in the sign-change of $\mathscr{N}_2$ at some finite value of St.

The parameter combinations (St, e, ν) at which $\mathscr{N}_2$ undergoes sign-reversal can be calculated by solving the following equation

$$\mathscr{N}_1 - 6\lambda^2 = 0, \tag{5.55}$$

along with (5.53) and (5.44). Figure 5.9(c) shows the variation of $St_\pm$ with restitution coefficient: $\mathscr{N}_2$ is positive and negative, respectively, below and above each line for a specified

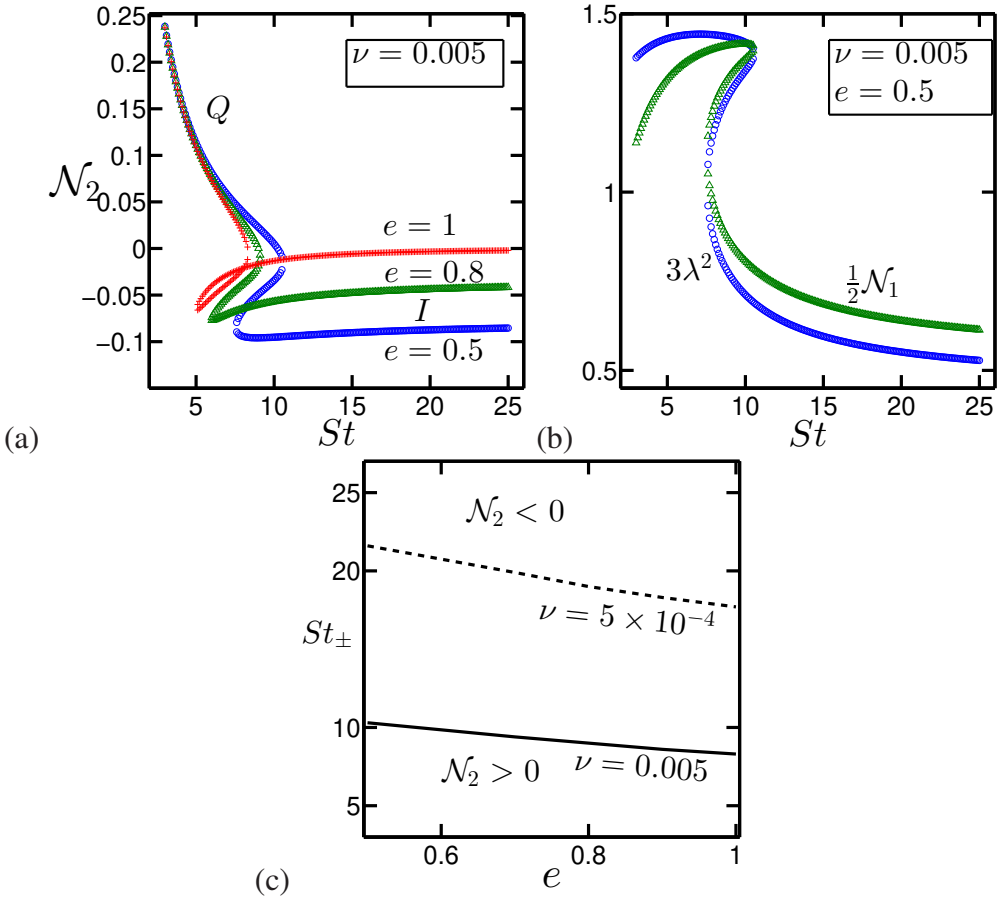

Fig. 5.9 (a) Variation of the second ($\mathcal{N}_2$) normal stress difference against Stokes number (St) for different values of the restitution coefficient; the particle volume fraction is $\nu = 0.005$. (b) Variations of $3\lambda^2$ (blue circles) and $\mathcal{N}_1/2$ (green triangles) with St for $e = 0.5$, with other parameters as in panel *a*. (c) Variations of the critical Stokes number $St_\pm$ (at which $\mathcal{N}_2 = 0$) with e for $\nu = 0.005$ (solid line) and $\nu = 0.0005$ (dashed line).

density ν. It is seen that the effect of inelastic dissipation is to increase the critical value of $St_{\pm}$ at which $\mathscr{N}_2$ changes its sign; reducing the mean-density increases $St_{\pm}$ at any e.

It may be noted that for a 'dense' sheared granular gas ($St \to \infty$), the second normal-stress difference undergoes sign-change (Alam & Luding 2005*b*; Saha & Alam 2016) at some critical density ($\nu_{\pm} \sim 0.2$), with $\mathscr{N}_2$ being negative and positive in the dilute and dense limit, respectively; the competition between (i) the collisional anisotropies in a dense system (that makes the particle-motion increasingly streamlined (Alam & Luding 2005*b*) with increasing density) and (ii) the second-moment anisotropies (ϕ, η, λ^2) is known to be responsible for this sign-change (Saha & Alam 2016). For the present case of a 'dilute' suspension, the behaviour of $\mathscr{N}_2$ in the quenched state resembles that in a sheared 'dense' granular fluid; this could possibly be due to the 'streamlined' particle motion in both systems, characterizing the underlying anisotropy.

5.5 Discussion: Comparison with Grad's moment-expansion (GME)

Recall that in figure 5.2, we have made a detailed comparison between the predictions of two moment theories: (i) the standard Grad's moment-expansion (GME) around a Maxwellian (Grad 1949; Tsao & Koch 1995; Sangani *et al.* 1996; Chamorro *et al.* 2015) using Hermite polynomials and (ii) the present anisotropic-Maxwellian moment-expansion (AME). Overall, the AME predictions for granular temperature are found to be more accurate (see insets in figure 5.2) than that of GME, especially at lower values of restitution coefficient, via a comparison with available simulation data. This conclusion holds for shear viscosity too (not shown) since $\mu \propto \sqrt{T}$ – in the following we focus on the predictive abilities of the present theory (AME) with reference to two normal-stress differences. (The reader is referred to Saha & Alam (2014) for details on AME that has been used to derive a generalized Fourier law for heat-flux vector, along with conductivity tensors; the heat-flux, however, vanishes in uniform shear flow as in the present case.)

5.5.1 Suspension of elastic and inelastic hard spheres: $\mathscr{N}_1$ and $\mathscr{N}_2$

From the present AME theory, the normal stress differences for elastic ($e = 1$) hard-sphere suspensions in the "ignited" state are given by (Appendix A)

$$\mathscr{N}_1 = \frac{18}{6+\Omega St^2} \quad \text{and} \quad -\mathscr{N}_2 = \frac{9(9+\Omega St^2)\Omega St^2}{(6+\Omega St^2)\left[252+87\Omega St^2+7\Omega^2 St^4\right]} > 0. \tag{5.56}$$

with

$$\Omega = \frac{1}{2St^2}\left[\left(St^2 - \frac{171}{7}\right) + \left(\left(St^2 - \frac{3}{7}\right)^2 - (12\sqrt{2})^2\right)^{1/2}\right]. \tag{5.57}$$

The last quantity Ω is positive for $St > St_{c_1} = \sqrt{171/7}$ (the critical Stokes number for "ignited-to-unstable" transition, viz. eqn. (3.7)), and asymptotically approaches unity, $\Omega(St \to \infty) = 1$, and hence $\Omega \in (0,1)$ at any $St > St_{c_1}$.

The AME-predictions (5.56) can be compared with the corresponding GME predictions for $\mathscr{N}_1$ and $\mathscr{N}_2$:

$$\mathscr{N}_1 = \frac{18}{6 + \Theta St^2} \quad \text{and} \quad -\mathscr{N}_2 = \frac{\frac{9}{14}\Theta}{6 + \Theta St^2} > 0, \tag{5.58}$$

where

$$\Theta = \frac{1}{2St^2}\left[\left(St^2 - \frac{171}{14}\right) + \left(\left(St^2 - \frac{171}{14}\right)^2 - 12^2\right)^{1/2}\right]. \tag{5.59}$$

In (5.58) that there is a minor correction in the expression for $\mathscr{N}_2$: the numerical factor $9/14$ in the numerator was taken as $9/7$ in Tsao & Koch (1995). The positivity of (5.59) follows from the positivity of its discriminant, resulting in $St > St_{c_1} = \sqrt{169.5/7}$, which is very close to $\sqrt{171/7}$ for the positivity of (5.57). It is worth pointing out that the functional dependence of both (5.57) and (5.59) yields almost identical values for Ω and Θ at any $St > St_{c_1}$.

Figure 5.10 shows a comparison of (5.56) (denoted by solid lines) for $\mathscr{N}_1$ and $\mathscr{N}_2$ with (i) the DSMC simulation data (symbols) of Tsao & Koch (1995) and (ii) the GME theory (5.58) (dashed lines) – the particle volume fraction is set to $\nu = 0.01$, representing a 'dilute' gas-solid suspension. It is seen that both (5.56) and (5.58) predict the correct behaviour of $\mathscr{N}_1$ – two theories are almost indistinguishable from each other, with excellent quantitative agreement with simulation. However, there is a significant disagreement (by a factor of about 2) between (5.58) and the DSMC data for the second normal-stress difference $\mathscr{N}_2$; in contrast, the predictions of AME (5.56) are uniformly good for both $\mathscr{N}_1$ and $\mathscr{N}_2$ over a range of Stokes number.

It may be noted that in GME the quadratic nonlinear-terms (proportional to $P^2_{\alpha\beta}$) need to be taken into account while evaluating the source term $\aleph_{\alpha\beta}$ (5.13) in order to obtain 'non-zero' second normal-stress difference as suggested by Herdegen & Hess (1982) for a Boltzmann (dilute) gas. A brief account of the related analysis for a gas-solid suspension of inelastic particles is provided in Appendix E – the resulting expressions for $\mathscr{N}_1$ and $\mathscr{N}_2$ reduce to (5.58)

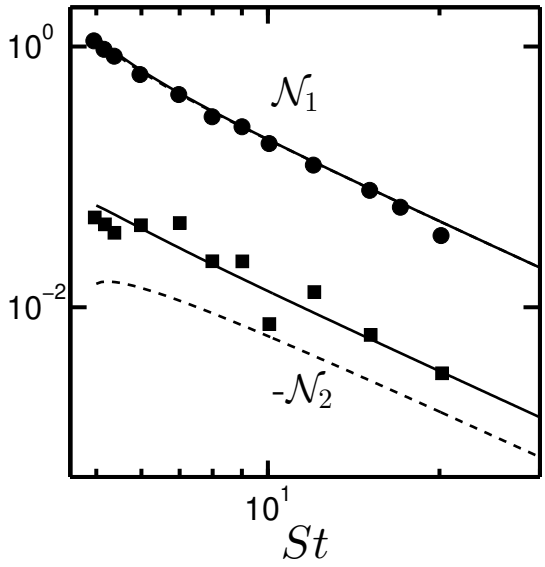

Fig. 5.10 Variations of the first (circles) and second (squares) normal-stress differences with Stokes number for a suspension of elastic ($e = 1$) hard-spheres – the particle volume fraction is $\nu = 0.01$, representing a 'dilute' suspension. The solid lines represent the present theory (5.56) and the dashed lines represent the standard Grad's moment theory (5.58); the DSMC simulation data (Tsao & Koch 1995) are denoted by symbols.

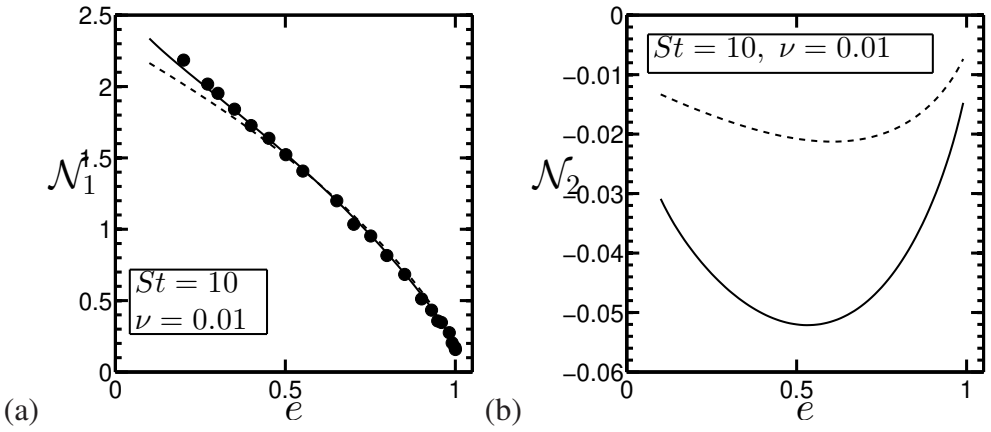

Fig. 5.11 Comparisons of (a) first and (b) second normal-stress differences at $St = 10$: (i) DSMC simulation (filled circles, Sangani *et al.* (1996)), (ii) present theory (solid lines), (iii) the standard Grad's moment expansion [dashed lines, see Appendix E].

for elastically-colliding particles. On the other hand, the analysis of Sangani *et al.* (1996) did not include such nonlinear Grad-terms, resulting in $\mathscr{N}_2 = 0$; the recent work of Chamorro *et al.* (2015) also confirmed that the nonlinear Grad-terms are necessary for $\mathscr{N}_2 \neq 0$. It has been verified that the quadratic non-linear terms do not noticeably affect the value of $\mathscr{N}_1$ as well as the shear viscosity.

The effect of inelasticity on $\mathscr{N}_1$ and $\mathscr{N}_2$ can be ascertained from figures 5.11(a) and 5.11(b), respectively, for a suspension with small Stokes number ($St = 10$); other parameters are as in figure 5.10. It is clear from panel *a* that the present predictions of $\mathscr{N}_1$ (solid line) agree well with simulation data for the whole range of e, but the GME-predictions (dashed and dot-dashed lines) are slightly lower at $e < 0.5$. On the other hand, the GME theory grossly under-predicts (by a factor of 3) the value of $\mathscr{N}_2$ for dissipative particles, see figure 5.11(b).

5.5.2 From sheared suspension to 'dry' ($St \to \infty$) granular gas

To further understand the predictions of normal stress differences ($\mathscr{N}_1$ and $\mathscr{N}_2$) from two theories (GME and AME) for dissipative particles ($e < 1$), we focus on the uniform shear flow of a dilute granular gas ($St \to \infty$) – the molecular-dynamics (MD) simulations of inelastic hard-spheres with Lees-Edward boundary conditions have been carried out for a range of restitution coefficients $e \in (0.3, 1)$ at a particle volume fraction of $\nu = 0.01$; a relatively small system with $N = 1000$ particles was simulated– other simulation details can be found in (Alam & Luding 2005*b*; Gayen & Alam 2008). From these simulations, it is easy to extract data on two anisotropy parameters, namely, (i) the shear-plane temperature anisotropy η [see (5.24)] and (ii) the excess temperature $T_z^{ex}/T = \lambda^2$ [see (5.26)], which are marked by filled-circles in figures 5.12(a) and 5.12(b), respectively. In each panel, the theoretical predictions of Saha & Alam (2016) are shown by solid lines. Overall, there is excellent agreement between AME theory and MD simulation.

Figures 5.13(a) and 5.13(b) compare the MD simulation data (symbols) for $\mathscr{N}_1$ and $\mathscr{N}_2$, respectively, with theory; the AME predictions, denoted by solid lines, are calculated from (5.53) and (5.54) by setting $St \to \infty$ (Saha & Alam 2016), and the corresponding GME-predictions (Appendix E) are denoted by dashed lines. In addition, the dot-dashed line in each panel represents the super-Burnett-order solution of Sela & Goldhirsch (1998), obtained from the Chapman-Enskog expansion of inelastic Boltzmann equation. It is clear that both GME and AME theories predict almost the same value of $\mathscr{N}_1$ for a range of restitution coefficient $e \in (0.3, 1)$, but the GME-prediction for $\mathscr{N}_2$ is consistently lower than that of AME and can be off by a factor of 3 at $e = 0.3$. On the other hand, the AME-predictions for both $\mathscr{N}_1$ and $\mathscr{N}_2$ are comparable to those of Chapman-Enskog solution for $e \geq 0.8$, but the latter becomes increasingly inaccurate for $e < 0.8$. Therefore, the quantitative predictions of the AME for two

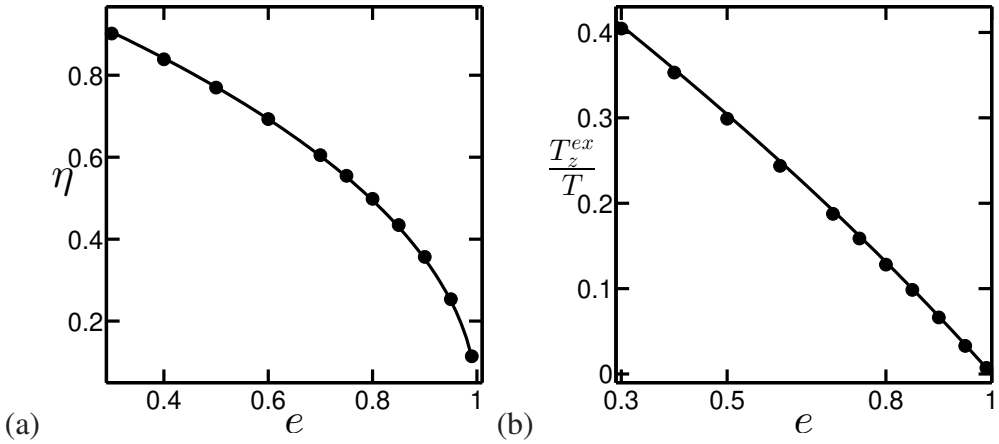

Fig. 5.12 Comparisons of (a) shear-plane temperature-anisotropy η and (b) the excess temperature $T_z^{ex}/T \equiv 2\lambda^2$ in uniform shear flow of a granular gas ($St = \infty$): MD simulation (symbols) and theory [solid line, Saha & Alam (2016)]. The particle volume fraction is $\nu = 0.01$ and the number of particles is $N = 1000$ in simulations.

normal stress differences are better than those of GME and Chapman-Enskog solution – this overall conclusion holds for both gas-solid and dry granular suspensions of inelastic particles.

5.6 Summary and Conclusion

The rheology of a dilute gas-solid suspension, consisting of inelastic spheres suspended in a Newtonian fluid, undergoing simple shear flow is analysed, with the effect of the gas-phase being modelled via a Stokesian drag force. The pertinent inelastic Boltzmann equation is solved using an anisotropic Gaussian as the single particle distribution function which is known to be appropriate for a sheared system. The resulting hydrodynamic model for the particle-phase consists of a 10-moment system $(\rho, \boldsymbol{u}, \boldsymbol{M})$ of density (ρ), hydrodynamic velocity ($\mathbf{u}$) and the second-moment ($\boldsymbol{M} = \langle \boldsymbol{CC} \rangle$) of fluctuation/peculiar velocity. One focus of the present work has been to analyse the anisotropy of $\boldsymbol{M}$ in the simple shear flow of a dilute gas-solid suspension and subsequently tie and explain the rheological quantities in terms of them.

The seond-moment tensor has been characterized by three parameters: (i) the non-coaxiality angle (ϕ, the angle between the principal eigen-direction of $\boldsymbol{M}$ and the shear tensor $\boldsymbol{D}$), (ii) the shear-plane temperature-anisotropy (η, the difference between the principal eigenvalues of $\boldsymbol{M}$ on the shear plane, $\eta \propto T_x - T_y$, where T_i is the granular temperature along i-th direction) and (iii) the excess temperature ($\lambda^2 \propto T - T_z$) along the vorticity direction; the first two [ϕ and η] are dubbed 'shear-plane' anisotropies and the last-one (λ^2) is dubbed vorticity-plane anisotropy. The closed-form expressions for three anisotropy parameters (ϕ, η, λ^2) and the

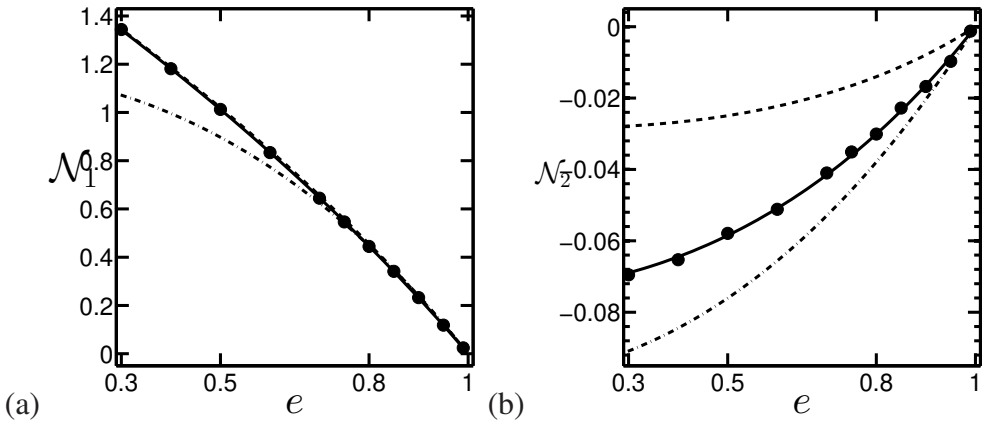

Fig. 5.13 Comparisons of (a) $\mathscr{N}_1$ and (b) $\mathscr{N}_2$ in uniform shear flow of a granular gas ($St = \infty$): (i) MD simulation (symbols), (ii) present theory [solid lines, Saha & Alam (2016)] and (iii) the standard Grad's moment theory (dashed line). The dot-dash line in each panel represent the super-Burnett-order Chapman-Enskog solution of Sela & Goldhirsch (1998). Parameter values as in figure 5.12.

granular temperature (T) have been obtained as functions of the Stokes number (St), the mean density (ν) and the restitution coefficient (e) by solving the second-moment balance equation; these are used to obtain analytical expressions for the particle-phase viscosity and two normal-stress differences. Scaling relations have been obtained in the limits of small and large St as well as small inelasticity $(1-e)$.

Static multiple states of high and low temperatures are found when the Stokes number is small enough, thereby recovering the original "ignited" (I) and "quenched" (Q) states of Tsao & Koch (1995) – the role of inelasticity on these states has been examined. The high-temperature ignited state, in which the randomness of the particle motion is high giving rise to a large value of granular temperature (T), exists above some minimum Stokes number (St_{c_1}) whose value increases with increasing e. In contrast, the low-temperature quenched state, in which most of the particles in the system follow the local fluid velocity, appears below a critical value of Stokes number (St_{c_2}) which is a decreasing function of both e and ν. Both these Stokes numbers (St_{c_1} and St_{c_2}) have been determined analytically as functions of ν and e, and the regions of co-existence of two states (quenched and ignited) along with the transition regimes have been identified in a three-dimensional (St, e, ν) phase diagram.

The effect of inelasticity is found to reduce the particle-phase viscosity on both ignited and quenched states, with shear-thickening behaviour (increasing viscosity with increasing shear rate) being found in both states. At any e, the shear-viscosity undergoes a discontinuous jump with increasing St at "$Q \to I$" transition, which can be interpreted as "discontinuous shear

thickening" (DST). The two normal stress differences also undergo similar first-order jump-transitions: (i) $\mathscr{N}_1$ from large to small positive values and (ii) $\mathscr{N}_2$ from positive to negative values. The sign-change of $\mathscr{N}_2$ (figure 5.9) has been identified with the system being making a "$Q \leftrightarrow I$" transition. The origin of this sign-change has been tied to a competition between (i) the excess temperature ($T_z^{ex} \propto 3\lambda^2$) and (ii) the shear-plane anisotropies ($\eta \sin 2\phi \equiv \mathscr{N}_1/2$) of the second-moment tensor: while the former dominates over the latter in the quenched state, the latter dominates in the ignited state, resulting in the sign-change of $\mathscr{N}_2$ at some finite value of St. For both granular and gas-solid suspensions, the excess temperature along the vorticity direction is responsible for the origin of $\mathscr{N}_2 \neq 0$, while the temperature anisotropy η and the non-coaxiality angle ϕ are responsible for $\mathscr{N}_1 \neq 0$.

The comparative analyses in figures 5.2, 5.10, 5.11, 5.12 and 5.13 can be summarized as follows: the moment expansion about an anisotropic-Maxwellian (AME) yields accurate transport coefficients (shear viscosity and normal stress differences) for dissipative particles ($e < 1$) in both small and large Stokes number limits, representative of gas-solid and dry granular suspensions, respectively. The standard Grad's moment-expansion (GME) significantly under-predicts the value of the second normal stress difference $\mathscr{N}_2$, although it is comparable with AME with respect to $\mathscr{N}_1$ up-to a restitution coefficient of $e = 0.5$. On the other hand, the latter theory (GME) also over-predicts the shear viscosity ($\mu \propto \sqrt{T}$, viz. figure 5.2) of small-St suspensions even for moderately dissipative ($e = 0.8$) particles; the mismatch between GME and simulation increases with decreasing e. Based on the present work we conclude that the superior predictive ability of the AME theory for hydrodynamics and rheology of 'dry' ($St \to \infty$) sheared granular gases (Saha & Alam 2014, 2016) carries over to small-St gas-solid suspensions of highly inelastic particles.

It would be interesting to check the applicability of this theory to dense gas-solid suspensions of inelastic particles (with frictional interactions) which can be taken up in future. The present work can also be extended to include a 'non-linear' drag law (dependence on particle Reynolds number) by modifying (5.5) via well-known empirical correlations. Lastly, the anisotropies (ϕ, η, λ^2) of the second-moment tensor should be measured from simulations of finite-St suspensions so that one-to-one comparisons with theory can be made in this regard.

Appendix A

Analysis in the ignited state for elastic hard-spheres

For a gas-solid suspension of elastic hard-spheres ($e = 1$), the collisional source of second-moment in the ignited state is given by

$$\begin{aligned}\aleph_{\alpha\beta} &= \frac{-24\rho_p \nu^2}{\sigma\pi^{\frac{3}{2}}}\int (k_\alpha j_\beta + k_\beta j_\alpha)(\boldsymbol{k}\cdot\boldsymbol{M}\cdot\boldsymbol{j})(\boldsymbol{k}\cdot\boldsymbol{M}\cdot\boldsymbol{k})^{\frac{1}{2}} d\boldsymbol{k} \\ &= -\frac{32\rho_p \nu^2 T^{3/2}}{35\sigma\sqrt{\pi}}\times \\ &\left[\begin{array}{ccc} \eta^2+21\lambda^2+21\eta\sin 2\phi & -21\eta\cos 2\phi & 0 \\ -21\eta\cos 2\phi & \eta^2+21\lambda^2-21\eta\sin 2\phi & 0 \\ 0 & 0 & -2(\eta^2+21\lambda^2) \end{array}\right], \end{aligned} \tag{A.1}$$

which is a function of ν,T, η, ϕ and λ^2.

Four independent equations of second-moment balance,

$$P_{\delta\beta}u_{\alpha,\delta} + P_{\delta\alpha}u_{\beta,\delta} + \frac{2\gamma}{St}P_{\alpha\beta} = \aleph_{\alpha\beta}, \tag{A.2}$$

can be rearranged to yield a quartic-order equation,

$$\omega^2\left[12096St^2\omega^2 + \left(10260St - 420St^3\right)\omega + 3225 - 175St^2\right] = 0, \tag{A.3}$$

where ω is the rescaled temperature

$$\omega = \frac{\nu}{\sqrt{\pi}}\frac{\sqrt{T}}{(\dot{\gamma}\sigma/2)}. \tag{A.4}$$

In the following, the temperature has been made dimensionless by dividing it by $(\dot{\gamma}\sigma/2)^2$. Three distinct solutions of (A.3) are

$$\sqrt{T_{is}} = \frac{5\pi^{\frac{1}{2}}}{144}\frac{St}{\nu}\Omega(St), \tag{A.5}$$

$$\sqrt{T_{us}} = \frac{5\pi^{\frac{1}{2}}}{144}\frac{St}{\nu}\left[\frac{7St^2 - 171 - \sqrt{49St^4 - 42St^2 - 14103}}{14St^2}\right], \tag{A.6}$$

$$T_{qs} = 0, \tag{A.7}$$

with $T_{is} > T_{us} > T_{qs}$, where

$$\Omega(St) = \left[\frac{7St^2 - 171 + \sqrt{49St^4 - 42St^2 - 14103}}{14St^2}\right] \equiv \frac{144}{5}\omega_{is}St^{-1}. \tag{A.8}$$

In the above expressions, T_{qs} corresponds to the quenched state temperature, T_{us} corresponds to an unstable temperature and T_{is} corresponds to the temperature in the ignited state. It is clear from (A.6) that a positive value for T_{us} requires the following condition on the Stokes number:

$$7St^2 - 171 \geqslant 0, \qquad \Rightarrow \qquad St \geqslant \sqrt{\frac{171}{7}} \approx 4.9425 \equiv St_{c_1}. \tag{A.9}$$

Therefore, St must be greater than or equal to St_{c_1}, and (A.9) provides a lower bound on St for the existence of the ignited state in a dilute sheared gas-solid suspension.

The remaining equations of (A.2) can be solved to yield solutions for η^2 and λ^2 in the ignited state:

$$\left.\begin{aligned} \eta^2 &= \frac{(9+\Omega St^2)}{4\left(1+\frac{29}{84}\Omega St^2+\frac{1}{36}\Omega^2St^4\right)} \\ \lambda^2 &= \frac{(7+\Omega St^2)}{14\left(1+\frac{29}{84}\Omega St^2+\frac{1}{36}\Omega^2St^4\right)} \end{aligned}\right\}; \tag{A.10}$$

the solution for the non-coaxilality angle is

$$\sin(2\phi) = \frac{\eta}{1+\lambda^2}. \tag{A.11}$$

Therefore, the normal stress differences in the ignited state are given by

$$\mathscr{N}_1 = \frac{15}{5+24St\omega} \equiv \frac{18}{6+\Omega St^2}, \tag{A.12}$$

$$-\mathscr{N}_2 = \frac{270St\omega(5+16St\omega)}{(5+24St\omega)(175+1740St\omega+4032St^2\omega^2)}. \tag{A.13}$$

In the ignited state, the expression for the shear viscosity of the particle phase is

$$\mu = -P_{xy}/\dot{\gamma} = \mu_N \Omega(St), \tag{A.14}$$

where

$$\mu_N = \frac{5\sqrt{\pi}}{96}\rho_p \sigma \sqrt{T} \tag{A.15}$$

is the Newtonian viscosity of a dilute gas. Therefore, $\Omega(St)$ [(A.8)] is a measure of the deviation of particle-phase viscosity from the Newtonian viscosity of a dilute hard-sphere gas.

Appendix B

Coefficients a_i

Explicit expressions of the individual coefficients a_i appearing in (5.34) are given by:

$$a_{10} = 86416243200(3-e)^4(1-e)^3(1+e)^7\pi St^6\nu^7, \tag{B.1}$$

$$a_9 = 28805414400(3-e)^3(1-e)^2(1+e)^6(19-13e)\pi^{(3/2)}St^5\nu^6, \tag{B.2}$$

$$\begin{aligned} a_8 = 28576800(3-e)^2(1-e)(1+e)^5\pi^2St^4\nu^5\Big(&252(197-278e+93e^2)\\ &+5(1747-1438e+363e^2)St^2\Big), \end{aligned} \tag{B.3}$$

$$\begin{aligned} a_7 = 3810240(3-e)(1+e)^4\sqrt{\pi}St^3\nu^4\Big(&2100(1-e)(241-284e+79e^2)\pi^2\\ &+25(12607-19952e+10099e^2-1746e^3)\pi^2St^2\\ &-3456(3-e)^3(1-e)^2(1+e)^4St^3\nu^3\Big), \end{aligned} \tag{B.4}$$

$$\begin{aligned} a_6 = 79380(1+e)^3\pi St^2\nu^3\Big(&21000(1-e)(871-854e+199e^2)\pi^2\\ &+500(56617-78677e+35629e^2-5361e^3)\pi^2St^2\\ &-125(1691+539e-1223e^2+337e^3)\pi^2St^4\\ &-27648(3-e)^3(1-e)(1+e)^4(29-23e)St^3\nu^3\Big), \end{aligned} \tag{B.5}$$

$$\begin{aligned} a_5 = 18900(1+e)^2\pi^{(3/2)}St\nu^2\Big(&441000(1-e)(23-11e)\pi^2\\ &+10500(3437-3093e+688e^2)\pi^2St^2-875(477+442e-247e^2)\pi^2St^4\\ &-580608(3-e)^2(1-e)(1+e)^4(11-7e)St^3\nu^3\\ &-1152(3-e)^2(1+e)^4(991-934e+279e^2)St^5\nu^3\Big), \end{aligned} \tag{B.6}$$

$$
\begin{aligned}
a_4 = {} & 63(1+e)\nu\Big(165375000(1-e)\pi^4 + 656250(2437-1069e)\pi^4 St^2 \\
& - 109375(107+193e)\pi^4 St^4 - 48384000(3-e)(1-e)(1+e)^4(37-19e)\pi^2 St^3\nu^3 \\
& - 288000(3-e)(1+e)^4(3917-3368e+843e^2)\pi^2 St^5\nu^3 \\
& - 3024000(3-e)^3(1+e)^4\pi^3 St^6\nu^3 + 7962624(3-e)^4(1-e)(1+e)^8 St^6\nu^6\Big), \qquad \text{(B.7)} \\
a_3 = {} & 2520\sqrt{\pi}St\Big(2296875\pi^4 - 504000(1-e)(1+e)^4(41-17e)\pi^2 St\nu^3 \\
& - 6000(1+e)^4(5617-4438e+933e^2)\pi^2 St^3\nu^3 - 189000(3-e)^2(1+e)^4\pi^3 St^4\nu^3 \\
& - 1000(1+e)^4(1203-1002e+247e^2)\pi^2 St^5\nu^3 \\
& + 663552(3-e)^3(1-e)(1+e)^8 St^4\nu^6\Big), \qquad \text{(B.8)} \\
a_2 = {} & -2400(1+e)^3\pi St\nu^2\Big(1323000(1-e)\pi^2 + 15750(383-151e)\pi^2 St^2 \\
& + 165375(3-e)\pi^3 St^3 + 875(789-305e)\pi^2 St^4 \\
& - 870912(3-e)^2(1-e)(1+e)^4 St^3\nu^3 - 1728(3-e)^2(1+e)^4(47-39e)St^5\nu^3\Big), \qquad \text{(B.9)} \\
a_1 = {} & -2000(1+e)^2\pi^{(3/2)}St^2\nu\Big(441000\pi^2 + 55125\pi^3 St + 98000\pi^2 St^2 \\
& - 580608(3-e)(1-e)(1+e)^4 St\nu^3 - 3456(3-e)(1+e)^4(47-39e)St^3\nu^3\Big), \qquad \text{(B.10)} \\
a_0 = {} & 1440000(1+e)^5\pi^2 St^2(4+St^2)\nu^3\Big(42(1-e)+(13-9e)St^2\Big). \qquad \text{(B.11)}
\end{aligned}
$$

Appendix C

Ordering analysis to determine three temperatures

We will solve (5.34) analytically in the asymptotic limit $\nu \ll 1$, $St \gg 1$, and $St^3\nu \ll 1$ (Tsao & Koch 1995), and three feasible solutions have been found as described below.

C.1 Temperature in the quenched state

For $\xi \sim O(St^{3/2}\sqrt{\nu})$, the leading order term in (5.34) is $O(St^{\frac{11}{2}}\nu^{\frac{3}{2}})$ and consequently we have

$$a_3\xi^3 + a_1\xi = 0, \tag{C.1}$$

where

$$a_3 = 5788125000\pi^{\frac{9}{2}}St, \qquad a_1 = -196000000\pi^{\frac{7}{2}}(1+e)^2St^4\nu. \tag{C.2}$$

The solution at this level of approximation is

$$T_{qs} = \xi^2 = \frac{32(1+e)^2}{945\pi}St^3\nu, \tag{C.3}$$

which corresponds to the temperature in the quenched state. Note that the quenched temperature increases with increasing both St and ν.

C.2 Unstable temperature

When $\xi \sim O(St^3\nu)^{-1}$, the highest-order term in (5.34) is $O(1/St^8\nu^3)$, and on neglecting terms smaller than this, we have at leading order

$$a_4\xi^4 + a_3\xi^3 = 0, \tag{C.4}$$

where

$$a_4 = -6890625(1+e)(107+193e)\pi^4 St^4\nu, \qquad a_3 = 5788125000\pi^{\frac{9}{2}}St. \tag{C.5}$$

Therefore, we have

$$\sqrt{T_{us}} = \xi = \frac{840\sqrt{\pi}}{(1+e)(107+193e)}\left(\frac{1}{St^3\nu}\right), \tag{C.6}$$

This is the temperature of an intermediate state which is unstable – note that T_{us} decreases with increasing St and ν.

C.3 Temperature in the ignited state

In the asymptotic limit of $\xi \sim O(St/\nu)$, the leading order term of $a_i\xi^i\, i = 0(1)11$ is $O(St^{12}/\nu^3)$ and consequently we have from (5.34)

$$a_7\xi^7 + a_6\xi^6 = 0, \tag{C.7}$$

where

$$\left.\begin{aligned} a_7 &= 95256000(3-e)(1+e)^4(12607-19952e+10099e^2-1746e^3)\pi^{\frac{5}{2}}St^5\nu^4, \\ a_6 &= -9922500(1+e)^3(1691+539e-1223e^2+337e^3)\pi^3St^6\nu^3. \end{aligned}\right\} \tag{C.8}$$

Therefore, the temperature at this order of approximation is

$$\sqrt{T_{is}} = \xi = \frac{5(1691+539e-1223e^2+337e^3)\sqrt{\pi}}{48(3-e)(1+e)(12607-19952e+10099e^2-1746e^3)}\left(\frac{St}{\nu}\right), \tag{C.9}$$

which corresponds to the temperature in the ignited state. While T_{is} increases with increasing St, it deceases with increasing the particle volume fraction ν.

Appendix D

Analytical determination of limit-points St_{c_1} and St_{c_2}

At the critical/limit points, two solution branches of (5.34) corresponding to two different states [(i) quenched (T_{qs}) and unstable (T_{us}) states and (ii) unstable (T_{us}) and ignited (T_{is}) states] meet and consequently we have saddle-node bifurcations from one stable state to another. Therefore, these limit points correspond to the double roots of (5.34) at which the following conditions must be satisfied:

$$\mathscr{G}(\xi_c) = 0 \quad \text{and} \quad \mathscr{G}'(\xi_c) = 0. \tag{D.1}$$

D.1 Determining St_{c_1}: discontinuous transition from "ignited" to "quenched" states

The critical Stokes number, St_{c_1}, for the transition from the ignited to quenched states corresponds to the limit point at which the temperatures corresponding to the ignited (T_{is}) and unstable (T_{us}) branches overlap with each other. Considering $\xi \sim O(\nu St)^{-1} \gg 1$, and retaining the highest-order terms, (5.34) reduces to

$$\mathscr{G} \approx a_7\xi^7 + a_6\xi^6 + a_5\xi^5 + a_4\xi^4 + a_3\xi^3 = 0 = a_7\xi^4 + a_6\xi^3 + a_5\xi^2 + a_4\xi + a_3, \tag{D.2}$$

and

$$4a_7\xi^3 + 3a_6\xi^2 + 2a_5\xi + a_4 = 0, \tag{D.3}$$

where

$$\left.\begin{aligned}
a_7 &= 95256000(3-e)(1+e)^4(12607-19952e+10099e^2-1746e^3)\pi^{\frac{5}{2}}St^5\nu^4,\\
a_6 &= 9922500(1+e)^3\pi^3St^4\Big(4(56617-78677e+35629e^2-5361e^3)\\
&\qquad -(1691+539e-1223e^2+337e^3)St^2\Big)\nu^3,\\
a_5 &= 16537500(1+e)^2\pi^{\frac{7}{2}}St^3\Big(12(3437-3093e+688e^2)\\
&\qquad -(477+442e-247e^2)St^2\Big)\nu^2,\\
a_4 &= 6890625(1+e)\pi^4St^2(6(2437-1069e)-(107+193e)St^2)\nu,\\
a_3 &= 5788125000\pi^{\frac{9}{2}}St.
\end{aligned}\right\} \tag{D.4}$$

Using the condition of equal roots of a fourth-degree polynomial (D.2), we obtain an expression for the critical Stokes number for the "ignited-to-unstable" transition:

$$St_{c_1} \approx 9.9 - 4.91e. \tag{D.5}$$

While decreasing the Stokes number along the ignited-state branch (see figure 5.2), the system jumps from the ignited to the quenched state at $St < St_{c_1}$ for all $\nu < \nu^l_{us}$ (3.8). Therefore, (D.5) represents the minimum/critical Stokes number below which (5.34) admits the unique "quenched" state solution.

D.2 Determining St_{c_2}: discontinuous transition from "quenched" to "ignited" state

The limit point corresponding to the overlap of the quenched and unstable branches of the system is denoted by the Stokes number St_{c_2} at which the temperatures associated with the quenched (T_{qs}) and unstable (T_{us}) states coincide – above this critical value of Stokes number the quenched state ceases to exist. Mathematically, St_{c_2} is the point of the double root $T_{is} = T_{us}$ of (5.34). above which there exists only one feasible solution T_{is} (corresponding to the ignited state) and the system jumps from the quenched state into the ignited state At this order of approximation $\xi \sim O(1)$ and the highest order terms are of the orders of νSt^4 and St. Therefore on neglecting the terms of $O(St^4\nu^2)$ and using the statement of $T_{is} = T_{us}$, we have from (5.34)

$$\mathscr{G}(\xi_c) \approx a_4\xi^4 + a_3\xi^3 + a_1\xi = 0 = a_4\xi^3 + a_3\xi^2 + a_1, \tag{D.6}$$

$$\text{and} \quad \mathscr{G}'(\xi_c) \approx 3a_4\xi^2 + 2a_3\xi = 0, \tag{D.7}$$

where

$$\left.\begin{aligned} a_4 &= -6890625(1+e)(107+193e)\pi^4 St^4 \nu, \\ a_3 &= 5788125000\pi^{\frac{9}{2}} St, \\ a_1 &= -196000000(1+e)^2\pi^{\frac{7}{2}} St^4 \nu. \end{aligned}\right\} \tag{D.8}$$

It follows from (D.7) that

$$\xi_c = \frac{-2a_3}{3a_4} = \frac{560\sqrt{\pi}}{(1+e)(170+193e)St^3\nu}. \tag{D.9}$$

On substituting (D.9) into (D.6) we obtain the *critical-surface*

$$St_{c_2}^3 \nu_c = \left(\frac{3087000\pi^2}{(1+e)^4(107+193e)^2}\right)^{\frac{1}{3}}, \tag{D.10}$$

above which only the ignited state exists.

Appendix E

Grad's moment expansion (GME) for inelastic gas-solid suspension

The standard Grad's moment expansion (GME) in terms of a truncated Hermite series around the Maxwellian (Grad 1949) has been employed by many researchers (Herdegen & Hess 1982; Tsao & Koch 1995; Chamorro *et al.* 2015) to analyse the Boltzmann equation for a "sheared" hard-sphere gas as well as gas-solid suspensions.

- Herdegen & Hess (1982)$\Rightarrow e=1,\ St=\infty$ (Dilute gas of elastic hard-spheres)
- Tsao & Koch (1995)$\Rightarrow e=1,\ St$ finite (Suspension of elastic hard-spheres)
- Chamorro *et al.* (2015)$\Rightarrow e\neq 1,\ St$ finite (Suspension of inelastic hard-spheres)

For the case of a dilute gas-solid suspension of "inelastic" hard-spheres, the collisional production term of the second moment has been evaluated as:

$$\aleph_{\alpha\beta} = -\frac{8\rho_p \nu^2(1-e^2)T^{\frac{3}{2}}}{\sqrt{\pi}\sigma}\delta_{\alpha\beta} - \frac{24\nu(1+e)(3-e)T^{\frac{1}{2}}}{5\sqrt{\pi}\sigma}P_{\langle\alpha\beta\rangle} + \frac{(1+e)}{35\sqrt{\pi}\sigma\rho_p T^{\frac{1}{2}}}\underline{\Big\{(5+3e)P_{\langle kl\rangle}P_{\langle kl\rangle}\delta_{\alpha\beta} + 12(e-3)P_{\langle\alpha l\rangle}P_{\langle l\beta\rangle}\Big\}}, \tag{E.1}$$

where the underlined terms represent the quadratic nonlinearity in the pressure deviator $P_{\langle\alpha\beta\rangle} = P_{\alpha\beta} - p\delta_{\alpha\beta}$, with $p = P_{\alpha\alpha}/3$; $\rho_p = m/(\pi\sigma^3/6)$ is the intrinsic/material density of particles, ν is the particle volume fraction and e is the restitution coefficient. In fact, the second normal-stress difference is zero ($\mathcal{N}_2 = 0$) in the absence of the underlined non-linear terms in (E.1), see the proof at the end of this appendix.

Defining the non-dimensional quantities as

$$P^* = \frac{P}{\rho_p \nu (\dot{\gamma}\sigma/2)^2}, \qquad T^* = \frac{T}{(\dot{\gamma}\sigma/2)^2}, \qquad \aleph^* = \frac{\aleph}{\rho_p \nu \dot{\gamma}^3 (\sigma/2)^2}, \tag{E.2}$$

and on omitting the $*$ signs, for convenience, the dimensionless second-moment balance for steady homogeneous shear flow,

$$P_{\delta\beta} u_{\alpha,\delta} + P_{\delta\alpha} u_{\beta,\delta} + \frac{2}{St} P_{\alpha\beta} = \aleph_{\alpha\beta}, \tag{E.3}$$

can be written in component form as follows:

$$\begin{aligned}
&(1+e)(5+3e)\left(P_{\langle xx\rangle}^2 + P_{\langle yy\rangle}^2 + P_{\langle zz\rangle}^2 + 2P_{xy}^2\right) - 12(1+e)(3-e)\left(P_{\langle xx\rangle}^2 + P_{xy}^2\right) \\
&\quad - 280(1-e^2)T^2 - 168(1+e)(3-e)TP_{\langle xx\rangle} - \frac{140\sqrt{\pi}\sqrt{T}P_{xy}}{\nu} \\
&\quad - \frac{140\sqrt{\pi}\sqrt{T}}{St\nu}(T + P_{\langle xx\rangle}) = 0,
\end{aligned} \tag{E.4}$$

$$\begin{aligned}
&(1+e)(5+3e)\left(P_{\langle xx\rangle}^2 + P_{\langle yy\rangle}^2 + P_{\langle zz\rangle}^2 + 2P_{xy}^2\right) - 12(1+e)(3-e)\left(P_{\langle yy\rangle}^2 + P_{xy}^2\right) \\
&\quad - 280(1-e^2)T^2 - 168(1+e)(3-e)TP_{\langle yy\rangle} - \frac{140\sqrt{\pi}\sqrt{T}}{St\nu}(T + P_{\langle yy\rangle}) = 0,
\end{aligned} \tag{E.5}$$

$$\begin{aligned}
&(1+e)(5+3e)\left(P_{\langle xx\rangle}^2 + P_{\langle yy\rangle}^2 + P_{\langle zz\rangle}^2 + 2P_{xy}^2\right) - 12(1+e)(3-e)P_{\langle zz\rangle}^2 \\
&\quad - 280(1-e^2)T^2 - 168(1+e)(3-e)TP_{\langle zz\rangle} - \frac{140\sqrt{\pi}\sqrt{T}}{St\nu}(T + P_{\langle zz\rangle}) = 0,
\end{aligned} \tag{E.6}$$

$$\begin{aligned}
&12(1+e)(3-e)P_{xy}P_{\langle zz\rangle} - 168(1+e)(3-e)TP_{xy} - \frac{70\sqrt{\pi}\sqrt{T}}{\nu}(T + P_{\langle yy\rangle}) \\
&\quad - \frac{140\sqrt{\pi}T^{\frac{1}{2}}}{St\nu}P_{xy} = 0,
\end{aligned} \tag{E.7}$$

along with constraint $\widehat{P}_{\alpha\alpha} = 0$. These equations have been solved numerically for specified values of e, St and ν to yield T, $P_{\langle\alpha\alpha\rangle}$ and P_{xy}; two normal stress differences $\mathcal{N}_1$ and $\mathcal{N}_2$ can be expressed in terms of $P_{\langle\alpha\alpha\rangle}$. These are dubbed "GME" solutions and their comparisons with the present theory (§5.4) based on anisotropic-Maxwellian expansion (AME) are shown in figures 5.10, 5.11 and 5.13, as discussed in §5.5.1 and §5.5.2.

Theorem 5.0.1. *The source term is uniquely decomposed as* $\aleph_{\alpha\beta} = \left(\frac{1}{3}\aleph_{\gamma\gamma}\right)\delta_{\alpha\beta} + \aleph_{\langle\alpha\beta\rangle}$. *If* $\aleph_{\langle\alpha\beta\rangle} = BP_{\langle\alpha\beta\rangle}$, *then* $\mathcal{N}_2 = 0$.

Proof. For the case of homogeneous shear $u_x = \dot{\gamma} y$, $u_y = 0$, $u_z = 0$; the balance of second moment for a granular gas is

$$\mathrm{P}_{\delta\beta}\mathrm{u}_{\alpha,\delta} + \mathrm{P}_{\delta\alpha}\mathrm{u}_{\beta,\delta} = \aleph_{\alpha\beta}. \tag{5.8}$$

Now, upon substituting $\alpha = 2$, $\beta = 2$ and $\alpha = 3$, $\beta = 3$ we have

$$\aleph_{22} = 0 = \aleph_{33}. \tag{5.9}$$

From $P_{ij} = p\delta_{ij} + P_{\langle ij\rangle}$, we can write

$$\mathscr{N}_2 = \left(P_{\langle 22\rangle} - P_{\langle 33\rangle}\right) = B^{-1}\left(\aleph_{\langle 22\rangle} - \aleph_{\langle 33\rangle}\right) = 0. \tag{5.10}$$

□

Of course, (5.10) is in contradiction with (i) the nonlinear expression (E.1) obtained from the standard Grad-moment expansion as well as with (ii) our choice of anisotropic Maxwellian distribution function, both yielding $\mathscr{N}_2 \neq 0$.

Chapter 6

Summary

In this Chapter a summary of the research work done in this thesis alongwith conclusion made are presented. We have tried to address the issues, which were raised in Chapter **Chapter 1** (Introduction). A brief discussion about the future work that can be derived from the thesis is also given. A chapter-wise summary of the present work is provided below.

A complete 14/10 moment theory for a "dense" granular gas using Grad's moment method Grad (1949) is proposed in **Chapter 2**. An expansion around the Gaussian is performed to obtain the non-equilibrium distribution function. A Grad like moment theory has been established in terms of the fourteen field variables: i) the mass density (ρ), ii) macroscopic flow velocity $(\boldsymbol{u})$, iii) kinetic stress $(\boldsymbol{P}^k)$, iv) kinetic heat flux $(\boldsymbol{q}^k)$ and v) the contracted fourth moment P_{iijj}. The collisional source and flux terms at different orders are calculated by including all the nonlinear terms arising from these hydrodynamic field variables and their gradients. The collisional dissipation or the cooling rate is derived for the whole range of volume fraction that includes second order derivatives of the hydrodynamic variables as well. A generalized Fourier law for granular heat flux is established using Maxwell iteration technique. It is observed that even at Navier-Stokes level (5 field theory) the thermal conductivity is an anisotropic-asymmetric tensor and the anisotropy follows from the presence of higher order nonlinear terms in $\aleph_{\alpha\beta\beta}$. The gradient of kinetic stress also drives a heat current at the 10 moment theory and these features are clear signatures for non-Fourier rheology. Finally, this 14 moment theory is applied to analyse the uniform shear flow of a 3-dimensional granular fluid. Analytical expressions of all the transport coefficients are determined as a function of the coefficient of restitution (e) and the solid volume fraction (ν) using this higher order theory. The non-Newtonian rheology appears in this granular uniform shear flow in terms of the normal stress differences is also appreciated. An effort has been made to develop a complete theory that can be applicable to granular flows at any choice of inelasticity and volume fraction.

In **Chapter 3**, an extended hydrodynamics equations, in terms of ten-moments (the density, the velocity vector and the second moment tensor), are proposed for a granular fluid that include the normal stress differences as well as the granular heat flux. For the steady uniform shear flow of smooth inelastic spheres, the constitutive relations are derived by choosing the anisotropic/triaxial Gaussian as the single-particle distribution function. The equation for the second moment of velocity fluctuations is solved semi-analytically, yielding closed-form expressions for the 'non-Newtonian' stress tensor, the shear viscosity and the collisional dissipation rate for the whole range of density (i.e. the volume fraction of particles). The first normal stress difference $\mathscr{N}_1$ is found to be positive in the dilute limit and decreases monotonically to zero in the dense limit. However, the second normal stress difference $\mathscr{N}_2$ is negative and positive in the dilute and dense limits, respectively, and the sign-change of $\mathscr{N}_2$ at a finite density is due to the sign-change of its kinetic component. The origin of $\mathscr{N}_1$ is tied to the *non-coaxiality* ($\phi \neq 0$) between the eigen-directions of the second-moment tensor $\boldsymbol{M}$ and those of the shear tensor $\boldsymbol{D}$; the non-coaxiality angle ϕ is maximum in the dilute limit and decreases with increasing density, resulting in *co-linear* (i.e. $\phi = 0$) eigen-directions between $\boldsymbol{M}$ and $\boldsymbol{D}$ and consequently $\mathscr{N}_1 \to 0$ in the maximum packing limit. In contrast, the origin of $\mathscr{N}_2$ in the dilute limit is tied to the 'excess' temperature ($T_z^{ex} = T - T_z$, where T_z and T are the z-component and the average of the granular temperature respectively) along the mean-vorticity (z) direction, whereas its origin in the dense limit is tied to the imposed shear field. Theoretical expressions for both $\mathscr{N}_1$ and $\mathscr{N}_2$ as well as for pressure and shear viscosity agree well with previous simulation data for the uniform shear flow of inelastic hard-spheres (Alam & Luding, *Powders & Grains*, 2005, pp. 1141-1145) for a large range of volume fractions spanning from the dilute to the dense regime. Based on our analytical solution for the dense limit, we show that the eigen-directions of the collisional stress tensor $\boldsymbol{P}^c$ are co-linear with those of the shear tensor $\boldsymbol{D}$ as is the case for the kinetic stress ($\boldsymbol{P}^k = \rho \boldsymbol{M}$) in the same limit. The proposed 10-moment hydrodynamic theory is made closed by deriving the constitutive relation for the granular heat flux via a perturbation expansion around the anisotropic Gaussian state. It is shown that the gradient of the kinetic stress also drives a heat current in addition to the standard Fourier-current driven by the temperature gradient, and the 'generalized' thermal conductivity is characterized by an anisotropic second-rank tensor. The leading off-diagonal terms of the conductivity tensor vary quadratically with the shear rate and hence its anisotropy is a Burnett-order effect. An improvement over the other Grad-level theories in terms of successful determination of the two normal stress differences for the whole range of density is discussed.

In **Chapter 4**, the normal stress differences along with other transport coefficients are analysed for the simple shear flow of a dense gas-solid suspension of inelastic hard spheres

suspended in a fluid of viscosity μ_g and experiencing a Stokes drag force. Viscous heating is compensated by dissipation via two mechanisms (i) the inelastic collisions between particles characterized by a coefficient of normal restitution e $(0 < e < 1)$ and (ii) the Stokes drag force which the surround fluid exerts on the particles. Rheology of the particle phase is analysed with anisotropic-Gaussian as the single particle distribution function. The first and second normal stress differences along-with other transport coefficients are computed for the whole range of density (ν) and inelasticity (e) with the scaled Stokes number $(St_d = St/R_{diss})$ varying from a very low limit 10 to the dry granular limit $St \to \infty$. An exact solution of the second moment balance of velocity fluctuations at Burnett order (i.e second order in the shear rate) has been derived, leading to analytical expressions for the first $(\mathscr{N}_1)$ and the second $(\mathscr{N}_2)$ normal stress differences. On assuming the Burnett order solution as the base state solution a perturbative solution at the super-super-Burnett order (i.e fourth order in the shear rate) is also derived and that improves the analytical base. It is observed that the first normal stress difference is maximum in the dilute regime and tends to zero at the dense limit but remains positive throughout, on the other hand the second normal stress difference is negative in the dilute limit undergoes a sign change at some finite density and becomes positive in the dense limit. The location of the critical density, where second normal stress difference changes its sign is determined and plotted as a 3-dimensional critical surface. This work is a direct extension of chapter 3 $(St \to \infty)$, including the interstitial fluid effects $(St = \text{finite})$. Finally, as we approach the limit of $St \to \infty$ $(\mu_g \to 0)$, results for the dry granular flows of chapter 3 are directly followed.

In **Chapter 5**, the hydrodynamics and rheology of a sheared dilute gas-solid suspension, consisting of inelastic hard-spheres suspended in a gas, are analysed using anisotropic Maxwellian as the single particle distribution function. The closed-form solutions for granular temperature (T) and three invariants of the second-moment tensor are obtained as functions of the Stokes number (St), the mean density (ν) and the restitution coefficient (e). Multiple states of high and low temperatures are found when the Stokes number is small, thus recovering the "ignited" and "quenched" states, respectively, of Tsao & Koch (1995) (J. Fluid Mech.,1995, vol. 296, pp. 211-246). The phase diagram is constructed in the three-dimensional (ν, St, e)-space that delineates the regions of ignited and quenched states and their coexistence. Analytical expressions for the particle-phase shear viscosity and the normal stress differences are obtained, along with related scaling relations on the quenched and ignited states. At any e, the shear-viscosity undergoes a discontinuous jump with increasing shear rate (i.e. discontinuous shear-thickening) at the "quenched-ignited" transition. The first $(\mathscr{N}_1)$ and second $(\mathscr{N}_2)$ normal-stress differences also undergo similar first-order transitions: (i) $\mathscr{N}_1$ jumps from large to small positive values and (ii) $\mathscr{N}_2$ from positive to negative values with increasing St, with

the sign-change of $\mathscr{N}_2$ identified with the system making a transition from the quenched to ignited states. The superior prediction of the present theory over the standard Grad's method and the Chapman-Enskog solution is demonstrated via comparisons of transport coefficients with simulation data for a range of Stokes number and restitution coefficient.

References

ABBAS, M., CLIMENT, E. & SIMONIN, O. 2009 Shear-induced self-diffusion of inertial particles in a viscous fluid. *Physical review E* **79** (3), 036313.

ABU-ZAID, S. & AHMADI, G. 1993 Analysis of rapid shear flows of granular materials by a kinetic model including frictional losses. *Powder technology* **77** (1), 7–17.

ALAM, M. 2005 Md simulation for a sheared granular gas: Non-newtonian and non-fourier rheologies. *Unpublished* .

ALAM, M. & LUDING, S. 2002 How good is the equipartition assumption for the transport properties of a granular mixture? *Granular Matter* **4** (3), 139–142.

ALAM, M. & LUDING, S. 2003*a* First normal stress difference and crystallization in a dense sheared granular fluid. *Physics of Fluids* **15** (8), 2298–2312.

ALAM, M. & LUDING, S. 2003*b* Rheology of bidisperse granular mixtures via event-driven simulations. *Journal of Fluid Mechanics* **476**, 69–103.

ALAM, M. & LUDING, S. 2005*a* Energy nonequipartition, rheology, and microstructure in sheared bidisperse granular mixtures. *Physics of Fluids* **17** (6), 063303.

ALAM, M. & LUDING, S. 2005*b* Non-newtonian granular fluids: simulation and theory. *Powders and Grains* p. 1141.

ALAM, M. & NOTT, P. R. 1997 The influence of friction on the stability of unbounded granular shear flow. *Journal of Fluid Mechanics* **343**, 267–301.

ALAM, M. & SAHA, S. 2017 Normal stress differences and beyond-navier-stokes hydrodynamics. In *EPJ Web of Conferences*, , vol. 140, p. 11014. EDP Sciences.

ANDERSON, T. B. & JACKSON, R. 1967 Fluid mechanical description of fluidized beds. equations of motion. *Industrial & Engineering Chemistry Fundamentals* **6** (4), 527–539.

ANSARI, I. H. & ALAM, M. 2016 Pattern transition, microstructure, and dynamics in a two-dimensional vibrofluidized granular bed. *Physical Review E* **93** (5), 052901.

ARAKI, S. 1988 The dynamics of particle disks: Ii. effects of spin degrees of freedom. *Icarus* **76** (1), 182–198.

ARAKI, S. & TREMAINE, S. 1986 The dynamics of dense particle disks. *Icarus* **65** (1), 83–109.

BAGNOLD, R. A. 1954 Experiments on a gravity-free dispersion of large solid spheres in a newtonian fluid under shear. In *Proceedings of the Royal Society of London A: Mathematical, Physical and Engineering Sciences*, , vol. 225, pp. 49–63. The Royal Society.

BARNES, H. 1989 Shear-thickening ("dilatancy") in suspensions of nonaggregating solid particles dispersed in newtonian liquids. *Journal of Rheology* **33** (2), 329–366.

BIZON, C., SHATTUCK, M., SWIFT, J. & SWINNEY, H. L. 1999 Transport coefficients for granular media from molecular dynamics simulations. *Physical Review E* **60** (4), 4340.

BOYER, F., POULIQUEN, O. & GUAZZELLI, É. 2011 Dense suspensions in rotating-rod flows: normal stresses and particle migration. *Journal of Fluid Mechanics* **686**, 5–25.

BRADY, J. F. & BOSSIS, G. 1985 The rheology of concentrated suspensions of spheres in simple shear flow by numerical simulation. *Journal of Fluid Mechanics* **155**, 105–129.

BRADY, J. F. & MORRIS, J. F. 1997 Microstructure of strongly sheared suspensions and its impact on rheology and diffusion. *Journal of Fluid Mechanics* **348**, 103–139.

BREY, J. J., DUFTY, J. W., KIM, C. S. & SANTOS, A. 1998 Hydrodynamics for granular flow at low density. *Physical Review E* **58** (4), 4638.

BREY, J. J., MORENO, F., GARCÍA-ROJO, R. & RUIZ-MONTERO, M. 2001 Hydrodynamic maxwell demon in granular systems. *Physical Review E* **65** (1), 011305.

BRILLIANTOV, N. & PÖSCHEL, T. 2003 Hydrodynamics and transport coefficients for dilute granular gases. *Physical Review E* **67** (6), 061304.

BRILLIANTOV, N. V. & PÖSCHEL, T. 2004 *Kinetic theory of granular gases*. Oxford University Press.

BRILLIANTOV, N. V., PÖSCHEL, T., KRANZ, W. T. & ZIPPELIUS, A. 2007 Translations and rotations are correlated in granular gases. *Physical review letters* **98** (12), 128001.

BROWN, E. & JAEGER, H. M. 2009 Dynamic jamming point for shear thickening suspensions. *Physical review letters* **103** (8), 086001.

BROWN, E. & JAEGER, H. M. 2012 The role of dilation and confining stresses in shear thickening of dense suspensions. *Journal of Rheology* **56** (4), 875–923.

BROWN, E. & JAEGER, H. M. 2014 Shear thickening in concentrated suspensions: phenomenology, mechanisms and relations to jamming. *Reports on Progress in Physics* **77** (4), 046602.

BUCHHOLTZ, V., PÖSCHEL, T. & TILLEMANS, H.-J. 1995 Simulation of rotating drum experiments using non-circular particles. *Physica A: Statistical Mechanics and its Applications* **216** (3), 199–212.

BURNETT, D. 1935 The distribution of velocities in a slightly non-uniform gas. *Proceedings of the London Mathematical Society* **2** (1), 385–430.

BUYEVICH, Y. A. 1971 Statistical hydromechanics of disperse systems part 1. physical background and general equations. *Journal of Fluid Mechanics* **49** (3), 489–507.

CAFIERO, R. & LUDING, S. 2000 Mean field theory for a driven granular gas of frictional particles. *Physica A: Statistical Mechanics and its Applications* **280** (1), 142–147.

CAFIERO, R., LUDING, S. & HERRMANN, H. J. 2002 Rotationally driven gas of inelastic rough spheres. *EPL (Europhysics Letters)* **60** (6), 854.

CAMPBELL, C. S. 1990 Rapid granular flows. *Annual Review of Fluid Mechanics* **22** (1), 57–90.

CANDELA, D. & WALSWORTH, R. 2007 Understanding the breakdown of fourier's law in granular fluids. *American Journal of Physics* **75** (8), 754–757.

CARNAHAN, N. F. & STARLING, K. E. 1969 Equation of state for nonattracting rigid spheres. *The Journal of Chemical Physics* **51**, 635.

CHAMORRO, M. G., REYES, F. V. & GARZÓ, V. 2015 Non-newtonian hydrodynamics for a dilute granular suspension under uniform shear flow. *Physical Review E* **92** (5), 052205.

CHAPMAN, S. & COWLING, T. G. 1970 *The mathematical theory of non-uniform gases: an account of the kinetic theory of viscosity, thermal conduction and diffusion in gases*. Cambridge university press.

CHOU, C.-S. & RICHMAN, M. W. 1998 Constitutive theory for homogeneous granular shear flows of highly inelastic spheres. *Physica A: Statistical Mechanics and its Applications* **259** (3), 430–448.

CLAVAUD, C., BÉRUT, A., METZGER, B. & FORTERRE, Y. 2017 Revealing the frictional transition in shear-thickening suspensions. *Proceedings of the National Academy of Sciences* p. 201703926.

COUTURIER, É., BOYER, F., POULIQUEN, O. & GUAZZELLI, É. 2011 Suspensions in a tilted trough: second normal stress difference. *Journal of Fluid Mechanics* **686**, 26–39.

DAVIDSON, J. F. & HARRISON, D. 1963 *Fluidised particles*. Cambridge Univ Press.

DBOUK, T., LOBRY, L. & LEMAIRE, E. 2013 Normal stresses in concentrated non-brownian suspensions. *Journal of Fluid Mechanics* **715**, 239–272.

DE GROOT, S. R. & MAZUR, P. 2013 *Non-equilibrium thermodynamics*. Courier Corporation.

DENN, M. M. & MORRIS, J. F. 2014 Rheology of non-brownian suspensions. *Annual review of chemical and biomolecular engineering* **5**, 203–228.

FERNANDEZ, N., MANI, R., RINALDI, D., KADAU, D., MOSQUET, M., LOMBOIS-BURGER, H., CAYER-BARRIOZ, J., HERRMANN, H. J., SPENCER, N. D. & ISA, L. 2013 Microscopic mechanism for shear thickening of non-brownian suspensions. *Physical review letters* **111** (10), 108301.

FORTERRE, Y. & POULIQUEN, O. 2008 Flows of dense granular media. *Annu. Rev. Fluid Mech.* **40**, 1–24.

FOSS, D. R. & BRADY, J. F. 2000 Structure, diffusion and rheology of brownian suspensions by stokesian dynamics simulation. *Journal of Fluid Mechanics* **407**, 167–200.

GARZÓ, V. 2012 Grad's moment method for a low-density granular gas. navier-stokes transport coefficients. *arXiv preprint arXiv:1211.5932* .

GARZÓ, V. 2013 Grad's moment method for a granular fluid at moderate densities: Navier-stokes transport coefficients. *Physics of Fluids* **25** (4), 043301.

GARZÓ, V. & DUFTY, J. 1999 Dense fluid transport for inelastic hard spheres. *Physical Review E* **59** (5), 5895.

GARZÓ, V. & DUFTY, J. W. 2002 Hydrodynamics for a granular binary mixture at low density. *Physics of Fluids* **14** (4), 1476–1490.

GARZÓ, V., TENNETI, S., SUBRAMANIAM, S. & HRENYA, C. 2012 Enskog kinetic theory for monodisperse gas–solid flows. *Journal of Fluid Mechanics* **712**, 129–168.

GAYEN, B. & ALAM, M. 2006 Algebraic and exponential instabilities in a sheared micropolar granular fluid. *Journal of Fluid Mechanics* **567**, 195–233.

GAYEN, B. & ALAM, M. 2008 Orientational correlation and velocity distributions in uniform shear flow of a dilute granular gas. *Physical review letters* **100** (6), 068002.

GAYEN, B. & ALAM, M. 2011 Effect of coulomb friction on orientational correlation and velocity distribution functions in a sheared dilute granular gas. *Physical Review E* **84** (2), 021304.

GIDASPOW, D. 1994 *Multiphase flow and fluidization: continuum and kinetic theory descriptions*. Academic press.

GOLDHIRSCH, I. 2003 Rapid granular flows. *Annual review of fluid mechanics* **35** (1), 267–293.

GOLDHIRSCH, I., NOSKOWICZ, S. & BAR-LEV, O. 2005 Nearly smooth granular gases. *Physical review letters* **95** (6), 068002.

GOLDREICH, P. & TREMAINE, S. 1978 The velocity dispersion in saturn's rings. *Icarus* **34** (2), 227–239.

GOLDSMITH, W. 1960 *Impact*. Edward Arnold, London.

GRAD, H. 1949 On the kinetic theory of rarefied gases. *Communications on pure and applied mathematics* **2** (4), 331–407.

GUAZZELLI, E. & MORRIS, J. F. 2011 *A physical introduction to suspension dynamics*, , vol. 45. Cambridge University Press.

GUPTA, V. K., SHUKLA, P. & TORRILHON, M. 2017 Higher-order moment theories for dilute granular gases of smooth hard-spheres. *arXiv preprint arXiv:1701.09052* .

HERDEGEN, N. & HESS, S. 1982 Nonlinear flow behavior of the boltzmann gas. *Physica A: Statistical Mechanics and its Applications* **115** (1-2), 281–299.

HOFFMAN, R. 1972 Discontinuous and dilatant viscosity behavior in concentrated suspensions. i. observation of a flow instability. *Transactions of the Society of Rheology* **16** (1), 155–173.

HOFFMAN, R. 1974 Discontinuous and dilatant viscosity behavior in concentrated suspensions. ii. theory and experimental tests. *Journal of Colloid and Interface Science* **46** (3), 491–506.

HOLWAY JR, L. H. 1966 New statistical models for kinetic theory: methods of construction. *Physics of Fluids (1958-1988)* **9** (9), 1658–1673.

HUANG, K. 1987 Statistical mechanics, 2nd. *Edition (New York: John Wiley & Sons)* .

HUTHMANN, M. & ZIPPELIUS, A. 1997 Dynamics of inelastically colliding rough spheres: Relaxation of translational and rotational energy. *Physical Review E* **56** (6), R6275.

IKENBERRY, E. & TRUESDELL, C. 1956 On the pressures and flux of energy in a gas according to {M} axwell\'s kinetic theory. *J. Rat. Mech. Anal.* **5**.

JACKSON, R. 2000 *The dynamics of fluidized particles*. Cambridge University Press.

JAEGER, H. M., NAGEL, S. R. & BEHRINGER, R. P. 1996 Granular solids, liquids, and gases. *Reviews of modern physics* **68** (4), 1259.

JANSSEN, H. 1895 Versuche über getreidedruck in silozellen. *Zeitschr. d. Vereines deutscher Ingenieure* **39** (35), 1045–1049.

JAYNES, E. T. 1957 Information theory and statistical mechanics. *Physical review* **106** (4), 620.

JENKINS, J. & RICHMAN, M. 1985*a* Grad's 13-moment system for a dense gas of inelastic spheres. *Archive of Rational Mechanics and Analysis* **87**, 647–669.

JENKINS, J. & RICHMAN, M. 1985*b* Kinetic theory for plane flows of a dense gas of identical, rough, inelastic, circular disks. *Physics of Fluids (1958-1988)* **28** (12), 3485–3494.

JENKINS, J. T. & RICHMAN, M. W. 1988 Plane simple shear of smooth inelastic circular disks: the anisotropy of the second moment in the dilute and dense limits. *J. Fluid Mech.* **192**, 313–328.

JENKINS, J. T. & ZHANG, C. 2002 Kinetic theory for identical, frictional, nearly elastic spheres. *Physics of Fluids* **14** (3), 1228–1235.

KADANOFF, L. P. 1999 Built upon sand: Theoretical ideas inspired by granular flows. *Reviews of Modern Physics* **71** (1), 435.

KOCH, D. L. 1990 Kinetic theory for a monodisperse gas–solid suspension. *Physics of Fluids A: Fluid Dynamics* **2** (10), 1711–1723.

KOCH, D. L. & HILL, R. J. 2001 Inertial effects in suspension and porous-media flows. *Annual Review of Fluid Mechanics* **33** (1), 619–647.

KOGAN, M. 1969 Rarefied gas dynamics. *Plenum Press, New York* **2**, l.

KREMER, G. M. 2010 *An introduction to the Boltzmann equation and transport processes in gases*. Springer Science & Business Media.

KREMER, G. M. & MARQUES JR, W. 2011 Fourteen moment theory for granular gases. *Kinet. Relat. Models* **4**, 317–331.

LAUN, H. 1994 Normal stresses in extremely shear thickening polymer dispersions. *Journal of non-newtonian fluid mechanics* **54**, 87–108.

LEES, A. & EDWARDS, S. 1972 The computer study of transport processes under extreme conditions. *Journal of Physics C: Solid State Physics* **5** (15), 1921.

LERNER, E., DÜRING, G. & WYART, M. 2012 A unified framework for non-brownian suspension flows and soft amorphous solids. *Proceedings of the National Academy of Sciences* **109** (13), 4798–4803.

LOUGE, M., MASTORAKOS, E. & JENKINS, J. 1991 The role of particle collisions in pneumatic transport. *Journal of Fluid Mechanics* **231**, 345–359.

LUDING, S., HUTHMANN, M., MCNAMARA, S. & ZIPPELIUS, A. 1998 Homogeneous cooling of rough, dissipative particles: Theory and simulations. *Physical Review E* **58** (3), 3416.

LUN, C. 1991 Kinetic theory for granular flow of dense, slightly inelastic, slightly rough spheres. *Journal of Fluid Mechanics* **233**, 539–559.

LUN, C., SAVAGE, S. B., JEFFREY, D. & CHEPURNIY, N. 1984 Kinetic theories for granular flow: inelastic particles in couette flow and slightly inelastic particles in a general flowfield. *J. Fluid Mech.* **140**, 223–256.

LUN, C. K. & SAVAGE, S. B. 2003 Kinetic theory for inertia flows of dilute turbulent gas-solids mixtures. In *Granular gas dynamics*, pp. 267–289. Springer.

LUTSKO, J. F. 2004 Rheology of dense polydisperse granular fluids under shear. *Physical Review E* **70** (6), 061101.

LUTSKO, J. F. 2005 Transport properties of dense dissipative hard-sphere fluids for arbitrary energy loss models. *Physical Review E* **72** (2), 021306.

MARANZANO, B. J. & WAGNER, N. J. 2001 The effects of particle size on reversible shear thickening of concentrated colloidal dispersions. *The Journal of chemical physics* **114** (23), 10514–10527.

MAW, N., BARBER, J. & FAWCETT, J. 1976 The oblique impact of elastic spheres. *Wear* **38** (1), 101–114.

MAXWELL, J. C. 1867 On the dynamical theory of gases. *Philosophical transactions of the Royal Society of London* **157**, 49–88.

MAXWELL, J. C. 1879 On stresses in rarified gases arising from inequalities of temperature. *Philosophical Transactions of the royal society of London* **170**, 231–256.

MCLENNAN, J. A. 1965 Convergence of the chapman-enskog expansion for the linearized boltzmann equation. *The Physics of Fluids* **8** (9), 1580–1584.

MONTANERO, J., GARZÓ, V., SANTOS, A. & BREY, J. 1999 Kinetic theory of simple granular shear flows of smooth hard spheres. *Journal of Fluid Mechanics* **389**, 391–411.

MONTANERO, J. M. & GARZÓ, V. 2003 Shear viscosity for a heated granular binary mixture at low density. *Physical Review E* **67** (2), 021308.

MONTANERO, J. M., GARZÓ, V., ALAM, M. & LUDING, S. 2006 Rheology of two-and three-dimensional granular mixtures under uniform shear flow: Enskog kinetic theory versus molecular dynamics simulations. *Granular Matter* **8** (2), 103.

OGAWA, S. 1978 Multitemperature theory of granular materials .

OTSUKI, M. & HAYAKAWA, H. 2011 Critical scaling near jamming transition for frictional granular particles. *Physical Review E* **83** (5), 051301.

OTTINO, J. & KHAKHAR, D. 2000 Mixing and segregation of granular materials. *Annual Review of Fluid Mechanics* **32** (1), 55–91.

PARMENTIER, J.-F. & SIMONIN, O. 2012 Transition models from the quenched to ignited states for flows of inertial particles suspended in a simple sheared viscous fluid. *J. Fluid Mech.* **711**, 147–160.

PIDDUCK, F. 1922 The kinetic theory of a special type of rigid molecule. *Proceedings of the Royal Society of London. Series A, Containing Papers of a Mathematical and Physical Character* **101** (708), 101–112.

PÖSCHEL, T. & BUCHHOLTZ, V. 1995 Molecular dynamics of arbitrarily shaped granular particles. *Journal de physique I* **5** (11), 1431–1455.

RAMÍREZ, R., PÖSCHEL, T., BRILLIANTOV, N. V. & SCHWAGER, T. 1999 Coefficient of restitution of colliding viscoelastic spheres. *Physical review E* **60** (4), 4465.

RAO, K. K. & NOTT, P. R. 2008 *An introduction to granular flow*. Cambridge University Press New York.

REIF, F. 2009 *Fundamentals of statistical and thermal physics*. Waveland Press.

REYES, F. V., SANTOS, A. & GARZÓ, V. 2013 Steady base states for non-newtonian granular hydrodynamics. *Journal of Fluid Mechanics* **719**, 431–464.

RICHMAN, M. W. 1989 The source of second moment in dilute granular flows of highly inelastic spheres. *Journal of Rheology* **33**, 1293.

RONGALI, R. & ALAM, M. 2014 Higher-order effects on orientational correlation and relaxation dynamics in homogeneous cooling of a rough granular gas. *Physical Review E* **89** (6), 062201.

ROSENAU, P. 1989 Extending hydrodynamics via the regularization of the chapman-enskog expansion. *Physical Review A* **40** (12), 7193.

SAHA, S. & ALAM, M. 2014 Non-newtonian stress, collisional dissipation and heat flux in the shear flow of inelastic disks: a reduction via grad's moment method. *J. Fluid Mech.* **757**, 251–296.

SAHA, S. & ALAM, M. 2016 Normal stress differences, their origin and constitutive relations for a sheared granular fluid. *J. Fluid Mech.* **795**, 549–580.

SAHA, S. & ALAM, M. 2017*a* Revisiting ignited-quenched transition and the non-newtonian rheology of a sheared dilute gas-solid suspension. *arXiv preprint arXiv:1706.04457* .

SAHA, S. & ALAM, M. 2017*b* Revisiting ignited–quenched transition and the non-newtonian rheology of a sheared dilute gas–solid suspension. *J. Fluid Mech.* **833**, 206–246.

SANGANI, A. S., MO, G., TSAO, H.-K. & KOCH, D. L. 1996 Simple shear flows of dense gas-solid suspensions at finite stokes numbers. *J. Fluid Mech.* **313**, 309–341.

SANTOS, A. 2008 Does the chapman–enskog expansion for sheared granular gases converge? *Physical review letters* **100** (7), 078003.

SANTOS, A., BREY, J. J. & DUFTY, J. W. 1986 Divergence of the chapman-enskog expansion. *Physical review letters* **56** (15), 1571.

SANTOS, A., GARZÓ, V. & DUFTY, J. W. 2004 Inherent rheology of a granular fluid in uniform shear flow. *Physical Review E* **69** (6), 061303.

SANTOS, A., KREMER, G. M. & DOS SANTOS, M. 2011 Sonine approximation for collisional moments of granular gases of inelastic rough spheres. *Physics of Fluids* **23** (3), 030604.

SAVAGE, S. & JEFFREY, D. 1981 The stress tensor in a granular flow at high shear rates. *J. Fluid Mech.* **110**, 255–272.

SCHWAGER, T. & PÖSCHEL, T. 1998 Coefficient of normal restitution of viscous particles and cooling rate of granular gases. *Physical review E* **57** (1), 650.

SELA, N. & GOLDHIRSCH, I. 1998 Hydrodynamic equations for rapid flows of smooth inelastic spheres, to burnett order. *Journal of Fluid Mechanics* **361**, 41–74.

SERERO, D., GOLDHIRSCH, I., NOSKOWICZ, S. & TAN, M.-L. 2006 Hydrodynamics of granular gases and granular gas mixtures. *Journal of Fluid Mechanics* **554**, 237–258.

SETO, R., MARI, R., MORRIS, J. F. & DENN, M. M. 2013 Discontinuous shear thickening of frictional hard-sphere suspensions. *Physical review letters* **111** (21), 218301.

SHANNON, C. 1948 Tech. 27 (1948) 379; ce shannon, bell syst. *Tech* **27**, 623.

SHUKHMAN, I. 1984 Collisional dynamics of particles in saturn's rings. *Soviet Astronomy* **28**, 574–585.

SIEROU, A. & BRADY, J. 2002 Rheology and microstructure in concentrated noncolloidal suspensions. *Journal of Rheology* **46** (5), 1031–1056.

SIMON, V. & JENKINS, J. T. 1994 On the vertical structure of dilute planetary rings. *Icarus* **110** (1), 109–116.

SINGH, A. & NOTT, P. R. 2003 Experimental measurements of the normal stresses in sheared stokesian suspensions. *Journal of Fluid Mechanics* **490**, 293–320.

TORQUATO, S. 1995 Nearest-neighbor statistics for packings of hard spheres and disks. *Physical Review E* **51** (4), 3170.

TORRILHON, M. & STRUCHTRUP, H. 2004 Regularized 13-moment equations: shock structure calculations and comparison to burnett models. *Journal of Fluid Mechanics* **513**, 171–198.

TRUESDELL, C. & MUNCASTER, R. G. 1980 *Fundamentals of Maxwel's Kinetic Theory of a Simple Monatomic Gas: Treated as a Branch of Rational Mechanics*, , vol. 83. Academic Press.

TRUJILLO, L., ALAM, M. & HERRMANN, H. J. 2003 Segregation in a fluidized binary granular mixture: Competition between buoyancy and geometric forces. *EPL (Europhysics Letters)* **64** (2), 190.

TRULSEN, J. 1971 Towards a theory of jet streams. *Astrophysics and Space Science* **12** (2), 329–348.

TRULSSON, M., ANDREOTTI, B. & CLAUDIN, P. 2012 Transition from the viscous to inertial regime in dense suspensions. *Physical review letters* **109** (11), 118305.

TSAO, H.-K. & KOCH, D. L. 1995 Simple shear flows of dilute gas-solid suspensions. *J. Fluid Mech.* **296**, 211–246.

UGAWA, H. & CORDERO, P. 2007 Extended hydrodynamics from enskog's equation for a two-dimensional system general formalism. *Journal of Statistical Physics* **127** (2), 339–358.

VAN NOIJE, T. & ERNST, M. 1998 Velocity distributions in homogeneous granular fluids: the free and the heated case. *Granular Matter* **1** (2), 57–64.

VERLET, L. & LEVESQUE, D. 1982 Integral equations for classical fluids: Iii. the hard discs system. *Molecular Physics* **46** (5), 969–980.

WAGNER, N. J. & BRADY, J. F. 2009 Shear thickening in colloidal dispersions. *Physics Today* **62** (10), 27–32.

WALTON, O. R. & BRAUN, R. L. 1986 Viscosity, granular-temperature, and stress calculations for shearing assemblies of inelastic, frictional disks. *Journal of Rheology* **30** (5), 949–980.

WYART, M. & CATES, M. 2014 Discontinuous shear thickening without inertia in dense non-brownian suspensions. *Physical review letters* **112** (9), 098302.

XU, Q., MAJUMDAR, S., BROWN, E. & JAEGER, H. M. 2014 Shear thickening in highly viscous granular suspensions. *EPL (Europhysics Letters)* **107** (6), 68004.

ZHANG, C. 1993 Kinetic theoryfor rapid granular flows. PhD thesis, Ph. D. Dis.

ZWANZIG, R. 2001 *Nonequilibrium statistical mechanics*. Oxford University Press.

Appendix F

Evaluation of Collision Integrals in Terms of Series Expansion

In (3.76-3.77), $\mathscr{H}^{\delta p}_{\alpha\beta\gamma}$, $\mathscr{J}^{\delta p}_{\alpha\beta\gamma}$ and $\mathscr{K}^{\delta p}_{\alpha\beta\gamma}$ have integral expressions over θ and φ:

$$\mathscr{H}^{\delta p}_{\alpha\beta\gamma}(\eta,R,\phi,\lambda) \equiv \int_{\theta=0}^{2\pi}\int_{\varphi=0}^{\pi} \sin^{\alpha}2\theta\cos^{\beta}2\theta\sin^{\delta}\varphi\cos^{p}\varphi \times \left(1-\eta\sin^{2}\varphi\cos 2\theta+\lambda^{2}(3\sin^{2}\varphi-2)\right)^{\frac{\gamma}{2}}\mathfrak{F}\left(\chi\left[\eta,R,\phi,\lambda;\theta,\varphi\right]\right)d\varphi d\theta, \quad \text{(F.1)}$$

$$\mathscr{J}^{\delta p}_{\alpha\beta\gamma}(\eta,R,\phi,\lambda) \equiv \int_{\theta=0}^{2\pi}\int_{\varphi=0}^{\pi} \sin^{\alpha}2\theta\cos^{\beta}2\theta\sin^{\delta}\varphi\cos^{p}\varphi \times \left\{1-\eta\sin^{2}\varphi\cos 2\theta+\lambda^{2}(3\sin^{2}\varphi-2)\right\}^{\frac{\gamma}{2}}\mathfrak{G}\left(\chi\left[\eta,R,\phi,\lambda;\theta,\varphi\right]\right)d\varphi d\theta, \quad \text{(F.2)}$$

$$\mathscr{K}^{\delta p}_{\alpha\beta}(\eta,R,\phi,\lambda) \equiv \int_{\theta=0}^{2\pi}\int_{\varphi=0}^{\pi} \sin^{\alpha}2\theta\cos^{\beta}2\theta\sin^{\delta}\varphi\cos^{p}\varphi\left[(1-2\lambda^{2})\{\sin(2\phi+2\theta)-\cos\varphi \times \cos(2\phi+2\theta)\}+\sin^{2}\varphi\{3\lambda^{2}\sin(2\phi+2\theta)-\eta\sin 2\phi\}\right]\mathfrak{G}\left(\chi\left[\eta,R,\phi,\lambda;\theta,\varphi\right]\right)d\varphi d\theta, \quad \text{(F.3)}$$

where $\mathfrak{F}(\chi)$ and $\mathfrak{G}(\chi)$ are given by (3.60) and (3.61), respectively.

After performing term by term integration, and neglecting the terms beyond fourth order in η, λ, R and $\sin 2\phi$, we have the integrals as

$$\mathscr{H}_{003}^{10} = \frac{\pi}{210}\Big\{840 + 2688R^2 + 1024R^4 + 768R^2\lambda^2 - 24\eta^2\lambda^2 + 84\Big(\eta^2 + 3\lambda^4\Big) + 3\eta^4 + 672\sqrt{\pi}R\eta\cos 2\phi - 64\eta^2R^2\Big(2 + \cos 4\phi\Big)\Big\}, \tag{F.4}$$

$$\mathscr{H}_{013}^{30} = -\frac{4\pi}{105}\Big[4\sqrt{\pi}R\Big(21 + 12\lambda^2 + 32R^2\Big)\cos 2\phi + \eta\Big\{42 - \eta^2 + 12\lambda^2 + 32R^2\Big(2 + \cos 4\phi\Big)\Big\}\Big], \tag{F.5}$$

$$\mathscr{H}_{103}^{30} = \frac{16\pi}{105}R\sin 2\phi\Big\{\sqrt{\pi}\Big(21 + 12\lambda^2 + 32R^2\Big) + 16\eta R\cos 2\phi\Big\}, \tag{F.6}$$

$$2\mathscr{H}_{003}^{12} - \mathscr{H}_{003}^{30} = -\frac{4\pi}{1155}\Big\{528\sqrt{\pi}R\eta\cos 2\phi + 1386\lambda^2 + 66\Big(\eta^2 - 3\lambda^4\Big) - 33\eta^2\lambda^2 + 1024R^4 + 3\eta^4 + 32R^2\Big(66 - 4\eta^2 + 33\lambda^2 - 2\eta^2\cos 4\phi\Big)\Big\}, \tag{F.7}$$

$$2\eta\Big(\mathscr{H}_{101}^{31} - \mathscr{H}_{011}^{32}\Big) + 6\lambda^2\mathscr{H}_{001}^{32} = \frac{8\pi}{1155}\Big\{22\eta^2 - 64\eta^2R^2 + \eta^4 + 462\lambda^2 + 1056\lambda^2R^2 - 11\eta^2\lambda^2 - 66\lambda^4 + 4\sqrt{\pi}R\Big(33 + 32R^2\Big)\eta\cos 2\phi - 32R^2\eta^2\cos 4\phi\Big\}, \tag{F.8}$$

$$\eta\Big(2\mathscr{H}_{111}^{31} - \mathscr{H}_{201}^{30} - \mathscr{H}_{021}^{32}\Big) + 3\lambda^2\Big(\mathscr{H}_{011}^{32} - \mathscr{H}_{101}^{31}\Big) = -\frac{4\pi}{105}\Big\{36\sqrt{\pi}\lambda^2R\cos 2\phi + \eta\Big(42 - \eta^2 + 12\lambda^2 + 160R^2 - 64R^2\cos 4\phi\Big)\Big\}, \tag{F.9}$$

$$\eta\Big(\mathscr{H}_{201}^{31} + \mathscr{H}_{111}^{30} - \mathscr{H}_{111}^{32} - \mathscr{H}_{021}^{31}\Big) + 3\lambda^2\Big(\mathscr{H}_{101}^{32} + \mathscr{H}_{011}^{31}\Big) = \frac{16\pi}{105}R\sin 2\phi\Big\{9\sqrt{\pi}\lambda^2 - 32\eta R\cos 2\phi\Big\}, \tag{F.10}$$

$$\mathscr{J}_{012}^{30} = -\frac{8\pi}{315}\Big\{21\sqrt{\pi}\eta + 4R\Big(42 - 3\eta^2 + 12\lambda^2 + 32R^2\Big)\cos 2\phi\Big\}, \tag{F.11}$$

$$\mathscr{J}_{102}^{30} = \frac{32\pi}{315}R\sin 2\phi\Big(42 - \eta^2 + 12\lambda^2 + 32R^2\Big), \tag{F.12}$$

$$\mathscr{J}_{002}^{30} = \frac{4\pi}{3465}\Big[33\sqrt{\pi}\Big(35 + 96R^2 + 14\lambda^2\Big) - 8R\eta\Big\{160R^2 - 3\Big(66 + 5\eta^2 - 22\lambda^2\Big)\Big\}\cos 2\phi\Big], \tag{F.13}$$

$$\mathscr{J}_{002}^{10} = \frac{2\pi}{315}\left[21\sqrt{\pi}\left(15+32R^2\right) - 8R\eta\left\{32R^2 - 3\left(14+\eta^2-4\lambda^2\right)\right\}\cos 2\phi\right], \tag{F.14}$$

$$\mathscr{J}_{002}^{12} = \frac{2\pi}{3465}\left[33\sqrt{\pi}\left(35+32R^2-28\lambda^2\right) - 8R\eta\left\{32R^2 - 3\left(22+\eta^2\right)\right\}\cos 2\phi\right], \tag{F.15}$$

$$\mathscr{K}_{00}^{31} = \frac{32\pi}{3465}R\left(66+6\eta^2-132\lambda^2+32R^2-24\sqrt{\pi}\eta R\cos 2\phi+3\eta^2\cos 4\phi\right), \tag{F.16}$$

$$\begin{aligned}\mathscr{K}_{10}^{30} - \mathscr{K}_{01}^{31} = \frac{4\pi}{3465}\Big[\sqrt{\pi}\Big\{693+32R^2\left(33+10\eta^2-18\lambda^2\right)\Big\}\cos 2\phi - 8R\eta\Big\{209 \\ +15\eta^2-91\lambda^2-\left(143+15\eta^2-37\lambda^2\right)\cos 4\phi+40\sqrt{\pi}R\eta\cos 6\phi\Big\}\Big],\end{aligned} \tag{F.17}$$

$$\mathscr{K}_{10}^{31} + \mathscr{K}_{01}^{30} = \frac{4\pi}{315}\sin 2\phi\left\{208\eta R\cos 2\phi+3\sqrt{\pi}\left(21+32R^2\right)\right\}. \tag{F.18}$$

Appendix G

Stress Tensor and Transport Coefficients in Terms of Collision Integrals

The non-zero components of the dimensionless stress tensor in USF,

$$\boldsymbol{P}^* = \frac{\boldsymbol{P}}{\rho_p U_R^2} = \begin{pmatrix} P_{xx}^* & P_{xy}^* & 0 \\ P_{yx}^* & P_{yy}^* & 0 \\ 0 & 0 & P_{zz}^* \end{pmatrix}, \tag{G.1}$$

can be expressed in terms of the collision integral $\mathscr{J}_{\alpha\beta\gamma}^{\delta p}(\eta, R, \phi, \lambda^2)$ as defined in (3.79) and (F.2),

$$P_{xx}^* = \nu T^* \left[(1+\lambda^2+\eta\sin 2\phi) + \frac{3\nu g_0(1+e)}{2\pi^{\frac{3}{2}}} \left(\mathscr{J}_{002}^{30} - \sin 2\phi\, \mathscr{J}_{012}^{30} - \cos 2\phi\, \mathscr{J}_{102}^{30} \right) \right], \tag{G.2}$$

$$P_{yy}^* = \nu T^* \left[(1+\lambda^2-\eta\sin 2\phi) + \frac{3\nu g_0(1+e)}{2\pi^{\frac{3}{2}}} \left(\mathscr{J}_{002}^{30} + \sin 2\phi\, \mathscr{J}_{012}^{30} + \cos 2\phi\, \mathscr{J}_{102}^{30} \right) \right], \tag{G.3}$$

$$P_{zz}^* = \nu T^* \left[(1-2\lambda^2) + \frac{3\nu g_0(1+e)}{\pi^{\frac{3}{2}}} \mathscr{J}_{002}^{12} \right], \tag{G.4}$$

$$P_{xy}^* = \nu T^* \left[-\eta\cos 2\phi + \frac{3\nu g_0(1+e)}{2\pi^{\frac{3}{2}}} \left(\cos 2\phi\, \mathscr{J}_{012}^{30} - \sin 2\phi\, \mathscr{J}_{102}^{30} \right) \right]. \tag{G.5}$$

In (G.1), $U_R = 2\dot{\gamma}\sigma$ is the reference velocity scale and $\rho_p = \rho/\nu$ is the material/intrinsic density of particles.

The dimensionless pressure is given by

$$p^* \equiv \frac{P_{xx}^* + P_{yy}^* + P_{zz}^*}{3} = \frac{\nu}{64R^2} \left[1 + \frac{\nu g_0(1+e)}{\pi^{3/2}} \mathscr{J}_{002}^{10} \right], \tag{G.6}$$

where T^* is the granular temperature

$$T^* = \frac{T}{{U_R}^2} = \frac{1}{64R^2}. \tag{G.7}$$

The expression for the dimensionless shear viscosity is given by

$$\mu^* = \nu T^* \left[\eta \cos 2\phi - \frac{3\nu g_0 (1+e)}{2\pi^{\frac{3}{2}}} \left(\cos 2\phi \, \mathscr{J}^{30}_{012} - \sin 2\phi \, \mathscr{J}^{30}_{102} \right) \right]. \tag{G.8}$$

The 'scaled' first and second normal stress differences are defined with respect to mean pressure via

$$\mathscr{N}_1 = \frac{P_{xx} - P_{yy}}{p} \qquad \text{and} \qquad \mathscr{N}_2 = \frac{P_{yy} - P_{zz}}{p}. \tag{G.9}$$

Appendix H

Fourth-order Perturbation Solutions at Finite Density

We look for perturbation solutions of second moment equations in the form

$$\left.\begin{aligned}\eta &= \eta^{(2)} + \varepsilon\eta^{(3)} + \varepsilon^2\eta^{(4)} \\ \lambda^2 &= \lambda^{(2)} + \varepsilon\lambda^{(3)} + \varepsilon^2\lambda^{(4)} \\ R &= R^{(2)} + \varepsilon R^{(3)} + \varepsilon^2 R^{(4)} \\ \sin 2\phi &= \sin 2\phi^{(2)} + \varepsilon \sin 2\phi^{(3)} + \varepsilon^2 \sin 2\phi^{(4)}\end{aligned}\right\}. \tag{H.1}$$

Plugging these perturbation series into corresponding third (super-Burnett) and fourth (super-super-Burnett) order equations, we obtain perturbation equations at different orders.

At super-Burnett order (third-order in the shear rate), the balance equations for the second moment are

$$\left.\begin{aligned}&20\sqrt{\pi}\Big\{1+\frac{4}{5}(1+e)\nu g_0\Big\}(\eta^{(3)}R^{(2)}+\eta^{(2)}R^{(3)})\cos 2\phi^{(2)} + 256(1+e)\nu g_0 R^{(2)}R^{(3)} \\ &\quad -6(1-e^2)\nu g_0\Big\{\eta^{(2)}\eta^{(3)} + 32R^{(2)}R^{(3)} + 4\sqrt{\pi}(\eta^{(3)}R^{(2)}+\eta^{(2)}R^{(3)})\cos 2\phi^{(2)}\Big\} = 0 \\ &35\sqrt{\pi}(\eta^{(3)}R^{(2)}+\eta^{(2)}R^{(3)})\cos 2\phi^{(2)} + 2(1+e)\nu g_0\Big\{32(1+3e)R^{(2)}R^{(3)} \\ &-3(3-e)(\eta^{(2)}\eta^{(3)}+21\lambda^{(2)}\lambda^{(3)}) - 8\sqrt{\pi}(4-3e)(\eta^{(3)}R^{(2)}+\eta^{(2)}R^{(3)})\cos 2\phi^{(2)}\Big\} = 0 \\ &5\sqrt{\pi}R^{(3)}\cos 2\phi^{(2)} - (1+e)\nu g_0\{3(3-e)\eta^{(3)} + 2(1-3e)\sqrt{\pi}R^{(3)}\cos 2\phi^{(2)}\} = 0 \\ &5(\eta^{(3)} - \sin 2\phi^{(3)}) + 2(1+e)(1-3e)\nu g_0 \sin 2\phi^{(3)} = 0\end{aligned}\right\}. \tag{H.2}$$

The solutions for third order corrections are zero. At fourth order in the shear rate, the perturbation equations are

$$
\left.\begin{aligned}
&1680\sqrt{\pi}\varepsilon^2(\eta^{(4)}R^{(2)}+\eta^{(2)}R^{(4)})\cos 2\phi^{(2)}-3(1-e^2)\nu g_0\Big(168\varepsilon^2\eta^{(2)}\eta^{(4)}+3\eta^{(2)^4}\\
&+5376\varepsilon^2R^{(2)}R^{(4)}+1024R^{(2)^4}-128R^{(2)^2}\eta^{(2)^2}+768R^{(2)^2}\lambda^{(2)^2}-24\eta^{(2)^2}\lambda^{(2)^2}\\
&+252\lambda^{(2)^4}+672\sqrt{\pi}\varepsilon^2(\eta^{(4)}R^{(2)}+\eta^{(2)}R^{(4)})\cos 2\phi^{(2)}-64\eta^{(2)^2}R^{(2)^2}\Big)\\
&+1344\sqrt{\pi}(1+e)\nu g_0\varepsilon^2(\eta^{(4)}R^{(2)}+\eta^{(2)}R^{(4)})\cos 2\phi^{(2)}\\
&+256(1+e)\nu g_0\Big\{R^{(2)^2}\Big(-3\eta^{(2)^2}+12\lambda^{(2)^2}+32R^{(2)^2}\Big)+84\varepsilon^2R^{(2)}R^{(4)}\Big\}=0\\
&2310\sqrt{\pi}\varepsilon^2(\eta^{(4)}R^{(2)}+\eta^{(2)}R^{(4)})\cos 2\phi^{(2)}+(1+e)\nu g_0\Big[32R^{(2)^2}\Big\{8\eta^{(2)^2}-165\lambda^{(2)^2}\\
&-12e\eta^{(2)^2}+99e\lambda^{(2)^2}\Big\}+4224(1+3e)\varepsilon^2R^{(2)}R^{(4)}-9(3-e)\Big\{\eta^{(2)^4}+44\varepsilon^2\eta^{(2)}\eta^{(4)}\\
&-11\eta^{(2)^2}\lambda^{(2)^2}+924\varepsilon^2\lambda^{(2)}\lambda^{(4)}-66\lambda^{(2)^4}\Big\}+1024(5+3e)R^{(2)^4}\\
&-528\sqrt{\pi}(4-3e)\varepsilon^2(\eta^{(4)}R^{(2)}+\eta^{(2)}R^{(4)})\cos 2\phi^{(2)}+64(2-3e)\eta^{(2)^2}R^{(2)^2}\Big]=0\\
&210\sqrt{\pi}\Big(\varepsilon^2R^{(4)}+\lambda^{(2)^2}R^{(2)}\Big)\cos 2\phi^{(2)}-(1+e)\nu g_0\big[12\sqrt{\pi}\big\{7(1-3e)\varepsilon^2R^{(4)}\\
&+4(4-3e)\lambda^{(2)^2}R^{(2)}-32(1+e)R^{(2)^3}\big\}\cos 2\phi^{(2)}+\eta^{(2)}\big\{126(3-e)\varepsilon^2\eta^{(4)}\\
&-3(3-e)\eta^{(2)^2}+36(3-e)\lambda^{(2)^2}+96(1-3e)R^{(2)^2}\big\}\big]=0\\
&105\sqrt{\pi}\big\{\varepsilon^2\eta^{(4)}-\lambda^{(2)^2}\sin 2\phi^{(2)}-\varepsilon^2\sin 2\phi^{(4)}\big\}-2(1+e)\nu g_0\Big[\big[16(5+3e)\eta^{(2)}R^{(2)}\cos 2\phi^{(2)}\\
&-3\sqrt{\pi}\big\{4(4-3e)\lambda^{(2)^2}-32(1+e)R^{(2)^2}\big\}\big]\sin 2\phi^{(2)}-21\sqrt{\pi}(1-3e)\varepsilon^2\sin 2\phi^{(4)}\Big]=0
\end{aligned}\right\}. \tag{H.3}
$$

The solution of these equations are

$$\varepsilon^2\eta^{(4)} = \Bigg[\Big[\sqrt{\pi}\nu g_0\cos 2\phi^{(2)}\{5-2(1+e)(1-3e)\nu g_0\}\Big\{1024(1+e)(5+3e)R^{(2)^4}$$
$$-192(1+e)(1+3e)R^{(2)^2}\Big(\eta^{(2)^2}-4\lambda^{(2)^2}\Big)-9(1-e^2)\Big(\eta^{(2)^4}-8\eta^{(2)^2}\lambda^{(2)^2}+84\lambda^{(2)^4}\Big)\Big\}\Big]$$
$$-\Big[8\Big\{5\sqrt{\pi}\eta^{(2)}\cos 2\phi^{(2)}+2(1+e)\nu g_0\Big(8(1+3e)R^{(2)}-(1-3e)\sqrt{\pi}\eta^{(2)}\cos 2\phi^{(2)}\Big)\Big\}$$
$$\times\Big\{210\sqrt{\pi}\lambda^{(2)^2}R^{(2)}\cos 2\phi^{(2)}-48(1+e)\sqrt{\pi}\nu g_0R^{(2)}\cos 2\phi^{(2)}\Big((4-3e)\lambda^{(2)^2}-8(1+e)R^{(2)^2}\Big)$$
$$-3(1+e)\nu g_0\eta^{(2)}\Big(32(1-3e)R^{(2)^2}-(3-e)(\eta^{(2)^2}-\lambda^{(2)^2})\Big)\Big\}\Big]\Bigg]$$
$$\Big[4\Big[\sqrt{\pi}\cos 2\phi^{(2)}\Big\{2\sqrt{\pi}\cos 2\phi^{(2)}\{5-2(1+e)(1-3e)\nu g_0\}R^{(2)}-3(1-e^2)\nu g_0\eta^{(2)}\Big\}$$
$$\times\{5-2(1+e)(1-3e)\nu g_0\}+6(3-e)(1+e)\nu g_0\Big\{5\sqrt{\pi}\eta^{(2)}\cos 2\phi^{(2)}$$
$$+2(1+e)\nu g_0\Big(8(1+3e)R^{(2)}-(1-3e)\sqrt{\pi}\eta^{(2)}\cos 2\phi^{(2)}\Big)\Big\}\Big]\Big], \tag{H.4}$$

$$\varepsilon^2\lambda^{(4)} = \frac{1}{238848\lambda^{(2)}}\Bigg(\Bigg[\frac{28}{(3-e)}\Big\{1024(5+3e)R^{(2)^4}$$
$$+96R^{(2)^2}\Big(2(2-3e)\eta^{(2)^2}-11(5-3e)\lambda^{(2)^2}\Big)-9(3-e)\Big(\eta^{(2)^4}-11\eta^{(2)^2}\lambda^{(2)^2}-66\lambda^{(2)^4}\Big)\Big\}\Bigg]$$
$$-\Bigg[132\Big[35\sqrt{\pi}\eta^{(2)}\cos 2\phi^{(2)}+8(1+e)\nu g_0\Big\{8(1+3e)R^{(2)}-(4-3e)\sqrt{\pi}\eta^{(2)}\cos 2\phi^{(2)}\Big\}\Big]$$
$$\times\Big[70\sqrt{\pi}\lambda^{(2)^2}R^{(2)}\cos 2\phi^{(2)}+(1+e)\nu g_0\Big\{16\sqrt{\pi}R^{(2)}\cos 2\phi^{(2)}\Big((1+e)R^{(2)^2}-(4-3e)\lambda^{(2)^2}\Big)$$
$$-32(1-3e)\eta^{(2)^2}R^{(2)}+3(3-e)\eta^{(2)}\Big(\eta^{(2)^2}-12\lambda^{(2)^2}\Big)\Big\}\Big]$$
$$\frac{}{(3-e)(1+e)\sqrt{\pi}\{5-2(1+e)(1-3e)\nu g_0\}\nu g_0\cos 2\phi^{(2)}}\Bigg]$$
$$+\Bigg[1848\varepsilon^2\eta^{(4)}\Bigg[\frac{\sqrt{\pi}\{35-8(1+e)(4-3e)\nu g_0\}R^{(2)}\cos 2\phi^{(2)}-6(3-e)(1+e)\nu g_0\eta^{(2)}}{(3-e)(1+e)\nu g_0}$$
$$+\frac{3\Big\{35\sqrt{\pi}\eta^{(2)}\cos 2\phi^{(2)}+8(1+e)\nu g_0\Big(8(1+3e)R^{(2)}-(4-3e)\sqrt{\pi}\eta^{(2)}\cos 2\phi^{(2)}\Big)\Big\}}{\sqrt{\pi}\{5-2(1+e)(1-3e)\nu g_0\}\cos 2\phi^{(2)}}\Bigg]\Bigg]\Bigg), \tag{H.5}$$

$$\varepsilon^2 R^{(4)} = \frac{1}{42\sqrt{\pi}\{5-2(1+e)(1-3e)\nu g_0\}\cos 2\phi^{(2)}}\Bigg[-210\sqrt{\pi}{\lambda^{(2)}}^2 R^{(2)}\cos 2\phi^{(2)}$$
$$+48(1+e)\sqrt{\pi}\nu g_0 R^{(2)}\cos 2\phi^{(2)}\Big\{(4-3e){\lambda^{(2)}}^2-8(1+e){R^{(2)}}^2\Big\}$$
$$+3(1+e)\nu g_0\eta^{(2)}\Big\{32(1-3e){R^{(2)}}^2-(3-e)\Big({\eta^{(2)}}^2-{\lambda^{(2)}}^2\Big)\Big\}$$
$$+\Big\{126(3-e)(1+e)\nu g_0\varepsilon^2\eta^{(4)}\Big\}\Bigg], \tag{H.6}$$

$$\varepsilon^2\sin 2\phi^{(4)} = \Big[105\sqrt{\pi}\Big({\lambda^{(2)}}^2\sin 2\phi^{(2)}-\varepsilon^2\eta^{(4)}\Big)+$$
$$2(1+e)\nu g_0\sin 2\phi^{(2)}\Big\{16(5+3e)\eta^{(2)}R^{(2)}\cos 2\phi^{(2)}-3\sqrt{\pi}\big(4(4-3e){\lambda^{(2)}}^2-32(1+e){R^{(2)}}^2\big)\Big\}\Big]$$
$$\overline{\qquad\qquad 21\sqrt{\pi}\{2(1+e)(1-3e)\nu g_0-5\}\qquad\qquad}. \tag{H.7}$$

Appendix I

Source of Second Moment Tensor

Retaining terms up-to $O(\eta^m \lambda^n R^n \sin^q(2\phi),\ m+n+p+q \leq 4)$, the expressions for the non-zero elements of the source of the second moment tensor (3.126) in USF are given by

$$
\begin{aligned}
\aleph_{xx} &= A_{xx} + \widehat{E}_{xx} + \widehat{G}_{xx} + 2\dot{\gamma}\Theta_{xy} \\
&= -\frac{(1-e^2)\rho\nu g_0 T^{\frac{3}{2}}}{385\sigma\pi^{\frac{1}{2}}}\Big[3080 + 12672R^2 + 5120R^4 + 396\eta^2 - 640\eta^2R^2 + 15\eta^4 \\
&+ 1848\lambda^2 + 4224\lambda^2R^2 - 132\eta^2\lambda^2 + 660\lambda^4 + 3168\sqrt{\pi}\eta R\cos 2\phi - 320\eta^2R^2\cos 4\phi \\
&+ 44\eta\sin 2\phi\Big\{42 + 32R^2 - \eta^2 + 12\lambda^2\Big\}\Big] \\
&- \frac{8(1+e)\rho\nu g_0 T^{\frac{3}{2}}}{385\sigma\pi^{\frac{1}{2}}}\Big[22\eta^2 - 64\eta^2R^2 + \eta^4 + 462\lambda^2 + 1056\lambda^2R^2 - 11\eta^2\lambda^2 - 66\lambda^4 \\
&+ 4\sqrt{\pi}R(33+32R^2)\eta\cos 2\phi - 32R^2\eta^2\cos 4\phi + 11\eta\sin 2\phi\Big\{42 + 224R^2 - \eta^2 + 12\lambda^2\Big\}\Big] \\
&- \frac{8(1+e)\rho\nu g_0 T\dot{\gamma}}{1155\pi^{\frac{1}{2}}}\Big[3\sqrt{\pi}\eta\left(77 - 32R^2\right)\cos 2\phi + 32R\Big\{66 + 48R^2 - 2\eta^2 \\
&- \eta^2\cos 4\phi - 44\eta\sin 2\phi\Big\}\Big],
\end{aligned}
\tag{I.1}
$$

$$
\begin{aligned}
\aleph_{yy} &= A_{yy} + \widehat{E}_{yy} + \widehat{G}_{yy} - 2\dot{\gamma}\Theta_{xy} \\
&= -\frac{(1-e^2)\rho\nu g_0 T^{\frac{3}{2}}}{385\sigma\pi^{\frac{1}{2}}}\Big[3080 + 12672R^2 + 5120R^4 + 396\eta^2 - 640\eta^2R^2 + 15\eta^4 \\
&+ 1848\lambda^2 + 4224\lambda^2R^2 - 132\eta^2\lambda^2 + 660\lambda^4 + 3168\sqrt{\pi}\eta R\cos 2\phi - 320\eta^2R^2\cos 4\phi \\
&- 44\eta\sin 2\phi\Big\{42 + 32R^2 - \eta^2 + 12\lambda^2\Big\}\Big] \\
&- \frac{8(1+e)\rho\nu g_0 T^{\frac{3}{2}}}{385\sigma\pi^{\frac{1}{2}}}\Big[22\eta^2 - 64\eta^2R^2 + \eta^4 + 462\lambda^2 + 1056\lambda^2R^2 - 11\eta^2\lambda^2 - 66\lambda^4 \\
&+ 4\sqrt{\pi}R(33 + 32R^2)\eta\cos 2\phi - 32R^2\eta^2\cos 4\phi - 11\eta\sin 2\phi\Big\{42 + 224R^2 - \eta^2 + 12\lambda^2\Big\}\Big] \\
&+ \frac{8(1+e)\rho\nu g_0 T\dot{\gamma}}{1155\pi^{\frac{1}{2}}}\Big[3\sqrt{\pi}\eta\Big(77 + 32R^2\Big)\cos 2\phi + 8R\Big\{198 + 160R^2 - 14\eta^2 \\
&+ 132\lambda^2 - 7\eta^2\cos 4\phi - 176\eta\sin 2\phi\Big],
\end{aligned}
\tag{I.2}
$$

$$
\begin{aligned}
\aleph_{zz} &= A_{zz} + \widehat{E}_{zz} + \widehat{G}_{zz} \\
&= -\frac{(1-e^2)\rho\nu g_0 T^{\frac{3}{2}}}{385\sigma\pi^{\frac{1}{2}}}\Big[3080 + 4224R^2 + 1024R^4 + 132\eta^2 - 128R^2\eta^2 + 3\eta^4 - 3696\lambda^2 \\
&+ 1452\lambda^4 + 1056\sqrt{\pi}R\eta\cos 2\phi - 64R^2\eta^2\cos 4\phi\Big] \\
&+ \frac{16(1+e)\rho\nu g_0 T^{\frac{3}{2}}}{385\sigma\pi^{\frac{1}{2}}}\Big[22\eta^2 - 64R^2\eta^2 + \eta^4 + 462\lambda^2 + 1056R^2\lambda^2 - 11\eta^2\lambda^2 - 66\lambda^4 \\
&+ 4\sqrt{\pi}R(33 + 32R^2)\eta\cos 2\phi - 32R^2\eta^2\cos 4\phi\Big] \\
&+ \frac{64(1+e)\rho\nu g_0 T\dot{\gamma}}{1155\pi^{\frac{1}{2}}}R\Big(66 + 32R^2 + 6\eta^2 - 132\lambda^2 - 24\sqrt{\pi}R\eta\cos 2\phi + 3\eta^2\cos 4\phi\Big),
\end{aligned}
\tag{I.3}
$$

$$
\begin{aligned}
\aleph_{xy} &= A_{xy} + \widehat{E}_{xy} + \widehat{G}_{xy} + \dot{\gamma}\left(\Theta_{yy} - \Theta_{xx}\right) \\
&= \frac{4(1-e^2)\rho\nu g_0 T^{\frac{3}{2}}}{35\sigma\pi^{\frac{1}{2}}}\left[4\sqrt{\pi}R(21+32R^2+12\lambda^2)+\eta(42+96R^2-\eta^2+12\lambda^2)\cos 2\phi\right] \\
&+ \frac{8(1+e)\rho\nu g_0 T^{\frac{3}{2}}}{35\sigma\pi^{\frac{1}{2}}}\left[36\sqrt{\pi}R\lambda^2+\eta(42+96R^2-\eta^2+12\lambda^2)\cos 2\phi\right] \\
&+ \frac{4(1+e)\rho\nu g_0 T\dot{\gamma}}{1155\sqrt{\pi}}\Big[\sqrt{\pi}(693+1056R^2-576R^2\lambda^2\cos^2 2\phi-462\eta\sin 2\phi) \\
&- 4R\eta(132+15\eta^2-145\lambda^2)\cos 2\phi+60R\eta^3\cos 6\phi \\
&- 148\eta\lambda^2 R\cos 6\phi+88R\eta^2\sin 4\phi\Big]. \qquad \text{(I.4)}
\end{aligned}
$$

Appendix J

Contracted Third-order Source Term ($\aleph_{\alpha\beta\beta}$) in the dilute limit

The contracted third-order source term $\aleph_{\alpha\beta\beta}$ in the evaluation of heat flux (3.166) has the following form

$$\begin{aligned}\aleph_{\alpha\beta\beta} &= \aleph[mC^2C_\alpha] \\ &= \frac{m\sigma^2}{2}\int\int\int_{\boldsymbol{g}\cdot\boldsymbol{k}>0}\Delta(C^2C_\alpha)f^{(2)}(\mathbf{c_1},\mathbf{r},\mathbf{c_2},\mathbf{r})(\boldsymbol{g}\cdot\boldsymbol{k})d\boldsymbol{k}d\boldsymbol{c}_1d\boldsymbol{c}_2. \end{aligned} \tag{J.1}$$

In the following we will evaluate this multi-dimensional integral to obtain a closed-form algebraic expression for $\aleph_{\alpha\beta\beta}$ as given by (3.161) in the main text.

Changing the variables of integration from $\boldsymbol{c}_1$, $\boldsymbol{c}_2$ to $\boldsymbol{g}=\boldsymbol{c}_1-\boldsymbol{c}_2=\boldsymbol{C}_1-\boldsymbol{C}_2$, $\boldsymbol{G}=(\boldsymbol{C}_1+\boldsymbol{C}_2)/2$; $d\boldsymbol{c}_1d\boldsymbol{c}_2{=}d\boldsymbol{C}_1d\boldsymbol{C}_2{=}d\boldsymbol{g}d\boldsymbol{G}$ and using

$$\begin{aligned}\Delta(C^2C_\alpha) = \Bigg[&(1+e)^2(\boldsymbol{g}\cdot\boldsymbol{k})^2G_\beta k_\beta k_\alpha-(1+e)(\boldsymbol{g}\cdot\boldsymbol{k})G_\beta(k_\beta g_\alpha+g_\beta k_\alpha) \\ &-\frac{1}{2}(1-e^2)(\boldsymbol{g}\cdot\boldsymbol{k})^2G_\alpha\Bigg],\end{aligned} \tag{J.2}$$

along with the molecular-chaos assumption for the two-body distribution function $f^{(2)}$, we can rewrite (J.1) as

$$\begin{aligned}\aleph_{\alpha\beta\beta} &= \frac{m\sigma^2 n^2}{16\pi^3|\boldsymbol{M}|}\int\int\int_{\boldsymbol{g}\cdot\boldsymbol{k}>0}\\ &\left[(1+e)^2(\boldsymbol{g}\cdot\boldsymbol{k})^3 G_\beta k_\beta k_\alpha - (1+e)(\boldsymbol{g}\cdot\boldsymbol{k})^2 G_\beta(k_\beta g_\alpha + g_\beta k_\alpha) - \frac{1}{2}(1-e^2)(\boldsymbol{g}\cdot\boldsymbol{k})^3 G_\alpha\right]\\ &\exp\left\{-\frac{1}{4}M_{ab}^{-1}(4G_aG_b + g_a g_b)\right\}\left[1 + 2a_iG_i + b_i f_i(\boldsymbol{g},\mathbf{G})\right]d\boldsymbol{G}d\boldsymbol{g}d\boldsymbol{k}\\ &= I^{(1)}_{\alpha\beta\beta} + I^{(2)}_{\alpha\beta\beta} + I^{(3)}_{\alpha\beta\beta}.\end{aligned} \tag{J.3}$$

where Einstein's summation convention has been used in repeated index and

$$\left.\begin{aligned} f_1 &= \tfrac{1}{2}(3g_1^2 + g_2^2 + g_3^2)G_1 + g_1(g_2G_2 + g_3G_3) + 2G_1\boldsymbol{G}^2,\\ f_2 &= \tfrac{1}{2}(g_1^2 + 3g_2^2 + g_3^2)G_2 + g_2(g_1G_1 + g_3G_3) + 2G_2\boldsymbol{G}^2,\\ f_3 &= \tfrac{1}{2}(g_1^2 + g_2^2 + 3g_3^2)G_3 + g_3(g_1G_1 + g_2G_2) + 2G_3\boldsymbol{G}^2.\end{aligned}\right\} \tag{J.4}$$

Now using the following results

$$\left.\begin{aligned} \int \exp\{-G_aM_{ab}^{-1}G_b\}d\boldsymbol{G} &= \pi^{\frac{3}{2}}|\boldsymbol{M}|^{\frac{1}{2}},\\ \int G_iG_j\exp\{-G_aM_{ab}^{-1}G_b\}d\boldsymbol{G} &= \tfrac{\pi^{\frac{3}{2}}}{2}|\boldsymbol{M}|^{\frac{1}{2}}M_{ij},\\ \int G_iG_jG_kG_l\exp\{-G_aM_{ab}^{-1}G_b\}d\boldsymbol{G} &= \tfrac{\pi^{\frac{3}{2}}}{4}|\boldsymbol{M}|^{\frac{1}{2}}(M_{ij}M_{kl} + M_{ik}M_{jl} + M_{il}M_{jk}),\end{aligned}\right\} \tag{J.5}$$

we can simplify the three integrals $I^{(k)}_{\alpha\beta\beta}$ in (J.3) as

$$\begin{aligned} I^{(1)}_{\alpha\beta\beta} &= \frac{m\sigma^2n^2(1+e)^2}{16\pi^{\frac{3}{2}}|\boldsymbol{M}|^{\frac{1}{2}}}\int\int_{\boldsymbol{g}\cdot\boldsymbol{k}>0}(\boldsymbol{g}\cdot\boldsymbol{k})^3k_\alpha k_\beta\exp\left\{-\frac{1}{4}g_aM_{ab}^{-1}g_b\right\}\\ &\times\left[\left\{a_1 + \frac{1}{2}b_1\left(3M_{xx} + M_{yy} + M_{zz}\right) + b_2M_{xy}\right\}M_{1\beta}\right.\\ &+\left\{a_2 + \frac{1}{2}b_2\left(M_{xx} + 3M_{yy} + M_{zz}\right) + b_1M_{xy}\right\}M_{2\beta}\\ &+\left\{a_3 + \frac{1}{2}b_3\left(M_{xx} + M_{yy} + 3M_{zz}\right)\right\}M_{3\beta}\\ &+\frac{1}{4}g_1^2\left(3b_1M_{1\beta} + b_2M_{2\beta} + b_3M_{3\beta}\right) + \frac{1}{4}g_2^2\left(b_1M_{1\beta} + 3b_2M_{2\beta} + b_3M_{3\beta}\right)\\ &+\frac{1}{4}g_3^2\left(b_1M_{1\beta} + b_2M_{2\beta} + 3b_3M_{3\beta}\right) + \frac{1}{2}g_1g_2\left(b_1M_{2\beta} + b_2M_{1\beta}\right)\\ &\left.+\frac{1}{2}g_1g_3\left(b_1M_{3\beta} + b_3M_{1\beta}\right) + \frac{1}{2}g_2g_3\left(b_2M_{3\beta} + b_3M_{2\beta}\right)\right]d\boldsymbol{g}d\boldsymbol{k}, \end{aligned} \tag{J.6}$$

$$
\begin{aligned}
I^{(2)}_{\alpha\beta\beta} = &-\frac{m\sigma^2 n^2(1+e)}{16\pi^{\frac{3}{2}}|\boldsymbol{M}|^{\frac{1}{2}}}\int\int_{\boldsymbol{g}\cdot\boldsymbol{k}>0}(\boldsymbol{g}\cdot\boldsymbol{k})^2\Big(k_\alpha g_\beta + g_\alpha k_\beta\Big)\exp\Big\{-\frac{1}{4}g_a M^{-1}_{ab} g_b\Big\}\\
&\times\Bigg[\Big\{a_1+\frac{1}{2}b_1\Big(3M_{xx}+M_{yy}+M_{zz}\Big)+b_2M_{xy}\Big\}M_{1\beta}\\
&+\Big\{a_2+\frac{1}{2}b_2\Big(M_{xx}+3M_{yy}+M_{zz}\Big)+b_1M_{xy}\Big\}M_{2\beta}\\
&+\Big\{a_3+\frac{1}{2}b_3\Big(M_{xx}+M_{yy}+3M_{zz}\Big)\Big\}M_{3\beta}\\
&+\frac{1}{4}g_1^2\Big(3b_1M_{1\beta}+b_2M_{2\beta}+b_3M_{3\beta}\Big)+\frac{1}{4}g_2^2\Big(b_1M_{1\beta}+3b_2M_{2\beta}+b_3M_{3\beta}\Big)\\
&+\frac{1}{4}g_3^2\Big(b_1M_{1\beta}+b_2M_{2\beta}+3b_3M_{3\beta}\Big)+\frac{1}{2}g_1g_2\Big(b_1M_{2\beta}+b_2M_{1\beta}\Big)\\
&+\frac{1}{2}g_1g_3\Big(b_1M_{3\beta}+b_3M_{1\beta}\Big)+\frac{1}{2}g_2g_3\Big(b_2M_{3\beta}+b_3M_{2\beta}\Big)\Bigg]d\boldsymbol{g}d\boldsymbol{k},
\end{aligned}
\tag{J.7}
$$

$$
\begin{aligned}
I^{(3)}_{\alpha\beta\beta} = &-\frac{m\sigma^2 n^2(1-e^2)}{32\pi^{\frac{3}{2}}|\boldsymbol{M}|^{\frac{1}{2}}}\int\int_{\boldsymbol{g}\cdot\boldsymbol{k}>0}(\boldsymbol{g}\cdot\boldsymbol{k})^3\exp\Big\{-\frac{1}{4}g_a M^{-1}_{ab} g_b\Big\}\\
&\times\Bigg[\Big\{a_1+\frac{1}{2}b_1\Big(3M_{xx}+M_{yy}+M_{zz}\Big)+b_2M_{xy}\Big\}M_{1\alpha}\\
&+\Big\{a_2+\frac{1}{2}b_2\Big(M_{xx}+3M_{yy}+M_{zz}\Big)+b_1M_{xy}\Big\}M_{2\alpha}\\
&+\Big\{a_3+\frac{1}{2}b_3\Big(M_{xx}+M_{yy}+3M_{zz}\Big)\Big\}M_{3\alpha}\\
&+\frac{1}{4}g_1^2\Big(3b_1M_{1\alpha}+b_2M_{2\alpha}+b_3M_{3\alpha}\Big)+\frac{1}{4}g_2^2\Big(b_1M_{1\alpha}+3b_2M_{2\alpha}+b_3M_{3\alpha}\Big)\\
&+\frac{1}{4}g_3^2\Big(b_1M_{1\alpha}+b_2M_{2\alpha}+3b_3M_{3\alpha}\Big)+\frac{1}{2}g_1g_2\Big(b_1M_{2\alpha}+b_2M_{1\alpha}\Big)\\
&+\frac{1}{2}g_1g_3\Big(b_1M_{3\alpha}+b_3M_{1\alpha}\Big)+\frac{1}{2}g_2g_3\Big(b_2M_{3\alpha}+b_3M_{2\alpha}\Big)\Bigg]d\boldsymbol{g}d\boldsymbol{k}.
\end{aligned}
\tag{J.8}
$$

To obtain closed-form expressions for integrals (J.6), (J.7) and (J.8), it remains to carry out integrations over $\boldsymbol{g}$ and $\boldsymbol{k}$. To carry out the integrations over $\boldsymbol{g}$ we use the following results:

$$
\int(\boldsymbol{g}\cdot\boldsymbol{k})^3\exp\Big\{-\frac{1}{4}g_a M^{-1}_{ab} g_b\Big\}d\boldsymbol{g} = 32\pi|\boldsymbol{M}|^{\frac{1}{2}}\vartheta^{\frac{3}{2}},
\tag{J.9}
$$

$$\int g_x^2(\boldsymbol{g}\cdot\boldsymbol{k})^3 \exp\left\{-\frac{1}{4}g_a M_{ab}^{-1} g_b\right\} d\boldsymbol{g}$$
$$= 16\pi|\boldsymbol{M}|^{\frac{1}{2}}\vartheta^{\frac{1}{2}}T^2\Big[7+3\eta^2+8\lambda^2+\lambda^4+6\Big\{\eta^2-(1+\lambda^2)^2\Big\}\cos 2\phi\sin^2\varphi\sin 2\theta$$
$$+2\eta(5+2\lambda^2)\sin 2\phi-3\cos 2\varphi\Big\{1+\eta^2+4\lambda^2+3\lambda^4+2\eta(1+2\lambda^2)\sin 2\phi\Big\}$$
$$-2\cos 2\theta\sin^2\varphi\Big\{8\eta(1+\lambda^2)+\Big(5\eta^2+3(1+\lambda^2)^2\Big)\sin 2\phi\Big\}\Big], \tag{J.10}$$

$$\int g_y^2(\boldsymbol{g}\cdot\boldsymbol{k})^3 \exp\left\{-\frac{1}{4}g_a M_{ab}^{-1} g_b\right\} d\boldsymbol{g}$$
$$= 16\pi|\boldsymbol{M}|^{\frac{1}{2}}\vartheta^{\frac{1}{2}}T^2\Big[7+3\eta^2+8\lambda^2+\lambda^4-6\Big\{\eta^2-(1+\lambda^2)^2\Big\}\cos 2\phi\sin^2\varphi\sin 2\theta$$
$$-2\eta(5+2\lambda^2)\sin 2\phi-3\cos 2\varphi\Big\{1+\eta^2+4\lambda^2+3\lambda^4-2\eta(1+2\lambda^2)\sin 2\phi\Big\}$$
$$-2\cos 2\theta\sin^2\varphi\Big\{8\eta(1+\lambda^2)-\Big(5\eta^2+3(1+\lambda^2)^2\Big)\sin 2\phi\Big\}\Big], \tag{J.11}$$

$$\int g_z^2(\boldsymbol{g}\cdot\boldsymbol{k})^3 \exp\left\{-\frac{1}{4}g_a M_{ab}^{-1} g_b\right\} d\boldsymbol{g}$$
$$= 32\pi|\boldsymbol{M}|^{\frac{1}{2}}\vartheta^{\frac{1}{2}}T^2(1-2\lambda^2)\Big[5-7\lambda^2+3(1-3\lambda^2)\cos 2\varphi-2\eta\cos 2\theta\sin^2\varphi\Big], \tag{J.12}$$

$$\int g_x g_y (\boldsymbol{g}\cdot\boldsymbol{k})^3 \exp\left\{-\frac{1}{4} g_a M_{ab}^{-1} g_b\right\} d\boldsymbol{g}$$
$$= 32\pi |\boldsymbol{M}|^{\frac{1}{2}} \vartheta^{\frac{1}{2}} T^2 \Big[\Big\{5\eta^2 + 3(1+\lambda^2)^2\Big\}\cos 2\phi \cos 2\theta \sin^2\varphi - \eta(5+2\lambda^2)\cos 2\phi$$
$$+ 3\eta(1+2\lambda^2)\cos 2\varphi \cos 2\phi + 3\Big\{\eta^2 - (1+\lambda^2)^2\Big\}\sin^2\varphi \sin 2\phi \sin 2\theta\Big], \quad \text{(J.13)}$$

$$\int g_x g_z (\boldsymbol{g}\cdot\boldsymbol{k})^3 \exp\left\{-\frac{1}{4} g_a M_{ab}^{-1} g_b\right\} d\boldsymbol{g}$$
$$= 48\sqrt{2}\pi |\boldsymbol{M}|^{\frac{1}{2}} \vartheta^{\frac{1}{2}} T^2 \sin 2\varphi (1-2\lambda^2)\Big[(1+\lambda^2)\Big\{\cos(\theta+\phi) - \sin(\theta+\phi)\Big\}$$
$$- \eta\Big\{\cos(\theta-\phi) + \sin(\theta-\phi)\Big\}\Big], \quad \text{(J.14)}$$

$$\int g_y g_z (\boldsymbol{g}\cdot\boldsymbol{k})^3 \exp\left\{-\frac{1}{4} g_a M_{ab}^{-1} g_b\right\} d\boldsymbol{g}$$
$$= 48\sqrt{2}\pi |\boldsymbol{M}|^{\frac{1}{2}} \vartheta^{\frac{1}{2}} T^2 \sin 2\varphi (1-2\lambda^2)\Big[(1+\lambda^2)\Big\{\cos(\theta+\phi) + \sin(\theta+\phi)\Big\}$$
$$- \eta\Big\{\cos(\theta-\phi) - \sin(\theta-\phi)\Big\}\Big], \quad \text{(J.15)}$$

$$\int g_x (\boldsymbol{g}\cdot\boldsymbol{k})^2 \exp\left\{-\frac{1}{4} g_a M_{ab}^{-1} g_b\right\} d\boldsymbol{g}$$
$$= 16\sqrt{2}\pi |\boldsymbol{M}|^{\frac{1}{2}} \vartheta^{\frac{1}{2}} T \sin\varphi \Big[(1+\lambda^2)\Big\{\cos(\theta+\phi) - \sin(\theta+\phi)\Big\}$$
$$- \eta\Big\{\cos(\theta-\phi) + \sin(\theta-\phi)\Big\}\Big], \quad \text{(J.16)}$$

$$\int g_y (\boldsymbol{g}\cdot\boldsymbol{k})^2 \exp\left\{-\frac{1}{4} g_a M_{ab}^{-1} g_b\right\} d\boldsymbol{g}$$
$$= 16\sqrt{2}\pi |\boldsymbol{M}|^{\frac{1}{2}} \vartheta^{\frac{1}{2}} T \sin\varphi \Big[(1+\lambda^2)\Big\{\cos(\theta+\phi) + \sin(\theta+\phi)\Big\}$$
$$- \eta\Big\{\cos(\theta-\phi) - \sin(\theta-\phi)\Big\}\Big], \quad \text{(J.17)}$$

$$\int g_z (\boldsymbol{g}\cdot\boldsymbol{k})^2 \exp\left\{-\frac{1}{4} g_a M_{ab}^{-1} g_b\right\} d\boldsymbol{g} = 32\pi |\boldsymbol{M}|^{\frac{1}{2}} \vartheta^{\frac{1}{2}} T (1-2\lambda^2)\cos\varphi, \quad \text{(J.18)}$$

$$\begin{aligned}
&\int g_x^3(\boldsymbol{g}\cdot\boldsymbol{k})^2 \exp\left\{-\frac{1}{4}g_a M_{ab}^{-1} g_b\right\} d\boldsymbol{g} \\
&\quad = \frac{8\sqrt{2}\pi|\boldsymbol{M}|^{\frac{1}{2}}T^3}{\vartheta^{\frac{1}{2}}} \sin\varphi\Big[(1+\lambda^2)\Big\{\cos(\theta+\phi)-\sin(\theta+\phi)\Big\} \\
&\qquad -\eta\Big\{\cos(\theta-\phi)+\sin(\theta-\phi)\Big\}\Big]\Big[13+\eta^2+8\lambda^2-5\lambda^4 \\
&\qquad +2\Big\{\eta^2-(1+\lambda^2)^2\Big\}\cos 2\phi \sin^2\varphi \sin 2\theta + 2\eta(7-2\lambda^2)\sin 2\phi \\
&\qquad -\cos 2\varphi\Big\{1+\eta^2+20\lambda^2+19\lambda^4+2\eta(1+10\lambda^2)\sin 2\phi\Big\} \\
&\qquad -2\cos 2\theta \sin^2\varphi\Big\{8\eta(1+\lambda^2)+\Big(7\eta^2+(1+\lambda^2)^2\Big)\sin 2\phi\Big\}\Big],
\end{aligned} \tag{J.19}$$

$$\begin{aligned}
&\int g_y^3(\boldsymbol{g}\cdot\boldsymbol{k})^2 \exp\left\{-\frac{1}{4}g_a M_{ab}^{-1} g_b\right\} d\boldsymbol{g} \\
&\quad = \frac{8\sqrt{2}\pi|\boldsymbol{M}|^{\frac{1}{2}}T^3}{\vartheta^{\frac{1}{2}}} \sin\varphi\Big[(1+\lambda^2)\Big\{\cos(\theta+\phi)+\sin(\theta+\phi)\Big\} \\
&\qquad -\eta\Big\{\cos(\theta-\phi)-\sin(\theta-\phi)\Big\}\Big]\Big[13+\eta^2+8\lambda^2-5\lambda^4 \\
&\qquad -2\Big\{\eta^2-(1+\lambda^2)^2\Big\}\cos 2\phi \sin^2\varphi \sin 2\theta - 2\eta(7-2\lambda^2)\sin 2\phi \\
&\qquad -\cos 2\varphi\Big\{1+\eta^2+20\lambda^2+19\lambda^4-2\eta(1+10\lambda^2)\sin 2\phi\Big\} \\
&\qquad -2\cos 2\theta \sin^2\varphi\Big\{8\eta(1+\lambda^2)-\Big(7\eta^2+(1+\lambda^2)^2\Big)\sin 2\phi\Big\}\Big],
\end{aligned} \tag{J.20}$$

$$\begin{aligned}
&\int g_z^3(\boldsymbol{g}\cdot\boldsymbol{k})^2 \exp\left\{-\frac{1}{4}g_a M_{ab}^{-1} g_b\right\} d\boldsymbol{g} \\
&\quad = \frac{32\pi|\boldsymbol{M}|^{\frac{1}{2}}T^3}{\vartheta^{\frac{1}{2}}}(1-2\lambda^2)^2\cos\varphi\Big[7-5\lambda^2+(1-11\lambda^2)\cos 2\varphi - 6\eta\cos 2\theta\sin^2\varphi\Big],
\end{aligned} \tag{J.21}$$

$$\int g_x^2 g_z (\boldsymbol{g}\cdot\boldsymbol{k})^2 \exp\Big\{-\frac{1}{4} g_a M_{ab}^{-1} g_b\Big\} d\boldsymbol{g}$$
$$= \frac{16\pi|\boldsymbol{M}|^{\frac{1}{2}} T^3}{\vartheta^{\frac{1}{2}}} (1-2\lambda^2)\cos\varphi \Big[5+\eta^2+4\lambda^2-\lambda^4$$
$$+2\Big\{\eta^2-(1+\lambda^2)^2\Big\}\cos 2\phi \sin^2\varphi \sin 2\theta + 6\eta \sin 2\phi$$
$$-\cos 2\varphi\Big\{1+\eta^2+8\lambda^2+7\lambda^4+2\eta(1+4\lambda^2)\sin 2\phi\Big\}$$
$$-2\cos 2\theta \sin^2\varphi\Big\{4\eta(1+\lambda^2)+\Big(3\eta^2+(1+\lambda^2)^2\Big)\sin 2\phi\Big\}\Big], \tag{J.22}$$

$$\int g_x g_z^2 (\boldsymbol{g}\cdot\boldsymbol{k})^2 \exp\Big\{-\frac{1}{4} g_a M_{ab}^{-1} g_b\Big\} d\boldsymbol{g}$$
$$= \frac{16\sqrt{2}\pi|\boldsymbol{M}|^{\frac{1}{2}} T^3}{\vartheta^{\frac{1}{2}}} (1-2\lambda^2)\sin\varphi \Big[(1+\lambda^2)\Big\{\cos(\theta+\phi)-\sin(\theta+\phi)\Big\}$$
$$-\eta\Big\{\cos(\theta-\phi)+\sin(\theta-\phi)\Big\}\Big]\Big[3-3\lambda^2+(1-5\lambda^2)\cos 2\varphi - 2\eta\cos 2\theta\sin^2\varphi\Big],$$

$$\int g_y^2 g_z (\boldsymbol{g}\cdot\boldsymbol{k})^2 \exp\Big\{-\frac{1}{4} g_a M_{ab}^{-1} g_b\Big\} d\boldsymbol{g}$$
$$= \frac{16\pi|\boldsymbol{M}|^{\frac{1}{2}} T^3}{\vartheta^{\frac{1}{2}}} (1-2\lambda^2)\cos\varphi \Big[5+\eta^2+4\lambda^2-\lambda^4$$
$$-2\Big\{\eta^2-(1+\lambda^2)^2\Big\}\cos 2\phi \sin^2\varphi \sin 2\theta - 6\eta \sin 2\phi$$
$$-\cos 2\varphi\Big\{1+\eta^2+8\lambda^2+7\lambda^4-2\eta(1+4\lambda^2)\sin 2\phi\Big\}$$
$$+2\cos 2\theta \sin^2\varphi\Big\{4\eta(1+\lambda^2)-\Big(3\eta^2+(1+\lambda^2)^2\Big)\sin[2\phi\Big\}\Big], \tag{J.23}$$

$$\int g_y g_z^2 (\boldsymbol{g}\cdot\boldsymbol{k})^2 \exp\Big\{-\frac{1}{4} g_a M_{ab}^{-1} g_b\Big\} d\boldsymbol{g}$$
$$= \frac{16\sqrt{2}\pi|\boldsymbol{M}|^{\frac{1}{2}} T^3}{\vartheta^{\frac{1}{2}}} (1-2\lambda^2)\sin\varphi \Big[(1+\lambda^2)\Big\{\cos(\theta+\phi)+\sin(\theta+\phi)\Big\}$$
$$-\eta\Big\{\cos(\theta-\phi)-\sin(\theta-\phi)\Big\}\Big]\Big[3-3\lambda^2+(1-5\lambda^2)\cos 2\varphi - 2\eta\cos 2\theta\sin^2\varphi\Big],$$

$$\int g_x g_y g_z (\boldsymbol{g}\cdot\boldsymbol{k})^2 \exp\Big\{-\frac{1}{4} g_a M_{ab}^{-1} g_b\Big\} d\boldsymbol{g}$$
$$= \frac{32\pi|\boldsymbol{M}|^{\frac{1}{2}} T^3}{\vartheta^{\frac{1}{2}}} (1-2\lambda^2)\cos\varphi \Big[\Big\{\eta^2-(1+\lambda^2)^2\Big\}\sin^2\varphi \sin 2\theta \sin 2\phi$$
$$-\cos 2\phi\Big\{3\eta-\eta(1+4\lambda^2)\cos 2\varphi-\Big(3\eta^2+(1+\lambda^2)^2\Big)\sin^2\varphi\cos 2\theta\Big\}\Big]. \tag{J.24}$$

Now retaining up to fourth-order terms in η, λ^2 in the expansion for ϑ we have

$$\vartheta = \boldsymbol{k}\cdot\boldsymbol{M}\cdot\boldsymbol{k} = T\{1-\eta\sin^2\varphi\cos 2\theta+\lambda^2(3\sin^2\varphi-2)\}, \tag{J.25}$$

$$\begin{aligned}
\vartheta^{\frac{3}{2}} \approx\; & T^{\frac{3}{2}}\Big[1-\frac{3}{2}\{\eta\sin^2\varphi\cos 2\theta-\lambda^2(3\sin^2\varphi-2)\} \\
& +\frac{3}{8}\{\eta\sin^2\varphi\cos 2\theta-\lambda^2(3\sin^2\varphi-2)\}^2+\frac{1}{16}\{\eta\sin^2\varphi\cos 2\theta-\lambda^2(3\sin^2\varphi-2)\}^3 \\
& +\frac{3}{128}\{\eta\sin^2\varphi\cos 2\theta-\lambda^2(3\sin^2\varphi-2)\}^4\Big], \qquad \text{(J.26)} \\
\vartheta^{\frac{1}{2}} \approx\; & T^{\frac{1}{2}}\Big[1-\frac{1}{2}\{\eta\sin^2\varphi\cos 2\theta-\lambda^2(3\sin^2\varphi-2)\} \\
& -\frac{1}{8}\{\eta\sin^2\varphi\cos 2\theta-\lambda^2(3\sin^2\varphi-2)\}^2-\frac{1}{16}\{\eta\sin^2\varphi\cos 2\theta-\lambda^2(3\sin^2\varphi-2)\}^3 \\
& -\frac{5}{128}\{\eta\sin^2\varphi\cos 2\theta-\lambda^2(3\sin^2\varphi-2)\}^4\Big], \qquad \text{(J.27)} \\
\vartheta^{-\frac{1}{2}} \approx\; & \frac{1}{T^{\frac{1}{2}}}\Big[1+\frac{1}{2}\{\eta\sin^2\varphi\cos 2\theta-\lambda^2(3\sin^2\varphi-2)\} \\
& +\frac{3}{8}\{\eta\sin^2\varphi\cos 2\theta-\lambda^2(3\sin^2\varphi-2)\}^2+\frac{5}{16}\{\eta\sin^2\varphi\cos 2\theta-\lambda^2(3\sin^2\varphi-2)\}^3 \\
& +\frac{35}{128}\{\eta\sin^2\varphi\cos 2\theta-\lambda^2(3\sin^2\varphi-2)\}^4\Big]. \qquad \text{(J.28)}
\end{aligned}$$

Using the information about the contact vector $\boldsymbol{k}$ given above and carrying out the remaining integrations over $\boldsymbol{k}$, we obtain the final expressions for the integrals $I^{(k)}_{\alpha\beta\beta}$ in (J.3):

$$
\begin{aligned}
I^{(1)}_{x\beta\beta} = {} & \frac{4\rho(1+e)^2T^{1/2}}{385\rho_p\sigma\pi^{1/2}\{16\eta^4+24\eta^2(1+2\lambda^4)+(5+4\lambda^2+8\lambda^4)^2\}} \\
& \times\Big[\Big[-8\eta^6(72-221\lambda^2)+2\eta^4(13379+5780\lambda^2-1352\lambda^4+2568\lambda^6) \\
& +(5+4\lambda^2+8\lambda^4)(6930+6930\lambda^2+14553\lambda^4+495\lambda^6-194\lambda^8+16\lambda^{10}) \\
& +\eta^2[38115+\lambda^2\{12573+8\lambda^2(10812+2651\lambda^2+4\lambda^4+881\lambda^6)\}] \\
& +\eta\{440\eta^6+6930(1+2\lambda^2)+2\eta^4(2125-928\lambda^2+1360\lambda^4) \\
& +\lambda^4(16137+16748\lambda^2+23146\lambda^4+2816\lambda^6+5040\lambda^8) \\
& +\eta^2(1683-6220\lambda^2+11196\lambda^4-576\lambda^6+5880\lambda^8)\}\sin 2\phi\Big]q_x \\
& -\Big[\eta\{440\eta^6+6930(1+2\lambda^2)+2\eta^4(2125-928\lambda^2+1360\lambda^4) \\
& +\lambda^4(16137+16748\lambda^2+23146\lambda^4+2816\lambda^6+5040\lambda^8) \\
& +\eta^2(1683-6220\lambda^2+11196\lambda^4-576\lambda^6+5880\lambda^8)\}\cos 2\phi\Big]q_y\Big],
\end{aligned}
\tag{J.29}
$$

$$
\begin{aligned}
I^{(1)}_{y\beta\beta} = {} & \frac{4\rho(1+e)^2T^{1/2}}{385\rho_p\sigma\pi^{1/2}\{16\eta^4+24\eta^2(1+2\lambda^4)+(5+4\lambda^2+8\lambda^4)^2\}} \\
& \times\Big[-\Big[\eta\{440\eta^6+6930(1+2\lambda^2)+2\eta^4(2125-928\lambda^2+1360\lambda^4) \\
& +\lambda^4(16137+16748\lambda^2+23146\lambda^4+2816\lambda^6+5040\lambda^8) \\
& +\eta^2(1683-6220\lambda^2+11196\lambda^4-576\lambda^6+5880\lambda^8)\}\cos 2\phi\Big]q_x \\
& +\Big[-8\eta^6(72-221\lambda^2)+2\eta^4(13379+5780\lambda^2-1352\lambda^4+2568\lambda^6) \\
& +(5+4\lambda^2+8\lambda^4)(6930+6930\lambda^2+14553\lambda^4+495\lambda^6-194\lambda^8+16\lambda^{10}) \\
& +\eta^2[38115+\lambda^2\{12573+8\lambda^2(10812+2651\lambda^2+4\lambda^4+881\lambda^6)\}] \\
& -\eta\{440\eta^6+6930(1+2\lambda^2)+2\eta^4(2125-928\lambda^2+1360\lambda^4) \\
& +\lambda^4(16137+16748\lambda^2+23146\lambda^4+2816\lambda^6+5040\lambda^8) \\
& +\eta^2(1683-6220\lambda^2+11196\lambda^4-576\lambda^6+5880\lambda^8)\}\sin 2\phi\Big]q_y\Big],
\end{aligned}
\tag{J.30}
$$

$$I^{(1)}_{z\beta\beta} = \frac{4\rho(1+e)^2T^{1/2}}{385\rho_p\sigma\pi^{1/2}(5+2\eta^2-8\lambda^2+14\lambda^4)}$$
$$\times\Bigg[\Big[6930-2\eta^4(10-23\lambda^2)-\lambda^2(13860-27027\lambda^2+7524\lambda^4+404\lambda^6+3482\lambda^8)$$
$$+\eta^2\{3465+12\lambda^2(3+\lambda^2)(11-7\lambda^2)\}\Big]q_z\Bigg], \tag{J.31}$$

$$I^{(2)}_{x\beta\beta} = \frac{8\rho(1+e)T^{1/2}}{385\rho_p\sigma\pi^{1/2}\{16\eta^4+24\eta^2(1+2\lambda^4)+(5+4\lambda^2+8\lambda^4)^2\}}$$
$$\times\Bigg[\Big[2600\eta^8+2\eta^6(1829+3164\lambda^2+14100\lambda^4)$$
$$-2\eta^4(16501-1365\lambda^2-24216\lambda^4-19336\lambda^6-36300\lambda^8)$$
$$-(5+4\lambda^2+8\lambda^4)(10010+10472\lambda^2+20823\lambda^4+1606\lambda^6-3174\lambda^8$$
$$+206\lambda^{10}-4980\lambda^{12})-\eta^2\{53537+2\lambda^2(9163+46074\lambda^2-18458\lambda^4$$
$$-61221\lambda^6-42092\lambda^8-44860\lambda^{10})\}-2\eta\{440(14+25\lambda^2)$$
$$-\eta^6(484+4240\lambda^2)+\eta^4(2926-3349\lambda^2+672\lambda^4-13440\lambda^6)$$
$$+\lambda^4(15994+7228\lambda^2+3614\lambda^4-26081\lambda^6-19416\lambda^8-6720\lambda^{10})$$
$$+2\eta^2(1375-5450\lambda^2-3990\lambda^4-13093\lambda^6-10610\lambda^8-12760\lambda^{10})\}\sin 2\phi\Big]q_x$$
$$+\Big[2\eta\{440(14+25\lambda^2)-\eta^6(484+4240\lambda^2)$$
$$+\eta^4(2926-3349\lambda^2+672\lambda^4-13440\lambda^6)$$
$$+\lambda^4(15994+7228\lambda^2+3614\lambda^4-26081\lambda^6-19416\lambda^8-6720\lambda^{10})$$
$$+2\eta^2(1375-5450\lambda^2-3990\lambda^4-13093\lambda^6-10610\lambda^8-12760\lambda^{10})\}\cos 2\phi\Big]q_y\Bigg], \tag{J.32}$$

$$I^{(2)}_{y\beta\beta} = \frac{8\rho(1+e)T^{1/2}}{385\rho_p\sigma\pi^{1/2}\{16\eta^4+24\eta^2(1+2\lambda^4)+(5+4\lambda^2+8\lambda^4)^2\}}$$
$$\times\Bigg[\Big[2\eta\{440(14+25\lambda^2)-\eta^6(484+4240\lambda^2)$$
$$+\eta^4(2926-3349\lambda^2+672\lambda^4-13440\lambda^6)$$
$$+\lambda^4(15994+7228\lambda^2+3614\lambda^4-26081\lambda^6-19416\lambda^8-6720\lambda^{10})$$
$$+2\eta^2(1375-5450\lambda^2-3990\lambda^4-13093\lambda^6-10610\lambda^8-12760\lambda^{10})\}\cos 2\phi\Big]q_x$$
$$+\Big[2600\eta^8+2\eta^6(1829+3164\lambda^2+14100\lambda^4)$$
$$-2\eta^4(16501-1365\lambda^2-24216\lambda^4-19336\lambda^6-36300\lambda^8)$$
$$-(5+4\lambda^2+8\lambda^4)(10010+10472\lambda^2+20823\lambda^4+1606\lambda^6-3174\lambda^8$$
$$+206\lambda^{10}-4980\lambda^{12})-\eta^2\{53537+2\lambda^2(9163+46074\lambda^2-18458\lambda^4$$
$$-61221\lambda^6-42092\lambda^8-44860\lambda^{10})\}+2\eta\{440(14+25\lambda^2)$$
$$-\eta^6(484+4240\lambda^2)+\eta^4(2926-3349\lambda^2+672\lambda^4-13440\lambda^6)$$
$$+\lambda^4(15994+7228\lambda^2+3614\lambda^4-26081\lambda^6-19416\lambda^8-6720\lambda^{10})$$
$$+2\eta^2(1375-5450\lambda^2-3990\lambda^4-13093\lambda^6-10610\lambda^8-12760\lambda^{10})\}\sin 2\phi\Big]q_y\Bigg], \tag{J.33}$$

$$I^{(2)}_{z\beta\beta} = \frac{8\rho(1+e)T^{1/2}}{385\rho_p\sigma\pi^{1/2}(5+2\eta^2-8\lambda^2+14\lambda^4)}$$
$$\times\Bigg[\Big[130\eta^6-154(65-136\lambda^2)+2\eta^4(139+241\lambda^2+885\lambda^4)$$
$$-\eta^2(4873-22\lambda^2-1580\lambda^4+428\lambda^6-5110\lambda^8)$$
$$-\lambda^4(39435-12650\lambda^2-14046\lambda^4+28598\lambda^6-34590\lambda^8)\Big]q_z\Bigg], \tag{J.34}$$

$$
\begin{aligned}
I^{(3)}_{x\beta\beta} = &-\frac{2\rho(1-e^2)T^{1/2}}{35\rho_p\sigma\pi^{1/2}\{16\eta^4+24\eta^2(1+2\lambda^4)+(5+4\lambda^2+8\lambda^4)^2\}} \\
&\times\Bigg[\Big[-24\eta^6(2-9\lambda^2)+2\eta^4(2161+840\lambda^2-24\lambda^4+376\lambda^6) \\
&\quad+3(5+4\lambda^2+8\lambda^4)(350+308\lambda^2+753\lambda^4-56\lambda^6+6\lambda^8-16\lambda^{10}) \\
&\quad+3\eta^2\{2063+4\lambda^2(155+1201\lambda^2+218\lambda^4+44\lambda^6+58\lambda^8)\} \\
&\quad+2\eta\{20\eta^6+30(7+26\lambda^2)+\eta^4(137-128\lambda^2+80\lambda^4) \\
&\quad-3\eta^2(97+220\lambda^2+14\lambda^4+80\lambda^6-60\lambda^8) \\
&\quad+3\lambda^4(13+220\lambda^2+347\lambda^4+16\lambda^6+120\lambda^8)\}\sin 2\phi\Big]q_x \\
&\quad-\Big[2\eta\{20\eta^6+30(7+26\lambda^2)+\eta^4(137-128\lambda^2+80\lambda^4) \\
&\quad-3\eta^2(97+220\lambda^2+14\lambda^4+80\lambda^6-60\lambda^8) \\
&\quad+3\lambda^4(13+220\lambda^2+347\lambda^4+16\lambda^6+120\lambda^8)\}\cos 2\phi\Big]q_y\Bigg],
\end{aligned}
\tag{J.35}
$$

$$
\begin{aligned}
I^{(3)}_{y\beta\beta} = &-\frac{2\rho(1-e^2)T^{1/2}}{35\rho_p\sigma\pi^{1/2}\{16\eta^4+24\eta^2(1+2\lambda^4)+(5+4\lambda^2+8\lambda^4)^2\}} \\
&\times\Bigg[-\Big[2\eta\{20\eta^6+30(7+26\lambda^2)+\eta^4(137-128\lambda^2+80\lambda^4) \\
&\quad-3\eta^2(97+220\lambda^2+14\lambda^4+80\lambda^6-60\lambda^8) \\
&\quad+3\lambda^4(13+220\lambda^2+347\lambda^4+16\lambda^6+120\lambda^8)\}\cos 2\phi\Big]q_x \\
&\quad+\Big[-24\eta^6(2-9\lambda^2)+2\eta^4(2161+840\lambda^2-24\lambda^4+376\lambda^6) \\
&\quad+3(5+4\lambda^2+8\lambda^4)(350+308\lambda^2+753\lambda^4-56\lambda^6+6\lambda^8-16\lambda^{10}) \\
&\quad+3\eta^2\{2063+4\lambda^2(155+1201\lambda^2+218\lambda^4+44\lambda^6+58\lambda^8)\} \\
&\quad-2\eta\{20\eta^6+30(7+26\lambda^2)+\eta^4(137-128\lambda^2+80\lambda^4) \\
&\quad-3\eta^2(97+220\lambda^2+14\lambda^4+80\lambda^6-60\lambda^8) \\
&\quad+3\lambda^4(13+220\lambda^2+347\lambda^4+16\lambda^6+120\lambda^8)\}\sin 2\phi\Big]q_y\Bigg],
\end{aligned}
\tag{J.36}
$$

$$I^{(3)}_{z\beta\beta} = -\frac{2\rho(1-e^2)T^{1/2}}{35\rho_p\sigma\pi^{1/2}(5+2\eta^2-8\lambda^2+14\lambda^4)} \times \Big[\Big[\eta^4(4+22\lambda^2)+3\eta^2(187+74\lambda^2+4\lambda^6) + 3(350-616\lambda^2+1329\lambda^4-218\lambda^6-12\lambda^8-118\lambda^{10})\Big]q_z\Big]. \tag{J.37}$$

Inserting the above integrals into (J.3), we obtain the following expression for the third order source term

$$\aleph_{\alpha\beta\beta} = I^{(1)}_{\alpha\beta\beta} + I^{(2)}_{\alpha\beta\beta} + I^{(3)}_{\alpha\beta\beta} = -\frac{2\rho(1+e)\sqrt{T}}{385\rho_p\sigma\sqrt{\pi}}\mathfrak{Q}_{\alpha\gamma}q_\gamma, \tag{J.38}$$

as in (3.161) in the main text, where q_γ is the heat flux and $\mathfrak{Q}_{\alpha\gamma}$ is a second-rank tensor whose elements are explicitly given in 3.12.2.

Appendix K

Integral Expression for Collisional Flux of Momentum ($\Theta_{\alpha\beta}$)

The collisional flux of momentum can be expressed as:

$$\begin{aligned}\Theta_{\alpha\beta} &= \Theta_{\alpha}[mC_{\beta}] \\ &= \frac{m(1+e)\sigma^3}{4}\int\int\int_{\boldsymbol{g}\cdot\boldsymbol{k}>0}(\boldsymbol{g}\cdot\boldsymbol{k})^2 k_{\alpha}k_{\beta}\int_0^1 f^{(2)}(\boldsymbol{c}_1,\boldsymbol{x}-\omega\sigma\boldsymbol{k},\boldsymbol{c}_2,\boldsymbol{x}+\sigma\boldsymbol{k}-\omega\sigma\boldsymbol{k})d\omega d\boldsymbol{k}d\boldsymbol{c}_1 d\boldsymbol{c}_2.\end{aligned} \tag{K.1}$$

Using the assumption of molecular chaos on $f^{(2)}$ and applying Taylor series expansion on $f^{(1)}$ along with change of variables from $\boldsymbol{c}_1$, $\boldsymbol{c}_2$, ω to $\boldsymbol{g}=\boldsymbol{c}_1-\boldsymbol{c}_2$, $\boldsymbol{G}=(\boldsymbol{C}_1+\boldsymbol{C}_2)/2$, $\omega = 1/2-\varepsilon(d\boldsymbol{c}_1 d\boldsymbol{c}_2 = d\boldsymbol{g}d\boldsymbol{G})$ we have

$$\begin{aligned}f^{(2)}(\boldsymbol{c}_1,\boldsymbol{x}-\omega\sigma\boldsymbol{k},\boldsymbol{c}_2,\boldsymbol{x}+\sigma\boldsymbol{k}-\omega\sigma\boldsymbol{k}) &= f^{(2)}\left(\boldsymbol{c}_1,\boldsymbol{x}+(\varepsilon-\frac{1}{2})\sigma\boldsymbol{k},\boldsymbol{c}_2,\boldsymbol{x}+(\varepsilon+\frac{1}{2})\sigma\boldsymbol{k}\right) \\ &= \frac{n^2 g_0}{8\pi^3|\boldsymbol{M}|}\exp\left\{-\frac{1}{4}\boldsymbol{M}^{-1}_{\alpha\beta}[(g_{\alpha}+V_{\alpha})(g_{\beta}+V_{\beta})+4(G_{\alpha}-\varepsilon V_{\alpha})(G_{\beta}-\varepsilon V_{\beta})]\right\},\end{aligned} \tag{K.2}$$

where

$$\boldsymbol{V}=\sigma\boldsymbol{k}\cdot\nabla\boldsymbol{u}. \tag{K.3}$$

Expression (K.2) is exact for simple shear. From (K.1) and (K.2), we arrive at

$$\Theta_{\alpha\beta} = \frac{m(1+e)n^2 g_0 \sigma^3}{32\pi^3|\boldsymbol{M}|} \int\int_{\boldsymbol{g}\cdot\boldsymbol{k}>0} (\boldsymbol{g}\cdot\boldsymbol{k})^2 k_\alpha k_\beta \exp\Big\{-\frac{1}{4}[(g_\alpha + V_\alpha)\boldsymbol{M}^{-1}_{\alpha\beta}(g_\beta + V_\beta)]\Big\}$$
$$\times\Big(\int_{-\frac{1}{2}}^{\frac{1}{2}}\int \exp\Big\{-[(G_\alpha - \varepsilon V_\alpha)\boldsymbol{M}^{-1}_{\alpha\beta}(G_\beta - \varepsilon V_\beta)]\Big\} d\boldsymbol{G}d\varepsilon\Big) d\boldsymbol{k}d\boldsymbol{g}. \quad \text{(K.4)}$$

Using the following identity

$$\int_{-\frac{1}{2}}^{\frac{1}{2}}\int \exp\Big\{-[(G_\alpha - \xi V_\alpha)\boldsymbol{M}^{-1}_{\alpha\beta}(G_\beta - \xi V_\beta)]\Big\} d\boldsymbol{G}d\xi = \pi^{\frac{3}{2}}\sqrt{T^3(\xi+1)(\varsigma+1)(\zeta+1)}$$
$$= \pi^{\frac{3}{2}}|\boldsymbol{M}|^{\frac{1}{2}}, \quad \text{(K.5)}$$

and carrying out the integration over $\boldsymbol{G}$ and ξ, we have

$$\Theta_{\alpha\beta} = \frac{\rho n(1+e)g_0\sigma^3}{32\pi^{\frac{3}{2}}|\boldsymbol{M}|^{\frac{1}{2}}} \int\int_{\boldsymbol{g}\cdot\boldsymbol{k}>0} (\boldsymbol{g}\cdot\boldsymbol{k})^2 k_\alpha k_\beta \exp\Big\{-\frac{1}{4}[(g_\alpha + V_\alpha)\boldsymbol{M}^{-1}_{\alpha\beta}(g_\beta + V_\beta)]\Big\} d\boldsymbol{k}d\boldsymbol{g}. \quad \text{(K.6)}$$

In terms of the function $\mathfrak{G}$ of $\chi \equiv \boldsymbol{V}\cdot\boldsymbol{k}/2\sqrt{(\boldsymbol{k}\cdot\boldsymbol{M}\cdot\boldsymbol{k})}$, (see Araki & Tremaine (1986); Jenkins & Richman (1988))

$$\mathfrak{G}(\chi) \equiv \pi^{\frac{1}{2}}(\frac{1}{2} + \chi^2)\mathrm{erfc}(\chi) - \chi\exp(-\chi^2), \quad \text{(K.7)}$$

the compact form for $\Theta_{\alpha\beta}$ (after integrating over $\boldsymbol{g}$) is found to be

$$\Theta_{\alpha\beta} = \frac{3(1+e)\rho\nu g_0}{\pi^{\frac{3}{2}}} \int k_\alpha k_\beta (\boldsymbol{k}\cdot\mathbf{M}\cdot\boldsymbol{k})\mathfrak{G}d\boldsymbol{k}, \quad \text{(K.8)}$$

the required expression for the collisional contribution of the stress tensor.

Appendix L

Integral Expression for Collisional Source of Second Moment ($\aleph_{\alpha\beta}$)

$$\aleph_{\alpha\beta} = \frac{m}{2}\int\int\int_{\boldsymbol{g}\cdot\boldsymbol{k}>0} \Delta(C_\alpha C_\beta) f^{(2)}(\boldsymbol{c}_1, \boldsymbol{x}-\sigma\boldsymbol{k}, \boldsymbol{c}_2, \boldsymbol{x})\sigma^2(\boldsymbol{g}\cdot\boldsymbol{k})d\boldsymbol{k}d\boldsymbol{c}_1 d\boldsymbol{c}_2, \tag{L.1}$$

$$\Delta(C_\alpha C_\beta) = -\frac{1}{2}(1+e)(\boldsymbol{g}\cdot\boldsymbol{k})[(1-e)(\boldsymbol{g}\cdot\boldsymbol{k})k_\alpha k_\beta + (\boldsymbol{g}\cdot\boldsymbol{j})(k_\alpha j_\beta + j_\alpha k_\beta)], \tag{L.2}$$

here $\boldsymbol{j}$ is the unit vector perpendicular to $\boldsymbol{k}$, that lies in the plane formed by $\boldsymbol{k}$ and $\boldsymbol{g}$. Using the Taylor series expansion and the molecular chaos assumption we can write

$$f^{(2)}(\boldsymbol{c}_1, \boldsymbol{x}-\sigma\boldsymbol{k}, \boldsymbol{c}_2, \boldsymbol{x}) = \frac{n^2 g_0}{8\pi^3|\boldsymbol{M}|}\exp\left\{-\frac{1}{2}\boldsymbol{M}^{-1}_{\alpha\beta}[(C_\alpha+V_\alpha)(C_\beta+V_\beta)+C_\alpha C_\beta]\right\}, \tag{L.3}$$

Changing the variables of integration from $\boldsymbol{c}_1$, $\boldsymbol{c}_2$ to $\boldsymbol{g} = \boldsymbol{c}_1 - \boldsymbol{c}_2$, $\boldsymbol{G} = (\boldsymbol{C}_1 + \boldsymbol{C}_2)/2$

$$\begin{aligned} &f^{(2)}(\boldsymbol{c}_1, \boldsymbol{x}-\sigma\boldsymbol{k}, \boldsymbol{c}_2, \boldsymbol{x}) \\ &\quad = \frac{n^2 g_0}{8\pi^3|\boldsymbol{M}|}\exp\left\{-\frac{1}{4}\boldsymbol{M}^{-1}_{\alpha\beta}[(g_\alpha+V_\alpha)(g_\beta+V_\beta)+(2G_\alpha+V_\alpha)(2G_\beta+V_\beta)]\right\}. \end{aligned} \tag{L.4}$$

Therefore

$$\aleph_{\alpha\beta} = -\frac{m(1+e)n^2 g_0 \sigma^2}{32\pi^3 |\boldsymbol{M}|} \int\int\int_{\boldsymbol{g}\cdot\boldsymbol{k}>0} [(1-e)(\boldsymbol{g}\cdot\boldsymbol{k})^3 k_\alpha k_\beta + (\boldsymbol{g}\cdot\boldsymbol{k})^2(\boldsymbol{g}\cdot\boldsymbol{j})(k_\alpha j_\beta + j_\alpha k_\beta)] \tag{L.5}$$

$$\exp\left\{-\frac{1}{4}\boldsymbol{M}^{-1}_{\alpha\beta}[(g_\alpha + V_\alpha)(g_\beta + V_\beta) + (2G_\alpha + V_\alpha)(2G_\beta + V_\beta)]\right\} d\boldsymbol{G} d\boldsymbol{g} d\boldsymbol{k}.$$

Using the following identity

$$\int \exp\left\{-\frac{1}{4}[(2G_\alpha + V_\alpha)\boldsymbol{M}^{-1}_{\alpha\beta}(2G_\beta + V_\beta)]\right\} d\boldsymbol{G} \equiv \pi^{\frac{3}{2}} |\boldsymbol{M}|^{\frac{1}{2}} \tag{L.6}$$

and carrying out the integration over $\boldsymbol{G}$, we have

$$\aleph_{\alpha\beta} = -\frac{m(1+e)n^2 g_0 \sigma^2}{32\pi^{\frac{3}{2}} |\boldsymbol{M}|^{\frac{1}{2}}} \int\int_{\boldsymbol{g}\cdot\boldsymbol{k}>0} [(1-e)(\boldsymbol{g}\cdot\boldsymbol{k})^3 k_\alpha k_\beta + (\boldsymbol{g}\cdot\boldsymbol{k})^2(\boldsymbol{g}\cdot\boldsymbol{j})(k_\alpha j_\beta + j_\alpha k_\beta)]$$
$$\times \exp\{-\frac{1}{4}[(g_\alpha + V_\alpha)\boldsymbol{M}^{-1}_{\alpha\beta}(g_\beta + V_\beta)]\} d\boldsymbol{k} d\boldsymbol{g}. \tag{L.7}$$

After performing the integration over $\boldsymbol{g}$, we obtain the following expression for the collisional source of second moment as (see Chou & Richman (1998))

$$\aleph_{\alpha\beta} = \Gamma_{\alpha\beta} + \Theta_{\alpha\delta} W_{\beta\delta} + \Theta_{\beta\delta} W_{\alpha\delta}, \tag{L.8}$$

where

$$\Gamma_{\alpha\beta} = A_{\alpha\beta} + \widehat{E}_{\alpha\beta} + \widehat{G}_{\alpha\beta}, \tag{L.9}$$

and the integral expressions of $A_{\alpha\beta}$, $\widehat{E}_{\alpha\beta}$ and $\widehat{G}_{\alpha\beta}$ are given in (3.55)-(3.57).

Appendix M

Uniform Shear Flow of Inelastic Disks: The Planar Analogue

In this section we derive an analytical solution at Burnett order for the uniform shear flow of identical disks. The number of parameters that are required to completely analyse the flow reduce to three viz. *i*) the temperature anisotropy (η), *ii*) the Savage-Jeffrey parameter (R) and *iii*) the non-coaxiality angle (ϕ). This work is the two-dimensional manifestation of the flow of spheres discussed in this chapter. We project the 3-d schematic of the co-ordinate reference displayed in figure 3.2 onto the *x*-*y* plane of motion as shown in figure M.1.

In this case the second moment of velocity fluctuations takes the form

$$\boldsymbol{M} \equiv T \begin{bmatrix} 1+\eta\sin 2\phi & -\eta\cos 2\phi \\ -\eta\cos 2\phi & 1-\eta\sin 2\phi \end{bmatrix} = T[\delta_{\alpha\beta}] + \widehat{\boldsymbol{M}}, \tag{M.1}$$

where η, T and ϕ have the same interpretations as in 3-d. The planar analogue of the anisotropic distribution function and the radial distribution function (Verlet & Levesque 1982) are

$$f(\boldsymbol{c},\boldsymbol{x},t) = \frac{n}{2\pi|\boldsymbol{M}|^{\frac{1}{2}}}\exp\left(-\frac{1}{2}\boldsymbol{C}\cdot\boldsymbol{M}^{-1}\cdot\boldsymbol{C}\right), \tag{M.2}$$

$$g_0(\nu) = \frac{(1-7\nu/16)}{(1-\nu)^2}, \tag{M.3}$$

with ν $(=n\pi\sigma^2/4)$ being the area fraction (density) of particles.

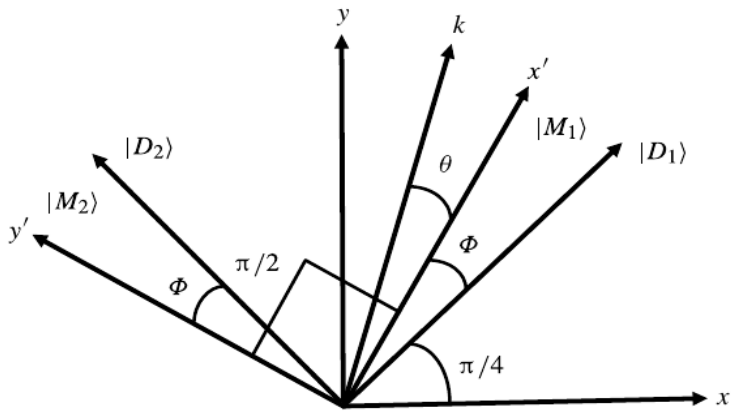

Fig. M.1 A sketch of the coordinate frame: $|D_1\rangle$ and $|D_2\rangle$ are the eigen-directions of the shear tensor $\boldsymbol{D}$, and $|M_1\rangle$ and $|M_2\rangle$ are the eigen-directions of the second moment tensor $\boldsymbol{M}$.

M.1 Burnett Order Analytical Solution for the Whole Range of Area Fraction

The second moment balance when truncated at second-order yields the related Burnett order equations

$$\left.\begin{aligned} 4\pi^{\frac{3}{2}}\eta R\cos 2\phi+(1+e)\nu g_0 R(16\pi R+2\pi^{\frac{3}{2}}\eta\cos 2\phi) &= \\ \nu g_0(1-e^2)(3\pi^{\frac{3}{2}}\eta R\cos 2\phi+2\pi+\tfrac{3}{8}\pi\eta^2+12\pi R^2) & \\ 4\pi^{\frac{3}{2}}R\cos 2\phi-(1+e)\nu g_0(2\pi\eta-2\pi^{\frac{3}{2}}R\cos 2\phi)=\nu g_0(1-e^2)(3\pi^{\frac{3}{2}}R\cos 2\phi+\tfrac{3}{2}\pi\eta) & \\ 4\pi^{\frac{3}{2}}R(\eta-\sin 2\phi)-2\pi^{\frac{3}{2}}(1+e)\nu g_0 R\sin 2\phi=-3\pi^{\frac{3}{2}}\nu g_0(1-e^2)R\sin 2\phi & \end{aligned}\right\}. \tag{M.4}$$

An analytical solution of the Burnett order equation is determined as a function of the coefficient of restitution (e), volume fraction (ν) and the radial distribution function (g_0). The solution we obtain looks like

$$\left.\begin{aligned} \tan(2\phi) &= \frac{8\sqrt{\pi}R}{(1+e)(7-3e)\nu g_0} \\ \eta &= \frac{1}{4}\Big\{4-(1+e)(1-3e)\nu g_0\Big\}\sin(2\phi) \end{aligned}\right\}, \tag{M.5}$$

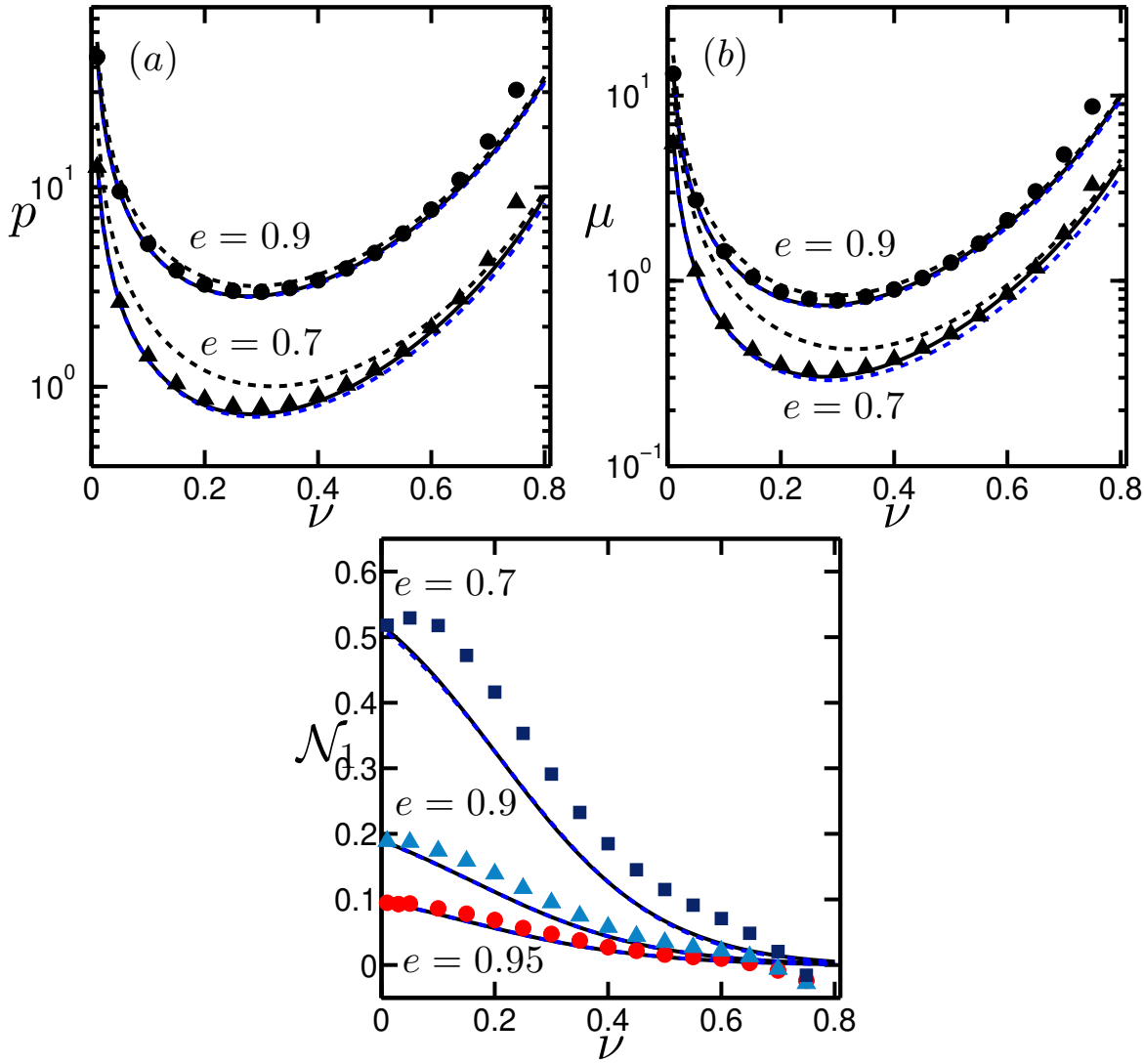

Fig. M.2 Comparison among (i) the full numerical solution (solid lines), (ii) Burnett order analytical solution (blue dashed lines) (ii) the Navier-Stokes model (black dashed lines, (Lutsko 2005)) and (iii) the simulation data (symbols, (Alam & Luding 2003*b*)) for the variation of (a) total pressure p and (b) shear viscosity μ with area fraction ν. Results for two values of the restitution coefficient ($e = 0.9$ and 0.7) are shown. In the second row variation of the scaled first normal stress difference $\mathcal{N}_1$ with area fraction ν is shown for three values of coefficients of restitution $e = 0.95, 0.9$ and 0.7 respectively.

where R satisfies

$$512(1+3e)\pi R^4 + \Big\{256(-1+e)\pi + 8(7-3e)^2(1+e)^2(1+3e)\nu^2 g_0^2 + (25-9e)\pi(4+(1+e)(-1+3e)\nu g_0)^2\Big\}R^2 + 4(7-3e)^2(-1+e)(1+e)^2\nu^2 g_0^2 = 0. \tag{M.6}$$

It must be noted that these solutions (M.5-M.6) are exact at second order, and hence differs from the "approximate" second-order solution of Saha & Alam (2014). The latter paper is attached at the end of this thesis.

Below we present the behaviours of the transport coefficients as obtained from Burnett-order analytical solution (M.5-M.6), full numerical solution and Navier-Stokes order hydrodynamics. The simulation results from Alam & Luding (2003*b*) are also superimposed.

For small dissipation $e = 0.9$, the analytical Burnett order solution (blue dashed lines) and the full numerical solution (solid lines) give rise to almost identical results, and it is almost impossible to distinguish these two results at least in naked eye. However at some moderate value at inelasticity $e = 0.7$ the Burnett-order solutions for shear viscosity (μ) slightly deviates from the full numerical solution for $\nu > 0.3$ nevertheless for first normal stress difference $(\mathscr{N}_1)$ the analytical Burnett order solution matches exactly with the numerical solution.

Supplementary Material

Saha & Alam (2014) J. Fluid Mech. 757, 251-296

J. Fluid Mech. (2014), *vol.* 757, *pp.* 251–296.
doi:10.1017/jfm.2014.489

Non-Newtonian stress, collisional dissipation and heat flux in the shear flow of inelastic disks: a reduction via Grad's moment method

Saikat Saha[1] **and Meheboob Alam**[1,†]

[1]Engineering Mechanics Unit, Jawaharlal Nehru Centre for Advanced Scientific Research, Jakkur P.O., Bangalore 560064, India

(Received 28 January 2014; revised 30 June 2014; accepted 21 August 2014)

The non-Newtonian stress tensor, collisional dissipation rate and heat flux in the plane shear flow of smooth inelastic disks are analysed from the Grad-level moment equations using the anisotropic Gaussian as a reference. For steady uniform shear flow, the balance equation for the second moment of velocity fluctuations is solved semi-analytically, yielding closed-form expressions for the shear viscosity μ, pressure p, first normal stress difference $\mathscr{N}_1$ and dissipation rate $\mathscr{D}$ as functions of (i) density or area fraction ν, (ii) restitution coefficient e, (iii) dimensionless shear rate R, (iv) temperature anisotropy η (the difference between the principal eigenvalues of the second-moment tensor) and (v) angle ϕ between the principal directions of the shear tensor and the second-moment tensor. The last two parameters are zero at the Navier–Stokes order, recovering the known exact transport coefficients from the present analysis in the limit $\eta, \phi \to 0$, and are therefore measures of the non-Newtonian rheology of the medium. An exact analytical solution for leading-order moment equations is given, which helped to determine the scaling relations of R, η and ϕ with inelasticity. We show that the terms at super-Burnett order must be retained for a quantitative prediction of transport coefficients, especially at moderate to large densities for small values of the restitution coefficient ($e \ll 1$). Particle simulation data for a sheared inelastic hard-disk system are compared with theoretical results, with good agreement for p, μ and $\mathscr{N}_1$ over a range of densities spanning from the dilute to close to the freezing point. In contrast, the predictions from a constitutive model at Navier–Stokes order are found to deviate significantly from both the simulation and the moment theory even at moderate values of the restitution coefficient ($e \sim 0.9$). Lastly, a generalized Fourier law for the granular heat flux, which vanishes identically in the uniform shear state, is derived for a dilute granular gas by analysing the non-uniform shear flow via an expansion around the anisotropic Gaussian state. We show that the gradient of the deviatoric part of the kinetic stress drives a heat current and the thermal conductivity is characterized by an anisotropic second-rank tensor, for which explicit analytical expressions are given.

Key words: granular media, kinetic theory, rheology

†Email address for correspondence: meheboob@jncasr.ac.in

1. Introduction

A driven system of macroscopic or non-Brownian particles (e.g. driven by external vibration or shearing) resembles a molecular gas in which the particles move around randomly but lose energy upon collision, with the latter being a major difference between a granular gas and its molecular counterpart. Such a non-equilibrium state of agitated particles is also known as a rapid granular fluid (Goldhirsch 2003), for which the dense-gas kinetic theory (Chapman & Cowling 1970) has been appropriately modified and successfully used for a variety of flow configurations over the past three decades (Savage & Jeffrey 1981; Jenkins & Richman 1985*a*,*b*; Brey *et al.* 1998; Sela & Goldhirsch 1998; Brilliantov & Pöschel 2004; Rao & Nott 2008). In this paper we investigate the non-Newtonian rheology of a sheared granular system via kinetic theory. For an N-particle system, the stress tensor has contributions from both kinetic and collisional mechanisms of transport:

$$\boldsymbol{P} = \boldsymbol{P}_{kin} + \boldsymbol{P}_{coll}. \tag{1.1}$$

The first mechanism is dominant in the dilute regime, whereas the second one dominates in the dense regime. This can be further decomposed as

$$\boldsymbol{P} = p\boldsymbol{I} + \widehat{\boldsymbol{P}}, \tag{1.2}$$

where $p \equiv P_{ii}/\mathrm{dim}$ is the isotropic pressure (dim is the dimension), $\boldsymbol{I}$ is the identity tensor and the deviatoric stress is $\widehat{\boldsymbol{P}}$. The off-diagonal components of $\widehat{\boldsymbol{P}}$ are related to shear viscosity, which, in general, depends on the deformation rate. At the Navier–Stokes (NS) order, the stress tensor is Newtonian (i.e. linear in the shear rate, with the proportionality constant being the shear viscosity) and its diagonal components are equal. The latter implies that the first and second normal stress differences, $\mathscr{N}_1 \sim P_{xx} - P_{yy}$ and $\mathscr{N}_2 \sim P_{yy} - P_{zz}$, respectively, are identically zero. The non-zero normal stresses and/or the shear-rate dependence of viscosity are signatures of the non-Newtonian rheology of the medium. In kinetic theory, the normal stresses appear at the Burnett order (Burnett 1935; Grad 1949; Chapman & Cowling 1970) and hence cannot be taken into account in the standard NS-order hydrodynamic equations. Higher-order theories such as the Burnett equations (Burnett 1935; Sela & Goldhirsch 1998) or Grad's 13-moment equations (Grad 1949; Jenkins & Richman 1985*a*,*b*; Torrilhon & Struchtrup 2004) should therefore be used to correctly model the nonlinear rheology of granular fluids. Although the rest state of the Burnett equations is known to be unstable for molecular gases, there are ways to regularize these equations (Rosenau 1989). Moreover, it has been established recently (Santos 2008) that the partial sum of the shear stress converges in the uniform shear of a granular fluid, with its radius of convergence increasing with increasing dissipation or inelasticity. On the other hand, in Grad's method the distribution function is expanded in a Hermite series around the local Maxwellian of thermal equilibrium, and the moment equations for an extended set of hydrodynamic fields are written down.

The sheared granular fluid is known to possess finite normal stress differences for the whole range of densities (Sela & Goldhirsch 1998; Alam & Luding 2003*a*,*b*, 2005*a*,*b*) and the rate dependence of viscosity seems to be an inherent feature of the uniform shear state of a granular fluid (Santos, Garzo & Dufty 2004). Figure 1 indicates that the first normal stress difference is finite in a sheared granular fluid for a range of densities and its magnitude increases with increasing dissipation. Detailed

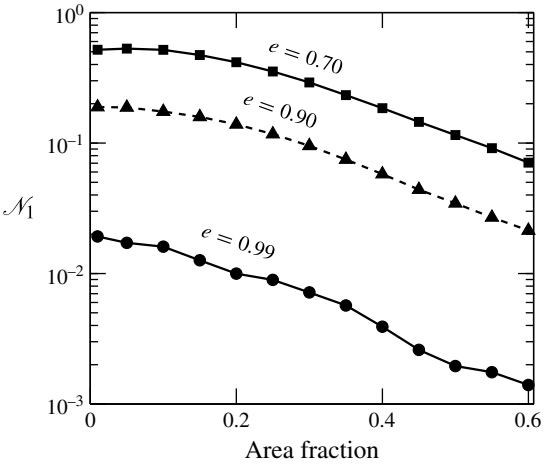

FIGURE 1. Variation of the first normal stress difference $\mathscr{N}_1 = 2(P_{xx} - P_{yy})/(P_{xx} + P_{yy})$ (see (4.21)) with area fraction of particles for different values of the restitution coefficient e. Data (symbols) correspond to event-driven simulations (Alam & Luding 2003*a*,*b*) for a sheared system of smooth inelastic hard disks with Lees–Edward boundary condition (see § 5.2 for details); lines are drawn to guide the eye.

simulations in two dimensions, i.e. for disks (Alam & Luding 2003*a*,*b*), and three dimensions, i.e. for spheres (Alam & Luding 2005*a*,*b*), have uncovered the following distinguishing features of normal stresses in a sheared granular fluid: (i) the first normal stress difference is positive in the dilute limit and undergoes a sign reversal at a finite density near the freezing point (depending on dissipation) in the dense limit; and (ii) the second normal stress difference is negative in the dilute limit and becomes positive beyond a moderate density. Both theory and simulation suggest that the magnitudes of the first and second normal stress differences increase with increasing dissipation.

Large normal stresses, such as those in figure 1, must be taken into account to correctly model a dissipative granular fluid in the rapid shear regime. Jenkins & Richman (1988) have incorporated normal stresses in their study of steady uniform shear flow (USF) of inelastic disks, following earlier kinetic theory work of Goldreich & Tremaine (1978) and Araki & Tremaine (1986) that used the anisotropic Gaussian as a reference state. They solved the second-moment balance equation in the two extreme limits of density, and derived analytical results for the stress tensor in dilute and dense flows, but the solutions for the full range of densities remain unexplored for the shear flow of inelastic disks. Chou & Richman (1998) analysed the USF of inelastic spheres and provided numerical solutions for the stress tensor for the full range of densities. More recently, Lutsko (2004) used an arbitrary Gaussian as a reference to solve the Enskog equation for a polydisperse mixture of inelastic hard spheres via the Hermite expansion (Grad 1949) around the anisotropic reference state, and the related kinetic integrals were simplified using a generating function technique. Focusing attention on the uniform shear state, he evaluated the stress tensor numerically and confirmed the previous numerical results of Chou & Richman (1998). It was further shown that the moment theory predictions for normal stress differences agree well with those obtained from the direct simulation Monte Carlo (DSMC) solution of the Enskog equation for a range of densities but can differ considerably

from molecular dynamics simulations of the same system for moderately dense binary mixtures. The reason for the latter disagreement remains unclear. It would greatly help our understanding of the nonlinear and non-Newtonian rheology of particulate media if such higher-order theories could be tackled analytically or semi-analytically to obtain closed-form constitutive relations – this forms the primary motivation of the present work.

In this paper, we derive closed-form analytical expressions for all components of the stress tensor as well as the collisional dissipation rate of steady USF for the whole range of densities by considering terms up to super-Burnett order (i.e. third order in shear rate and temperature anisotropy). To achieve the above goal, we follow the anisotropic version of Grad's moment method (Jenkins & Richman 1988) and solve the balance equation for the second-moment of velocity fluctuations semi-analytically for the USF of smooth inelastic hard disks. In addition, we generalize this method for the non-uniform shear state and derive an explicit constitutive relation for heat flux. Our primary focus is to decipher an analytical understanding of how all the transport coefficients (shear viscosity, pressure and first normal stress difference) depend on different control parameters (e.g. density, restitution coefficient, shear rate, etc.) when one goes beyond the 'linear' NS regime via Grad's moment equations. Our second goal is to check whether the resulting moment theory can yield quantitative predictions for normal stress differences and other transport coefficients for the whole range of densities and restitution coefficients (e.g. at small values of the restitution coefficient). Both goals are achieved successfully from our super-Burnett-order constitutive relations as demonstrated in § 4. Furthermore, the validation of the derived nonlinear constitutive relations, via a comparison with molecular dynamics simulations (§ 5), at different densities confirms the appropriateness of the Enskog kinetic equation to describe the dense shear flow of inelastic hard disks.

The rest of this paper is organized as follows. Section 2 provides a brief overview of the kinetic theory, the Grad-level (second or higher order in gradients) hydrodynamic equations and the anisotropic Gaussian distribution function. The construction of the second-moment tensor and its anisotropy in the USF, and the formulation of the second-moment equation in a rotated coordinate frame, are described in § 3. The collision integrals in the moment equations are approximated by an infinite series as outlined in § 4, followed by the explicit forms of resulting moment equations at Burnett and super-Burnett orders. An exact analytical solution for 'leading-order' moment equations is derived in § 4.1. The super-Burnett-order expressions for all components of the stress tensor, along with shear viscosity, pressure and first normal stress difference, are discussed in § 4.2. That the Grad-level dissipation rate depends on both the shear rate and the temperature anisotropy is discussed in § 4.3. The degenerate nature of the uniform shear state is discussed in § 4.4 in terms of its inherent 'non-Newtonian' rheology. The accuracy of our super-Burnett-order constitutive relations is verified in § 5.1 via a comparison with the full numerical solution. In addition to comparing with the molecular dynamics simulation data, § 5.2 establishes the superior predictions of the present moment theory with respect to an NS-order constitutive model (Lutsko 2005; Garzo, Santos & Montanero 2007). A comparative discussion of our results with another Grad-level theory (Kremer & Marques 2011; Garzo 2012) as well as with a Chapman–Enskog-based Burnett-order theory (Sela, Goldhirsch & Noskowicz 1996) for a dilute system is made in § 5.3. In § 6 we consider the non-uniform shear state and outline a procedure to derive the constitutive relation for the 'non-Fourier' heat flux. The conclusions are given in § 7.

2. Overview of Enskog kinetic theory and Grad-level moment equations

Let us consider a dense granular gas consisting of N randomly moving smooth inelastic hard disks of diameter σ and mass m. Let $\boldsymbol{c}_1$ and $\boldsymbol{c}_2$ be the velocities of two disks before a collision, with $\boldsymbol{c}_1'$ and $\boldsymbol{c}_2'$ being their post-collisional velocities, respectively. The collision dynamics for instantaneous and binary collisions is governed by

$$(\boldsymbol{g}' \cdot \boldsymbol{k}) = -e(\boldsymbol{g} \cdot \boldsymbol{k}), \tag{2.1}$$

where $\boldsymbol{g} \equiv \boldsymbol{g}_{12} = \boldsymbol{c}_1 - \boldsymbol{c}_2$ and $\boldsymbol{g}' = \boldsymbol{c}_1' - \boldsymbol{c}_2'$ are the pre- and post-collisional relative velocities, respectively, and $\boldsymbol{k} \equiv \boldsymbol{k}_{12} = (\boldsymbol{x}_2 - \boldsymbol{x}_1)/|\boldsymbol{x}_2 - \boldsymbol{x}_1|$ is the unit contact vector joining the centre of disk 1 to that of disk 2 at collision. In (2.1), e is the coefficient of normal restitution, with $e = 1$ and 0 referring to perfectly elastic and sticking collisions, respectively. Since the disks are assumed to be smooth, there is no change in their tangential component of relative velocity (i.e. $\boldsymbol{k} \times \boldsymbol{g}' = \boldsymbol{k} \times \boldsymbol{g}$).

At the mesoscopic level, this system is described by the Liouville equation for an N-particle distribution function, which can be reduced to an infinite hierarchy of evolution equations of distribution functions (one-body, two-body, three-body, etc.), known as the BBGKY (for Bogoliubov–Born–Green–Kirkwood–Yvon) hierarchy (Chapman & Cowling 1970). The first member of this hierarchy deals with the evolution of the single-particle distribution function $f(\boldsymbol{c}, \boldsymbol{x}, t)$, which, in the absence of any body force, reads

$$\left(\frac{\partial}{\partial t} + \boldsymbol{c} \cdot \boldsymbol{\nabla}\right) f = J(f^{(2)}), \tag{2.2}$$

where $\boldsymbol{\nabla}$ is the gradient operator in the configuration space and $J(f^{(2)})$ is the collision integral, which that depends on the two-particle distribution function $f^{(2)}(\boldsymbol{c}_1, \boldsymbol{x}_1, \boldsymbol{c}_2, \boldsymbol{x}_2, t)$. The transition from the mesoscopic to the macroscopic level is made via the hydrodynamic or coarse-grained fields, which are nothing but the moments of $f(\boldsymbol{c}, \boldsymbol{x}, t)$ of various orders. In addition to (i) the mass density

$$\rho(\boldsymbol{x}, t) \equiv m\, n(\boldsymbol{x}, t) = m \int f(\boldsymbol{c}, \boldsymbol{x}, t)\, \mathrm{d}\boldsymbol{c}, \tag{2.3}$$

where $n(\boldsymbol{x}, t) = N/V$ is the number density of particles, and (ii) the coarse-grained velocity

$$\boldsymbol{u}(\boldsymbol{x}, t) \equiv \langle \boldsymbol{c} \rangle = \frac{1}{n(\boldsymbol{x}, t)} \int \boldsymbol{c} f(\boldsymbol{c}, \boldsymbol{x}, t)\, \mathrm{d}\boldsymbol{c}, \tag{2.4}$$

we choose (iii) the full second-moment tensor

$$\boldsymbol{M}(\boldsymbol{x}, t) \equiv \langle \boldsymbol{C}\boldsymbol{C} \rangle = \frac{1}{n(\boldsymbol{x}, t)} \int \boldsymbol{C}\boldsymbol{C} f(\boldsymbol{c}, \boldsymbol{x}, t)\, \mathrm{d}\boldsymbol{c}, \tag{2.5}$$

where $\boldsymbol{C} \equiv \boldsymbol{c} - \boldsymbol{u}$ is the peculiar or fluctuation velocity of the particles, as a separate hydrodynamic field. The trace of (2.5) is the granular temperature

$$T(\boldsymbol{x}, t) \equiv \left\langle \frac{1}{2} \boldsymbol{C} \cdot \boldsymbol{C} \right\rangle = \frac{1}{2n(\boldsymbol{x}, t)} \int \boldsymbol{C}^2 f(\boldsymbol{c}, \boldsymbol{x}, t)\, \mathrm{d}\boldsymbol{c}, \tag{2.6}$$

which constitutes a hydrodynamic field at the NS order. Note that this definition of temperature (2.6) is commonly used in the granular mechanics community (Savage & Jeffrey 1981; Jenkins & Richman 1985*a*,*b*; Goldhirsch 2003; Rao & Nott 2008),

although the usual definition (Chapman & Cowling 1970) incorporating the mass m and the Boltzmann constant k_B has also been adopted by many (Brilliantov & Pöschel 2004; Santos *et al.* 2004; Lutsko 2005). In either case, it must be noted that the granular temperature is not a thermodynamic temperature (Goldhirsch 2003).

The evolution equations for hydrodynamic fields are obtained from the kinetic equation (2.2) by multiplying it by a particle property $\psi = \psi(\boldsymbol{c})$ and integrating it over the velocity space, resulting in the following master balance equation:

$$\frac{\partial}{\partial t}\langle n\psi\rangle = -\boldsymbol{\nabla}\cdot\langle n\boldsymbol{c}\psi\rangle + \mathfrak{C}[\psi]. \tag{2.7}$$

Here

$$\left.\begin{aligned}\mathfrak{C}[\psi] &= \iiint_{\boldsymbol{g}\cdot\boldsymbol{k}>\boldsymbol{0}} (\psi_2' - \psi_2) f^{(2)}(\boldsymbol{c}_1, \boldsymbol{x} - \sigma\boldsymbol{k}, \boldsymbol{c}_2, \boldsymbol{x}, t)\, \sigma\,(\boldsymbol{k}\cdot\boldsymbol{g})\, \mathrm{d}\boldsymbol{k}\, \mathrm{d}\boldsymbol{c}_1\, \mathrm{d}\boldsymbol{c}_2 \\ &= \iiint_{\boldsymbol{g}\cdot\boldsymbol{k}>\boldsymbol{0}} (\psi_1' - \psi_1) f^{(2)}(\boldsymbol{c}_1, \boldsymbol{x}, \boldsymbol{c}_2, \boldsymbol{x} + \sigma\boldsymbol{k}, t)\, \sigma\,(\boldsymbol{k}\cdot\boldsymbol{g})\, \mathrm{d}\boldsymbol{k}\, \mathrm{d}\boldsymbol{c}_1\, \mathrm{d}\boldsymbol{c}_2\end{aligned}\right\} \tag{2.8}$$

is the collisional rate of production of ψ per unit area, with $\boldsymbol{g}\cdot\boldsymbol{k} > 0$ referring to the constraint of impending collisions. It is straightforward to decompose (2.8) into the form (Jenkins & Richman 1985*a*,*b*; Rao & Nott 2008)

$$\mathfrak{C}[\psi] = \aleph[\psi] - \boldsymbol{\nabla}\cdot\boldsymbol{\Theta}[\psi] - \boldsymbol{\Theta}\left[\frac{\partial\psi}{\partial\boldsymbol{C}}\right] : \boldsymbol{\nabla}\boldsymbol{u}, \tag{2.9}$$

where $\boldsymbol{\Theta}[\psi]$ and $\aleph[\psi]$ are the collisional flux and production or source terms, respectively, whose integral expressions are given in §§ A.1 and A.2, respectively. Note that the origin of the collisional flux $\boldsymbol{\Theta}[\psi]$ is tied to the excluded volume of the 'macroscopic' particles and hence this term vanishes for a 'dilute' system of point particles. Combining (2.9) and (2.7), the master balance equation simplifies to (Jenkins & Richman 1985*a*,*b*, 1988)

$$\frac{\partial}{\partial t}\langle n\psi\rangle = -\left\langle n\left(\frac{\partial}{\partial t} + \boldsymbol{c}\cdot\boldsymbol{\nabla}\right) u_\alpha \frac{\partial\psi}{\partial C_\alpha}\right\rangle - \boldsymbol{\nabla}\cdot(\langle n\boldsymbol{c}\psi\rangle + \boldsymbol{\Theta}[\psi]) - \boldsymbol{\Theta}\left[\frac{\partial\psi}{\partial\boldsymbol{C}}\right] : \boldsymbol{\nabla}\boldsymbol{u} + \aleph[\psi]. \tag{2.10}$$

Substituting $\psi = 1$, c_α and $C_\alpha C_\beta$ into (2.10), we obtain the balance equations

$$\frac{\mathrm{D}\rho}{\mathrm{D}t} = -\rho u_{\alpha,\alpha}, \tag{2.11}$$

$$\rho\frac{\mathrm{D}u_\alpha}{\mathrm{D}t} = -P_{\alpha\beta,\alpha}, \tag{2.12}$$

$$\rho\frac{\mathrm{D}M_{\alpha\beta}}{\mathrm{D}t} = -Q_{\gamma\alpha\beta,\gamma} - P_{\delta\beta}u_{\alpha,\delta} - P_{\delta\alpha}u_{\beta,\delta} + \aleph_{\alpha\beta}, \tag{2.13}$$

for the mass, momentum and second moment, respectively. In the above, $\mathrm{D}/\mathrm{D}t = \partial/\partial t + u_\alpha(\partial/\partial x_\alpha)$ is the convective derivative, the subscript following a comma denotes a partial derivative (i.e. $u_{\alpha,\alpha} \equiv \partial u_\alpha/\partial x_\alpha$) with Einstein's summation convention over

repeated indices, and

$$P_{\alpha\beta} = \rho\langle \boldsymbol{C}_\alpha \boldsymbol{C}_\beta\rangle + \Theta_\alpha[mC_\beta] \equiv \rho M_{\alpha\beta} + \Theta_{\alpha\beta}, \tag{2.14}$$

$$Q_{\gamma\alpha\beta} = \rho\langle C_\gamma C_\alpha C_\beta\rangle + \Theta_\gamma[mC_\alpha C_\beta] \equiv \rho M_{\gamma\alpha\beta} + \Theta_{\gamma\alpha\beta}, \tag{2.15}$$

$$\aleph_{\alpha\beta} = \aleph[mC_\alpha C_\beta] \tag{2.16}$$

are the total stress tensor (momentum flux), the flux of the second moment, and the collisional source of the second moment (dissipation), respectively. In (2.14) and (2.15), the first term represents the kinetic contribution and the second term is its collisional contribution.

The trace of (2.13) yields the well-known balance equation for granular energy,

$$\rho\frac{\mathrm{D}T}{\mathrm{D}t} = -q_{\alpha,\alpha} - P_{\alpha\beta}u_{\beta,\alpha} - \mathscr{D}, \tag{2.17}$$

where

$$\mathscr{D} \equiv -\tfrac{1}{2}\aleph_{\beta\beta} = -\tfrac{1}{2}\aleph[mC^2] \tag{2.18}$$

is the rate of dissipation of energy per unit area (i.e. in two dimensions) and

$$q_\alpha \equiv \tfrac{1}{2}Q_{\alpha\beta\beta} = \tfrac{1}{2}\rho M_{\alpha\beta\beta} + \tfrac{1}{2}\Theta_{\alpha\beta\beta} \tag{2.19}$$

is the heat-flux vector. In (2.13), we assume that the deviatoric part of $Q_{\gamma\alpha\beta}$, i.e.

$$\widehat{Q}_{\gamma\alpha\beta} = Q_{\gamma\alpha\beta} - \tfrac{1}{4}(Q_{\gamma\xi\xi}\delta_{\alpha\beta} + Q_{\alpha\xi\xi}\delta_{\gamma\beta} + Q_{\beta\xi\xi}\delta_{\alpha\gamma}), \tag{2.20}$$

is zero, thus leaving only the contracted third moment $M_{\alpha\beta\beta} = \langle C_\alpha C_\beta C_\beta\rangle$ as the relevant hydrodynamic variable at third order.

In summary, the balance equations (2.11), (2.12) and (2.13), along with the constraint $\widehat{Q}_{\gamma\alpha\beta} = 0$, constitute the minimal Grad-level description of a fluidized granular matter in terms of moment equations that incorporates normal stress difference. The second-moment balance equation (2.13) can be replaced by its deviatoric part and the standard granular energy equation (2.17); the former equation is identically satisfied at the NS-level description. To close the balance equations (2.11)–(2.13), we need constitutive relations for the stress tensor (2.14), the collisional dissipation rate $\mathscr{D}$ (or the second-moment source term $\aleph_{\alpha\beta}$, (2.16)) and the heat flux (2.19). While the expressions for the first two constitutive quantities are derived for the uniform shear state as discussed in §§ 3 and 4, the heat flux requires a consideration of the non-uniform shear flow since the temperature gradient vanishes in the USF, which is dealt in § 6.

2.1. *Anisotropic Gaussian distribution function*

The constitutive relations require an evaluation of the collision integrals (see appendix A), which involve the two-particle distribution function. We adopt Boltzmann's *stosszahlansatz* (molecular chaos assumption) for which

$$f^{(2)}(\boldsymbol{c}_1, \boldsymbol{x} - \sigma\boldsymbol{k}, \boldsymbol{c}_2, \boldsymbol{x}, t) = g_0(\nu) f(\boldsymbol{c}_1, \boldsymbol{x} - \sigma\boldsymbol{k}, t) f(\boldsymbol{c}_2, \boldsymbol{x}, t). \tag{2.21}$$

Here $g_0(\nu)$ is the contact value of the radial distribution function whose functional form is taken to be (Verlet & Levesque 1982)

$$g_0(\nu) = \frac{(1 - 7\nu/16)}{(1-\nu)^2}, \tag{2.22}$$

with ν $(= n\pi\sigma^2/4)$ being the area fraction (density) of particles. As in the work of Jenkins & Richman (1988), we assume that the single-particle velocity distribution is an 'anisotropic' Gaussian

$$f(\boldsymbol{c}, \boldsymbol{x}, t) = \frac{n}{2\pi|\boldsymbol{M}|^{1/2}} \exp\left(-\frac{1}{2}\boldsymbol{C}\cdot\boldsymbol{M}^{-1}\cdot\boldsymbol{C}\right), \tag{2.23}$$

where $|\boldsymbol{M}| = \det(\boldsymbol{M})$ is the determinant of the second moment, which reduces to the standard Maxwellian or Gaussian distribution function for the case of isotropic $M_{\alpha\beta} = T\delta_{\alpha\beta}$. The ansatz of (2.23) as a solution for the homogeneous sheared system is tantamount to choosing an extended set of hydrodynamic fields, since the anisotropic Gaussian is a function of all components of the second moment, $\boldsymbol{M} = \langle \boldsymbol{CC}\rangle$, of the fluctuation velocity. Such an approach of choosing the generalized or anisotropic Gaussian as the reference state for a non-equilibrium system has been pioneered in the planetary physics community (Goldreich & Tremaine 1978; Shukhman 1984; Araki & Tremaine 1986; Schmidt *et al.* 2001; Latter & Ogilvie 2006) dealing with the modelling of Saturn's ring (Esposito 2006). This formalism has also been adopted by the granular matter community (Jenkins & Richman 1988; Chou & Richman 1998; Lutsko 2004) and can be applied to study the rheology of an arbitrary sheared state (as a perturbation of the homogeneous sheared system) via the well-known Hermite expansion (Lutsko 2004). This differs from Grad's original moment method (Grad 1949; Jenkins & Richman 1985*a*,*b*; Torrilhon & Struchtrup 2004; Vega Reyes, Santos & Garzo 2013) in which the reference state is a Gaussian representing the rest state of thermal equilibrium, and the deviations from the 'local' equilibrium are modelled via a Hermite expansion with unknown coefficients. In § 6, we will discuss an orthonormal expansion around (2.23) to derive the constitutive relation for the heat flux.

3. Steady uniform shear and the second-moment tensor

Let us focus on the two-dimensional coordinate system (since we are dealing with an assembly of disks) as depicted in figure 2, with x and y denoting the flow and gradient directions, respectively. The USF is described by the velocity-gradient tensor

$$\boldsymbol{\nabla u} = \begin{bmatrix} 0 & 2\dot{\gamma} \\ 0 & 0 \end{bmatrix} \equiv \boldsymbol{D} + \boldsymbol{W}, \tag{3.1}$$

such that the velocity field is $\boldsymbol{u} = (u, v) = (2\dot{\gamma}y, 0)$, where $2\dot{\gamma} = \mathrm{d}u/\mathrm{d}y$ is the uniform (constant) shear rate. The shear and spin tensors are given by

$$\boldsymbol{D} = \begin{bmatrix} 0 & \dot{\gamma} \\ \dot{\gamma} & 0 \end{bmatrix} \quad \text{and} \quad \boldsymbol{W} = \begin{bmatrix} 0 & \dot{\gamma} \\ -\dot{\gamma} & 0 \end{bmatrix}. \tag{3.2a,b}$$

The eigenvalues of $\boldsymbol{D}$ are $\pm\dot{\gamma}$ with respective eigenvectors

$$|D_1\rangle = \begin{bmatrix} \cos\frac{1}{4}\pi \\ \sin\frac{1}{4}\pi \end{bmatrix} \quad \text{and} \quad |D_2\rangle = \begin{bmatrix} -\sin\frac{1}{4}\pi \\ \cos\frac{1}{4}\pi \end{bmatrix}. \tag{3.3a,b}$$

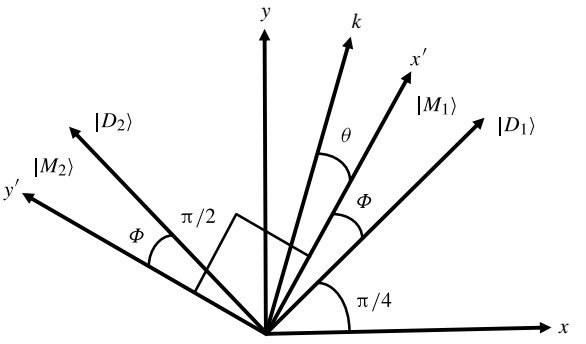

FIGURE 2. A sketch of the coordinate frame: $|D_1\rangle$ and $|D_2\rangle$ are the eigen-directions of the shear tensor $\boldsymbol{D}$, and $|M_1\rangle$ and $|M_2\rangle$ are the eigen-directions of the second-moment tensor $\boldsymbol{M}$.

These eigen-directions are sketched in figure 2. To formulate the anisotropic moment theory for the USF in two dimensions, we follow the work of Jenkins & Richman (1988) in §§ 3.1 and 3.2. Next we simplify our analysis of the second-moment balance by working in a rotated coordinate frame as discussed in § 3.3.

3.1. *Anisotropy in the second-moment tensor*

Here we analyse the second-moment tensor $\boldsymbol{M}$ in terms of its eigenvalues and eigenvectors. Let M_1 and M_2 be the eigenvalues of $\boldsymbol{M}$, with associated eigenvectors $|M_1\rangle$ and $|M_2\rangle$, respectively. We assume that the eigenvector $|M_1\rangle$ makes an angle ϕ with the eigenvector $|D_1\rangle$ of the shear tensor $\boldsymbol{D}$ (see (3.3)). Since $|M_1\rangle$ and $|M_2\rangle$ are orthogonal, the eigenvector $|M_2\rangle$ makes the same angle ϕ with $|D_2\rangle$; this is illustrated in figure 2. The expression for the second-moment tensor $\boldsymbol{M}$ is

$$\begin{aligned}\boldsymbol{M} &= M_1 \begin{bmatrix}\cos(\phi+\frac{1}{4}\pi)\\ \sin(\phi+\frac{1}{4}\pi)\end{bmatrix}\begin{bmatrix}\cos(\phi+\frac{1}{4}\pi) & \sin(\phi+\frac{1}{4}\pi)\end{bmatrix}\\ &\quad + M_2 \begin{bmatrix}-\sin(\phi+\frac{1}{4}\pi)\\ \cos(\phi+\frac{1}{4}\pi)\end{bmatrix}\begin{bmatrix}-\sin(\phi+\frac{1}{4}\pi) & \cos(\phi+\frac{1}{4}\pi)\end{bmatrix}\\ &\equiv T\begin{bmatrix}1+\eta\sin 2\phi & -\eta\cos 2\phi\\ -\eta\cos 2\phi & 1-\eta\sin 2\phi\end{bmatrix} = T[\delta_{\alpha\beta}] + \widehat{\boldsymbol{M}},\end{aligned} \tag{3.4}$$

where we have defined the following variables:

$$2T \equiv M_{\alpha\alpha} = M_1 + M_2, \tag{3.5}$$

$$\eta \equiv (M_2 - M_1)/2T, \tag{3.6}$$

and $\widehat{\boldsymbol{M}}$ is the deviatoric part of the second moment,

$$\widehat{\boldsymbol{M}} = \eta T\begin{bmatrix}\sin 2\phi & -\cos 2\phi\\ -\cos 2\phi & -\sin 2\phi\end{bmatrix}. \tag{3.7}$$

It is clear from (3.4) that the diagonal elements of $\boldsymbol{M}$ are not equal, and η is a measure of the anisotropy of the second-moment tensor. Moreover, the angle ϕ (see figure 2)

measures the rotation that makes $\boldsymbol{M}$ diagonal (see § 3.3). It is straightforward to verify that

$$|\boldsymbol{M}| = T^2(1-\eta^2), \tag{3.8}$$

$$M_1 = T(1-\eta) \quad \text{and} \quad M_2 = T(1+\eta), \tag{3.9a,b}$$

with $M_2 > M_1$.

Let us introduce the 'Savage–Jeffrey' number (Savage & Jeffrey 1981)

$$R = \frac{\sigma\dot{\gamma}}{4\sqrt{T}} \equiv \frac{\dot{\gamma}}{4\sqrt{T/\sigma^2}}, \tag{3.10}$$

which can be interpreted as the scaled or dimensionless shear rate and also as the inverse of the square root of the dimensionless temperature. It is evident from (3.4) and (3.10) that R, η and ϕ are three unknown parameters that completely characterize the anisotropic second-moment tensor $\boldsymbol{M}$ in USF. Recall that the stress tensor (2.14) is $\boldsymbol{P} \equiv \rho\boldsymbol{M}$ in the dilute limit. Hence the anisotropy of $\boldsymbol{M}$ is responsible for the first normal stress difference ($P_{xx} - P_{yy} \sim \eta \sin 2\phi$) in the dilute limit, which is one signature of the stress tensor being non-Newtonian.

3.2. *The second-moment balance equation in uniform shear flow*

For the steady USF, the number density n, velocity gradient $\boldsymbol{\nabla u}$, granular temperature T and the components of $\boldsymbol{M}$ are constant, and therefore the mass and momentum balance equations are identically satisfied. The balance equation for the second-moment tensor (2.13) reduces to

$$P_{\delta\beta}u_{\alpha,\delta} + P_{\delta\alpha}u_{\beta,\delta} = \aleph_{\alpha\beta}, \tag{3.11}$$

where

$$P_{\alpha\beta} = \rho M_{\alpha\beta} + \varTheta_{\alpha\beta} \tag{3.12}$$

is the total stress tensor. The kinetic stress $\rho M_{\alpha\beta}$ is calculated from (3.4), and the collisional stress can be written as (see § A.1)

$$\varTheta_{\alpha\beta} = \frac{2(1+e)\rho\nu g_0(\nu)}{\pi^{3/2}} \int k_\alpha k_\beta (\boldsymbol{k}\cdot\boldsymbol{M}\cdot\boldsymbol{k})\mathfrak{G}(\chi)\,\mathrm{d}\boldsymbol{k}. \tag{3.13}$$

The collisional source of second moment $\aleph_{\alpha\beta}$ in (3.11) can be decomposed as (Jenkins & Richman 1988)

$$\aleph_{\alpha\beta} = A_{\alpha\beta} + \widehat{B}_{\alpha\beta} = A_{\alpha\beta} + \widehat{E}_{\alpha\beta} + \widehat{G}_{\alpha\beta} + \varTheta_{\alpha\gamma}W_{\beta\gamma} + \varTheta_{\beta\gamma}W_{\alpha\gamma}, \tag{3.14}$$

where

$$A_{\alpha\beta} = -\frac{4(1-e^2)\rho\nu g_0(\nu)}{\sigma\,\pi^{3/2}} \int k_\alpha k_\beta (\boldsymbol{k}\cdot\boldsymbol{M}\cdot\boldsymbol{k})^{3/2}\mathfrak{F}(\chi)\,\mathrm{d}\boldsymbol{k}, \tag{3.15}$$

and $\widehat{B}_{\alpha\beta}$, $\widehat{E}_{\alpha\beta}$ and $\widehat{G}_{\alpha\beta}$ represent traceless tensors, which also possess similar integral expressions as detailed in § A.2. The contact vector $\boldsymbol{k}$ over which the above integrations have to be performed and its unit normal $\boldsymbol{j}$ can be expressed as

$$\boldsymbol{k} = \begin{bmatrix} \cos(\theta+\phi+\frac{1}{4}\pi) \\ \sin(\theta+\phi+\frac{1}{4}\pi) \end{bmatrix} \quad \text{and} \quad \boldsymbol{j} = \begin{bmatrix} \sin(\theta+\phi+\frac{1}{4}\pi) \\ -\cos(\theta+\phi+\frac{1}{4}\pi) \end{bmatrix}. \tag{3.16a,b}$$

We have assumed that θ is the angle between $\boldsymbol{k}$ and $|M_1\rangle$ (the eigenvector corresponding to the smaller eigenvalue of $\boldsymbol{M}$, (3.9)) as illustrated in figure 2. It is straightforward to verify that

$$\boldsymbol{k}\cdot\boldsymbol{M}\cdot\boldsymbol{k}\equiv T+\boldsymbol{k}\cdot\widehat{\boldsymbol{M}}\cdot\boldsymbol{k}=T(1-\eta\cos 2\theta)\quad\text{and}\quad\boldsymbol{j}\cdot\boldsymbol{M}\cdot\boldsymbol{k}=-T\eta\sin 2\theta. \tag{3.17a,b}$$

In (3.13) and (3.15) and related collision integrals, the integrands are expressed in terms of two analytic functions $\mathfrak{F}(\chi)$ and $\mathfrak{G}(\chi)$ defined as (Araki & Tremaine 1986; Jenkins & Richman 1988):

$$\mathfrak{F}(\chi)\equiv-\sqrt{\pi}(\tfrac{3}{2}\chi+\chi^3)\operatorname{erfc}(\chi)+(1+\chi^2)\exp(-\chi^2), \tag{3.18}$$

$$\mathfrak{G}(\chi)\equiv\sqrt{\pi}(\tfrac{1}{2}+\chi^2)\operatorname{erfc}(\chi)-\chi\exp(-\chi^2), \tag{3.19}$$

where

$$\chi=\frac{\sigma(\boldsymbol{k}\cdot\boldsymbol{\nabla u}\cdot\boldsymbol{k})}{2\sqrt{\boldsymbol{k}\cdot\boldsymbol{M}\cdot\boldsymbol{k}}}=\frac{2R\cos 2(\theta+\phi)}{(1-\eta\cos 2\theta)^{1/2}}\equiv\chi(\eta,R,\phi,\theta). \tag{3.20}$$

It is clear from (3.16), (3.17) and (3.20) that the integrations over $\boldsymbol{k}$ in (3.13)–(3.15) are to be carried out over θ via $\mathrm{d}\boldsymbol{k}=\mathrm{d}\theta$, with $\theta\in(0,2\pi)$. It is worth pointing out that $\chi=0$ in the dilute limit, since the origin of this term is tied to the excluded-volume effects of macroscopic particles.

With the aid of (3.12) and (3.14), the balance of second moment (3.11) finally reduces to

$$\rho M_{\delta\beta}(D_{\alpha\delta}+W_{\alpha\delta})+\Theta_{\delta\beta}D_{\alpha\delta}+\rho M_{\delta\alpha}(D_{\beta\delta}+W_{\beta\delta})+\Theta_{\delta\alpha}D_{\beta\delta}=A_{\alpha\beta}+\widehat{E}_{\alpha\beta}+\widehat{G}_{\alpha\beta}. \tag{3.21}$$

This is the central equation that must be solved to obtain the rheological quantities (shear viscosity, pressure and first normal stress difference) of USF for the whole range of densities ν. Furthermore, the Grad-level collisional dissipation rate is calculated from (3.14).

3.3. *Reduced second-moment equations in rotated coordinate frame*

Equation (3.21) is significantly simplified if $\boldsymbol{M}$ is made diagonal. This is achieved by using

$$\mathscr{R}=\begin{bmatrix}\cos(\phi+\frac{1}{4}\pi) & -\sin(\phi+\frac{1}{4}\pi)\\ \sin(\phi+\frac{1}{4}\pi) & \cos(\phi+\frac{1}{4}\pi)\end{bmatrix} \tag{3.22}$$

as the rotation matrix with respect to the coordinate frame $x'y'$, with x' and y' being directed along $|M_1\rangle$ and $|M_2\rangle$, respectively (see figure 2). In the rotated $x'y'$ frame, the second-moment tensor is diagonal,

$$\boldsymbol{M}'=T\begin{bmatrix}1-\eta & 0\\ 0 & 1+\eta\end{bmatrix}, \tag{3.23}$$

with the prime indicating that the quantity is evaluated in this new frame, and

$$\boldsymbol{k}' = \begin{bmatrix} \cos\theta \\ \sin\theta \end{bmatrix}, \quad \boldsymbol{j}' = \begin{bmatrix} \sin\theta \\ -\cos\theta \end{bmatrix}, \tag{3.24a,b}$$

$$\boldsymbol{u}' = 2\dot{\gamma}[x' \sin(\phi + \tfrac{1}{4}\pi) + y' \cos(\phi + \tfrac{1}{4}\pi)] \begin{bmatrix} \cos(\phi + \frac{1}{4}\pi) \\ -\sin(\phi + \frac{1}{4}\pi) \end{bmatrix}, \tag{3.25}$$

and

$$\boldsymbol{D}' = \dot{\gamma} \begin{bmatrix} \cos 2\phi & -\sin 2\phi \\ -\sin 2\phi & -\cos 2\phi \end{bmatrix}, \quad \boldsymbol{W}' = \dot{\gamma} \begin{bmatrix} 0 & 1 \\ -1 & 0 \end{bmatrix}. \tag{3.26a,b}$$

It is clear from (3.23) that the anisotropy of $\boldsymbol{M}$ is characterized solely by the temperature difference η as defined in (3.6). Note that the non-zero component of vorticity is in the direction orthogonal to the plane of the motion, and hence the spin tensor is invariant under the planar rotation (3.22).

In the rotated coordinate frame, the components of (3.21) are its trace

$$-2\eta\rho T\dot{\gamma} \cos 2\phi + \dot{\gamma}(\Theta_{x'x'} - \Theta_{y'y'}) \cos 2\phi - 2\dot{\gamma}\Theta_{x'y'} \sin 2\phi = \tfrac{1}{2}(A_{x'x'} + A_{y'y'}), \tag{3.27}$$

the deviatoric component

$$2\rho T\dot{\gamma} \cos 2\phi + \dot{\gamma}(\Theta_{x'x'} + \Theta_{y'y'}) \cos 2\phi = \tfrac{1}{2}(A_{x'x'} - A_{y'y'}) + \widehat{E}_{x'x'} + \widehat{G}_{x'x'}, \tag{3.28}$$

and the off-diagonal component

$$2\rho T\dot{\gamma}(\eta - \sin 2\phi) - \dot{\gamma}(\Theta_{x'x'} + \Theta_{y'y'}) \sin 2\phi = A_{x'y'} + \widehat{E}_{x'y'} + \widehat{G}_{x'y'}. \tag{3.29}$$

The integral terms appearing in (3.27)–(3.29) can be expressed as

$$\left.\begin{aligned}
A_{x'x'} + A_{y'y'} &= \frac{-4\rho\nu g_0(1-e^2)T^{3/2}}{\sigma\pi^{3/2}} \mathscr{H}_{003}(\eta, R, \phi), \\
A_{x'x'} - A_{y'y'} &= \frac{-4\rho\nu g_0(1-e^2)T^{3/2}}{\sigma\pi^{3/2}} \mathscr{H}_{103}(\eta, R, \phi), \\
A_{x'y'} &= \frac{-2\rho\nu g_0(1-e^2)T^{3/2}}{\sigma\pi^{3/2}} \mathscr{H}_{013}(\eta, R, \phi), \\
\widehat{E}_{x'x'} &= \frac{4\rho\nu g_0(1+e)T^{3/2}\eta}{\sigma\pi^{3/2}} \mathscr{H}_{021}(\eta, R, \phi), \\
\widehat{E}_{x'y'} &= -\frac{4\rho\nu g_0(1+e)T^{3/2}\eta}{\sigma\pi^{3/2}} \mathscr{H}_{111}(\eta, R, \phi),
\end{aligned}\right\} \tag{3.30}$$

$$\left.\begin{aligned}
\widehat{G}_{x'x'} &= \frac{2\rho\nu g_0(1+e)T\dot{\gamma}}{\pi^{3/2}} [\cos 2\phi \, \mathscr{J}_{020}(\eta, R, \phi) \\
&\quad + \sin 2\phi \, \mathscr{J}_{110}(\eta, R, \phi) - \eta \sin 2\phi \, \mathscr{J}_{010}(\eta, R, \phi)], \\
\widehat{G}_{x'y'} &= -\frac{2\rho\nu g_0(1+e)T\dot{\gamma}}{\pi^{3/2}} [\cos 2\phi \, \mathscr{J}_{110}(\eta, R, \phi) \\
&\quad + \sin 2\phi \, \mathscr{J}_{200}(\eta, R, \phi) - \eta \sin 2\phi \, \mathscr{J}_{100}(\eta, R, \phi)], \\
\Theta_{x'x'} + \Theta_{y'y'} &= \frac{2\rho\nu g_0(1+e)T}{\pi^{3/2}} \mathscr{J}_{002}(\eta, R, \phi), \\
\Theta_{x'x'} - \Theta_{y'y'} &= \frac{2\rho\nu g_0(1+e)T}{\pi^{3/2}} \mathscr{J}_{102}(\eta, R, \phi), \\
\Theta_{x'y'} &= \frac{\rho\nu g_0(1+e)T}{\pi^{3/2}} \mathscr{J}_{012}(\eta, R, \phi).
\end{aligned}\right\} \tag{3.31}$$

Here $\mathscr{H}_{\alpha\beta\gamma}$ and $\mathscr{J}_{\alpha\beta\gamma}$ possess the integral expressions

$$\mathscr{H}_{\alpha\beta\gamma}(\eta, R, \phi) \equiv \int_0^{2\pi} \cos^\alpha 2\theta \sin^\beta 2\theta\, (1-\eta\cos 2\theta)^{\gamma/2} \mathfrak{F}(\chi[\eta, R, \phi, \theta])\, \mathrm{d}\theta, \quad (3.32)$$

$$\mathscr{J}_{\alpha\beta\gamma}(\eta, R, \phi) \equiv \int_0^{2\pi} \cos^\alpha 2\theta \sin^\beta 2\theta\, (1-\eta\cos 2\theta)^{\gamma/2} \mathfrak{G}(\chi[\eta, R, \phi, \theta])\, \mathrm{d}\theta, \quad (3.33)$$

with $\mathfrak{F}(\chi)$ and $\mathfrak{G}(\chi)$ given by (3.18) and (3.19).

Equations (3.27)–(3.29) represent a system of nonlinear integro-algebraic equations, which we solve using two different methods: (i) semi-analytical method and (ii) numerical method. In § 4 we outline a semi-analytical series solution (which reduces to the solution of Jenkins & Richman (1988) in the dense limit) and verify *a posteriori*, via a comparison with the full numerical solution (see § 5.1), that the adopted power-series representation of integrals (3.32) and (3.33) holds for the whole range of densities. More importantly, this helps to achieve our primary goal of deriving closed-form analytical expressions for nonlinear transport coefficients as well as for the dissipation rate that are valid from dilute to dense flows as we show in §§ 4.2 and 4.3, respectively.

4. Non-Newtonian stress tensor and dissipation rate: constitutive relations

The solution of (3.27)–(3.29) involves evaluating the integrals in (3.32) and (3.33) whose integrands are functions of $\mathfrak{F}(\chi)$ and $\mathfrak{G}(\chi)$ as defined in (3.18) and (3.19), respectively, with χ being given by (3.20). Using the power-series representation for the complementary error function and the exponential, the two functions $\mathfrak{F}(\chi)$ and $\mathfrak{G}(\chi)$ can be compactly expressed as

$$\begin{aligned}\mathfrak{F}(\eta, R, \phi, \theta) &= -\sqrt{\pi}\left[\frac{3}{2}\frac{2R\cos(2\phi+2\theta)}{(1-\eta\cos 2\theta)^{1/2}} + \left(\frac{2R\cos(2\phi+2\theta)}{(1-\eta\cos 2\theta)^{1/2}}\right)^3\right] \\ &\quad + \sum_{m=0}^{\infty} \frac{(-1)^m}{m!}\frac{3}{(2m-1)(2m-3)}\left[\frac{2R\cos(2\phi+2\theta)}{(1-\eta\cos 2\theta)^{1/2}}\right]^{2m}, \quad (4.1)\end{aligned}$$

$$\begin{aligned}\mathfrak{G}(\eta, R, \phi, \theta) &= \sqrt{\pi}\left[\frac{1}{2} + \frac{4R^2\cos^2(2\phi+2\theta)}{(1-\eta\cos 2\theta)}\right] \\ &\quad + \sum_{m=0}^{\infty} \frac{(-1)^m}{m!}\frac{2}{4m^2-1}\left[\frac{2R\cos(2\phi+2\theta)}{(1-\eta\cos 2\theta)^{1/2}}\right]^{2m+1}. \quad (4.2)\end{aligned}$$

Substituting (4.1) and (4.2) into (3.32) and (3.33) and carrying out term-by-term integrations over $\theta \in (0, 2\pi)$ results in an infinite series in η and R for each integral in (3.32) and (3.33) (see appendix B). To progress further, we need to truncate each series after a finite number of terms.

Retaining terms up to second order in η and R (i.e. $O(\eta^2)$, $O(\eta R)$ and $O(R^2)$) in the integral expressions for $\mathscr{H}_{\alpha\beta\gamma}$ ((3.32) and (B 6) in appendix B) and for $\mathscr{J}_{\alpha\beta\gamma}$ ((3.33)

and (B 7) and (B 8) in appendix B), (3.27)–(3.29) simplify to

$$\left.\begin{aligned}
&4\pi^{3/2}\eta R\cos 2\phi + (1+e)\nu g_0 R(16\pi R + 2\pi^{3/2}\eta\cos 2\phi)\\
&\quad = \nu g_0(1-e^2)(3\pi^{3/2}\eta R\cos 2\phi + 2\pi + \tfrac{3}{8}\pi\eta^2 + 12\pi R^2),\\
&4\pi^{3/2}R\cos 2\phi - (1+e)\nu g_0(2\pi\eta - \tfrac{1}{16}\pi\eta^3 - 2\pi^{3/2}R\cos 2\phi - 12\pi^{3/2}R^3\cos 2\phi\\
&\qquad - 4\pi\eta R^2 + 8\pi\eta R^2\sin^2 2\phi)\\
&\quad = \nu g_0(1-e^2)[3\pi^{3/2}R\cos 2\phi + \tfrac{3}{2}\pi\eta],\\
&4\pi^{3/2}R(\eta - \sin 2\phi) - (1+e)\nu g_0 R(2\pi^{3/2}\sin 2\phi + 12\pi^{3/2}R^2\sin 2\phi + 4\pi\eta R\sin 4\phi)\\
&\quad = -3\pi^{3/2}\nu g_0(1-e^2)R\sin 2\phi.
\end{aligned}\right\} \tag{4.3}$$

At the third order in η and R (i.e. up to $O(\eta^3)$, $O(\eta^2 R)$, $O(\eta R^2)$ and $O(R^3)$) they are

$$\left.\begin{aligned}
&4\pi^{3/2}\eta R\cos 2\phi + (1+e)\nu g_0 R(16\pi R + 16\pi R^3 + 2\pi^{3/2}\eta\cos 2\phi - \tfrac{1}{2}\pi\eta^2 R\\
&\qquad - \pi R\eta^2\cos^2 2\phi)\\
&\quad = \nu g_0(1-e^2)(3\pi^{3/2}\eta R\cos 2\phi + 2\pi + \tfrac{3}{8}\pi\eta^2 + 12\pi R^2),\\
&4\pi^{3/2}R\cos 2\phi - (1+e)\nu g_0(2\pi\eta - \tfrac{1}{16}\pi\eta^3 - 2\pi^{3/2}R\cos 2\phi - 12\pi^{3/2}R^3\cos 2\phi\\
&\qquad + 8\pi\eta R^2\sin^2 2\phi - 4\pi R^2\eta)\\
&\quad = \nu g_0(1-e^2)[3R\pi^{3/2}\cos 2\phi + 6\pi^{3/2}R^3\cos 2\phi + \tfrac{3}{2}\pi\eta + \tfrac{3}{2}\pi\eta R^2(2+\cos 4\phi)],\\
&4\pi^{3/2}R(\eta - \sin 2\phi) - (1+e)\nu g_0 R\left(2\pi^{3/2}\sin 2\phi + 12\pi^{3/2}R^2\sin 2\phi + 4\pi\eta R\sin 4\phi\right)\\
&\quad = -\nu g_0(1-e^2)(3\pi^{3/2}R\sin 2\phi + 6\pi^{3/2}R^3\sin 2\phi + \tfrac{3}{2}\pi\eta R^2\sin 4\phi).
\end{aligned}\right\} \tag{4.4}$$

It is clear that we have three unknowns η, R and ϕ to solve for at each order, provided the restitution coefficient e and the area fraction ν are specified. Both sets of coupled algebraic equations, (4.3) and (4.4), can be easily solved using the Newton–Raphson method.

Equations (4.3) and (4.4) can be thought of as analogues of the Burnett-order (quadratic in shear rate) and super-Burnett-order (cubic in shear rate) equations, respectively, and this will become evident in § 4.1, where we show that $\eta \sim O(R)$ to leading order. In principle we can retain further higher-order terms to solve the above three equations but stop at the cubic order as they provide adequate accuracy to recover the exact numerical solution, as we shall demonstrate in § 5.1.

4.1. *Exact solution at leading order: scaling relations*

Before moving to numerical solution of (4.3) and (4.4), it is illuminating to consider the leading-order moment equations that admit an exact solution, which helps to understand the scaling relations for the three unknowns η, R and ϕ in terms of the restitution coefficient e. Retaining only the zeroth-order terms in η and R in the integral expressions for $\mathscr{H}_{\alpha\beta\gamma}$ and $\mathscr{J}_{\alpha\beta\gamma}$ (see (B 6)–(B 8) in appendix B), the following equations for the second-moment balance are obtained:

$$\left.\begin{aligned}
2\sqrt{\pi}\eta R\cos 2\phi - (1-e^2)\nu g_0 &= 0,\\
2\sqrt{\pi}R\cos 2\phi - (1+e)\nu g_0\eta + \sqrt{\pi}(1+e)\nu g_0 R\cos 2\phi &= 0,\\
2(\eta - \sin 2\phi) - (1+e)\nu g_0\sin 2\phi &= 0.
\end{aligned}\right\} \tag{4.5}$$

These equations are amenable to analytical solution, and yield

$$\left.\begin{aligned} \eta &= \sqrt{(1-e)(1+\tfrac{1}{2}(1+e)\nu g_0)} \sim (1-e)^{1/2}, \\ R &= \frac{\sqrt{(1-e^2)(1+e)}\,\nu g_0}{\sqrt{2\pi(2e+(1+e)\nu g_0)}} \sim (1-e)^{1/2}, \\ \sin 2\phi &= \sqrt{\frac{2(1-e)}{2+(1+e)\nu g_0}} \sim (1-e)^{1/2}, \\ \cos 2\phi &= \sqrt{\frac{2e+(1+e)\nu g_0}{2+(1+e)\nu g_0}}, \\ \frac{\eta}{R} &= \frac{\sqrt{\pi(2+(1+e)\nu g_0)(2e+(1+e)\nu g_0)}}{(1+e)\nu g_0}, \end{aligned}\right\} \tag{4.6}$$

with each quantity being a function of e and ν only. Note further that

$$\frac{\eta}{R}\cos 2\phi = \sqrt{\pi}\left(1+\frac{2e}{(1+e)\nu g_0}\right). \tag{4.7}$$

It is clear from (4.6) that the temperature anisotropy η, the shear rate R and $\sin 2\phi$ scale as $\epsilon \equiv (1-e)^{1/2}$ (a measure of the inelasticity of particle collisions). More importantly, that both η and R are of the same order lends credence to the adopted power-series expansion of the collision integrals (3.32) and (3.33) in terms of η and R (see appendix B). The leading-order scaling of R and η with ϵ implies that the NS-, Burnett- and super-Burnett-order terms in the USF are of order $O(\epsilon)$, $O(\epsilon^2)$ and $O(\epsilon^3)$, respectively, although we have not attempted to establish this connection at higher orders (see the discussion in § 4.4). In the rest of this paper, the second- and third-order terms in R and η are referred to as Burnett and super-Burnett order, respectively.

4.2. *Non-Newtonian stress tensor: analytical expressions for transport coefficients*

The dimensionless stress tensor can be written as

$$\boldsymbol{P}^* = \frac{\boldsymbol{P}}{\rho_p U_R^2} = \begin{pmatrix} P^*_{xx} & P^*_{xy} \\ P^*_{yx} & P^*_{yy} \end{pmatrix} \equiv \begin{pmatrix} p^* & 0 \\ 0 & p^* \end{pmatrix} - \begin{pmatrix} -\mathscr{N}^*_{1/2} & \mu^* \\ \mu^* & \mathscr{N}^*_{1/2} \end{pmatrix}, \tag{4.8}$$

where $p^* = (P^*_{xx}+P^*_{yy})/2$ is the pressure, $\mu^* = -P^*_{xy}$ is the shear viscosity and $\mathscr{N}_1^* = P^*_{xx}-P^*_{yy}$ is the first normal stress difference. Here ρ_p is the material (intrinsic) density of particles and $U_R = 2\dot{\gamma}\sigma$ is the reference velocity scale. We will express constitutive relations in terms of the dimensionless temperature, which is defined as

$$T^* = \frac{T}{U_R^2} \equiv \frac{1}{64R^2}. \tag{4.9}$$

The power series (4.2) for $\mathfrak{G}(\eta, R, \phi)$ is inserted into (3.13) to evaluate the collisional stress, and the total stress tensor is subsequently obtained from (3.12). In the following we present only the final analytical expressions for the components of the stress tensor, thus leaving the related algebraic details to appendix C.

4.2.1. *Shear viscosity: up to super-Burnett order*

Retaining terms up to the third order in temperature anisotropy η and shear rate R, the dimensionless shear stress takes the following form (see appendix C):

$$\frac{P^*_{xy}}{\nu T^*} = -\eta\cos 2\phi - \frac{4\nu g_0(1+e)}{\sqrt{\pi}}\left[R\left(1+\frac{\sqrt{\pi}}{8}\frac{\eta}{R}\cos 2\phi\right) + \underbrace{R^3\left(1-\frac{\eta^2}{32R^2}(1+2\cos^2 2\phi)\right)}\right] + O(\eta^m R^n, m+n\geqslant 4). \tag{4.10}$$

The first term on the right-hand side represents its kinetic contribution and the remaining part its collisional contribution. Recall from (4.7) that $(\eta/R)\cos 2\phi \sim O(1)$, and hence the underbraced terms in (4.10) are of super-Burnett ($O(R^3)$) order.

The expression for the dimensionless shear viscosity, $\mu^* = \mu/\rho_p\sigma U_R \equiv -P_{xy}/\rho_p U_R^2 = -P^*_{xy}$, follows from (4.10):

$$\mu^* = \frac{\nu\sqrt{T^*}}{8}\left[\frac{\eta}{R}\cos 2\phi + \frac{4\nu g_0(1+e)}{\sqrt{\pi}}\left(1+\frac{\sqrt{\pi}}{8}\frac{\eta}{R}\cos 2\phi + \underbrace{R^2-\frac{\eta^2}{32}(1+2\cos^2 2\phi)}\right)\right] + O(\eta^m R^n, m+n\geqslant 4). \tag{4.11}$$

The nonlinear dependence of viscosity on the shear rate R and the temperature anisotropy η is evident from the underbraced terms in (4.11).

For a check, we consider the NS-order shear viscosity

$$\mu^* = \frac{\nu\sqrt{T^*}}{8}\left[\frac{\eta}{R}\cos 2\phi + \frac{4\nu g_0(1+e)}{\sqrt{\pi}}\left(1+\frac{\sqrt{\pi}}{8}\frac{\eta}{R}\cos 2\phi\right)\right] + O(R^2), \tag{4.12}$$

which follows from (4.11) by neglecting the nonlinear terms. Substituting the leading-order solution (4.7) into (4.12), we obtain the expressions for the kinetic and collisional parts of the shear viscosity as

$$\mu^*_k \equiv \frac{\nu\sqrt{T^*}}{8}\left(\frac{\eta}{R}\cos 2\phi\right) = \frac{\nu\sqrt{T^*}}{8}\sqrt{\pi}\left(1+\frac{2e}{(1+e)\nu g_0}\right), \tag{4.13}$$

$$\mu^*_c = \frac{\nu^2 g_0(1+e)\sqrt{T^*}}{2\sqrt{\pi}}\left[1+\frac{\pi}{8}\left(1+\frac{2e}{(1+e)\nu g_0}\right)\right], \tag{4.14}$$

respectively, at NS order. These expressions (4.13) and (4.14) with $e=1$ agree perfectly with the known results for the shear viscosity (Jenkins & Richman 1985*a*) of an elastic hard-disk system.

4.2.2. *Pressure: up to super-Burnett order*

At the third-order approximation in η and R, the diagonal components of the stress tensor are

$$\frac{P^*_{xx}}{\nu T^*} = (1+\eta\sin 2\phi) + \nu g_0(1+e)\left(1+\frac{1}{2}\eta\sin 2\phi + 4R^2 + \frac{2}{\sqrt{\pi}}\eta R\cos 2\phi - \frac{1}{4\sqrt{\pi}}R\eta^2\sin 2\phi\cos 2\phi\right) + O(\eta^m R^n, m+n\geqslant 4), \tag{4.15}$$

$$\frac{P_{yy}^*}{\nu T^*} = (1-\eta\sin 2\phi) + \nu g_0(1+e)\left(1-\frac{1}{2}\eta\sin 2\phi + 4R^2 + \frac{2}{\sqrt{\pi}}\eta R\cos 2\phi + \frac{1}{4\sqrt{\pi}}R\eta^2\sin 2\phi\cos 2\phi\right) + O(\eta^m R^n, m+n\geqslant 4). \tag{4.16}$$

Note that both contain odd-order terms in η and R having opposite signs, and hence they cancel each other, resulting in the following expression for the mean pressure:

$$p^* = \nu T^*\left[1+\nu g_0(1+e)\left(1+\underbrace{4R^2+\frac{2}{\sqrt{\pi}}\eta R\cos 2\phi}\right)\right] + O(\eta^m R^n, m+n\geqslant 4). \tag{4.17}$$

This expression holds at both second and third order of approximation in η and R. In any case, it is clear that the collisional part of the pressure depends on the shear rate R and the temperature anisotropy η, revealing the nonlinear dependence of pressure at the Burnett order $O(R^2)$ and beyond. Neglecting the 'underbraced' terms in (4.17), we arrive at the textbook expression for pressure,

$$p^* = \nu T^*(1+\nu g_0(1+e)), \tag{4.18}$$

which holds at NS order.

4.2.3. *First normal stress difference*

Subtracting (4.16) from (4.15), we obtain an expression for the first normal stress difference:

$$P_{xx}^* - P_{yy}^* = 2\eta\sin(2\phi)\nu T^* + \nu^2 g_0(1+e)T^*\left(\eta\sin 2\phi - \frac{1}{2\sqrt{\pi}}R\eta^2\sin 2\phi\cos 2\phi\right) + \text{h.o.t.} \tag{4.19}$$

The leading term in (4.19) is of order $O(R^2)$, since $\eta\sin 2\phi = O(1-e) = O(R^2)$ following (4.6), and the terms of order $O(R)$ in (4.15) and (4.16) do not contribute to the normal stress difference. The leading correction in (4.19) comes from the collisional part of the stress tensor,

$$R\eta^2\sin 2\phi\cos 2\phi \equiv R^2(\eta\sin 2\phi)\left(\frac{\eta}{R}\cos 2\phi\right) = O(R^4), \tag{4.20}$$

which is fourth order in the shear rate.

Retaining terms up to $O(R^4)$ in (4.19), the scaled first normal stress difference is given by

$$\mathscr{N}_1 = \frac{P_{xx}-P_{yy}}{p} = \frac{\eta\sin 2\phi\left(2+\nu g_0(1+e)\left(1-\frac{1}{2\sqrt{\pi}}R\eta\cos 2\phi\right)\right)}{1+\nu g_0(1+e)\left(1+4R^2+\frac{2}{\sqrt{\pi}}\eta R\cos 2\phi\right)}, \tag{4.21}$$

which is a measure of the normal stress with respect to the mean/isotropic pressure (4.17). Focusing on the dilute limit ($\nu\to 0$), (4.21) becomes

$$\mathscr{N}_1 = 2\eta\sin 2\phi = 2(1-e)\sim R^2\sim\dot{\gamma}^2, \tag{4.22}$$

which scales quadratically with the shear rate. This confirms that the normal stress difference is a Burnett-order effect (Sela & Goldhirsch 1998). Note from (4.21) that $\mathscr{N}_1 \sim \eta \sin 2\phi$ at any density and it approaches zero for $\eta \to 0$ and/or $\phi \to 0$. The origin of the normal stress difference is, therefore, tied to (i) the temperature anisotropy η and (ii) the angle ϕ between the eigen-directions of the shear tensor $\boldsymbol{D}$ and the second-moment tensor $\boldsymbol{M}$ – both are shear-induced effects.

It should be noted that the elastic limit ($e \to 1$) remains non-singular even though the temperature diverges ($T \sim R^{-2} \to \infty$ as $e \to 1$). The latter divergence is due to the absence of any mechanism to compensate the shear work, but this can be fixed by using a thermostat. Therefore, the normal stress difference is finite for perfectly elastic collisions (Sela *et al.* 1996; Alam & Luding 2003*a*,*b*):

$$\mathscr{N}_1 = 0.679 \frac{\dot{\gamma}^2 l_f^2}{T}, \tag{4.23}$$

where l_f is the mean free path. Note, however, that $\mathscr{N}_1 \sim O(10^{-20})$ in a sheared molecular gas at standard temperature and pressure with $\dot{\gamma} = O(1)$ and hence is negligible. The expression (4.23) can be understood from (4.22) by tying the in-built mechanism of energy replenishment in a granular gas with a thermostat in its molecular counterpart.

4.3. *Dissipation rate: dependence on shear rate and normal stress*

Employing the series solution for integrals, the collisional dissipation rate in the energy balance equation can be calculated from (3.14) as

$$\begin{aligned}
\mathscr{D} &\equiv -\frac{1}{2}\aleph_{\beta\beta} = -\frac{1}{2}(A_{\beta\beta} + \widehat{B}_{\beta\beta}) = -\frac{1}{2}(A_{x'x'} + A_{y'y'}) \\
&= \frac{2\rho\nu g_0(1-e^2)T^{3/2}}{\sigma\,\pi^{3/2}}\mathscr{H}_{003}(\eta, R, \phi) \\
&= \frac{4\rho\nu g_0(1-e^2)T^{3/2}}{\sigma\sqrt{\pi}}\left(1 + 6R^2\left(1 + \frac{\sqrt{\pi}}{4}\frac{\eta}{R}\cos 2\phi\right) + \frac{3}{16}\eta^2 + \text{h.o.t.}\right).
\end{aligned} \tag{4.24}$$

The neglected terms in (4.24) are of order $O(\eta^m R^n)$ with $m+n \geqslant 4$: the leading-order corrections are second order in both R and η but the odd-order terms ($m+n=1,3,\ldots$) are zero. Hence the expression (4.24) is exact up to the super-Burnett order. In the isotropic limit of zero normal stress difference ($\eta \to 0$ and $\phi \to 0$), (4.24) reduces to

$$\mathscr{D} = \mathscr{D}^{(0)}(1 + 6R^2 + O(R^4)), \tag{4.25}$$

which contains a rate-dependent correction term at the leading order. The origin of this correction is tied to the excluded-volume effects (3.20) of a dense gas. In (4.25),

$$\mathscr{D}^{(0)} = \frac{4\rho_p \nu^2 g_0(1-e^2)T^{3/2}}{\sigma\sqrt{\pi}} \tag{4.26}$$

is the dissipation rate for a system of inelastic hard disks (Jenkins & Richman 1985*a*), which holds at both Euler and NS orders. Equation (4.26), however, differs

from related NS-order theories (Lutsko 2005; Garzo *et al.* 2007) that are built around the homogeneous cooling state as a reference.

Returning to (4.24), we note that the correction terms beyond the NS order depend quadratically on both (i) the shear rate ($\dot{\gamma} \sim R \sim \epsilon \equiv (1-e)^{1/2}$) and (ii) the temperature anisotropy η ($\sim \epsilon$). The latter finding uncovers a novel dependence of the collisional dissipation rate on the normal stress difference since $\eta \sim \mathscr{N}_1$. As clarified in § 4.1, the above quadratic-order corrections in (4.24) can also be translated into an effective correction of $O(\epsilon^2)$, which agrees qualitatively with the related Burnett-order expression for $\mathscr{D}$ derived by Sela & Goldhirsch (1998) and Brilliantov & Pöschel (2003), who used the Chapman–Enskog method to solve the Boltzmann equation in three dimensions up to the Burnett order (i.e. the second order in the gradients of hydrodynamic fields). Note that the latter work analysed the homogeneous cooling state of a granular gas of viscoelastic particles by incorporating the second-order gradient terms in the two-particle distribution function.

4.4. *Inherent non-Newtonian rheology of uniform shear flow*

Let us now remark on the dependence of various transport coefficients on (i) the shear rate R, (ii) the temperature anisotropy η, (iii) the non-coaxiality angle ϕ, (iv) the restitution coefficient e and (v) the density or area fraction ν that we uncovered in §§ 4.2 and 4.3. It is clear from (4.6) that there is an intertwined relationship among R, η and ϕ via their dependence on e and ν in the uniform shear state, and this survives at any order. For example, (4.4) can be solved perturbatively by using (4.6) as the zeroth-order solution, leading to an approximate solution for η, R and ϕ as a function of $\epsilon = (1-e)^{1/2}$ for the whole range of densities. Substituting these values into (4.11) results in an expression for the shear viscosity as a function of e and ν. This implies that specifying ν and e with Lees–Edward boundary condition (Alam & Luding 2003*a*,*b*, 2005*a*,*b*; Gayen & Alam 2008) sets the granular temperature and the shear rate simultaneously, which is a consequence of the 'in-built' thermostat of collisional dissipation that balances the shear work. Therefore, it would not be possible to isolate the shear-rate dependence of viscosity (and other transport coefficients) from its dependence on inelasticity if we were to measure shear viscosity from the molecular dynamics simulation (§ 5.2) of a granular fluid under uniform shear.

What is measured in simulations is nothing but the non-Newtonian viscosity, since the shear rate is always finite, and hence the rheology of the uniform shear state of a granular fluid is inherently non-Newtonian (Santos *et al.* 2004) unlike in its elastic counterpart. The comparisons of transport coefficients in § 5.2 will validate their dependence on the density and the restitution coefficient at any arbitrary shear rate. On the other hand, the explicit rate dependence of transport coefficients can be checked in future with simulations of boundary-driven shear (with imposed temperature gradient) where the shear rate and the restitution coefficient can be independently varied (Vega Reyes *et al.* 2013).

5. Validation of constitutive relations and comparison with particle simulation

5.1. *Validation of constitutive relations: are super-Burnett terms required?*

Here we validate the constitutive relations for all transport coefficients as detailed in § 4.2. This is done by carrying out a comparison between the transport coefficients obtained from (i) the full numerical solution of moment equations and (ii) those obtained from their analytical expressions at Burnett (i.e. quadratic order in R and η) and super-Burnett (i.e. cubic order in R and η) orders. The goal is to check whether

we need to go beyond the Burnett order for an accurate representation of transport coefficients at any restitution coefficient for the whole range of densities.

For the complete numerical solution of the moment equations, we evaluate the integrals in $\boldsymbol{A}$, $\widehat{\boldsymbol{E}}$, $\widehat{\boldsymbol{G}}$ and Θ in (3.27)–(3.29) using the standard quadrature rule. Next we solve the resulting system of three nonlinear algebraic equations by the Newton–Raphson method, yielding values of η, R and ϕ for specified values of the area fraction ν and the restitution coefficient e. This helps to determine (see appendix C) the pressure p, the shear viscosity μ and the first normal stress difference $\mathscr{N}_1$ as functions of ν and e.

The comparison between the full moment theory and the series solutions at second and third orders is given in figure 3: panels (*a*)–(*d*), respectively, display the variations of pressure, shear viscosity, granular temperature and first normal stress difference with area fraction, for four values of the restitution coefficient ($e = 0.99$, 0.9, 0.6 and 0.3). In each panel, the continuous (black) and dashed (red online) lines represent the series solution at third- and second-order approximation, respectively, and the symbols denote the exact solution (full numerical solution) of the moment equations. We observe excellent agreement between the third-order series solution and the exact solution even at a strong dissipation of $e = 0.3$. In contrast, the second-order series solution does well only up to $e = 0.6$ for the normal stress difference (see panel (*d*)), although the pressure, viscosity and temperature are well predicted by the second-order solution even at $e = 0.3$.

On the whole, figure 3 confirms that, while the Burnett-order expressions yield accurate transport coefficients in the dilute limit, the super-Burnett-order terms are required to reproduce the correct behaviour of all transport coefficients at higher densities ($\nu > 0.2$) for the whole range of restitution coefficients ($0 \leqslant e \leqslant 1$).

To see why the adopted series expansion (4.1) and (4.2) works well, we plot the variations of η, R and ϕ in figure 4(*a–c*), respectively. Again, we observe excellent agreement between the exact solution (symbols) and the third-order series solution (solid line) for the whole range of densities up to a restitution coefficient of $e = 0.3$. However, the second-order solution (dashed line) for η in panel (*a*) is seen to deviate significantly from its exact solution at $e = 0.6$ beyond a moderate density of $\nu \sim 0.35$, and this disagreement occurs at a much lower density ($\nu \sim 0.2$) for $e = 0.3$. It is clear that both R and η are small in the dilute and dense limits, respectively, but they tend to become of order one in opposite limits. Nevertheless, the series representation (4.1) and (4.2) and the resulting power-series expansion of integrals (3.32) and (3.33) in terms of η and R (appendix B) works excellently for the whole range of densities even at strong dissipations, as illustrated in figure 4, if we retain the third-order terms as in (4.4).

5.2. *Comparison of anisotropic moment theory with simulation and Navier–Stokes model*

In this section we make a detailed comparison for all transport coefficients of the non-Newtonian stress tensor as obtained in § 4.2 from the moment theory with (i) particle simulations and (ii) an NS order model. The NS-order transport coefficients are taken from those of Lutsko (2005) as detailed in appendix D. Note that Lutsko's model holds for both disks and spheres; Garzo *et al.* (2007) also derived NS-level transport coefficients in arbitrary dimension using a modified Sonine expansion, and confirmed that the viscosity, pressure and dissipation rate are hardly affected in both approaches. It may be noted that both works carry out a Chapman–Enskog expansion around

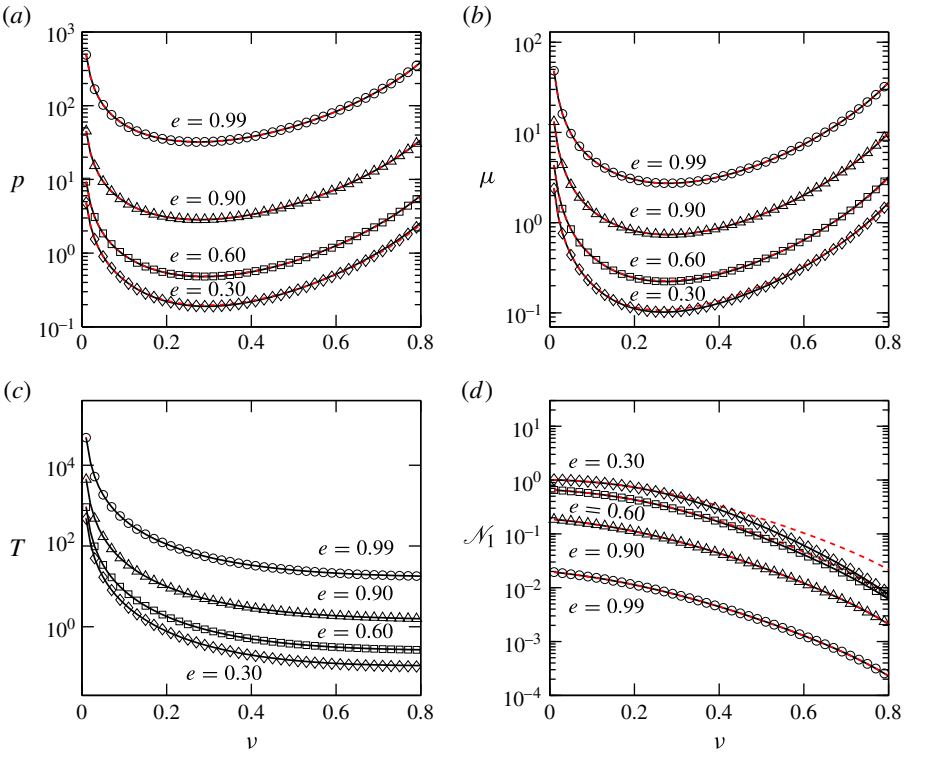

FIGURE 3. (Colour online) Comparison of the numerical solution for the moment theory (symbols) with approximate series solution: second-order (red dashed lines) and third-order (black solid line) series solutions for the (*a*) pressure, (*b*) shear viscosity, (*c*) granular temperature and (*d*) first normal stress difference.

the homogeneous cooling state, and the NS-level transport coefficients thus obtained are assumed to hold for all values of the restitution coefficient, since they made no assumption about the smallness of inelasticity or dissipation.

The event-driven simulation of the USF of inelastic hard disks (i.e. in two dimensions) has been carried out by Alam & Luding (2003*a*,*b*) and we take their data to compare with the present theory. The disks interact via the standard binary collision rule of smooth particles, (2.1), for a specified value of the restitution coefficient. The state of uniform shear is achieved by employing the Lees–Edward boundary condition (Lees & Edwards 1972). All simulations have been carried out in a square box with $N = 1024$ disks for two values of the restitution coefficient, $e = 0.9$ and 0.7, for a range of densities (area fractions) $\nu \in (0.01, 0.8)$ spanning from the dilute to the dense regime.

Figure 5 shows a comparison for the pressure field between (i) the exact moment theory (solid line, numerical solution), (ii) the NS-order model (dashed line) and (iii) simulation data (symbols). Panels (*a*)–(*c*), respectively, correspond to the total pressure ($p = p_k + p_c$), and its kinetic (p_k) and collisional (p_c) components; the data for $e = 0.9$ and 0.7 are marked in each panel. The analogue of figure 5 for the shear viscosity is displayed in figure 6. For both pressure and viscosity, we observe that the NS model overpredicts the simulation data, and the degree of discrepancy increases

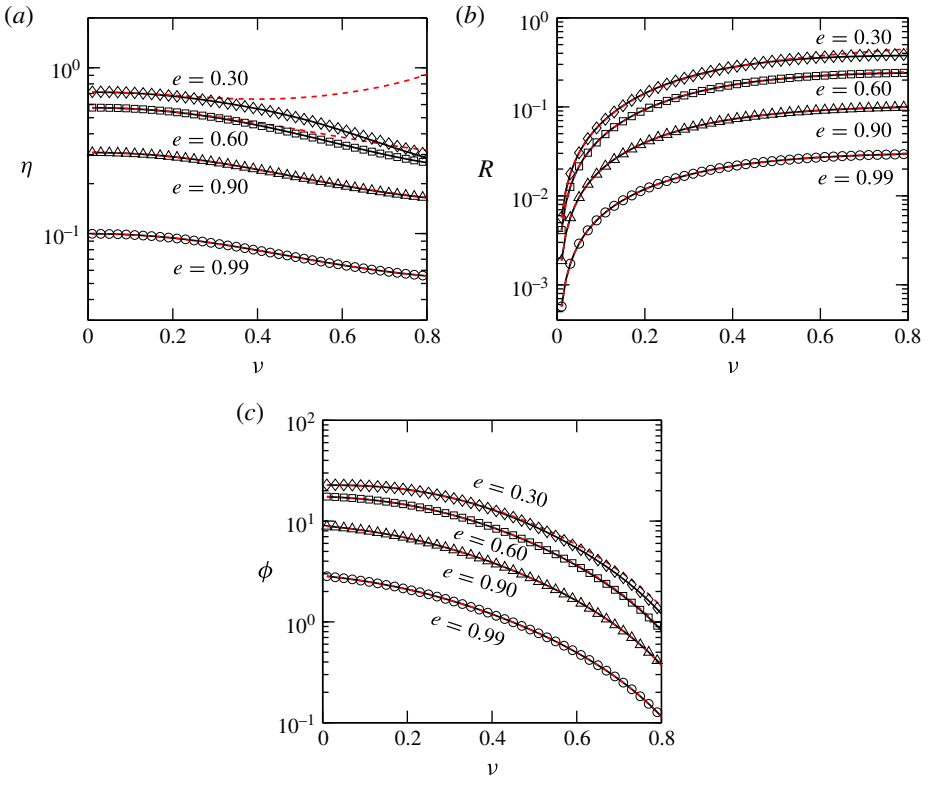

FIGURE 4. (Colour online) Comparison between the 'exact' (numerical solution) moment theory and the approximate series solution for a range of densities: variations of (*a*) η, (*b*) R and (*c*) ϕ (degrees) with area fraction. The symbols, dashed (red) and solid (black) lines represent the full numerical solution, second-order and third-order series solutions, respectively.

with decreasing value of e (i.e. with increasing dissipation). It is noteworthy that the deviation between the NS model and the simulation is more prominent for dilute flows at any restitution coefficient. In contrast, the predictions of the moment theory agree excellently with simulation even at $e = 0.7$ for a large range of densities – up to $\nu \sim 0.65$, which is close to the freezing point density $\nu_f \approx 0.69$ (see figures 5 and 6). A possible reason for quantitative discrepancies at large densities could be the breakdown of the molecular chaos assumption (§ 2.1), especially beyond the freezing density (Mitarai & Nakanishi 2007).

Figures 7 and 8 show the variations of the scaled pressure p/T and the scaled viscosity $\mu/\sqrt{T}$, respectively. In each figure, panels (*a*) and (*b*) correspond to $e = 0.9$ and 0.7, respectively, with the solid line, dashed line and symbols denoting the moment theory, NS theory and simulation data, respectively. Recall that both these scaled quantities ($p/T = f_1(\nu, e, \ldots)$ and $\mu/\sqrt{T} = f_2(\nu, e, \ldots)$) are functions solely of the density and restitution coefficient in the NS-level theory; however, they have additional dependence on the shear rate ($\dot{\gamma} \sim R$) as well as on the normal stress difference ($\mathscr{N}_1 \sim \eta$). Figure 7 indicates that the dependence of f_1 on R and η is negligible in dilute to moderately dense flows even at $e = 0.7$, but a slight deviation

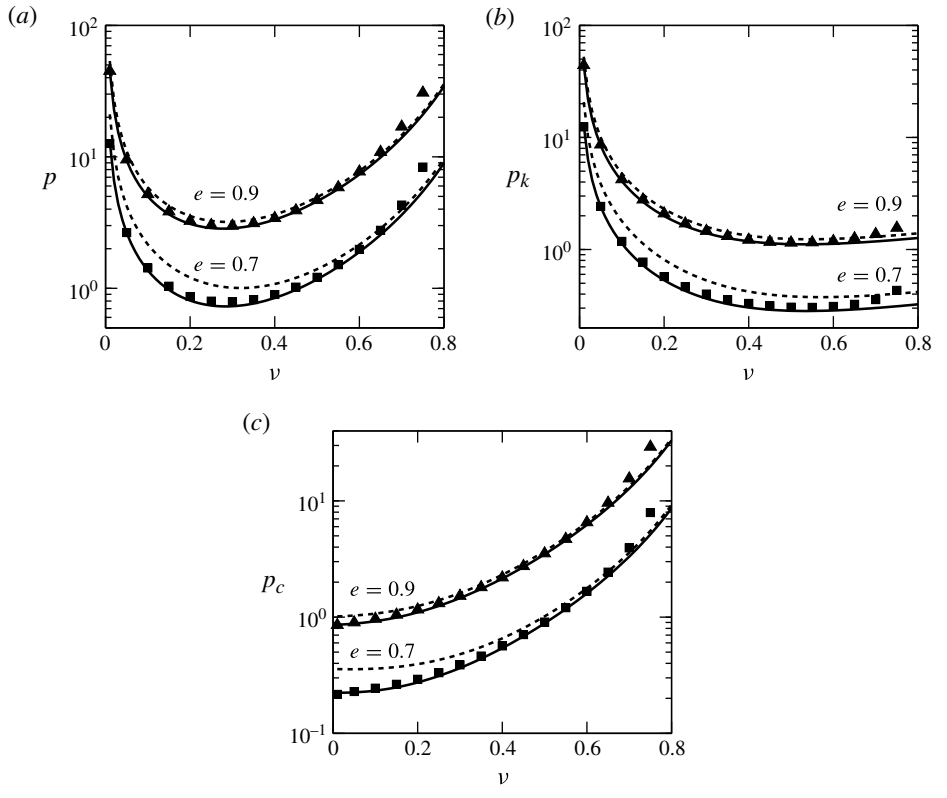

FIGURE 5. Comparison among the full moment theory (solid line, present work), the NS model (dashed line, Lutsko 2005) and simulation data (symbols) for the variation of pressure with area fraction: (*a*) total pressure $p = p_k + p_c$, (*b*) kinetic pressure p_k and (*c*) collisional pressure p_c. Results for two values of the restitution coefficient ($e = 0.9$ and 0.7) are shown.

(between the moment theory and the NS-level theory) is noticeable in the dense limit, which becomes more prominent with increasing dissipation. On the other hand, the viscosity function f_2 deviates strongly from its NS prediction in the dilute limit even at $e = 0.9$.

Figure 9 shows the variation of the scaled first normal stress difference $\mathscr{N}_1 = (P_{xx} - P_{yy})/p$ with density for three values of $e = 0.95$, 0.9 and 0.7. The lines correspond to the moment theory and the symbols to simulation data. Recall that $\mathscr{N}_1 = 0$ for all NS-order constitutive models. The prediction of the moment theory agrees well with simulation data for $e = 0.95$ and 0.9, but there are quantitative differences between theory and simulation that increase with increasing dissipation. Although the theoretical prediction remains good in the dilute limit ($\nu \to 0$) even at $e = 0.7$ (see also § 5.3 and figure 10), increasing the density leads to an underprediction of simulation data – this might be related to enhanced density correlations at finite densities. The latter assertion is supported by additional simulations at $e = 0.5$ (with other simulation parameters being fixed at finite densities) that show the emergence of particle clusters spanning over the whole system. Another noteworthy point in figure 9 is that the theory predicts $\mathscr{N}_1 \to 0$ in the dense limit, but

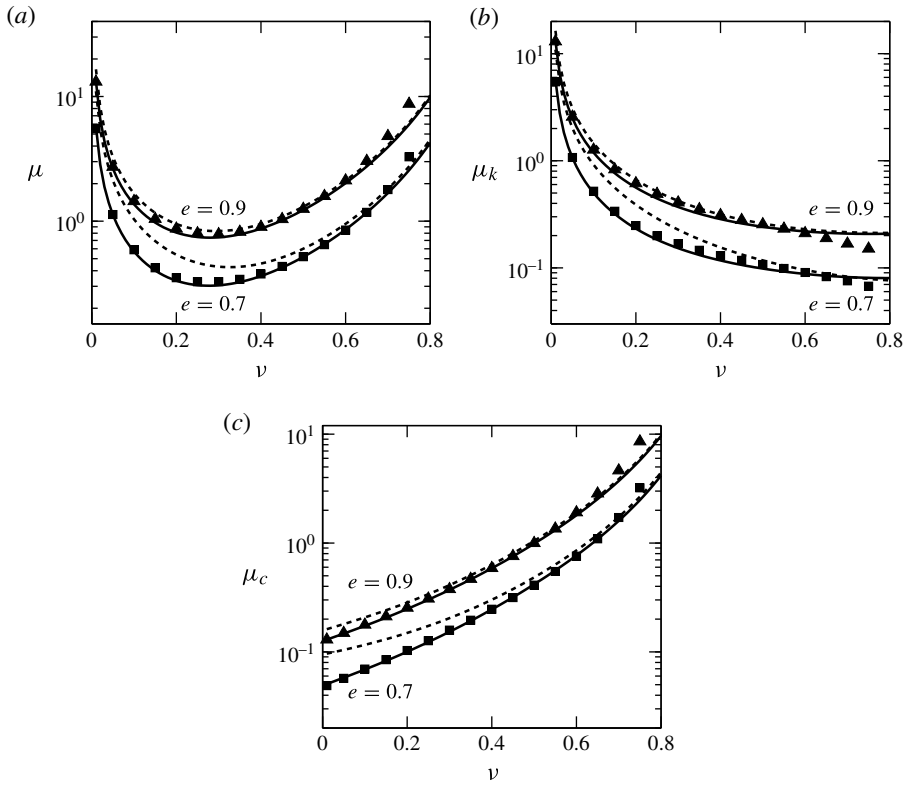

FIGURE 6. Same as figure 5 but for the variation of shear viscosity with area fraction: (*a*) total viscosity $\mu = \mu_k + \mu_c$, (*b*) kinetic viscosity μ_k and (*c*) collisional viscosity μ_c.

the simulation shows a sign reversal of $\mathscr{N}_1$ at some critical density (near the freezing density). This sign reversal of $\mathscr{N}_1$ is, in fact, tied to changes in the microstructure (Alam & Luding 2003*a*,*b*), i.e. changes in the pair correlation function and its relaxation under shear. The latter effect is not incorporated in the present theory, which is likely to be responsible for the disagreement between theory and simulation in the dense regime.

On the whole, we find that the Grad-level moment theory with anisotropic Gaussian can quantitatively predict the pressure and shear viscosity for a range of densities up to the freezing point at very strong dissipations ($e = 0.3$). In contrast the NS model (Lutsko 2005; Garzo *et al.* 2007), which is assumed to hold at any dissipation, shows quantitative discrepancies even at moderate dissipations ($e = 0.9$) and the degree of disagreement increases with decreasing restitution coefficient e. Last but not least, the missing ingredient of any NS-order constitutive model, the normal stress difference ($\mathscr{N}_1$, figure 9), is well predicted by our anisotropic moment theory, although quantitative discrepancy remains at finite densities for large dissipations.

5.3. *Comparison with another Grad-level theory in the dilute limit*

In this section we compare our analytical transport coefficients (§ 4.2) with those derived from another variant of Grad's method (Kremer & Marques 2011; Garzo 2012). In the latter two works, the moment theory was developed using a Hermite

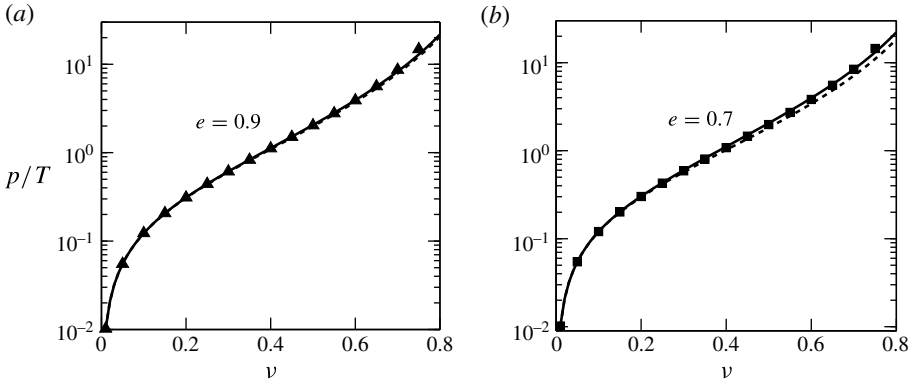

FIGURE 7. Variation of p/T (dimensionless) with area fraction for (*a*) $e = 0.9$ and (*b*) $e = 0.7$. The solid and dashed lines represent the exact moment theory (i.e. the full numerical solution) and the NS-order model (Lutsko 2005), respectively, and the symbols denote simulation data.

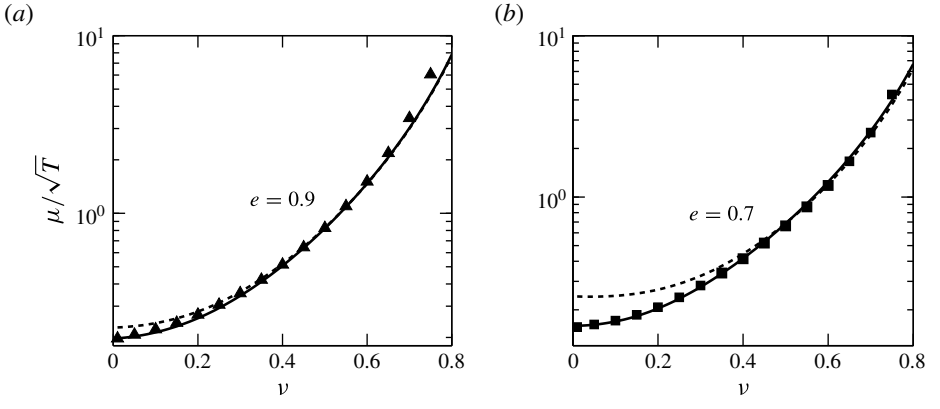

FIGURE 8. Variation of $\mu/\sqrt{T}$ (dimensionless) with area fraction for (*a*) $e = 0.9$ and (*b*) $e = 0.7$. The solid and dashed lines represent the exact moment theory (i.e. the full numerical solution) and the NS-order model (Lutsko 2005), respectively, and the symbols denote simulation data.

expansion around an isotropic Gaussian state, in contrast to the anisotropic Gaussian reference in our work. Leaving aside the mathematical details, we note that the balance equation for the second moment in the steady uniform shear state is the same as (3.11) as elaborated in § 3.2. An approximate expression for the source term has been determined for hard disks (Garzo 2012):

$$\aleph_{\alpha\beta} = -\varphi_\mu \widehat{P}_{\alpha\beta} - \zeta p \delta_{\alpha\beta}, \tag{5.1}$$

where $\widehat{P}_{\alpha\beta} = P_{\alpha\beta} - p\delta_{\alpha\beta}$ is the pressure deviator. The equation of state is $p \equiv (P_{xx} + P_{yy})/2 = \rho T$, and the expressions for the cooling rate ζ, collision frequency φ_μ (related to shear viscosity) and the coefficient of the fourth velocity cumulant α_2 $(= \langle C^4 \rangle / \langle C^4 \rangle^{(0)} - 1$, with the superscript '0' denoting its evaluation for a Gaussian or

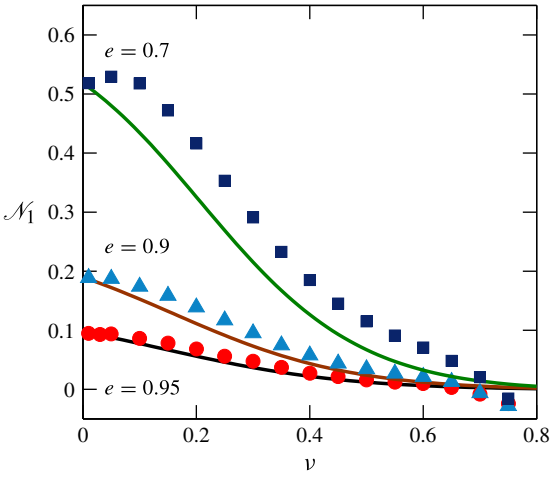

FIGURE 9. (Colour online) Variation of the scaled first normal stress difference $\mathscr{N}_1$ with area fraction. The symbols and lines represent the molecular dynamics simulation data and the present moment theory, respectively.

Maxwellian) are given by

$$\left.\begin{aligned} \zeta &= \frac{4\nu}{\sigma\sqrt{\pi}}(1-e^2)\left(1+\frac{3\alpha_2}{16}\right)\sqrt{T}, \\ \varphi_\mu &= \frac{\nu}{\sigma\sqrt{\pi}}(7-3e)(1+e)\left(1-\frac{\alpha_2}{32}\right)\sqrt{T}, \\ \alpha_2 &\equiv \left(\frac{\langle C^4\rangle}{\langle C^4\rangle^{(0)}}-1\right) = \frac{16(1-e)(1-2e^2)}{57-25e+30(1-e)e^2}. \end{aligned}\right\} \tag{5.2}$$

Note that $\alpha_2 = 0$ for a Maxwellian distribution function.

With the aid of (5.1) and taking the overall shear rate in the USF as $\mathrm{d}u/\mathrm{d}y = 2\dot{\gamma}$ (defined in (3.1)), (3.11) can be decomposed into its component forms:

$$\left.\begin{aligned} \varphi_\mu P_{xy} &= -2\dot{\gamma}P_{yy}, \\ (\varphi_\mu-\zeta)P_{xx} &= (\varphi_\mu+\zeta)P_{yy}, \\ 8\dot{\gamma}P_{xy} &= -(\varphi_\mu+\zeta)P_{xx}+(\varphi_\mu-\zeta)P_{yy}. \end{aligned}\right\} \tag{5.3}$$

The solution of (5.3) yields the diagonal components of the stress tensor,

$$\frac{P_{xx}}{4\rho_p\dot{\gamma}^2\sigma^2} = \frac{\nu}{64R^2}\left(\frac{\varphi_\mu+\zeta}{\varphi_\mu}\right) \quad \text{and} \quad \frac{P_{yy}}{4\rho_p\dot{\gamma}^2\sigma^2} = \frac{\nu}{64R^2}\left(\frac{\varphi_\mu-\zeta}{\varphi_\mu}\right), \tag{5.4a,b}$$

and the dimensionless shear rate R is

$$R^2 = \frac{\dot{\gamma}^2\sigma^2}{16T} = \frac{\nu^2(7-3e)^2(1+e)^2(1-e)(1-\frac{1}{32}\alpha_2)^2(1+\frac{3}{16}\alpha_2)}{16\pi(3+e-\frac{1}{32}\alpha_2(31-27e))}. \tag{5.5}$$

The expression for the first normal stress difference is

$$\mathscr{N}_1 = \frac{2(P_{xx}-P_{yy})}{(P_{xx}+P_{yy})} = \frac{2\zeta}{\varphi_\mu} = \frac{8(1-e)(1+\frac{3}{16}\alpha_2)}{(7-3e)(1-\frac{1}{32}\alpha_2)} \sim (1-e) \sim R^2, \tag{5.6}$$

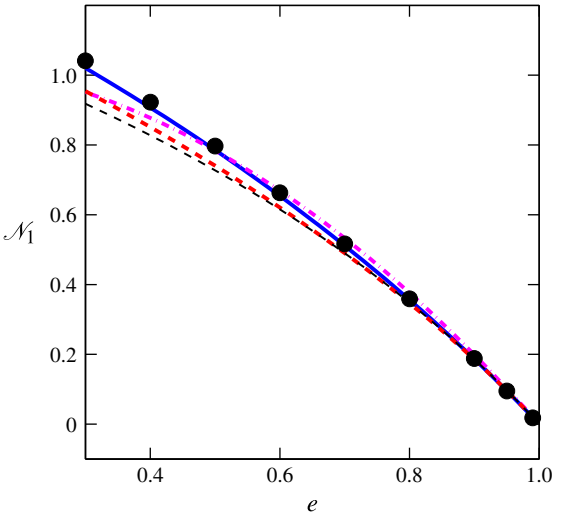

FIGURE 10. (Colour online) Comparison of the first normal stress difference obtained from simulation (symbols) with the present anisotropic Gaussian theory (blue solid line), the Grad-level theory of Garzo (thick red dashed line, (5.6)) and the Burnett-order theory of Sela & Goldhirsch (magenta dot-dashed line). The 'thin' black dashed line corresponds to (5.6) with $\alpha_2 = 0$ (see the text in § 5.3 for details). The area fraction is set to $\nu = 0.01$.

which scales quadratically with the shear rate and hence is a Burnett-order effect as confirmed in § 4.2.3.

The comparison of (5.6) with the present theory and the particle simulation data is shown in figure 10, marked by the red dashed line, the blue solid line and the circles, respectively; the simulations were carried out for an average area fraction of $\nu = 0.01$. The Burnett-order expression of Sela *et al.* (1996), obtained from the Chapman–Enskog expansion, is also displayed on the same figure (magenta dot-dashed line). We observe that the simulation data agree uniformly with the present anisotropic Gaussian theory for a large range of restitution coefficients $e \in (0.3, 0.99)$, but the Grad-level expression (5.6) of Garzo underpredicts the simulation results for $e < 0.8$. On the other hand, the Burnett theory of Sela *et al.* agrees well with simulation and present theory up to $e = 0.5$ and underpredicts $\mathscr{N}_1$ for $e < 0.5$. To ascertain the relative importance of the fourth velocity cumulant α_2 for a quantitative prediction of $\mathscr{N}_1$, we set $\alpha_2 = 0$ in (5.6) and plot the resulting expression as the 'thin' black dashed line in figure 10. It is clear that the fourth velocity cumulant does not affect $\mathscr{N}_1$ noticeably up to a restitution coefficient of $e \approx 0.6$ but underpredicts it slightly for smaller e.

From (5.3) and (5.4), the expressions for shear viscosity $\mu = -P_{xy}/2\dot{\gamma}$ and pressure $p = (P_{xx} + P_{yy})/2$ can be obtained as

$$\frac{\mu}{2\rho_p \dot{\gamma}\sigma^2} = \frac{\nu^2(1-e^2)(1+\frac{3}{16}\alpha_2)}{128\sqrt{\pi}R^3} \quad \text{and} \quad \frac{p}{4\rho_p \dot{\gamma}^2\sigma^2} = \frac{\nu}{64R^2}, \tag{5.7a,b}$$

with R being given by (5.5). These two expressions (5.7) are compared in figure 11, denoted by the red dashed lines, with (i) the particle simulation (denoted by symbols) and (ii) the present anisotropic Gaussian theory (blue solid lines). The curves for two variants of the NS-level theory (Lutsko 2005, green dot-dashed lines;

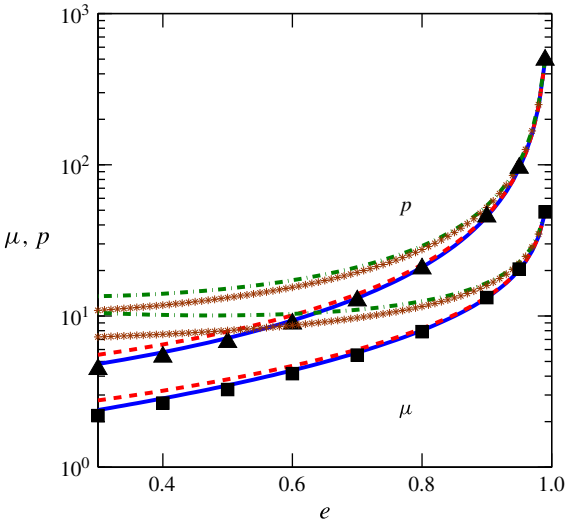

FIGURE 11. (Colour online) Comparison for dimensionless pressure and shear viscosity obtained from molecular dynamics simulation (symbols) with the present anisotropic Gaussian theory (blue solid lines), the Grad-level theory of Garzo (red dashed lines, (5.7)), the NS-level theory of Lutsko (2005, green dot-dashed lines) and the NS-level theory of Jenkins & Richman (1985*a*, magenta starred lines). Other parameters are as in figure 10.

and Jenkins & Richman 1985*a*, magenta starred lines) are also displayed. We see excellent agreement of simulation data with the present theory, but the isotropic version of the moment theory slightly overpredicts both p and μ for $e < 0.5$. In contrast, both the NS-level theories overpredict the simulation data even at $e = 0.9$, and the quantitative disagreement worsens significantly with further decrease of restitution coefficient. It is surprising that the NS theory of Jenkins & Richman provides a better quantitative prediction for p and μ in comparison to Garzo and Lutsko's theory, since the latter theory incorporates the fourth velocity cumulant α_2 and makes no assumption about the smallness of the restitution coefficient.

On the whole, figures 10 and 11 confirm that the present anisotropic Gaussian theory provides better prediction for all transport coefficients ($\mathscr{N}_1$, μ and p) for the whole range of restitution coefficients in comparison to two existing theories (in the dilute limit) that are based on (i) the Chapman–Enskog expansion (Sela *et al.* 1996) and (ii) the isotropic version of Grad's moment expansion (Kremer & Marques 2011; Garzo 2012).

6. Constitutive relation for granular heat flux in the dilute limit

Lastly, we outline a procedure to derive the constitutive relation for granular heat flux focusing on the dilute limit of granular shear flow. Note that the heat flux vanishes in the uniform shear state since $\boldsymbol{\nabla} T = 0$, and hence we need to consider non-uniform shear flow ('non-USF') in which the gradients of hydrodynamic fields are non-zero, i.e. $\boldsymbol{\nabla}(n, T, \dot{\gamma}) \neq 0$. Carrying out an orthonormal expansion around the anisotropic Gaussian state, we will show that the heat-flux vector depends on the gradients of temperature and the second-moment tensor, and the thermal conductivity is characterized by an anisotropic second-rank tensor.

6.1. *Distribution function for non-uniform shear flow: expansion around the anisotropic Gaussian*

Following Grad (1949), we choose $(1, C_x, C_y, C_x^2, C_xC_y, C_y^2, C^2C_x, C^2C_y)$ as the basis set that incorporates the third-degree polynomials. Let us define an inner product,

$$\langle \chi, \psi \rangle = \frac{1}{2\pi|\boldsymbol{M}|^{1/2}} \int \chi\psi \exp\left(-\frac{1}{2}\boldsymbol{C}\cdot\boldsymbol{M}^{-1}\cdot\boldsymbol{C}\right) \mathrm{d}\boldsymbol{C}, \tag{6.1}$$

with respect to the anisotropic Gaussian as the weight function. The related orthonormal basis $(1, \xi_x, \xi_y, \xi_x^2, \xi_x\xi_y, \xi_y^2, \xi^2\xi_x, \xi^2\xi_y)$ is obtained by applying the Gram–Schmidt orthogonalization procedure.

We assume that the single-particle distribution function for the non-uniform shear flow (non-USF) can be expanded as

$$f = f_0(a + a_i\xi_i + a_{ij}\xi_i\xi_j + b_i\xi^2\xi_i), \tag{6.2}$$

where the anisotropic Gaussian

$$f_0 = \frac{n}{2\pi|\boldsymbol{M}|^{1/2}} \exp\left(-\frac{1}{2}C_\alpha M_{\alpha\beta}^{-1}C_\beta\right) \tag{6.3}$$

is the zeroth state representing the USF. The coefficients a, a_i, a_{ij} and b_i in (6.2) are to be chosen such that the basic hydrodynamic fields

$$(n, \boldsymbol{u}, \langle \boldsymbol{CC}\rangle) \tag{6.4}$$

are recovered at any order. This implies that the following 'compatibility' conditions must be satisfied:

$$\left.\begin{aligned} n(\boldsymbol{x}, t) &= \int f(\boldsymbol{c}, \boldsymbol{x}, t)\,\mathrm{d}\boldsymbol{c} = \int f_0(\boldsymbol{c}, \boldsymbol{x}, t)\,\mathrm{d}\boldsymbol{c}, \\ \int \boldsymbol{C} f(\boldsymbol{c}, \boldsymbol{x}, t)\,\mathrm{d}\boldsymbol{c} &= 0 = \int \boldsymbol{C} f_0(\boldsymbol{c}, \boldsymbol{x}, t)\,\mathrm{d}\boldsymbol{c}, \\ M_{\alpha\beta} = \int C_\alpha C_\beta f(\boldsymbol{c}, \boldsymbol{x}, t)\,\mathrm{d}\boldsymbol{c} &= \int C_\alpha C_\beta f_0(\boldsymbol{c}, \boldsymbol{x}, t)\,\mathrm{d}\boldsymbol{c} = M_{\alpha\beta}^{(0)}. \end{aligned}\right\} \tag{6.5}$$

This yields $a = 1$, $a_i = 0$, $a_{ij} = 0$ and $b_i \neq 0$. Therefore, the distribution function for non-USF is given by

$$\begin{aligned} f = \frac{n}{2\pi|\boldsymbol{M}|^{1/2}} \exp\left(-\frac{1}{2}C_\alpha M_{\alpha\beta}^{-1}C_\beta\right) \Bigg[1 &+ \frac{q_x\{C_x^3 + C_xC_y^2 - (3M_{xx} + M_{yy})C_x - 2M_{xy}C_y\}}{\rho\{M_{xx}(3M_{xx}^2 + 6M_{xy}^2 + M_{yy}^2) + 2M_{xy}^2M_{yy}\}} \\ &+ \frac{q_y\{M_{xx}(3M_{xx}^2 + 6M_{xy}^2 + M_{yy}^2) + 2M_{xy}^2M_{yy}\} - q_xM_{xy}(3M_{xx}^2 + 2M_{xx}M_{yy} + 4M_{xy}^2 + 3M_{yy}^2)}{\rho(M_{xx}M_{yy} - M_{xy}^2)\{M_{xx}^2(3M_{xx}^2 + 12M_{xy}^2 + 10M_{yy}^2) - 4M_{xy}^2(2M_{xx}M_{yy} - 4M_{xy}^2 - 3M_{yy}^2) + 3M_{yy}^4\}} \\ &\times \Bigg\{ C_x^2C_y + C_y^3 + \frac{3M_{xy}(M_{xx} + M_{yy})^3}{M_{xx}(3M_{xx}^2 + 6M_{xy}^2 + M_{yy}^2) + 2M_{xy}^2M_{yy}} C_x \\ &- \frac{M_{xx}^2(3M_{xx}^2 + 9M_{yy}M_{xx} + M_{yy}^2) + M_{xx}M_{yy}(3M_{yy}^2 + 16M_{xy}^2) - 8M_{xy}^4}{M_{xx}(3M_{xx}^2 + 6M_{xy}^2 + M_{yy}^2) + 2M_{xy}^2M_{yy}} C_y \\ &- \frac{M_{xy}(4M_{xy}^2 + 3M_{xx}^2 + 3M_{yy}^2 + 2M_{xx}M_{yy})}{M_{xx}(3M_{xx}^2 + 6M_{xy}^2 + M_{yy}^2) + 2M_{xy}^2M_{yy}} (C_x^3 + C_xC_y^2) \Bigg\} \Bigg], \end{aligned} \tag{6.6}$$

where

$$q_\alpha = \frac{m}{2}\int C^2 C_\alpha f(\boldsymbol{c},\boldsymbol{x},t)\,\mathrm{d}\boldsymbol{c} \tag{6.7}$$

is the 'kinetic' heat-flux vector.

6.2. *Generalized Fourier law from the balance of contracted third moment*

In the dilute limit, the collisional fluxes ($\varTheta(\cdot)=0$) are neglected and hence the balance equation for the contracted third moment $M_{\alpha\beta\beta}=\langle C_\alpha C_\beta C_\beta\rangle$ is obtained from (2.10) as

$$\rho\frac{\mathrm{D}M_{\alpha\beta\beta}}{\mathrm{D}t} + Q_{n\alpha\beta\beta,n} - 3M_{(\alpha\beta}P_{\beta)n,n} + 3Q_{n(\alpha\beta}u_{\beta),n} = \aleph_{\alpha\beta\beta}, \tag{6.8}$$

where $Q_{n\alpha\beta}\equiv\rho M_{n\alpha\beta}$ and the second term on the left-hand side is a contracted fourth-order moment,

$$Q_{n\alpha\beta\beta} = m\int C_n C_\alpha C^2 f(\boldsymbol{x},\boldsymbol{c},t)\,\mathrm{d}\boldsymbol{c}, \tag{6.9}$$

and the subscript under $(\ldots)$ on the third and fourth terms is defined such that

$$Q_{n(\alpha\beta}u_{\beta),n} = \tfrac{1}{3}(2Q_{n\alpha\beta}u_{\beta,n} + Q_{n\beta\beta}u_{\alpha,n}), \tag{6.10}$$

$$M_{(\alpha\beta}P_{\beta)n,n} = \tfrac{1}{3}(2M_{\alpha\beta}P_{\beta n,n} + M_{\beta\beta}P_{\alpha n,n}), \tag{6.11}$$

with the comma on the subscript denoting a partial derivative. The source term in (6.8) has the following integral expression:

$$\aleph_{\alpha\beta\beta}\equiv\aleph[C_\alpha C_\beta C_\beta] = \frac{m\sigma}{2}\iiint_{\boldsymbol{g}\cdot\boldsymbol{k}>0}\Delta(C^2C_\alpha)f(\boldsymbol{c}_1,\boldsymbol{x})f(\boldsymbol{c}_2,\boldsymbol{x})(\boldsymbol{g}\cdot\boldsymbol{k})\,\mathrm{d}\boldsymbol{k}\,\mathrm{d}\boldsymbol{c}_1\,\mathrm{d}\boldsymbol{c}_2, \tag{6.12}$$

where $\Delta(C^2C_\alpha)$ is defined in § A.3.

Inserting the distribution function (6.6) into (6.12), changing to new integration variables $(\boldsymbol{c}_1,\boldsymbol{c}_2)\to(\boldsymbol{g},\boldsymbol{G})$, and evaluating the integrals over $\boldsymbol{G}$, $\boldsymbol{g}$ and $\boldsymbol{k}$ (see § A.3), we obtain

$$\aleph_{\alpha\beta\beta} = -\frac{\rho(1+e)\sqrt{T}}{32\rho_p\sigma\sqrt{\pi}}\varOmega_{\alpha\gamma}q_\gamma, \tag{6.13}$$

where $\boldsymbol{q}=(q_x,q_y)$ is the heat-flux vector. Note that we have neglected quadratic nonlinear terms in q_γ to derive (6.13). The elements of $\varOmega=[\varOmega_{\alpha\gamma}]$ are

$$\varOmega=[\varOmega_{\alpha\gamma}] = \frac{1}{1+\eta^2+\eta^4}\begin{bmatrix}\overline{\varOmega}_{11} & \overline{\varOmega}_{12}\\ \overline{\varOmega}_{21} & \overline{\varOmega}_{22}\end{bmatrix}, \tag{6.14}$$

where

$$\left.\begin{aligned}
\overline{\varOmega}_{11} &= 608+714\eta^2+831\eta^4+82\eta^6-e(480+594\eta^2+606\eta^4-33\eta^6)\\
&\quad+\eta\sin2\phi(160+124\eta^2+148\eta^4+105\eta^6+e(-96+63\eta^2-84\eta^4)),\\
\overline{\varOmega}_{12} &= -\eta\cos2\phi(160+124\eta^2+148\eta^4+105\eta^6+e(-96+63\eta^2-84\eta^4))\\
&= \overline{\varOmega}_{21}\\
\overline{\varOmega}_{22} &= 608+714\eta^2+831\eta^4+82\eta^6-e(480+594\eta^2+606\eta^4-33\eta^6)\\
&\quad-\eta\sin2\phi(160+124\eta^2+148\eta^4+105\eta^6+e(-96+63\eta^2-84\eta^4)).
\end{aligned}\right\} \tag{6.15}$$

It is clear from (6.13) that the source term $\aleph_{\alpha\beta\beta}$ is a combination of q_x and q_y and depends on the restitution coefficient e, the temperature anisotropy η and the non-coaxiality angle ϕ.

6.2.1. *Heat flux from Maxwell iteration: thermal conductivity tensor*

Now we apply the well-known Maxwell iteration scheme (Truesdell & Muncaster 1980) to the contracted third-moment equation (6.8) to obtain the constitutive relation for heat flux. For this purpose, we rewrite (6.8) as

$$\aleph_{\alpha\beta\beta}=2\frac{\mathrm{D}q_\alpha}{\mathrm{D}t}+2q_\alpha\frac{\partial u_\beta}{\partial x_\beta}+\frac{\partial Q_{n\alpha\beta\beta}}{\partial x_n}-2(M_{\alpha\beta}+T\delta_{\alpha\beta})\frac{\partial P_{\beta n}}{\partial x_n}+2(Q_{n\alpha\beta}+q_n\delta_{\alpha\beta})\frac{\partial u_\beta}{\partial x_n}, \quad (6.16)$$

where q_α is defined in (6.7). In the Maxwell iteration scheme, the terms on the right-hand side of (6.16) are replaced by their zeroth-order values obtained by using the anisotropic Gaussian (6.3) as the distribution function. For the USF (i.e. at the zeroth order), it is straightforward to verify that

$$\left.\begin{aligned} P^{(0)}_{\alpha\beta} &= \rho M^{(0)}_{\alpha\beta}\equiv\rho M_{\alpha\beta},\\ q^{(0)}_{\alpha} &= 0=Q^{(0)}_{\alpha\beta\gamma},\\ Q^{(0)}_{n\alpha\beta\beta} &= 2\rho(T\delta_{\alpha\beta}+M_{\alpha\beta})M_{n\beta},\end{aligned}\right\} \quad (6.17)$$

and hence

$$\left.\begin{aligned} M^{(0)}_{\alpha\beta}P^{(0)}_{\beta n,n} &= \frac{\partial\rho}{\partial x_n}M_{\alpha\beta}M_{\beta n}+\rho M_{\alpha\beta}\frac{\partial M_{\beta n}}{\partial x_n},\\ \frac{1}{2}Q^{(0)}_{n\alpha\beta\beta,n} &= \frac{\partial\rho}{\partial x_n}TM_{n\alpha}+\rho\frac{\partial T}{\partial x_n}M_{n\alpha}+\rho T\frac{\partial M_{n\alpha}}{\partial x_n}\\ &\quad+\frac{\partial\rho}{\partial x_n}M_{n\beta}M_{\alpha\beta}+\rho\frac{\partial M_{n\beta}}{\partial x_n}M_{\alpha\beta}+\rho M_{n\beta}\frac{\partial M_{\alpha\beta}}{\partial x_n}.\end{aligned}\right\} \quad (6.18)$$

Inserting (6.17) and (6.18) into the right-hand side of (6.16) and equating the resulting expression with (6.13), we obtain the desired constitutive relation for the heat flux:

$$q_\gamma=-\frac{64\rho_p\sigma\sqrt{\pi}}{(1+e)\sqrt{T}}\,\mathfrak{Q}^{-1}_{\gamma\alpha}\left(2M_{\alpha n}\frac{\partial T}{\partial x_n}+M_{\beta n}\frac{\partial\widehat{M}_{\alpha\beta}}{\partial x_n}\right), \quad (6.19)$$

where $\widehat{M}_{\alpha\beta}$ is the deviatoric part of the second-moment tensor $M_{\alpha\beta}=T\delta_{\alpha\beta}+\widehat{M}_{\alpha\beta}$, with $\mathfrak{Q}_{\gamma\alpha}$ being given by (6.14) and (6.15). (A similar expression for the heat flux was used by Simon & Jenkins (1994) in the context of modelling planetary rings, made of inelastic spheres (i.e. in three dimensions), but they did not present the related derivation.) Equation (6.19) should be treated as a generalized Fourier law, since the gradient of the deviatoric part of the second moment (or the kinetic stress) also creates a heat flux, in addition to the standard Fourier contribution due to the temperature gradient. This indicates that there could be a heat flux even in the absence of a temperature gradient, driven solely by the gradient of the deviatoric stress $\widehat{M}_{\alpha\beta}$. Such a stress-gradient-driven heat flux is well known in rarefied gases (Grad 1949; Kogan 1969; Chapman & Cowling 1970); in fact, applying the Maxwell iteration scheme to equation (5.38) of Grad (1949) leads to a similar constitutive relation for the heat flux as in (6.19). In any case, identifying the coefficient of the temperature gradient in (6.19) with the thermal conductivity, we find that the thermal conductivity,

$$\kappa_{\gamma n}=\frac{128\rho_p\sigma\sqrt{\pi}}{(1+e)\sqrt{T}}\,\mathfrak{Q}^{-1}_{\gamma\alpha}M_{\alpha n}, \quad (6.20)$$

is a second-rank tensor that is anisotropic ($\kappa_{xx} \neq \kappa_{yy}$ and $\kappa_{xy} \neq 0$). The anisotropy of (6.20) is a consequence of the imposed shear field, since the 'cross' thermal conductivity coefficient κ_{xy} is proportional to $\eta \sim \dot{\gamma}$. Therefore, (6.20) can aptly be dubbed the 'shear-induced' anisotropic thermal conductivity tensor. One consequence of this anisotropy is the well-known rarefaction effect of heat flow along a direction orthogonal to the temperature gradient (Kogan 1969).

6.2.2. *Thermal conductivity at Navier–Stokes order: verification*

As a check, we consider the limit of vanishing temperature anisotropy, $\eta \to 0$, for which the following relations hold:

$$M_{\alpha\beta} = T\delta_{\alpha\beta}, \quad \widehat{M}_{\alpha\beta} = 0 \quad \text{and} \quad \mathfrak{Q}^{-1}_{\gamma\alpha} = \frac{-1}{32(15e-19)}\delta_{\gamma\alpha}. \tag{6.21a–c}$$

Inserting these into (6.19) and (6.20), we obtain

$$q_\gamma = -\frac{16m\sqrt{T}}{\sqrt{\pi}\sigma(19+4e-15e^2)}\frac{\partial T}{\partial x_\gamma} \equiv -\kappa\frac{\partial T}{\partial x_\gamma}, \tag{6.22}$$

where

$$\kappa = \frac{16m\sqrt{T}}{\sqrt{\pi}\sigma(19+4e-15e^2)}. \tag{6.23}$$

Equation (6.23) agrees exactly with the expression for thermal conductivity for a dilute system of inelastic hard disks at NS order (Jenkins & Richman 1985*a*).

To summarize this section, we have found a generalized Fourier law (6.19) and determined the explicit expressions for the elements of the thermal conductivity tensor (6.20) in terms of e, η and ϕ for a sheared system of a dilute granular gas in two dimensions. This should be extended to a dense granular gas to obtain an expression for the thermal conductivity tensor for the whole range of densities.

7. Conclusions and outlook

We analysed the Grad-level moment equations (Grad 1949; Jenkins & Richman 1988) for the plane shear flow of smooth inelastic disks, with a goal to obtain closed-form expressions for the non-Newtonian stress tensor, the collisional dissipation rate and the granular heat flux. In this moment approach, an anisotropic Gaussian (Goldreich & Tremaine 1978; Araki & Tremaine 1986), which is a function of all components of the second moment of the fluctuation velocity ($\boldsymbol{M} = \langle \boldsymbol{CC} \rangle$), was taken as the single-particle distribution function representing the base state of USF. The mass and momentum balance equations are identically satisfied for USF, and the equation for the second-moment tensor of velocity fluctuations was solved semi-analytically via a series expansion of certain collision integrals.

We derived closed-form expressions for all the transport coefficients (shear viscosity μ, pressure p and first normal stress difference $\mathscr{N}_1$) and the collisional dissipation rate $\mathscr{D}$ in terms of five parameters: (i) density or area fraction ν, (ii) restitution coefficient e, (iii) shear rate R (see (3.10)), (iv) temperature anisotropy η (see (3.6)) and (v) angle ϕ between the principal eigenvectors of the shear tensor $\boldsymbol{D} = (\boldsymbol{\nabla u} + (\boldsymbol{\nabla u})^{\mathrm{T}})/2$ and the second-moment tensor $\boldsymbol{M}$. The last two parameters (η and ϕ) are zero at the NS order (i.e. at the linear order in the shear rate) and are, therefore, a measure of the non-Newtonian rheology of the medium. In the uniform shear state, we found that R, η

and $\sin 2\phi$ scale with inelasticity $\epsilon = (1-e)^{1/2}$ at the leading order (see (4.6) and discussion in § 4.4), and therefore the shear-rate dependence of transport coefficients can be translated into their dependence on ϵ in USF. The nonlinear nature of the rheology was analysed by retaining terms up to the super-Burnett order (i.e. third order in R and η) in the transport coefficients, and our analytical expressions for transport coefficients reduced to known exact expressions for the Newtonian rheology when they were truncated at the NS order. The origin of the first normal stress difference was shown to be tied to (i) the non-coaxiality ($\phi \neq 0$) of the principal directions of the shear and second-moment tensors and (ii) the temperature anisotropy ($\eta \neq 0$). Both are shear-induced effects and appear at the Burnett-order approximation of transport coefficients. In particular, both $\sin 2\phi$ and η are finite and are of the same order in the dilute limit, leading to $\mathscr{N}_1 \neq 0$ as $\nu \to 0$.

From a comparison of analytically derived constitutive relations with those obtained from the full numerical solution of moment equations (see figure 3), we showed that, while the Burnett-order terms (i.e. second order in R and η) are sufficient for accurate predictions of all transport coefficients (μ, p and $\mathscr{N}_1$) in the dilute limit, the super-Burnett-order terms must be retained to achieve similar accuracy for dense flows, especially at large dissipations. The resulting super-Burnett-order transport coefficients were further validated via a comparison with the event-driven simulation data for the USF of an inelastic hard-disk system. We found good agreement between simulation and moment theory for p, μ and $\mathscr{N}_1$ (figures 5–9) for a range of densities spanning from the dilute to close to the freezing point. In contrast, the transport coefficients obtained from an NS-order constitutive model (which is assumed to hold at any dissipation (Lutsko 2005; Garzo *et al.* 2007)) were shown to deviate significantly from both simulation and the moment theory even at moderate values of the restitution coefficient ($e \sim 0.9$). The success of the anisotropic Gaussian to predict transport coefficients in the uniform shear state seems to be tied to the fact that the terms of all orders in the shear rate and the temperature anisotropy are implicitly incorporated in the anisotropic Gaussian distribution function.

Going beyond the uniform shear state, we derived a constitutive relation for the granular heat flux in the dilute limit (§ 6) using a perturbation expansion around the anisotropic Gaussian and subsequently employing the Maxwell iteration scheme on the balance equation for the contracted third moment ($M_{\alpha\beta\beta} = \langle C_\alpha C^2 \rangle$) of fluctuation velocity. We found that the granular heat flux follows a generalized Fourier law (6.19) in which the gradients of the deviatoric part of the second-moment tensor drive a heat current in addition to the standard Fourier conduction driven by the temperature gradient. This non-Fourier contribution is a rarefaction effect, which appears at the Grad-level (second order in gradients) description of the granular shear flow, and has an analogue in rarefied molecular gases too (Grad 1949). The thermal conductivity is found to be characterized by an anisotropic second-rank tensor (6.20), for which we derived an explicit expression in terms of the restitution coefficient e, temperature anisotropy η and non-coaxiality angle ϕ. In the limits of $\eta \to 0$ and $\phi \to 0$, we recovered the expression for the scalar thermal conductivity that holds at the NS order.

In addition to considering the three-dimensional case of spheres, the present anisotropic moment theory can be extended to include the full contracted fourth moment ($M_{\alpha\alpha\beta\beta} = \langle C^4 \rangle$) as a separate hydrodynamic field, which is likely to recover the density-gradient-dependent term in the constitutive relation for heat flux (Saha & Alam 2014). This will also generate additional contributions (in terms of the fourth velocity cumulant, $\alpha_2 = \langle C^4 \rangle / \langle C^4 \rangle^{(0)} - 1$) to (i) the shear viscosity μ (4.11) and (ii) the dissipation rate $\mathscr{D}$ (4.24) that can be checked in future work. For the

three-dimensional case, the existing Grad-level theories that are based on an expansion around the isotropic Gaussian state (e.g. Kremer & Marques 2011) predict that the second normal stress difference is zero, which is in contrast to both the particle simulation data (Alam & Luding 2005*a*,*b*) and the Burnett-order theory (Sela & Goldhirsch 1998) based on Chapman–Enskog expansion. On the other hand, the theories based on the anisotropic Gaussian (Chou & Richman 1998; Lutsko 2004) predict non-zero values for both normal stress differences. Therefore, the present semi-analytical formalism of the anisotropic moment theory should be extended to derive closed-form constitutive relations for spheres too. Another direction of research would be to extend the present approach: (i) to include the rotational motion for a rough frictional granular gas (Jenkins & Richman 1985*a*; Mitarai, Nakanishi & Hayakawa 2002; Rongali & Alam 2014); and (ii) to consider a sheared binary or polydisperse granular mixture (Alam *et al.* 2002; Lutsko 2004; Montanero *et al.* 2006). The present constitutive relations for the stress tensor (§ 4.2) and the heat flux (§ 6) along with extended hydrodynamic equations (2.11)–(2.13) can also be tested in dynamic simulations of granular flows, including the stability analyses of shear flows (Gayen & Alam 2006; Shukla & Alam 2009, 2011*a*,*b*).

Acknowledgements

One of us (M.A.) learned much about the related literature on 'planetary rings' while attending a conference on 'Non-Equilibrium Dynamics in Astrophysics and Material Science' (November 2011), held at Yukawa Institute for Theoretical Physics, Kyoto University, Japan, and is grateful to Professor H. Hayakawa for the invitation and hospitality for the same. M.A. would like to thank Professor J. T. Jenkins for a fruitful coffee-table discussion on this topic during this conference as well as Dr J. Schmidt for discussions on Saturn's ring and sharing many related references.

Appendix A. Integral expressions for collisional flux and source terms

A.1. *Collisional flux of momentum ($\Theta_{\alpha\beta}$) at second order*

For a dense system of disks, the collisional flux of momentum can be expressed as (Jenkins & Richman 1985*a*,*b*, 1988):

$$\begin{aligned}\Theta_{\alpha\beta} &= \Theta_\alpha[mC_\beta]\\ &= \frac{m(1+e)\sigma^2}{4}\iiint_{\boldsymbol{g}\cdot\boldsymbol{k}>0}(\boldsymbol{g}\cdot\boldsymbol{k})^2 k_\alpha k_\beta\\ &\quad\times\int_0^1 f^{(2)}(\boldsymbol{c}_1,\boldsymbol{x}-\omega\sigma\boldsymbol{k},\boldsymbol{c}_2,\boldsymbol{x}+\sigma\boldsymbol{k}-\omega\sigma\boldsymbol{k})\,\mathrm{d}\omega\,\mathrm{d}\boldsymbol{k}\,\mathrm{d}\boldsymbol{c}_1\,\mathrm{d}\boldsymbol{c}_2\\ &= \frac{m(1+e)\sigma^2}{4}\iiint_{\boldsymbol{g}\cdot\boldsymbol{k}>0}(\boldsymbol{g}\cdot\boldsymbol{k})^2 k_\alpha k_\beta\\ &\quad\times\int_{-1/2}^{1/2} f^{(2)}\left(\boldsymbol{c}_1,\boldsymbol{x}+\left(\xi-\frac{1}{2}\right)\sigma\boldsymbol{k},\boldsymbol{c}_2,\boldsymbol{x}+\left(\xi+\frac{1}{2}\right)\sigma\boldsymbol{k}\right)\mathrm{d}\xi\,\mathrm{d}\boldsymbol{G}\,\mathrm{d}\boldsymbol{k}\,\mathrm{d}\boldsymbol{g}. \end{aligned}\tag{A 1}$$

The latter expression has been obtained via a change of variables: $(\boldsymbol{c}_1,\,\boldsymbol{c}_2,\,\omega)\to(\boldsymbol{g},\,\boldsymbol{G},\,\xi)$, with $\boldsymbol{g}=\boldsymbol{c}_1-\boldsymbol{c}_2$, $\boldsymbol{G}=(\boldsymbol{C}_1+\boldsymbol{C}_2)/2$, $\xi=1/2-\omega$ and $\mathrm{d}\boldsymbol{c}_1\,\mathrm{d}\boldsymbol{c}_2=\mathrm{d}\boldsymbol{g}\,\mathrm{d}\boldsymbol{G}$. With the molecular chaos assumption and using the Taylor series expansion on the single-particle distribution $f^{(1)}$, the two-particle distribution in (A 1) can be

simplified to

$$f^{(2)}\left(\boldsymbol{c}_1, \boldsymbol{x}+\left(\xi-\frac{1}{2}\right)\sigma\boldsymbol{k}, \boldsymbol{c}_2, \boldsymbol{x}+\left(\xi+\frac{1}{2}\right)\sigma\boldsymbol{k}\right)$$
$$=\frac{n^2 g_0}{4\pi^2|\boldsymbol{M}|}\exp\left\{-\frac{1}{4}M^{-1}_{\alpha\beta}[(g_\alpha+V_\alpha)(g_\beta+V_\beta)+4(G_\alpha-\xi V_\alpha)(G_\beta-\xi V_\beta)]\right\}, \quad \text{(A 2)}$$

where $|\boldsymbol{M}|\equiv\det(\boldsymbol{M})$ and $\boldsymbol{V}=\sigma\boldsymbol{k}\cdot\boldsymbol{\nabla}u$.

Combining (A 1) and (A 2), we obtain

$$\begin{aligned}\Theta_{\alpha\beta} &= \frac{m(1+e)n^2 g_0\sigma^2}{16\pi^2|\boldsymbol{M}|}\iint_{\boldsymbol{g}\cdot\boldsymbol{k}>0}(\boldsymbol{g}\cdot\boldsymbol{k})^2 k_\alpha k_\beta \exp\left\{-\frac{1}{4}\left[(g_\alpha+V_\alpha)M^{-1}_{\alpha\beta}(g_\beta+V_\beta)\right]\right\}\\ &\quad\times\left(\int_{-1/2}^{1/2}\int\exp\{-[(G_\alpha-\xi V_\alpha)M^{-1}_{\alpha\beta}(G_\beta-\xi V_\beta)]\}\,\mathrm{d}\boldsymbol{G}\,\mathrm{d}\xi\right)\mathrm{d}\boldsymbol{k}\,\mathrm{d}\boldsymbol{g}\\ &= \frac{\rho n(1+e)g_0\sigma^2}{16\pi|\boldsymbol{M}|^{1/2}}\iint_{\boldsymbol{g}\cdot\boldsymbol{k}>0}(\boldsymbol{g}\cdot\boldsymbol{k})^2 k_\alpha k_\beta\exp\left\{-\frac{1}{4}[(g_\alpha+V_\alpha)M^{-1}_{\alpha\beta}(g_\beta+V_\beta)]\right\}\mathrm{d}\boldsymbol{k}\,\mathrm{d}\boldsymbol{g}.\end{aligned} \quad \text{(A 3)}$$

To arrive at (A 3), the identity $\int\int(\cdot)\,\mathrm{d}\boldsymbol{G}\,\mathrm{d}\xi=\pi\sqrt{|\boldsymbol{M}|}$ has been used. Carrying out the integration over $\boldsymbol{g}$, a compact expression for the collisional flux of momentum is obtained as given by (3.13).

A.2. *Collisional source of second moment ($\aleph_{\alpha\beta}$) at second order*

Using the molecular chaos assumption and the Taylor series expansion of a single-particle distribution about $\boldsymbol{x}$, the two-particle distribution function can be written as

$$\begin{aligned}&f^{(2)}(\boldsymbol{c}_1, \boldsymbol{x}-\sigma\boldsymbol{k}, \boldsymbol{c}_2, \boldsymbol{x})\\ &\quad=\frac{n^2 g_0}{4\pi^2|\boldsymbol{M}|}\exp\left\{-\frac{1}{2}M^{-1}_{\alpha\beta}[(C_\alpha+V_\alpha)(C_\beta+V_\beta)+(C_\alpha C_\beta)]\right\}\\ &\quad=\frac{n^2 g_0}{4\pi^2|\boldsymbol{M}|}\exp\left\{-\frac{1}{4}M^{-1}_{\alpha\beta}[(g_\alpha+V_\alpha)(g_\beta+V_\beta)+(2G_\alpha+V_\alpha)(2G_\beta+V_\beta)]\right\},\end{aligned} \quad \text{(A 4)}$$

where the last expression involves a change of variables $(\boldsymbol{c}_1, \boldsymbol{c}_2)\to(\boldsymbol{g}, \boldsymbol{G})$ and $\boldsymbol{V}=\sigma\boldsymbol{k}\cdot\boldsymbol{\nabla}\boldsymbol{u}$.

The collisional source of the second moment can be expressed as (Jenkins & Richman 1985*a*,*b*, 1988)

$$\begin{aligned}\aleph_{\alpha\beta} &\equiv \aleph_{\alpha\beta}[mC_\alpha C_\beta]\\ &= \frac{m\sigma}{2}\iiint_{\boldsymbol{g}\cdot\boldsymbol{k}>0}\Delta(C_\alpha C_\beta)f^{(2)}(\boldsymbol{c}_1, \boldsymbol{x}-\sigma\boldsymbol{k}, \boldsymbol{c}_2, \boldsymbol{x})(\boldsymbol{k}\cdot\boldsymbol{g})\,\mathrm{d}\boldsymbol{k}\,\mathrm{d}\boldsymbol{c}_1\,\mathrm{d}\boldsymbol{c}_2\\ &= \frac{mn^2 g_0\sigma}{8\pi^2|\boldsymbol{M}|}\iint_{\boldsymbol{g}\cdot\boldsymbol{k}>0}\Delta(C_\alpha C_\beta)(\boldsymbol{g}\cdot\boldsymbol{k})\exp\left\{-\frac{1}{4}[(g_\alpha+V_\alpha)M^{-1}_{\alpha\beta}(g_\beta+V_\beta)]\right\}\\ &\quad\times\left(\int\exp\left\{-\frac{1}{4}[(2G_\alpha+V_\alpha)M^{-1}_{\alpha\beta}(2G_\beta+V_\beta)]\right\}\mathrm{d}\boldsymbol{G}\right)\mathrm{d}\boldsymbol{k}\,\mathrm{d}\boldsymbol{g}\end{aligned}$$

$$= \frac{m\sigma n^2 g_0}{8\pi|\boldsymbol{M}|^{1/2}} \iint_{\boldsymbol{g}\cdot\boldsymbol{k}>0} \Delta(C_\alpha C_\beta)(\boldsymbol{g}\cdot\boldsymbol{k}) \exp\left\{-\frac{1}{4}[(g_\alpha + V_\alpha)M^{-1}_{\alpha\beta}(g_\beta + V_\beta)]\right\} \mathrm{d}\boldsymbol{k}\,\mathrm{d}\boldsymbol{g}$$

$$= \frac{\rho\nu g_0}{2\pi^2\sigma|\boldsymbol{M}|^{1/2}} \iint_{\boldsymbol{g}\cdot\boldsymbol{k}>0} \Delta(C_\alpha C_\beta)(\boldsymbol{g}\cdot\boldsymbol{k}) \exp\left\{-\frac{1}{4}[(g_\alpha + V_\alpha)M^{-1}_{\alpha\beta}(g_\beta + V_\beta)]\right\} \mathrm{d}\boldsymbol{k}\,\mathrm{d}\boldsymbol{g}. \tag{A 5}$$

The last expression results from $\int(\cdot)\,\mathrm{d}\boldsymbol{G} = \pi\sqrt{|\boldsymbol{M}|}$. Note further that

$$\Delta(C_\alpha C_\beta) = -\tfrac{1}{2}(1-e^2)(\boldsymbol{g}\cdot\boldsymbol{k})^2 k_\alpha k_\beta - \tfrac{1}{2}(1+e)(\boldsymbol{g}\cdot\boldsymbol{k})(\boldsymbol{g}\cdot\boldsymbol{j})(j_\alpha k_\beta + k_\alpha j_\beta), \tag{A 6}$$

where $\boldsymbol{j}$ is a unit vector perpendicular to the contact vector $\boldsymbol{k}$.

Inserting (A 6) into (A 5) and performing integrations over $\boldsymbol{g}$, a compact expression for $\aleph_{\alpha\beta}$ is obtained,

$$\aleph_{\alpha\beta} = A_{\alpha\beta} + \widehat{B}_{\alpha\beta}, \tag{A 7}$$

where $A_{\alpha\beta}$ is given by (3.15), and the traceless part, $\widehat{B}_{\alpha\beta}$, can be further decomposed into

$$\widehat{B}_{\alpha\beta} = \widehat{E}_{\alpha\beta} + \widehat{F}_{\alpha\beta}, \tag{A 8}$$

where

$$\widehat{E}_{\alpha\beta} = -\frac{4(1+e)\rho\nu g_0(\nu)}{\sigma\pi^{3/2}} \int (j_\alpha k_\beta + k_\alpha j_\beta)(\boldsymbol{j}\cdot\boldsymbol{M}\cdot\boldsymbol{k})(\boldsymbol{k}\cdot\boldsymbol{M}\cdot\boldsymbol{k})^{1/2}\mathfrak{F}(\chi)\,\mathrm{d}\boldsymbol{k}, \tag{A 9}$$

$$\begin{aligned}\widehat{F}_{\alpha\beta} &= \frac{2(1+e)\rho\nu g_0(\nu)}{\sigma\pi^{3/2}} \int (j_\alpha k_\beta + k_\alpha j_\beta)(\boldsymbol{V}\cdot\boldsymbol{M}^{-1}\cdot\boldsymbol{j})|\boldsymbol{M}|\mathfrak{G}(\chi)\,\mathrm{d}\boldsymbol{k} \\ &= \frac{2(1+e)\rho\nu g_0(\nu)}{\pi^{3/2}} \int (j_\alpha k_\beta + k_\alpha j_\beta)(\boldsymbol{k}\cdot(\boldsymbol{W}+\boldsymbol{D})\cdot\boldsymbol{M}^{-1}\cdot\boldsymbol{j})|\boldsymbol{M}|\mathfrak{G}(\chi)\,\mathrm{d}\boldsymbol{k} \\ &= \Theta_{\alpha\gamma}W_{\beta\gamma} + \Theta_{\beta\gamma}W_{\alpha\gamma} + \widehat{G}_{\alpha\beta},\end{aligned} \tag{A 10}$$

and

$$\widehat{G}_{\alpha\beta} = \frac{2(1+e)\rho\nu g_0(\nu)}{\pi^{3/2}} \int (j_\alpha k_\beta + k_\alpha j_\beta)k_\xi j_\gamma (TD_{\gamma\xi} - D_{\delta\xi}\widehat{M}_{\delta\gamma})\mathfrak{G}(\chi)\,\mathrm{d}\boldsymbol{k}, \tag{A 11}$$

with $\widehat{\boldsymbol{M}}$ being the deviatoric part of $\boldsymbol{M}$. The expression for $\mathfrak{F}(\chi)$ is given by (3.18), with χ as in (3.20).

A.3. *Third-order source term ($\aleph_{\alpha\beta\beta}$) to calculate heat flux in the dilute limit*

In the dilute limit, the third-order source term in (6.8) has the following integral expression:

$$\begin{aligned}\aleph_{\alpha\beta\beta} &= \aleph[mC^2C_\alpha] \\ &= \frac{m\sigma}{2} \iiint_{\boldsymbol{g}\cdot\boldsymbol{k}>0} \Delta(C^2C_\alpha) f^{(1)}(\boldsymbol{c}_1,\boldsymbol{x}) f^{(1)}(\boldsymbol{c}_2,\boldsymbol{x})(\boldsymbol{g}\cdot\boldsymbol{k})\,\mathrm{d}\boldsymbol{k}\,\mathrm{d}\boldsymbol{c}_1\,\mathrm{d}\boldsymbol{c}_2.\end{aligned} \tag{A 12}$$

Changing the variables of integration from $(\boldsymbol{c}_1,\boldsymbol{c}_2)\to(\boldsymbol{g},\boldsymbol{G})$, with $\mathrm{d}\boldsymbol{c}_1\,\mathrm{d}\boldsymbol{c}_2 = \mathrm{d}\boldsymbol{C}_1\,\mathrm{d}\boldsymbol{C}_2 = \mathrm{d}\boldsymbol{g}\,\mathrm{d}\boldsymbol{G}$ and

$$\begin{aligned}\Delta(C^2C_\alpha) = {} & [(1+e)^2(\boldsymbol{g}\cdot\boldsymbol{k})^2 G_\beta k_\beta k_\alpha - \tfrac{1}{2}(1-e^2)(\boldsymbol{g}\cdot\boldsymbol{k})^2 G_\alpha \\ & - (1+e)(\boldsymbol{g}\cdot\boldsymbol{k})G_\beta(k_\beta g_\alpha + g_\beta k_\alpha)],\end{aligned} \tag{A 13}$$

we can write

$$\begin{aligned}\aleph_{\alpha\beta\beta} &= \frac{m\sigma n^2}{8\pi^2|\boldsymbol{M}|}\iiint_{\boldsymbol{g}\cdot\boldsymbol{k}>0}\Big[(1+e)^2(\boldsymbol{g}\cdot\boldsymbol{k})^3 G_\beta k_\beta k_\alpha \\ &\quad -\frac{1}{2}(1-e^2)(\boldsymbol{g}\cdot\boldsymbol{k})^3 G_\alpha - (1+e)(\boldsymbol{g}\cdot\boldsymbol{k})^2 G_\beta(k_\beta g_\alpha + g_\beta k_\alpha)\Big] \\ &\quad \times \exp\left\{-\frac{1}{4}M_{ab}^{-1}(4G_aG_b + g_ag_b)\right\}[Xf_1(\boldsymbol{g},\boldsymbol{G}) + Yf_2(\boldsymbol{g},\boldsymbol{G})]\,\mathrm{d}\boldsymbol{G}\,\mathrm{d}\boldsymbol{g}\,\mathrm{d}\boldsymbol{k} \\ &\equiv I^{(1)}_{\alpha\beta\beta} + I^{(2)}_{\alpha\beta\beta} + I^{(3)}_{\alpha\beta\beta},\end{aligned} \tag{A 14}$$

where

$$X = \frac{q_x}{2\rho(M_{xx}(3M_{xx}^2 + 6M_{xy}^2 + M_{yy}^2) + 2M_{xy}^2M_{yy})}, \tag{A 15}$$

$$Y = \frac{q_y(M_{xx}(3M_{xx}^2 + 6M_{xy}^2 + M_{yy}^2) + 2M_{xy}^2M_{yy}) - q_xM_{xy}(3M_{xx}^2 + 2M_{xx}M_{yy} + 4M_{xy}^2 + 3M_{yy}^2)}{\rho|\boldsymbol{M}|(M_{xx}^2(3M_{xx}^2 + 12M_{xy}^2 + 10M_{yy}^2) + 4M_{xy}^2(-2M_{xx}M_{yy} + 4M_{xy}^2 + 3M_{yy}^2) + 3M_{yy}^4)} \tag{A 16}$$

$$f_1(\boldsymbol{g},\boldsymbol{G}) = \{3g_x^2G_x + g_y^2G_x + 4G_x^3 + 2g_xg_yG_y + 4G_xG_y^2 - 4(3M_{xx} + M_{yy})G_x - 8M_{xy}G_y\}, \tag{A 17}$$

$$\begin{aligned}f_2(\boldsymbol{g},\boldsymbol{G}) &= \Big\{\frac{3}{2}g_y^2G_y + \frac{1}{2}g_x^2G_y + 2G_y^3 + g_xg_yG_x + 2G_x^2G_y \\ &\quad + \frac{6M_{xy}(M_{xx}+M_{yy})^3}{3M_{xx}^3 + 6M_{xy}^2M_{xx} + M_{xx}M_{yy}^2 + 2M_{xy}^2M_{yy}}G_x \\ &\quad - \frac{2(3M_{xx}^4 + 9M_{yy}M_{xx}^3 + M_{yy}^2M_{xx}^2 + 3M_{yy}^3M_{xx} + 16M_{xy}^2M_{yy}M_{xx} - 8M_{xy}^4)}{3M_{xx}^3 + 6M_{xy}^2M_{xx} + M_{yy}^2M_{xx} + 2M_{xy}^2M_{yy}}G_y \\ &\quad - \frac{M_{xy}(4M_{xy}^2 + 3M_{xx}^2 + 3M_{yy}^2 + 2M_{xx}M_{yy})}{3M_{xx}^3 + 6M_{xy}^2M_{xx} + M_{yy}^2M_{xx} + 2M_{xy}^2M_{yy}} \\ &\quad \times \left(\frac{3}{2}g_x^2G_x + \frac{1}{2}g_y^2G_x + 2G_x^3 + g_xg_yG_y + 2G_xG_y^2\right)\Big\}.\end{aligned} \tag{A 18}$$

Now using

$$\int \exp\{-G_aM_{ab}^{-1}G_b\}\,\mathrm{d}\boldsymbol{G} = \pi|\boldsymbol{M}|^{1/2}, \tag{A 19}$$

$$\int G_iG_j\exp\{-G_aM_{ab}^{-1}G_b\}\,\mathrm{d}\boldsymbol{G} = \frac{\pi}{2}|\boldsymbol{M}|^{1/2}M_{ij}, \tag{A 20}$$

$$\int G_iG_jG_kG_l\exp\{-G_aM_{ab}^{-1}G_b\}\,\mathrm{d}\boldsymbol{G} = \frac{\pi}{4}|\boldsymbol{M}|^{1/2}(M_{ij}M_{kl} + M_{ik}M_{jl} + M_{il}M_{jk}), \tag{A 21}$$

we carry out the integrations over $\boldsymbol{G}$ to obtain

$$\begin{aligned}I^{(1)}_{\alpha\beta\beta} &= \frac{m\sigma n^2(1+e)^2}{8\pi|\boldsymbol{M}|^{1/2}}\iint_{\boldsymbol{g}\cdot\boldsymbol{k}>0}\exp\left\{-\frac{1}{4}g_aM_{ab}^{-1}g_b\right\}(\boldsymbol{g}\cdot\boldsymbol{k})^3k_\beta k_\alpha \\ &\quad \times\Big[X\left(\frac{3}{2}g_x^2M_{x\beta} + \frac{1}{2}g_y^2M_{x\beta} + g_xg_yM_{y\beta} - (3M_{xx}+M_{yy})M_{x\beta} - 2M_{xy}M_{y\beta}\right)\end{aligned}$$

$$+Y\left\{\frac{3}{4}g_y^2M_{y\beta}+\frac{1}{4}g_x^2M_{y\beta}+\frac{1}{2}g_xg_yM_{x\beta}+\frac{1}{2}(M_{xx}+3M_{yy})M_{y\beta}+M_{xy}M_{x\beta}\right.$$
$$+\frac{3M_{xy}M_{x\beta}(M_{xx}+M_{yy})^3}{3M_{xx}^3+6M_{xy}^2M_{xx}+M_{xx}M_{yy}^2+2M_{xy}^2M_{yy}}$$
$$-\frac{(3M_{xx}^4+9M_{yy}M_{xx}^3+M_{yy}^2M_{xx}^2+3M_{yy}^3M_{xx}+16M_{xy}^2M_{yy}M_{xx}-8M_{xy}^4)}{3M_{xx}^3+6M_{xy}^2M_{xx}+M_{yy}^2M_{xx}+2M_{xy}^2M_{yy}}M_{y\beta}$$
$$-\frac{4M_{xy}^3+3M_{xx}^2M_{xy}+3M_{yy}^2M_{xy}+2M_{xx}M_{yy}M_{xy}}{3M_{xx}^3+6M_{xy}^2M_{xx}+M_{yy}^2M_{xx}+2M_{xy}^2M_{yy}}$$
$$\left.\left.\times\left(\frac{3}{4}g_x^2M_{x\beta}+\frac{1}{4}g_y^2M_{x\beta}+\frac{1}{2}g_xg_yM_{y\beta}+\frac{1}{2}(3M_{xx}+M_{yy})M_{x\beta}+M_{xy}M_{y\beta}\right)\right\}\right]\mathrm{d}\boldsymbol{g}\,\mathrm{d}\boldsymbol{k},\tag{A 22}$$

$$I^{(2)}_{\alpha\beta\beta}=-\frac{m\sigma n^2(1-e^2)}{16\pi|\boldsymbol{M}|^{1/2}}\iint_{\boldsymbol{g}\cdot\boldsymbol{k}>0}\exp\left\{-\frac{1}{4}g_aM^{-1}_{ab}g_b\right\}(\boldsymbol{g}\cdot\boldsymbol{k})^3$$
$$\times\left[X\left(\frac{3}{2}g_x^2M_{x\alpha}+\frac{1}{2}g_y^2M_{x\alpha}+g_xg_yM_{y\alpha}-(3M_{xx}+M_{yy})M_{x\alpha}-2M_{xy}M_{y\alpha}\right)\right.$$
$$+Y\left\{\frac{3}{4}g_y^2M_{y\alpha}+\frac{1}{4}g_x^2M_{y\alpha}+\frac{1}{2}g_xg_yM_{x\alpha}+\frac{1}{2}(M_{xx}+3M_{yy})M_{y\alpha}+M_{xy}M_{x\alpha}\right.$$
$$+\frac{3M_{xy}M_{x\alpha}(M_{xx}+M_{yy})^3}{3M_{xx}^3+6M_{xy}^2M_{xx}+M_{xx}M_{yy}^2+2M_{xy}^2M_{yy}}$$
$$-\frac{(3M_{xx}^4+9M_{yy}M_{xx}^3+M_{yy}^2M_{xx}^2+3M_{yy}^3M_{xx}+16M_{xy}^2M_{yy}M_{xx}-8M_{xy}^4)}{3M_{xx}^3+6M_{xy}^2M_{xx}+M_{yy}^2M_{xx}+2M_{xy}^2M_{yy}}M_{y\alpha}$$
$$-\frac{4M_{xy}^3+3M_{xx}^2M_{xy}+3M_{yy}^2M_{xy}+2M_{xx}M_{yy}M_{xy}}{3M_{xx}^3+6M_{xy}^2M_{xx}+M_{yy}^2M_{xx}+2M_{xy}^2M_{yy}}$$
$$\left.\left.\times\left(\frac{3}{4}g_x^2M_{x\alpha}+\frac{1}{4}g_y^2M_{x\alpha}+\frac{1}{2}g_xg_yM_{y\alpha}+\frac{1}{2}(3M_{xx}+M_{yy})M_{x\alpha}+M_{xy}M_{y\alpha}\right)\right\}\right]\mathrm{d}\boldsymbol{g}\,\mathrm{d}\boldsymbol{k},\tag{A 23}$$

$$I^{(3)}_{\alpha\beta\beta}=-\frac{m\sigma n^2(1+e)}{8\pi|\boldsymbol{M}|^{1/2}}\iint_{\boldsymbol{g}\cdot\boldsymbol{k}>0}\exp\left\{-\frac{1}{4}g_aM^{-1}_{ab}g_b\right\}(\boldsymbol{g}\cdot\boldsymbol{k})^2(k_\beta g_\alpha+g_\beta k_\alpha)$$
$$\times\left[X\left(\frac{3}{2}g_x^2M_{x\beta}+\frac{1}{2}g_y^2M_{x\beta}+g_xg_yM_{y\beta}-(3M_{xx}+M_{yy})M_{x\beta}-2M_{xy}M_{y\beta}\right)\right.$$
$$+Y\left\{\frac{3}{4}g_y^2M_{y\beta}+\frac{1}{4}g_x^2M_{y\beta}+\frac{1}{2}g_xg_yM_{x\beta}+\frac{1}{2}(M_{xx}+3M_{yy})M_{y\beta}+M_{xy}M_{x\beta}\right.$$
$$+\frac{3M_{xy}M_{x\beta}(M_{xx}+M_{yy})^3}{3M_{xx}^3+6M_{xy}^2M_{xx}+M_{xx}M_{yy}^2+2M_{xy}^2M_{yy}}$$
$$-\frac{(3M_{xx}^4+9M_{yy}M_{xx}^3+M_{yy}^2M_{xx}^2+3M_{yy}^3M_{xx}+16M_{xy}^2M_{yy}M_{xx}-8M_{xy}^4)}{3M_{xx}^3+6M_{xy}^2M_{xx}+M_{yy}^2M_{xx}+2M_{xy}^2M_{yy}}M_{y\beta}$$

$$- \frac{4M_{xy}^3 + 3M_{xx}^2 M_{xy} + 3M_{yy}^2 M_{xy} + 2M_{xx}M_{yy}M_{xy}}{3M_{xx}^3 + 6M_{xy}^2 M_{xx} + M_{yy}^2 M_{xx} + 2M_{xy}^2 M_{yy}}$$
$$\times \left(\frac{3}{4} g_x^2 M_{x\beta} + \frac{1}{4} g_y^2 M_{x\beta} + \frac{1}{2} g_x g_y M_{y\beta} + \frac{1}{2}(3M_{xx} + M_{yy}) M_{x\beta} + M_{xy} M_{y\beta} \right) \Bigg\} \Bigg] \, \mathrm{d}\boldsymbol{g}\mathrm{d}\boldsymbol{k}. \tag{A 24}$$

To carry out the integrations over $\boldsymbol{g}$, we need the following results:

$$\int (\boldsymbol{g}\cdot\boldsymbol{k})^3 \exp\left\{-\frac{1}{4} g_a M_{ab}^{-1} g_b\right\} \mathrm{d}\boldsymbol{g} = 16\pi^{1/2} |\boldsymbol{M}|^{1/2} \vartheta^{3/2}, \tag{A 25}$$

$$\int g_x^2 (\boldsymbol{g}\cdot\boldsymbol{k})^3 \exp\left\{-\frac{1}{4} g_a M_{ab}^{-1} g_b\right\} \mathrm{d}\boldsymbol{g} = 128\pi^{1/2} |\boldsymbol{M}|^{1/2} \vartheta^{1/2} \left[\{\vartheta k_x + \varpi k_y\}^2 + \frac{1}{4} |\boldsymbol{M}| k_y^2 \right], \tag{A 26}$$

$$\int g_x g_y (\boldsymbol{g}\cdot\boldsymbol{k})^3 \exp\left\{-\frac{1}{4} g_a M_{ab}^{-1} g_b\right\} \mathrm{d}\boldsymbol{g}$$
$$= 128\pi^{1/2} |\boldsymbol{M}|^{1/2} \vartheta^{1/2} [\{\vartheta k_x + \varpi k_y\}\{\vartheta k_y - \varpi k_x\} - \frac{1}{4} |\boldsymbol{M}| k_x k_y], \tag{A 27}$$

$$\int g_y^2 (\boldsymbol{g}\cdot\boldsymbol{k})^3 \exp\left\{-\frac{1}{4} g_a M_{ab}^{-1} g_b\right\} \mathrm{d}\boldsymbol{g} = 128\pi^{1/2} |\boldsymbol{M}|^{1/2} \vartheta^{1/2} \left[\{\vartheta k_y - \varpi k_x\}^2 + \frac{1}{4} |\boldsymbol{M}| k_x^2 \right], \tag{A 28}$$

$$\int g_x (\boldsymbol{g}\cdot\boldsymbol{k})^2 \exp\left\{-\frac{1}{4} g_a M_{ab}^{-1} g_b\right\} \mathrm{d}\boldsymbol{g} = 16\pi^{1/2} |\boldsymbol{M}|^{1/2} \vartheta^{1/2} \{\vartheta k_x + \varpi k_y\}, \tag{A 29}$$

$$\int g_y (\boldsymbol{g}\cdot\boldsymbol{k})^2 \exp\left\{-\frac{1}{4} g_a M_{ab}^{-1} g_b\right\} \mathrm{d}\boldsymbol{g} = 16\pi^{1/2} |\boldsymbol{M}|^{1/2} \vartheta^{1/2} \{\vartheta k_y - \varpi k_x\}, \tag{A 30}$$

$$\int g_x^3 (\boldsymbol{g}\cdot\boldsymbol{k})^2 \exp\left\{-\frac{1}{4} g_a M_{ab}^{-1} g_b\right\} \mathrm{d}\boldsymbol{g}$$
$$= \frac{32\pi^{1/2} |\boldsymbol{M}|^{1/2}}{\vartheta^{1/2}} \{\vartheta k_x + \varpi k_y\}[4\{\vartheta k_x + \varpi k_y\}^2 + 3|\boldsymbol{M}| k_y^2], \tag{A 31}$$

$$\int g_x^2 g_y (\boldsymbol{g}\cdot\boldsymbol{k})^2 \exp\left\{-\frac{1}{4} g_a M_{ab}^{-1} g_b\right\} \mathrm{d}\boldsymbol{g}$$
$$= \frac{32\pi^{1/2} |\boldsymbol{M}|^{1/2}}{\vartheta^{1/2}} [4\{\vartheta k_y - \varpi k_x\}\{\vartheta k_x + \varpi k_y\}^2 - 2|\boldsymbol{M}| k_x k_y \{\vartheta k_x + \varpi k_y\}$$
$$+ |\boldsymbol{M}| k_y^2 \{\vartheta k_y - \varpi k_x\}], \tag{A 32}$$

$$\int g_x g_y^2 (\boldsymbol{g}\cdot\boldsymbol{k})^2 \exp\left\{-\frac{1}{4} g_a M_{ab}^{-1} g_b\right\} \mathrm{d}\boldsymbol{g}$$
$$= \frac{32\pi^{1/2} |\boldsymbol{M}|^{1/2}}{\vartheta^{1/2}} [4\{\vartheta k_x + \varpi k_y\}\{\vartheta k_y - \varpi k_x\}^2 - 2|\boldsymbol{M}| k_x k_y \{\vartheta k_y - \varpi k_x\}$$
$$+ |\boldsymbol{M}| k_x^2 \{\vartheta k_x + \varpi k_y\}], \tag{A 33}$$

$$\int g_y^3 (\boldsymbol{g}\cdot\boldsymbol{k})^2 \exp\left\{-\frac{1}{4} g_a M_{ab}^{-1} g_b\right\} \mathrm{d}\boldsymbol{g}$$
$$= \frac{32\pi^{1/2} |\boldsymbol{M}|^{1/2}}{\vartheta^{1/2}} \{\vartheta k_y - \varpi k_x\}[4\{\vartheta k_y - \varpi k_x\}^2 + 3|\boldsymbol{M}| k_x^2], \tag{A 34}$$

where

$$\vartheta = \boldsymbol{k}\cdot\boldsymbol{M}\cdot\boldsymbol{k} = T(1-\eta\cos 2\theta) \quad \text{and} \quad \varpi = -T\eta\sin 2\theta, \tag{A 35a,b}$$

and the contact vector $\boldsymbol{k}$ (cf. figure 2) is given by

$$\boldsymbol{k} = \begin{bmatrix} \cos(\theta+\phi+\frac{1}{4}\pi) \\ \sin(\theta+\phi+\frac{1}{4}\pi) \end{bmatrix}. \tag{A 36}$$

Note that

$$(\vartheta k_x + \varpi k_y) = T[\cos(\theta+\phi+\tfrac{1}{4}\pi) - \eta\cos(\theta-\phi-\tfrac{1}{4}\pi)], \tag{A 37}$$

$$(\vartheta k_y - \varpi k_x) = T[\sin(\theta+\phi+\tfrac{1}{4}\pi) + \eta\sin(\theta-\phi-\tfrac{1}{4}\pi)], \tag{A 38}$$

and to within an error of $O(\eta^3)$ we have

$$\vartheta^{3/2} \approx T^{3/2}(1-\tfrac{3}{2}\eta\cos 2\theta + \tfrac{3}{8}\eta^2\cos^2 2\theta), \tag{A 39}$$

$$\vartheta^{1/2} \approx T^{1/2}(1-\tfrac{1}{2}\eta\cos 2\theta - \tfrac{1}{8}\eta^2\cos^2 2\theta), \tag{A 40}$$

$$\vartheta^{-1/2} \approx \frac{1+\frac{1}{2}\eta\cos 2\theta + \frac{3}{8}\eta^2\cos^2 2\theta}{T^{1/2}}. \tag{A 41}$$

Using the above results we can carry out the integrations over $\boldsymbol{g}$ and $\boldsymbol{k}$ to yield

$$\begin{aligned} I^{(1)}_{x\beta\beta} &= \frac{3\rho(1+e)^2T^{1/2}}{32\rho_p\sigma\pi^{1/2}(1+\eta^2+\eta^4)} \\ &\quad\times[\{96+114\eta^2+118\eta^4-7\eta^6+\eta\sin 2\phi(24-5\eta^2+20\eta^4)\}q_x \\ &\quad+\{\eta\cos 2\phi(-24+5\eta^2-20\eta^4)\}q_y], \end{aligned} \tag{A 42}$$

$$\begin{aligned} I^{(1)}_{y\beta\beta} &= \frac{3\rho(1+e)^2T^{1/2}}{32\rho_p\sigma\pi^{1/2}(1+\eta^2+\eta^4)}[\{\eta\cos 2\phi(-24+5\eta^2-20\eta^4)\}q_x \\ &\quad+\{96+114\eta^2+118\eta^4-7\eta^6-\eta\sin 2\phi(24-5\eta^2+20\eta^4)\}q_y], \end{aligned} \tag{A 43}$$

$$\begin{aligned} I^{(2)}_{x\beta\beta} &= -\frac{3\rho(1-e^2)T^{1/2}}{8\rho_p\sigma\pi^{1/2}(1+\eta^2+\eta^4)}[\{16+21\eta^2+21\eta^4-\eta^6+2\eta(1-\eta^2)^2\sin 2\phi\}q_x \\ &\quad+\{-2\eta(1-\eta^2)^2\cos 2\phi\}q_y], \end{aligned} \tag{A 44}$$

$$\begin{aligned} I^{(2)}_{y\beta\beta} &= -\frac{3\rho(1-e^2)T^{1/2}}{8\rho_p\sigma\pi^{1/2}(1+\eta^2+\eta^4)}[\{-2\eta(1-\eta^2)^2\cos 2\phi\}q_x \\ &\quad+\{16+21\eta^2+21\eta^4-\eta^6-2\eta(1-\eta^2)^2\sin 2\phi\}q_y], \end{aligned} \tag{A 45}$$

$$\begin{aligned} I^{(3)}_{x\beta\beta} &= -\frac{\rho(1+e)T^{1/2}}{32\rho_p\sigma\pi^{1/2}(1+\eta^2+\eta^4)} \\ &\quad\times[\{704+804\eta^2+933\eta^4+73\eta^6+\eta\sin 2\phi(208+157\eta^2+184\eta^4+105\eta^6)\}q_x \\ &\quad+\{-\eta\cos 2\phi(208+157\eta^2+184\eta^4+105\eta^6)\}q_y], \end{aligned} \tag{A 46}$$

$$\begin{aligned} I^{(3)}_{y\beta\beta} &= -\frac{\rho(1+e)T^{1/2}}{32\rho_p\sigma\pi^{1/2}(1+\eta^2+\eta^4)}[\{-\eta\cos 2\phi(208+157\eta^2+184\eta^4+105\eta^6)\}q_x \\ &\quad+\{704+804\eta^2+933\eta^4+73\eta^6-\eta\sin 2\phi(208+157\eta^2+184\eta^4+105\eta^6)\}q_y]. \end{aligned} \tag{A 47}$$

Substituting (A 42)–(A 47) into (A 14), we obtain the final expressions (6.13)–(6.15) for the third-order source term.

Appendix B. Series representation for collision integrals

Recall from § 3.2 that the integration over the contact vector $\boldsymbol{k}$ is transformed into the integration over another variable $\theta \in (0, 2\pi)$ (the angle between $\boldsymbol{k}$ and $|M_1\rangle$, the eigenvector corresponding to the smaller eigenvalue of the second-moment tensor $\boldsymbol{M}$; cf. figure 2). The expressions for the integrals appearing in (3.27)–(3.29) are

$$\mathscr{H}_{\alpha\beta\gamma}(\eta, R, \phi) \equiv \int_0^{2\pi} \cos^\alpha 2\theta \sin^\beta 2\theta\, (1-\eta\cos 2\theta)^{\gamma/2} \mathfrak{F}(\eta, R, \phi, \theta)\, \mathrm{d}\theta, \tag{B 1}$$

$$\mathscr{J}_{\alpha\beta\gamma}(\eta, R, \phi) \equiv \int_0^{2\pi} \cos^\alpha 2\theta \sin^\beta 2\theta\, (1-\eta\cos 2\theta)^{\gamma/2} \mathfrak{G}(\eta, R, \phi, \theta)\, \mathrm{d}\theta. \tag{B 2}$$

Now substituting the infinite series representation for $\mathfrak{F}$ and $\mathfrak{G}$, as given in (4.1) and (4.2), into above integrals, a term-by-term integration can be carried out for both integrals $\mathscr{H}_{\alpha\beta\gamma}$ and $\mathscr{J}_{\alpha\beta\gamma}$. For example, the series representation for $\mathscr{H}_{003}$ is

$$\begin{aligned}
\mathscr{H}_{003}(\eta, R, \phi) \;=\; & 3\pi^{3/2}\eta R\cos 2\phi + \sum_{n=0}^{\infty} \Lambda(\tfrac{3}{2}, 2n)\pi^{1/2}\eta^{2n}\frac{2\Gamma(n+\frac{1}{2})}{n!} \\
& + 12R^2 \sum_{n=0}^{\infty} \Lambda\left(\frac{1}{2}, 2n\right)\eta^{2n}\frac{\pi^{1/2}(1+n+n\cos 4\phi)\Gamma(n+\frac{1}{2})}{(n+1)!} \\
& + 8R^4\left[\frac{3}{4}\pi + \frac{3}{64}\pi\eta^2(3+2\cos 4\phi) + O(\eta^4)\right] + O(R^6),
\end{aligned} \tag{B 3}$$

$$\begin{aligned}
\mathscr{J}_{020}(\eta, R, \phi) \;=\; & \frac{1}{2}\pi^{3/2} - 4R\sum_{n=0}^{\infty} \Lambda(2n+\frac{1}{2}, 2n+1)\eta^{2n+1}\frac{\pi^{1/2}\cos 2\phi\,\Gamma(n+\frac{3}{2})}{(n+2)!} \\
& + 2\pi R^2 \sum_{n=0}^{\infty} \eta^{2n}\frac{\{2+n+(n-1)\cos 4\phi\}\Gamma(n+\frac{1}{2})}{(n+2)!} \\
& - \frac{8}{3}R^3 \sum_{n=0}^{\infty} \Lambda\left(2n+\frac{3}{2}, 2n+1\right)\eta^{2n+1} \\
& \frac{\pi^{1/2}\cos 2\phi\{6+n+(n-3)\cos 4\phi\}\Gamma(n+\frac{3}{2})}{(n+3)!} + O(R^5),
\end{aligned} \tag{B 4}$$

where

$$\Lambda(\alpha, \beta) \equiv \frac{\Gamma(\alpha+1)}{\beta!\Gamma(\alpha+1-\beta)}, \tag{B 5}$$

with similar expressions for other integrals of $\mathscr{H}_{\alpha\beta\gamma}$ and $\mathscr{J}_{\alpha\beta\gamma}$.

Each of the above infinite series at the third-order approximation in R and η, with error $O(R^m\eta^n)$ and $(m+n) \geqslant 4$, can be simplified to

$$\left.\begin{aligned}
&\mathscr{H}_{003}(\eta, R, \phi) = 2\pi + 12\pi R^2 + 3\pi^{3/2}\eta R\cos 2\phi + \tfrac{3}{8}\pi\eta^2 + O(R^m\eta^n), \\
&\mathscr{H}_{103}(\eta, R, \phi) = -3\pi^{3/2}R\cos 2\phi - \tfrac{3}{2}\pi\eta \underbrace{- 6\pi^{3/2}R^3\cos 2\phi - \tfrac{3}{2}\pi\eta R^2(2+\cos 4\phi)}, \\
&\mathscr{H}_{013}(\eta, R, \phi) = 3\pi^{3/2}R\sin 2\phi + \underbrace{6\pi^{3/2}R^3\sin 2\phi + \tfrac{3}{2}\pi\eta R^2\sin 4\phi}, \\
&\mathscr{H}_{021}(\eta, R, \phi) = \pi - \tfrac{1}{32}\pi\eta^2 + 3\pi R^2(2-\cos 4\phi), \\
&\mathscr{H}_{111}(\eta, R, \phi) = -3\pi R^2\sin 4\phi,
\end{aligned}\right\} \tag{B 6}$$

$$\left.\begin{aligned}
\mathscr{J}_{020}(\eta, R, \phi) &= \tfrac{1}{2}\pi^{3/2} - \tfrac{1}{2}\pi R\eta\cos 2\phi + \pi^{3/2}R^2(2-\cos 4\phi),\\
\mathscr{J}_{110}(\eta, R, \phi) &= \tfrac{1}{2}\pi R\eta\sin 2\phi - \pi^{3/2}R^2\sin 4\phi,\\
\mathscr{J}_{010}(\eta, R, \phi) &= 4\pi R\sin 2\phi - \underbrace{\pi^{3/2}\eta R^2\sin 4\phi + \tfrac{3}{8}\pi R\eta^2\sin 2\phi + 4\pi R^3\sin 2\phi}, \\
\mathscr{J}_{200}(\eta, R, \phi) &= \tfrac{1}{2}\pi^{3/2} - \tfrac{3}{2}\pi R\eta\cos 2\phi + \pi^{3/2}R^2(2+\cos 4\phi),\\
\mathscr{J}_{100}(\eta, R, \phi) &= -4\pi R\cos 2\phi + \underbrace{\pi^{3/2}\eta R^2(2+\cos 4\phi) - \tfrac{9}{8}\pi R\eta^2\cos 2\phi - 4\pi R^3\cos 2\phi},
\end{aligned}\right\} \quad \text{(B 7)}$$

$$\left.\begin{aligned}
\mathscr{J}_{102}(\eta, R, \phi) &= -4\pi R\cos 2\phi - \tfrac{1}{2}\pi^{3/2}\eta + \underbrace{\tfrac{3}{8}\pi R\eta^2\cos 2\phi - 4\pi R^3\cos 2\phi},\\
\mathscr{J}_{012}(\eta, R, \phi) &= 4\pi R\sin 2\phi - \underbrace{\tfrac{1}{8}\pi R\eta^2\sin 2\phi + 4\pi R^3\sin 2\phi},\\
\mathscr{J}_{002}(\eta, R, \phi) &= \pi^{3/2} + 4R^2\pi^{3/2} + 2\pi\eta R\cos 2\phi.
\end{aligned}\right\} \quad \text{(B 8)}$$

Removing the underbraced terms yields second-order series approximation for the above integral expressions. Note that some of the above quantities have zero contribution at third order, and hence they are equal at both second- and third-order approximation.

Appendix C. Evaluation of stress tensor for uniform shear flow

Here we present explicit expressions for the transport coefficients of the USF as obtained from series solutions. The components of the dimensionless stress tensor are

$$\begin{aligned}
P^*_{xx} &= \frac{P_{xx}}{\rho_p {U_R}^2}\\
&= \nu T^*\left((1+\eta\sin 2\phi) + \frac{\nu g_0(1+e)}{\pi^{3/2}}[\mathscr{J}_{002}(\eta, R, \phi)\right.\\
&\quad \left. - \cos 2\phi\,\mathscr{J}_{012}(\eta, R, \phi) - \sin 2\phi\,\mathscr{J}_{102}(\eta, R, \phi)]\right), \qquad \text{(C 1)}\\
P^*_{yy} &= \frac{P_{yy}}{\rho_p {U_R}^2}\\
&= \nu T^*\left((1-\eta\sin 2\phi) + \frac{\nu g_0(1+e)}{\pi^{3/2}}[\mathscr{J}_{002}(\eta, R, \phi)\right.\\
&\quad \left. + \cos 2\phi\,\mathscr{J}_{012}(\eta, R, \phi) + \sin 2\phi\,\mathscr{J}_{102}(\eta, R, \phi)]\right), \qquad \text{(C 2)}\\
P^*_{xy} &= \frac{P_{xy}}{\rho_p {U_R}^2}\\
&= \nu T^*\left(-\eta\cos 2\phi + \frac{\nu g_0(1+e)}{\pi^{3/2}}[\cos 2\phi\,\mathscr{J}_{102}(\eta, R, \phi) - \sin 2\phi\,\mathscr{J}_{012}(\eta, R, \phi)]\right), \qquad \text{(C 3)}
\end{aligned}$$

where ρ_p is the density of particles, and the reference velocity scale for non-dimensionalization is $U_R = 2\dot{\gamma}\sigma$. Substituting the power-series expressions for $\mathscr{J}_{002}$, $\mathscr{J}_{012}$ and $\mathscr{J}_{102}$ as given by (B 8) in appendix B, we obtain the super-Burnett-order, $O(R^3)$, expression for the stress tensor in § 4.2.

The pressure $p = (P_{xx} + P_{yy})/2$ is calculated from the average of (C 1) and (C 2), which can be further decomposed into its kinetic and collisional parts:

$$p^* = \frac{p}{\rho_p {U_R}^2} = p_k^* + p_c^* = \nu T^* \left[1 + \frac{\nu g_0(1+e)}{\pi^{3/2}} \mathscr{J}_{002}(\eta, R, \phi)\right], \tag{C 4}$$

$$p_k^* = \nu T^*, \tag{C 5}$$

$$p_c^* = \frac{\nu g_0(1+e)}{\pi^{3/2}} T^* \mathscr{J}_{002}(\eta, R, \phi). \tag{C 6}$$

The dimensionless shear viscosity and its kinetic and collisional components are given by

$$\begin{aligned} \mu^* &= \frac{-P_{xy}}{\rho_p {U_R}^2} = \mu_k^* + \mu_c^* \\ &= \frac{\nu}{64R^2}\left[\eta \cos 2\phi - \frac{\nu g_0(1+e)}{\pi^{3/2}}\{\cos 2\phi\, \mathscr{J}_{102}(\eta, R, \phi) - \sin 2\phi\, \mathscr{J}_{012}(\eta, R, \phi)\}\right], \end{aligned} \tag{C 7}$$

$$\mu_k^* = \frac{\nu\eta \cos 2\phi}{64R^2}, \tag{C 8}$$

$$\mu_c^* = -\frac{\nu^2 g_0(1+e)}{64\pi^{3/2}R^2}[\cos 2\phi\, \mathscr{J}_{102}(\eta, R, \phi) - \sin 2\phi\, \mathscr{J}_{012}(\eta, R, \phi)]. \tag{C 9}$$

The granular temperature (3.5) is given by

$$T = \frac{M_{xx} + M_{yy}}{2} \quad \Longrightarrow \quad T^* = \frac{T}{{U_R}^2} = \frac{1}{64R^2}. \tag{C 10}$$

For the full numerical solution of the moment equations (3.29)–(3.31), the transport coefficients are calculated from (C 1)–(C 9) by evaluating the integrals $\mathscr{J}_{002}$, $\mathscr{J}_{102}$ and $\mathscr{J}_{012}$ in (B 2) by using standard quadrature rules.

On the other hand, for the series solution, (4.3) or (4.4) (at second order or third order, respectively) are solved for η, R and ϕ. Next the series expressions for $\mathscr{J}_{002}$, $\mathscr{J}_{102}$ and $\mathscr{J}_{012}$ ((B 8) from appendix B) are inserted into (C 1)–(C 9) in order to calculate the transport coefficients.

Appendix D. Constitutive model of Navier–Stokes order (Lutsko 2005)

The constitutive model for an inelastic hard-disk system is taken from Lutsko (2005), which is almost identical to that of Garzo *et al.* (2007) up to the first Sonine approximation:

$$g_0 = \frac{16 - 7\nu}{16(1-\nu)^2}, \tag{D 1}$$

$$\alpha_2 = \frac{16(1-e)(1-2e^2)}{57 - 25e + 30(1-e)e^2}, \tag{D 2}$$

$$\varphi_\mu^* = g_0\left(1 - \tfrac{1}{8}(1-e)(1-3e)\right), \tag{D 3}$$

$$\zeta^* = \tfrac{1}{2} g_0(1-e^2). \tag{D 4}$$

The dimensionless pressure with its kinetic and collisional parts are given by

$$p^* = \nu T^*(1 + (1+e)\nu g_0) = p_k^* + p_c^*, \tag{D 5}$$

$$p_k^* = \nu T^*, \tag{D 6}$$

$$p_c^* = (1+e)\nu^2 g_0 T^*, \tag{D 7}$$

and the dimensionless viscosity is

$$\mu^* = \mu_k^* + \mu_c^*, \tag{D 8}$$

$$\mu_k^* = \frac{\sqrt{\pi}}{8} T^{*1/2} \frac{(1 - \frac{1}{4}(1+e)(1-3e)\nu g_0)}{(\varphi_\mu^* - \frac{1}{2}\zeta^*)}, \tag{D 9}$$

$$\mu_c^* = \frac{\sqrt{\pi}}{8} T^{*1/2} \left[\frac{(1+e)\{1 - \frac{1}{4}(1+e)(1-3e)\nu g_0\}\nu g_0}{2(\varphi_\mu^* - \frac{1}{2}\zeta^*)} + \frac{4(1+e)(1 - \frac{1}{16}\alpha_2)\nu^2 g_0}{\pi} \right]. \tag{D 10}$$

The expression for the dimensionless temperature follows from the energy balance equation:

$$T^* = \frac{\pi(1 - \frac{1}{4}(1+e)(1-3e)\nu g_0)(1 + \frac{1}{2}(1+e)\nu g_0)}{32(1-e^2)(1 + \frac{3}{16}\alpha_2)(\varphi_\mu^* - \frac{1}{2}\zeta^*)\nu^2 g_0} + \frac{1 - \frac{1}{16}\alpha_2}{8(1-e)(1 + \frac{3}{16}\alpha_2)}. \tag{D 11}$$

REFERENCES

ALAM, M. & LUDING, S. 2003*a* First normal stress difference and crystallization in sheared granular fluid. *Phys. Fluids* **15**, 2298–2312.

ALAM, M. & LUDING, S. 2003*b* Rheology of bidisperse granular mixtures via event-driven simulations. *J. Fluid Mech.* **476**, 69–103.

ALAM, M. & LUDING, S. 2005*a* Energy non-equipartition, rheology and microstructure in sheared bidisperse granular mixtures. *Phys. Fluids* **17**, 063303.

ALAM, M. & LUDING, S. 2005*b* Non-Newtonian granular fluid: simulation and theory. In *Powders and Grains* (ed. R. Garcia-Rojo, H. J. Herrmann & S. McNamara), pp. 1141–1144. A. A. Balkema.

ALAM, M., WILLITS, J. T., ARNARSON, B. O. & LUDING, S. 2002 Kinetic theory of a binary mixture of nearly elastic disks with size and mass disparity. *Phys. Fluids* **14**, 4085–4087.

ARAKI, S. & TREMAINE, S. 1986 The dynamics of dense particle disks. *Icarus* **65**, 83–109.

BREY, J. J., DUFTY, J. W., KIM, C. S. & SANTOS, A. 1998 Hydrodynamics for granular flow at low density. *Phys. Rev.* E **58**, 4638–4653.

BRILLIANTOV, N. V. & PÖSCHEL, T. 2003 Hydrodynamics and transport coefficients for dilute granular gases. *Phys. Rev.* E **67**, 061304.

BRILLIANTOV, N. V. & PÖSCHEL, T. 2004 *Kinetic Theory of Granular Gases*. Oxford University Press.

BURNETT, D. 1935 The distribution of velocities in a slightly non-uniform gas. *Proc. Lond. Math. Soc.* **39**, 385–430.

CHAPMAN, S. & COWLING, T. G. 1970 *The Mathematical Theory for Non-Uniform Gases*. Cambridge University Press.

CHOU, C. S. & RICHMAN, M. W. 1998 Constitutive theory for homogeneous granular shear flows of highly inelastic spheres. *Physica* A **259**, 430–448.

ESPOSITO, L. 2006 *Planetary Rings*. Cambridge University Press.

GARZO, V. 2012 Grad's moment method for a low density granular gas: Navier–Stokes transport coefficients. *AIP Conf. Proc.* **1501**, 1031–1037.

GARZO, V., SANTOS, A. & MONTANERO, J. M. 2007 Modified Sonine approximation for the Navier–Stokes transport coefficients of a granular gas. *Physica* A **376**, 94–107.

GAYEN, B. & ALAM, M. 2006 Algebraic and exponential instabilities in a sheared micropolar granular fluid. *J. Fluid Mech.* **567**, 195–231.

GAYEN, B. & ALAM, M. 2008 Orientational correlation and velocity distributions in uniform shear flow of a dilute granular gas. *Phys. Rev. Lett.* **100**, 068002.

GOLDHIRSCH, I. 2003 Rapid granular flows. *Annu. Rev. Fluid Mech.* **35**, 267–293.

GOLDREICH, P. & TREMAINE, S. 1978 The velocity dispersion in Saturn's rings. *Icarus* **34**, 227–239.

GRAD, H. 1949 On the kinetic theory of rarefied gases. *Commun. Pure Appl. Maths* **2**, 331–407.

JENKINS, J. T. & RICHMAN, M. W. 1985*b* Grad's 13-moment system for a dense gas of inelastic spheres. *Arch. Rat. Mech. Anal.* **87**, 355–377.

JENKINS, J. T. & RICHMAN, M. W. 1985*a* Kinetic theory of plane flows of a dense gas of identical, rough, inelastic, circular disks. *Phys. Fluids* **28**, 3485–3494.

JENKINS, J. T. & RICHMAN, M. W. 1988 Plane simple shear of smooth inelastic circular disks. *J. Fluid Mech.* **192**, 313–328.

KOGAN, M. N. 1969 *Rarefied Gas Dynamics*. Plenum Press.

KREMER, G. M. & MARQUES, W. 2011 Fourteen moment theory for granular gases. *Kinet. Relat. Models* **4**, 317–331.

LATTER, H. N. & OGILVIE, G. I. 2006 The linear stability of dilute particulate rings. *Icarus* **184**, 498–516.

LEES, A. W. & EDWARDS, S. 1972 The computer study of transport processes under extreme conditions. *J. Phys.* C **5**, 1921–1929.

LUTSKO, J. F. 2004 Rheology of dense polydisperse granular fluids under shear. *Phys. Rev.* E **70**, 061101.

LUTSKO, J. F. 2005 Transport properties of dense dissipative hard-sphere fluids for arbitrary energy loss models. *Phys. Rev.* E **72**, 021306.

MITARAI, N. & NAKANISHI, H. 2007 Velocity correlations in dense granular shear flows: effects on energy dissipation and normal stress. *Phys. Rev.* E **75**, 031305.

MITARAI, N., NAKANISHI, H. & HAYAKAWA, H. 2002 Collisional granular flow as a micropolar fluid. *Phys. Rev. Lett.* **88**, 174301.

MONTANERO, J. M., GARZO, V., ALAM, M. & LUDING, S. 2006 Rheology of two- and three-dimensional granular mixtures under uniform shear flow: Enskog kinetic theory versus molecular dynamics simulations. *Granul. Matt.* **8**, 103–115.

RAO, K. K. R. & NOTT, P. R. 2008 *An Introduction to Granular Flow*. Cambridge University Press.

RONGALI, R. & ALAM, M. 2014 Higher-order effects on orientational correlation and relaxation dynamics in homogeneous cooling of a rough granular gas. *Phys. Rev.* E **89**, 062201.

ROSENAU, P. 1989 Extending hydrodynamics via the regularization of the Chapman–Enskog expansion. *Phys. Rev.* A **40**, 7193–7196.

SAHA, S. & ALAM, M. 2014 Conductivity and Dufour tensors in a sheared granular gas (in preparation).

SANTOS, A. 2008 Does the Chapman–Enskog expansion for sheared granular gases converge? *Phys. Rev. Lett.* **100**, 078003.

SANTOS, A., GARZO, V. & DUFTY, J. W. 2004 Inherent rheology of a granular fluid in uniform shear. *Phys. Rev.* E **69**, 061303.

SAVAGE, S. B. & JEFFREY, D. J. 1981 The stress tensor in a granular flow at high shear rates. *J. Fluid Mech.* **110**, 255–272.

SCHMIDT, J., SALO, H., SPAHN, F. & PETZSCHMANN, O. 2001 Viscous overstability in Saturn's B-ring: hydrodynamic theory and comparison to simulations. *Icarus* **153**, 316–331.

SELA, N. & GOLDHIRSCH, I. 1998 Hydrodynamic equations for rapid flows of smooth inelastic spheres. *J. Fluid Mech.* **361**, 41–74.

SELA, N., GOLDHIRSCH, I. & NOSKOWICZ, S. H. 1996 Kinetic theoretical study of a simply sheared two-dimensional granular gas to Burnett order. *Phys. Fluids* **8**, 2337–2353.

SHUKHMAN, G. 1984 Collisional dynamics of particles in Saturn's rings. *Sov. Astron.* **28**, 547–584.

SHUKLA, P. & ALAM, M. 2009 Order parameter description of shear-banding in granular Couette flow via Landau equation. *Phys. Rev. Lett.* **103**, 068001.

SHUKLA, P. & ALAM, M. 2011*a* Nonlinear stability and patterns in granular plane Couette flow: Hopf and pitchfork bifurcations, and evidence for resonance. *J. Fluid Mech.* **672**, 147–195.

SHUKLA, P. & ALAM, M. 2011*b* Weakly nonlinear theory of shear-banding instability in granular plane Couette flow: analytical solution, comparison with numerics and bifurcation. *J. Fluid Mech.* **666**, 204–253.

SIMON, V. & JENKINS, J. T. 1994 On the vertical structure of dilute planetary rings. *Icarus* **110**, 109–116.

TORRILHON, M. & STRUCHTRUP, H. 2004 Regularized 13-moment equations: shock structure calculations and comparison to Burnett models. *J. Fluid Mech.* **513**, 171–198.

TRUESDELL, C. & MUNCASTER, R. G. 1980 *Fundamentals of Maxwell's Kinetic Theory of a Simple Monatomic Gas*. Academic Press.

VEGA REYES, F., SANTOS, A. & GARZO, V. 2013 Steady base states for non-Newtonian granular hydrodynamics. *J. Fluid Mech.* **719**, 431–464.

VERLET, L. & LEVESQUE, D. 1982 Integral equations for classical fluids III. The hard disk system. *Mol. Phys.* **46**, 969–980.

List of Corrections in Updated Thesis

The thesis has been updated and reorganized following the suggestions of two reviewers.

Chapter 1

1. $1\mu m$ is changed to 1mm.

Chapter 2

1. In expressions (2.51)-(2.52), the colour is changed to "blue".
2. Text quoted from the work of Garzo (2013) is modified and made in italic font.
3. A footnote is added to explain the word "dense" in page 19.

Chapter 3

1. Appendices A-H have been renamed as appendices F-M and pushed to the end of the thesis.

Chapter 4

Major changes are made in this chapter. Initially in the first draft of my thesis I mistakenly assumed terms like $\frac{\lambda^2 R}{St_d}$ are of third order in shear rate. But actually it is a Burnett order term (second order in shear rate) and therefore should appear in the Burnett order equations of second moment balance and consequently there will be changes in the super-Burnett and super-super-Burnett order equations as well. This inclusion in the Burnett order approximations of the second moment balance produces quantitative and qualitative improvement of the analytical solutions at various orders which are manifested in the figures for comparison with full numerical solution. In summary the list of changes made in chapter 4 are as follows:

1. The Burnett order equations (4.56) are modified and therefore there is some modification in Sec 4.5.
2. Related results for dry granular gas of Chapter 3 are recovered and a new subsection 4.5.1 is devoted to this.
3. The super- Burnett and super-super-Burnett order equations are modified and are listed in subsection 4.5.2.
4. The expression for shear viscosity for a dry granular gas is derived in 4.6.2.
5. Figures 4.3-4.12 are updated.

Chapter 5

1. Appendices I-M are renamed to Appendices A-E.

Journal Publications

1. Non-Newtonian stress, collisional dissipation and heat flux in the shear flow of inelastic disks: a reduction via Grad's moment method,
   Saikat Saha & Meheboob Alam,
   Journal of Fluid Mechanics, vol. **757**, pp. 251-296, 2014.

   [Added as a supplementary material]

2. Normal stress differences, their origin and constitutive relations for a sheared granular fluid,
   Saikat Saha & Meheboob Alam,
   Journal of Fluid Mechanics, vol. **795**, pp. 549-580, 2016. [Chapter 3]

3. Revisiting ignited-quenched transition and the non-Newtonian rheology of a sheared dilute gas-solid suspension,
   Saikat Saha & Meheboob Alam,
   Journal of Fluid Mechanics, vol. **833**, pp. 206-246, 2017. [Chapter 5]

In Preparation

1. Anisotropy and nonlinear rheology of a sheared gas-solid suspension: Theory and simulation ,
   Saikat Saha, Ronak Gupta & Meheboob Alam (2017), [Chapter 4]

2. Higher-order theories for a dense granular fluid: normal stress differences and heat flux,
   Saikat Saha & Meheboob Alam (2018), [Chapter 2]

Conference Proceeding

1. Normal stress differences and beyond-Navier-Stokes hydrodynamics,
   Meheboob Alam & **Saikat Saha**,
   EPJ. Conf., *8th International Conference on Micromechanics of Granular Media*, vol. **140**, pp. 11014, 2017.